NASA Conference Publication 2287

Refrigeration for Cryogenic Sensors

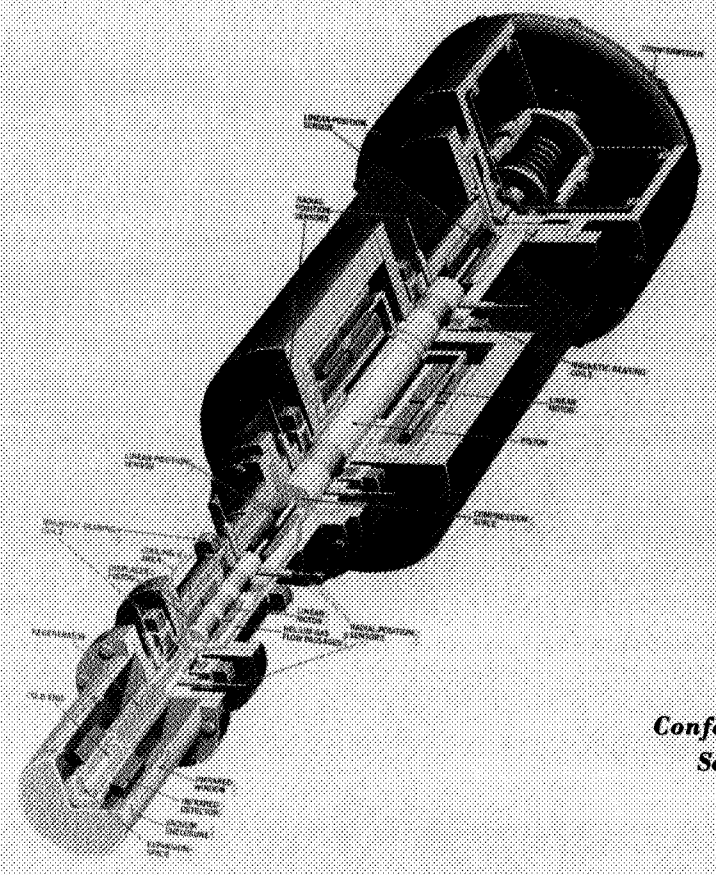

Proceedings of the Second Biennial Conference on Refrigeration for Cryogenic Sensors and Electronic Systems held at NASA Goddard Space Flight Center Greenbelt, Maryland December 7-8, 1982

25th Anniversary
1958-1983

NASA

NASA Conference Publication 2287

Refrigeration for Cryogenic Sensors

Max Gasser, *Editor*
Goddard Space Flight Center

Proceedings of the Second Biennial Conference on Refrigeration for Cryogenic Sensors and Electronic Systems held at NASA Goddard Space Flight Center Greenbelt, Maryland December 7-8, 1982

National Aeronautics and Space Administration

Scientific and Technical Information Branch

1983

INTRODUCTION

This document contains the proceedings of the Second Biennial Conference on Refrigeration for Cryogenic Sensors and Electronic Systems. The Conference was held at the National Aeronautics and Space Administration's Goddard Space Flight Center, Greenbelt, Maryland, on December 7-8, 1982.

The first cryogenic refrigeration conference was held at the National Bureau of Standards, Boulder, Colorado, in October 1980. Its objective was to report and discuss the state of cryocooler technology in a temperature range below 20 K with cooling capacity below 10 K. The conference was extremely beneficial to the cryocooler community, and as a result, the participants voted unanimously to meet again.

The objectives of the second conference were similar to the first. The emphasis was to be on low temperature, closed cycle cooler technology; however, higher temperature coolers (77 K), with technology applicable to the low temperature coolers, were considered to be within the scope of the meeting.

The importance of cryocooler technology cannot be overemphasized. The utilization of superconducting and other cryogenic instruments, on the ground and in space, rests heavily on the development of reliable, compact, low-cost cryocoolers. To this end, we hope the second conference made a contribution.

The Editors

Second Biennial Conference on
Refrigeration for Cryogenic Sensors and Electronic Systems

Mr. Edgar A. Edelsack
Office of Naval Research

Dr. Martin Nisenoff
Naval Research Laboratory

Dr. Allan Sherman
NASA/Goddard Space Flight Center

Mr. Max G. Gasser
NASA/Goddard Space Flight Center

Dr. Ralph C. Longsworth
Air Products and Chemicals Inc.

Dr. Peter J. Kerney
CTI-Cryogenics

CONTENTS

CONTENTS (continued)

CONTENTS (continued)

CONTENTS (continued)

U.S. NAVY PROGRAM IN SMALL CRYOCOOLERS

M. Nisenoff
Naval Research Laboratory
Washington, D.C. 20375 USA

E. A. Edelsack
Office of Naval Research
Arlington, VA 22217 USA

ABSTRACT

If superconducting and cryogenically cooled electronic instrumentation are to be deployed in future Naval operational systems, there is an strong need for compact, highly reliable cryogenic refrigerators. Accordingly, several years ago, a Navy program was initiated to develop fractional-watt cryocoolers capable of operating below 10 K. Several varieties of Stirling coolers have been built and are under evaluation. In addition, helium gas compressors designed for use with small, closed cycle Joule-Thomson coolers are under development. An overview of the technical aspects of the program are presented. Many of the individual efforts supported under this program are discussed in detail elsewhere at this Conference.

INTRODUCTION

Superconductive electronic systems are fast becoming a practical reality. In addition, there is interest in the use of semiconductor devices and circuits operating at temperatures of 77 K and below. With the possible exception of cryogenic high speed, high density computer application, the required cooling capacity for most applications are quite modest, from microwatts to fractions of a watt at the operating temperature. Efficient, highly reliable, fractional watt closed cycle refrigeration systems ("cryocoolers") have been developed for operating temperatures near 77 K. However, there has been only limited activity in developing fractional watt coolers for the temperature region below about 50 K.

The realization that closed cycle refrigerators are essential to make cryogenic electronics a viable technology is not new. For example, Prof. S. C. Collins, the inventor of the Collins cryostat, made the following observations in 1958 when he was awarded the Kamerlingh Onnes Medal on the occasion of the 50th anniversary of the liquefaction of helium:[1]

> In recent years we hear much about ingenious devices for computer elements and amplifiers which require a very low temperature environment. . . . At long last it seems that a practical application for superconductivity has been found. The technical problems yet to

be solved may be formidable but, if one may judge by the vigor and optimism with which many competent people are attacking these problems, solutions will soon be found.

The matter of suitable refrigeration presents a different kind of problem. It too, must be resolved before success is complete. For very large computers a supply of liquid helium might be accepted with reluctance. What is really demanded is a closed-cycle helium refrigerator of great reliability which can provide the required refrigeration at temperatures down to 1.2 K without interruption for months at a time. For large installations such a refrigerator, I believe, can now be produced and its performance guaranteed. But the field of application is much broader if one can have compact refrigerators of small power which can be plugged into a wall socket, as you do a household refrigerator. This is more difficult because small machines are much more sensitive to trouble of all sorts. Several groups, however, have set out to produce just such a unit. There is a general feeling that by the time the physicists are ready for them the refrigerators will be available.

These comments, both in regard to superconductivity as well as to small refrigerators, are true today as they were 24 years ago.

The U.S. Navy is exploring the feasibility of using superconductive electronic devices, circuits and systems in surveillance, communications and data processing applications. Since the highest known value of a superconducting transition temperature is 23 K, the refrigeration interest is in the region below 20 K, with strong interest below 10 K. In the research laboratory, the use of liquid cryogens such as boiling liquid hydrogen (20.4 K) and liquid helium (4.2 K) are commonly used to provide the needed cryogenic environment. However, if such systems are to be used away from the laboratory, the logistics of providing a continuous supply of liquid cryogens can be both tedious and difficult. Furthermore, the use of liquid hydrogen or helium is often considered too exotic for non-cryogenic specialists. Therefore, to expedite the introduction of superconductive or cooled semiconductor electronic systems in operational situations, a program was initiated several years ago by the Office of Naval Research to develop small, highly reliable, energy-efficient cryocoolers for the temperature region near 10 K.

SPECIFICATIONS

A summary of various 4 K refrigeration systems and the range of required cooling capacity is presented in Table I. In response to demand, commercial refrigerators are available with cooling capacities greater than several watts.[2] However, whenever there is a fractional watt requirement, larger refrigerators are used even though the weight, volume, electrical input power and cost may be excessive for the specific application. A survey of available coolers, both those operating near 10 K as well as at higher temperatures indicated that the efficiency (that is, the percent of Carnot efficiency for the particular operating and ambient temperatures) of small, fractional watt

coolers was low compared to that realized in larger capacity machines (see Fig. 1).[3,4] Furthermore, it appears that there was a distinct penalty in weight, volume, electrical input power and cost in 4 K machines compared to coolers that operate near 10 K.[5] Since minimizing all of these parameters are crucial if superconductive electronic systems are to be deployed in most operational systems, the decision was made to develop closed cycle refrigerators operating below 10 K.

In considering the various applications in which superconductive and cooled semiconductor devices and circuits might be used in research, industrial or military situations, it became evident that no one set of parameters could satisfy all potential applications. In formulating goals for this program, a set of desired specifications was selected. However, throughout the program, the contractors performed trade-off studies to determine how varying one parameter influenced the other parameters.

The tentative design goals selected for the parameters of the cryocoolers to be developed under this Program are given in Table II. The weight and volume of the cooled package are typical for a superconducting gradiometer sensor and coil systems.[6] In many applications, both weight and volume to be cooled might be considerably smaller. The ultimate temperature of less than 8 K was chosen so that superconductive circuits fabricated from niobium (transition temperature of 9.2 K) might be used with these coolers. The reserved cooling capacity and three electrical loads were specified to emphasize that efficient use of intermediate cooling stations should be made and that coolers should have some reserve capacity for handling active loads at the low temperature. The goal for the electrical input power is 100 watts while a figure of 250 watts might be acceptable. (The input power figure includes all power required for the operation of the cryocooler such as vacuum pumps, cooling systems, etc.) These input power values correspond to a cooler coefficient of performance from 2,000 to 10,000 watts/watts, which is compatible with the data shown in Fig. 1. The total system weight and volume should, of course, be minimal. The time between routine maintenance and Mean Time Before Failure should be as long as possible, certainly months, while at times approaching a year of continuous operation would be desirable. Since one application of superconducting instrumentation is the SQUID magnetometer and magnetic gradiometer, care should be exercised to minimize the magnetic signature and mechanical vibration spectrum by proper design and the use of suitable materials. Although the sensitivity of SQUID systems is in the range of 10^{-14} tesla rms per root hertz (10^{-10} gauss rms per root hertz), the requirements for magnetic signature and vibration spectrum of cold finger were somewhat relaxed for this phase of the program. In subsequent phases of the program which may focus on interfacing cryocoolers with SQUID magnetic instrumentation, these specifications will probably have to be modified to reduce the interference signals from the cooler. The cool down time for a cryocooler is extremely dependent on the end use; in some cases, the system must be cooled from ambient temperature to operating temperature in minutes or less while in other applications, cool down time is irrelevant as the total system, once cooled, would be maintained at operating temperature for extremely long times. For this phase, it was specified that with the maximum mass to be cooled, the cooldown time could be as long as 24 hours although shorter times would be desirable.

PROGRAM

At the start of this program in 1980, new and novel concepts in cryocooler design were solicited which would satisfy the design goal outlined above. In addition to the complete system design, responses were also solicited in the areas of components, such as compressors, shaft seals, regenerative materials, etc. Some fifteen proposals were received and evaluated. In addition to these proposals inputs to the program were received from NBS-Boulder where development of a nylon and fiberglass Stirling cycle cooler had begun earlier under ONR support,[7,8] and from the U.S. Army Night Vision and Electro-Optics Laboratory, which had previously developed single stage Stirling coolers operating at 77 K, proposed to extend their technology to the 10 K region.[9]

The individual contracts thus far supported under this program are outlined in Tables III, IV and V. The entries in Table III are relate to Stirling cycle coolers. Descriptions of many of these activities can be found elsewhere in these Proceedings.

The second area of R&D under this program has been in the area of small Joule-Thomson cycle coolers and small helium gas compressors to enable small J-T coolers to be operated in a closed cycle mode. A J-T "cooler-on-a-chip" was developed by Little under ONR support.[10] More recently these efforts have been directed toward developing a small metal diaphragm compressor for use with this type of cooler-on-a-chip and eventually toward staging three J-T systems to achieve temperatures near 4 K. The Jet Propulsion Laboratory is working on polyurethane membrane compressors for (conventional) tubular J-T coolers, while Collins is developing a neoprene sleeve diaphragm compressor.

The final area of interest under this program has been to understand the problems associated with the use of cryocoolers to provide the required cryogenic environment for superconductive SQUID magnetometers and magnetic gradiometers. Zimmerman has operated one of his Stirling coolers with a SQUID gradiometer and has identified some of the interface problems and will be attempting to mitigate them.[6] Another effort is to document the sensitivity of SQUID magnetometers to the environment, such as temperature variation, vibrations etc. Finally, a facility has been established at the Naval Research Laboratory to study the magnetic signatures of cryocooler systems especially those to be used with magnetic sensors.

CURRENT STATUS OF PROGRAM

At the end of the Navy program on small cryocoolers in 1985, the goal is to have one or more complete systems, either Stirling or J-T, for integration with some cryogenic electronic device or circuit to demonstrate the feasibility of a closed cycle refrigeration system. This demonstration model will elucidate the interference problems and yield valuable information on how optimal system integration can be achieved without degrading the performance capabilities of the electronic device or circuit.

FUTURE DIRECTIONS

The completion of the Navy program in small, energy-efficient, highly reliable cryocoolers will not be the end of Navy interest in this technology. The current program will demonstrate the state of the art in this class of cooler and subsequent programs would be directed at interfacing and integrating these coolers into operational systems that will satisfy Navy requirements. In the non-military community, these cryocoolers may find their first use in cooling SQUID biomagnetic instrumentation. In this application, the major problem would be to minimize interference produced by the vibration and magnetic signature of the cooler which is probably the most serious problem to be encountered in integrating cryocoolers with electronic packages.

Because of the limited funds available under this program, many design concepts for cryocoolers have not been pursued. For example, in the case of cooling a magnetic sensor system, a split system might be used in which the motors and other moving parts would be located at a distance from the sensor to take advantage of the inverse cube fall-off of the magnetic signature. The motors, compressors and moving displacer would be remotely located from the cold station and the "cooling power" of the system transmitted by some means from the refrigerator to the electronic package to be cooled. If magnetic measurements do not have to be made continuously, for example, if a 10% duty cycle for measurements is acceptable, a thermal reservoir of large heat capacity might be used to maintain the SQUID system at the required operating temperature while measurements are being made and the cooler is not operating. Another area of interest is in extremely low power coolers which would operate for very long times but for which the cooldown could be done over a very long period of time or with the use of auxiliary cooldown modes using either liquid nitrogen or liquid helium.

These are only a few possibilities for new concepts and possible directions in small cryogenic refrigeration. They are only suggested here to indicate that the present Navy program is just touching the tip of the iceberg of cryogenic refrigeration. New and novel concepts in refrigeration are still welcome and encouraged so that this technology can continue to grow and mature.

Table 1. Cryogenic refrigeration requirements near 4 K.

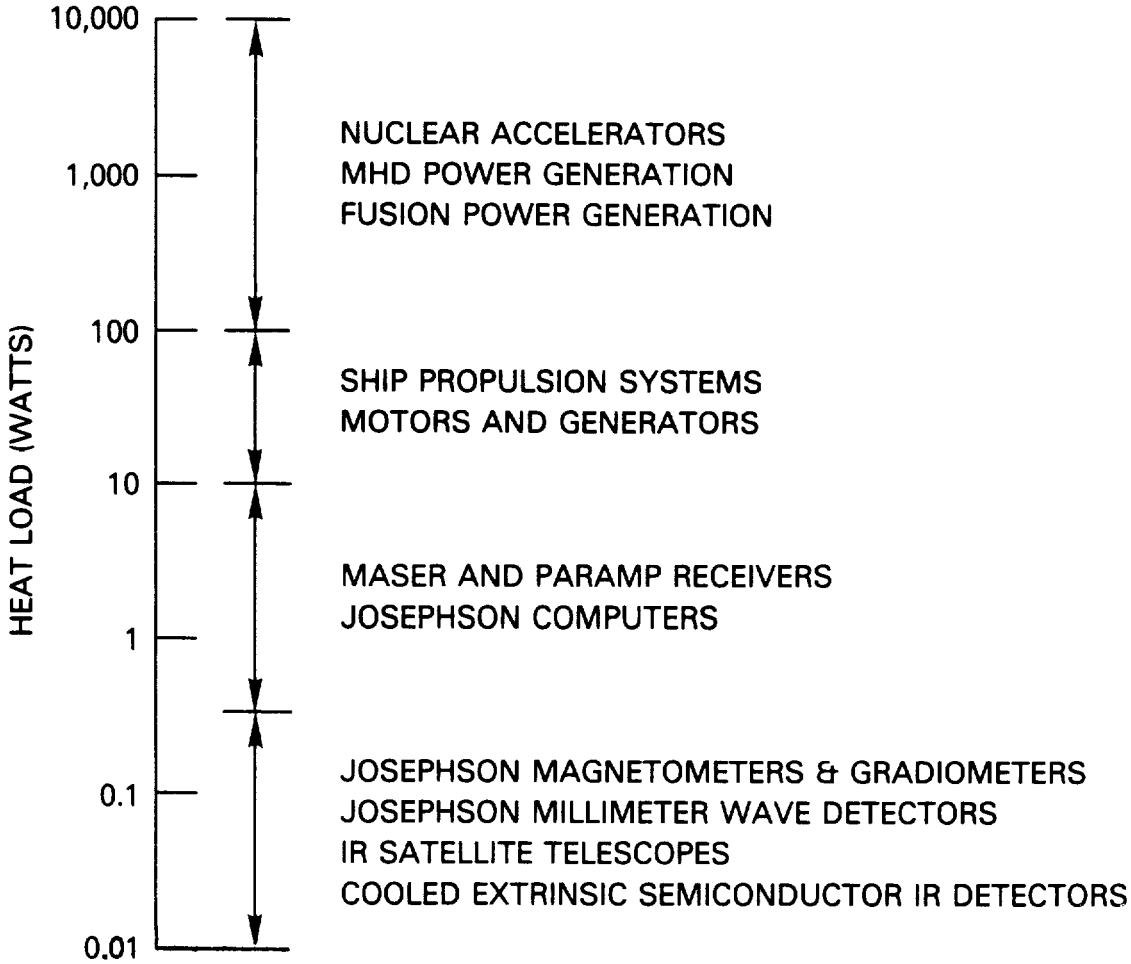

Table II. Cryocooler Specifications

PARAMETER	GOAL
Volume to be cooled	4 cm diam. x 15 cm long
Mass to be cooled	300 grams
Electrical leads into cold volume	3 coaxial leads
Ultimate operating temperature	< 8 K
Reserve cooling power at 10 K	50 mw
Temperature stability (without electrical heater feedback)	$\pm 10^{-2}$ K
Electrical input power	100 watts
System weight	4.5 kg
System volume	10^{4} cc
Routine maintenance	4000 hours
Mean Time Before Failure	8000 hours
Cooldown time	~ 8 hours
Mechanical vibration at cold station	$<10^{-7}$ rads
Magnetic signature at cold station	$<10^{-8}$ gauss rms/$\sqrt{Hz}$

Table III. Research in Stirling Cycle Cryocoolers

Organization	Investigators	Cooler Concept
National Bureau of Standards Boulder, CO	J. E. Zimmerman D. B. Sullivan	Nyon and fiberglass working materials: ceramic compressors
SHE Corporation San Diego, CA	R. Sagar	Nylon and fiberglass: He gas regenerator 3He working fluid
Cryogenic Technology, Inc. Waltham, MA	P. J. Kerney W. Prittle	MACOR[11] working material
Phillips Laboratories Briarcliffe Manor, NY	W. Newman A. Daniels	Triple expansion system: counterbalanced liner drive motor
Rockwell International Anaheim, CA	W. Hartwig	Gas adsorption compressors
Lake Shore-Cryotronics Westville, OH	W. Pierce	Pneumatic drive mechanism
Night Vision & Electro-Optics Laboratory Fort Belvoir, VA	W. Horn	Staged version of 77 K Stirling cooler

Table IV. Research in J-T coolers and small helium compressors

Organizations	Investigators	Concepts
MMR Technologies, Inc. Mountain View, CA	W. A. Little	J-T "cooler-on-a-chip"; grooves sandblasted in glass slides; metal diaphragm compressor
Jet Propulsion Laboratory Pasadena, CA	E. Tward	Polyurethene membrane compressor
Naval Research Laboratory Washington, D.C.	S. C. Collins	Neoprene sleeve compressor

Table V. Research in interfacing of cryocoolers to electronic systems

Organizations	Investigators	Concepts
Quantum Design, Inc. San Diego, CA	M. Simmonds	Interfacing SQUIDs to cryocoolers
Naval Research Laboratory Washington, D.C.	M. Nisenoff H. Weinstock	Facility to measure magnetic signatures of coolers

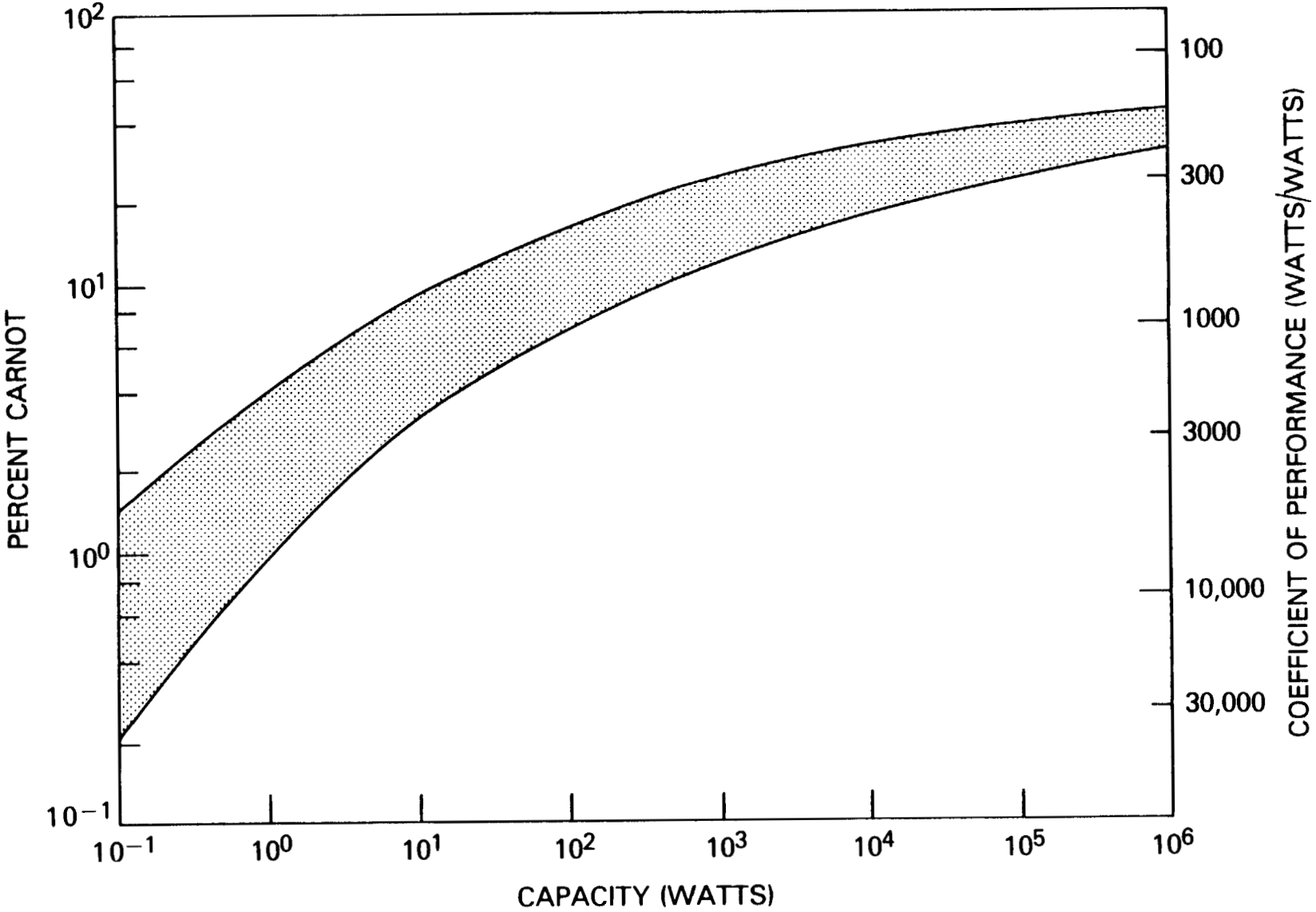

Fig. 1. Percentage of Carnot efficiency and Coefficient of Performance (COP) for 4 K closed cycle refrigerators as a function of cooling capacity. (The high temperature reservoir temperature was assumed to be 293 K.)

REFERENCES

1. Collins, S. C.: Recent Growth in Low Temperature Applications. Comm. Leiden, Suppl. 114c, 1958.

2. Crawford, A. H.: Specifications for Cryogenic Refrigerators. Cryogenics 10, 28 (1970).

3. Strobridge, T. R., and Chelton, D. B.: Size and Power Requirements of 4.2°K Refrigerators. Advances in Cryogenic Engineering, Vol. 12 (Plenum Press, New York, 1967), pp. 576-584.

4. Strobridge, T. R.: Cryogenic Refrigerators - An Updated Survey. NBS Technical Note 655 (Superintendent of Documents, U.S. Government Printing Office, Washington, D.C. 20402, Catalogue No. C13.46:655; 1974).

5. Nisenoff, M.: Current Status of High Temperature Josephson Device Technology. Refrigeration for Cryogenic Sensors and Electronic Systems; NBS Special Publication 607 (Superintendent of Documents, U.S. Government Printing Office, Washington, D.C. 20402, USA, 1981), pp. 195-209.

6. Sullivan, D. B., Zimmerman, J. E., and Ives, J. T.: Operation of a Practical SQUID Gradiometer in a Low-Power Stirling Cryocooler. Ibid., pp. 186-194.

7. Sullivan, D. B., and Zimmerman, J. E.: Very Low-Power Stirling Cryocooler Using Plastic and Composite Materials. Internat. J. Refrig. 2, 211 (1979).

8. Zimmerman, J. E., and Radebaugh, R.: Operation of a SQUID in a Very Low-Power Cryocooler. Applications of Closed Cycle Cryocoolers to Small Superconducting Devices; NBS Special Publication 508 (Superintendent of Documents, U.S. Government Printing Office, Washington, D.C. 20402, USA; Catalogue No. 003-003-01910-1; 1978), pp. 59-66.

9. Horn, S. B., and Asher, M. S.: Theoretical Analysis of a 3-stage Stirling Cycle Cryocooler. Refrigeration for Cryogenic Sensors and Electronic Systems; NBS Special Publication 607 (Superintendent of Documents, U.S. Government Printing Office, Washington, D.C. 20402, USA; 1981), pp. 30-48.

10. Little, W. A.: Design Considerations for Microminiature Refrigerators Using Laminar Flow Heat Exchangers. Refrigeration for Cryogenic Sensors and Electronic Systems. NBS Special Publication 607 (Superintendent of Documents, U.S. Government Printing Office, Washington, D.C. 20402, USA, 1981), pp. 154-160.

11. MACOR is a registered trademark for a machineable ceramic manufactured by Corning Glass Works, Inc., Corning, NY, USA.

NASA NEEDS AND TRENDS IN CRYOGENIC COOLING

Allan Sherman
NASA/Goddard Space Flight Center

INTRODUCTION

There are increasing numbers of NASA space instruments that require cryogenic cooling to accomplish their objectives. These include instruments for Earth observation, atmospheric science, gamma-ray and X-ray astronomy, infrared astronomy, and basic research. Potential future space applications for cryogenic cooling include instruments for high energy astronomy, radio-astronomy, relativity measurements, and a variety of instruments and systems employing superconducting devices.

The elements of the instruments that may require cooling are radiation detectors, optical components, baffles, or in some cases, the whole instrument. Cryogenic cooling is necessary to provide the required detector response, reduce pre-amplifier noise, and/or reduce background radiation.

The objectives of the discussion herein are to indicate the projected NASA needs in spaceborne cryogenic systems and to describe recent results from NASA cryogenic cooling technology efforts. Much background information has been extracted from References 1 and 2. However, the emphasis will be placed upon future cryogenic cooling applications. Only areas where there are large efforts and significant projected needs will be covered.

INSTRUMENT SYSTEM NEEDS

Earth Observation

Observation of the Earth's surface from satellites* is accomplished at wavelength bands for which the Earth's atmosphere is transparent. Two of these "clear air" bands are from .3 - 2μm and from 8 - 14μm. The former band is utilized to measure reflected sunlight from the Earth while the latter is used to detect the Earth's radiant emission.

Earth observation in the .3 - 2μm band does not usually require cryogenic cooling. In the 8 - 14μm regime, cryogenic cooling of the detector and, perhaps some optical components, is required.

The most common form of detector used by NASA to-date for the 8 - 14μm band has been Hg Cd Te. Cryogenic cooling of the detectors has been accomplished with radiant coolers.[3] For example, the AVHRR (Advanced High

*Satellites are defined here as free-flying spacecraft, unattached to the Shuttle or a space platform or station.

Resolution Radiometer) aboard the TIROS series of spacecraft utilizes a radiant cooler to maintain Hg Cd Te detectors at 95°K. The Landsat-D spacecraft, which was launched in 1982, employs a radiant cooler to provide 87°K for the Thematic Mapper instrument Hg Cd Te detectors. The instrument cooling loads for the cited examples are 35 mW and 85 mW, respectively. Schematic of typical radiant coolers are shown in Figure 1.

The Earth observation instruments to-date are usually scanner type--i.e., there is a moving mirror which scans a swath of the Earth normal to the orbit plane. The input radiation for each mirror position is separated into the desired wavelength bands and focused on single detectors, each appropriately designed and doped for the particular wavelength.

A new concept for Earth observation instruments utilizes a large number of detectors arranged in a line to essentially take a "picture" of a swath of the Earth at each orbital position, at a particular wavelength band.

The prime advantage of linear array systems over scanner systems is the potential for improved spectral and spacial resolution. This occurs because each detector has a much larger integration time over a partiuclar swath of the Earth.

The thermal band (i.e., $\sim 12\mu m$) of a multi-linear array (MLA) instrument might consist of 2,000 Hg Cd Te detectors and associated electronics. Typical cooling requirements are on the order of several watts at 90 - 100°K. The mid-infrared (3-6μm) band and perhaps the 1-2.5μm band would also require cryogenic temperatures with cooling loads of 1 or more watts.

Mission lifetime for an MLA instrument would be at least 3 years. Thus, it is clear that a closed cycle refrigerator would be of extreme benefit for a linear array instrument and is probably the only practical cooler for it. Figure 2 is a schematic of the NASA/GSFC, long-lifetime, Stirling cycle cooler, presently being developed, coupled to an MLA-type instrument.

The MLA class of instruments, then, clearly require coolers with larger capacity than present day scanning instruments. It is unclear, however, when the NASA MLA instruments will be developed and operational.

Atmospheric Science

Measurements of the atmosphere composition, temperature, pressure and wind are made at a variety of wavelengths for which the atmosphere is not transparent. These measurements fall into two general categories--direct emission and occultation instruments. In the first case, radiometric measurements are made directly at the particular emission wavelength of the constituent of interest. In the second case, the absorption lines from an emission source, such as the sun, are observed through the limb* of the atmosphere.

*Limb measurements refer to observing from the spacecraft in a direction tangent to the Earth and through the atmosphere.

Examples of previous atmospheric science instruments are the LRIR (Limb Radiance Inversion Radiometer) which was placed in orbit aboard Nimbus-6, and LIMS (Limb Infrared Monitoring of the Stratosphere) which was aboard Nimbus-7. The LRIR measured Earth-limb radiance in four spectral bands ranging from 8.6 to 27μm. The LIMS obtained stratospheric data in six bands ranging from 6.08 to 17.24μm. In both cases, Hg Cd Te detectors were employed.

Both the LRIR and LIMS instruments utilized a two-stage, solid cryogen cooler produced by Lockheed Palo Alto Research Laboratories. The primary cryogen was methane at a nominal temperature of 65^{o}K and an instrument heat load of 52 mW. The secondary stage employed ammonia at a nominal temperature of 152^{o}K with a instrument heat load of 91 milliwatts.

A new NASA atmospheric science satellite presently being designed is the Upper Atmosphere Research Satellite (UARS). This spacecraft accommodates 11 instruments, 2 of which utilize cryogenics. It is anticipated that the UARS will be launched in 1988.

The UARS Cryogenic Limb Array Etalon Spectrometer (CLAES) instrument will utilize a solid hydrogen cooler for cooling 23 Si (Ga) detectors and the spectrometer optics to 12^{o}K. The cooler vent line will vapor cool the telescope baffle to 130^{o}K. The 12^{o}K Si (Ga) detectors, together with the low instrument background temperature, provide very sensitive measurements of atmospheric constituents with emission spectra in the 3.5 - 13μm regime. The cooling load to the 12^{o}K hydrogen is .3 W, while the baffle load is 2.4 W.

The CLAES cooler will be the first to utilize solid hydrogen in space, although ground testing of a small flight-type, solid cryogenic cooler has been successfully accomplished.[3] A schematic of the CLAES solid hydrogen cooler is shown in Figure 3. The anticipated weight of the system is 354 Kg, including 78 Kg of hydrogen.

The low temperature requirement of the instrument limited the cooler design to either solid hydrogen or supercritical helium. Hydrogen was selected over helium because of its higher cryogenic cooling efficiency, which becomes critical for a system with an 18 month lifetime requirement. A 10^{o}K, closed-cycle cooler would offer very significant weight benefits over the solid hydrogen cooler, as well as a longer lifetime. However, a 10^{o}K, long-lifetime, closed-cycle cooler is not yet developed.

A second cryogenic instrument that will be aboard the UARS spacecraft is the Improved Stratospheric and Mesospheric Sounder (ISAMS). The ISAMS has 12 spectral channels over the 4 - 100μm regime.

The ISAMS infrared channels will be cooled by two Stirling cycle coolers that are presently being developed. Although nothing has been published, the coolers will employ linear drive motors and dry lubricated pistons. Required capacity of each machine will be 1 watt at 80^{o}K. The minimum lifetime requirements for the coolers is 18 months.

The UARS and other future atmospheric science missions once again demonstrate the need for a long-lifetime mechanical cooler. In addition, in the case where a stored cryogen system is expedient to employ, methods for extending lifetime for a given size cooler must be developed. For example, a large fraction of the heat leak between a stored cryogen cooler outer vacuum shell and the inner cryogen tank is by conduction through the support structure connecting the shell to the tank. This structure is required for the cooler system to survive launch loads, but is considerably overdesigned for orbital conditions. The development of a structural system that could essentially disengage after the cooler is in orbit would reduce the heat load to the cryogen and greatly extend cooler lifetime.

Infrared Astronomy

For NASA infrared astronomy missions, liquid helium cooling is essential. The first of the infrared astronomy missions will be the Infrared Astronomy Satellite (IRAS), which is to be launched into a polar orbit in January 1983. This joint U.S., Netherlands, and U.K. satellite system utilizes doped silicon detectors to survey the sky and to make selected point source measurements in a wavelength range of 8 to 129 μm.

The IRAS will utilize a 540 liter, 1.8^{o}K, superfluid helium dewar manufactured by Ball Aerospace Systems Division. As shown in Figure 4, the superfluid helium is contained in a torroidal-shaped, 5083 aluminum main cryogen tank. The infrared telescope system fits into the center of the torroid and is mounted to the telescope mounting ring. Structural support is achieved through nine fiberglass-epoxy bands which terminate at the main shell. Additional thermal protection is provided by three vapor-cooled shields and multilayer insulation in the vacuum space. The main shell will operate at about 200^{o}K via radiant cooling in orbit to further reduce heat leaks to the cryogen tank. Liquid-to-vapor phase separation in zero gravity is accomplished by a porous plug located at the entrance to the vent line. The dewar cover, which is jettisoned during the initial stages after achieving orbit, utilizes a supercritical helium tank to reduce its heat leak. From ground test data and mathematical modeling, the operational orbital lifetime for the IRAS dewar is predicted to be about 7 months.

The same basic IRAS dewar will be used for the Cosmic Background Explorer (Cobe) mission, which has recently been approved as a new NASA program. Modifications to the IRAS dewar for Cobe include deletion of the aperture cover tank, additional support straps for Shuttle launch (versus Delta for IRAS), improved valves, and a lower main shell temperature.

In addition to photoconductor detectors (as on IRAS), Cobe will utilize infrared bolometers. Consequently, it is desirable to operate the dewar at as low a temperature as possible, which is 1.6^{o}K.

Future infrared astronomy missions indicate the need for even lower temperatures for bolometers. One mission is the Shuttle Infrared Telescope

Facility (SIRTF). This facility will fly as an attached payload to the Shuttle (Figure 5). The basic cooling system will consist of a combination of liquid helium and supercritical helium cryostats. However, an instrument attached to the facility will be capable of carrying its own "booster" cooling system as well. The facility, then, will make multiple flights with a different complement of instruments on each flight.

It is clear that some of the instruments that will fly with SIRTF will carry ultra-low temperature coolers to provide bolometer temperatures of .1 to .3°K. Greatly increased bolometer performance will result at these ultra-low temperatures.

One other infrared astronomy mission is the Small Helium-Cooled Infrared Telescope that will fly aboard the Shuttle in 1984. The requirements for this system, however, are not technology drivers. The technology drivers for infrared astronomy missions are the need for lower tempratures for infrared bolometers and long-lifetime dewars for future free-flyer and space station instruments.

Other Liquid Helium Systems

There are other NASA payloads that will require liquid helium. These include, for example, the Gravity Probe B Satellite, the Superfluid Helium Properties Experiment, and possible future payloads employing superconducting components. The cryogenic needs for these systems are similar to those of infrared astronomy.

X-Ray and Gamma Ray Astronomy

Cryogenic cooling is required for X-ray spectrometer instruments for both the detectors (e.g., Si(Li)) and Field Effect Transistors (FETs). The temperature requirement is about 100-120°K for the detector and 130°K for the FETs.

The High Energy Astronomical Observatory-B (HEAO-B) utilized a two-stage, solid methane/ammonia cooler for its X-ray instrument. Launched in 1978, the cooler maintained a nominal 80°K primary temperature and 150°K secondary temperature for 11 months. The cooler was manufactured by Ball Aerospace Systems Division.

A future X-ray observatory that is in the planning stages at NASA is the Advanced X-ray Astronomical Facility. Although the instruments have not yet been selected for this satellite, it is likely that at least one will require cryogenic cooling.

In the area of gamma ray astronomy, the HEAO-C satellite was launched in 1979. This satellite utilized the same cooler design as HEAO-B to perform X-ray and gamma ray spectroscopy. However, the HEAO-C cooler achieved a lifetime of only 8 months.

For both the HEAO-B and C satellites, it is clear that a long-lifetime,

closed cycle cooler would have been a tremendous asset. Of course, a much larger stored cryogen cooler, which is more feasible in the Shuttle era, would also have helped. Additionally, a launch support release mechanism for the stored cryogen system would have extended lifetime by several months. With possible higher heat loads and longer lifetime requirements of future X-ray and gamma ray instruments, it is clear that a closed cycle cooler will be required.

Space Station

NASA is presently proposing the development of a space station. Although the exact nature of the station has not been defined, it would appear that resupplying cryogens to scientific payloads may be a reasonable thing to do. This could take the form of "refueling in space" or replacement of a cooler and/or instrument. In one sense, this may alleviate the cryogen lifetime problem; however, from a cost and risk viewpoint, one would want to have a long service interval. The cryogenic system design drivers and needs for a space station system are essentially unknown at this time.

Summary of NASA Needs

It is clear there is a pressing need for a long-lifetime, closed cycle cooler. A device of this nature in the 65^{o}K temperature range would find wide spread utilization for earth observation, and X-ray and gamma ray astronomy missions. A 10^{o}K, closed cycle cooler would find application for atmospheric science instruments. Another potential use would be to provide the cooling for radiation shields and the inner support structure of stored cryogen systems for both instruments and long-term storage of cryogenic propellants in space.

For infrared astronomy and other liquid helium systems, improvement in lifetime of the cryogenic systems is needed. The development of structural support release systems for dewars would certainly be of great benefit. It is also about time to consider closed cycle liquefaction systems for space.

Additionally, for infrared astronomy missions, flight-worthy ultra-low temperature systems, such as a helium-3 and adiabatic demagnetization refrigerators, will be needed.

The refueling of Orbit Transfer Vehicle cryogenic propulsion systems is already in NASA's plans. A cryogenic fluid transfer technology experiment should fly aboard the Shuttle in the late 1980's. This technology may also be of use in developing systems for the servicing of cryogenic coolers from a space station.

RECENT PROGRESS IN NASA TECHNOLOGY PROGRAMS

Reference 1 summarizes the progress in NASA efforts to develop the technology to satisfy the stated needs. The following is a brief discussion of significant progress since Reference 1 was published.

The most exciting achievement over the past year has been the successful

testing of the first model of the NASA/Goddard long-lifetime, 5W, 65°K, Stirling cycle cooler (Figure 6). This cooler, which is being developed for NASA by Philips Laboratories, utilizes magnetic bearings to eliminate rubbing of the piston and displacer against the cylinder walls. Additional design features include (1) linear drive systems for both the piston and displacer, (2) elimination of organic materials and the resultant contamination inside the working volumes, (3) electronic control of piston/displacer axial motions and phase angle, and (4) dynamic balance.

As of this writing, the cooler has successfully completed over 300 hours of operation and 100 start/stop cycles. All performance design goals have been met. Details of the latest test results are in Reference 6.

The next step in the long-life, Stirling cycle cooler program is to develop a second 65°K, 5W model of the cooler. The second model will improve the technology of the system to a level where a flight program would commit to using it. Follow-on plans include extending the technology to lower temperature (12°K) machines.

Results have also been reported during the past year in the development of stored cryogen system structural release systems. For example, Reference 7 describes the design of a NASA 3-year, liquid helium dewar utilizing the Lockheed Passive-Orbital-Disconnect-Strut System. Another NASA contract to design a structural release system has recently been awarded to Ball Aerospace Systems Division.

The systems being developed are the passive type, as illustrated in Figure 7. In the series passive design, the launch load is transmitted through the pin between the tubular structural support and end fitting. When in orbit, there is only a thin fiberglass band connecting the end fitting and tube, and there is a clearance around the pin. In this way, the thermal conductance in orbit is very low. In the parallel design, the thin outer tube is the in-orbit support, while during launch, the central structural member supports the load. These "bumper" type systems do not require any activation other than the launch loads themselves. More work is needed to flight qualify these systems.

Work has also progressed over the last year in the development of adsorption coolers. Tests have begun on a $LaNi_5$ adsorption type Joule Thomson refrigerator that achieves 29°K. This system offers advantages for outer planet missions, where radioactive power system waste heat is available and a 77°K first stage temperature can be achieved via radiant cooling. Details of these results are in Reference 8.

Additional NASA work of significance over the past year includes studies on the development of a zero-g, .3°K, ^{3}He system. The results of experiments on a copper matrix fluid retention system for such a device are reported in Reference 9.

CONCLUSION

A variety of NASA needs in cryogenic cooling has been identified. Efforts to provide the technology for these needs have produced outstanding results. However, much remains to be done.

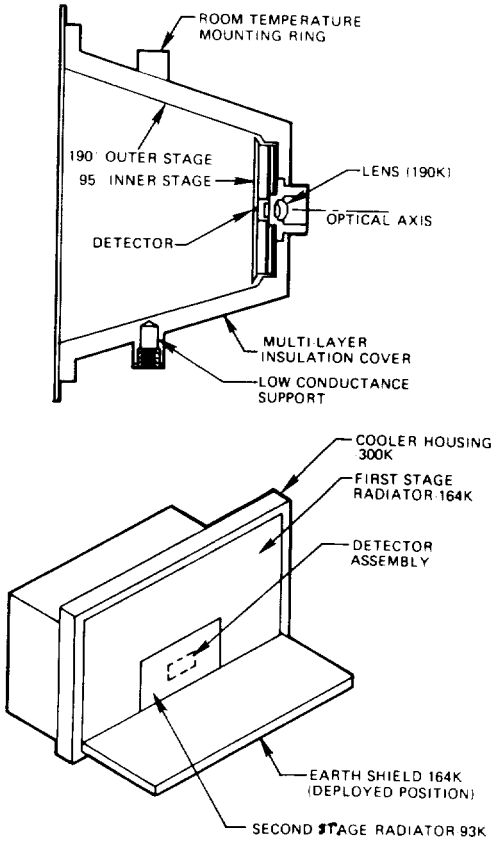

Figure 1. Radiant Coolers: A.D. Little (top), ITT (bottom).

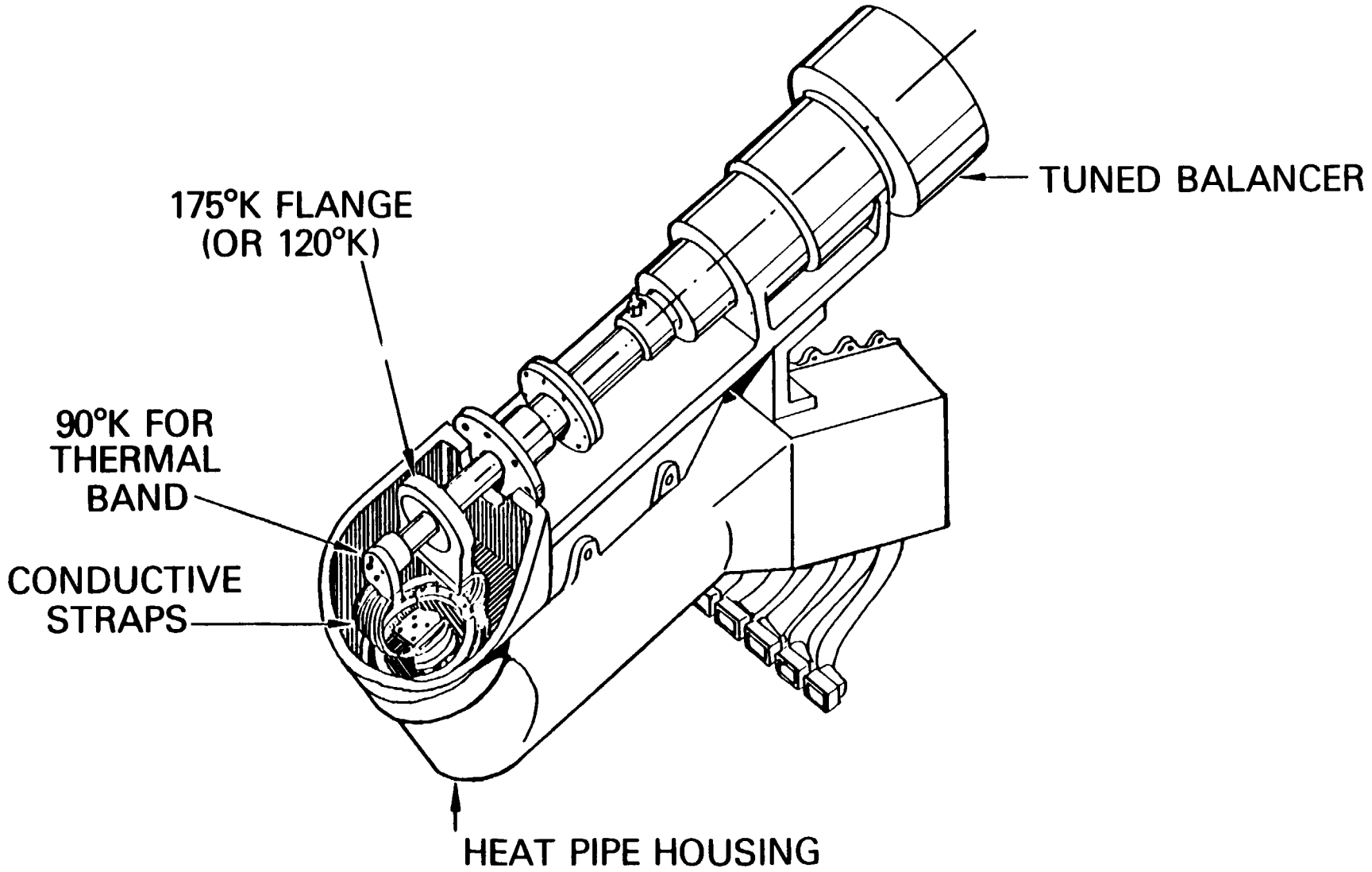

Figure 2 MLA Instrument Coupled to a Stirling Cooler
(extracted from Reference 4)

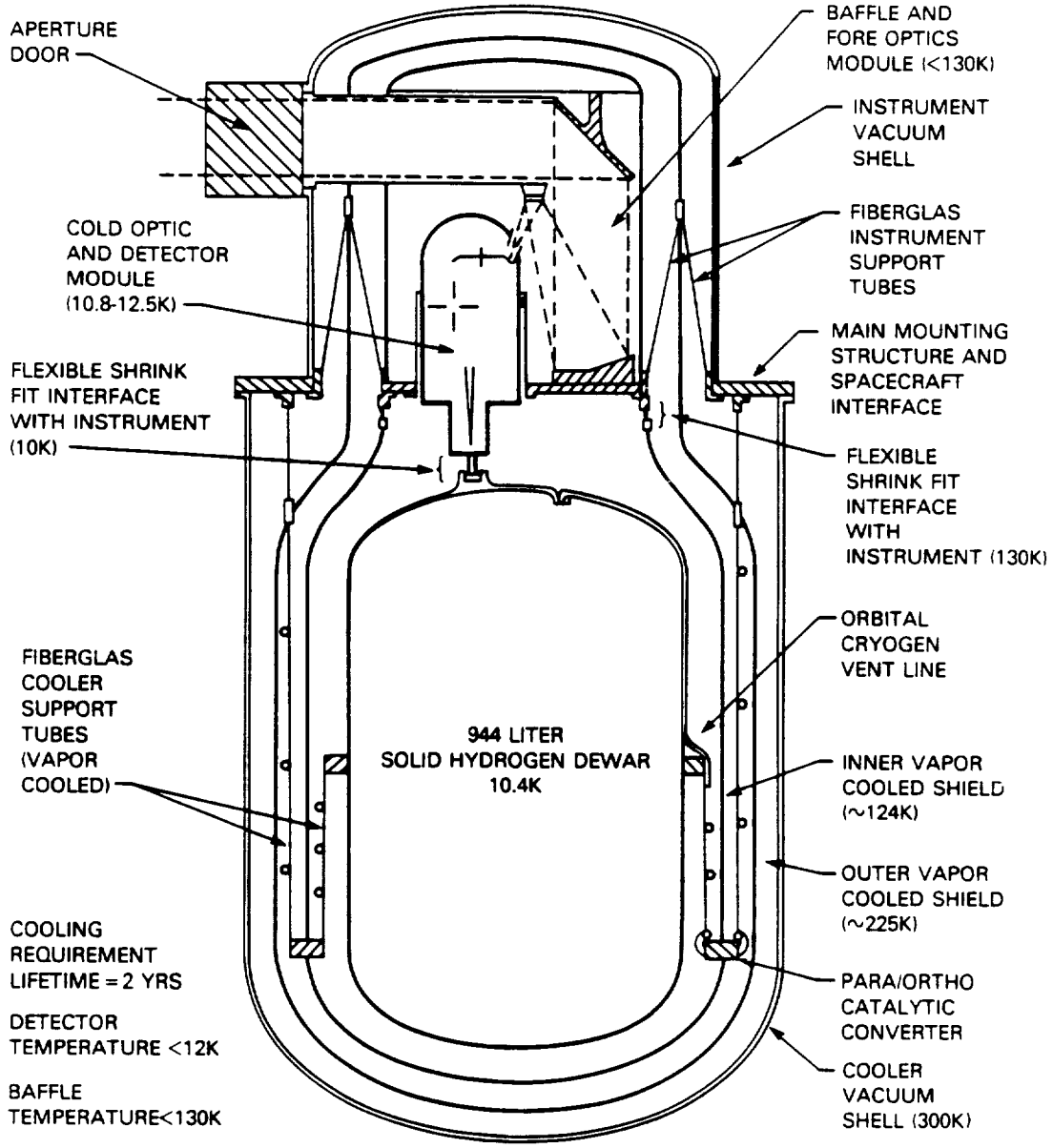

Figure 3 CLAES Solid Hydrogen Cooler Concept

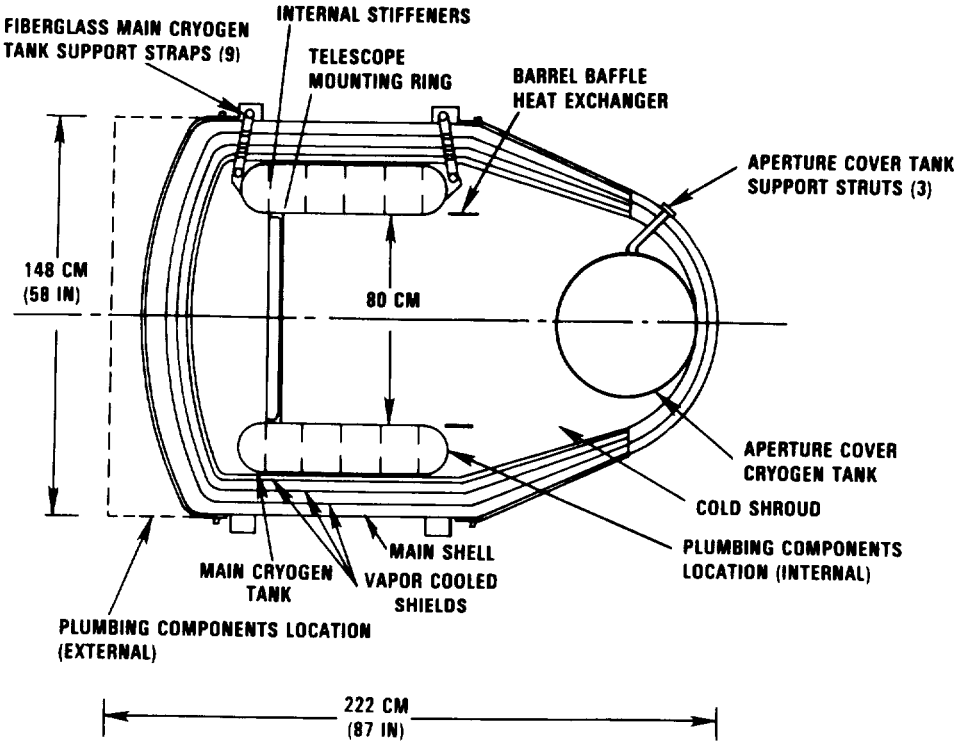

Figure 4. IRAS Superfluid Helium Dewar.

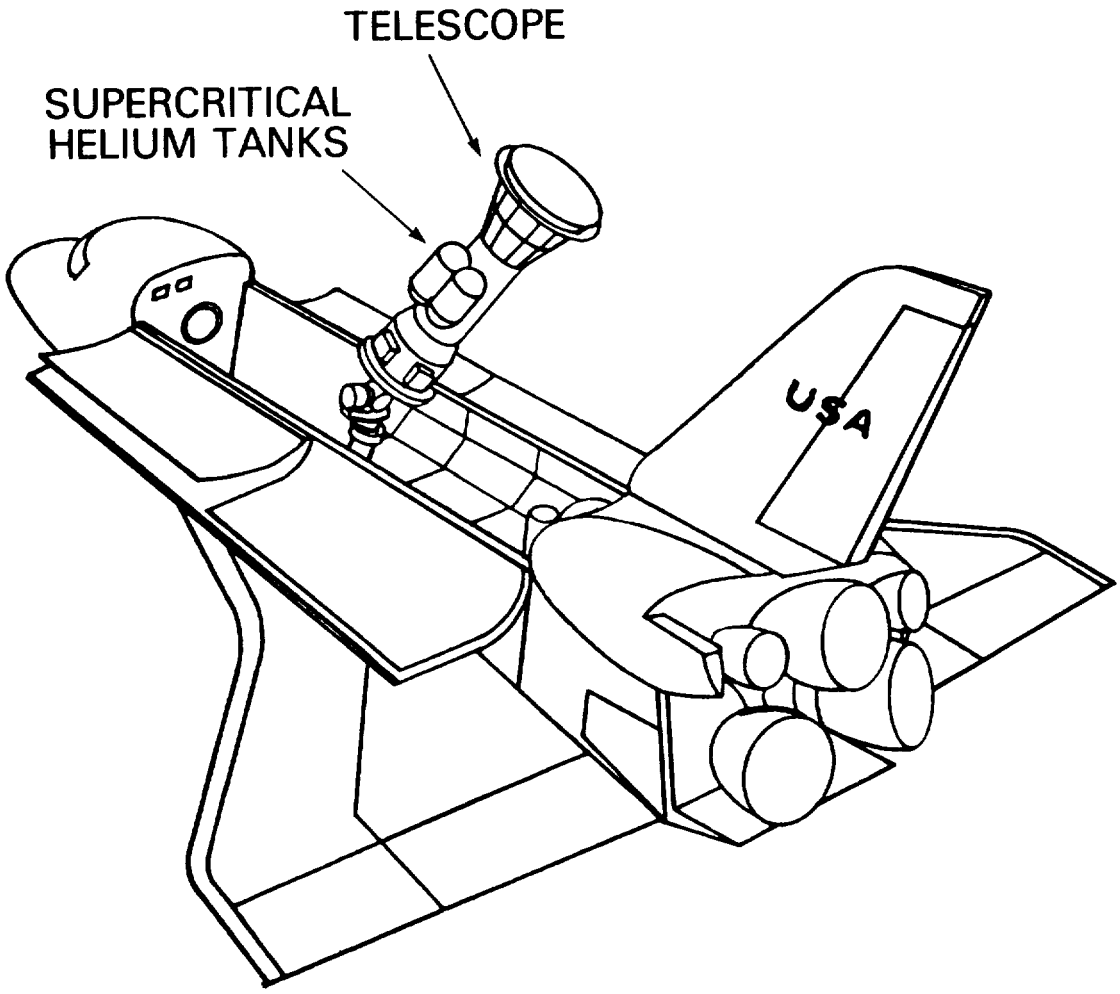

Figure 5. SIRTF Concept.

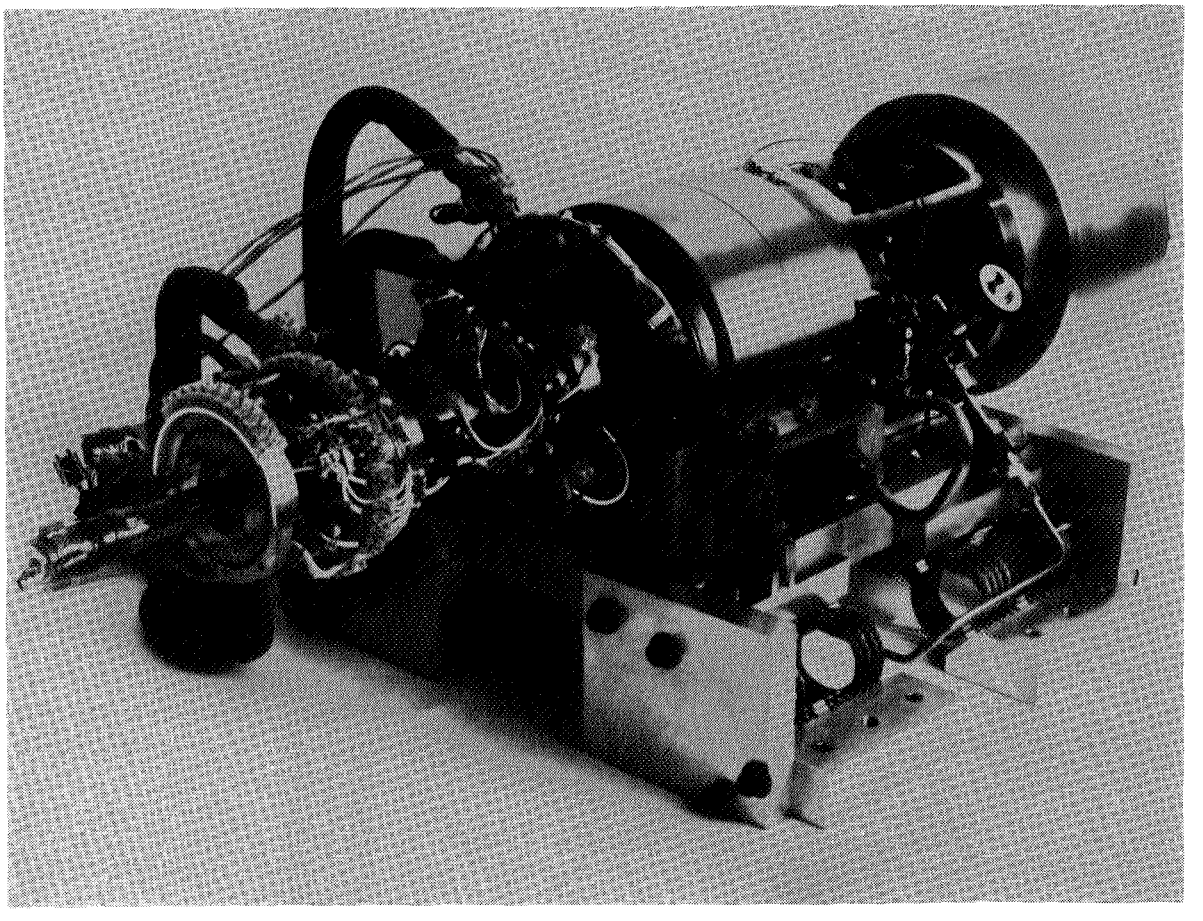

Figure 6. Photograph of NASA Stirling Cycle Cooler developed by Philips Laboratories.

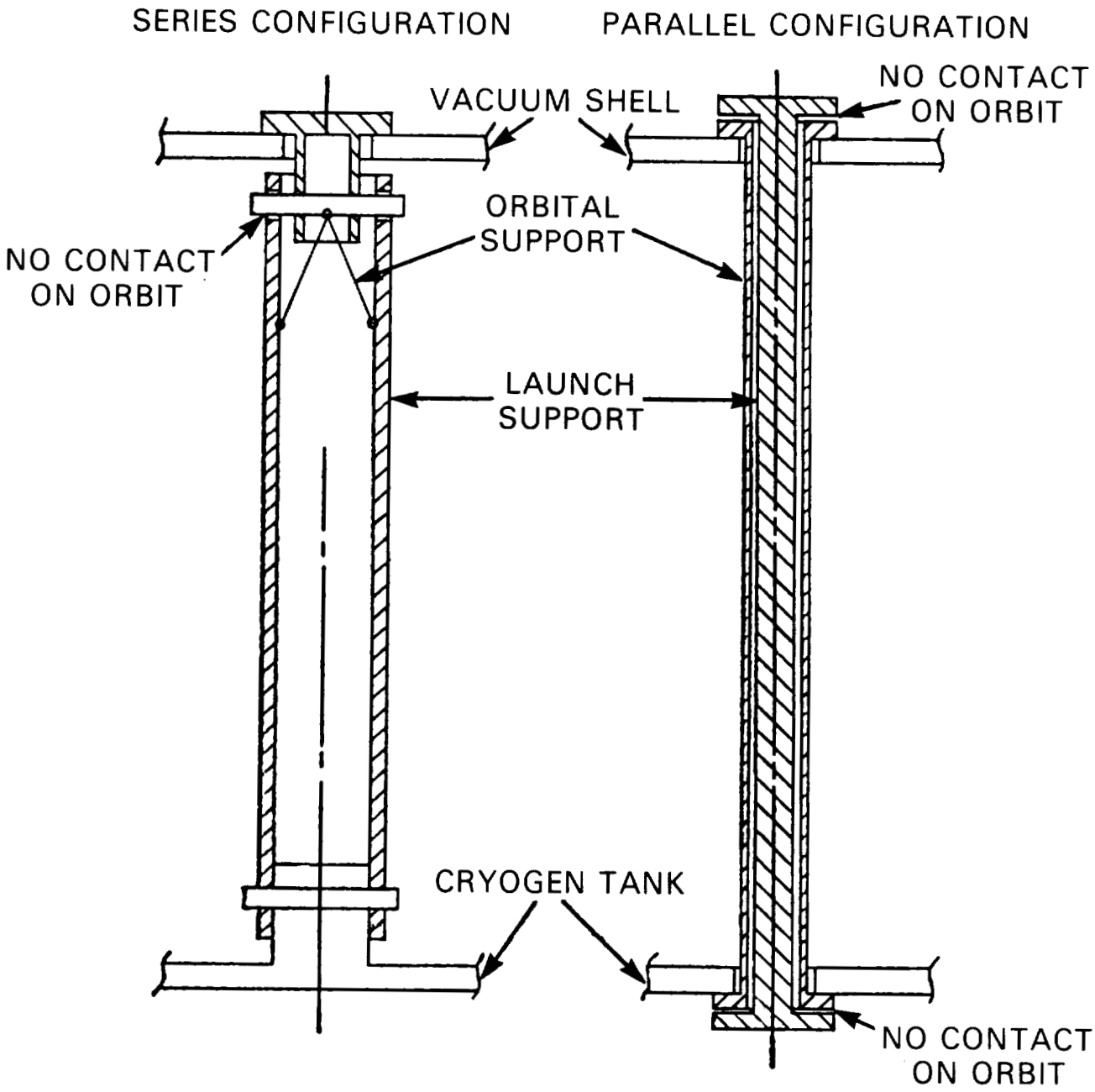

Figure 7. Series and Parallel Launch Support Release System for Stored Cryogen Systems.

REFERENCES

1. Sherman, A., "History, Status and Future Applications of Spaceborne Cryogenic Systems," Advances in Cryogenic Engineering, Vol. 27, 1981, p. 1007.

2. Vorreiter, J., "Cryogenic Systems for Spacecraft," Contemporary Physics, Vol. 21, No. 3, 1980, p. 201.

3. Donohoe, M., Sherman, A., and Hickman, D., "Radiant Coolers - Theory, Flight History, Design Comparisons, and Future Applications," AIAA Paper 75-184, AIAA 13th Aerospace Sciences Meeting, Pasadena, California, January 1975.

4. SBRC MLA/ELOS Final Review; presented at NASA/Goddard Space Flight Center, May 1982.

5. Nast, T., Study of a Solid Hydrogen Cooler for Spacecraft Instruments and Sensors, LMSC-D-766177, Final Report for NAS5-25792, August 1980.

6. Stolfi, F., Goldowsky, M., Ricciaredelli, J., and Shapiro, P., "A Magnetically Suspended, Linearly Driven Cryogenic Refrigerator," Second Biennial Conference on Refrigeration for Cryogenic Sensors and Electronic Systems, December 1982, NASA/GSFC, Greenbelt, MD.

7. Parmley, R., Feasibility Study for Long Lifetime Helium Dewar, NASA CR-166254, December 1981.

8. Jones, J., "$LaNi_5$ Hydride Cryogenic Refrigerator Test Hardware Results," Second Biennial Conference on Refrigeration for Cryogenic Sensors and Electronic Systems, December 1982, NASA/GSFC, Greenbelt, MD.

9. Kittel, P., Ennis, E., Brooks, W., and Miller, A., "A He^3 Refrigerator Employing Capillary Confinement of Liquid Cryogen," Second Biennial Conference on Refrigeration for Cryogenic Sensors and Electronic Systems, December 1982, NASA/GSFC, Greenbelt, MD.

CRYOCOOLER ACTIVITIES IN CHINA

Ralph C. Longsworth

ABSTRACT

A glimpse of cryocooler activity in China was obtained during a two week visit in June 1982 as a member of a trade mission organized by the American Vacuum Equipment Manufacturers Association and the China Council for the Promotion of International Trade. Seminars on cryopumping were given in Beijing, Shenyang, and Shanghai during which we met people actively involved in refrigerator research and development and saw several research facilities and factories that are developing and manufacturing vacuum equipment and some related cryogenic equipment.

INTRODUCTION

The Government of the Peoples Republic of China is encouraging technical exchange with more advanced countries by sending Chinese scientists and engineers overseas to study and work, as well as having foreign trade missions visit China. Prior to visiting China I met with Mr. Xie Lun, an engineer in the Cryogenic and Superconductivity Laboratory of the Research Institute of Automation for the Machine Building Industry in Beijing (Peking), who is presently studying in the United States at George Washington University. He provided a list of facilities where cryogenic work is being done. This information is included here to provide a more complete picture than I was able to obtain firsthand. Related work in the field of Superconducting Materials Research was recently reported by Dew-Hughes (Ref. 1).

BEIJING

What seem to be the most extensive research programs on small refrigerators in China are being pursued at the Research Institute of Physics, Chinese Academy of Science. Professor C. S. Hong, one of the editors of Cryogenics, leads the program. One of his students, Mr. Chang Liang, said that they had developed a helium dilution refrigerator and a Gifford McMahon refrigerator and were working on a magnetic cold stage. It was reported that they are also working on small gas bearing turbines. (Ref. 2)

At the General Research Institute for Nonferrous Metals, Professor Zhou Li is directing a program to develop a superconducting magnet for ore separation. The refrigeration system is the responsibility of the Research

Institute of Automation for Machine Building, also in Beijing. It is reported that the latter group is manufacturing Gifford McMahon refrigerators and NMR cryostats.

SHENYANG

Jiang Xie Chang, Director of the Chinese Vacuum Association and Vice Chief Engineer of the Shenyang Vacuum Technology Institute, arranged for a tour of their research facility. Equipment seen included a vacuum gauge calibration unit with diffusion pumps, zirconium getter ion pumps, a 300 mm turbo molecular pump, a 200 mm cryopump with a Gifford McMahon refrigerator, a small high Q ion pump, an ion plasma deposition unit for decorative plating of gold, and miscellaneous vacuum instruments. The G-M refrigerator has an oil lubricated compressor and an expander with a scotch yoke drive similar to the CTI unit. Capacity is reported to be 4 W at 20 K plus 10 W at 77 K.

We also visited the Scientific Instrument Factory which is affiliated with the Chinese Academy of Sciences, Sun Da-Zheng, Director. They manufacture diffusion pumps, ion pumps, cold traps, and valves and incorporate them in instruments for Auger, ESCA, MBE, and ion milling. The workmanship was of high quality.

SHANGHAI

We visited the Shu-Guang Machinery Works Corporation, headed by Chen Yun Long, where we saw liquid helium and liquid nitrogen dewars being built. Vacuum equipment being built included a wide range of diffusion pumps, large and small coating chambers, vacuum gauges, and film thickness monitors.

The Shanghai Mechanical Institute has a group of people, including Sun Chong Giu, studying small cryogenic refrigerators.

I was told that a small helium liquefier is being built in Shanghai which has a capacity of 10 L/hr with LN precooling.

OTHER LOCATIONS (not visited)

A group at Nanjing University is developing cryopumps (Ref. 3) and is reported to have built their own G-M refrigerator. Another group is reported to be working on cryopumps in Lanzhou.

The University at Hefei is reported to have a low temperature laboratory, and the University at Weihai is reported to have a small refrigerator research program including work on J-T refrigerators. Work on air separation

is reportedly being pursued at Hangzhou and Xian University.

CONCLUSIONS

At this time the Chinese seem to be at a point in the development of cryogenic refrigeration equipment where we in the United States were about ten to fifteen years ago. One is impressed with the number, quality, and dedication of the people involved in this work. Although their resources are meager, they seem to be making good progress in catching up to western technology.

REFERENCES

1. Dew-Huges, D.: Superconducting Materials Research in the People's Republic of China. Cryogenics, Oct. 1982, pp. 505-508.

2. Munday, A. J. and Yang, K. J.: A Grooved Self-acting Gas Bearing for Use in Cryogenic Expansion Turbines. Presented at AICHE Annual Meeting, Los Angeles, 18 November 1982.

3. Bing-kun Liu; Jia-sheng Ren; and Xiu-hua Cui: Cryosorption Pumping of Hydrogen with the ZDB-150 Type Cryopump Cooled by a Two-Stage Closed-Cycle Refrigerator. J. Vac. Sci. Technology, 20(4), April 1982, pp. 1000-1004.

JAPANESE ACTIVITIES IN REFRIGERATION TECHNOLOGY

T. Fujita, T. Ohtsuka and Y. Ishizaki*

Department of Physics, Tohoku University, Sendai 980, Japan

ABSTRACT

This paper reviews recent activities in refrigeration technology in Japan, which are stimulated strongly by growing induxtirial demands and big national projects. At present, the JNR project on the MAGLEV train is the most powerful one and requires all knowledges of cryogenics including various scales of refrigeration. In fact, several R & D works are now in progress for various types of refrigerators. Currently research activities have also started in developing Stirling cycle refrigerators and magnetic refrigerators for applications in a wider area.

INTRODUCTION

Research in the field of cryogenic refrigeration below 20 K in Japan was initiated at Tohoku University as a study of low temperature physics. Besides the accumulation of basic physical data, some effort was also made to construct helium liquefiers in this early period of study. However, the first helium liquefier in Japan was an imported ADL Collins machine, which was installed at Tohoku University in 1952. Following Tohoku University, some other univeristies, national laboratories and companies installed the same type of helium liquefiers successively during the next decade. In 1958, a group at the Institute for Solid State Physics, the University of Tokyo, succeeded in producing liquid helium by the first Japanese liquefier of cascade type with an output of 4 liters per hour. Helium liquefiers in this period were used mainly for laboratory experiments. Industrial needs for larger machines have grown up in conjunction with progress in superconducting magnet technology and its applications.

As for cryocoolers, the Gifford-McMahon cycle was first investigated at Hitachi Ltd. The first test machine was reported to operate successfully but it was not directly followed by a practical machine. A recent application of the Gifford-McMahon refrigerator will be described by Matsubara and Yasukochi in this Conference [1]. Supported by the group in the University of Tokyo, Osaka Oxygen Industries developed a small cryocooler of a modified Solvay cycle in 1971. A commercial version of this machine "Cryo-mini" is now

---

* Technical Consultant.

available with a capacity of 1 W at 15 K, being applied mainly for cryopumps. Basic study of Stirling cycle cryocooler was carried out at the University of Tokyo and 30 K was reached in 1972 [2]. An improved version of this test machine will be discussed later.

Recent activities in refrigeration technology in Japan are strongly stimulated by big national projects. Of such stimulants, the Japanese National Railways (JNR) project on the superconducting magnetically levitated (MAGLEV) vehicles is the most powerfull one at present. As part of the project, R & D works are now in progress for various types of on-board refrigerators including Claude cycle, Stirling cycle and Gifford-McMahon cycle machines. Some of them are expected to meet general demands for applications in a wider area, such as for cryopumps. Superconductive electronics also is one of the recent R & D targets in Japan which require cryogenic environment. However there have been practically no activities in developing small, low-noise cryocoolers for this purpose. As a rare exception. the present authors have just started to develop small Stirling cycle cryocoolers for high temperature SQUIDs. Research activities have also started in developing magnetic refrigerators. In the following, the current activities are reviewed on development of such cryocoolers which produce low temperatures particularly below 20 K.

MAGLEV REFRIGERATION SYSTEM

The JNR MAGLEV project was initiated formally in 1970 following technical, economical and environmental assessments. After a variety of laboratory tests, the first running test by a 1/2 scale model vehicle ML500 was conducted in 1977, using the 1.3 km section of guideway constructed in Miyazaki prefecture. At this early stage of running tests, a sealed-off cryostat system for superconducting magnets was employed [3]. In parallel, research was also made on developing small scale "on-board" refrigerators. In 1978, an on-board refrigerator with a capacity of 30 W at 4.4 K was installed on ML500R and tested at 200 km/hr. A series of tests with ML500 were successfully completed in 1979 with achievement of a record speed of 517 km/hr on the 7 km full scale test track in Miyazaki [4].

For performance tests on more practical vehicles containing all essential feature required commercially, the test track was converted in 1980 from the inverted T-shape to a U-shaped guideway (Fig. 1). In parallel, a test train MLU001 was constructed. As shown in fig. 2, the final configuration of the new model consists of three connected vehicles, each of which has eight superconducting magnets. Figure 3 shows the arrangement of compressors, refrigerators, cryostats, and superconductive magnets. Two superconducting magnets are installed in one cryostat on the first and third cars (MLU001-1 and -3), whereas each magnet is installed individually in one cryostat on the second car (MLU001-2). To compensate for heat leak to cryostats, one refrigerator per car system is employed on MLU001-1, but one refrigerator per cryostat system is employed on MLU001-2 and -3. The configuration is expected to allow critical comparison between various systems.

A remarkable progress has been made in cryostat design during the past ten years. Finally, a cooling capacity of 2.5 W per magnet was specified for the cryocooler to compensate the heat leak. JNR is developing various on-board refrigerators in collaboration mainly with three industrial groups: Hitachi Ltd., Toshiba Co./ Sumitomo Heavy Industries Ltd., and Mitsubishi Electric Co./ Aisin Seiki Co.

Figure 4 shows a Claude cycle refrigerator of type A with a capacity of 30 W at 4.4 K developed for MLU001-1. Specifications of the machine are listed in the Table 1. The machine has 5 stages of heat exchangers, 2 expansion engines and a Joule-Thomson valve.

Claude cycle refrigerators of type B with a capacity of 5 W at 4.5 K were independently developed and installed on MLU001-2 and -3. Figure 5 shows one of the machines attached on the cryostat. The heat exchangers which were adopted for this type of refrigerators will be described by Koizumi et al. in this Conference [5].

An on-board refrigerator of type C which consists of Stirling cycle and Joul-Thomson loop, was also developed for MLU001-2. The J-T loop has four heat exchangers, three precoolers and a J-T valve. Each stage of the precoolers is cooled by a three stage Stirling cycle refrigerator, which is operated at 4.93 Hz with helium gas pressure of 16 kg/cm^2. The coldest stage of the refrigerator reached 11.1 K. The overall cooling capacity of this machine is 8 W at 4.37 K. Further effort is concentrated on developing a Stirling cycle machine which can reach 4 K without J-T loop.

In November of 1982, JMR succeeded in the manned test run with three connected cars train MLU001 which carries these various types of refrigerators.

OTHER DEVELOPMENTS

STIRLING CYCLE CRYOCOOLER

After basic investigation on regenerators and refrigeration cycles, Ishizaki and his co-workers at the University of Tokyo designed some Stirling cycle cryocoolers in the early 1970s. A three-phase Stirling cycle machine was constructed to obtain optimal design figures. Especially the effect of phase angle on refrigeration output was investigated with different compression and expansion volume ratios. Based on the result, they next constructed a four-phase Stirling cycle cryocooler, in which the pistons were driven with a swash plate. This machine produced a refrigeration output of 45 W at 78 K [2]. A four-phase regenerator, which consists of multi-layers of metal plate fixed with adhesives and small metal balls inside was also developed for compact design and improvement in thermal efficiency.

More recently, Ishizaki cooperated with a group of Aisin Seiki in developing a commercial Stirling cycle cryocooler. Figure 6 shows the 2 stage Stirling cycle cryocooler developed for general purposes including application

to cryopumps. A swash plate driving mechanism is employed to convert motor rotation to reciprocal motions of four pistons which are arranged at 90 degree intervals. A pair of the counter pistons is for the second stage of 20 K cooling circuit, whereas the other pair is for the first stage of 90 K cooling circuit which is used to precool the 2nd stage. Cooling capacities of 20 W and 150 W are reported at the first stage temperature of 90 K respectively with cooling down time of about 15 minutes.

A low noise Stirling cycle cryocooler is also investigated for cooling SQUID sensors. Recently, we developed Nb_3Ge SQUIDs which operate satisfactorily at temperatures approaching 18 K [6]. Our device has a relatively wide range of operating temperature. High temperature and wide range operation make the cryocooler design more practical with sufficient margin. In collaboration with Aisin Seiki, our group at Tohoku University constructed a two stage Stirling cycle cryocooler, in which small lead balls of 0.1 mm in diameter were used for the coldest part of the regenerators. A front view of our machine and an enlarged view of the cold heads are shown in Fig.7. This cryocooler was built to test a design for compact, light weight, easy-to-handle refrigerators for eventual use in cooling cryogenic sensors. Measurements are now undertaken on cooling performance, mechanical vibration, temperature fluctuation, electromagnetic noise, etc. Specification are listed in Table 2. Expected cooling capacity is 50 mW at 15 K. Although the tests with this trial machine have not been completed, a non-metalic structure and the use of heat pipe are now under consideration as a next step for reducing magnetic noise and temperature fluctuation respectively.

MAGNETIC REFRIGERATION

A study group on magnetic refrigeration was formed at the Society of Non-traditional Technology in 1980 to look into the possibility of its future use in refrigeration ranging from sub-room temperatures down to superfluid helium temperature ($\sim$1.8 K). More recently, a group at the Tokyo Institute of Technology lead by Hashimoto and a group at Toshiba have cooperated in constructing a prototype machine aimed at establishing the feasibility of a magnetic refrigerator working between 20 K and 4.2 K. The working substance used is Gadolinium Gallium Garnet (GGG) single crystal which has a relatively high entropy density, high heat conductivity and reasonably high Debye temperature ($\sim$500 K). As the lattice entropy is small compared to the spin entropy below 20 K for GGG, the refrigerator may , in principle, be operated in a Carnot cycle. Heat of magnetization at the high temperature isothermal was removed by gaseous helium flowing through a pipe P (Fig.8). The lower end of GGG was attached to a thermosiphon, the cold end of the thermosiphon was used to condense helium gas. By measuring the rate of liquefication of helium, the refrigeration capacity at 4.2 K for a cycle starting at 16 K and 6.7 T using 1.7 mole of GGG was estimated to be 42 J when the field was reduced at a rate of 0.67 T per sec [7]. The magnetic field for this experiment was changed by energizing and de-energizing a superconducting pulse magnet at various sweep rates. This mode of altering the magnetic field is not favourable for practical use due to extra losses incurred in operation of the superconducting magnet. The experiment is still in its initial stage, however, and the method was used to investigate problems in the magnetic

refrigeration cycle proper.

CONCLUSION

Groups engaged in R & D works on cryocoolers in Japan are summarized in Table 3. Almost all cryocooler activities are more or less stimulated by big national projects as pointed out in the introduction.

JNR invested more than 20 billion yen in the MAGLEV project and since 1979 the government has been subsidizing the project with an annual outlay of 600 million yen. However, the amount of the funds alloted to the refrigeration technology is not known.

Science and Technology Agency appropriated 463 million yen in the 1982 fiscal year budget for promoting R & D studies for establishing the technological base of applied superconductivity and cryogenics. Out of the total fund, about 95 million yen is to be alloted for refrigeration technology regarding Stirling cycle cryocoolers and magnetic refrigerators.

Ministry of Education and Culture supported university research on superconductive electronics with a grant of 600 million yen for the period 1979 to 1981. Although the need for small cryocoolers gained gradual recognition in this area, development efforts are still minor.

Although basic research and digital application of superconductivity are in progress at various industries, Nippon Telegraph and Telephon Public Corporation, and Electrotechnical Laboratory. However, no explicit activities have not been reported on refrigeration at present.

The authors would like to thank Y. Kyotani for providing them with a mass of information on the JNR project.

Table 1 Specifications of JNR MAGLEV On-Board Refrigerators

Type	A	B	C
Ref. Cycle	Claude	Claude	Stirling+J-T
Cooling Capacity at 4.4 K (W)	30	5	8
He Flow Rate (Nm^3/h)	150	30	17.2
Inlet Pressure (kg/cm^2G)	15	16	18.9
Size diam (mm) length (mm)	400 1400	300 800	296 796
Weight (Kg)	140	40	33.9

Table 2 Specifications of the Cryocooler Built in Tohoku University to Test a Design for Eventual Use in Cooling Cryogenic Sensors.

Item	Specification
Refrigeration Cycle	Stirling cycle
Output (cooling capacity)	50 mW at 15 K
Lowest temperature	$\sim$ 10 K
Working gas	Helium
Input power	150 W
Dimension	260mm x 290mm x 540 mm
Weight	24 Kg
Drive	$\lesssim$ 5 Hz

Table 3 List of Groups Working with Cryocoolers in Japan

Group	Leader	Object	Refrigeration Cycle
Aisin Seiki Co. Ltd.	T. Tani	Mag. Lev. Cryopump SQUID	Stirling + J-T Stirling Stirling
Consultant	Y. Ishizaki	Mag. Lev. Josephson Computer Cryopump	Stirling Cycle Machine Cryogenic System
Hitachi Ltd.	T. Fujinaga	Mag. Lev.	Claude
JNR	Y. Kyotani	Mag. Lev.	Stirling G-M + J-T Claude
Mitsubishi Electric Corporation	Y. Furuta	Mag. Lev.	G-M + J-T
Sumitomo Heavy Industries, Ltd.	T. Koizumi	Mag. Lev.	Claude
Toshiba Corporation	M. Yamaji H. Nakagome	Mag. Lev. Superfluid ^{4}He	Claude Magnetic Refrigerator
Nihon University	Y. Matsubara	Study of Regenerator	Regenerative Cycle
Tohoku University	T. Ohtsuka T. Fujita	SQUID	Stirling
Tokyo Institute of Technology	T. Hashimoto	Superfluid ^{4}He	Magnetic Refrigerator

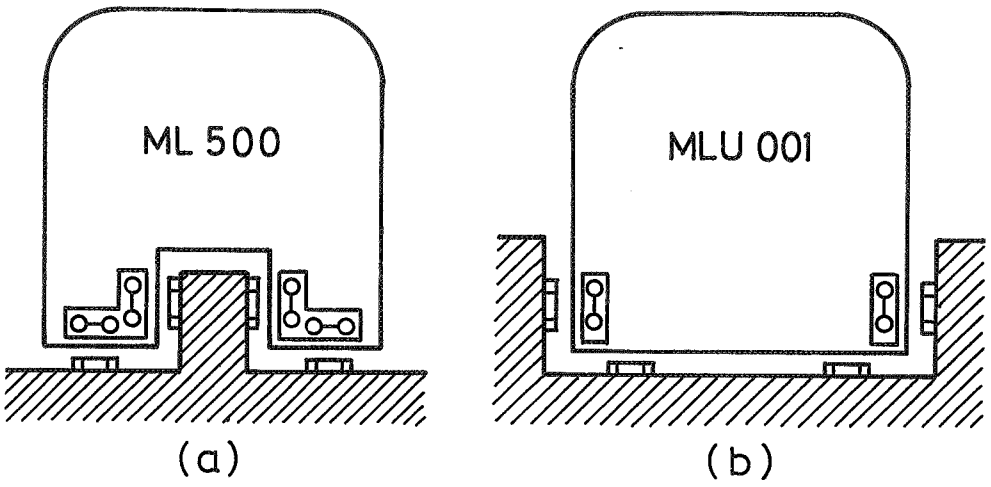

Figure 1. Schematic views of (a) ML500 on the inverted T-shaped guideway and (b) MLU001 on the U-shaped guideway. The vehicles carry liquid helium cryostat systems of L-shape and I-shape respectively.

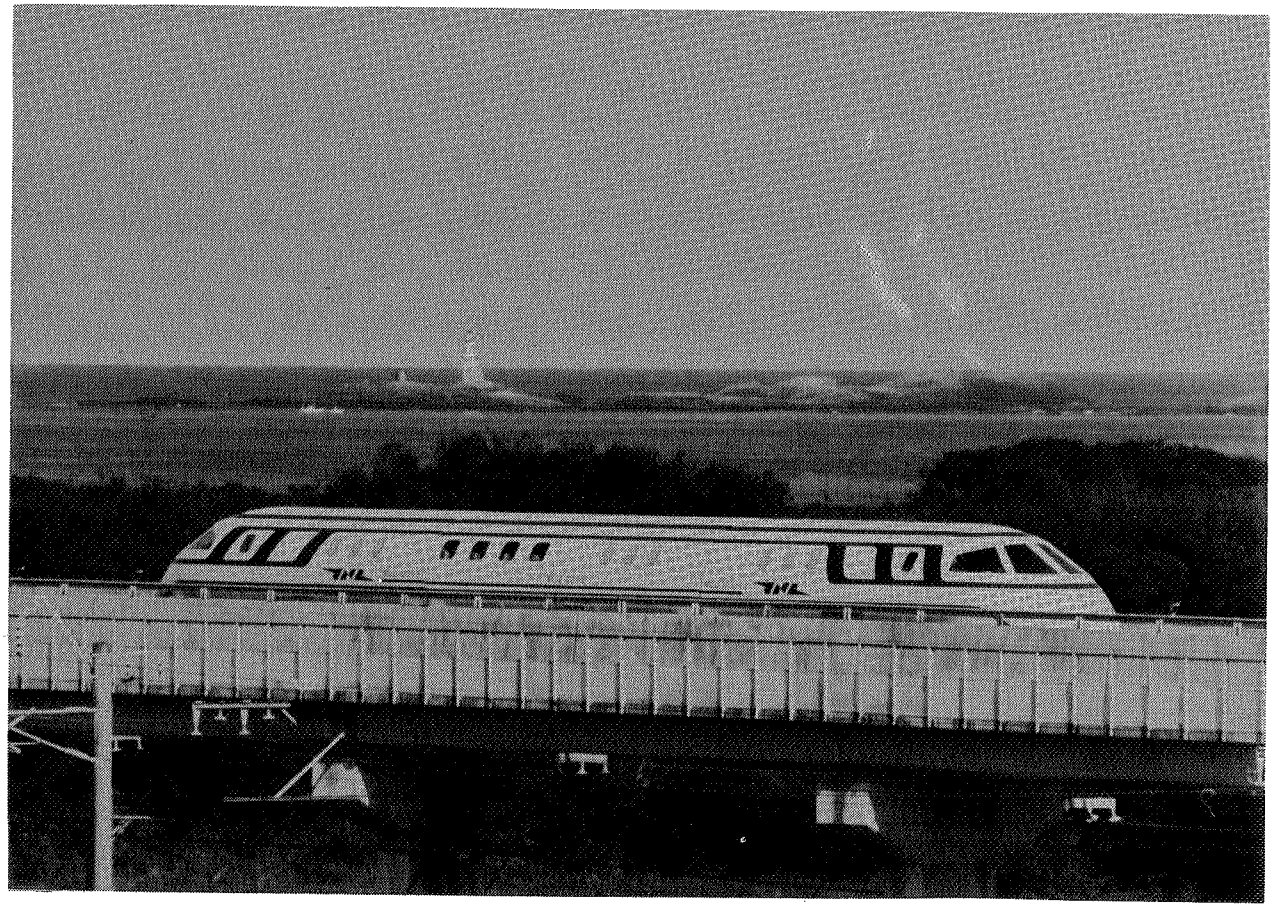

Figure 2. Photograph of MLU001 running on the test track.

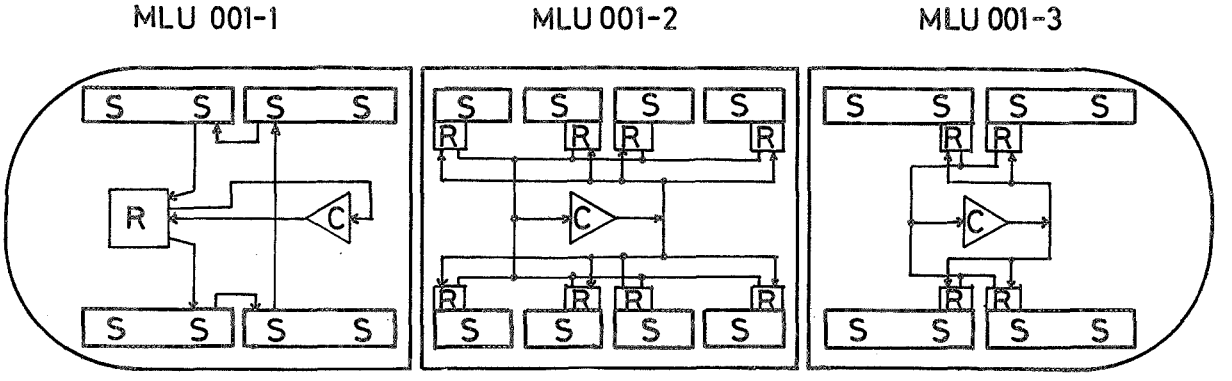

Figure 3. Schematic diagram of the cryogenic system on MLU001. S : Superconducting magnet, R : Refrigerator, C : Compressor.

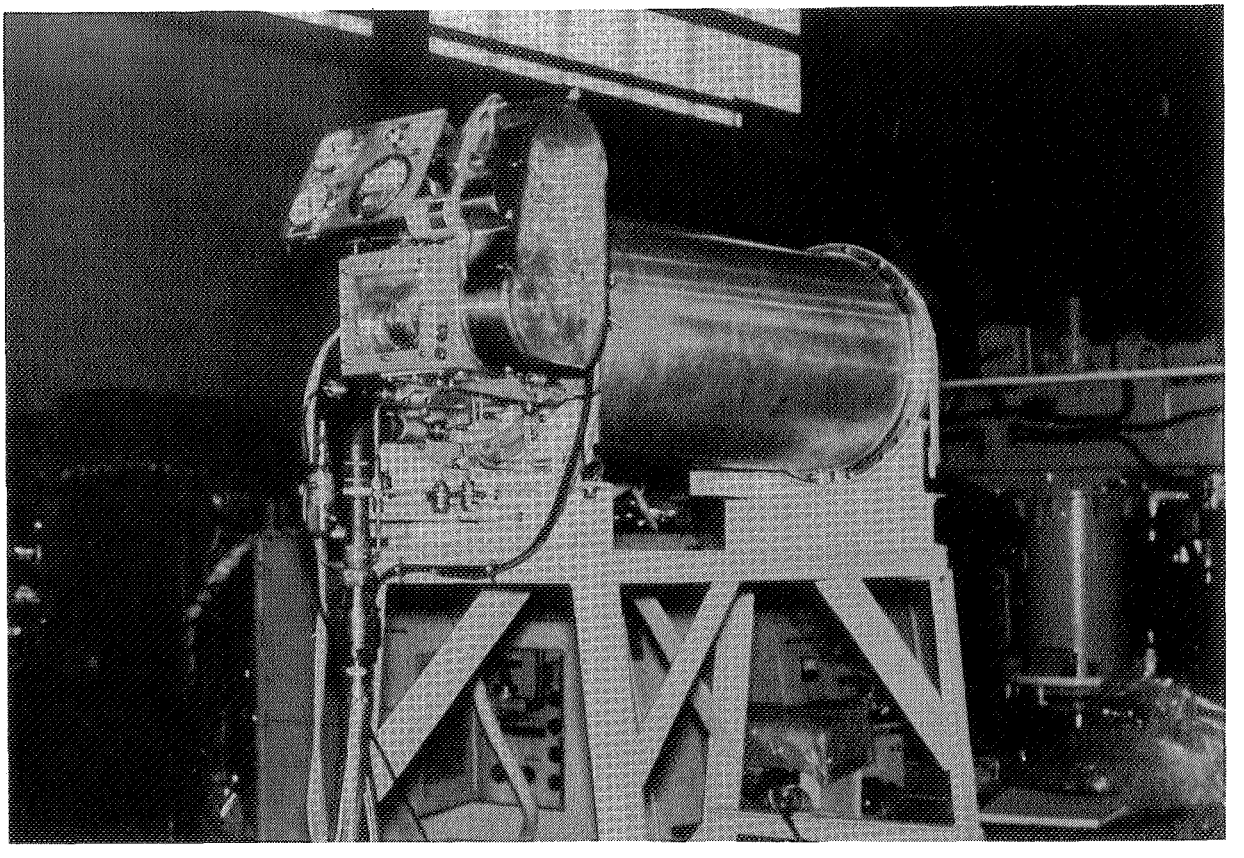

Figure 4. A Claude cycle on-board refrigerator of type A.

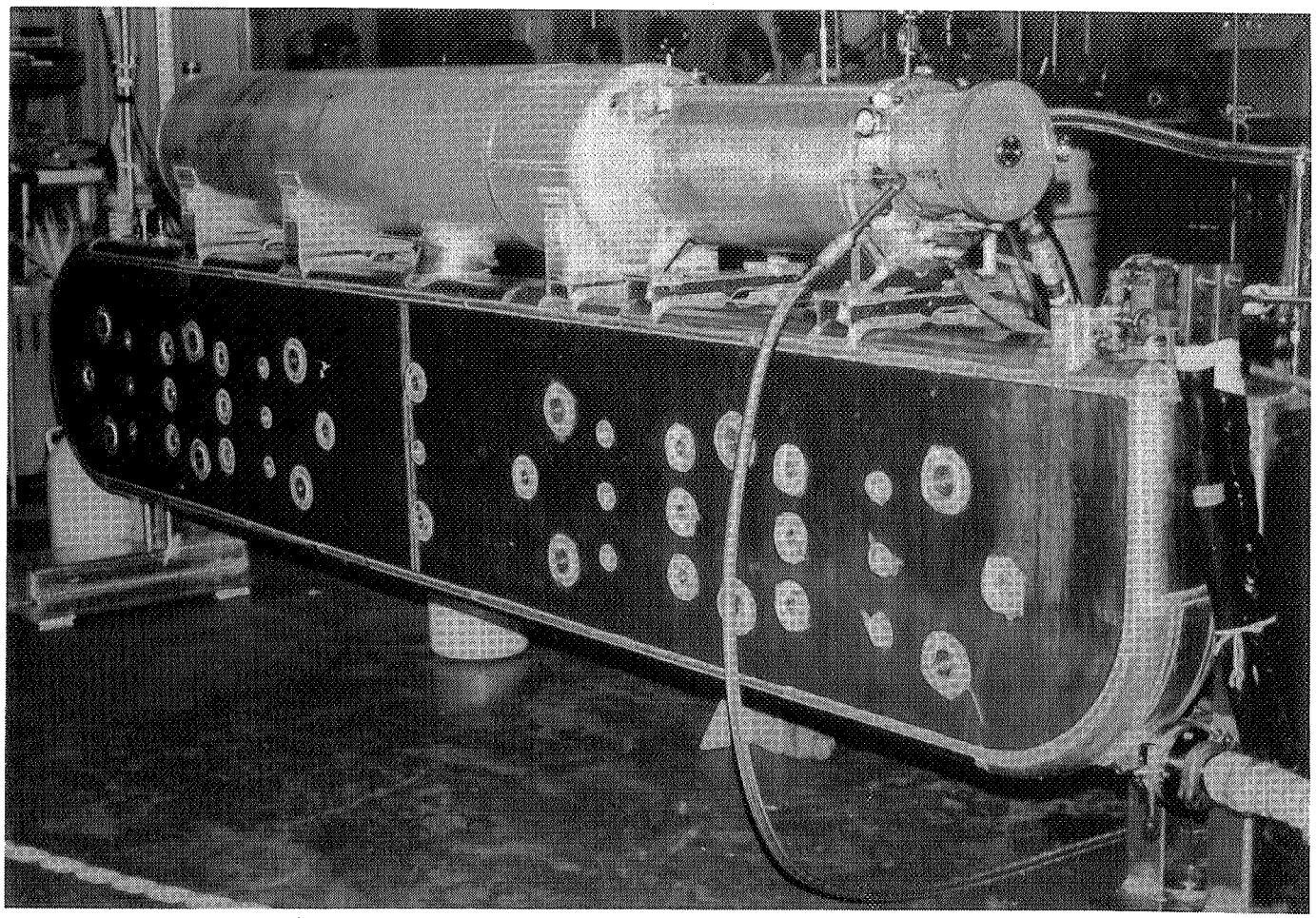

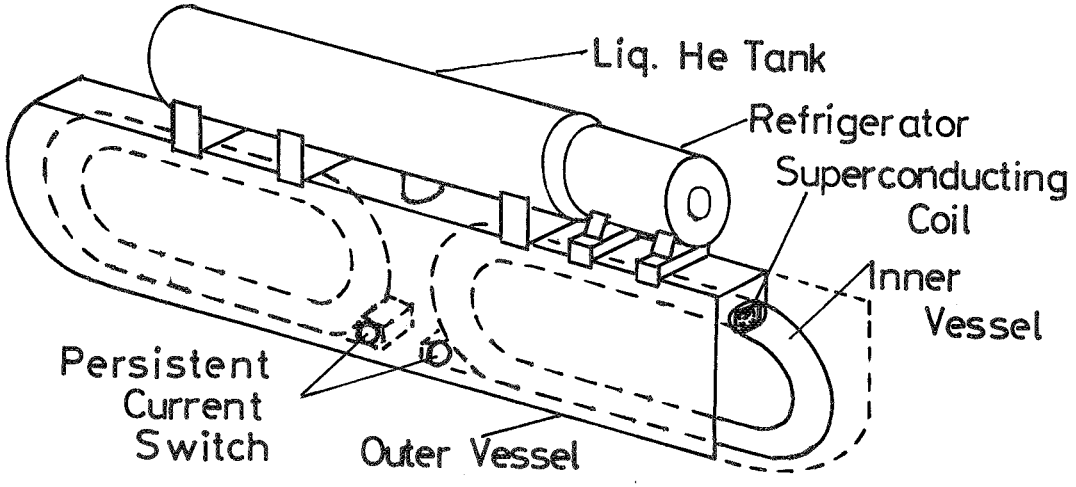

Figure 5. Photograph (upper) of an on-board refrigerator mounted on the I-shaped cryostat system. The structure is outlined in the schematic drawing (lower).

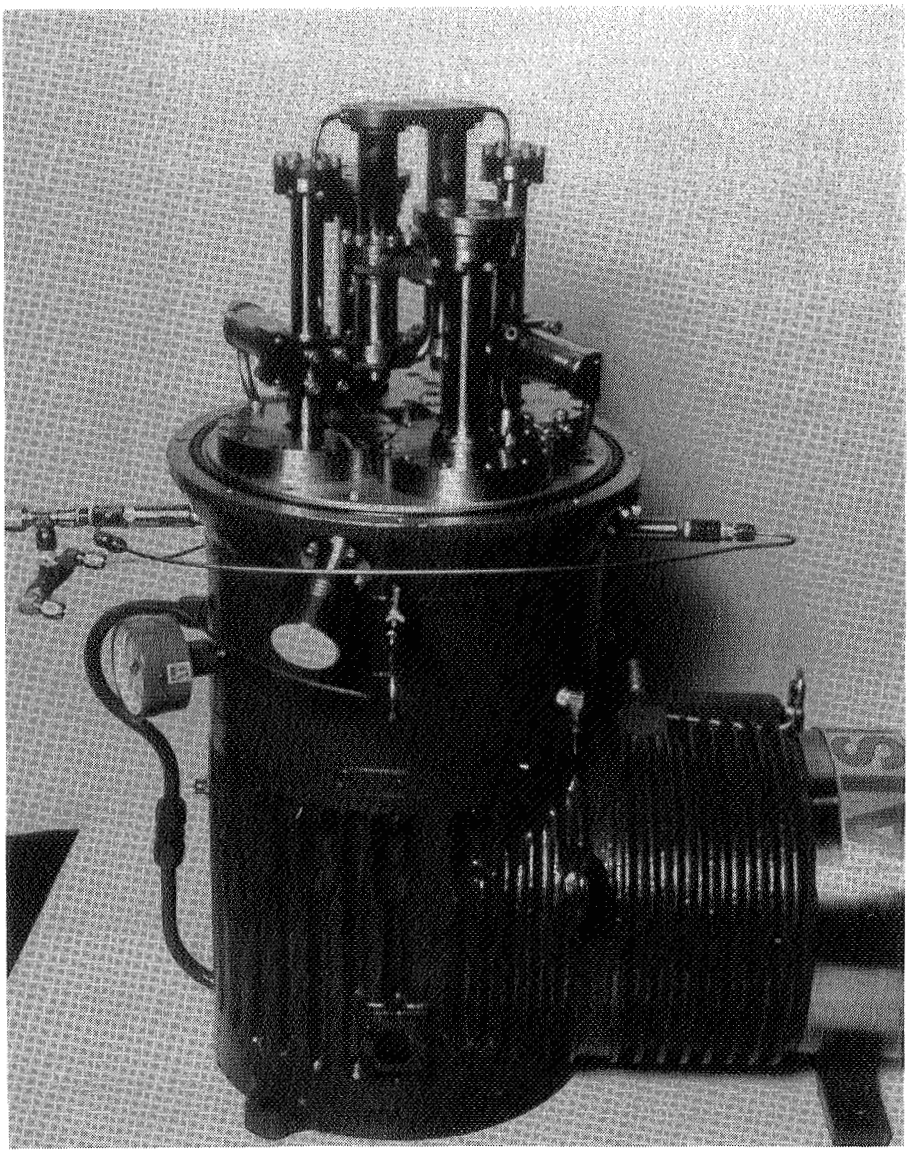

Figure 6. A 2-stage Stirling cycle cryocooler commercially developed for general purposes.

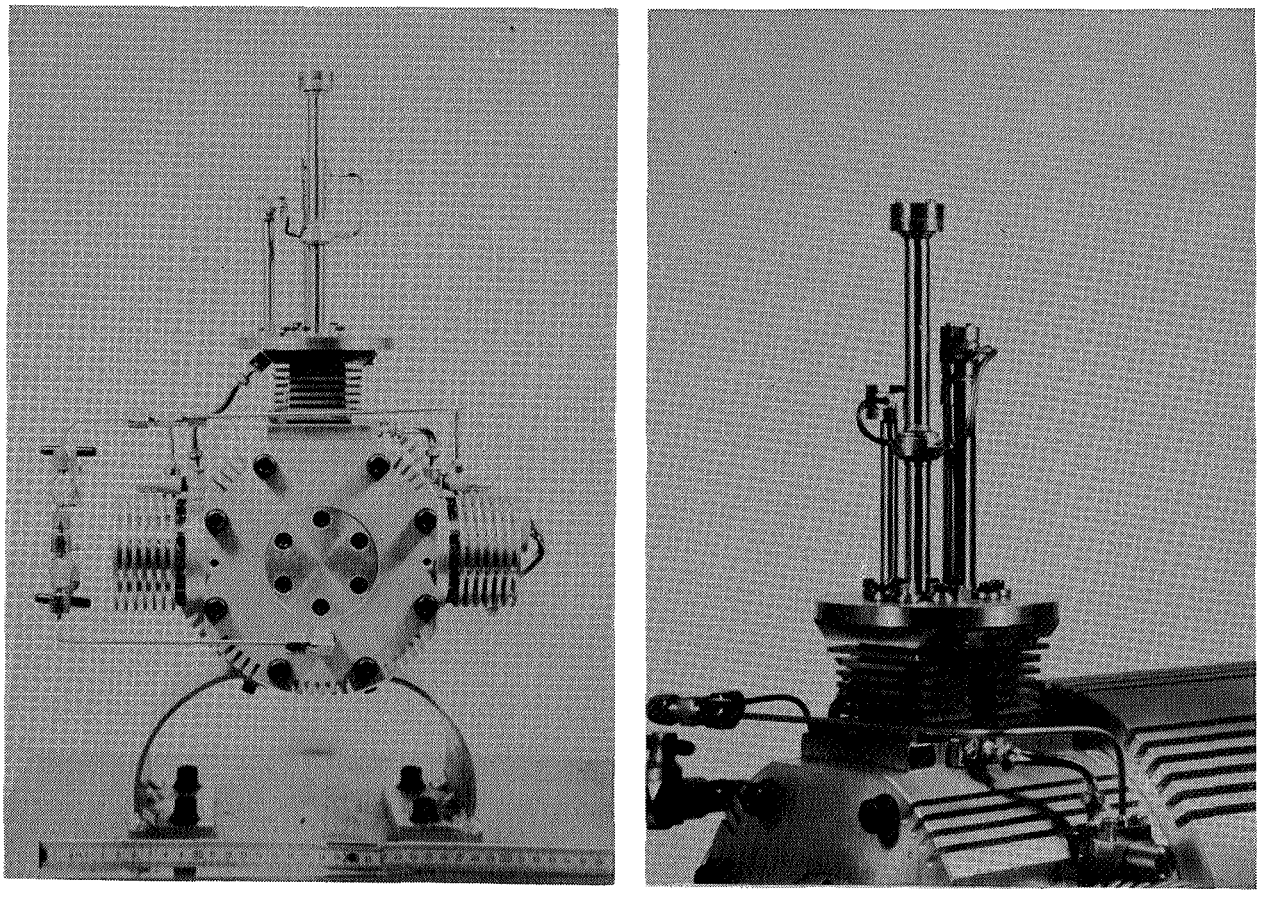

(a) (b)

Figure 7. A test model of low-power Stirling cycle cryocooler for SQUID sensors: (a) front view and (b) cold head

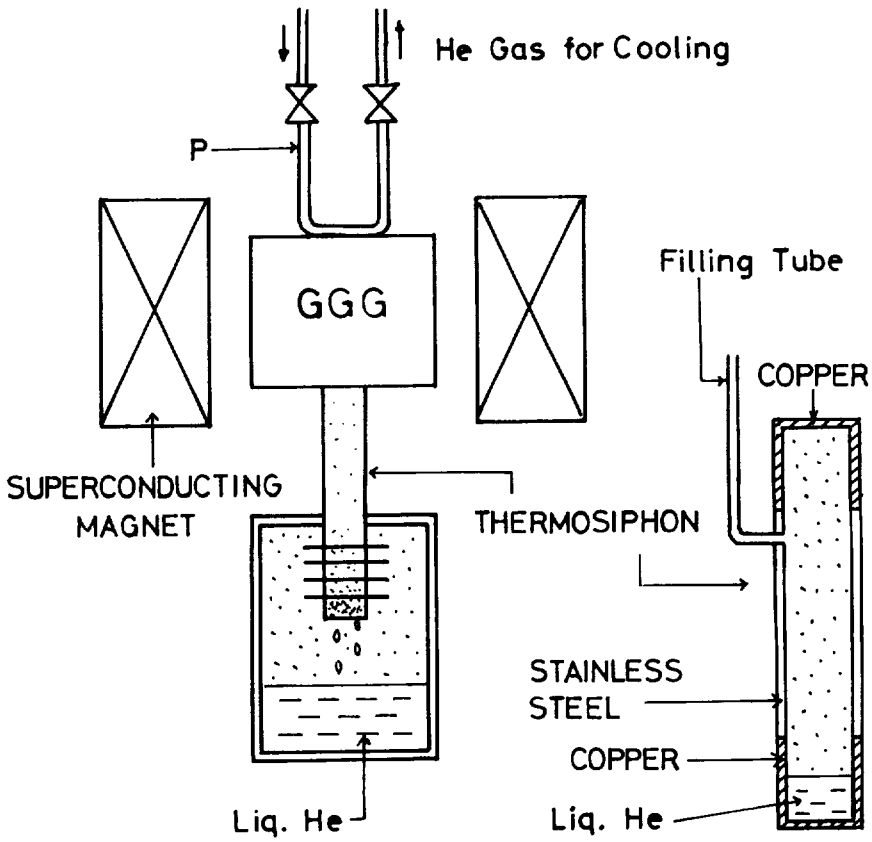

Figure 8. Schematic arrangement of experiments on magnetic refrigeration

REFERENCES

[1] Matsubara, Y. and Yasukochi, K.: An Application of Gap Regenerator/ Expander Precooled by Two State G-M Refrigerator (This Conference).

[2] Oshima, K. and Ishizaki, Y.: Refrigeration Technology in Japan, Proc. 5th International Cryogenic Engineering Conference, Kyoto, edited by K. Mendelssohn, IPC Science and Technology Press (1974) pp.357-360.

[3] Ishizaki, Y., Kuroda, T. and Ohtsuka, T.: Sealed Cryostat System for Magnetically Levitated Vehicles, ibid., pp.102-105.

[4] Ohtsuka, T. and Kyotani Y.: Recent Progress in Superconducting Magnetic Levitation Tests in Japan, IAS Conference Record, CH1575-0/80/0000-0238, IEEE (1980) pp.238-243.

[5] Koizumi, T., Kanazawa, M., Takahashi, M., Uchida, T. and Suzuki, M.: A Small and Light Weight Heat Exchanger for On-Board Helium Refrigerator (This Conference).

[6] Fujita, T., Suzuki, M., Ikegawa S., Ohtsuka, T. and Anayama, T.: High Temperature Operation of Nb_3Ge SQUIDs, Proc. 9th International Cryogenic Engineering Conference, Kobe, edited by K. Yasukochi and H. Nagano, Butterworth & Co. (1982) pp369-372.

[7] Hashimoto, T.: private communication.

SPACECRAFT-BORNE LONG LIFE CRYOGENIC REFRIGERATION

STATUS AND TRENDS

Dr. Alfred L. Johnson
The Aerospace Corporation, El Segundo, California

ABSTRACT

The status of cryogenic refrigerator development intended for, or possibly applicable to, long life spacecraft-borne application is reviewed. Based on these efforts, the general development trends are identified. Using currently projected technology needs, the various trends are compared and evaluated. The linear drive, non-contacting bearing Stirling cycle refrigerator concept appears to be the best current approach that will meet the technology projection requirements for spacecraft-borne cryogenic refrigerators. However, a multiply redundant set of lightweight, moderate life, moderate reliability Stirling cycle cryogenic refrigerators using high-speed linear drive and sliding contact bearings may possibly suffice.

INTRODUCTION

To establish bounds for this overview, figure 1 illustrates possible spacecraft-borne long life cryogenic cooling needs, while suggested methods are shown in figure 2 and current program design regimes appear in figure 3. Expendable mass cryogenic heat sinks are excluded from consideration due to the excessive weight and volume that results when such a system is sized to the long life requirement (5 to 10 years). A hybrid system which would use a refrigerator to balance the tankage heat leaks and a stored cryogen for the actual cooling effect may, in some instances, prove to be the optimum system; however, such integrated systems are beyond the purview of this paper.

---

* This study was supported by the Space Division, Air Force Systems Command under Contract No. F04701-82-C-0083.

For the higher cryogenic temperatures, the use of conductive-radiative or convective-radiative cooling methods, possibly incorporating heat of fusion thermal storage, cryogenic heat pipes (conventional, variable conductance, and diode), and/or thermal switches will suffice--especially if the vehicle orbit, orientation, and configuration can be somewhat constrained. With the exception of diode heat pipes and cryogenic thermal switches, this segment of spacecraft cryogenic cooling technology is sufficiently well developed to be immediately applicable. However, some areas could be improved, e.g., spectrally selective surface coatings, improved insulation, and low specific weight radiator designs.

For low heat loads at intermediate range cryogenic temperatures, thermoelectric (Peltier) cooling is an available mature technology that will suffice when coupled with low temperature radiators. Lockheed Research Laboratories are currently developing Nernst-Ettinghausen thermo-magneto-electric cryogenic cooling materials. This is a high risk program that might result in developing materials with improved direct conversion efficiencies; however, even if the material development is successful, engineering hardware probably will not be available until 1990.

Adiabatic demagnetization is the thermodynamic process used to obtain extremely low temperatures. Recently, Stegert (ref. 1) at Los Alamos has suggested that this technique might be extended to develop a high efficiency cryogenic refrigerator applicable to the "midband" region (5 - 50K; 1-10 W). At this time, it appears to be a high risk endeavor due to the complex mechanical system configuration, extremely high magnetic field requirements (superconducting magnetics), and the lack of materials with significant magnetocaloric properties to cover the temperature range from heat source to heat sink.

As evidenced in figures 1 and 2, the majority of the spacecraft-borne long life cryogenic cooling needs can be met effectively only with the use of mechanical refrigerators. Projections of the performance characteristics of such hardware which could be developed, up to the year 2000, are summarized in table I.

STATUS

The lack of reliable cryogenic refrigerators for spacecraft use has been recognized as a constraining technology for over 20 years. Tens of millions of dollars of federal research funds have been spent on this technology. A totally successful product has yet to be developed. The status of four current programs specifically directed towards the development of long life spacecraft-borne refrigerators is summarized below followed by comments on other cryogenic refrigerator programs which exhibit features potentially adaptable to this development.

1. Arthur D. Little Rotary Reciprocating Refrigerator (fig. 4). This design uses rotary motion to create a gas bearing effect as well as reciprocating motion for compression and expansion to create the refrigeration effect. This concept has been under development since 1962. The

design can be thermodynamically configured as either an Ericsson cycle or a Stirling cycle. In the Ericsson cycle configuration, the rotary motion is synchronized with the reciprocating motion so that slide valve porting can be simply accommodated. The bearing and porting requirements imposed on the low temperature displacer result in the need for a close tolerance, small clearance part which has proven to be difficult to make. The Stirling cycle configuration should reduce this problem, since the valving would be eliminated, much higher rotational speed could be used, and the clearance could thereby be increased. The Ericsson cycle hardware has not yet successfully operated as a complete system. The Stirling cycle hardware has not yet been built. Component-demonstrated life is approximately 10,000 hr.

2. Hughes Aircraft Company Vuilleumier Refrigerator (fig. 5). This design is based on the Vuilleumier cycle which uses heat rather than mechanical energy to cyclically pressurize the working gas. The hardware has been in development since 1967. The design uses sliding composite seals and riders and a rotary to reciprocating mechanical drive to shuttle the displacers while a 90° phase angle is maintained between the relative positions of the hot and cold displacers. The drive mechanism uses dry-lubricated ball bearings and Bendix flexure bearings. The design is wear and fatigue life limited.

Maximum demonstrated life is approximately 6,000 hr. The design has low efficiency due to the thermodynamic losses in the conversion of electrical energy to heat to mechanical energy. The Hughes Vuilleumier refrigerator appears to be an acceptable unit for a one-year mission; however, the electrical power required is high in comparison to the alternatives, resulting in increased vehicle weight and cost unless on-board heat (e.g. nuclear) is provided.

3. AiResearch/Garrett Turbo Brayton Refrigerator (fig. 6). This design uses foil-type gas bearings, a high-speed compressor, and a turbo-alternator expander. The hardware has been under development since 1977. Full system operation has been demonstrated; however, the system did not meet design goals due to a design error in the cold regenerator. The performance test is scheduled to be rerun with a larger cold regenerator and improved insulation. There have been less than 1000 hr of full system operation. This design is based on concepts and principles that should result in a five-year service life, high reliability unit, although further life testing will be required to verify this. The power required is high when compared to most other refrigerator configurations in the design regimes of current interest.

4. Philips Laboratories, U.S.A., Magnetic Bearing-Free Piston Stirling Cycle Refrigerator (fig. 7). This concept has been under development since 1978 and had a successful first run in March 1982. Magnetic bearings are used to support the moving elements thereby eliminating mechanical wear, thus trading mechanical simplicity with wear for electro-magnetic complexity with zero wear. The design offers promise of being a successful long life, high reliability, efficient cryogenic refrigerator, but it will be necessary to perform further life tests to

establish the reliability of the magnetic bearing system. The existing design will need modification for spacecraft use; however, the test data from the development model show that all performance requirements, including zero wear, have been met. A multi-stage linear Stirling refrigerator would offer the same advantages as the single stage; unfortunately, such a unit is yet to be built and demonstrated.

5. Other Programs of Interest. Philips designed and constructed a "one-year" rhombic drive cryogenic refrigerator, four of which were flown on the STP 78-1 spacecraft experiment (fig. 8). Three of the refrigerators have continued to operate (periodically) for over 36 months, but with a continually degrading performance primarily due to helium leakage. Probably some contamination of the regenerator also exists due to the rhombic drive lubricant and seal wear. The design could be improved by replacing the elastometric static seals with hermetic welded joints to eliminate helium leakage and by adding a bellows (not included in the flight versions due to unsatisfactory performance) to separate the working gas from the gear lubricants to eliminate regenerator contamination. In this way, a two- to three-year life design should result. (Test data on candidate metal bellows show seal failure at 10,000 hr.) It is probably more cost-effective and energy efficient, however, to complete the redesign and qualification of the NASA Goddard single stage linear Stirling refrigerator.

Philips Einhoven, Netherlands, has developed a line of extremely simple linear drive, free piston, Stirling cycle refrigerators. These units, intended initially for laboratory use, are guaranteed for 2,500 hr. The basis of this claim is an experiment in which five units were operated 23 hr/day until 5,000 hr were accumulated on each unit. Apparently no significant change occurred in performance after the first few hundred hours. Philips Einhoven is currently developing several different militarized versions of this refrigerator. Schematics of the units are shown in figure 9. (These machines are not designed for spacecraft operation.)

Davey (ref. 2) has reported on the development of a long life, high reliability, spacecraft-intended split Stirling component refrigerator which appears to be very similar in configuration to the Philips Einhoven unit, except that flexure bearings have been incorporated to support the compressor piston to eliminate wear, and a linear drive has been added to the displacer in order to control the phase angle. The flexure bearing design is apparently derived from that developed by Johnston (ref. 3) for an artificial heart Stirling engine. The current status of this development is uncertain. Figure 10 is a schematic of this unit.

A linear drive helium prototype compressor was developed at Mechanical Technology, Inc., and a mating prototype reciprocating helium expander/liquifier was developed at Cryogenic Technology, Inc. The development, which was not completely successful, was intended to be used for a shipboard liquid helium source, but the technology may be applicable to spacecraft-borne use. There are similarities between the Arther D. Little and the Mechanical Technology, Inc., linear compressors; both are linear resonance

machines using gas springs. However, the Mechanical Technology Inc., design uses hydrostatic gas bearings, reed valves, and a linear magnetic induction motor, whereas the Arthur D. Little compressor uses hydrodynamic bearings, slide valves, and a linear solenoid motor.

The Night Vision Laboratory is funding the development of a split component Stirling cycle refrigerator somewhat similar to the Philips Einhoven/Davey-Oxford designs. Although intended for ground and airborne use, the unit might prove useful in spacecraft applications.

TRENDS

Considering the thermodynamic cycles suitable for cryogenic refrigerators, the current state of the art of the elements used in long duration spacecraft cryogenic refrigerators, and the active development programs, it is possible to create a morphological array which provides some insight into possible future trends in the technology. The thermodynamic cycles of interest are the Stirling, Ericsson (Brayton), and Claude/Collins. The Vuilleumier refrigerator can be considered to be a Stirling power engine driving a Stirling refrigerator. Possible bearing systems are low pressure sliding contact, flexures, hydrodynamic gas, hydrostatic gas, and electromagnetic. For linear refrigerators, the motor choice includes moving coil, moving iron, and moving magnet. For rotary dynamic refrigerators, induction and permanent magnet rotor motors are possible, the latter being superior due to higher efficiency. The three variables--thermodynamic cycle, bearing type, and motor type--can be used to generate a morphological array. The current development efforts are noted on the resulting map (fig. 11). Apparently, very few of the possible combinations are currently being pursued. As an additional possibility for bearing systems, Mechanical Technology, Inc., has suggested that piezoelectrically energized squeeze film bearings might be developed for this type of hardware. Similarly, piezoelectric drives ("benders") or magnetostrictive drives might prove useful as an alternative to linear electromagnetic motors, especially as displacer actuators.

To establish a basis for evaluating trends, note that three major design parameters of importance to spacecraft-borne cryogenic refrigerators are: service life/reliability (which implies a mean time between failure), cooling capacity at temperature, and specific power (power in per cooling effect) at temperature. Technology projection values for these parameters, in essence "design requirements," have been presented in table I for the 1980-2000 time period. It is interesting to compare these design parameters against the intrinsic capabilities of the generic type of refrigerator typified by each of the four major development programs currently being funded: the Arthur D. Little Rotary Reciprocating Refrigerator, the Hughes Vuilleumier Refrigerator, the AiResearch Turbo-Brayton Refrigerator, and the Philips Linear Drive, Magnetic Bearing Stirling Refrigerator.

First consider the service life/reliability parameter. The close tolerance, small clearance development problem of the Arthur D. Little Refrigerator development must be resolved before the design can meet the

one-year/85% reliability requirement. If a suitable thermally stable material can be found, if the unit is designed so that all materials used are never stressed beyond the fatigue limit, and if the position sensor life proves to be adequate, the design may meet the five-year service life/90% reliability. To develop a longer life/higher reliability version, advanced materials and/or alternate concepts/applications are considered necessary. These items are addressed later in this paper.

The Hughes Vuilleumier Refrigerator program must complete the regenerator composite seal development effort before the design is considered to have met the one-year/85% reliability requirement. To proceed much beyond this point, a complete redesign is required to eliminate wear, reduce material fatigue stresses, and stop working fluid leakage. This could be accomplished by changing to a linear drive (thereby eliminating the Bendix flexure and the dry-lubricated ball bearings), changing from sliding contact composite seals to clearance seals, and converting from a bolted flange, O-ring seal to a welded enclosure which is designed so that the stresses remain well within the material fatigue limit. To meet the 10-year service life/95% reliability, advanced materials and/or alternate concepts/applications are considered necessary.

The thrust bearing currently used in the AiResearch Turbo-Brayton Refrigerator turbo-expander/alternator unit may not be the design recommended for the flight configuration. When this question is resolved, the design should be capable of meeting the five-year service life/90% reliability requirement if the motor stator end windings can survive and if the shutdown/restart cycles do not wear the foil bearings excessively. Ten-year service life with 95% reliability appears to be beyond the capabilities of this design unless advanced materials and/or alternate concepts/applications are utilized.

The Philips Linear Drive Magnetic Bearing Stirling Refrigerator was conceived and designed to meet the five-year service life/90% reliability requirement. The existing hardware is an engineering development design configuration, thus the refrigerator needs to be redesigned to a flight configuration. If the unit is designed so that all materials used are never stressed beyond the fatigue limit, and if the position sensor life proves adequate, the fundamental design would appear to meet the 5-year, 190% reliability requirement. Figure 12 graphically summarizes the service life/reliability development issues discussed above.

If a thermally stable material can be obtained for the close tolerance, small clearance requirements of the Arthur D. Little Rotary Refrigerator design, then all four development concepts can be considered as capable of meeting both the 5 W at 65°K to 20 W at 20°K design spectrum and the 0.2 W at 10°K to 2 W at 10°K design spectrum by appropriate component sizing and/or staging. To meet the 0.1 W at 4°K to 5 W at 4°K design spectrum, an additional stage would be required for the AiResearch Turbo-Brayton design incorporating a final stage recuperator and a Joule-Thompson (J-T) valve (possibly aided with a jet pump). This effectively changes the configuration to a Collins cycle, as shown in figure 13. The Arthur D. Little,

Hughes, and Philips designs would require a secondary loop using recuperators, a compressor, and a J-T valve (possibly aided by a jet pump) to meet the 0.1 W at 4°K to 5 W at 4°K design spectrum. Figure 14 graphically shows the essence of this hybrid configuration. The cooling capacity at temperature development issues discussed above are illustrated in figure 15.

Considerations of the issues relating to specific power at temperature show that the Arthur D. Little and Philips refrigerator concepts can be utilized, subject to appropriate sizing, staging, and incorporation of additional components, to meet the design requirements for all three spectra identified. The Hughes Vuilleumier design concept can only meet the specific power at temperature requirements in the 10 kW power-in/W cooling at 10°K region--effectively the 1980 technology point. The AiResearch Turbo-Brayton refrigerator concept can be sized to meet the specific power at temperature design requirements, but only if the cooling loads are greater than those identified under the cooling capacity at temperature design requirements. Figure 16 shows the comparison between the four refrigerator concepts for the specific power and temperature development issues.

To meet the technology projections, "advanced materials" may be required. Some candidate materials and their potential use are summarized in Table II. Of particular interest are dimensionally stable materials with low, isotropic coefficients of thermal expansion suitable for use down to 4°K, materials with high fatigue limit strength at 10^9 cycles, and materials suitable for non-wearing sliding contact bearings.

Alternate approaches to meet the technology projections exist. One method would be to use a number of moderate life, high reliability, lightweight, high efficiency refrigerators coupled in parallel to the cryogenic load through cryogenic thermal diodes. If one unit failed, another unit would be activated. Figure 17 depicts such a redundancy-based refrigeration system. The Philips Einhoven, Davey-Oxford, and Night Vision Laboratory split component Stirling cycle designs are candidate refrigerators for this concept. A second method would be to incorporate a large cryogenic heat sink with a greatly oversized non-wearing refrigerator (and a cryogenic thermal diode) that could operate with a low duty cycle and still provide the average cooling needs. The number of stop-start cycles would necessarily increase; however, the total running time on the refrigerator would decrease and the efficiency would increase (due to the unit being sized to a larger heat load). Overall system advantages might also result, since a better match could be obtained between power needs and power availability. These alternate approaches have not been examined in sufficient detail to validate their usefulness nor to influence the design parameters used in the current development programs.

CLOSURE

In order to meet the life-reliability requirements identified for spacecraft-borne long duration applications, cryogenic refrigerators should be designed to eliminate component wear, material fatigue, working fluid

contamination, and working fluid leakage. The Turbo-Brayton refrigerator design appears to satisfy these criteria; there is no sliding contact (other than startup), no pressure cycling, no sources for contamination in contact with the working fluid, and effectively no leakage (The entire unit is welded together thereby hermetically sealing the working gas.). The compressor and turbine wheel blades are subjected to low level, high frequency cyclic stresses as are the unsupported copper end windings and the ferromagnetic laminations in the motor. Proper material selection and structural design should result in keeping the stresses in these elements well below the fatigue limit. Unfortunately, this design does exhibit a relatively low efficiency in comparison to the periodic refrigerator designs in the mid-cryogenic temperatures, mid-cooling effect region. Several technology innovations exist which could be developed and incorporated in the Turbo-Brayton design to improve efficiency (three-dimensional flow turbine/compressor "wheels," higher speed components, magnetic bearing on the turboalternator, lower loss rotors, higher effectiveness heat exchangers, a more efficient insulation system); however, even if all the improvements were successfully incorporated, the design still would only be power competitive in the higher cryogenic temperature or the higher heat load regions.

The Vuilleumier cycle refrigerator, as embodied in the Hughes Aircraft Corporation design, experiences wear (bearings, seals, riders), material fatigue (flextures, housing pressure cycling), potential working fluid contamination (breakdown of organic wear products), and working fluid leakage (bolted closures-elastometric seals). Through conversion to a linear drive, incorporation of clearance seals, and enclosure of the unit in a hermetic housing, most of these difficulties could be eliminated (except for housing pressure cycling). The design would still be considerably less efficient than the Stirling and Ericsson cycle refrigerators; thus it would be non-competitive from an effective total weight basis unless an on-board low penalty heat source were available (waste heat, nuclear, solar thermal).

The Rotary Reciprocating Refrigerator, as designed by Arthur D. Little, and the magnetic bearing-supported linear Stirling cycle refrigerator as developed by Philips Laboratories both appear to possess most of the attributes deemed necessary for long life, high reliability operation together with relatively high operation efficiency. The Stirling cycle variant of the Rotary Reciprocating Refrigerator seems to be superior to the Ericsson cycle version due to a less critical displacer clearance requirement, the inherent simplicity of a regenerator in comparison to a recuperator, and a higher overall cycle efficiency (due to the higher effectiveness obtained from a regenerator in comparison to a recuperator). (Only the Ericsson cycle version is presently under development.) Both the Arthur D. Little and the Philips Laboratories designs have potential failure modes which have not been completely evaluated, one being the failure of the position sensor(s) necessary for the proper operation of the unit, and the other possibility being enclosure failure from material pressure cycle fatigue. Neither appears to be an insurmountable problem.

At this time, the linear drive non-contacting bearing Stirling cycle refrigerator concept appears to be the best approach to meet the technology

projection requirements for spacecraft-borne cryogenic refrigerators; however, a system based on the use of a number of lightweight, moderate life, moderate reliability cryogenic refrigerators (e.g., Philips Einhoven, Davey-Oxford, Mico-Vision Laboratory) coupled in parallel via cryogenic thermal diodes may prove to be competitive, especially since any spacecraft system specification will probably mandate the incorporation of at least one redundant refrigerator.

REFERENCES

1. Stegert, W.A.: "Stirling-Cycle Rotating Magnetic Refrigeration and Heat Engines for Use Near Room Temperature," J. Appl. Phys., Vol. 49, no. 3 March 1978.

2. Davey, G.: "The Oxford University Miniature Cryogenic Refrigerator," International Conference on Advanced Infrared Detectors and Systems, Institute of Electrical Engineers, London, October 1982.

3. Walker, G.: "Stirling Engines," Clarendon Press, Oxford, 1980.

TABLE I. - SPACECRAFT-BORNE CRYOGENIC REFRIGERATORS
TECHNOLOGY PROJECTIONS

ITEM \ YEAR	1980	1985	1990	1995	2000
SERVICE LIFE/RELIABILITY (MTBF* - HR)	1 YR/85% ($5X10^4$)		5 YRS/90% ($4X10^5$)		10 YRS/95% ($2X10^6$)
COOLING CAPACITY @ TEMP.	0.2W @ 10K	2W @ 10K 5W @ 65K	0.1W @ 4K	20W @ 20K	5 W @ 4K
SPECIFIC POWER @ TEMP. - POWER IN PER WATT COOLING	10KW/W @ 10K	2.5 KW/W @ 10K 30 W/W @ 65K	10 KW/W @ 4K	250 W/W @ 20K	2.5 KW/W @ 4K

* MTBF - Mean Time Between Failure

TABLE II. - SPACECRAFT–BORNE CRYOGENIC REFRIGERATORS
POTENTIALLY USEFUL MATERIALS

ITEM	USE
SINGLE CRYSTAL METALS	HIGH FATIGUE LIMIT PARTS
CERAMICS	CLOSE TOLERANCE,, SMALL CLEARANCE PARTS
GLASSY METALS	HIGH MAGNETIC PERMEABILITY MATERIAL
RARE EARTH ELEMENTS/COMPOUNDS	REGENERATOR MATRIX MATERIAL HIGH ENERGY PRODUCT HIGH COHESIVE STRENGTH MAGNETICS - FOR MOTOR/MAGNETIC BEARINGS
ADVANCED COMPOSITES	HIGH STRENGTH FATIGUE RESISTANT HOUSINGS; OTHER MEMBERS
PIEZO ELECTRIC/MAGNETOSTRICTIVE MATERIALS	LINEAR MOTORS/FLEXURES (BENDERS) SQUEEZE FILM GAS BEARING GENERATORS
DIAMOND MATRIX COMPOSITES	HARD-ON-HARD SLIDING CONTACT BEARINGS

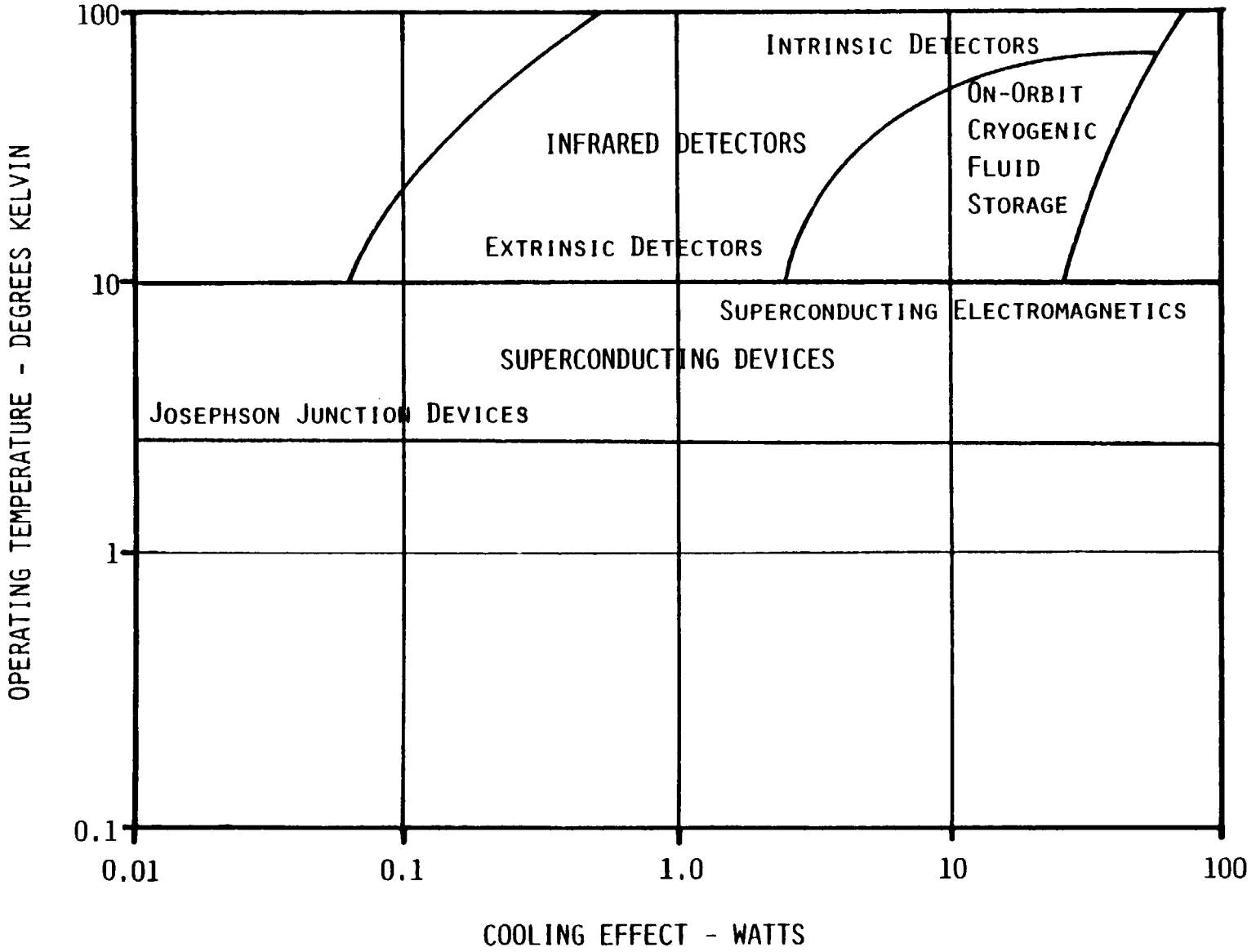

Figure 1. Cryogenic Cooling Considerations for Long Duration Spacecraft Applications--Needs

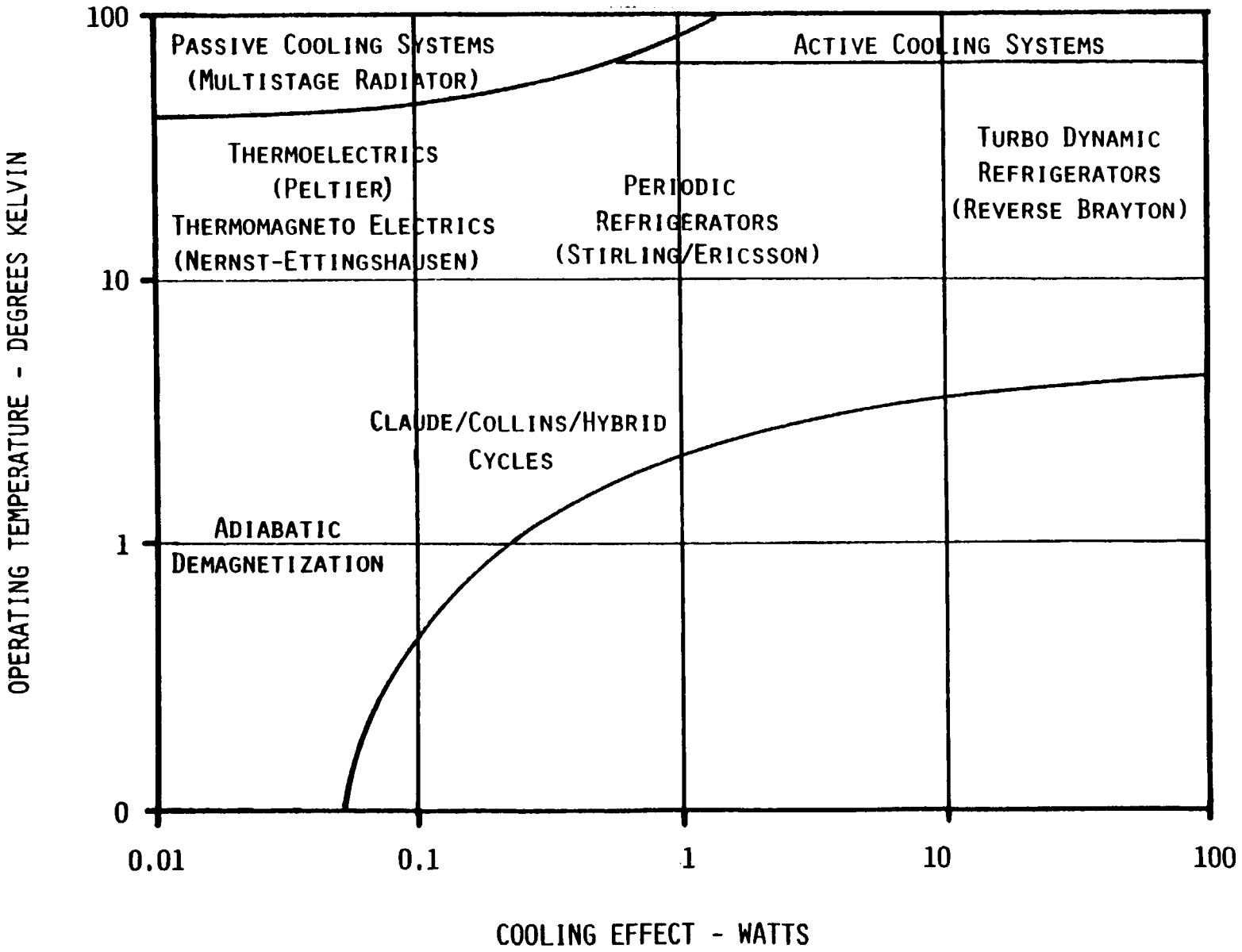

Figure 2. Cryogenic Cooling Considerations for Long Duration Spacecraft Applications--Methods

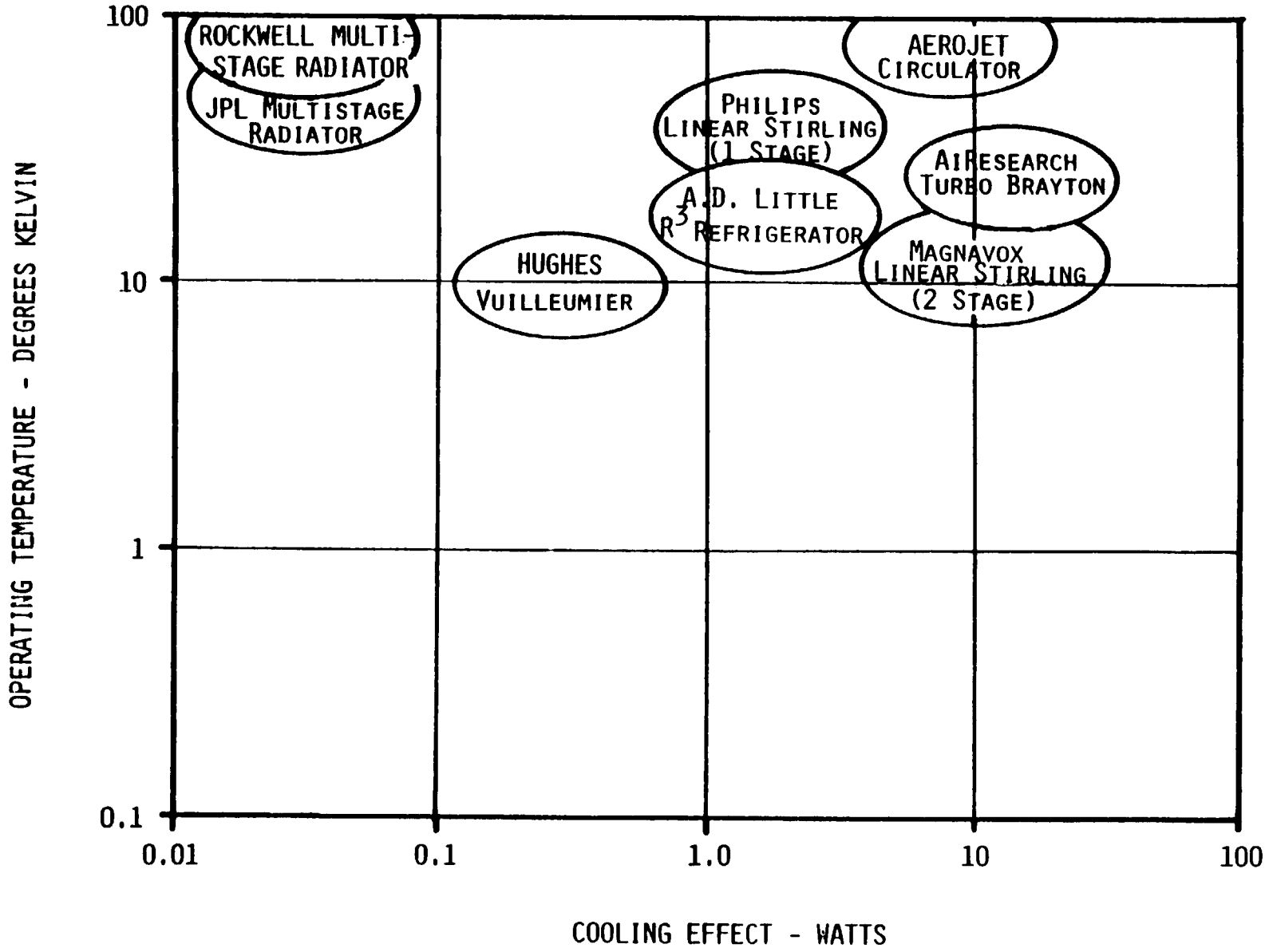

Figure 3. Cryogenic Cooling Considerations for Long Duration Spacecraft Applications--Developments

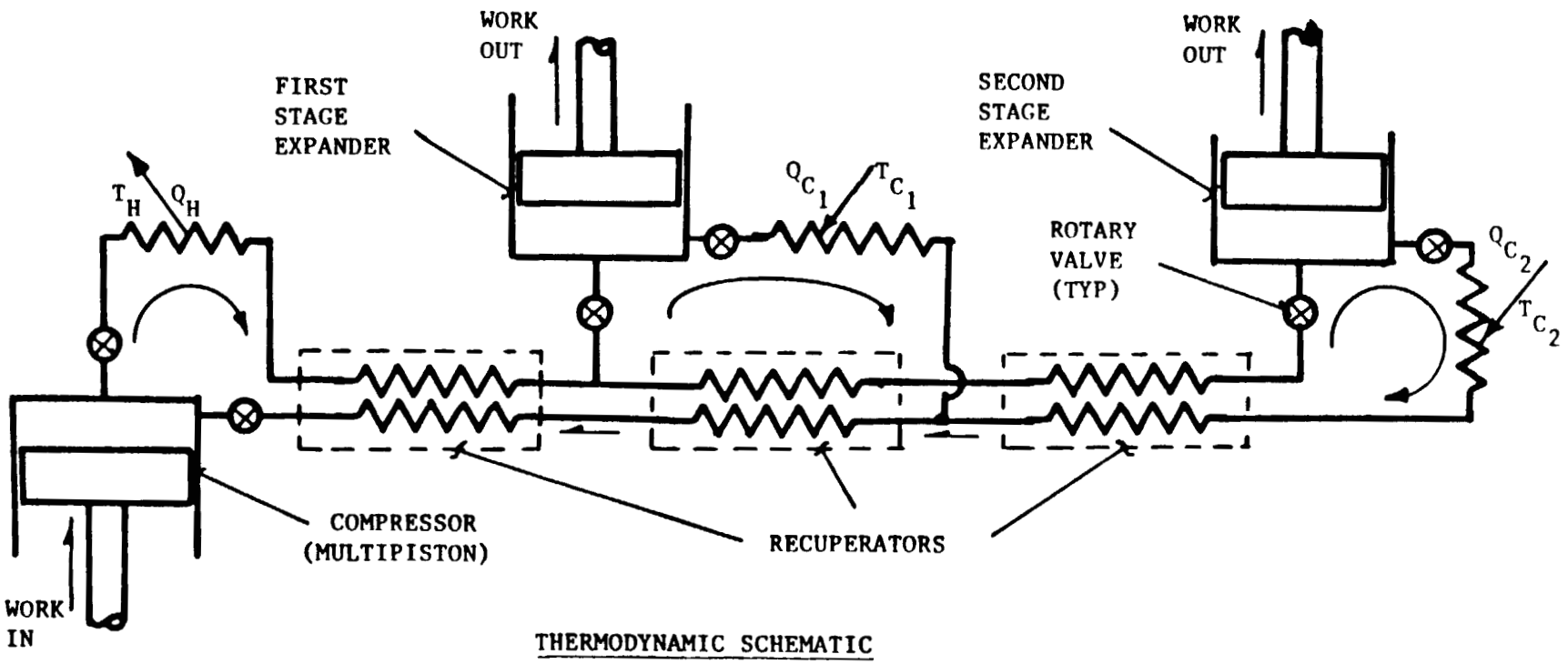

Figure 4a. Arthur D. Little Two-Stage Rotary Reciprocating Refrigerator

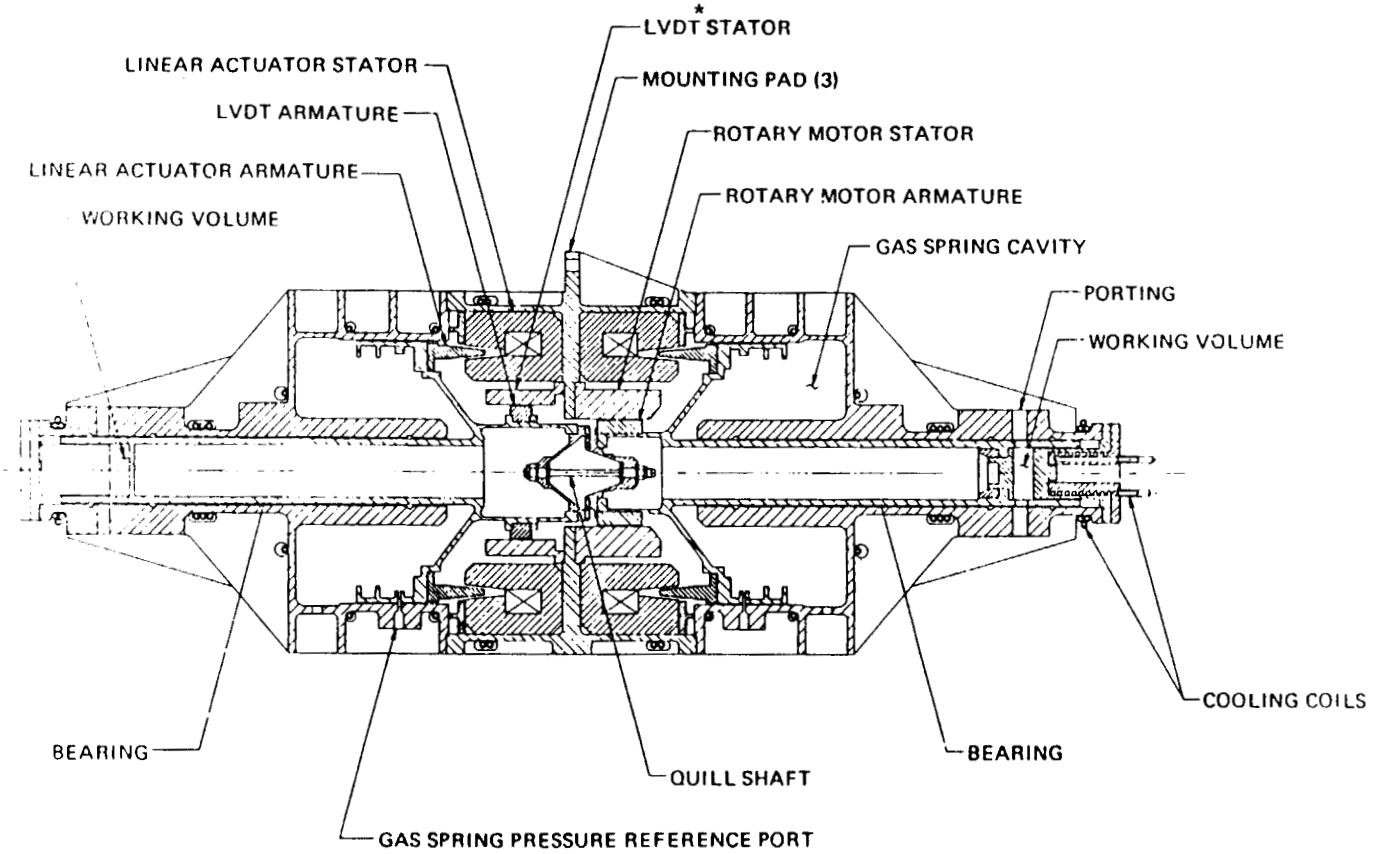

Figure 4b. Arthur D. Little Rotary Reciprocating Refrigerator Compressor details.

Ref.: Breckenridge, R.W., "Refrigerators for Cooling Spaceborne Sensors," Proceedings of the Society of Photo-Optical Instrumentation Engines, 29-30 July 1980, San Diego, CA.

*Linear Variable Displacement Transducer

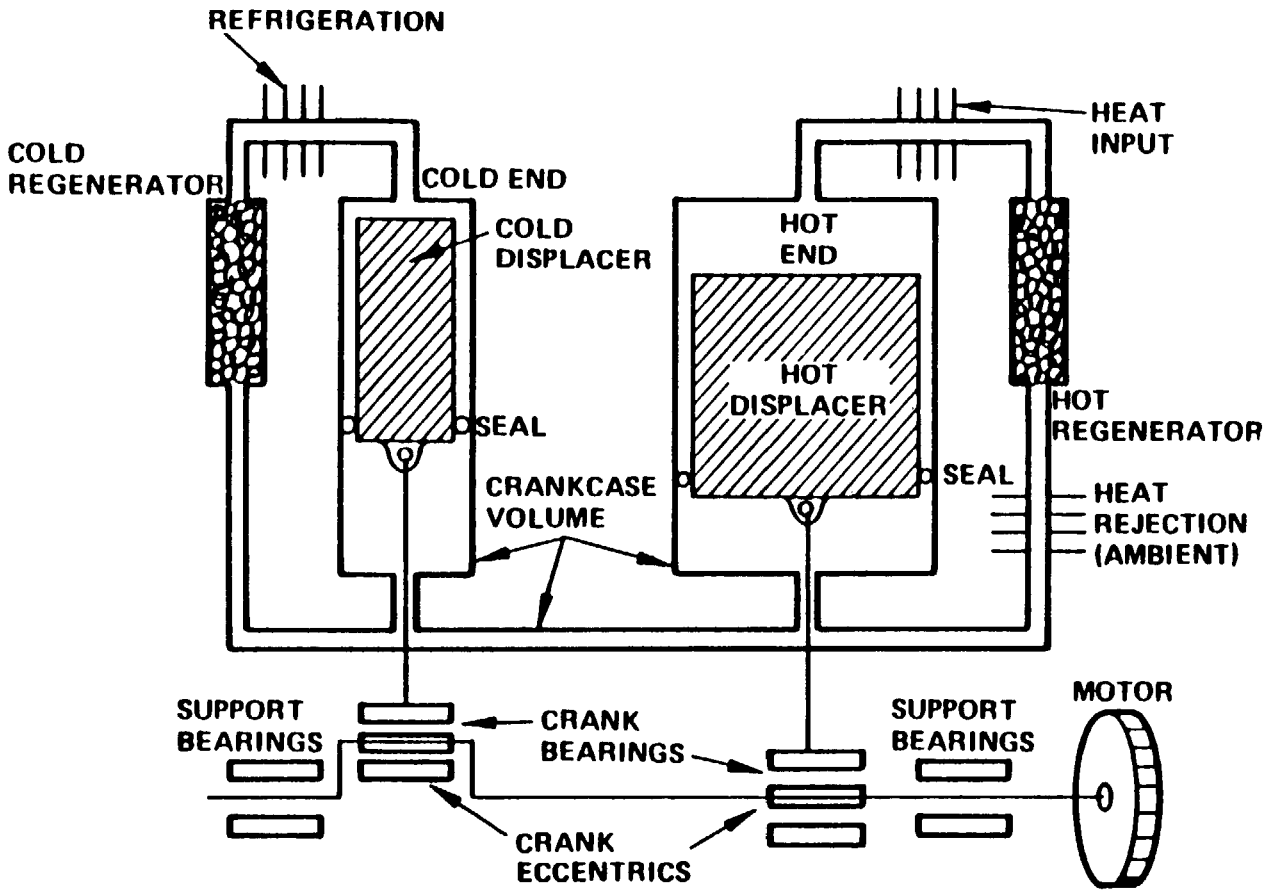

- CONSTANT VOLUME MACHINE
- MOTOR MAKES UP FRICTION IN MACHINE
- 90^{o} PHASING ELIMINATES NEEDS FOR VALVES

Figure 5a. Hughes Vuilleumier Cycle Refrigerator fundamnetal schematic.

Ref.: Doody, R.D., "The High Capacity Spaceborne Vuilleumier Refrigerator," Proceedings of the Society of Photo-Optical Instrumentation Engines, 29-30 July 1980, San Diego, Ca.

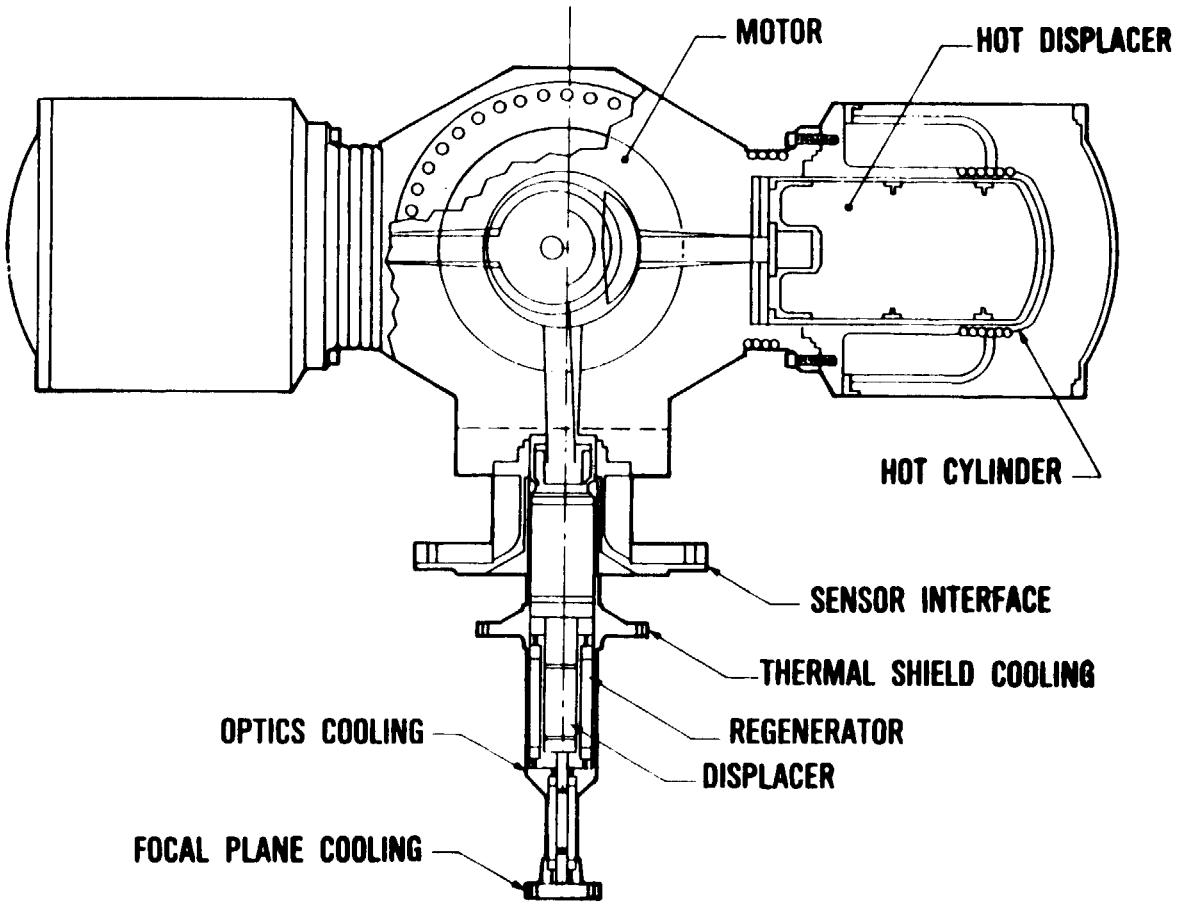

Figure 5b. Hughes Vuilleumier Cycle Refrigerator general layout.

Ref.: Doody, R.D., "The High Capacity Spaceborne Vuilleumier Refrigerator," Proceedings of the Society of Photo-Optical Instrumentation Engines, 29-30 July 1980, San Diego, CA.

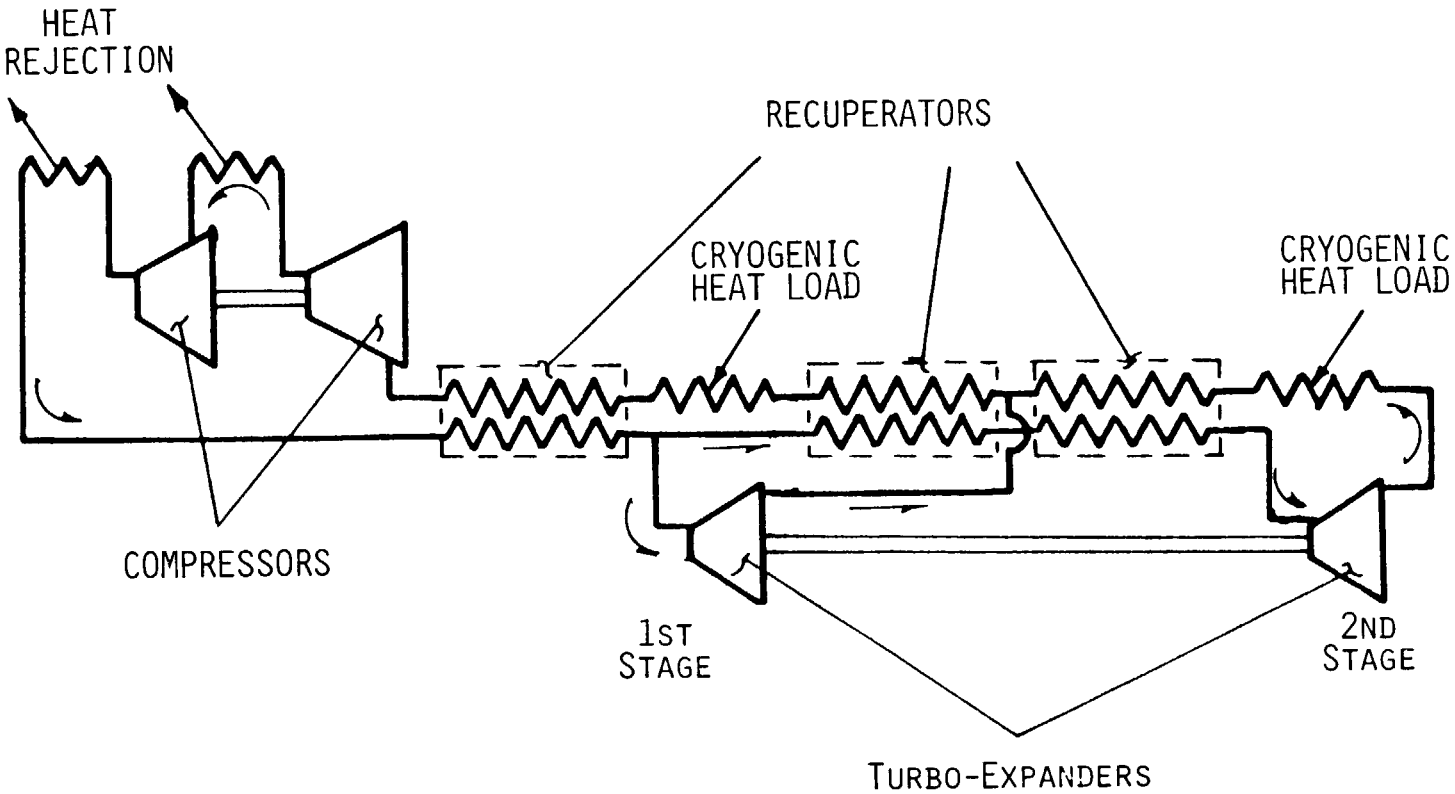

Figure 6a. AiResearch Turbo Brayton Refrigerator schematic.

Ref.: Wapato, P.G. and Norman, R.H., "Long Duration Cryogenic Cooling with Reversed Brayton Turbo-Refrigeration," Proceedings of the Society of Photo-Optical Instrumentation Engines, 29-30 July 1980, San Diego, CA.

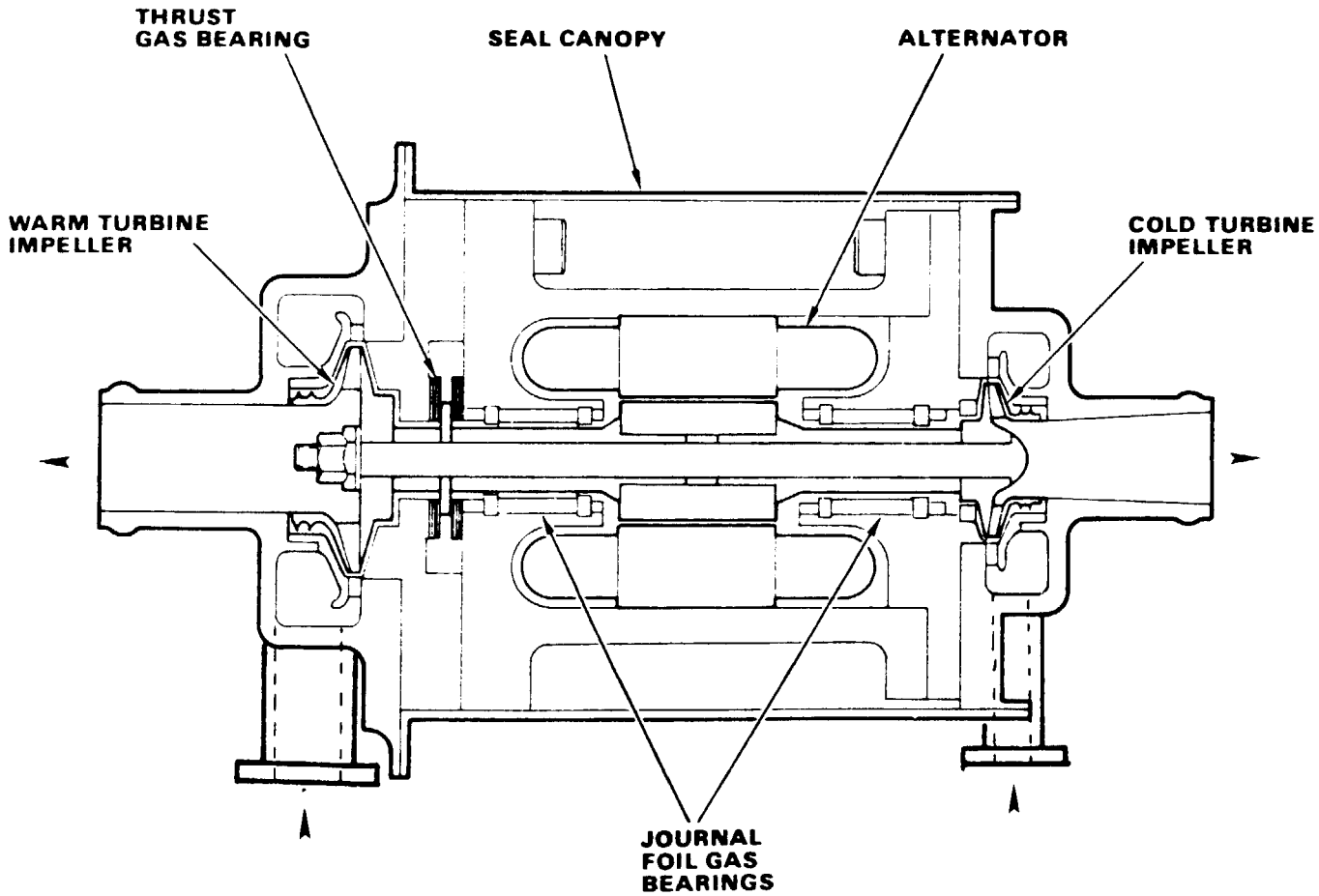

Figure 6b. AiResearch Turbo Brayton Refrigerator, Single Shaft, Integrated Turboalternator.

Ref.: Wapato, P.G. and Norman, R.H., "Long Duration Cryogenic Cooling with Reversed Brayton Turbo-Refrigeration," Proceedings of the Society of Photo-Optical Instrumentation Engines, 29-30 July 1980, San Diego, CA.

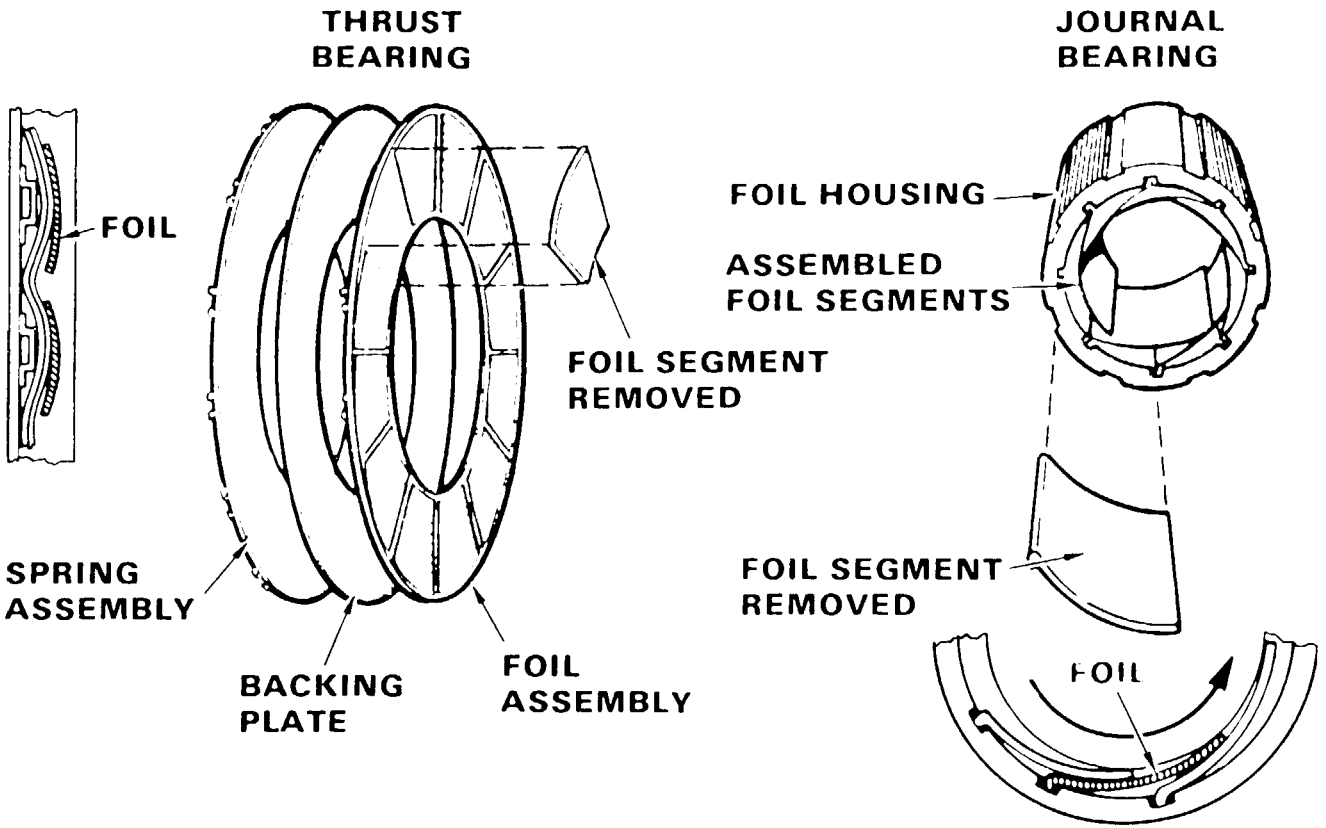

Figure 6c. AiResearch Turbo Brayton Refrigerator, Foil Gas Bearing Concept.

Ref.: Wapato, P.G. and Norman, R.H., "Long Duration Cryogenic Cooling with Reversed Brayton Turbo-Refrigeration," Proceedings of the Society of Photo-Optical Instrumentation Engines, 29-30 July 1980, San Diego, CA.

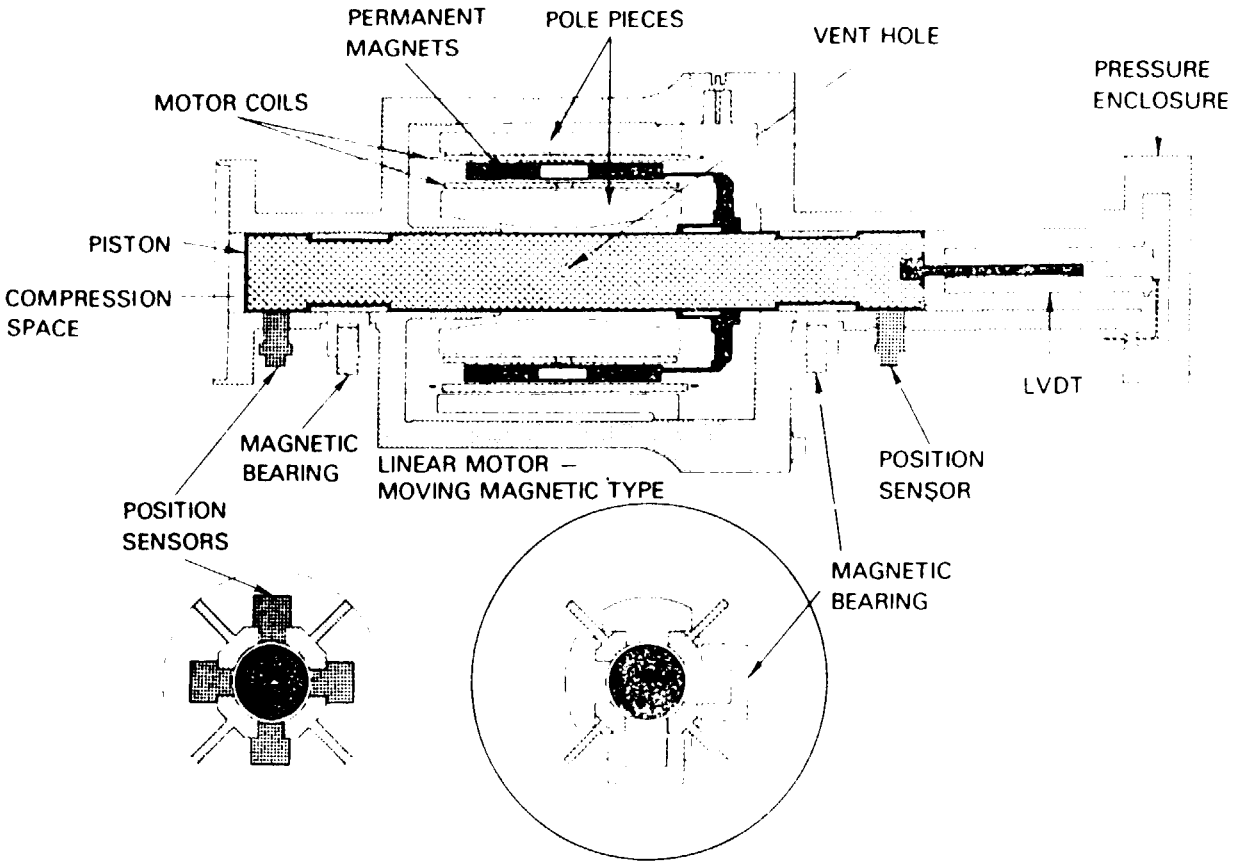

Figure 7a. Philips Laboratories Linear Stirling Cycle Compression Section.

Ref.: Gassen, M.G., Sherman, A., and Beale, W., "Developments Towards Achievement of a 3-5 Year Lifetime Stirling Cycle Refrigerator for Space Applications," Refrigeration for Cryogenic Sensors and Electronic Systems, U.S. Separtment of Commerce, NBS Special Publication 607, May 1981.

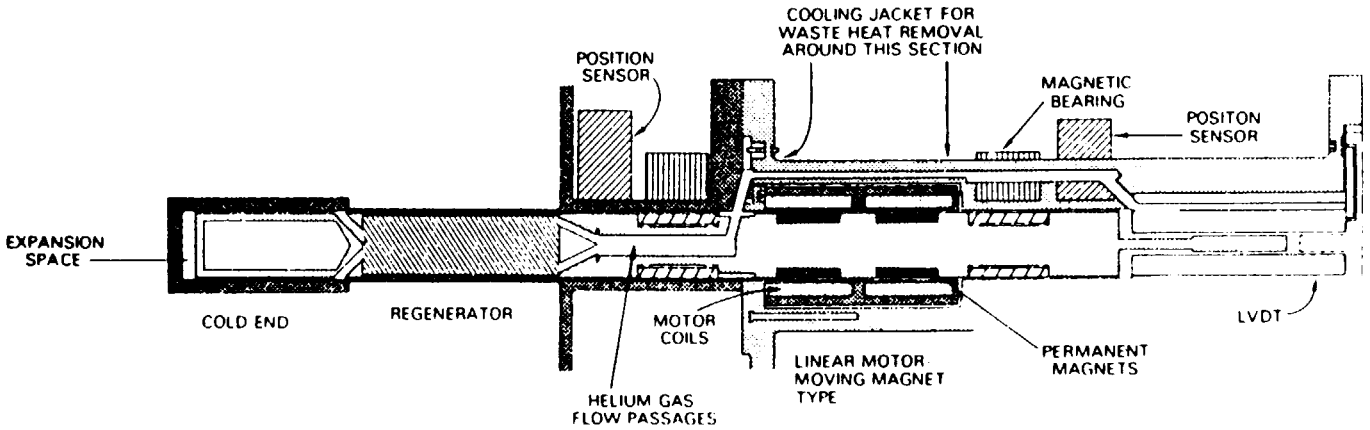

Figure 7b. Philips Laboratories Linear Stirling Cycle Expansion Section.

Ref.: Gassen, M.G., Sherman, A., and Beale, W., "Developments Towards Achievement of a 3-5 Year Lifetime Stirling Cycle Refrigerator for Space Applications," Refrigeration for Cryogenic Sensors and Electronic Systems, U.S. Department of Commerce, NBS Special Publication 607, May 1981.

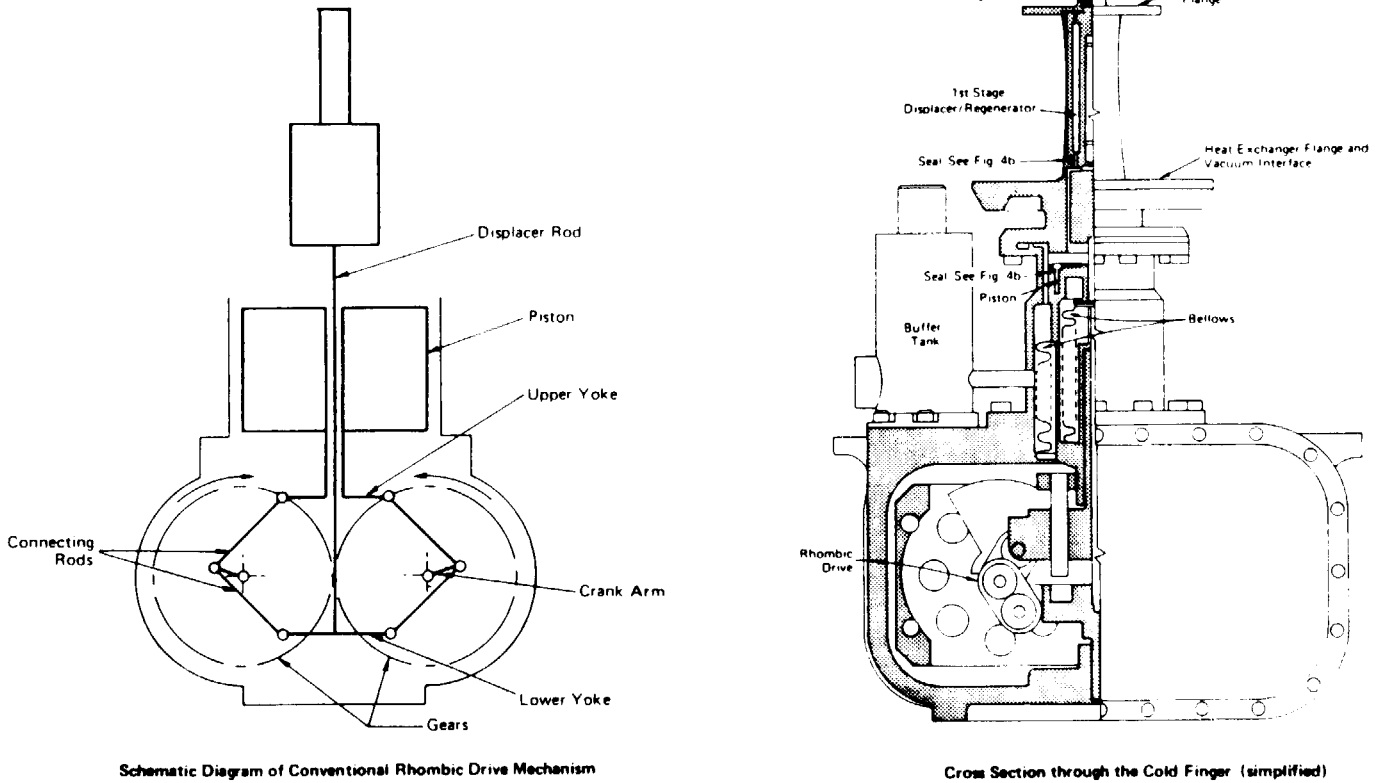

Figure 8. Philips Two-Stage Rhombic Drive Spacecraft Stirling Refrigerator, STP-78-1.

Ref.: Leffel, C.S. and Vonbriesen, R., "The APL Satellite Refrigerator Program--Final Report," Johns Hopkins University, Applied Physics Laboratory, March 1981.

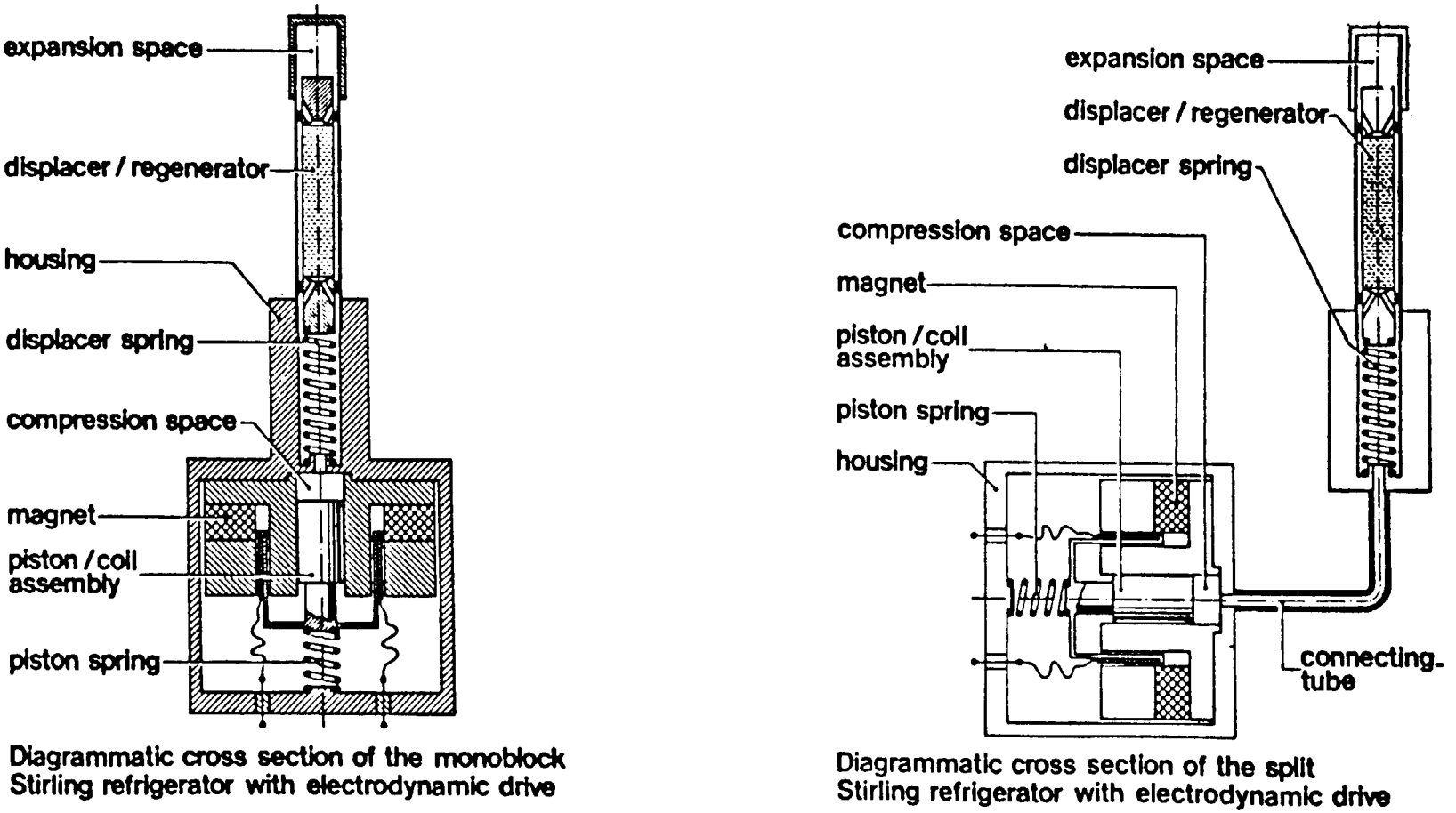

Figure 9. Philips-Einhoven Miniature Stirling Cycle Cryogenic Refrigerators.

Ref.: deJonge, A.K., "A Small Free-Piston Stirling Refrigerator," Proceedings of the 14th Intersociety Energy Conversion Engineering Conference, Boston, 5-10 August 1979.

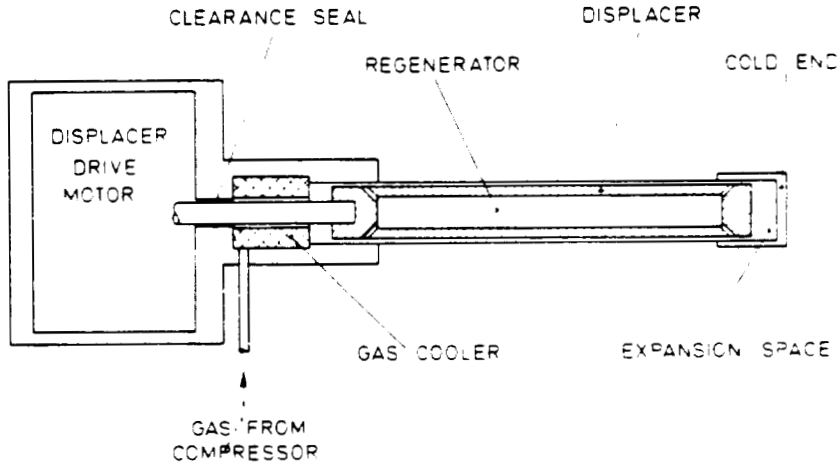

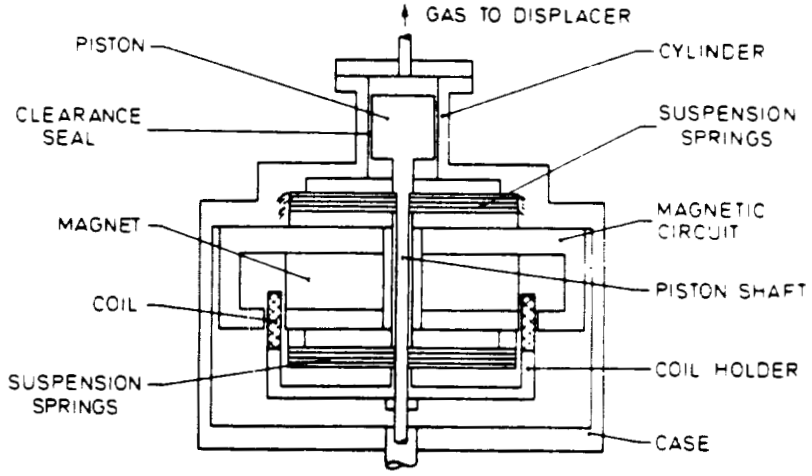

Figure 10. Oxford University Miniature Cryogenic Refrigerator.

Ref.: Davey, G., "the Oxford University Miniature Stirling Refrigerator," International Conference on Advanced Infrared Detectors and Systems, IEE, London, 29-30 October, 1981.

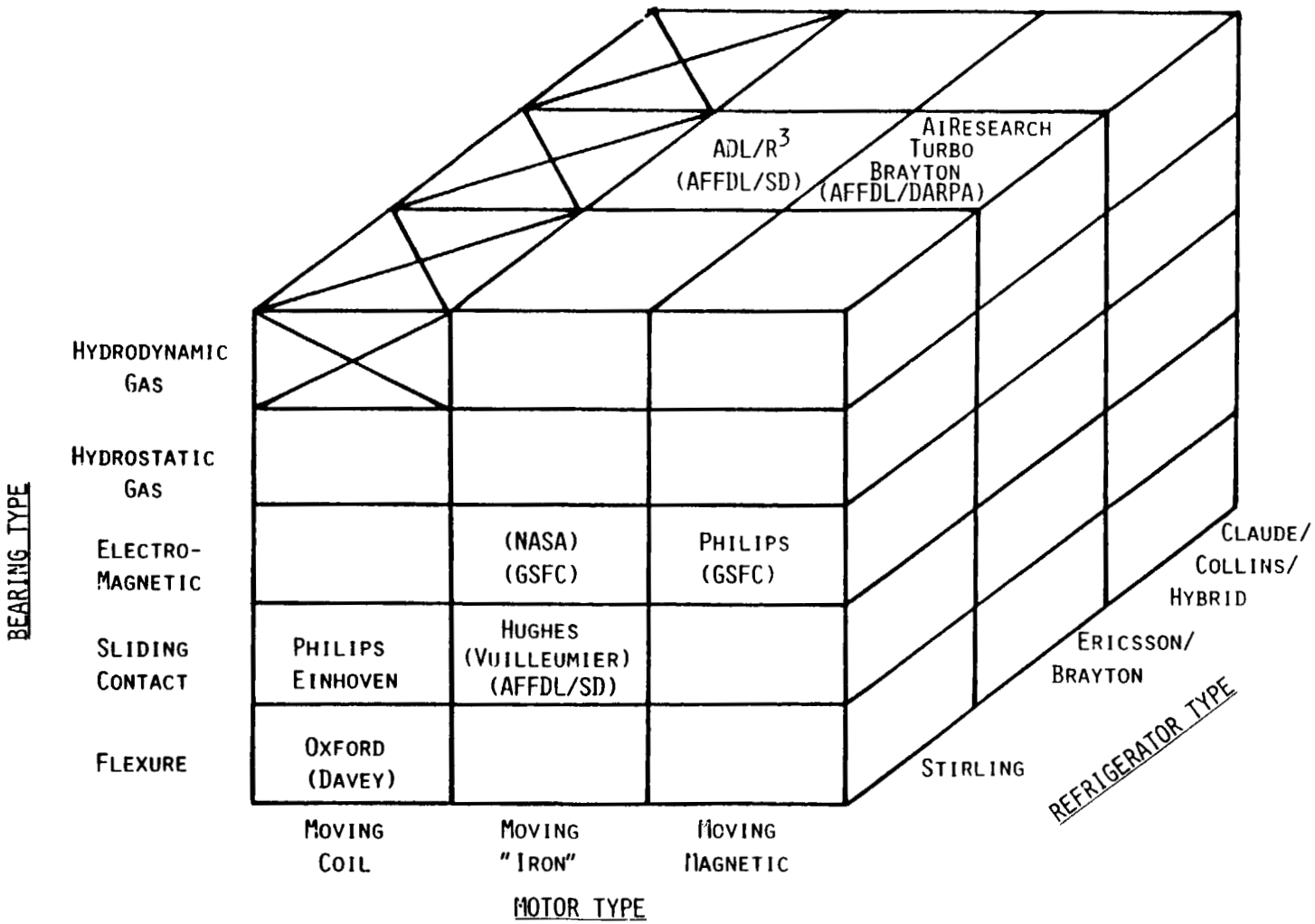

Figure 11. Long Life Spacecraft-Borne Cryogenic Rfrigerator Morphological Array

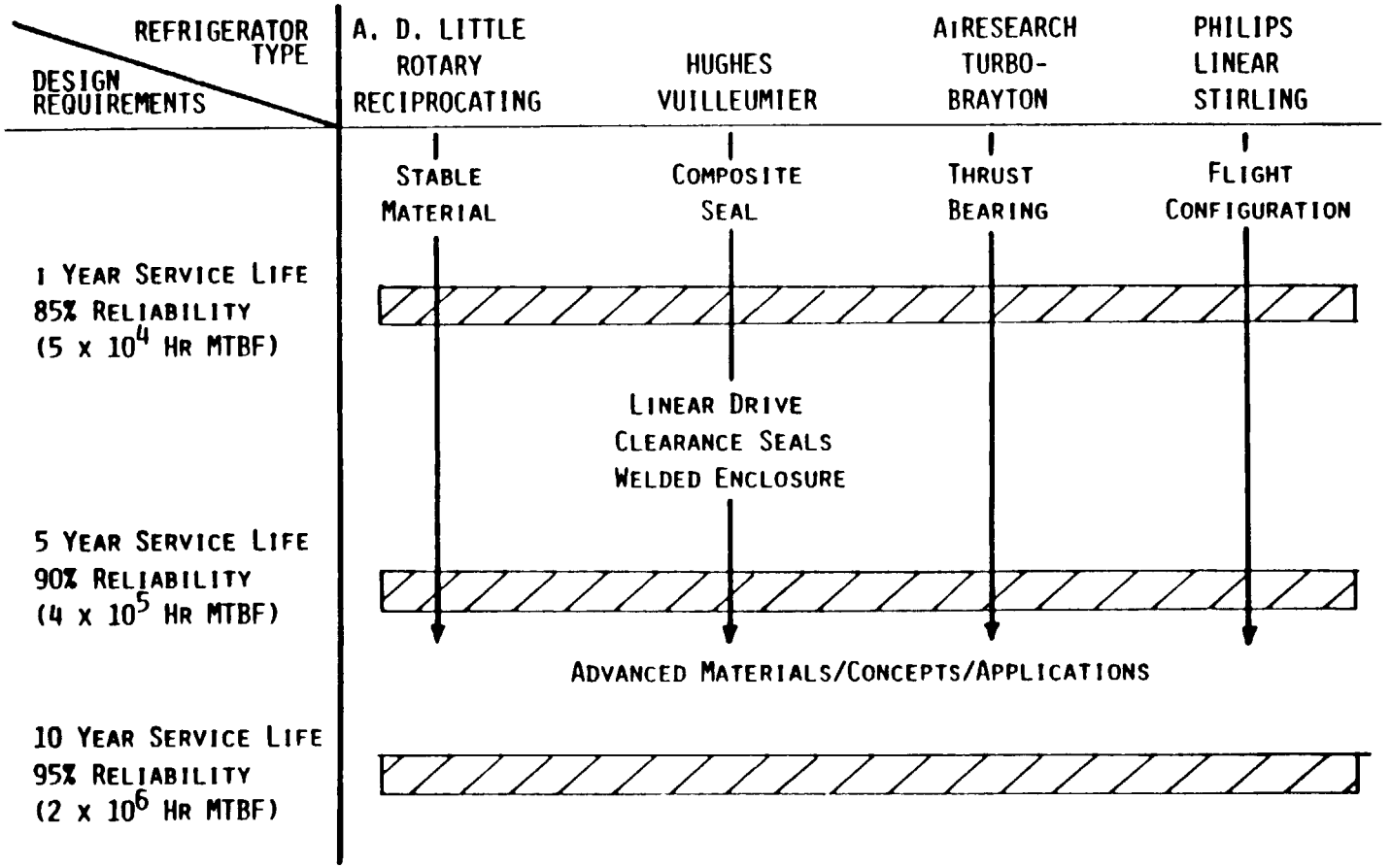

Figure 12. Spacecraft-Borne Cryogenic Refrigerators, Service Life/Reliability Development Issues

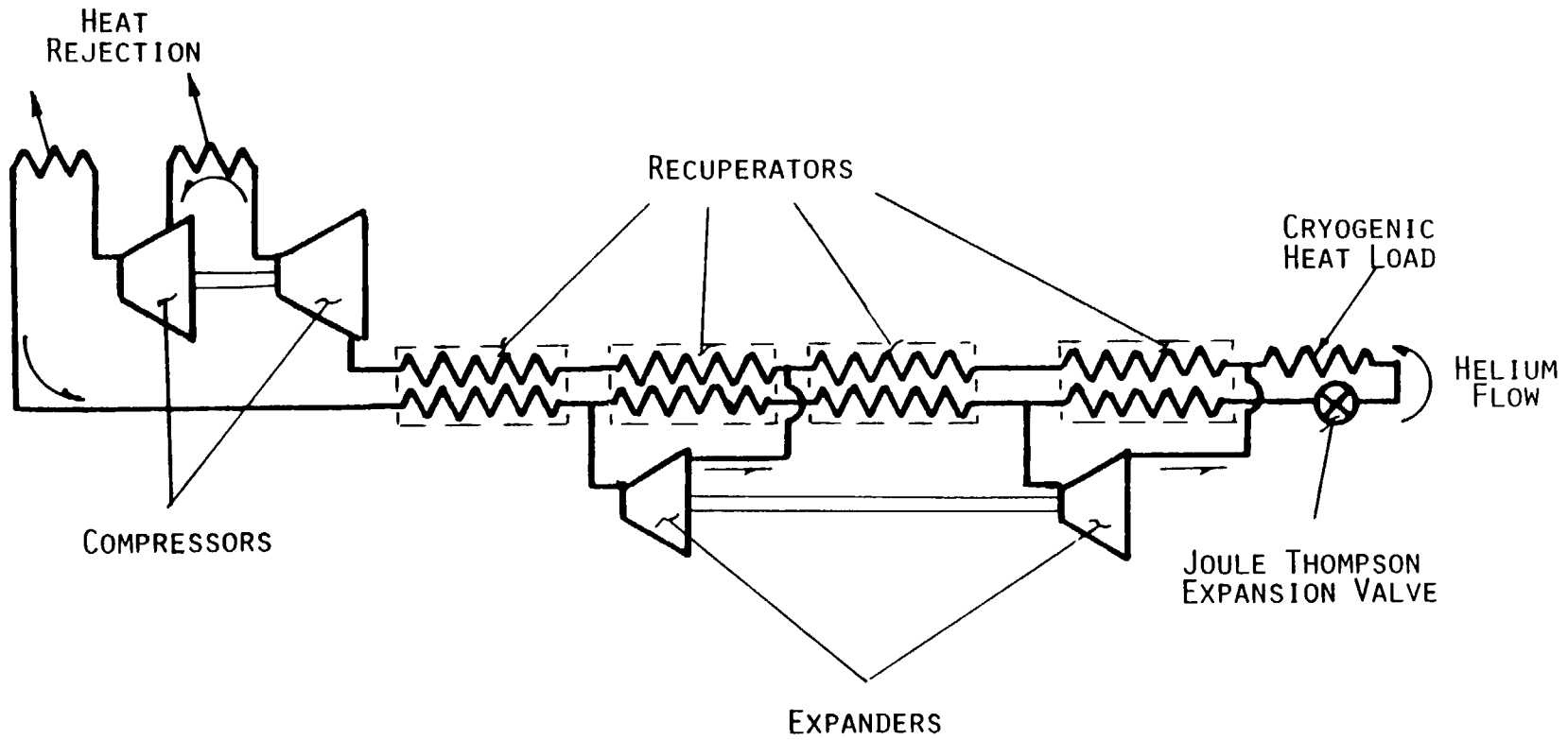

Figure 13. Collins Cycle Cryogenic Refrigerator

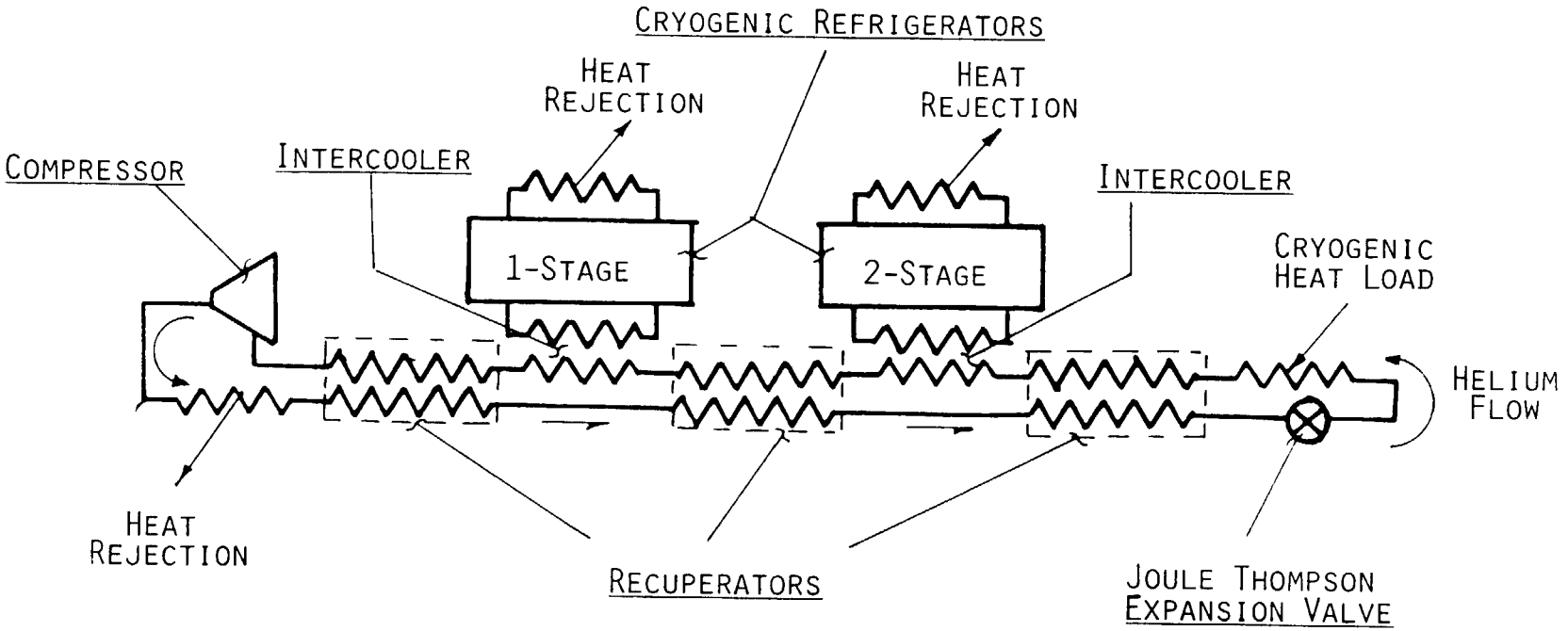

Figure 14. Hybrid Cryogenic Refrigerator Schematic

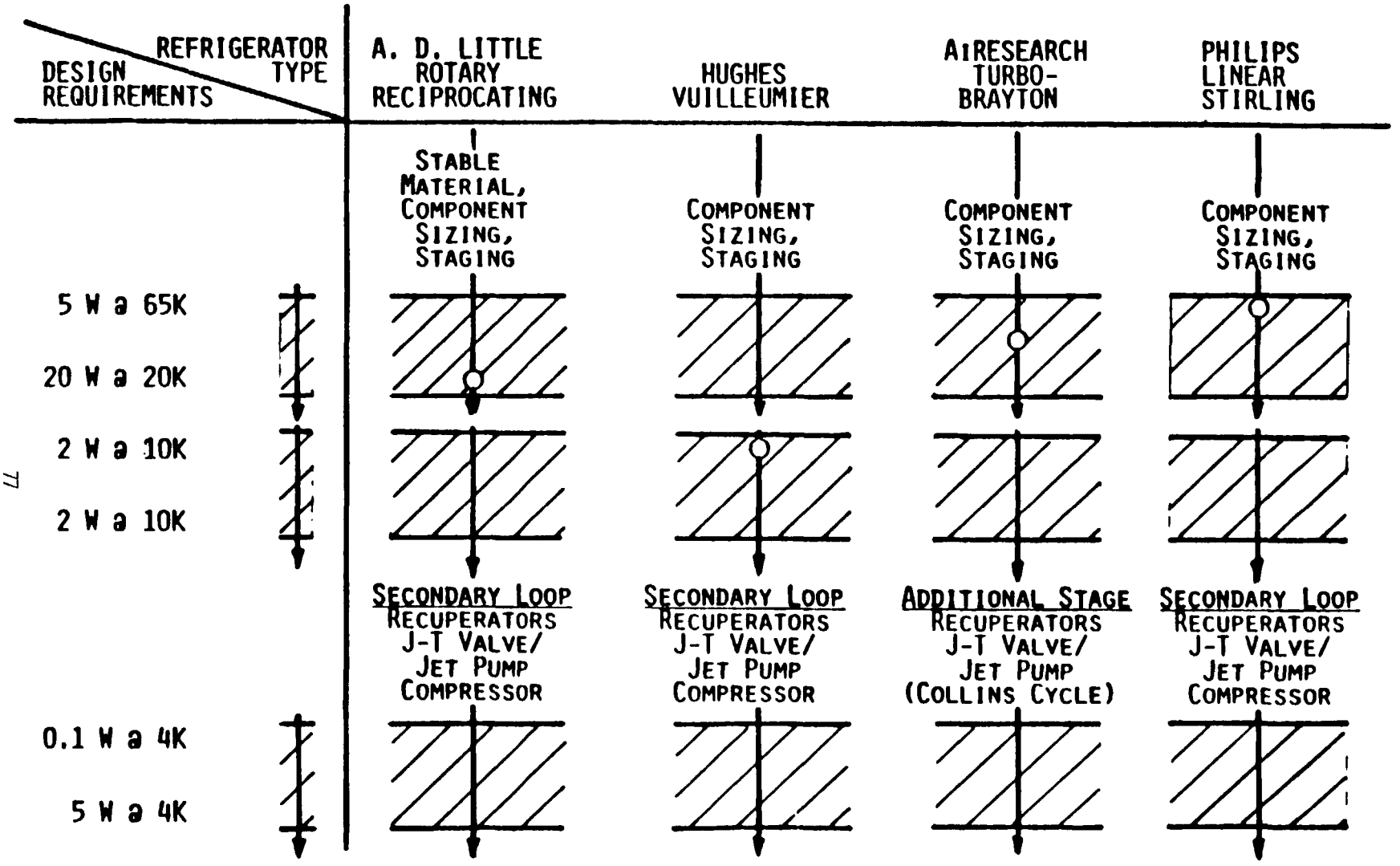

Figure 15. Spacecraft-Borne Cryogenic Refrigerators, Cooling Capacity at Temperature Development Issues

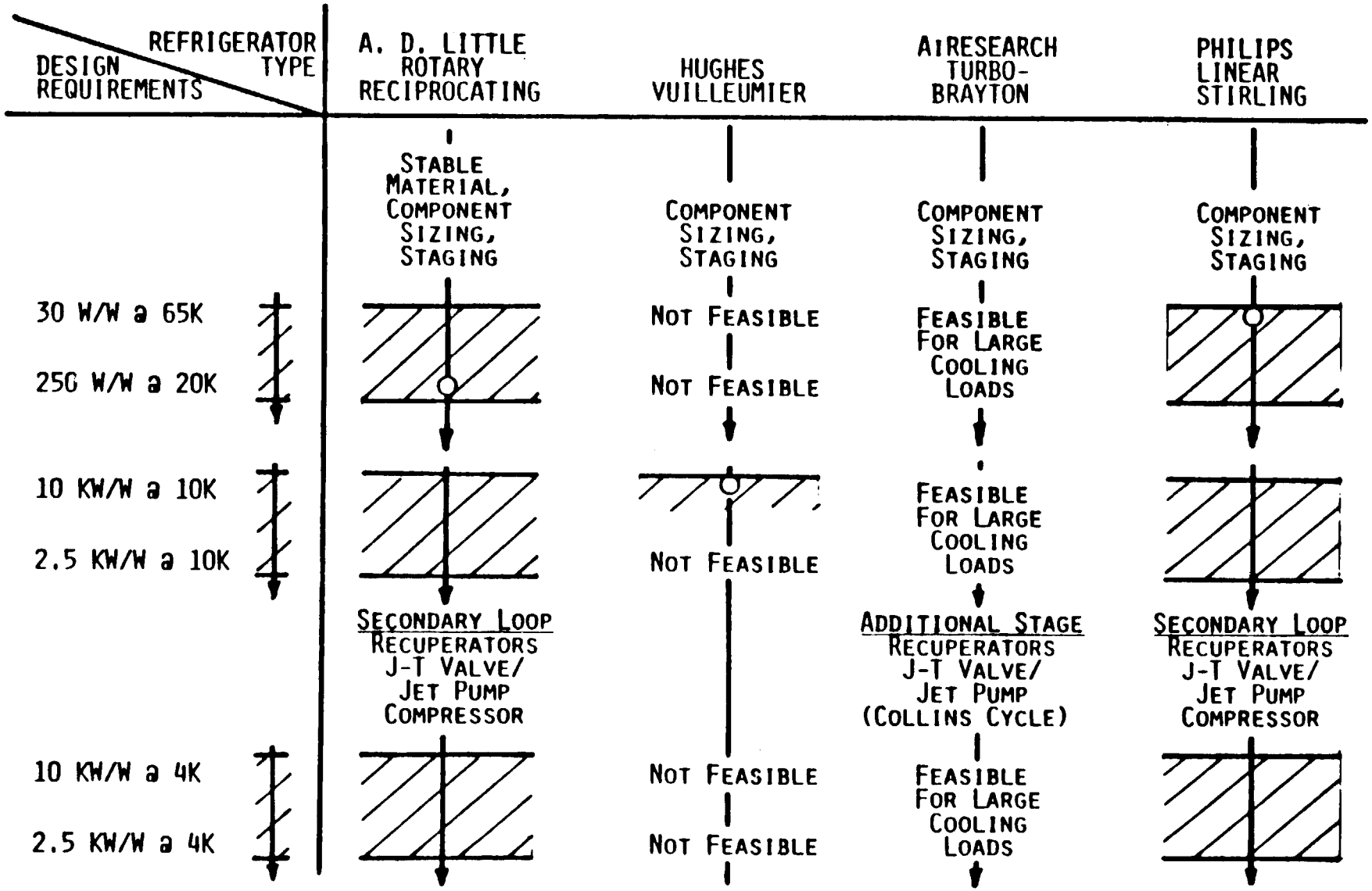

Figure 16. Spacecraft-Borne Cryogenic Refrigerators, Specific Power at Temperature Development Issues

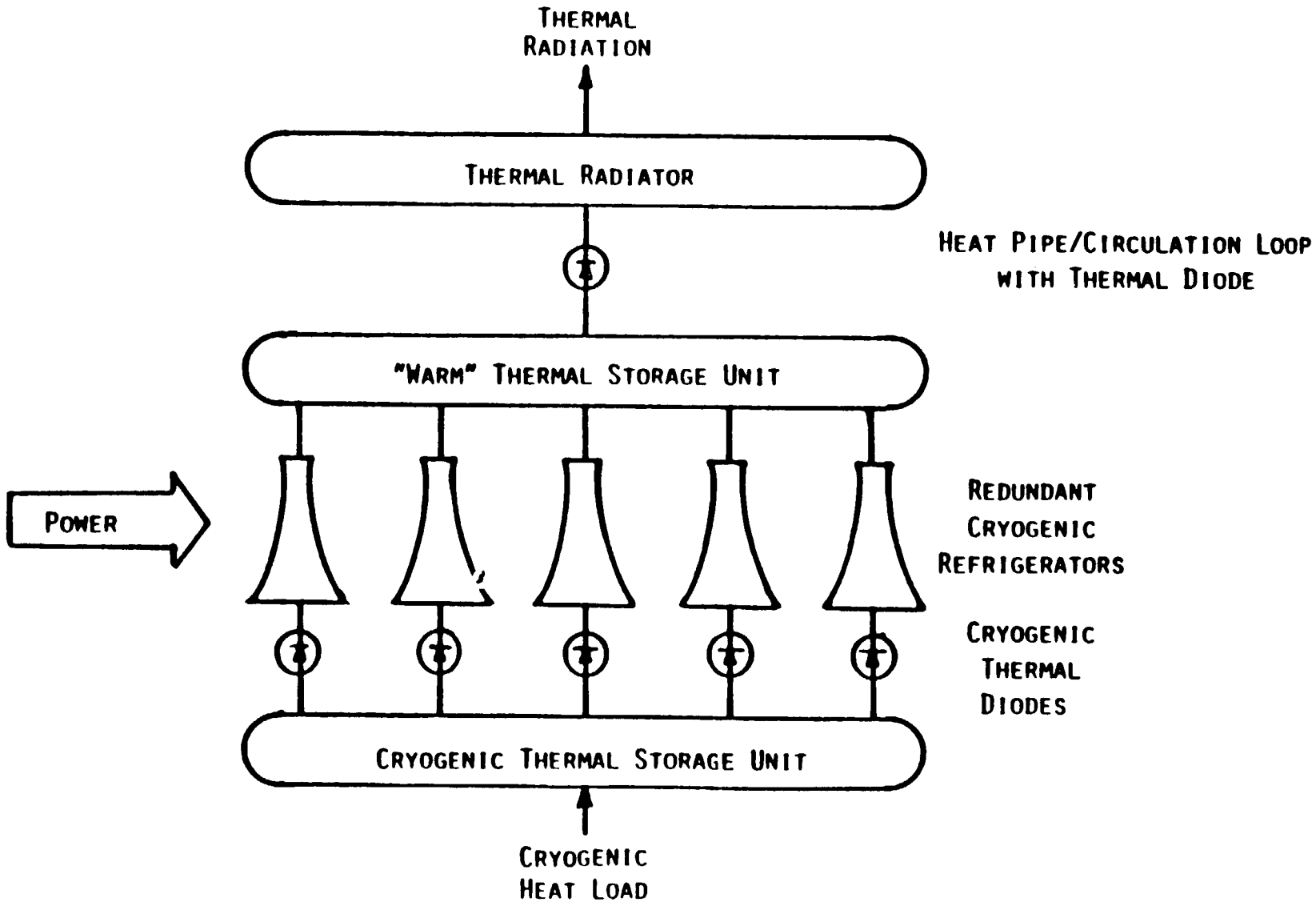

Figure 17. Redundancy-Based Spacecraft-Borne Long Life Cryogenic Refrigeration

REGENERATION EXPERIMENTS BELOW 10K IN A REGENERATIVE-CYCLE CRYOCOOLER*

Ronald E. Sager**

AND

Douglas N. Paulson

S.H.E. Corporation, 4174 Sorrento Valley Blvd., San Diego CA 92121

ABSTRACT

At temperatures below 10K, regenerative cycle cryocoolers are limited by regeneration losses in the helium working fluid which result from the decreasing heat capacity of the regenerating material and the increasing density of helium. Our experiments are examining several approaches to improving the low-temperature regeneration in a four-stage regenerative cycle cooler constructed primarily of fiberglass materials. Using an interchangeable fourth stage, the experiments have included configurations with multiple regeneration passages, and a static helium volume for increased heat capacity. Experiments using helium-3 as the working fluid and a Malone stage are planned. Results indicate that, using these techniques, it should be possible to construct a regenerative cycle cooler which will operate below 6K.

*Work supported by Department of Energy, Division of Advanced Energy Projects.

**Present address: Quantum Design, 11404 Sorrento Valley Road, San Diego, CA.

INTRODUCTION

The low temperature performance of regenerative cycle coolers is determined by fundamental physical properties of the solid regenerating material and the helium working fluid. Specifically, the decreasing heat capacity of solid regenerators precludes proper regeneration of the working fluid below about 10 K. In our experimental cooler, the thermal conductivity of the cylinder walls and displacer is of added importance since we use no regeneration matrix, but depend only on regeneration at the walls of a single regeneration gap. Our experiments, which are an extension of the work pioneered by Zimmerman and others [1-4] on plastic cryocoolers, are aimed at improving the regeneration properties of the coldest stage of a four-stage cooler, with the ultimate goal of obtaining temperatures below 5K.

THEORETICAL MODEL FOR REGENERATION LOSS

For estimating the effects of different fourth stage configurations on the low temperature performance of the cooler, we have developed a mathematical model for the regeneration loss in a cooler using single gap regeneration. The model assumes laminar flow along the gap, and that the fluid in direct contact with the walls is at the same temperature as the wall at that point. There will then be a temperature difference between the walls and the fluid in the middle of the gap due to the finite thermal conductivity of the fluid and its velocity along the gap.

Solving the heat flow equation for the temperature gradient in the fluid and the resulting thermal oscillation in the walls, we can compute the net enthalpy flow along the gap by averaging over one cycle of the cooler. For sinusoidal gas flow, the regeneration loss for a single stage of the cooler operating between temperature T_1 and T_2 will be given by:

$$\dot{Q}_R = \left(\frac{17}{280}\right)\left(\frac{d}{\pi DL}\right)(M\dot{n}_o)^2\left[\int_{T_1}^{T_2}\left(\frac{C_p^2}{K_f}\right)dT + \left(\frac{1.16\sqrt{\tau}}{d}\right)\int_{T_1}^{T_2}\frac{C_p^2}{\sqrt{K_w C_w}}\,dT\right] \quad (1)$$

Here d is width of regenerator gap, D is the displacer diameter, L is the length of the stage, M is the atomic weight of the working fluid (in grams/mole), $\dot{n}_o$ is the molar flow rate along the gap, τ is the period of the cooler cycle, C_w and K_w are respectively the heat capacity and thermal conductivity of the walls, and C_p and K_f are respectively the heat capacity at constant pressure (per gram) and thermal conductivity of the helium working fluid. The integrals account for the variation of C_w, K_w, C_p, and K_f over the temperature gradient, $\nabla_z T$ which is constant along the stage.

Since our experimental cooler uses a Gifford-McMahon cycle rather than a true sinusoidal Stirling cycle, the sinusoidal assumption is probably the most significant approximation in the calculation. However, the approximation should affect only the multiplicative constant in equation (1), not its functional form, and when applied to a nonsinusoidal gas flow, the essential

error is an uncertainty in the value of the molar flow rate. To account for this problem in making comparisons with our experiments, we have used the molar flow rate as an adjustable parameter. We expect that this will not be necessary in future experiments with a true Stirling cooler since the molar flow rate should be more well defined.

The two terms in equation (1) arise from two different aspects of the regeneration process. The first term, which depends only on the heat capacity and thermal conductivity of the working fluid, arises from the temperature difference between the middle and the edges of the gap. Physically this term represents the regeneration loss incurred by imperfect regeneration of the fluid in the middle of the gap. The second term, which depends on the heat capacity and thermal conductivity of the walls, represents the ability of the walls to accept heat from the working fluid as it flows toward the cold end of the machine. At temperatures below about 10K the thermal conductivity and heat capacity of the walls become very small, so the walls can absorb less and less heat from the gas. The problem is made substantially worse at these temperatures by the rapidly increasing density (and increasing heat capacity per unit volume) of the helium.

It is interesting to evaluate the regeneration loss for a single stage constructed of nylon having a single regeneration gap and with its warm end operating at about 30K. The results are shown in Figure 1. The calculation assumed a gap width of .0025 cm, displacer diameter of .47 cm, length of 15 cm for the stage, and a maximum molar flow rate of .0043 moles/sec. This molar flow rate should be roughly characteristic of a cooler operating at one Hertz with a 0.7 cm stroke between pressures of 0.2 and 0.8 MPa.

Since the regeneration loss completely dominates other internal losses below about 15K, we expect the operating temperature of the cooler to be the point at which the internal regeneration loss just balances the total cooling power. The solid line in Figure 1 shows the estimated regeneration loss; the broken line gives the estimated cooling power assuming isothermal expansion. The peak in the cooling power at 5.2K, which reflects the behavior of the isobaric expansion coefficient for helium near its critical point, will probably be less dramatic in practice since the expansion will not be truly isothermal.

From this simple model, we would predict an operating temperature of about 10K for this stage. For comparison with experiment, the assumed operating parameters are those reported by Zimmerman for his four-stage machine which operated at about 8.5K. The discrepancy may arise from our assumption that the full pressure fluctuation is developed in the final stage of the cooler, which would assume a higher molar flow rate than actually exists in the cooler. In any event, the qualitative nature of the regeneration loss should accurately reflect the difficulty in achieving temperatures below about 8K. This seems to be consistent with Zimmerman's later results in which his five stage cooler reached about 7K, only a 1.5K improvement after adding an entire stage to his four stage machine.[3]

The dashed line in Figure 1 shows the contribution to the regeneration loss from the first term in equation (1). Physically this curve represents the regeneration loss to be expected if there were infinite heat capacity in the walls of the cylinder and displacer. While the contribution from this term is not insignificant, especially below about 6K, the comparison clearly demonstrates the requirement for first solving the heat capacity problem. The experiments we describe below specifically address the question of trying to improve the regeneration capacity of the cylinder and displacer walls at temperatures below 15K.

Although our primary interest is the thermodynamic behavior of the coldest stage, we have modeled the performance of the machine in terms of conduction, viscous, and shuttle heat losses, as well as radiation loading on the cooler. Our models for shuttle and conduction losses [2,5] have been verified in separate measurements [6]. Calculations for viscous and radiation losses are sufficiently straightforward that we do not expect any major errors in these estimates.

THE EXPERIMENTAL APPARATUS

To perform the experiments we have constructed a four stage cylinder and displacer, similar to Zimmerman's, having dimensions as given in Table I. The displacer is driven by a variable speed stepping motor through a scotch yoke, and a standard compressor of the type used for commercial cryocoolers provides the high and low pressure sources for the expansion/compression cycle. Electrically actuated pneumatic valves which control expansion and compression in the cooler are triggered from the displacer drive such that the phase of the displacer stroke and the duration of both expansion and compression can be adjusted.

While the eventual goal of our work is a more self-contained compact device, we felt that the Gifford-McMahon configuration provided added flexibility for the basic experiments with which to investigate in detail the effects of different parameters on the operation of the cooler. Another convenient aspect of the apparatus is the detachable fourth stage which allows quick modifications to the most interesting part of the cooler. This design, which uses an indium O-ring to make the seal, has functioned well, and we have had no particular problem repeatedly achieving a vacuum tight seal, at least for our pressures of up to about 1.0 MPa.

In the experiments, we are pursuing essentially three different ideas for improving the low temperature regeneration in the cooler. First, the heat capacity per unit volume of helium increases at low temperature rather than decreasing. This suggests the possibility of trying to use static helium fluid residing in the cylider walls of the last stage to provide the requisite heat capacity[7]. A possible configuration is shown in Figure 2a.

Thermal contact with the static helium must be provided by constructing a cylinder which has an extremely anisotropic thermal conductivity -- very high

in the radial direction to allow heat transfer between the working fluid and the static helium, but very low parallel to the cylinder axis to prevent thermal conduction down the cooler. Ideally one might use a thin-walled laminated tube consisting of alternating rings of copper and stainless steel bonded together, but in practice the fabrication of such a structure which is helium leak tight has proven to be extremely difficult. Nonetheless, we have achieved a partial success, and have collected some data from a cooler using this type of assembly.

Our second technique is to use helium-3 as the working fluid in the cooler. Obviously for a Gifford-McMahon cycle, or any large cooler, this becomes prohibitively expensive. However, a small Stirling cooler could be charged with helium-3 for a few hundred dollars. If the cooler were constructed completely without dynamic seals, it should be able to operate for years before the helium charge would require replenishment.

The advantage of using helium-3 is that both its critical pressure and critical temperature are substantially lower than those of helium-4. At temperatures and pressures near their critical points, the density and other thermodynamic properties of the two isotopes will scale approximately as the ratio of their critical temperatures and pressures. Since the increasing density of the fluid contributes to the regeneration problem, we expect an improvement when using helium-3 since its density and heat capacity per unit volume will be somewhat less than those of helium-4 at the same temperature. Furthermore, since our type of cooler is designed to operate at low pressures, typically between 0.2 and 1 MPa, the lower critical pressure will be advantageous by allowing the cooler to operate completely above the critical pressure of the helium-3 and avoid the density and heat capacity problems encountered at the critical point of helium-4.

Finally, we are also investigating the use of a somewhat different type of refrigeration cycle for the final stage of the cooler. Allen, et al,[8] have observed that the counterflow heat exchange used in a Malone cycle[9] might help alleviate the problem of vanishing heat capacity in the regenerator. In the Malone cycle the helium is forced to flow through one channel as it moves toward the cold end of the machine, and through a second parellel channel as it returns to the warm end of the cooler. As shown in Figure 2b, heat exchange occurs across the wall separating the two channels, providing regeneration through a type of counterflow heat exchanger. In a cryocooler using a Malone stage, we are testing a tandem design in which the reciprocating flow of a staged Stirling cryocooler feeds the pulsating unidirectional flow of the Malone engine using a pressure seal and check valves. An essential quality of the Malone engine is the use of a pulsating, unidirectional fluid flow in which the regenerator behaves similarly to a counterflow heat exchanger so that, as constant pressure, the working fluid regenerates itself. Consequently, the thermal load on the Malone regenerator is greatly reduced over that in a Stirling machine. This is is particularly advantageous from the standpoint of the heat capacity problem.

There are two disadvantages to this approach, however. First, the reciprocating fluid flow in the upper three stages of the cooler must be converted to a pulsating unidirectional flow in the final stage. This will require check valves between the third and fourth stages to provide preferred paths for the incoming and outgoing fluid. Secondly, while the outgoing fluid stream can provide the heat capacity for regenerating the incoming fluid, the Malone regenerator requires a substantially larger regenerator dead volume, which introduces an additional heat capacity problem. Specifically, the larger dead volume means that a significant amount of helium remains in the fourth stage regenerator during the compression cycle. Hence, there must still be sufficient heat capacity available in the walls and displacer of the final stage to absorb the heat of compression of the fluid remaining in the regenerator. Because of this effect, a cooler using only a Malone-style regenerator in the fourth stage may not achieve a temperature significantly below one having only a loaded regenerator. However, we feel that there is considerable merit in the combination of a Malone stage operating inside a helium loaded regenerator.

EXPERIMENTAL RESULTS TO DATE

To provide a simple system for comparison with calculation, and to compare with Zimmerman's experiments, we first ran the cooler with no fourth stage at all. The operating temperatures of the three stages for this configuration are given in Table II. Since we imposed no external load on the machine (other than that produced by the radiation shields), each stage should operate at the temperature where the inherent thermal losses in the machine plus the radiation loading just equal the refrigeration produced by the stage.

To determine the refrigeration power which the cooler was producing, we measured the P-V function at the top of the cooler using an absolute pressure transducer with the volume axis simulated by a sinewave generator synchronized with the displacer. Over several measurements with different cooler configurations, we found that the P-V diagram thus generated gave a value for the total refrigeration very close to that predicted for a sinusoidal pressure fluctuation. Consequently, for later experiments we simply used that approximation.

For making comparisons between experiment and theory, we used the observed operating temperatures of the various cryocooler stages as data points, then computed the total thermal loading and cooling power expected at each stage of the cooler. Table II shows the comparison for the experiments with the three stage cooler. On the basis of our independent measurements of shuttle and conduction losses, we believe these estimates to be accurate to within a few percent. Futhermore, the estimates for the viscous losses are nearly negligible as are the radiation losses in stages two and three. Since the relative magnitudes of the other losses change dramatically over the length of the cooler, the overall agreement gave us reasonable confidence in our model.

In our first experiment with a four stage machine we used nested cylindrical sleeves as shown in Figure 2c for the final stage. The initial concept was that the additional regeneration passages would allow a greater volume of fiberglass in the cylinder walls to participate in the regeneration process. However, later investigation showed that the heat capacity of the fiberglass drops so quickly below 15K that even if the entire volume of the last stage participates in the regeneration, there is still far too little heat capacity to provide proper regeneration below about 10K.

Results from this configuration are given in Table III. The lowest operating temperature we achieved in this configuration was 7.6K, which compares favorably with the 8.5K obtained by Zimmerman in his four stage machine[1]. The improvement is probably due to a combination of the larger volume of fiberglass provided in the fourth stage and also perhaps to our use of a Gifford-McMahon cycle rather than the Stirling cycle. Although the actual operating parameters were somewhat different from those reported by Zimmerman, estimates for the regeneration loss and refrigeration power in our cooler are qualitatively the same as those in Figure 1. In particular, the regeneration effectiveness in our configuration also decreases precipitously below 10K, producing a virtual wall at about 8K.

As with the three stage experiments, the calculations for the estimated losses and the cooling power in the first three stages in the machine show reasonable agreement with the observed operating temperatures. While the estimates for the fourth stage are clearly incorrect the error is not surprising considering the complicated geometry of the cooler. The regeneration loss for the fourth stage was estimated by assuming that the fluid flow divided among the various regeneration passages in proportion to the flow impedances of each passage. The loss was then computed separately for each gap. This model is reasonable so long as the thermal penetration depth in the fiberglass is less than half of the radial distance between the gaps. In fact, for our geometry this approximation breaks down between 10 and 15K, so it is not surprising that the value in Table III underestimates the regeneration loss in the fourth stage.

In more recent experiments we have operated the cooler with the fourth stage constructed as in Figure 2a. Table IV gives the operating temperatures of the cooler with this fourth stage configuration using alternating rings of copper and stainless steel. As in the other experiments, the comparison between the observed operating temperatures and calculated losses in the machine is reasonable, with the exception of the third stage. We believe that the failure of this configuration to achieve a temperature of less than 7K resulted from a small leak between the static helium volume and working volume of the cooler. Our measurements of the leak rate suggested that the cyclical pressure fluctuations in the static volume would be a few percent of those in the working volume of the engine. Since even small pressure fluctuations in the relatively large static helium volume will involve a substantial heat of compression, we believe that such a leak could significantly degrade the cooler performance. Also viscous heating of liquid flowing through the leak will introduce an additional thermal load on the cold end of the machine. For the same reasons, the comparison with calculation is suspect.

An additional potential problem with our design is that the thermal conductivity of the static helium itself is rather poor in this temperature regime, so it becomes difficult to effectively access the inherent heat capacity of the static fluid. The spacing of the thermally conductive discs was based on the effective thermal penetration depth of the static fluid, so that ideally all of the static fluid could participate in the regeneration process. However, more effective thermal contact with the static fluid may be possible using a packed screen mesh or similar construction to provide the thermal contact between the static and working fluid [5].

Nonetheless, this four stage machine did achieve an ultimate temperature of 7.1K which is a significant improvement over the 7.6K performance of the machine with just a fiberglass regenerator. A quantitative feeling for the improvement can be obtained from noting in Figure 1 that a decrease in operating temperature from 7.6K to 7.1K represents a change from 370 mW to 530 mW in the regeneration loss in a fiberglass regenerator. We believe that the performance of a cooler with a helium-loaded final stage can be further improved with a completely sealed static volume, and we are currently developing more reliable techniques to fabricate this structure.

We are also presently preparing for experiments with a Malone-stage displacer and helium-3 as the working fluid. Experiments using both of these concepts should be completed within a few months. Nonetheless, the major problem is still to provide the proper regenerative heat capacity in the fourth stage, and we feel that the use of some type of static helum loading represents one of the best approaches to that problem.

COMMENTS AND CONCLUSIONS

We feel that our results to date provide encouragement for further work in trying to develop a small low-power cooler which can achieve a temperature of about 5K. We have, however, encountered several experimental problems which must also be addressed, and will probably require some clever engineering to completely solve. One of our most persistent problems has been the diffusion of helium through both the O-ring seals and the plastic materials of which the cooler is constructed. In our laboratory apparatus we have simply pumped on the vacuum container continuously to prevent thermal loading of the cooler via conduction through residual helium gas. Monitoring the vacuum can with a helium leak detector has provided quantitative information on the effectiveness of that approach. To guarantee the proper thermal isolation, the residual helium pressure will have to be kept below 10^{-5} Torr or so, which is a stringent long term requirement when using materials which allow helium diffusion. Zimmerman has begun to address the problem by incorporating metal-foil diffusion barriers in his more recent cooler,[10] but a complete solution will probably also require some innovative application of hermetic sealing techniques.

Our immediate problem has been that the possiblility of residual helium in the vacuum container has introduced a certain level of uncertainty in the

interpretation of our data. While comparisons with calculation do not show any major thermal loading, the balance between internal losses and cooling power in the coldest part of the machine could be substantially altered by even a very small residual heat leak.

In addition to this uncertainty, we have encountered some problem of reproducibility in our experiments from run to run, most notably in reproducing the results of our initial experiments with the fiberglass regenerator. Part of the problem probably arises from an orientational effect in the displacer. Specifically, since the upper three stages of our machine use a rigid displacer, the interstage alignment is critical. In recent experiments we have seen a significant effect on the coldest stage by rotating the displacer to different azimuthal orientations. This result was completely unexpected since the displacer has centering stubs which should keep it properly aligned and it has not been observed to bind inside the cylinder even when cold. Two possible explanations are that the centering stubs have worn or that certain orientations produce enough frictional heating to adversely affect the coldest stage. On examination, we did find some wear on the centering stubs, but not enough to account for the effect. In future coolers it will probably be advisable to allow for some type of self-aligning mechanism between adjacent stages.

To summarize, we feel that our results to date provide hope for the eventual realization of a small low-power cooler which can operate below 6K. Eventually we hope to push that limit to below 5K. Although many practical problems still remain to be solved, once a prototype device has been demonstrated, its potential applications should generate a substantial interest in solving those remaining problems.

Table I. Physical dimensions of four stage experimental cooler. All values in centimeters.

Stage	1	2	3	4
Displacer Dia.	3.40	2.02	1.21	0.52
Cylinder O.D.	3.96	2.49	1.52	1.52
Displacer length	16.0	15.5	15.6	16.0
Regenerator gap	.0152	.0102	.0102	.002

Table II. Estimated losses and refrigeration in three stage cooler. All values are given in milliwatts. Stroke = .75 cm, Speed = 2.1 sec, P_{hi} = .78 MPa, and P_{lo} = .14 MPa.

Stage	1	2	3
Operating Temp (K)	164	53	12
Regeneration	170	185	168
Shuttle	178	46	5
Conduction	476	110	9
Viscous	33	14	0
Radiation	222	7	0
Total Losses	1079	362	182
Total Refrigeration	1064	372	208
Discrepancy	1.4%	2.7%	12.5%

Table III. Estimated losses and refrigeration in four stage cooler with multiple sleeve regenerator. All values are given in milliwatts. Stroke = 1.5 cm, Speed = 1.5 sec, P_{hi} = .79 MPa, and P_{lo} = .15 MPa.

Stage	1	2	3	4
Operating Temp (K)	164	68	30	7.6
Regeneration	578	464	286	45
Shuttle	760	179	25	6
Conduction	503	87	10	4
Viscous	97	23	4	2
Radiation	220	7	0	0
Total Losses	2158	760	325	56
Total Refrigeration	2210	774	354	152

Table IV. Estimated losses and refrigeration in four stage cooler with helium loaded refrigerator. Stroke = 1.0 cm, Speed = 1.75 sec, L_4 = 16 cm, P_{hi} = .75 MPa, and P_{lo} = .15 MPa.

Stage	1	2	3	4
Operating Temp (K)	164	76	26	7.1
Regeneration	330	306	358	83
Shuttle	341	90	16	1
Conduction	473	61	13	3
Viscous	76	42	4	9
Radiation	220	7	0	0
Total Losses	1440	506	391	96
Total Refrigeration	1528	534	245	121

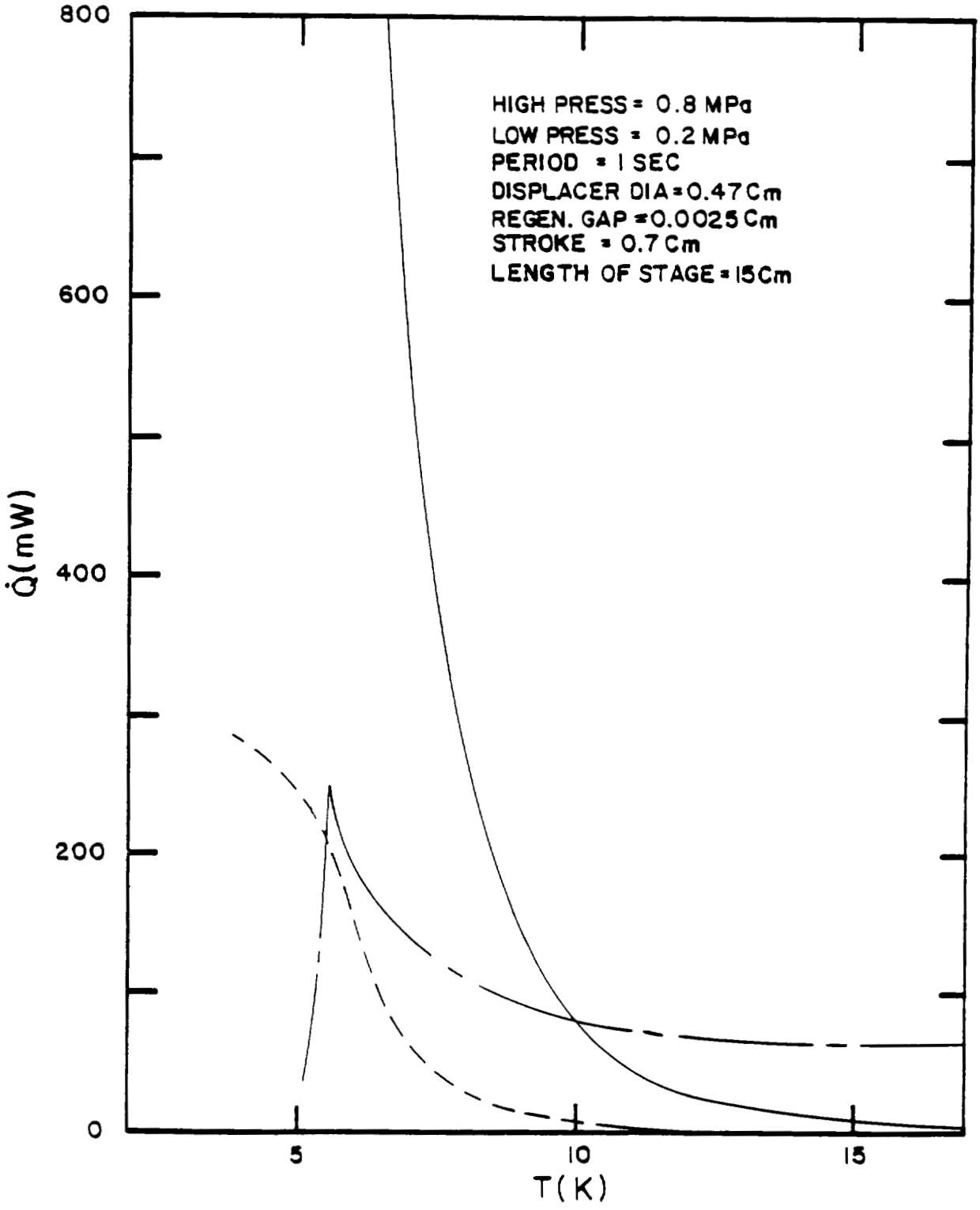

Figure 1. Estimates for regeneration loss and refrigeration for coldest stage of a Stirling-cycle cryocooler. The solid line shows the regeneration loss for operating parameters shown. The broken line (——————) shows the expected refrigeration produced by the stage, and the dashed line (- - -) gives the contribution to the regeneration loss from the finite thermal conductivity of the fluid in the regenerator gap.

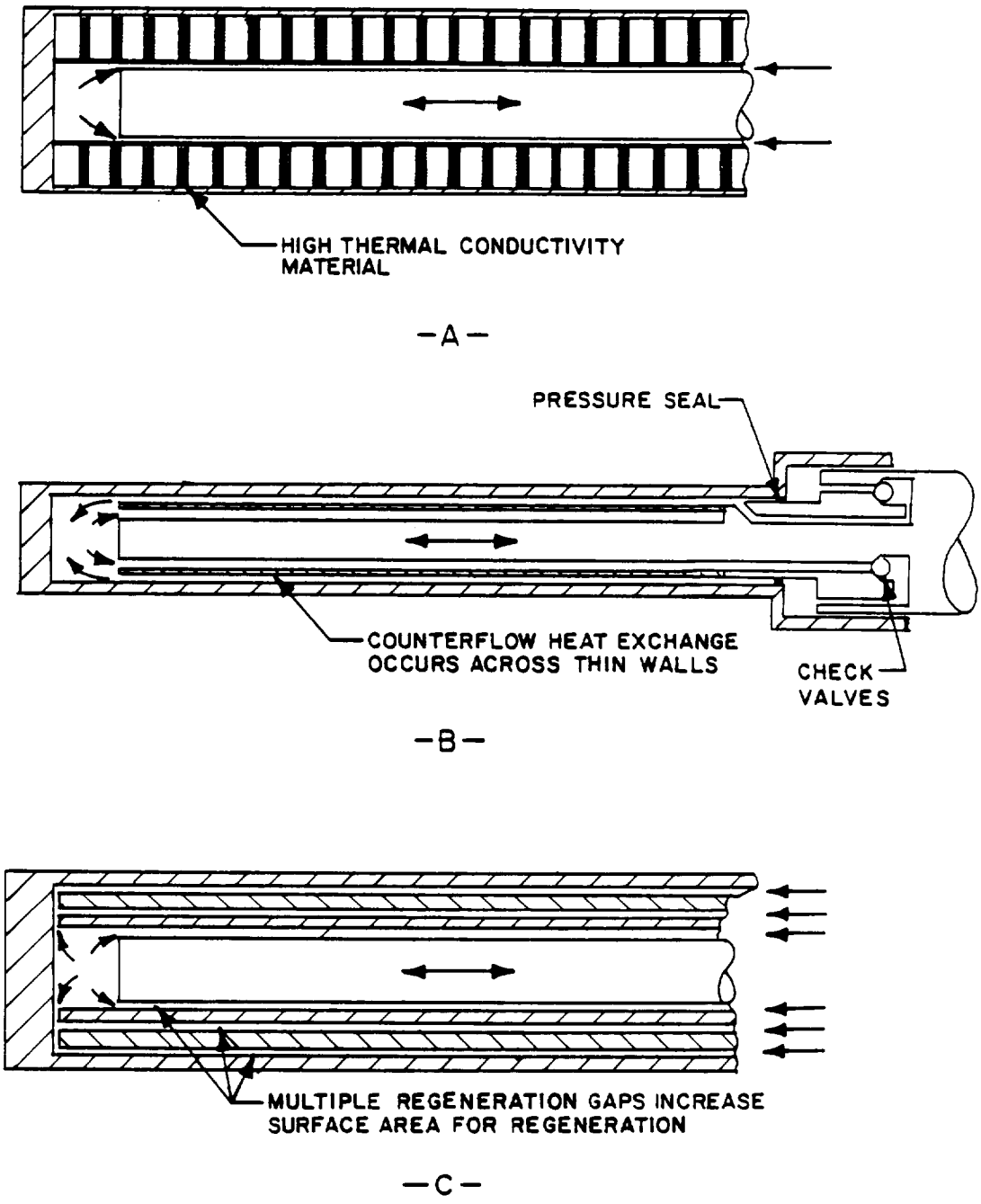

Figure 2. Part (a) shows scheme for loading the final stage of a Stirling cooler with static helium to provide additional heat capacity for regeneration. Part (b) shows counterflow heat exchange mechanism in a Malone cycle, and part (c) shows regeneration gap configuration in first experiments with a 4-stage Stirling cooler.

REFERENCES

1. J. E. Zimmerman and R. Radebaugh, "Operation of a SQUID in a Very Low-Power Cryocooler", NBS Special Publication 508, National Bureau of Standards, 59 (1978).

2. R. Radebaugh and J. E. Zimmerman, "Shuttle Heat Transfer in Plastic Displacers at Low Speeds"', NBS Special Publication 508, National Bureau of Standards, 68 (1978).

3. D. B. Sullivan, J. E. Zimmerman, and J. T. Ives, "Operation of a Practical SQUID Gradiometer in a Low-Power Stirling Cryocooler", NBS Special Publication 607, National Bureau of Standards, 186, (1980).

4. K. Myrtle, C. Winter, and S. Gygax, Cryogenics 22, 139 (1982).

5. J. C. Wheatley, unpublished.

6. R. E. Sager, unpublished.

7. R. B. Fleming, "Regenerators in Cryogenic Refrigerators", Tech Report AFFDL-TR-68-143 (Wright Patterson AFB, Ohio, 1968).

8. P. C. Allen, W. R. Knight, D. N. Paulson, and J. C. Wheatley, Proc Nat Acad Sci 77 #1, 39 (1980), and P.C. Allen, D.N. Paulson, and J.C. Wheatley, Proc Nat Acad Sci 78 #1, 31 (1980), and P.C. Allen, G.H. Fisher, W.R. Knight, D.N. Paulson, and J.C. Wheatley, J. of Appl. Phys. 52, 3876 (1981).

9. J. F. J. Malone, J. R. Soc. Arts (London) 79, 679 (1983).

10. J. E. Zimmerman, private communication.

A Cryocooler for Applications Requiring Low Magnetic and Mechanical Interference*

J. E. Zimmerman, D. E. Daney, and D. B. Sullivan
National Bureau of Standards
Electromagnetic Technology Division
Boulder, CO 80303

ABSTRACT

A very low-power, low-interference Stirling cryocooler is being developed based on principles and techniques described in several previous publications over the last four years. It differs in several important details from those built previously. It uses a tapered displacer based upon an analytical optimization procedure. The displacer is driven by an auxiliary piston and cylinder (rather than by mechanical linkage) using some of the working fluid itself to provide the driving force. This provides smooth, vibration-free motion, and, more importantly, allows complete mechanical and spatial separation of the cryostat from the pressure-wave generator. Either of two different pressure-wave generators can be used. One is a non-contaminating, unlubricated ceramic piston and cylinder. The other is a compressed-air-operated rubber diaphragm with motor-driven valves to cycle the pressure between appropriate limits.

INTRODUCTION

For several years we have been investigating new variations on the well-known split Stirling mechanism for cooling very low-power cryoelectronic devices [1, 2, 3, 4]. The variations have included (1) the use of plastic and composite materials for the low-temperature stationary and moving parts and for the regenerator, (2) optimizing the geometry and other parameters to minimize the input power required, (3) electronic stabilization of the low temperature end, (4) simple construction which permits considerable design flexibility at moderate cost, (5) as many as five stages of refrigeration, (6) operation at sub-atmospheric pressures to enhance regenerator efficiency and permit operation at temperatures approaching 3 K. As part of these investigations we have demonstrated operation of a SQUID at 8.2 K in a four-stage cryocooler and a SQUID gradiometer at 7 K in a five-stage cryocooler.

* This work has been supported primarily by the Office of Naval Research.

This paper covers what may be regarded as the final phase of this line of development, including (1) use of a compressed-air-actuated neoprene diaphragm pressure-wave generator which permits removing the electric-motor drive and accompanying interference from the vicinity of the cryocooler, (2) an unlubricated alumina piston and cylinder for a long-life non-contaminating pressure-wave generator, (3) preliminary results on manufacturing an epoxy- glass-composite tapered displacer and sleeve incorporating a titanium-foil diffusion barrier, (4) a low-vibration gas drive for the displacer, in which part of the working fluid itself is conducted through a phase-shift mechanism to an auxiliary piston connected to the displacer. A fifth item on this list, the computer derivation of the optimum distribution of refrigeration, is described in the accompanying paper [4].

The first two items on the preceding list represent alternate mechanisms for producing a pressure wave in the working fluid, as required by the thermodynamic cycle. There are several reasons why one or the other of these mechanisms might be preferred for a particular application. For example, the diaphragm pressure-wave generator is relatively very cheap to manufacture, but outgassing of the rubber and helium diffusion through it may cause problems where long-term continuous operation is required.

The present developments are aimed toward the production of a low-interference cryocooler for highly critical applications such as SQUID-based instruments, which at the same time offers reasonable reliability, portability, ease of operation, and moderate cost.

THE CONCEPT OF A LOW-INTERFERENCE CRYOCOOLER

The essential elements (to be described in the following sections) of a low-interference cryocooler are shown in figure 1. The principle element which qualifies it as "low interference" is the gas-drive mechanism for the displacer. The mechanism has only one moving part with only one degree of freedom, and the gas drive is inherently "soft". Thus, vibrational interference associated with the displacer motion should be greatly reduced compared to that produced by the rotary-reciprocating mechanical drive used previously. In addition, since there is no mechanical connection to the pressure-wave generator, the latter can be placed an arbitrary distance from the cryostat, subject only to the requirement that it have the capacity to handle the extra volume of a long gas line. This physical separation of the two sections of the cryocooler essentially eliminates the pressure-wave generator and its drive mechanism as a source of magnetic interference or vibration, and it also makes the system flexible in that different generators may be interchanged depending upon the requirements of different applications. Two different types of generators have been built. One is electric-motor driven and uses an unlubricated close-fitting alumina (Al_2O_3) piston and cylinder for long-term continuous operation without gaseous contamination. The other is a neoprene diaphragm driven by compressed air alternately applied to the back side of the diaphragm and released to the atmosphere by a pair of cam-operated valves. A third possible way to generate the pressure wave

is to use a commercial helium compressor and purification system, alternately admitting high-pressure helium directly to the refrigerator and releasing it to the compressor input with cam-operated valves. A small commercial helium compressor should have the capacity to simultaneously operate several refrigerators of the size we are studying.

The tapered displacer and sleeve (with gap regenerator) was envisioned as a configuration that could be easily manufactured, with whatever profile would provide the optimum distribution of refrigeration as derived by the optimization procedure described in the accompanying paper. The sleeve incorporates a thin metal-foil barrier to block helium diffusion into the vacuum space. Lacking such a barrier, our earlier cryocoolers would not maintain a low temperature for more than a few minutes without continuous pumping. The bottom end of the sleeve also has molded into it an aluminum thermal link between the expansion space and the device chamber.

The system as sketched in figure 1 has been assembled and operated, but with only partial success. In particular, problems have been encountered in fabricating a leak-tight displacer sleeve. Current tests are being run using the five-stage displacer and sleeve described previously, in which a temperature below 7 K was maintained. It should be emphasized that nearly every component of the system represents a significant departure from previous practice, and so some practical difficulties might have been anticipated. On a positive note, none of the defects appear to be conceptual or fundamental, and the remedies are fairly obvious.

The following paragraphs describe the design and tests of the various components.

AIR-DRIVEN DIAPHRAGM PRESSURE-WAVE GENERATOR

Figure 2 shows a cross-section of a neoprene rubber diaphragm, 1.5 mm thick, clamped between circular aluminum plates with smoothly machined surfaces. The surfaces were given a sinusoidal contour so that the rubber is not sharply bent at any point when pressed against either surface (whether or not a sinusoidal contour is optimum for this purpose has not been determined). Several narrow, 1/2 by 1/2 mm, radial grooves were cut in each surface to prevent gas being trapped in case the center of the diaphragm should contact the surface first and block the port. Each port consisted of several small holes rather than one large hole, again for the purpose of preventing stresses on the diaphragm due to sharp bends.

The air-control system, shown schematically in figure 2, consists of a pair of "miniature" bellows-sealed valves, operated by cams to alternately admit high-pressure air ($\sim$ 0.6 MPa) to the diaphragm and release it to the atmosphere, at a rate adjustable around one cycle per second.

PRESSURE-WAVE GENERATOR USING CERAMIC PISTON AND CYLINDER

For some applications (as when compressed air is not available) a conventional generator using a motor-driven piston and cylinder is more convenient. The idea of using hard, unlubricated (or gas-lubricated) sliding surfaces to avoid contamination of the cryostat by liquid lubricants is fairly well known. An alumina (Al_2O_3) piston and cylinder has been operated at 1 cps for over 7000 hours without significant increase of leakage after the first 1000 hours [1]. The leakage rate ("blowby") amount to less than one percent of the total gas leaking past the piston during each compression and expansion cycle. This evidence indicates that the unit should be good for several years of continuous operation at pressures in the neighborhood of a few atmospheres and a speed of 1 Hz.

The pushrod seal is a potential source of contamination both from condensable gases in the grease and, perhaps, from air which might be trapped in the grease and dragged past the O-ring. A double seal was used in an attempt to greatly reduce the contamination. Two O-rings were separated a distance equal to the piston stroke, so that air trapped in the grease would not be dragged all the way from the outside atmosphere into the cylinder in each stroke. Air that is dragged into the intermediate space was diluted by being vented into a small auxiliary helium reservoir. An extra benefit of this arrangement is that grease applied to the pushrod between the O-rings will be pushed into a circumferential ridge which alternately contacts each O-ring at the limits of the stroke - in effect, the O-rings act as grease retainers for each other.

TAPERED DISPLACER AND SLEEVE WITH DIFFUSION BARRIER

The accompanying paper [4] describes the analytical procedure for optimizing the distribution of refrigeration vs. temperature through the use of a tapered displacer and matching sleeve (here we have chosen the term "sleeve", since "cylinder" obviously is not appropriate). A conical glass-epoxy displacer and sleeve, with which a temperature of 9 K was achieved, has been constructed by Myrtle et al [5], showing that the concept is viable. We have attempted to add several features to the concept. Our experimental units are filament-wound except at the small end, a technique which should give better structural homogeneity than cloth layers, and may be more suitable for commercial production (even better might be injection molding, a technique that has not been tried). An aluminum thermal link, molded into the bottom end of the sleeve, is an important feature (figure 3). It should increase the refrigeration efficiency by providing a low-resistance connection between the expansion space and the thermal load, resulting in more nearly isothermal expansion. An essential feature is a 30 μm titanium-foil diffusion barrier laminated into the sleeve about a millimeter from the inner surface, and extending from the top down about three-quarters of the total length. It was considered too difficult to extend the foil all the way to the bottom, but this should not be necessary since diffusion should be negligible at the cold end.

The manufacturing process, which was done by a commercial firm, consisted of filament-winding a thick layer of glass thread and epoxy over a stainless-steel conical form, the small end of which was held in a steady-rest made of 9 mm rod. After curing and removing the form and rod, the 9 mm hole in the small end was filled with a mixture of chopped fibers and epoxy and cured again. This constituted the "blank" for the displacer, which was then machined on a lathe to the desired tapered shape and wall thickness. The displacer itself was used as the form for the sleeve, which was fabricated by exactly the same process. The diffusion barrier was incorporated during filament winding, and the aluminum thermal link was put in place in the small end along with the mixture of chopped fibers and epoxy. The sleeve was then machined to the appropriate external shape.

Filament-winding has been highly successful for construction of cryogenic pressure and vacuum vessels of various shapes. However, our requirements posed some unique problems. The first sleeve that was built appeared not to have a good bond between the titanium foil and the epoxy, and also leaked along the aluminum thermal link. The latter was corrected, after a number of unsuccessful attempts by other methods, by pressing an aluminum cup with epoxy sealant over the bottom end so as to completely enclose the external part of the thermal link. In a second displacer and sleeve that has just been built, but not yet tested, the titanium foil was rough-etched with dilute hyroflouric acid to improve the bonding to the epoxy.

DISPLACER DRIVE

The most significant and unusual feature of the present cryocooler system is a displacer drive which uses some of the helium gas from the pressure wave generator, acting on a small auxiliary piston, to move the displacer (figure 3). The correct amplitude and phase relation between the pressure wave and the displacer motion are obtained by a pair of metering (needle) valves and a small adjustable auxiliary volume, as shown schematically in figure 1. In the absence of friction, no force should be required to move the displacer, and so, ideally, a single metering valve between the helium line and the auxiliary piston should provide $\pi/2$ phase shift. In an electronic system, the valve is analagous to a resistance and the movable piston is analagous to an infinite capacitance. The auxiliary volume and second valve, analogous to a second capacitance and resistance, provides additional phase shift, at the expense of requiring more helium gas (the analog of electric charge). Friction between the moving and stationary parts reduces the available phase shift, and requires more helium gas for a given phase shift. Since friction is difficult to predict and may vary with time, the auxiliary piston was made considerably larger than was estimated to be necessary in order to reduce the relative effects of friction and of gas leakage past the piston. Owing to this and other uncertainties, it is also difficult to predict the amount of gas, and the concomitant extra pressure-wave generator capacity, needed to operate the displacer drive.

The auxiliary cylinder was made of aluminum tubing with a thin stainless-steel inner liner, precisely ground to a uniform bore. The piston was made from a cylindrical cup-shaped aluminum piece with an outer nylon sleeve to rub against the stainless steel cylinder liner, with a radial clearance of perhaps 20 μm. The pushrod seal is a double O-ring arrangement with the same grease-retaining feature as the one described above in connection with the ceramic piston and cylinder.

The dead volume above the auxiliary piston acts as a nearly constant-pressure ballast reservoir, at a pressure slightly less than the average pressure below the piston, owing to the weight of the piston and displacer. In operation, the weight causes the displacer to rest briefly at the bottom of its stroke during each cycle - a very useful feature since it insures minimal dead volume in the expansion space (in zero gravity, this function could be provided by a lightweight spring). Another desirable feature of this type of displacer drive is that, although it is properly characterized as "soft", it is relatively stiff at the bottom of the stroke, owing to the nearly zero volume beneath the auxiliary piston. That is, the gas entering the zero volume will immediately provide a large force if the displacer does not immediately start moving upwards. Since any friction or viscous drag between a tapered displacer and sleeve should occur mainly at the bottom of the stroke (where the two surfaces nominally come into contact) the gas drive is relatively stiff precisely where stiffness is needed and not during the rest of the stroke. In normal operation, the displacer has not been observed to stick appreciably except when impurities have been frozen into the lower part of the regenerator gap. This latter condition must be prevented in the ultimate system, but when produced experimentally it is compensated for to a large extent by the stiffness of the drive mechanism.

This type of displacer drive is related to the so-called "free-displacer" mechanisms that have been used or tested rather extensively for small high-speed (> 10 Hz) cryocoolers for infrared detectors. These generally achieve the appropriate phase relation between displacer motion and pressure wave by tuning the mechanical resonant system consisting of the displacer-plus-piston mass and a gas spring - the mechanical analog of inductance and capacitance. So far as we are aware, there is no previous report of our type of drive, consisting of the analog of resistance and capacitance.

We might reiterate here again the feature of the gas drive which is of most profound significance from the point of view of eliminating magnetic interference and vibration, namely that it allows essentially perfect mechanical and spatial isolation of the pressure-wave generator from the cryostat.

PRELIMINARY TESTS OF THE SYSTEM

When an operating system like that shown in figure 1 was first assembled, using the components described in the preceding paragraphs, it achieved a temperature in the neighborhood of 30 K - exceedingly poor

performance relative to the expected 6 or 7 K. Since the displacer and sleeve wall thicknesses had been machined somewhat greater than the design analysis called for, ($\sim$ 5 mm instead of 3 mm), conduction heat input was expected to be correspondingly larger. The sleeve was subsequently machined to a thickness of 3 mm, but in so doing the machine tool cut into the titanium-foil diffusion barrier near the lower end, which caused a leak. On the basis of this and related evidence, it was concluded that the epoxy had not bonded well to the titanium. We were not successful in repairing the leak, so this particular displacer and sleeve was abandoned. Currently, the system is operating in the neighborhood of 10 K using the 5-stage displacer and sleeve described in earlier papers [1,3], still considerably short of expectations. Basically, the problem is that the amount of gas required for the displacer drive was underestimated, so neither the ceramic pressure-wave generator nor the diaphragm type has sufficient displacement (70 cm^3 and 100 cm^3, respectively) to produce the compression ratio of 3.7 at which a bottom end temperature below 7 K was previously achieved with the 5-stage displacer. Corrections to the present system would seem to be fairly obvious and straightforward, and the performance of the optimized system will be the subject of a future report.

With regard to reliability, no problems have been encountered. Except for the ceramic pressure-wave generator, none of the new components of the system has had extensive testing. The displacer drive mechanism has been operated about 1000 hours and the neoprene-diaphragm pressure-wave generator for over 2000 hours.

NOTE ADDED IN PROOF: Since this paper was submitted, two cryocoolers have been put into operation, using a concept which has evolved significantly beyond that shown in figure 1. A compressed-air-driven diaphragm, labeled (b) in figure 1, is used to produce the pressure wave in the working fluid, as shown. The displacer drive piston, however, is actuated through a separate helium line by a second, smaller air-driven diaphragm. The "phase-shift" components indicated in the figure are therefore dispensed with. The air-control valves for the two diaphragms are electric solenoid types, and their opening and closing times are programmed through a low-cost, fully dedicated microcomputer. The merits of this system as an experimental developmental device can hardly be adequately described in one paragraph, and full details will be submitted for publication later. The programmable control system allows independent control of onset, rate of change, and amplitude of both the pressure changes and the displacer motion; in other words, it provides arbitrary independent control of every part of the thermodynamic cycle, and the computer can be programmed to go through an optimization procedure in which each of a large number of parameters are successively varied to achieve lowest temperature, or most efficient operation at a particular temperature, or whatever is desired.

The two cryocoolers presently operating incorporate the 4-stage and the 5-stage displacers taken from cryocoolers described earlier [1,2,3], which used conventional piston-type pressure-wave generators and mechanical displacer drives. Both of the new systems reach temperatures

significantly below what was reported previously, 7.6 K compared to 8.2 K for the 4-stage displacer, and comparable improvement for the 5-stage displacer, although owing to thermometer malfunction the latter has not been precisely measured.

Our attention now has returned to the task of fabricating and testing a continuously tapered displacer shaped according to the analysis given in the accompanying paper [4].

REFERENCES

[1]. J. E. Zimmerman and D. B. Sullivan, "A Study of Design Principles for Refrigerators for Low-Power Cryoelectronic Devices," NBS Tech. Note 1049. U. S. Government Printing Office, Washington, D. C. (Jan. 1982). (This and the following two references are available free from the authors. Address: National Bureau of Standards, Mail Stop 724.03, Boulder, CO 80303).

[2]. J. E. Zimmerman and T. M. Flynn, "Applications of Closed-Cycle Cryocoolers to Small Superconducting Devices," NBS Special Publication 508, U. S. Government Printing Office, Washington, D. C. (April 1978).

[3]. J. E. Zimmerman, D. B. Sullivan, and S. E. McCarthy, "Refrigeration for Cryogenic Sensors and Electronic Systems," NBS Special Publication 607, U. S. Government Printing Office, Washington, D. C. (May 1981).

[4]. D. B. Sullivan, R. Radebaugh, D. E. Daney, and J. E. Zimmerman, "An Approach to Optimization of Low-Power Stirling Cryocoolers," Second Biennial Conference on Refrigeration for Cryogenic Sensors and Electronic Systems, NASA CP- , 1983. (Paper of this compilation.)

[5]. K. Myrtle, W. Winter, and S. Gygax, "A 9-K Conical Stirling-cycle Cryocooler," Cryogenics 22, 139 (1982).

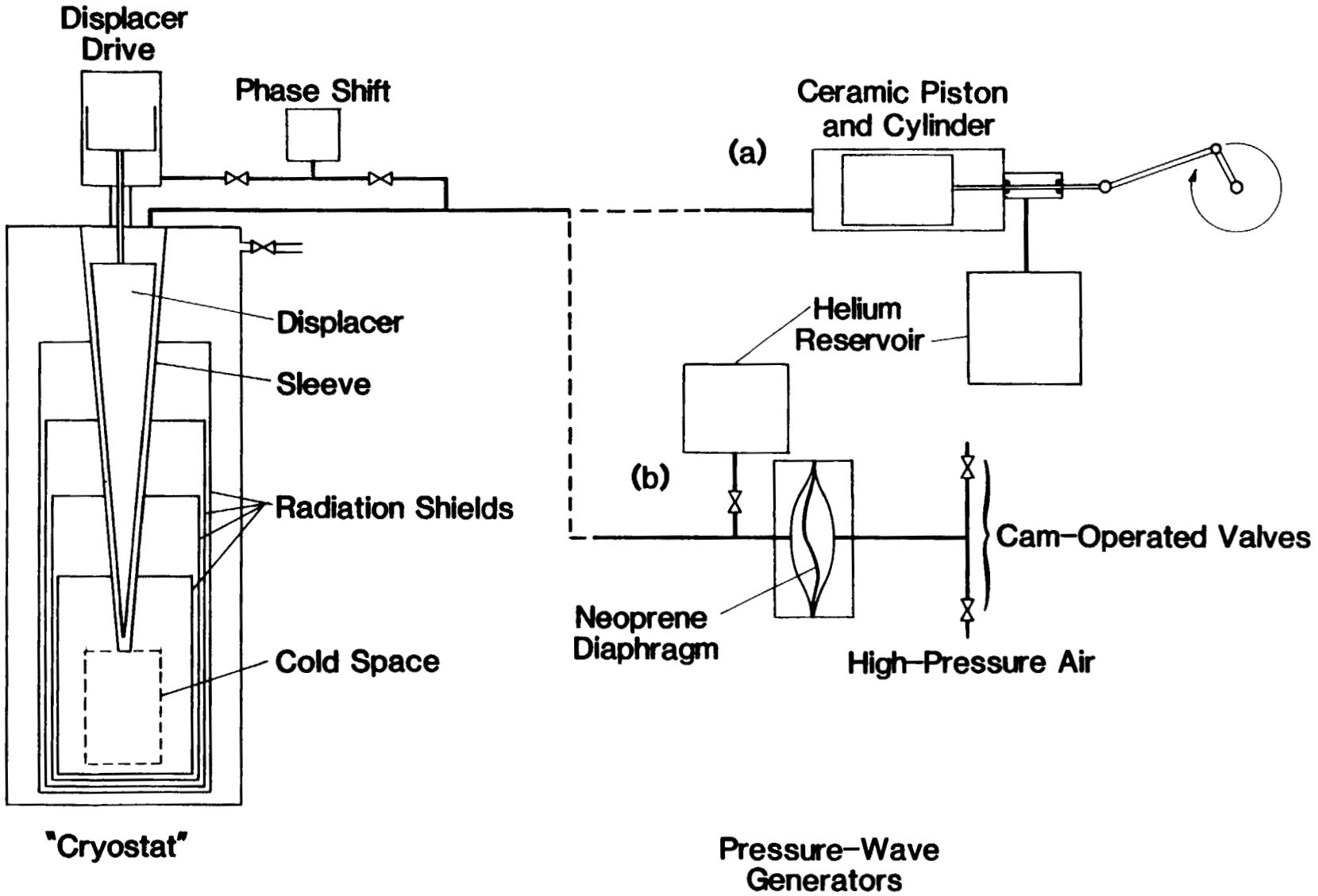

Figure 1. Conceptual Design of a Low-interference Cryocooler, with Two Different Options for the Pressure-wave Generator (a and b)

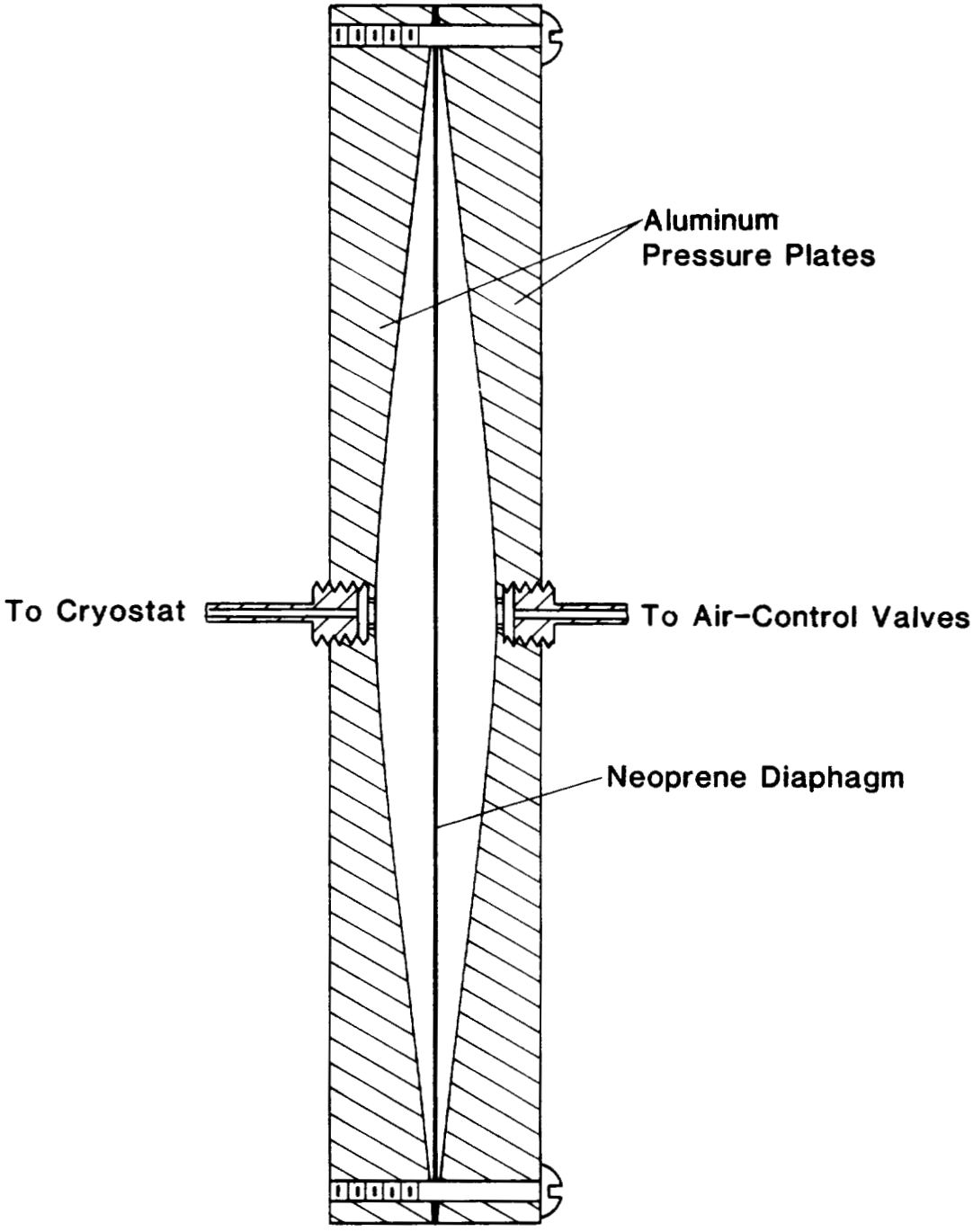

Figure 2. Diaphragm Pressure-wave Generator Driven by Compressed Air

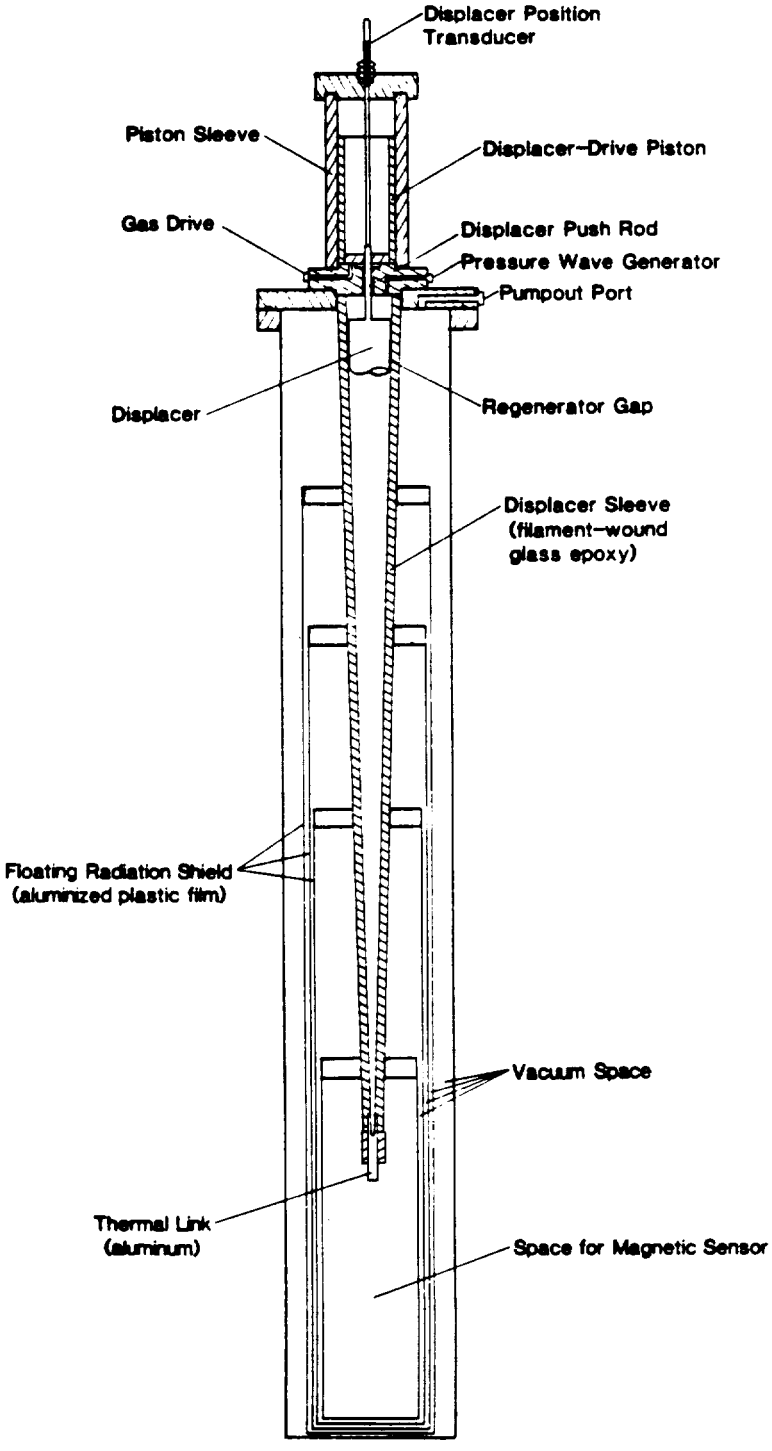

Figure 3. Tapered Displacer and Sleeve, Drive Mechanism, Radiation Shields, and Vacuum Jacket (collectively referred to in the text as the "cryostat")

An Approach to Optimization of Low-Power Stirling Cryocoolers*

D. B. Sullivan, R. Radebaugh, D. E. Daney, and J. E. Zimmerman
National Bureau of Standards
Electromagnetic Technology Division
Boulder, CO 80303

ABSTRACT

We describe a method for optimizing the design (shape of the displacer) of low-power Stirling cryocoolers relative to the power required to operate the systems. A variational calculation which includes static conduction, shuttle, and radiation losses, as well as regenerator inefficiency, has been completed for coolers operating in the 300 K to 10 K range. While the calculations apply to tapered displacer machines, comparison of the results with stepped-displacer cryocoolers indicates reasonable agreement.

INTRODUCTION

The general wisdom of intercepting heat transfer from a warm to a cold region by refrigeration at intermediate temperature levels has long been appreciated. The Carnot coefficient, $T_{amb}/T-1$, which governs the power required to refrigerate at a temperature, T, below the ambient temperature, T_{amb} is at the heart of this thought. Cryocoolers are commonly designed to fit an *a priori*, and often highly subjective, choice of refrigeration power at one or more low temperatures. One measure of performance is the efficiency of the cryocooler at the specified refrigeration power, that is, the ratio of the actual drive power to the ideal drive power as calculated using the Carnot coefficient. It is implicit in this approach that if such a machine is used in an application requiring very much less than the specified refrigeration power, the total system may be grossly inefficient. There is now a need to provide refrigeration for a number of very low-power cryoelectronic devices which require almost negligible refrigeration power (less than a milliwatt) at temperatures below about 8 K. In this case optimal interception of heat flow is of paramount importance and efficiency becomes a meaningless measure of performance. In this paper we consider such optimization for a class of low-power Stirling cryocoolers which use plastic materials in a gap-type regenerator [1-3]. In the course of this study we would like to propose alternate measures of performance for such machines which could provide for a rational comparison of different concepts.

* This work was supported in part by the Office of Naval Research under contract number N00014-82-F-0040.

As a preliminary problem, we consider the optimum refrigeration distribution for leads and support structures which connect room temperature to low temperature regions. This problem leads naturally to the consideration of the geometrical configuration of a Stirling cryocooler which provides for optimum cooling (that is, minimum drive power), which is the thrust of this work.

OPTIMAL REFRIGERATION DISTRIBUTION FOR CONDUCTION LOSSES

The problem considered here is that of interception of heat flowing along a support rod or electrical lead with the minimum amount of work performed by the refrigerator. For simplicity we assume a uniform cross section of area, A, for the heat conducting element and a thermal conductivity, k, which is independent of temperature. The optimization takes the form of a variational calculus problem [4] in which the direct output is the axial temperature distribution which results in the minimum work performed by the refrigerator. From this temperature distribution we can readily calculate the continuous refrigeration distribution which our imaginary refrigerator must provide.

The conduction heat flow is simply

$$\dot{Q} = kA \frac{dT}{dx} \quad . \tag{1}$$

The net work, w, done by the refrigerator in cooling from ambient temperature, T_{amb} at x to some lower temperature, T_o, at x = 0 is given by

$$w = \int_0^a \left(\frac{T_{amb}}{T} - 1 \right) \frac{d\dot{Q}}{dx} \, dx = \int_0^a \left(\frac{T_{amb}}{T} - 1 \right) kA \frac{d^2T}{dx^2} \, dx \quad , \tag{2}$$

We consider variations of T and find the T(x) for which w is stationary, that is, at an extremum. Application of the calculus of variations [4] leads to the differential equation

$$T \frac{d^2T}{dx^2} - \left(\frac{dT}{dx} \right)^2 = 0 \quad , \tag{3}$$

which has the solution

$$T = T_o e^{\alpha x} , \tag{4}$$

where

$$\alpha = \frac{1}{a} \ln (T_{amb}/T_o). \tag{5}$$

This exponential temperature distribution is the optimum one for this situation (constant k and uniform cross section). The distribution of refrigeration is calculated using equation 2.

If the thermal conductivity has the form $k = k_n T^n$, (n is a positive integer) the variational method leads to a differential equation

$$T \frac{d^2T}{dx^2} + \frac{1}{2} (n-2) \left(\frac{dT}{dx}\right)^2 = 0 \tag{6}$$

which except for n = 0 has the solution

$$T = (T_o^{n/2} - \beta x)^{2/n} , \tag{7}$$

where

$$\beta = (T_{amb}^{n/2} - T_o^{n/2})/a . \tag{8}$$

This type of calculation need not be restricted to elements of uniform cross section. For example, the optimum temperature distribution for heat flow along a truncated cone (big end at higher temperature) can be shown by a similiar approach to be derived from the differential equation

$$\frac{d^2T}{dx^2} + (\frac{n}{2} - 1) \frac{1}{T} \left(\frac{dT}{dx}\right)^2 + \frac{2}{x} \frac{dT}{dx} = 0 , \tag{9}$$

where n is the power of the temperature in the thermal conductivity (as before).

The conduction loss is given rigorously by the equation

$$\dot{Q}_{con} = kA \frac{dT}{dx} = \pi k(r + t)^2 \frac{dT}{dx} \quad , \tag{10}$$

where the thermal conductivity, k, is a function of temperature, T, and the cross-sectional area, A, is taken to be a function of the position, x, along the displacer, since we wish to consider variations of the displacer shape and thus of its area. In the second form of this equation, the area has been expressed in terms of the displacer radius, r, and the sleeve wall thickness, t.

For plastic displacers operating at low speed, Radebaugh and Zimmerman [5] have shown that a conduction-like form, devoid of gas properties, is appropriate for the description of shuttle heat loss.

$$\dot{Q}_{shu} = r\, S^2 \sqrt{\pi \hat{n} k C_v / 2} \frac{dT}{dx} = \beta \sqrt{k C_v}\, r \frac{dT}{dx} \quad . \tag{11}$$

Here r, the radius of the displacer, is a function x. S is the stroke, $\hat{n}$ is the frequency and k and C_v the thermal conductivity and specific heat of the displacer and sleeve walls, both being explicit functions of temperature. The factor β includes all of the constants in the equation. The assumptions are that (i) solid thermal properties are only weak functions of temperature, (ii) thermal resistance of the gas gap is negligible, (iii) the effect of gas-pressure cycling is negligible, i.e., heat capacity of the gas in the gap is negligible and regeneration is complete, (iv) interaction of the axial conduction effects in the displacer and wall are negligible, and (v) motion of the displacer is sinusoidal. The authors showed good experimental agreement with this equation for temperatures down to 102^{o} K. Assumption (iii) concerning the heat capacity of the gas might be expected to break down as the temperature falls below 10^{o} K where regeneration problems arise.

For the sake of this calculation we wish to consider an alternate, distributed form for the radiation loss [6]. We assume that 4 or 5 radiation shields will be attached along the length of the machine to intercept the radiation at higher temperatures where refrigeration efficiency is better and that liberal use of multiple super-insulation layers will be made between radiation shields. If Δx is the spacing (axially) between grounded radiation shields and n is the number of super-insulation layers per unit length (again axially), then we write

$$\dot{Q}_{rad} = (2\varepsilon\sigma A_s)\ (\Delta x/(n\Delta x+1))T^3 \frac{dT}{dx} = \gamma T^3 \frac{dT}{dx}\ , \qquad (12)$$

where A_s is surface area of the radiation shields (assumed to be the same for all shields), σ is the Stephan Boltzman constant and ε the emissivity of the superinsulation layers (taken to be 0.5 for the usual aluminized plastic material. In the abbreviated form γ collects together all of the constant terms. To be sure, this is a very rough sort of estimate, but it can be left so for several reasons. First, with sufficient shielding radiation losses can be held to a level which is significantly below other losses (10 to 20%) and second, radiation losses can be made negligible at the low temperature end where most of the real refrigeration problems arise. Finally, since we are approximating a discrete process (4 or 5 grounded shields) with a differential equation we should not take the exact form too seriously since the heat loss is, in fact, not distributed continuously along the displacer.

Radebaugh [7] has expressed the regenerator inefficiency for low-speed, plastic-displacer Stirling coolers in a form which is suitable for our purposes.

$$\dot{Q}_{reg} = (mC_p)^2 \frac{\dot{n}}{4r} (2\pi k C_v/\dot{n})^{-1/2} \frac{dT}{dx} = \delta(mC_p)^2/(r\sqrt{kC_v})\ . \qquad (13)$$

Here m is the total helium mass flow into the expansion space and C_p is the specific heat of helium at constant pressure. Again, δ is a collection of all the constants. The assumptions here are many: (i) temperature variation at the surface is sinusoidal, (ii) surface temperature is the gas temperature, (iii) gas volume in the regenerator is negligible, (iv) sinusoidal heat flow is only in the radial direction, (v) the expansion and compression space are isothermal, and (vi) various heat flows to the expansion space are independent of one another. Assumptions (i) and (v) are of greatest concern. The mass flow is only approximately sinusoidal, but the assumption greatly simplifies the form of the equation. Radebaugh shows that assumption (v) yields errors about a factor of 2 at 5 K and these reduce rapidly as temperature is increased.

A final loss term accounting for the non-ideal properties of helium gas might also be included. Like the regenerator inefficiency the non-ideal gas term (alternatively referred to as the enthalpy deficit) also depends on the gas flow and thus the calculations of the two terms should be similar. There is an important qualitative difference between the two terms however. The steeply decreasing heat capacity of many regenerator materials at low temperatures and the consequent steeply rising regenerator efficiency makes it difficult to achieve temperatures below 5 or 6 K (although a temperature approaching 3 K was achieved by operating a regenerative machine at sub-atmospheric pressure [3].

According to our preliminary calculations, the non-ideal gas properties of helium do not particularly limit the temperature that can be achieved, and in fact it is conceivable that they might be used to advantage in certain situations. We will assume ideal-gas behavior for the present calculation, but the non-ideal behavior could be added later as a refinement of the model.

The differential refrigeration, dW, is

$$dW = \begin{pmatrix}\text{Pressure}\\ \text{Change}\end{pmatrix}\begin{pmatrix}\text{Differential}\\ \text{Volume}\end{pmatrix}\begin{pmatrix}\text{Cycle}\\ \text{Rate}\end{pmatrix} \tag{14}$$

$$= (P_u - P_\ell)\,(2\pi S r dr)\,(\dot{n}) \quad ,$$

where P_u and P_ℓ are the upper and lower pressures, respectively. Integrating, the refrigeration is found to be

$$W = Br^2 \quad , \tag{15}$$

where $B = \pi S\dot{n}\,(P_u - P_\ell)$ is a constant. W is thus a function of the radius, r, and r is a function of the position, x, along the displacer. This form is valid where the displacer follows a square wave motion. Where sinusoidal motion is used, the Schmidt analysis should be applied, but for simplicity we simply reduce equation 14 by the multiplicative factor $2/\pi$.

Also, equation 14 applies only to the case where there is no pressure change during the displacement parts of the thermodynamic cycle. The ideal cycle (consisting of two isothermal and two isobaric processes) is commonly called the Ericsson cycle. In the ideal Stirling cycle (two isothermal and two constant-volume processes), there are pressure changes during all parts of the cycle and consequently a significant amount of refrigeration occurs during displacement as well as during expansion by the piston [8]. We have not tried to take account of this effect since it is not yet clear whether the Stirling or the Ericsson cycle (or some other idealization) is a better approximation to the actual operation of the machines to which these calculations are to be applied.

HEAT CONTENT OF THE WORKING FLUID

In equation 13, the term mC_p, which is a function of x, represents the heat content of all the gas which moves down past the point x on the displacer. It clearly depends on the geometry of the displacer and thus is not known until the displacer shape is known. It can be expressed as

$$mC_p = NC_{pm} = \frac{PV}{RT} C_{pm} = \frac{5}{2} \frac{PV}{T} \quad . \tag{16}$$

Here N is the number of moles of gas and $C_{pm} = \frac{5}{2} R$ is the specific heat per mole for helium gas. The volume, V, and temperature are functions of x and we choose to fix the pressure at P_u, a point to which we will return. Then we may write

$$mC_p = \frac{5}{2} P_u \int_o^V \frac{dV}{T} = \frac{5}{2} P_u \left[\frac{V_o}{T_o} + S \int_o^x \frac{2\pi r}{T} \frac{dr}{dx} dx \right] \tag{17}$$

$$= \left[\frac{r_o^2}{T_o} + 2 \int_o^x \frac{r}{T} \frac{dr}{dx} dx \right] \quad ,$$

where $\lambda = 5\pi SP_u/2$, r_o is the radius of the displacer at the bottom end, and $V_o = \pi r_o^2 S$ is the expansion volume at the bottom end. That the displacer should be blunt (of finite radius) at the bottom end can be understood by noting that some finite heat is always transferred all the way to the bottom end and thus some finite refrigeration is required at that point. Conduction through the sleeve wall is just one of the ways in which heat arrives at the bottom end.

In general the maximum pressure, P_u, is not coincident with the minimum volume in a Stirling machine, so, in principle, some pressure between P_u and P_ℓ should be used in equation 17. However, the regenerator loss term is calculated under the assumption that the temperature variation is sinusoidal and this also is not quite right. This last consideration suggests that equation 13 will underestimate the regenerator loss. Thus, we choose to use P_u in calculating mC_p since this increases the regenerator inefficiency term and compensates to some degree for the effect of non-sinusoidal temperature variation.

GENERAL APPROACH TO OPTIMIZATION

The approach which we have chosen involves variation of solutions to arrive at the optimum solution from an initial, rather arbitrary guess.

We select a power series to represent the temperature distribution along the displacer.

$$T(x) = T_o + T_1 x + T_2 x^2 + T_3 x^3 + \ldots . T_7 x^7 \ . \qquad (18)$$

If the top end temperature is constrained to be ambient temperature, T_{amb}, (e.g. 300^o K) and the bottom temperature (at x = 0) is fixed at T_o (e.g. 10 K), the normalization of x to the length, L, of the refrigerator yields the constraint

$$T_1 + T_2 + T_3 + \ldots . T_7 = T_{amb} - T_o \ , \qquad (19)$$

since x = 1 at the top end. A simple initial guess is that the temperature distribution is linear, that is, $T_1 = T_{amb} - T_o$ and the other coefficients are zero. This also fixes the initial guess for the temperature derivative, dT/dx.

Referring to figure 1 for nomenclature, the radius, r_o, of the displacer at the cold end (x = 0) can be found by equating the refrigeration term (equation 15) to the sum of the loss terms (equations 10, 11, 12, and 13). Since mC_p (given by equation 17) is known at the bottom in terms of r_o we can insert that into the regenerator loss term. The result is

$$Br_o^2 = \left[\pi k(r_o + t)^2 + \beta\sqrt{kC_v}\, r_o + \gamma T^3 + \delta\lambda^2 r_o^3/\sqrt{kC_v}\right] \frac{dT}{dx} \ . \qquad (20)$$

In terms of the initial guess for T(x), a consistent value for r_o can be obtained from this cubic equation since all elements in it are known.

In general we cannot use this procedure to obtain r at other positions along the displacer because the value for mC_p at points above the bottom end depends on the shape of the displacer which is as yet undetermined. However, assuming that the regenerator term is not the overwhelming one, an iterative process (by computer) can be used to arrive at a displacer shape which provides for consistency between mC_p as a function of x and the balance of refrigeration and losses. The balance equation is now

$$Br^2 = \left[\pi k(r+t)^2 + \beta\sqrt{kC_v}\, r + \gamma T^3 + \delta\,(mC_p)^2/(r\sqrt{kC_v})\right] \frac{dT}{dx} \ . \qquad (21)$$

Here we must use equation 17 for mC_p. We break the range of x into increments of Δx and, for $x = \Delta x$ calculate a value for r from this equation using the value of mC_p at $x = 0$. mC_p at $x = \Delta x$ can now be calculated from equation 17. We proceed to subsequent increments using the same procedure (that is, using the value of mC_p from the previous increment) until the entire range of x is covered. This procedure generates a first approximation for r(x) and for mC_p as a function of x. The values for mC_p are then shifted down one increment (Δx) since they are really associated with the values of r at those points. In the next iteration we use this information to improve upon the first approximation, that is, a new r(x) (and thus mC_p) is calculated using the old mC_p. The process is repeated until convergence is achieved, at which point we have a self consistent solution (mC_p and displacer shape). In practice this convergence is rather rapid, requiring less than 10 iterations.

For this particular guess at the optimum solution, the net power required to operate the machine can now be calculated using equation 2 where dQ/dx is the sum of the derivatives of the loss terms. Since this sum equals the derivative of the refrigeration power, that could equally well be used to calculate the net power (this is a convenient internal check on the consistency of the calculation).

Having calculated the net power to run this particular refrigerator, we can proceed to search for the optimum design, that is, the temperature distribution and displacer shape which minimize the drive power. The process involves variation of the coefficients in the expansion of T (see equation 18) consistent with the constraint given by equation 19. The variations which yield reductions in the power requirement are followed until further variations of any of the coefficients yield no further decrease.

We now assert (without proof) that this is the optimum solution. On general grounds one can argue that this could represent a local minimum (a sort of metastable solution) and that a solution of still lower power requirement might yet exist. In fact, we can offer no general proof that this is not true, but uniqueness of the solution can be tested by trying a variety of initial guesses for T(x). These will produce a different history in the search for the optimum solution, but arrival at the same solution will add confidence to the validity of the final result. A final point should be made. The problems on conduction loss considered in section 2.0 all had unique solutions and these were produced by a more rigorous method. While the refrigerator problem is more complex, the loss terms (Q's) in most reasonable situations (certainly in all cases which we have considered) are rather simple monotonically increasing functions of postion along the displacer and thus we don't expect the general character of the solutions to be significantly different from those derived in section 2.0.

As mentioned at the beginning of this section (3.0), additional support members or electrical leads can be included if necessary. The implicit assumption of this assertion is that the only loss for these

elements will be by conduction and that the temperature profile for them will be identical with that for the cooler itself. In general, this will require a number of thermal tie points between these elements and the cooler. With this condition, the additional loss can be added directly to equations 20 and 21. The cross sectional area for such members could be constant or some fixed function of x. Another reasonable modification which we have incorporated is the allowance for a hollow displacer (to cut down on conduction loss). For simplicity of description this has not been included explicitly, but the process involves a simple modification of the conduction term in equations 20 and 21. Actually we assume that the hollow space is filled with helium gas and include conductive but not convective heat transfer in the gas (i.e. convection eliminated by filling with glass fiber or some cellular material). Finally, if we add a constant power to these two equations we can provide for dissipation at the bottom end. In effect, the solution thus obtained will produce a refrigeration power equal to this constant.

The method used to attack this refrigerator problem parallels the simpler problem described in section 2.0. In both cases we consider variations in T for which the work integral, equation 2, is stationary with the constraint that temperature is fixed at the hot and cold ends. The primary difference of a general nature is that the system is really taken through the variations in the one case where an identification of the stationary solution based on the formal variational calculus is used in the other.

DESCRIPTION OF THE COMPUTER CODE

A simplified version of the flow chart which describes the computer code is shown in figure 2. Care should be used in literal use of this flow chart since there are implied actions which have been omitted for simplicity. These will be mentioned in the step by step description of the program. The numbers below refer to the segments of the program as shown in the figure. (1) The T(I) referred to here are the seven coefficients in the expansion of temperature as a power series in x (equation 18). Thus the index I which identifies the particular coefficient runs from 1 to 7. J is an integer which indexes the particular passage through the calculation for a particular value of I. It is reset to 0 for each change of I. (2) In this step the radius of the displacer at the bottom end is calculated using equation 20. J is also advanced at this step. (3 and 4) The procedures for these steps are described rather completely in section 3.3. The pertinent equations are 17 and 21. (5) The power integral to be calculated is given by equation 2. In this equation dQ/dx is the sum of the derivatives of the loss terms given by equations 10, 11, 12, and 13. In general these are expressed not only as functions of r, k, and C_v but also of dr/dx, dK/dT, dC_v/dT, dT/dx, and d^2T/dx^2. These are readily generated from information already available at this point. The power integral includes the power required for refrigeration in the bottom expansion volume. (6) J = 1 means this is the first pass for a particular value of I and thus, before proceeding, a variation must be made in T so as to have two values of

power for comparison. The process for varying T, depicted by the box here, involves addition of a fixed increment to one coefficient. Actually, to fulfill the requirement of equation 19 (boundary condition for temperature), an addition to one coefficient must be balanced by an equal reduction in one or more of the other coefficients. This will be discussed in more detail shortly. (7 and 8) Here the power just calculated in step 5 is compared with the value calculated in the previous pass. If this new value is smaller, the variation is pursued for another pass. If the new power is larger either the current round of variations has been played out for this particular value of I or this is the second pass and the variation should be reversed to see whether reduced power is found for the opposite variation. If J = 2 (i.e. second pass), it should be clear that the reversed variation must take one back beyond the first pass selection. We do this by reversing the increment and doubling its value of this one pass. Also, once the variation is reversed, the program should retain that sign for subsequent passes so that a yes answer at step 7 results in a further variation in the profitable direction. (9) Once the variations for a particular coefficient I are completed (no further reduction in power) the program moves on. In making this step the power (and the coefficient value associated with it) must be the lowest value just found. This simply means that one must go back to the previous pass since the logic has forced exit from step 8 after an increase in the power. In step 9, a test is done to see if all coefficients have been varied. If not the next one is selected and the process restarted. (10) If all of the coefficients have been varied, this set is compared with the set from the previous pass (the initial set if this is the first time through to this point). If the two sets are not identical, the whole process is rerun to generate another set of coefficients. This process is repeated until the coefficients do not change with further variations. (11) At this point a further refinement of the result can be achieved by a reduction of the increment used in the variational process. The integration increment used in step 5 could also be reduced to improve that process. Then, with the last set of temperature coefficients as a starting point, the entire procedure could be repeated until some preset measure of convergence is met. We have found that the computer costs at this stage are not negligible and have chosen to run through the whole process no more than 2 or 3 times. In general, the degree of convergence has generally been quite acceptable where a variational increment of 1.5 K and 50 steps per integral was used. (12) The final step involves output and is highly subjective in form. We have chosen to generate plots of T, r, mC_p, Q, and W (the power integral) as functions of x. The Q and W output can be broken down into the separate loss terms to show the relative importance of the different losses along the displacer.

The rate of convergence on the solution depends upon the exact form of the variation in step 6. We have tried only two. First (to satisfy equation 19), we have simply added to one coefficient and subtracted from the adjacent one. While this works sometimes, it can lead to difficulty and we have achieved better results including faster convergence with another simple procedure. The increment which is added to one coefficient is simply divided by 7 and that amount is subtracted from every

coefficient. This procedure more clearly emphasizes the one coefficient. The program could be improved (faster convergence) by more careful consideration of the form of the variation.

At times it has been difficult to arrive at a satisfactory initial guess for the coefficients. Without the regenerator term almost any simple guess works (e.g. T_1 = 290 K and all others are zero). But when the regenerator term is included this is not the case. The solution of equation 20 for the bottom end radius becomes highly dependent upon dT/dx at x = 0. If this derivative is too large there is no real, positive solution to the cubic equation 20 which simply means that the selected temperature derivative is inconsistent with any realizable refrigerator. For sufficiently small values of dT/dx at x = 0, two real, positive solutions are found and we always select the smaller of the two. The program can potentially run into unrealistic situations on its own. This happens particularly where the initial temperature profile is dramatically removed from the final one or as the calculation is pushed into regions where realizable results simply aren't expected for other reasons. For example, as the length of the displacer (an externally fixed constant) is reduced, the power requirement increases without bound and it becomes increasingly difficult to find any initial temperature profile which does not cause problems. Another type of problem arises when dT/dx goes to zero at any point along the displacer. Here, equations 20 and 21 become indeterminant, that is, no solution can be found for r (or r_0). The net effect of these considerations is a need to build certain tests into the program to assure proper exit and diagnostics when an unrealistic solution is encountered.

RESULTS OF THE CALCULATION

Based on earlier experimental work [1-3] on coolers of this type (stepped rather than tapered displacers), we have selected a set of parameters for a 'standard' low-power cryocooler. These parameters are given in Table I and represent the base from which we vary an individual parameter to study its effect. The remaining figures in the paper refer to this standard set of parameters. The displacer is taken to be hollow (as mentioned in section 3.3) so the table also includes a displacer wall thickness as well as a sleeve wall thickness.

The thermal conductivity is that of spun glass epoxy (designated G-10 by the National Electronic Manufacturers Association), which we represent by

$$k = 5.7 \times 10^{-2} + 5.03 \times 10^{-3}T - 2.02 \times 10^{-5}T^2 + 3.6 \times 10^{-8}T^3 ,$$

where the units are W/K·m. Similarly, the specific heat of the G-10 material is represented by

$$C_v = -1.36 \times 10^4 + 4.4 \times 10^3 T + 17.9 T^2 - 8.72 \times 10^{-2} T^3 + 1.3 \times 10^{-4} T^4,$$

where the units are J/km^3.

Figure 3 shows the results for $T_0 = 5$ K, a lower temperature than might be justified by the assumptions, but which emphasizes the effects of inclusion of the regenerator loss term. The upper two boxes show the optimized temperature profile and displacer shape in cases both including and excluding regenerator loss. In the bottom box we present the work integral (equation 2) for each loss term as a function of position along the displacer. Each point on one of these curves represents the total drive power required to take care of the particular loss term below the associated value of x. The curves in this lower box are associated with the profiles which include regenerator loss in the upper two boxes.

Several points should be noted. First, while regenerator losses are only significant at the cold end, radiation losses can be effectively intercepted at higher temperature. The inclusion of regenerator loss forces an elongated narrow end to the displacer which might be approximated by two conical sections. The temperature profile is similarly distorted. The importance of shuttle heat transfer is clear and its similarity to conductive heat transfer is perhaps surprising.

Note the slight irregularity at the upper end of the displacer for the case which excludes regenerator loss. We often find distortions (both positive and negative) in this region which we attribute to the lack of emphasis given this part of the displacer by the calculation. That is, the contribution to the power integral at the upper end is almost negligible and thus the variations simply emphasize the regions of the displacer which contribute significantly to the work integral. Presumably, such distortion would be eliminated with complete convergence, but with little further change in the power requirement. This is born out in a study of several iterations with successively smaller variational increment (see section 3.4).

Figures 4, 5, 6, and 7 display the effects of altering the stroke, length, frequency, and bottom-end dissipation for $T_0 = 10$ K. The curves represent the total power for each loss element (the value of the respective parts of the work integral at the top of the cooler). The refrigerator has been optimized for every value of the independent variable (e.g. stroke) where all the other parameters are maintained at the standard values shown in Table 1.

Several general comments can be made. Except where length is varied, the radiation loss is independent of the other parameters. This simply means that modest variations of the temperature profile have no marked effect on radiation loss. The linear increase of radiation loss with length (figure 5) seems reasonable since radiation surface area is also

linearly dependent on length. Regenerator loss is strongly dependent on the expansion volume at the bottom end. For example, as stroke is increased (figure 4) the regenerator loss increases as expected. The increases of regenerator loss with decreasing stroke in the limit of short stroke can be understood as arising from the precipitous increase in bottom end radius in this region. Remember that these curves represent a continuous set of optimized refrigerators, not a single refrigerator of fixed geometry. The regenerator loss dependence on expansion volume is clearly seen in equation 17 where the heat content of the fluid depends on how much gas is present. This plays an important role in the loss term (equation 13).

Shuttle heat transfer and conduction loss dominate these figures with only minor contributions from radiation and regeneration. The strong cross- over of the two leading terms with variation of stroke (figure 4) produces the most notable minimum in total power. The minimum appears to be at about 3 mm rather than the 5 mm value of the standard parameter set. For alterations of length (figure 5) and frequency (figure 6), the most notable effect is a sharp rise in power for small values of these parameters. Conduction and shuttle losses generally increase with increase in the size (radius) of the displacer. This is consistent with their respective dependences on displacer cross sectional area and surface area. The exception to this rule occurs where decrease in stroke results in decreasing shuttle loss even though the displacer size is rising rapidly.

For modest heat dissipation at the cold end, the power requirement rises almost linearly as seen in figure 7. Actually the only loss term which is not essentially linear over this range is regenerator loss. This is the only case where the drive power required for the cold end expansion space becomes really significant, rising to 0.36 watts at a refrigeration power of 10 mW from 0.03 watts with no dissipation. As discussed in section 3.4, the optimization includes the power required for this bottom end cooling, but it is not shown in figures 4, 5, 6, and 7 because it is so small.

Figure 8 shows a comparison between this theory and a stepped displacer cryocooler [3] which fits all of the standard set of parameters (Table I). The quantitative agreement is very good considering the number and nature of the approximations described in section 3.1 and the fact that the comparison is between a tapered and a stepped displacer. We have measured the pressure-volume (P-V) diagram for this 4-stage machine, with the helium pressure adjusted to give 10 K at the cold end. The area of the P-V diagram multiplied by the operating speed gave 2 watts as the mechanical power actually performed on the working fluid. Correcting for non-isothermal compression reduced this to a net power of 1.3 watts. The analytical result is 0.48 watts, surprisingly good agreement considering that the stepped displacer is not the optimum shape and that it is approximately twice as large as the calculated optimum.

CONCLUSIONS AND DISCUSSION

This last comparison with experiment adds confidence to the results of the calculations and suggests that they can provide reliable guidance in the design of such cryocoolers. The insight into the balance between the different loss terms in different parts of the refrigerator may also prove useful. It is reassuring to find that each loss term varies in a manner which can be qualitatively rationalized. The fact that regenerator losses rise sharply in the region below 10 K is consistent with real refrigerator experience. Thus, the model may eventually prove useful in evaluating the real benefits of new regenerator materials prior to tedious experimental tests.

The model could be improved in a number of ways. First, further thought given to the variational method could lead to more rapid convergence and hence savings of computer time. The effects of non-sinusoidal motion and helium mass flow should be more exactly included in the shuttle and regenerator terms to improve their accuracy. The non-ideal properties of the working fluid should be included, a proposition which may not be too difficult since a mechanism for including gas effects (the regenerator term) has already been included. There are, of course, other refinements which might be made since the loss terms rest upon numerous assumptions. Careful study of these assumptions should be used as a guide to such improvements. The Schmidt analysis should probably be included to account for the realistic motion of the displacer in the refrigeration term (equation 15). The fact that the regenerator gap does not go precisely to zero, giving a finite dead volume and increased mass flow should also be included.

As mentioned in the introduction, efficiency is not an adequate measure of performance for low-power cryocoolers such as these. Where we require no refrigeration at all, efficiency is zero. To utilize a refrigerator which has non-zero efficiency providing some finite refrigeration power implies a waste in drive power, since no refrigeration is required by the application.

The simplest and most universal measure of performance for low-power cryocoolers is the absolute value of the power required to run them and maintain a fixed temperature with no dissipation at the cold end. All refrigeration then goes to the interception of heat losses. In principle there is no finite minimum value to this power. In fact, if all heat transfer to some cold volume is reduced to zero, it takes no power at all to maintain that temperature.

While the simple measure of drive power can be broadly applied to intercompare different low power cryocoolers, another measure of performance within particular classes of cryocoolers may prove useful. This is simply to state an efficiency based upon the ratio of the optimum drive power and the actual drive power. Thus, if it takes 50 watts to run the refrigerator shown in figure 8, then the efficiency would be (0.78/50) x 100 = 1.56% since the optimum occurs for a drive power of 0.78 watts. The inefficiency includes not only inefficiencies in the refrigeration

process, but also in the compressor and drive machinery. This performance measure could be useful where other constraints are imposed. For example, suppose the application requires the use of many electrical leads to the cold space. These could be included in the analysis and the performance measure thus generated (through the optimization) would relate specifically to the application. This is more reasonable than using absolute drive power since, although no significant refrigeration power is required, the leads do require additional refrigeration along the length of the machine.

The authors would like to acknowledge the assistance of Ms. Diane Ulibarri with the computer code.

TABLE I

'Standard' Refrigerator Parameters

Stroke	= 5 mm	Frequency	= 1 Hz
Length	= 0.5 mm	Radiation Shield Diameter	= 80 mm
Cylinder Wall Thickness	= 3.0 mm	Displacer Wall	= 3.0 mm
Upper Pressure	= 5.7×10^5 Pa	Lower Pressure	= 1.6×10^5 Pa
Ambient Temperature	= 300 K		
Number of Grounded Rad. Shields	= 4	Number of Super-insulation Layers*	= 40

Power dissipation at bottom end = 0.0 W

* Around each grounded radiation shield.

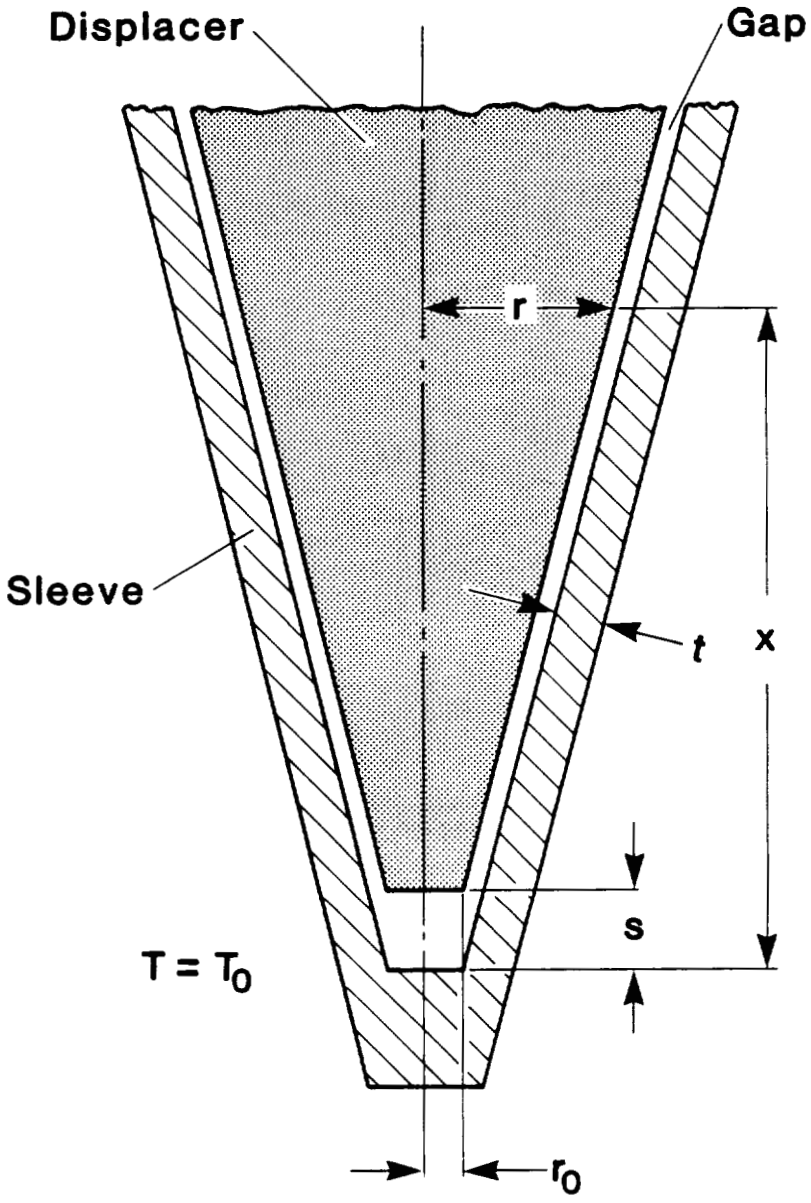

Figure 1. Schematic drawing of the tapered displacer and sleeve. The machine is shown at the top of the stroke, S. x is measured from the bottom end where the temperature is T_0 and the radius of the displacer is r. The sleeve wall thickness, t, is constant. While the taper shown here is conical, r is not generally expected to be a linear function of x.

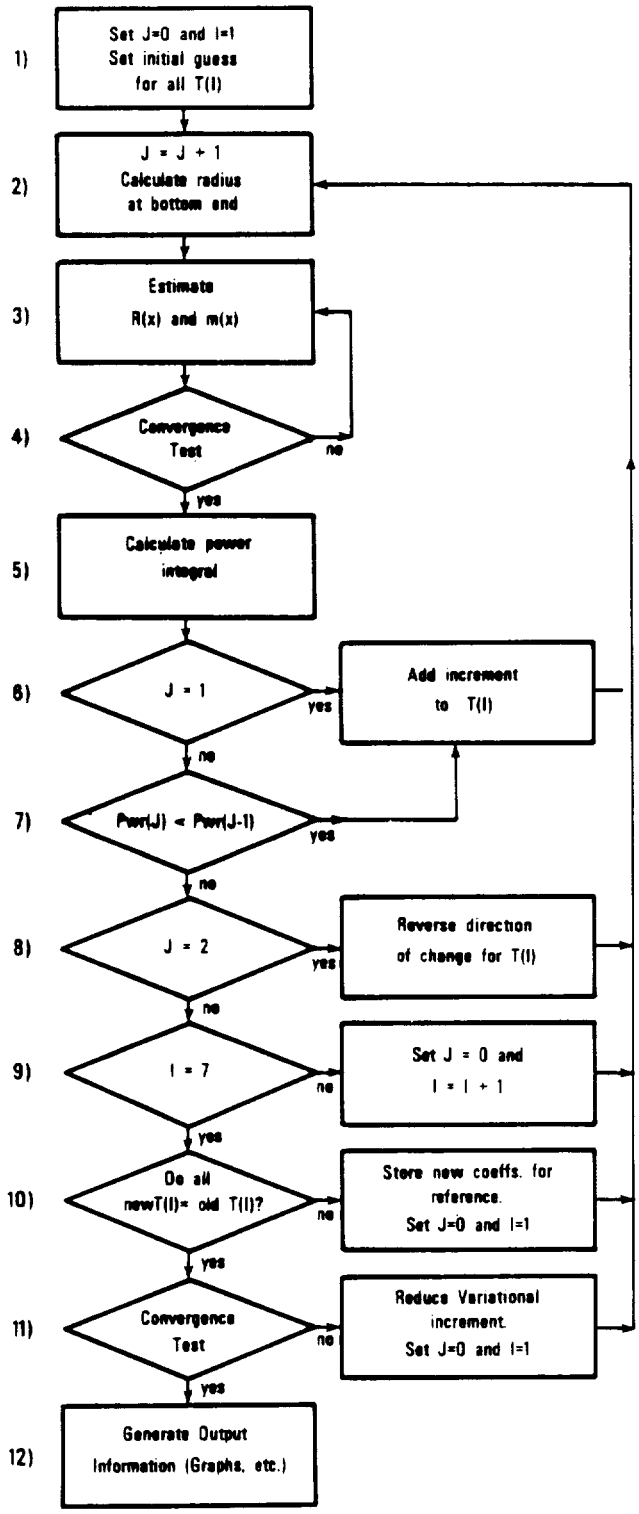

Figure 2. Flow chart for the computer program. The numbers on the left refer to descriptions of the specific steps within the text.

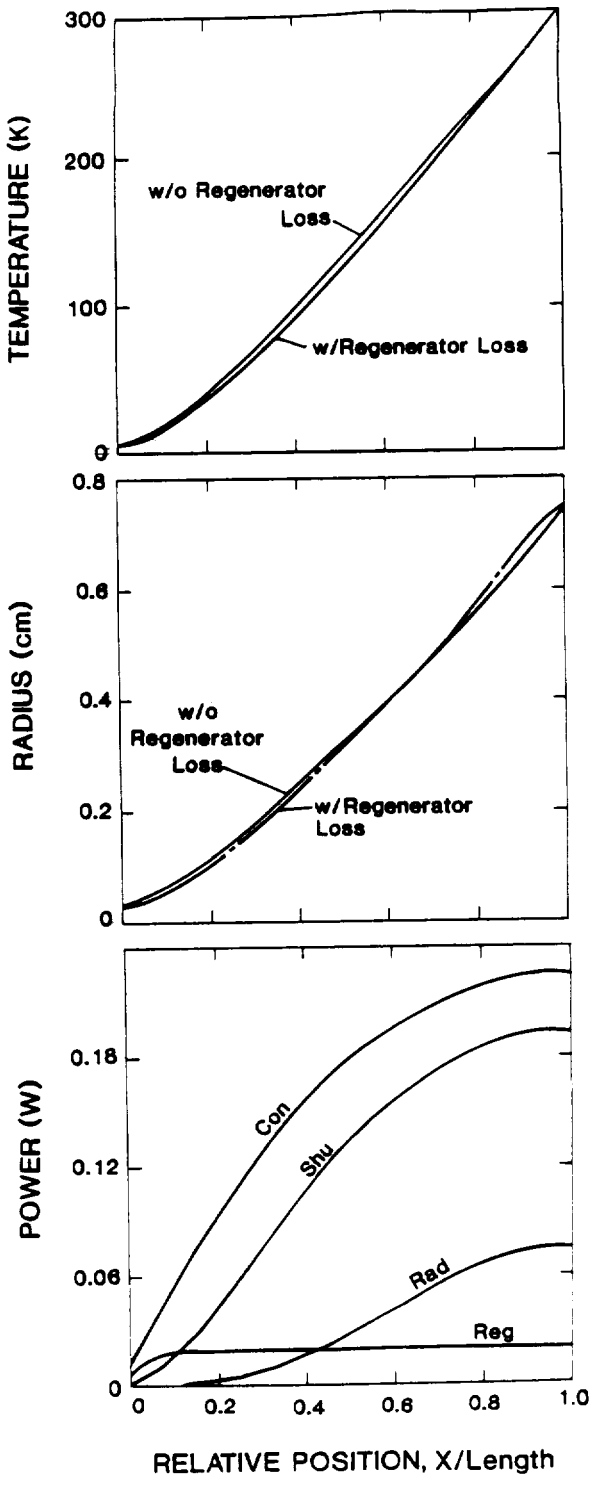

Figure 3. Results of the calculations for T_0 = 5 K and the parameters shown in Table I. The curves in the top 2 boxes represent the optimum results both with and without inclusion of the regenerator inefficiency. The bottom box refers to the case including this loss term. The power is that required to take care of the particular loss term (CON = Conduction, SHU = Shuttle, REG = Regenerator, and RAD = Radiation) below the associated value of x.

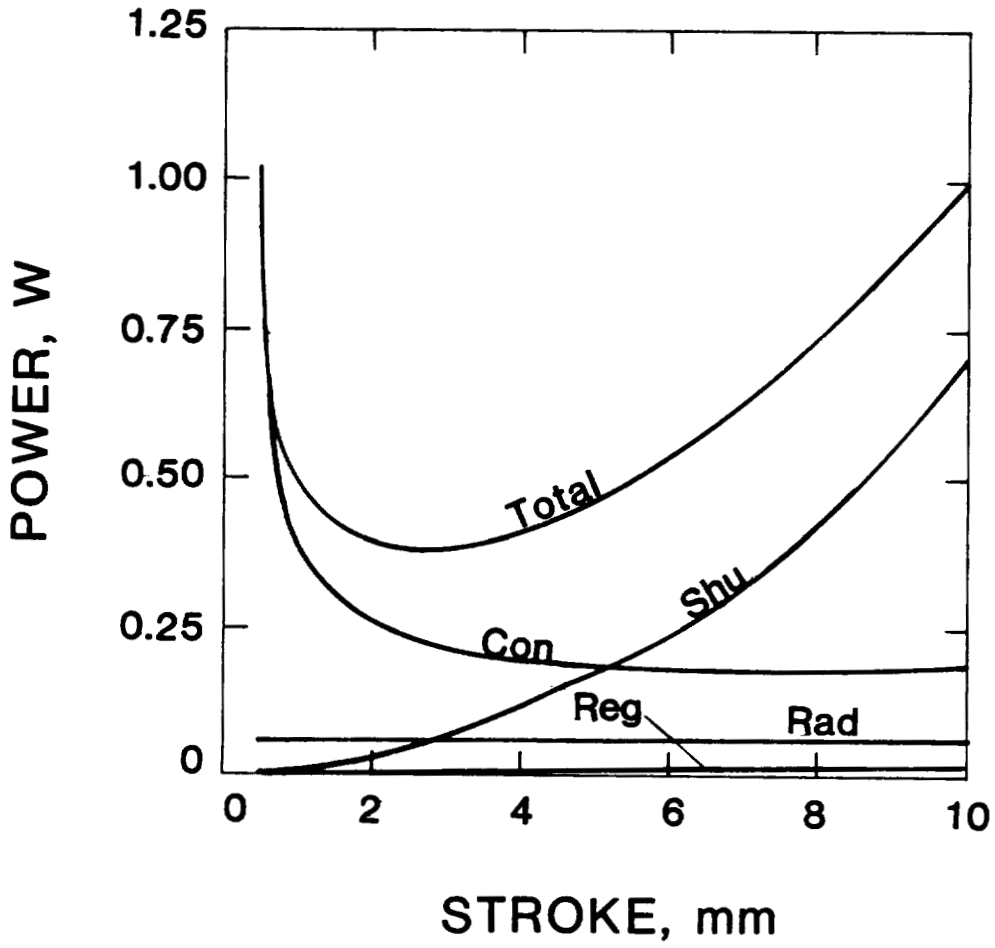

Figure 4. Bottom and top radii for the displacer and power requirement as a function of stroke for T_0 = 10 K and the parameters shown in Table I. The total power which includes the conduction, shuttle, radiation and regenerator terms shown in the figure also includes a small contribution which goes to provide refrigeration in the bottom expansion space. This contribution is negligible on this scale.

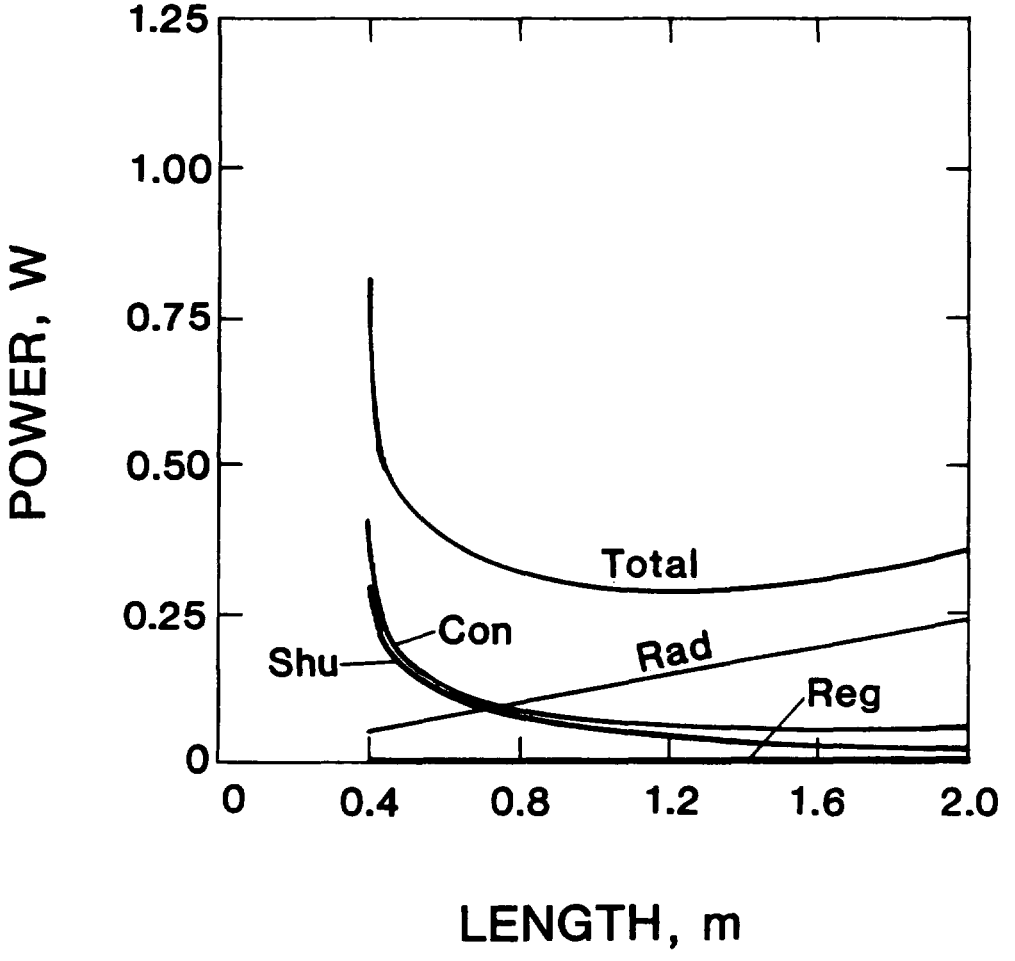

Figure 5. Bottom and top radii for the displacer and power requirement as a function of length for T_0 = 10 K and the parameters shown in Table I. The total power which includes the conduction, shuttle, radiation and regenerator terms shown in the figure also includes a small contribution which goes to provide refrigeration in the bottom expansion space. This contribution is negligible on this scale.

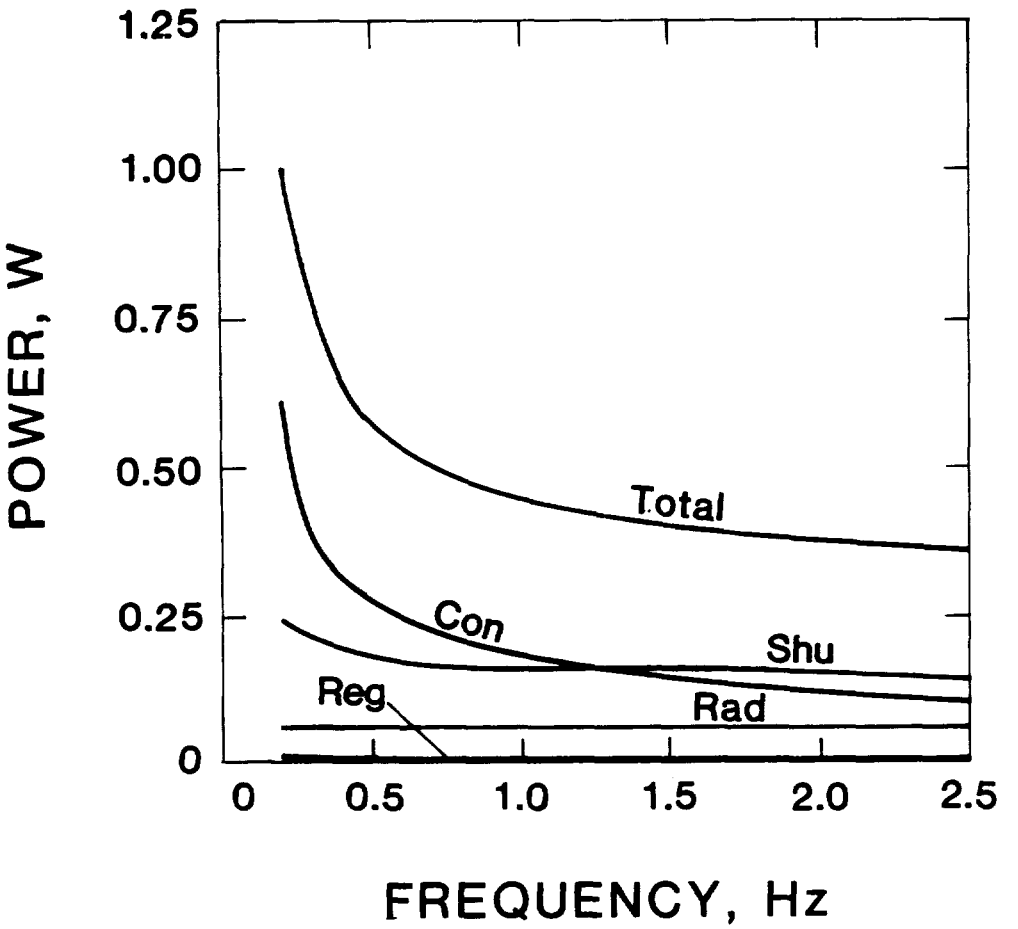

Figure 6. Bottom and top radii for the displacer and power requirement as a function of frequency for T_0 = 10 K and the parameters shown in Table I. The total power which includes the conduction, shuttle, radiation and regenerator terms shown in the figure also includes a small contribution which goes to provide refrigeration in the bottom expansion space. This contribution is negligible on this scale.

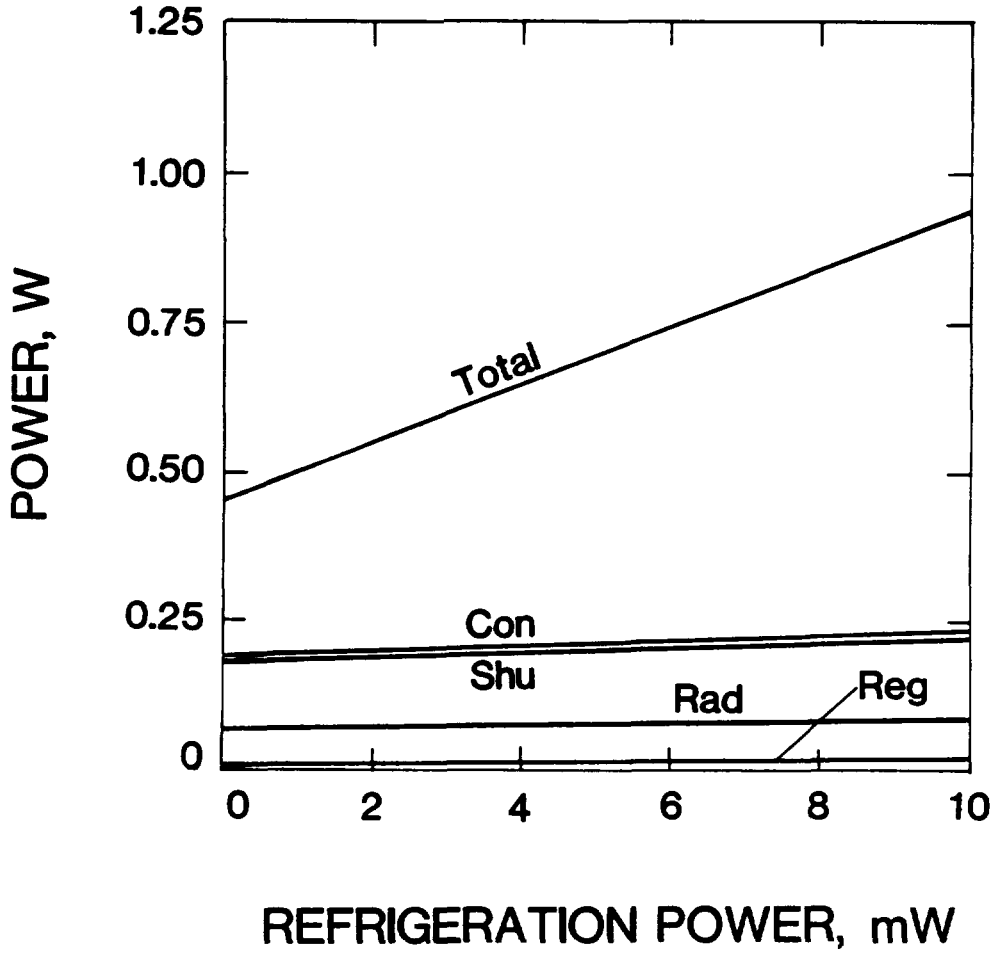

Figure 7. Bottom and top radii for the displacer and power requirement as a function of refrigeration power for T_o = 10 K and the parameters shown in Table I. The total power which includes the conduction, shuttle, radiation and regenerator terms shown in the figure also includes a small contribution which goes to provide refrigeration in the bottom expansion space. This contribution is negligible at refrigeration power = 0, but rises to 0.36 watts at 10 mW (the right intercept).

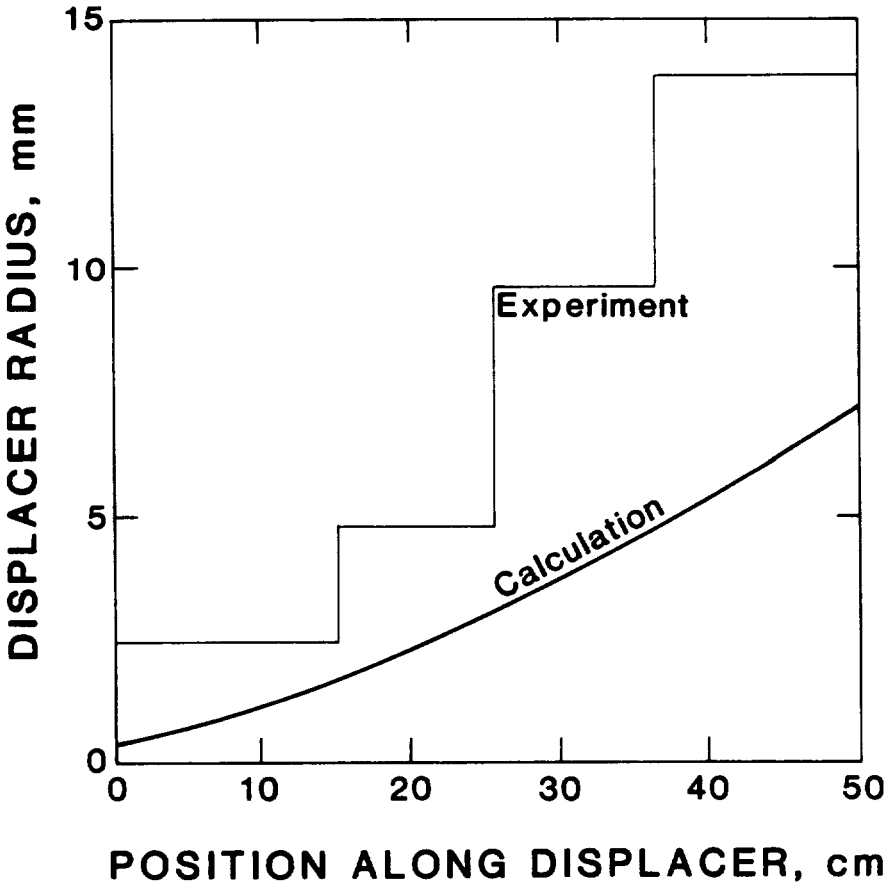

Figure 8. Comparison of a stepped displacer cryocooler with the calculation. The values of the parameters used in the calculation and which describe the refrigerator are shown in Table I.

REGENERATION EFFICIENCY, SHUTTLE HEAT LOSS AND THERMAL CONDUCTIVITY IN EPOXY-COMPOSITE ANNULAR GAP REGENERATORS FROM 4K TO 80K [1]

Ken Myrtle, Suso Cygax, Chris Plateel and Calvin Winter

Department of Physics, Simon Fraser University,
Burnaby, B.C., Canada V5A 1S6

ABSTRACT

Several groups have built epoxy-glass Stirling-cycle cryocoolers which utilize the annular gap between the displacer and the stationary outer sleeve as a regenerator. The cooling power and ultimate cold temperature achieved with cryocoolers of this design are primarly limited by regeneration inefficiency at the low temperature end of the cryocooler. This is because of the rapid decrease in the specific heat and thermal conductivity of the epoxy composite at low temperatures.

A test apparatus designed to simulate a section of a cryocooler has been built. Measurements of regeneration efficiency, shuttle heat loss and thermal conductivity are reported for several regenerator test sections. The test composites were epoxy-glass, epoxy-glass with lead particles, epoxy-glass with activated charcoal and epoxy-graphite. Losses measured for these materials were approximately the same. Losses are in good agreement with those calculated theoretically for an epoxy-glass (G-10) composite. The implications of these results on cryocooler design are discussed.

INTRODUCTION

Stirling-cycle cryocoolers, in which the annular gap between a displacer and a stationary outer cylinder is used as a regenerator, have been demonstrated recently. Zimmerman and Sullivan have demonstrated a five-stage cyrocooler made from a commercial spun glass-epoxy (G-10) outer cylinder and a solid nylon displacer [1]. They report reaching 7K. We have demonstrated operation of a cryocooler at 9K [2]. Our cryocooler was a single-stage conical device with a hollow displacer. Both the displacer and the outer cylinder were made from an epoxy-glass cloth composite.

These research efforts are directed toward the development of a reliable, low-power, closed-cycle cryocooler for operating superconducting devices, especially SQUIDS. The temperatures achieved are already low enough to allow operation of some "high temperature" types of SQUIDS [3,4]. Nevertheless, it would be highly desirable to improve the cryocooler design and reach temperatures below the critical temperature of helium (5.2K). This would have two major advantages. One is that many other types of

---

[1]This research was funded by the British Columbia Science Council. We are grateful to Simon Fraser University for a grant to allow the presentation of these results at this conference.

superconducting materials could be used. The second is that the superconducting apparatus could be immersed in a bath of liquid helium. A liquid bath would provide a large heat reservoir which would damp out rapid temperature fluctuations. If the liquid helium bath was connected to a sealed reservoir of gas at room temperature the bath temperature would be at the boiling point of liquid helium. Long term temperature drifts could be eliminated by monitoring the vapor pressure and using electronic feedback. The use of a liquid helium bath would therefore result in a large reduction in the noise, due to thermal fluctuations, observed in SQUIDS mounted directly on closed cycle cryocoolers [4].

This study of regeneration efficiency is directed toward the problem of designing a cryocooler capable of operation below 10K. The ultimate temperature of the cold end of a Stirling-cycle cryocooler is limited by various heat loss mechanisms. The ultimate temperature is reached when the refrigeration capacity of the volume of gas displaced at the cold end is equal to the heat transferred to the cold end by the loss mechanisms. The amount of heat lost by various mechanisms can be calculated theoretically and these calculations are consistent with experimental ultimate cryocooler temperatures observed [5,2]. Unfortunately, it is very difficult to study the loss mechanisms at low temperature in an experimental cryocooler. This is because the cryocooler performance depends on a combination of loss mechanisms over a wide range of temperatures, as well as on the refrigeration. We have built a special test facility to enable direct measurement of losses under conditions similar to those in an actual cryocooler.

HEAT LOSS MECHANISMS

Heat loss mechanisms present in a cryocooler include regeneration loss, shuttle heat loss, friction, conduction loss, radiation loss and the enthalpy deficit. Convection loss was also present in this test apparatus.

Regeneration loss is the net heat carried by the cycling of helium gas at constant pressure between the warm end and the cold end. When the regenerator is operating efficiently the majority of the heat carried by the helium gas is absorbed and released by the plastic walls of the displacer and cylinder as the helium flows in the annular gap between them. Theoretical formulae for regeneration loss are given in the appendix. Note that, for a fixed pressure and a fixed stroke, the regeneration loss is a strong function of temperature. Both regeneration loss terms are proportional to the square of the mass of helium gas transferred in one cycle. One regeneration loss term is inversely proportional to the conductivity of helium gas and inversely proportional to the gap between the displacer and the cylinder. The other regeneration loss term is inversely proportional to the square root of the product of the heat capacity and thermal conductivity of the plastic. The total regeneration loss therefore has a temperature dependence between T^{-3} and T^{-4}. Regeneration loss is the dominant loss term for temperatures below 20K.

Shuttle heat loss is the net heat carried by the specific heat of the displacer and transferred to the cylinder by the movement of the displacer. It varies approximately as T and is the dominant loss term above 20K. Over a wide range of pressures the shuttle heat loss is independent of the

pressure of the working gas, since the thermal conductivity of the gas does not depend on pressure. Losses measured at low pressures in the test apparatus were therefore primarily shuttle heat loss.

Friction was a significant source of heat in our test facility. It was approximately independent of pressure and temperature and was usually in the neighbourhood of 1 milliWatt. Friction is also very significant in a cryocooler. A common failure mode of cryocoolers is heating due to an increase in friction caused by solidification of impurities in the gap at the low temperature end.

Conduction loss and radiation loss are insignificant at the cold end (<20K) of a properly designed cryocooler. Conduction loss was also measured with this test apparatus.

The enthalpy deficit occurs in a non-ideal gas because the total enthalpy flow from the high temperature to the low temperature is greater than the enthalpy flow in the reverse direction due to pressure variations [5]. This is due to changes in the specific heat with pressure. It can be calculated from the physical properties of helium [6]. As our measurements were done at constant pressure they do not include the enthalpy deficit.

Convection of helium gas is a heat loss mechanism in our test apparatus which is not normally present in a cryocooler (unless the cryocooler is operated upside down). Unfortunately, our test apparatus was "upside down", with the cold end above the warm end. At high pressures convection losses were significant in our tests. The heat loss measurements, reported in Figs. 3 and 4, have been corrected for convection losses, as explained in the section on experimental results.

EXPERIMENTAL APPARATUS

A diagram of the heat loss test apparatus is shown as Fig. 1. The apparatus simulates a section of an actual cryocooler. A displacer (C) is moved up and down with a sinusoidal cycle by means of a stainless steel rod going to room temperature. When the displacer is moved, helium gas in the working space (5) is forced to slide past the displacer, in the gap between the displacer and the outer cylinder (B). The upper working volume is maintained at a fixed temperature by means of an electronic temperature controller. The controller is connected to a heater and a carbon glass thermometer in the copper plate (A). A known amount of heat is applied to the lower working volume by means of a heater in the copper end cap of the cylinder (E). In operation, the lower end of the cylinder (E), is hotter than the upper end (D). We define the "effective thermal conduction" or "heat loss" of the test section as the heat input at (E) divided by the temperature difference between (E) and (A). This "heat loss" is a function of the pressure of helium in the working space (5), the frequency and stroke of the displacer, the mean gap between the displacer and the outer cylinder and the mean temperature of the test section.

The test section is surrounded by a pumped evacuated space (3) and a copper radiation shield at the temperature of the upper (cold) end of the test section. Tests may be made over a wide temperature range by using either liquid nitrogen or liquid helium as a low temperature bath (1). Depending on the temperature desired, different pressures of exchange gas (2) were used to facilitate the electronic temperature regulation.

This design has the special feature that the test section is attached to the flange (A) with bolts and an indium O-ring to facilitate changing test sections. The displacer is fitted with copper end caps (F) and (G) which are always within the copper sections, (D) and (E) respectively, of the cylinder. This feature ensures that the temperature of the ends of the displacer remain fixed at the same values as the ends of the cylinder.

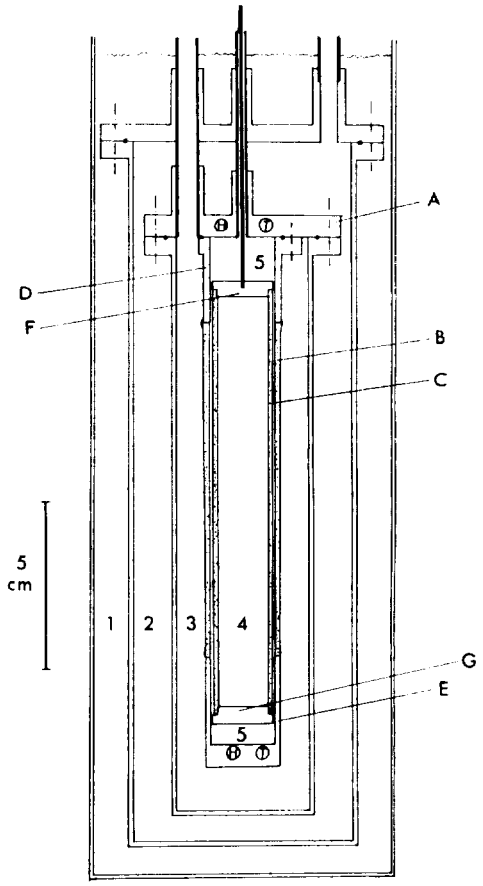

Fig. 1: Regenerator test apparatus.

A Upper copper mounting flange. It is held at a fixed temperature by heater (H) and thermometer (T).
B Conical glass-epoxy cylinder under test. (The taper of the cone is too slight to be noticable in the figure.)
C Conical glass-epoxy displacer under test.
D Copper cylinder flange mounted with an indium seal.
E Copper cylinder end with heater (H) to generate a temperature gradient and a thermometer (T).
F,G Copper displacer end plugs.

The volumes are filled as follows: 1 - Liquid helium, 2 - Exchange gas (helium), 3 - Hard vacuum, 4 - Vacuum (air frozen out) and 5 - Helium working gas.

The impedance of the regenerator to the flow of gas is low. Therefore, the difference in gas pressure between one end of the regenerator and the other is always negligible. The working gas (5) is connected to a large room temperature volume of helium gas. The pressure of the working gas is, therefore, to a good approximation, constant.

This design imposed some limitations. The gas line for the working volume goes through the liquid helium bath. This limited the pressure of the working gas to less than one atmosphere.

MATERIALS TESTED

The test displacer and cylinder sections were made by laying up the epoxy-composite material on a tapered mandril. The wall thicknesses of both the displacers and the cylinders were 1.3 mm. The inside diameter of the cylinder varied from 2.03 cm to 1.78 cm along its 7.6 cm length. Four materials were tested: epoxy-glass, epoxy-glass with 10wt% activated charcoal, epoxy-glass with 60wt% powdered lead and epoxy-graphite cloth. In all cases the displacer was sealed full of air, hence would be evacuated at temperatures below the freezing point of air. The epoxy-graphite displacer was filled with air but was stuffed with glass wool and layers of aluminized mylar to eliminate any convection of gas inside the displacer.

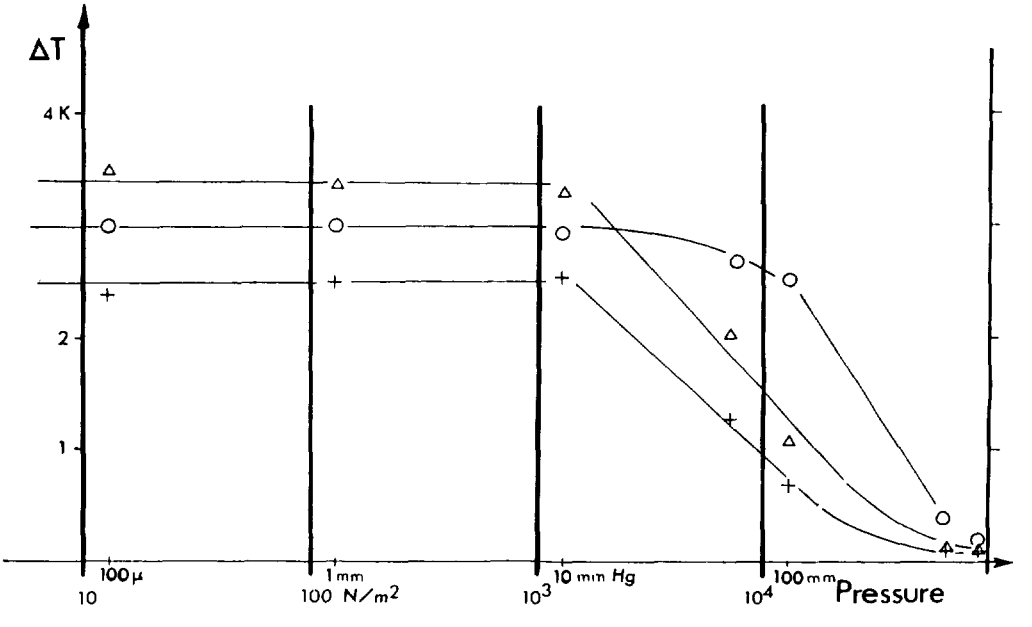

Fig. 2.

Temperature difference between the upper and lower ends of the cylinder, as a function of helium gas pressure, with the upper end held at a temperature of 6.0K.

- o Displacer stationary, heater on (0.65 mW), ΔT_1.
- \+ Displacer moving 0.625Hz 1.3cm stroke, heater off, ΔT_2.
- Δ Displacer moving 0.625Hz 1.3cm stroke, heater on (0.65mW), ΔT_3.

EXPERIMENTAL RESULTS

Typical experimental measurements are shown in Fig. 2 for an epoxy-glass displacer and an epoxy-glass cylinder. The temperature of the upper end of the cylinder was 6K for all of the data points shown. At each pressure three data points were taken. First, 0.65mW was applied to the lower heater, with the displacer held stationary. The temperature difference ΔT_1 between the two ends of the cylinder is plotted in the figure. This is related to the sum of thermal conductivity in the glass-epoxy and to the convection of helium gas in the working space. Measurements at low pressures have negligible convection, and allow calculation of the thermal conductivity of the glass-epoxy.

A second set of data points was taken with the heater turned off, but with the displacer moving up and down at 0.63 Hz, with a stroke of 1.3 cm. As a result of the slight taper of the displacer and cylinder the annular gap varied from 0.2 to 0.4 mm throughout the stroke. The temperature difference ΔT_2 between the upper and lower ends of the cylinder was again measured. This measurement is utilized to determine the amount of frictional heating which resulted from the movement of the displacer.

A third set of data points were taken with the heater turned on (0.65mW) and with the displacer moving giving the temperature differences ΔT_3.

These measurements allow us to estimate the sizes of the various heat loss mechanisms. First, the effective thermal conductivity of the cylinder and displacer (plus convection losses significant at higher pressures) is $\dot{Q}_c/\Delta T_1 = 0.65\text{mW}/\Delta T_1$. The values of thermal conductivity measured for the four materials are in close agreement with the published values for epoxy-glass G-10 [1]. The amount of frictional heating may be determined from the ratio of the temperature rise caused by friction, to that caused by electrical heating. The frictional heat is therefore: $H_f = 0.65\text{mW}\ \Delta T_2/(\Delta T_3 - \Delta T_2)$. The effective conductivity between the upper and lower ends of the cylinder due to regenerator inefficiency and shuttle heat transfer is:

$$\frac{\dot{Q}_{rs}}{\Delta T_3} = \frac{0.65\text{mW} + H_f - \dot{Q}_c}{\Delta T_3} = \frac{0.65\text{mW}}{(\Delta T_3 - \Delta T_2)} - \frac{0.65\text{mW}}{\Delta T_1} \qquad (1)$$

The term on the right corrects for conduction and convection losses. It is also possible to determine the shuttle and regeneration losses separately from this data. The regeneration loss is proportional to the pressure (helium mass flow) squared, whereas the shuttle heat loss is almost independent of pressure for pressures above 10 pascals (0.1 torr). Fig. 3 shows the measured pressure dependence of the sum of regeneration and shuttle heat losses, for a fixed temperature.

The temperature dependence of these two losses is shown plotted in Fig. 4 for a fixed pressure (0.65×10^5 Nt/m^2). Experimental data points are shown for the four types of materials tested. The theoretical shuttle heat loss and regeneration loss, calculated with the equations given in the appendix, are also shown plotted in the figure. The theory is in good agreement with the experimental data points. The four materials tested gave approximately the same losses in spite of their compositional differences.

This is because the thermal properties of the four materials were all dominated by the properties of their major constituent, epoxy. It should be noted that for a mean gap of 0.3 mm the thermal conductivity of helium is low enough that it imposes a significant limitation on regeneration, even if the specific heat of the plastic was higher.

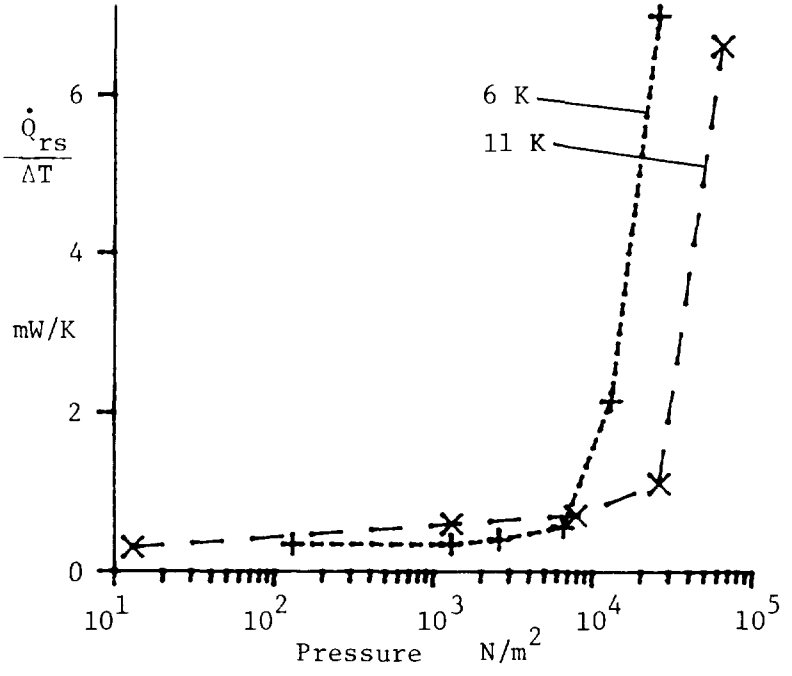

Fig. 3.

Regeneration and shuttle heat loss as a function of helium gas pressure, for two temperatures. Cylinder was epoxy-glass and the displacer was epoxy-glass plus 60% by wt. lead.

CONCLUSIONS

The good agreement obtained between experimental measurements of losses and the theoretical calculations encourages us to examine the implications of the theoretical loss calculations on cryocooler design. Examination of Fig. 4 shows that for temperatures above 20K the shuttle loss is dominant, whereas below 20K regeneration losses are dominant. The equations in the appendix show that an increase in the radial gap between the displacer and the cylinder causes an increase in the regeneration loss and a decrease in the shuttle heat loss. This suggests that the total loss due to regeneration and shuttle heat transfer can be reduced by increasing the radial gap in the warmer parts of the cryocooler and decreasing it at the cold end. This can be effected in a conical cryocooler by decreasing the pitch of the cone at the cold end, since the pitch of the cone is

related to the mean gap if the displacer and outer cylinder touch everywhere at the bottom of a stroke.

Unfortunately, the poor regeneration at low temperatures will not be greatly improved by reducing the radial gap as it is limited by the low heat capacity of the epoxy. The addition of lead to the epoxy should improve this somewhat, but the most we were able to add was 60wt%, which did not make a huge difference in the specific heat.

Regeneration losses at low temperatures will be very large for all regenerator materials. They can be reduced somewhat by decreasing the thermal gradient by extending the tip of the displacer. The result of this modification would be a shape somewhat like that of an exponential horn rather than the simple cone used in our earlier cryocooler.

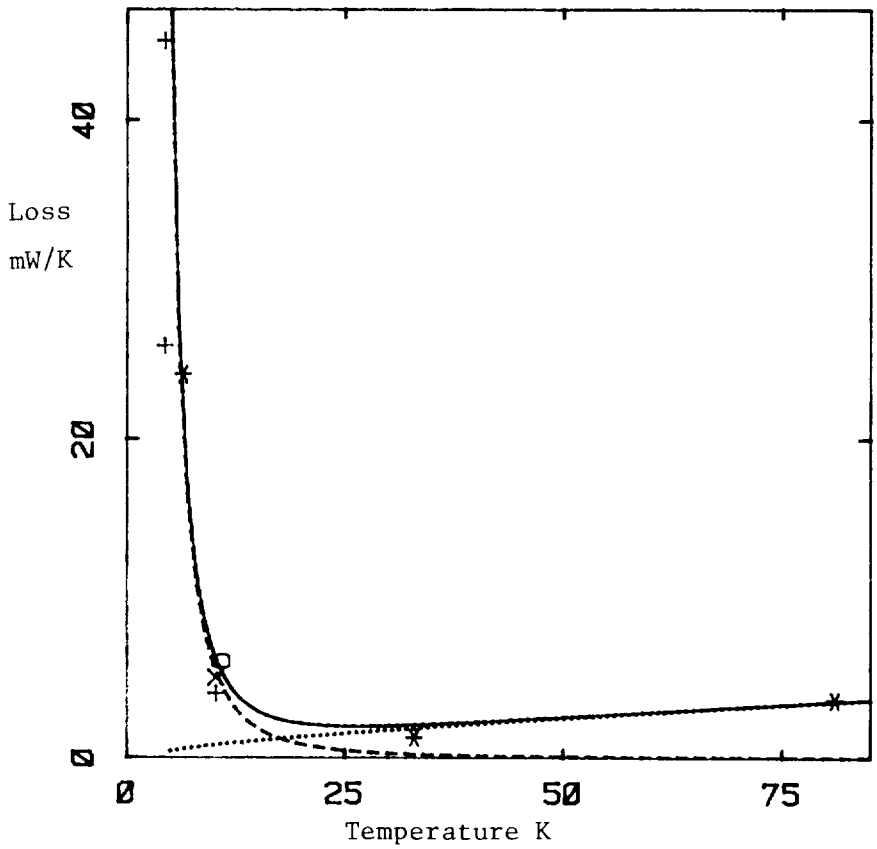

Fig. 4.

Regeneration and shuttle heat loss as a function of temperature for a pressure of 60000 Pascals (0.6 atmosphere).

——— Theoretical regeneration plus shuttle heat loss.

····· Theoretical shuttle heat loss.

- - - - Theoretical regeneration loss.

Experimental data.

* Epoxy glass.

X Epoxy glass plus 60% by weight lead.

\+ Epoxy glass plus 10% by weight charcoal.

o Epoxy with graphite fibers.

APPENDIX: THEORETICAL HEAT LOSS EQUATIONS

The theoretical regeneration and shuttle heat losses plotted in Fig. 4 are derived from published equations for regeneration [2], shuttle heat loss [7], the physical properties of epoxy-glass G-10 [1], and the physical properties of helium [6]. The equations used are reproduced below for convenience.

The regeneration loss $\dot{Q}_{regeneration}$ is the sum of a term due to the finite effective heat capacity of the plastic ($\dot{Q}_{rP}$) and a term due to the limited thermal conductivity of the helium gas ($\dot{Q}_{rHe}$). The Reynolds number is about half that for the onset of turbulent flow even at the lowest temperatures, consequently the conductivity of the gas is calculated for laminar flow conditions.

$$\frac{\dot{Q}_{regeneration}}{\Delta T} = \frac{\dot{Q}_{rP}}{\Delta T} + \frac{\dot{Q}_{rHe}}{\Delta T} \tag{2}$$

$$\frac{\dot{Q}_{rP}}{\Delta T} = \frac{\omega}{16\pi DL} (C_{pHe} M_o)^2 \left(\frac{\omega}{2\rho_P C_P K_P}\right)^{\frac{1}{2}} \tag{3}$$

$$\frac{\dot{Q}_{rHe}}{\Delta T} = \frac{17}{1120} \frac{\omega^2 g}{\pi DLK_{He}} (C_{pHe} M_o)^2 \tag{4}$$

M_o is the mass of helium moved in one cycle. The mass flow is assumed to be sinusoidal, therefore the peak mass flow rates are $+/- \omega M_o/2$.

For our test conditions the $\dot{Q}_{rP}$ term was about twice the $\dot{Q}_{rHe}$ term between 5K and 10K.

The shuttle heat loss $\dot{Q}_{shuttle}$ is due to the effective conduction of the plastic $\dot{Q}_{sP}$ in series with the effective conduction of the helium gas in the gap $\dot{Q}_{sHe}$.

$$\frac{\dot{Q}_{shuttle}}{\Delta T} = \left(\frac{\Delta T}{\dot{Q}_{sP}} + \frac{\Delta T}{\dot{Q}_{sHe}}\right)^{-1} \tag{5}$$

$$\frac{\dot{Q}_{sP}}{\Delta T} = \frac{D S^2}{4L} (\omega K_P C_P)^{\frac{1}{2}} \tag{6}$$

$$\frac{\dot{Q}_{sHe}}{\Delta T} = \frac{K_{He} D S^2}{2gL} \tag{7}$$

For our test conditions the $\dot{Q}_{sHe}$ term dominated the $\dot{Q}_{sP}$ term by more than a factor of two. This indicates the importance of a large gap in reducing shuttle loss at high temperatures.

The thermal conductivity K_p in mW/(cm-K) and the specific heat per unit volume $\rho_p C_p$ in mJ/(K-cm^3) for epoxy-glass G-10 for temperatures from 5K to 300K may be expressed as [1] :

$$K_p(T) = 0.917 + 0.0319\ T - 3.67 \times 10^{-5}\ T^2, \text{ and} \quad (8)$$

$$\rho_p C_p(T) = -14.9 + 3.75\ T + 0.0335\ T^2 - 9.21 \times 10^{-5}\ T^3. \quad (9)$$

SYMBOLS:
D - diameter of the displacer (1.9 cm)
ω - 2π times the frequency of cycling (0.63Hz x 2π)
K_{He} - Thermal conductivity of helium gas.
C_{pHe} - Heat capacity per unit mass of helium gas.
K_p - Thermal conductivity of the plastic (G-10).
ρ_p - Density of the plastic.
C_p - Heat capacity per unit mass of plastic.
ΔT - Temperature difference between the ends of the test section.
g - Mean radial gap between the displacer and cylinder (0.3 mm)
L - Length of test section (7.6 cm).
S - Stroke (1.3 cm)

DISCUSSION

Ronald E. Sager - Was your radiation shield isothermal or did it match the temperature gradient of the experimental apparatus?
Calvin Winter - The radiation shield was isothermal. It was held at the temperature of the coldest (top) end of the regenerator under test. The effects of radiation were negligible for tests at 6K and 11K.
Donald B. Sullivan - Does variation of the gap affect the operation of tapered displacer cryocoolers?
Calvin Winter - Yes. The tip region of the displacer will have a smaller slope and therefore a smaller variation in the gap when the displacer is moved, than the base region of the displacer. A smaller average gap at the tip than at the base will tend to reduce losses. Unfortunately, it is not possible to make the gap at the tip small enough because the resultant friction will render the cryocooler inoperative.

REFERENCES

[1] Zimmerman, J.E., Sullivan, D.B., National Bureau of Standards Technical Note 1049 (1982).
[2] Myrtle, K., Winter, C. and Gygax, S., Cryogenics, 22:139 (1982).
[3] Nisenoff, M., National Bureau of Standards Special Publication 607, page 195 (1981).
[4] Sullivan, D.B., Zimmerman, J.E. and Ives, J.T., ibid [3] page 186. Also published in NBS Technical note 1049, page 96 (1982).
[5] Radebaugh, R., XV International Congress of Refrigeration, Venice, September 1979, paper number A 1/2-16.
[6] McCarty, R.D., Thermophysical properties of He-4, NBS Technical Note 631, (1972).
[7] Zimmerman, J.E., Radebaugh, R., ibid [3] page 59. Also published in ibid [1] page 45.

A 10°K TRIPLE-EXPANSION STIRLING-CYCLE CRYOCOOLER

W. Newman and C. S. Keung
Philips Laboratories, Briarcliff Manor, New York 10510

ABSTRACT

This paper describes the design of a triple-expansion closed cycle Stirling cryocooler optimized for a cooling load of 50 mW at 10°K. The cooler has been designed with the objectives of low power, low weight, compactness, low mechanical motion, low electromagnetic noise, and low output temperature fluctuations. The design employs a direct drive linear motion piston motor and a triple-expansion free displacer. Piston motion is controlled by feedback from an optical position transducer. Mechanical vibrations are attenuated with a passive resonant counterbalance. Electromagnetic noise is attenuated with layered high permeability magnetic shielding. The regenerators move with the displacer within a thin titanium cold finger. The piston and displacer oscillate at 8.33 Hz on bearings and seals of reinforced Teflon™. The cooler is designed to provide the desired 50 mW of cooling at 10°K with a power input of less than 100 W. The piston can be driven at a greater stroke to produce up to 200 mW of cooling with an input power of 250 W. A lead and copper cold tip heat exchanger will limit temperature fluctuations to within 0.01°K. The cooler weight estimate is 35.9 kg for the thermodynamic components, 17 kg for the vibration absorber, and 8.6 kg for the electromagnetic interference (EMI) shielding. The cooler length without Dewar and vibration absorber is 710 mm.

INTRODUCTION

Development of small, efficient cryogenic refrigerators has been fostered by the requirements of infra-red detection systems. Infra-red system cryocooler requirements typically include high efficiency, compactness, low weight, low vibrations and long, maintainance-free operation in the 20 to 80°K temperature range. Stirling cycle coolers have proven to be well suited to these requirements. More recently, stricter requirements have arisen from increasing interest in superconducting quantum interference devices (SQUID) and magnetic gradiometers. For these devices, it is desirable to have coolers which operate at temperatures below 10°K. In addition to the efficiency, compactness, weight, vibration and reliability considerations, SQUID devices require that the associated coolers produce extremely low magnetic noise and low temperature fluctuations.

This paper describes the design of a Stirling cryocooler which was funded by the Office of Naval Research with the objective of bringing cryocooler technology closer to meeting SQUID requirements in a practical unit. The goals for this design were to produce 50 mW of cooling at 10°K with less

than 250 W power consumption in a reliable unit with minimum weight, size, vibrations, temperature variations, and electromagnetic noise. The design presented herein has not yet been fabricated. However, the performance is projected with confidence, since it is based on an earlier low temperature machine, analysis by the Philips Stirling cycle optimization program, and techniques proven in existing (albeit higher temperature) Philips coolers. The cold finger design of the unit described below is similar to an experimental machine which attained a minimum no-load temperature of 7.8°K [refs. 1,2]. In addition, bearing, seal and driver techniques were adapted from various Philips designs, including the MC-80 [ref. 3], the Johns-Hopkins University of Applied Physics Laboratory cooler [refs. 4,5], and the NASA-Goddard unit [ref. 6].

DESIGN APPROACH

THERMODYNAMIC CONSIDERATIONS

The present design employs three stages of expansion and three metal matrix regenerators which oscillate with the displacer within a thin walled titanium cold finger. The choice of metal regenerators was an early pivotal decision since metal in motion near a sensitive magnetometer might produce unacceptable interference. An alternative approach is to use extended gap regeneration and a non-metallic displacer. The extended gap approach typically suffers the disadvantages of an unusally long displacer, low cooling capacity, potential electromagnetic interference (EMI) from static electric charge accumulation on the moving displacer, and short duration of continuous operation due to possible cryopumping of organic vapors toward the cold tip.

Thermodynamically, the metal regenerators were found to be adequate down to the 10°K cooling range, both by experiment and by analysis. The magnetic interference produced by eddy currents induced in the moving metal displacer by the earth's magnetic field were estimated to be extremely low. This is due to the relatively high electrical resistivity and thin construction of the titanium displacer shell, as well as the low displacer amplitude and frequency. Interference originating from the displacer will be dominated by noise generated by even the best, shielded, compressor motors. Further, displacer originating interference has the compensating characteristic, like the motor interference, of being periodic. Thus, it was decided to proceed with metal regenerators.

After choosing the regenerator material, the cooler parameters were optimized. Optimization is performed by constraining the magnitude and temperature of cooling at the cold tip, then searching for the combination of variables which result in minimum power input. The optimal search is normally halted at the judgement of the designer in order to include considerations of total size and weight. Thus, the total cold finger length and piston displacer volume were chosen as a compromise between total size and efficiency.

DYNAMIC CONSIDERATIONS

After optimizing the thermodynamics, the mechanical dynamics were analyzed. The thermodynamic optimization resulted in specifications on the displacer amplitude, speed and phase shift with respect to the piston. This motion can be produced by a mechanical linkage connected to a crank drive, or by a separate displacer linear motor, or by resonance (alias "free displacer"). Since the mechanical linkage requires extra bearings and seals, and a separate driver requires more space and power, the resonant approach was chosen. When the piston mass and diameter are selected to achieve resonance with the compression pressure wave, the motor load is optimized. When the piston is not in resonance, the motor must also supply substantial reactive power resulting in lower efficiency. The equations for interfacing piston and displacer dynamics with the Stirling cycle thermodynamics for free-piston free-displacer machines have been presented by A. K. de Jonge in reference 3.

The resonance condition for the piston left a single design degree of freedom along a constrained line of piston mass versus amplitude at constant compressor displaced volume. Various linear motor designs were then analyzed to find the combination of piston mass and stroke which permitted the minimum weight motor to supply the necessary compressor power with 250 W electrical input power.

Since attaining the desired cooling at 10°K was essential, weight and size minimization were relaxed somewhat to arrive at a success oriented design. Thus, the cooler was optimized for 200 mW of cooling at 10°K with an input power of 250 W rather than the specified goal of 50 mW at 10°K with the same input power. The resulting design is flexible; power consumpion can be reduced for a reduced cooling load by running at a decreased piston stroke while keeping the piston in resonance. Predicted power consumption for a 50 mW load at 10°K is less than 100 W, including electronic driver losses. Further power reduction is possible for lower cooling loads, and excess cooling capacity can be used to accelerate cooldown time. Most importantly, the design has a high probabiliy of meeting the specified power versus cooling requirement. Temperature fluctuations of the cold tip are compensated by the cold tip heat exchanger, which has a high heat capacity. Mechanical vibrations are reduced with the use of an external passive vibration absorber. EMI attenuation is accomplished by enclosing the motor, the dominant source of low frequency noise, with layered, high-permeability, magnetic shielding.

A layout drawing of the resulting design is shown in figure 1. Table I summarizes the design objectives and table II lists the thermodynamic design values. The basic subsystems of the cooler are described in the following sections, viz., piston/motor, displacer, cold finger, vibration absorber, EMI shielding, and additional peripheral components.

SUBSYSTEM DESIGN

PISTON/MOTOR

The piston assembly includes a cylindrical piston and a concentric, linear-motor armature. The piston is driven directly by a linear motor. The motor and its housing dominate the weight of the thermodynamic components, and thus merit particular attention in their design. These components are shown in figure 2.

The thermodynamic optimization requires that the piston sweep a volume of 153 cc, with a resultant pressure wave of 0.34 to 0.69 MPa. For optimal system efficiency with a linear drive motor, the diameter of the piston and mass of the piston assembly should be selected so that the assembly resonates with the spring force of the compression space, at the cooler speed.

The geometry and dimensions of the motor were optimized with finite-element mappings of the stator and gap flux densities. The finite-element, magnetic-field program permitted the inclusion of analytically intractable effects such as nonlinear hard and soft magnetic materials, saturation, and leakage. Eddy current losses are reduced by laminating the stator with radial cuts. The motor design values are given in table III.

To minimize the side loads on the piston seal and bearings and to meet the mass requirement for the piston assembly, a moving-coil rather than moving-magnet motor design was chosen. Power transfer to the moving coil throughout its relatively large excursion is accomplished with rolling leads consisting of strips of beryllium copper. During operation, the circular deformation of the strips results in an acceptable peak oscillating stress of 275 MPa (40,000 psi), nonreversing.

The long piston excursion makes a mechanical spring impractical as a position centering device. Therefore, the piston motion is controlled with position feedback to the motor drive amplifier. An optical transducer was selected as the position sensor.

The piston seal and bearings consist of thin layers of Rulon™ (a reinforced Teflon™) bonded to the contacting surfaces of the piston assembly. The Rulon™ surface, sliding along the cylindrical wall of the compression space, acts as a bearing as well as a seal. A second bearing at the opposite end of the piston assembly also consists of a Rulon™ surface sliding on a guide which prevent rotation of the piston assembly. To facilitate maintenance the bearings are easily removable and replaceable.

The piston assembly is made of titanium to minimize armature weight and to match the thermal expansion of the Permendure motor stator. Shock pads located at both extremes of the stroke prevent damage during transit or in the event of overstroke during operation. The remainder of the motor housing is made of aluminum for low weight, low cost, and ready availability of material in the required dimensions. All motor housing joints use reusable metal C-rings for low leakage and for ease in disassembly.

DISPLACER/REGENERATOR

The displacer and regenerator are the most critical components of a Stirling cycle cooler. The displacer in this cooler has three stages of regeneration with three corresponding expansion spaces. The regenerators oscillate as an integral part of the displacer. The displacer is not independently driven, but oscillates with a mechanical spring in response to the compressor pressure wave. The regenerator must be designed for efficient transient gas-solid heat transfer, yet have low conduction heat leak and low flow losses. The transient heat transfer and thermal energy storage must be compatible with the charge pressure and speed of the cooler. The above requirements dictate an optimal displacer amplitude and phase shift relative to the piston. Furthermore, practical requirements, such as reasonable length, weight, and reliability, must be met. The resulting design values are listed in table IV.

Rulon™ bearing/seal surfaces similar to those of the piston are used at the two link locations and at the warm end of the first (warmest) regenerator. Though not be as easily replaceable as the piston seals. such replacement will be infrequent because the displacer seals will have a lower wear pressure and a much lower wear velocity. Furthermore, some leakage past partially worn regenerator seals will not have a serious effect, since the pressure drop across the seals is low, and the leakage flow will experience some gap regeneration in the displacer clearance space.

Lead was chosen as the third-stage regenerator material because of its ability to maintain its heat capacity at low temperatures.

Annulus-type heat exchangers are used to remove thermodynamic waste heat and to transfer heat from the device to be cooled to the working fluid. A linear variable differential transformer (LVDT) monitors the displacer position. The signal from this transducer can be used to measure the displacer amplitude and phase shift in order to optimize the mass and spring stiffness which are adjustable in the cooler design. The LVDT is packaged concentric with the mechanical spring and thus adds no additional length to the machine.

COLD FINGER

The cold finger and Dewar are shown in figure 3. The cold finger is the thin pressure vessel which contains the displacer. It must be thin to minimize the heat leak from the warm end of the cold tip, yet have the structural integrity to support the mass of the displacer, the cold-tip heat exchanger, and the device to be cooled. Also, it must contain a varying helium pressure without fatigue and not be excited in any vibration modes due to the displacer dynamics. For low heat leak and high mechanical strength, the cold finger is made of titanium. For the design dimensions and materials, a conservative stress analysis predicts:

Lowest mode frequency:	> 100 Hz
Worst case deflection due to all masses:	< 0.01 mm
Hoop stress from peak pressure:	< 27 MPa (4,000 psi)

At the cold tip there is a lead cap for damping temperature variations. The lead provides a large heat capacity for thermal damping. The mass of the lead is 500 g. Its thermal mass will attenuate the temperature variations to less than $\pm$ 0.01°K.

Stainless-steel coaxial signal leads (Uniform Tubes UT-85SS) are provided for connection to the cryogenically cooled device which is attached to the end of the cold finger. The leads are cooled continuously along their length by coiling them about the cold finger in contact with the titanium wall. Further, several turns of the leads are in thermal contact with two titanium disks extending radially from the first and second expansion spaces. These two disks act as heat exchangers for the leads as well as axial thermal radiation shields.

The cold finger is enclosed by an evacuated Dewar. Its interior surface is covered with layered superinsulation which provides radial radiation shielding with minimal conduction losses.

VIBRATION ABSORBER

The linearly reciprocating motions of the piston and displacer give rise to an axial momentum imbalance. This imbalance can be compensated with a third mass oscillating in opposition. Such a mass in resonance with a linear mechanical spring will be excited to absorb vibrations at its natural frequency.

Because the piston oscillates against the nonlinear gas spring of the compression space, the resulting piston motion is nonsinusoidal. The imbalance force is, therefore, composed of a large force at a fixed frequency plus superimposed higher harmonic imbalances. A passive absorber will attenuate only the imbalance at the fundamental frequency. For additional compensation, thecooler's position sensors can be used. The higher harmonics of the piston can be attenuated by using the optical sensor in position feedback to the piston motor to enforce pure sinusoidal motion. If further vibration attenuation is required, an active vibration compensator could be built to replace the passive design.

A passive vibration absorber (see fig. 4) was designed for this cooler. It is an external unit which bolts to the back plate of the motor housing, coaxial with the piston and displacer. Resonance tuning is accomplished with a removable mass tuning ring on the moving countermass. Spring linearity is maintained with relieved helical spring mounts. To insure low damping, the countermass is supported only by its springs. Since the countermass is not guided in linear bearings, it must be designed so that its various degrees of freedom do not have resonant frequencies close to the speed of the cooler. Optimization criteria of the countermass included low spring stress, low weight, and separation of modal frequencies. The resulting design values are given in table V.

EMI SHIELDING

The dominant source of electromagnetic interference from this cooler is the piston motor. The motor coil current, which oscillates at 8.3 Hz, induces a large, time-varying, magnetic field. This interference is attenuated by the surrounding motor stator, and further attenuated by shielding that encloses the piston motor. For a conservative calculation of shielding effectiveness, the stator attenuation was ignored. A two-dimensional, finite-element, magnetic field program was used to analyze the static field due to the peak current in the coil within the symmetric enclosure. Since the coil excitation is low frequency, shielding effectiveness is dominated by reluctance considerations rather than by eddy-currents; thus, a quasi-static analysis is valid.

Figure 5 shows a magnetic flux plot for one quadrant of the cross section of the motor coil in free space. There is rotational symmetry, as well as reflected symmetry, in the negative axial direction. The magnetic material chosen, Hipernom (Carpenter Technology Corp.) alloy, has a minimum permeability of 100,000 and a saturation flux density of 0.4 Tesla. Figure 6 shows the effect of enclosing the coil with a Hipernom cylindrical can connecting the two end plates. The peak field within the enclosure is 0.02 Tesla. The peak field within the 0.76 mm (0.030") thick shield is 0.24 Tesla. The peak field at the cold tip location is less than 0.1 micro Tesla. Additional layers of shielding material at the end plates produce further attenuation, but their influence is beyond the numerical accuracy of the field program. Multiple radial shielding layers for the cylindrical can will provide no additional attenuation of EMI at the cold tip.

The shielding design consists of a single layer of 0.76 mm (0.030") Hipernom supported by a shell of aluminum for the radial shielding, and multiple layers of Hipernom at the end plates for axial shielding. The end plates consist of three disk layers of 0.76 mm (0.030") Hipernom separated by two layers of 5 mm (0.200") copper. The separating copper disks provide an optimal reluctance gap as well as high-frequency eddy current shielding. Both end plates experience some leakage through bolt holes. The hole locations are placed off axis, as far as possible, to reduce the contribution of this leakage to the magnetic noise at the cold tip. Also, gas passages for helium flow between the compressor and displacer have been designed to minimize the effects of magnetic leakage.

The rear end plate and cylindrical can are external, and thus easily removable from the cooler. The end plate which forms the manifold between the displacer and piston can be removed if it is replaced with a similar plate to form the gas manifold and seat the C-seals. Thus, the shielding can be increased, if necessary, or removed, if not needed.

PERIPHERAL EQUIPMENT

Peripheral support equipment for the cooler consists of motor driver electronics and an ambient, forced-convection cooling system. The piston motor requires a dc power supply of at least 200 V, 250 W. The motor

driver is a pulse-width-modulated amplifier which can achieve a power transfer efficiency of 85%.

The cooling system is required to remove the heat of compression and the motor losses from the ambient heat exchanger. This can be accomplished with a closed-cycle recirculating bath, or with an open-cycle flow of any available liquid at ambient temperature. The flow requirements of 3 liters per minute through a pressure drop of 0.2 MPa (3 psi) can be satisified with a small water pump consuming less than 5 W.

The peripheral equipment is commercially available, although custom design would reduce power, weight, and size. This support equipment can be easily detached and transported separately.

DISCUSSION OF RESULTS

The given design meets or betters the goals for cooling and power consumption. Extensive effort was expended to minimize vibrations and EMI; the resulting noise, however, may not meet the demanding design goals. The total system weight is substantially higher than that of the goal; a weight breakdown is given in table VI. The limiting factors and trade-offs are discussed below.

The thermodynamic efficiency of the cooler is primarily limited by the regenerator efficiency. The responsible effect is the loss of specific heat of all materials at low temperature - a problem that has long been recognized. An improvement in regenerator efficiency would require an impractical geometry for an operational cooler (excessively long displacer) or a breakthrough in materials development. Nonetheless, the current displacer design meets the specified thermodynamic objectives.

The cooler will provide cold in excess of the prescribed 50 mW; specifically, 200 mW of cooling at 10°K at the maximum allowed input power of 250 W. By reducing the piston amplitude, the machine would provide the 50 mW of cooling with less than 100 W input power. For lower, steady-state cooling loads, the piston amplitude and corresponding input power requirements can be decreased even further. Conversely, at full power, the reserve cooling capacity can be used to accelerate the cooldown time. At 50 mW net cooling, the cooldown time is expected to be about six (6) hours.

The vibrations and EMI of the cooler were attenuated as far as practical with reasonable weight, size, power, and complexity. Additional attenuation could be achieved with added mass, active vibration compensation, more EMI shielding, active field compensation, or with a motor design stressing noise reduction rather than weight and efficiency. Each of these approaches involves penalties in system weight or power, for only a marginal reduction of noise.

Further noise attenuation could be accomplished through a major design revision. The cooler could be redesigned as a split system, allowing the compressor, the primary offending component, to be separated from the

displacer. This approach also would involve some penalties in efficiency and weight.

An option, if permissible to the operational constraints of the superconducting device, would be to run the cooler intermittently. Assuming 50 mW of excess cooling capability at 10°K decreasing to 0 W cooling at 8.5°K, the cooler could lower the temperature of the cold-tip thermal mass from 10°K to 9°K in roughly 60 seconds. Upon shutting off the cooler power, the vibrations and EMI noise generated by the cooler would cease. The heat leak through the regenerator matrix and stagnant helium, coaxial leads, cold finger wall, plus the Dewar losses, would cause the cold tip temperature to rise at a rate of roughly 2°K/minute. This would clearly not meet the desired temperature regulation of $\pm$ 0.01°K. However, a known, repeatable, smooth monotonic temperature ramp may be an acceptable disturbance subject to electronic compensation at the device output. This approach would satisfy the desired noise requirement and result in considerable weight savings, since the vibration absorber and EMI shielding could be eliminated.

DISCUSSION

Question by S. Shtrikman, Weizmann Institute of Science, Rehovoth, Israel: What is the phase angle between the motion of the displacer and that of the pressure pulse? To what is this angle optimized?

Answer by author: The phase angle is estimated to be 30°. For designs in which the displacer is driven by the pressure wave created by the piston motion. The optimized phase angle is the one that maximizes cold production for a given piston stroke.

Question by D.E. Daney, National Bureau of Standards, Boulder, Colorado: In computing the refrigeration capacity, do you see $\oint$Vdp or $\oint\alpha$Vdp where α is the dimensionless thermal expansivity?

Answer by author: In calculating the gross cold production, the expression $\oint$pdV, which is based on the isothermal model, is used. Non-isothermal effects are included in the calculation of net cold production.

TABLE I. DESIGN OBJECTIVES.

Cold production:	50 mW @ 10°K
Input power:	< 250 W
Weight:	minimize (25 kg goal)
Magnetic noise:	minimize (1.0 micro Gauss goal)
Vibrations:	minimize (goal of 0.1 micro-radian rotation of cold tip)
Cold tip temperature regulation:	fluctuations < 0.01°K
Cooldown time:	< 24 hours

TABLE II. THERMODYNAMIC DESIGN VALUES.

Mean pressure:	0.49 MPa (4.84 atm)
Speed:	8.33 Hz (500 cpm)
Piston amplitude:	45 mm (1.77")
Piston diameter:	46.5 mm (1.83")
Piston mass:	2.6 kg
Displacer amplitude:	3.73 mm (0.147")
Displacer diameters:	18, 25, 40 mm
Displacer phase shift:	52°
Displacer mass:	0.55 kg
Displacer spring stiffness:	14.5 kN/m (82.8 lbf/in.)
Expansion space temperatures:	10, 53, 105°K
Maximum pressure:	0.69 MPa (6.83 atm)
Minimum pressure:	0.34 MPa (3.37 atm)
Cold Production:	200 mW @ 10°K
Mechanical input power:	180 W

TABLE III. MOTOR DESIGN VALUES.

		Stator	
Magnets:	Material		$samarium_3cobalt$
	Energy product		160 kJ/m^3 (20 MG-Oe)
	Magnetic ring		
	Dimensions:	Axial length	72.5 mm
		Inside diameter	105.3 mm
		Outside diameter	127.3 mm
Yoke:	Material		vanadium Permendure
	Stator flux density		2.1 Tesla
	Gap flux density		0.45 Tesla
		Armature	
Coil:	No. of turns		336
	Resistance		1.54 ohms
	Inductance		71.0 mH
	Peak current		4.4 A
	Peak voltage		87 V
	Electrical input power		192 W
	Mechanical output power		175 W
	Efficiency		91%
	Dimensions:	Axial length	72.5 mm
		Inside diameter	98.2 mm
		Outside diameter	105.0 mm

TABLE IV. REGENERATOR DESIGN VALUES.

Regenerators

Temperature (°K)	10	55	105
Type	lead spheres	phosphor bronze mesh	phosphor bronze mesh
Length (mm)	50.0	27.2	50.0
Area (sq. mm)	227.0	452.0	1163.0
Fill factor	0.63	0.42	0.34
Sphere or wire dia. (mm)	0.135	0.041	0.041

TABLE V. VIBRATION ABSORBER DESIGN VALUES.

Springs: Combined pair	
Combined axial stiffness	32.6 kN/m
Combined lateral stiffness	52.2 kN/m
Moving Mass:	
Mass	11.9 kg
Polar inertia	0.029 kg-m^2
Rocking mode moment of inertia	0.050 kg-m^2
Modal Frequencies:	
Axial translation	52.3 rad/sec
Lateral translation	66.2
Rotation about axis	22.5
Rocking mode	80.2
Operating Conditions:	
Peak force	350 N
Peak amplitude	11.0 mm
Peak spring stress	122.0 MPa (18,000 psi)

TABLE VI. WEIGHT SUMMARY.

Compressor	27.2 kg
Expander	8.7 kg
EMI Shielding	8.6 kg
Countermass	17.0 kg
Total	61.50 kg

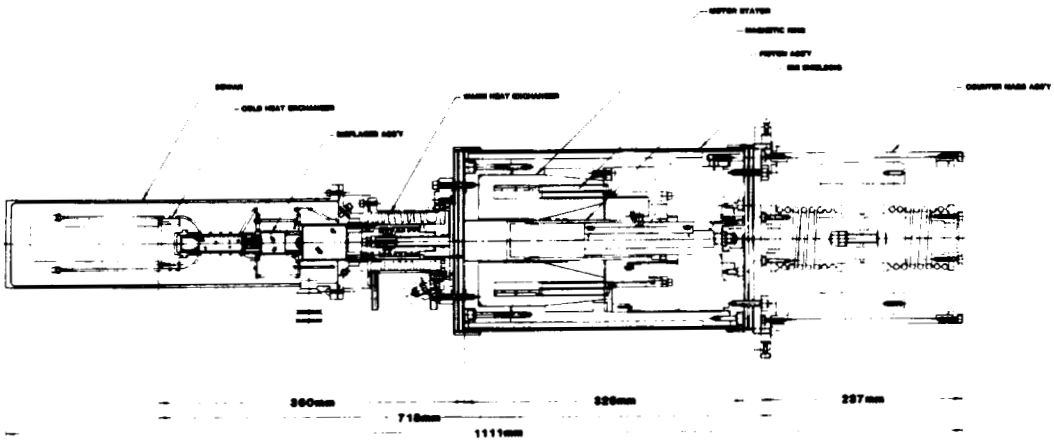

Fig. 1. Layout drawing of 10°K Stirling cycle cooler.

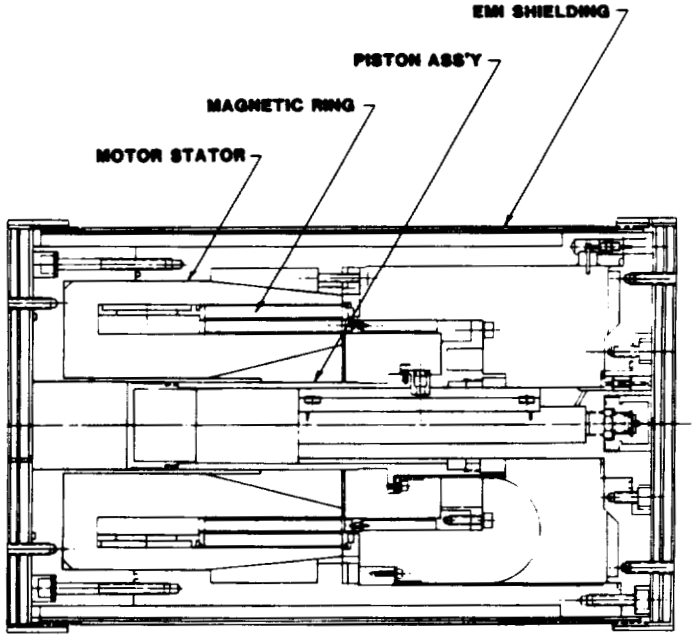

Fig. 2. Layout drawing of piston/motor section with piston at mid-stroke.

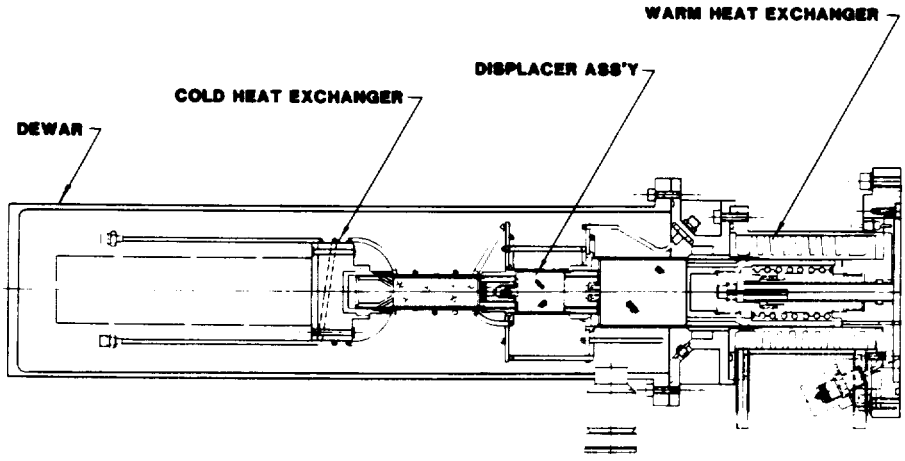

Fig. 3. Layout drawing of displacer section.

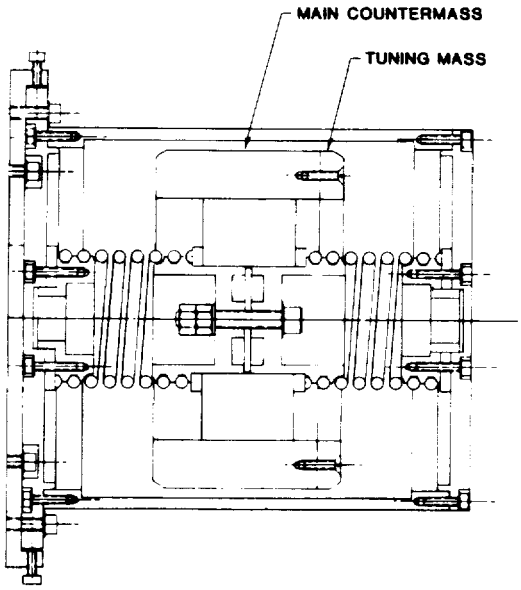

Fig. 4. Layout drawing of vibration absorber.

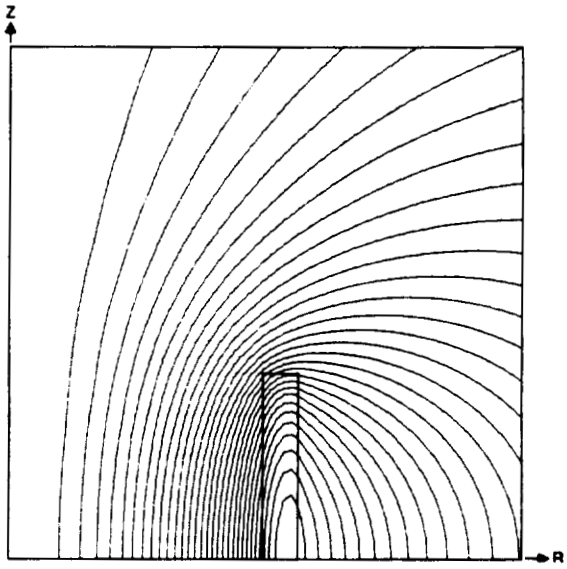

Fig. 5. Flux plot of cylindrical coil in free space.

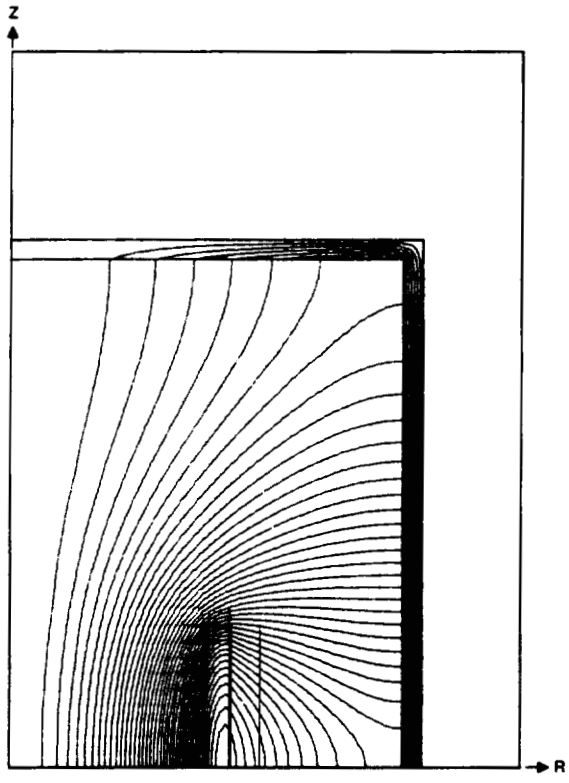

Fig. 6. Flux plot of coil enclosed by magnetic shielding.

REFERENCES

1. Daniels, A. and du Pre, F.K. "Triple-Expansion Stirling-Cycle Refrigerator", Advances in Cryogenic Engineering, Vol. 16, pp. 178-184, 1971.

2. Daniels, A. and du Pre, F.K. "Miniature Refrigerator for Electronic Devices", Philips Tech. Rev., Vol. 32, No. 2, pp. 49-56, (1971).

3. de Jonge, A.K., "A Small Free-Piston Stirling Refreigerator", Proceedings of the 14th IECEC, Boston, Mass, (Aug. 1979).

4. Naes, L.G. and Nast, T.C. "Long-Life Orbital Operationn of Stirling Cycle Mechanical Refrigerators", SPIE 24th Annual International Technical Symposium and Exhibit, (July 1980).

5. Leffel, C.S. and Vonbriesen, R. "The APL Satellite Refrigerator Program", JHU/APL,QM-80-178, March 1981.

6. Gasser, M.G. and Sherman, A. "Developments Toward Achievement of a 3-5 Year Lifetime Stirling Cycle Refrigerator for Space Applications", In Refrigeration for Cryogenic Sensors and Electronic System, NBS Special Publication 607, May 1981.

AN APPLICATION OF GAP REGENERATOR/EXPANDER PRECOOLED BY TWO STAGE G-M REFRIGERATOR

Y. Matsubara and K. Yasukochi

Atomic Energy Research Institute
College of Science and Technology
Nihon University

ABSTRACT

The degradation of regenerator effectiveness below 10K is due to the imbalance of the heat capacity of the regenerator material and helium gas as a working fluid. One of the attractive methods to increase this efficiency could be realized by a gap regenerator system regarding helium gas property.

This paper describes an experiment using pressurized helium gas as a regenerator material. A two stage G-M cycle refrigerator has been used for precooling the gap regenerator system. With this method, minimum temperature below 5K has been obtained when the precooling temperature maintained at 10K.

INTRODUCTION

In order to obtain the liquid helium temperature effectively by a regenerative cycle cryocooler, such as Stirling cycle or Gifford-McMahon cycle, we need to know the thermal behavior of regenerator material and property of helium gas as a working fluid. One of the solutions to obtaining the liquid helium temperature is to use the gap regenerator method with plastic cylinder and displacer which has been successfully developed by Zimmerman, et al.(1).

This paper describes the experimental results of a gap regenerator /expander which is made of plastic piston and stainless steel cylinder with helium gas annulus, precooled by two stage Gifford-McMahon refrigerator.

REGENERATOR CONFIGURATION

One of the features of a gap regenerator, when compared to lead shot type regenerator, is that the contents of working gas in the regenerator can be kept to minimum. This effect is particularly noticeable at a temperature level below 10K where the volumetric specific heat of the

helium gas increases, as pointed out by Radebaugh(2) and Daney (3).

On the other hand, the heat transfer area of a gap regenerator is limited to the finite displacer length and its cylinder surface, therefore, the regenerator heat capacity of wall materials becomes very small at a temperature level below 10K. For this reason, it then becomes necessary to balance the heat capacity ratio of the regenerator material and working gas.

Figure 1 shows the volumetric specific heat of helium gas below 15K, as compared to those of lead and G-10, explaining this fact very well. This also indicates that the high operating pressure may not be applicable due to the imbalance of the heat capacity ratio when lead or G-10 is used as a regenerator material.

To change the view point, high pressure helium gas seems to be a good regenerator material below 10K, if the thermal diffusion coefficient is maintained at a level high enough to create a reasonable operating cycle speed. This is because the low thermal diffusion coefficient would necessitate the cycle speed to be lowered to an unacceptable value for the regenerative cycle. Performance as a regenerator material when the operating speed is constant can be explained as follows:

Considering the sinusoidal temperature fluctuation on the surface of semi-infinite solid, the quantity of heat accumulated by the regenerative material during the half cycle is expressed as (4)

$$Q=\Delta T \cdot A \sqrt{\lambda C_p \rho \frac{2}{\pi} \tau_0} \ ,$$

where ΔT is the amplitude of temperature oscillation on the surface of the solid, A is the surface area, τ_0 is the period of oscillation, λ is the thermal conductivity, C_p is the specific heat and ρ is the density. Therefore, the value of $\sqrt{\lambda C_p \rho}$ represents the effectiveness of the material as a regenerator.

Fig. 2 shows this effectiveness of the helium gas compared to that of G-10, and it shows the pressurized helium gas ranging between 0.4-1.0 MPa becomes a regenerative material superior to G-10 in the temperature range below 8K.

EXPERIMENTAL APPARATUS

Fig. 3 shows the schematics of our experimental apparatus. The purpose of this study is related to the effectiveness of the regenerator operating below 10K. Therefore, we used two stage Gifford-McMahon cycle refrigerator as a precooler for the test section, which gives the warm heat station of 50K and cold heat station of 10K. With this arrangement, gap

regenerator/expander system as a test section can be made with a pair of single cylinder and displacer. This precooler was also constructed in our laboratory, which has a pneumatically controlled displacer, electronically controlled valves, copper mesh regenerator for warm stage and lead-shot regenerator for cold stage.

Details of the test section are shown on Fig. 4. Cylinder of the test section is made of stainless steel having an outer diameter of 13 mm and a thickness of 0.5 mm. Displacer is made of cotton-cloth reinforced phenolic resin, which has a diameter of 11.9 mm and a total length of 65 cm. Between the cold heat station and the cold end of the test section, the cylinder is covered with another stainless steel tube which has an outer diameter of 15 mm, a thickness of 0.4 mm, and a length of 24.5 cm.

Helium gas as a regenerator material is introduced from the capillary tube to this annular space where the carbon fiber was packed for the purpose of preventing convection. In this experiment, a small amount of lead-shots were also used as a regenerative material around 10K. Lead-shots of 0.3 mm diameter immersed in the epoxy resin were coated on the surface of the lower part of the displacer with its diameter rearranged to 11.9 mm by lathe.

A stepping motor was used to drive the displacer. The timing of the intake and exhaust valves were controlled by means of a computer using an input signal of the diaplacer position. Pressure change was measured by the strain guage bonded on the cold end cap.

RESULTS AND DISCUSSIONS

Fig. 5 shows the P-V diagrams obtained at the cold end volume with the displacer stroke of 8 mm and intake and exhaust pressure of 0.6 and 0.12 MPa, respectively. The reason of decreased pressure ratio of (b)-(e) compared to (a) is explained as follows:

This test section basically forms a G-M cycle which has a maximum refrigeration work per one cycle when it has a rectangular P-V diagram. This condition will result if the intake valve is opened when the expansion volume is at its minimum, and exhaust valve is opened when the expansion volume is at its maximum. However this condition increases the regenerator load due to the effect of the incomplete expansion of the excessive intaked mass of the helium gas. In the example of Fig. 5 to reduce this effect, early cut-off of the intake valve was executed.

When the expansion volume is maintained at room temperature, P-V diagram shows a rectangular shape, even when the early cut-off has been excuted. However, if the temperature of the expansion volume decreases, area of P-V diagram decreases due to the condensation of the gas at the expansion volume. The turning corner at upper right position on the P-V diagram is a point at which the exhaust valve is opened.

Mass velocity of the helium gas passing through the gap regenerator can be controlled by changing the valve timing with the appropriate displacer position. The difference between (c) and (d) is caused by this timing change.

Fig. 6 shows the minimum temperature, T_{min}, obtained at the cold end of the test section with an operating pressure of 0.6MPa-0.12MPa and constant temperature of the cold heat station at 10K. Fig. 6 (a) shows the effect of helium gas pressure inside of the annulas, P_{reg}, with a fixed cycle speed at 17rpm. This result indicates that the helium gas in the annulus acts as a regenerative material. The cold end temperature below 6K did not obtained without helium gas in this annulus space. Fig. 6 (b) shows the effect of cycle speed with a fixed P_{reg}.

As expected, optimum cycle speed is very low and we obtained minimum cold end temperature of 4.8K at 12rpm. Below this speed, cold end temperature increases again. The expander work calculated from the P-V diagram of Fig. 5 (e) is about 22mwatts. At this condition, a heat input of 8mwatts was added to the cold end. Cold end minimum temperature increased to 5.8K and expander work also increased to 24mwatts , therefore, thermal efficiency of the test section will be about 35% and main losses will be caused by shuttle loss, insufficient heat transfer area, and excess enthalpy flow into the expansion volume due to the non-ideality of helium gas.

CONCLUSION

While our data were not complete enough, our experimental results indicate that in the gap regenerator/expander system it is very effective to use pressurized helium gas as a regenerator material at a temperature level below 10K. We found a refrigeration temperature below 5K can be obtained under this method with the precooling temperature of 10K. Although, under the regenerator design as shown in Fig. 4, optimum cycle speed was as low as around 12 rpm, the highest possible cycle speed is desirable as regenerative cycle, as far as the pressure loss permits. We thus propose as follows:

The highest possible cycle speed should be obtained through the regenerator fabricated by putting the pressurized helium gas into fin- or wool-state of materials (such as copper, lead or other pure metal) which are high in its thermal conductivity, while low in its specific heat, in the temperature range below 10K. In our experiments, in order to know the optimum P-V diagram we employed such G-M cycle which can change the valve timing and we also used a different type refrigerator in the precooling system to avoid the effect on the upper stage to be caused by change in temperature.

Our experimental results suggest that we would be able to obtain the helium temperature from the room temperature by employing this system at the final stage of multistage Stirling cycle, without using the different

type precooling system.

We wish to thank S.Uosaki and T.Munekata for technical assistance.

REFERENCES

1. J.E.Zimmerman and D.B.Sullivan,"A Study of Design Principles for Power Cryoelectronic Devices", NBS Technical Note 1049 (1982)

2. R.Radebaugh,"Prospects for Small Cryocoolers", Proceeings of the 9th Int'l Cryog. Eng. Conf.,P.761,(1982).

3. D.E.Daney,"cooling Capacity of Stirling Cryocoolers the split cycle and nonideal gas effects", Cryogenics 22, 531 (1982)

4. S.Kutateladze,"Fundamentals of Heat Transfer", p.134, Academic Press. (1963)

DISCUSSION

Question by C. Winter, Simon Fraser University: Please descrive the mounting of the strain gage pressure transducer on the cold end cap. What was its sensitivity to pressure changes?

Answer by author: A foil strain gage is glued on the membrance of the cold end cap. Effective diameter and the thickness of the membrance is 8mm and 0.5mm respectively. This gauge (as shown in Fig. 7) consists of four different gauges which give signals proportional to a radial and a tangential strain of the membrance. Calibrated sensitivity of this pressure transducer was (3.48±0.02)KPa/Volt below 1MPa, using strain amplifier with the voltage gain of 350.

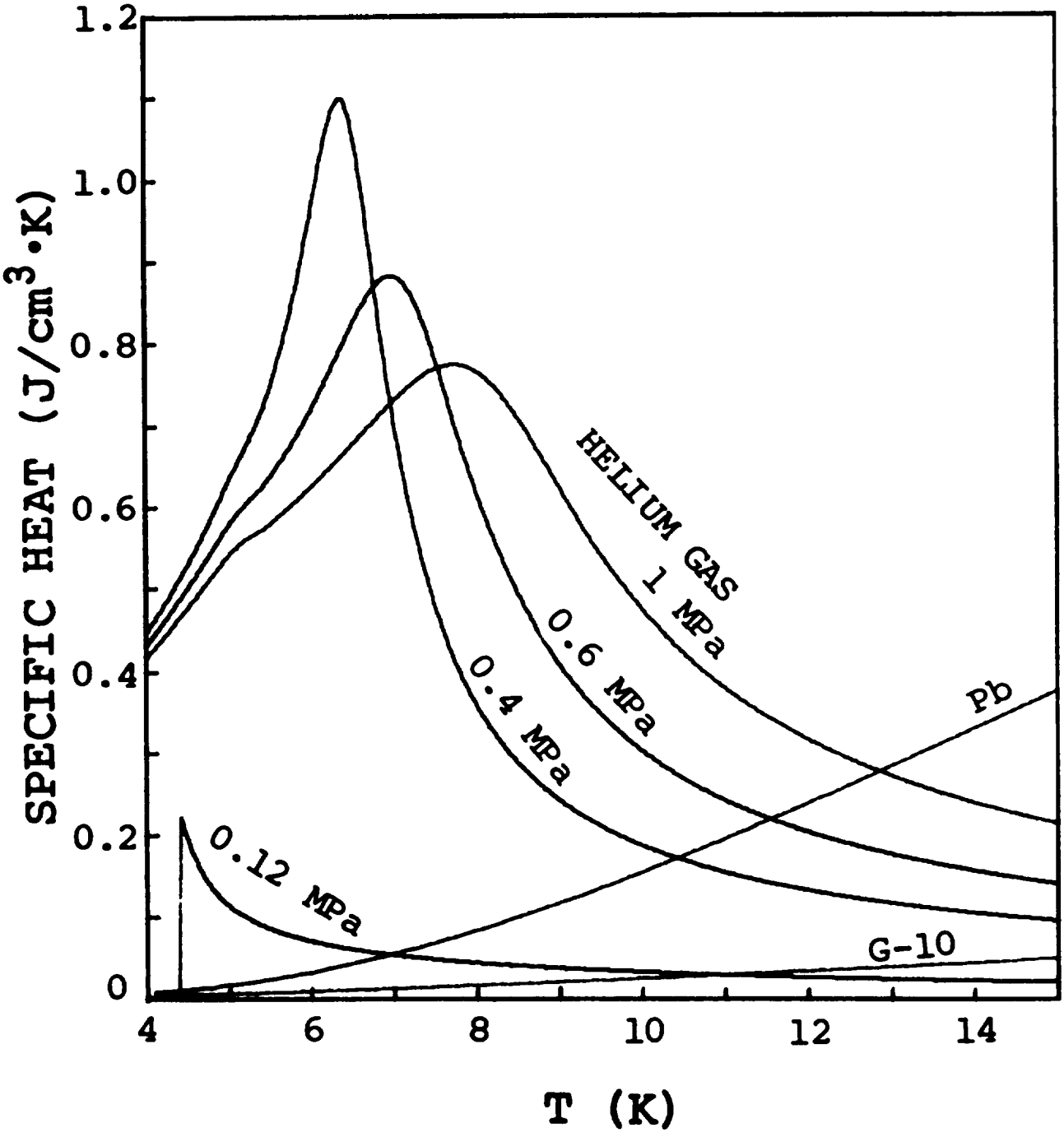

Figure 1. Volumetric heat capacity of helium, lead and G-10.

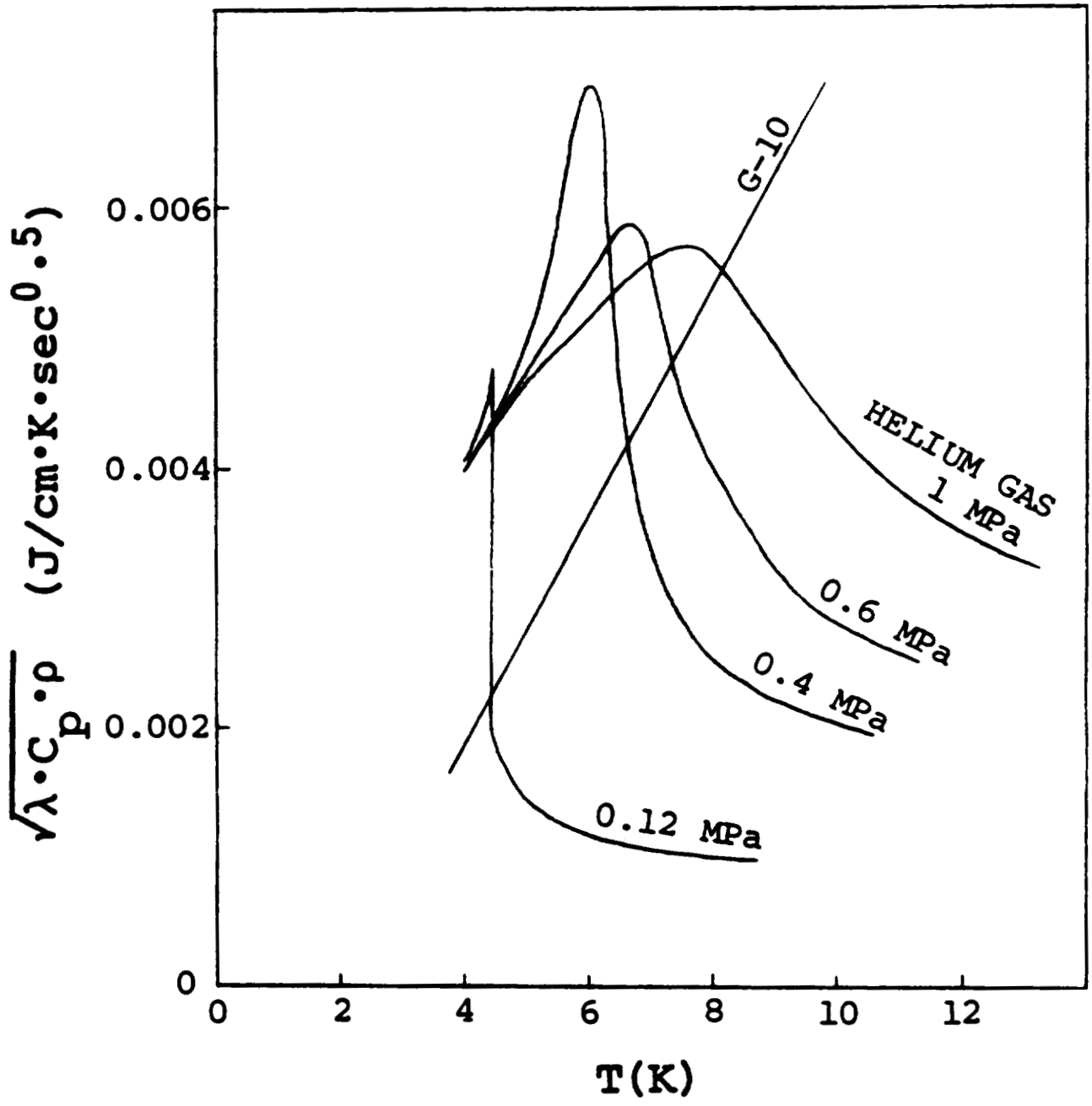

Fig.2 Performance of helium gas as a regenerative material.

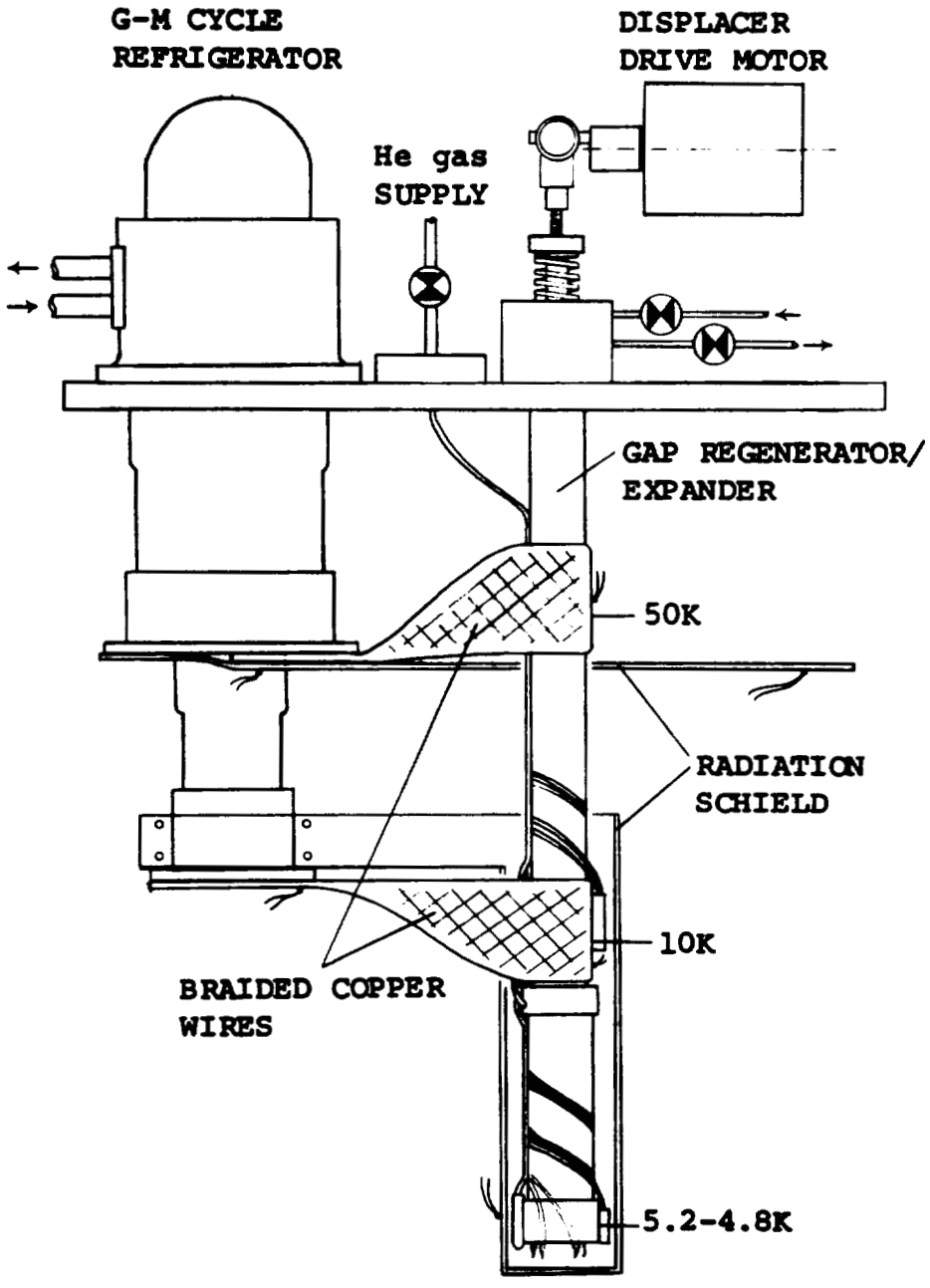

Figure 3. Schematic of experimental arrangement.

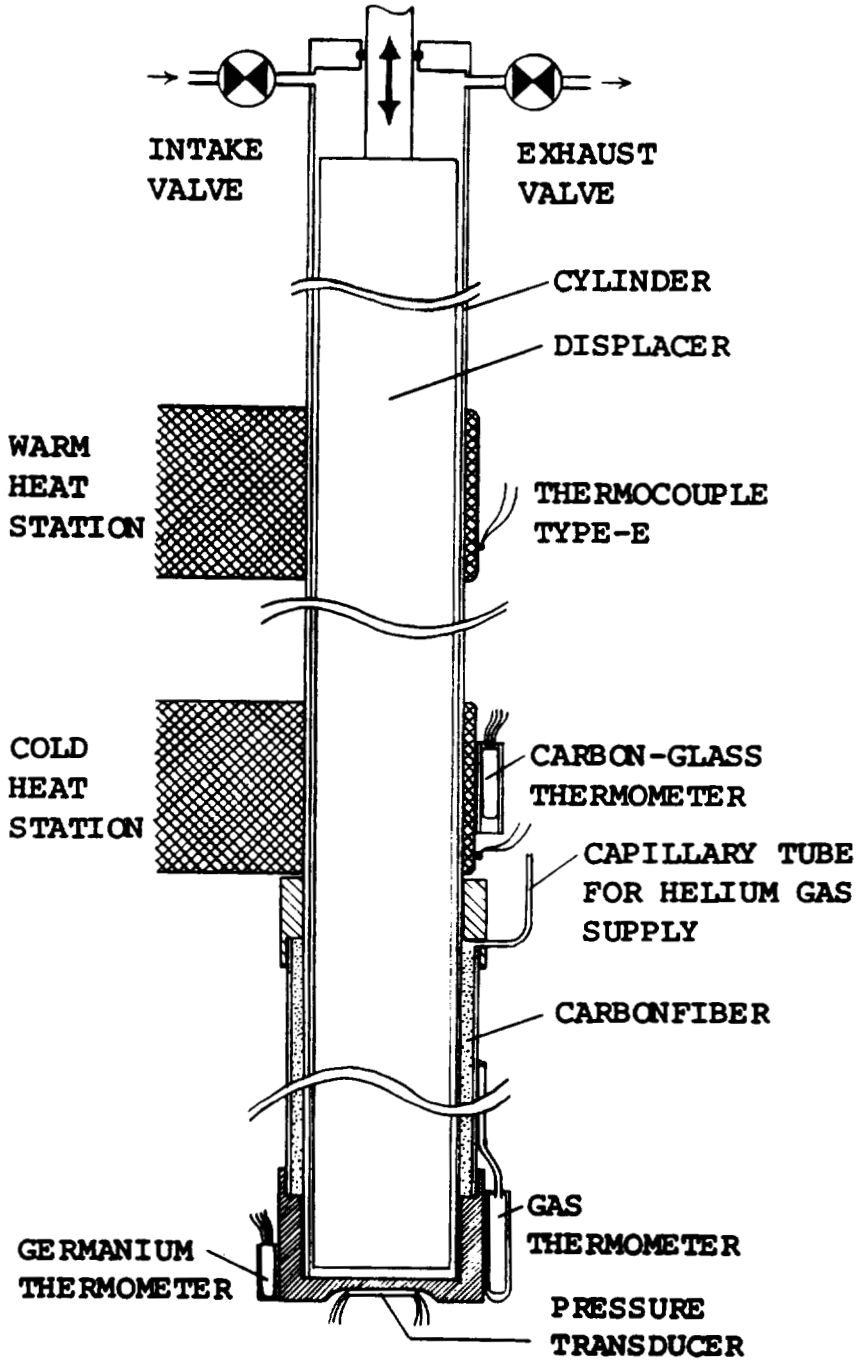

Figure 4. Gap regenerator/expander with pressurized helium gas annulus.

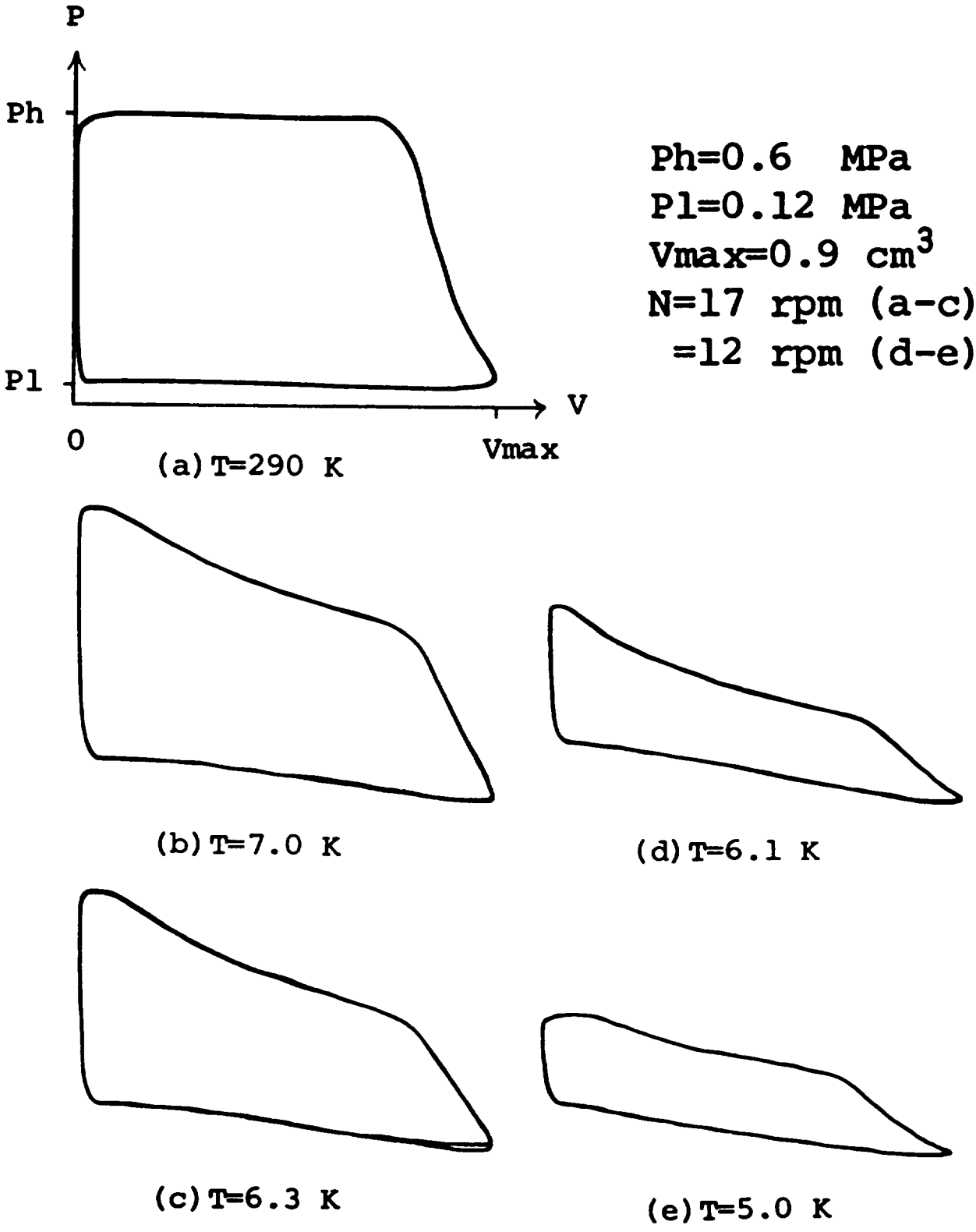

Figure 5. P-V diagrams of the expander.

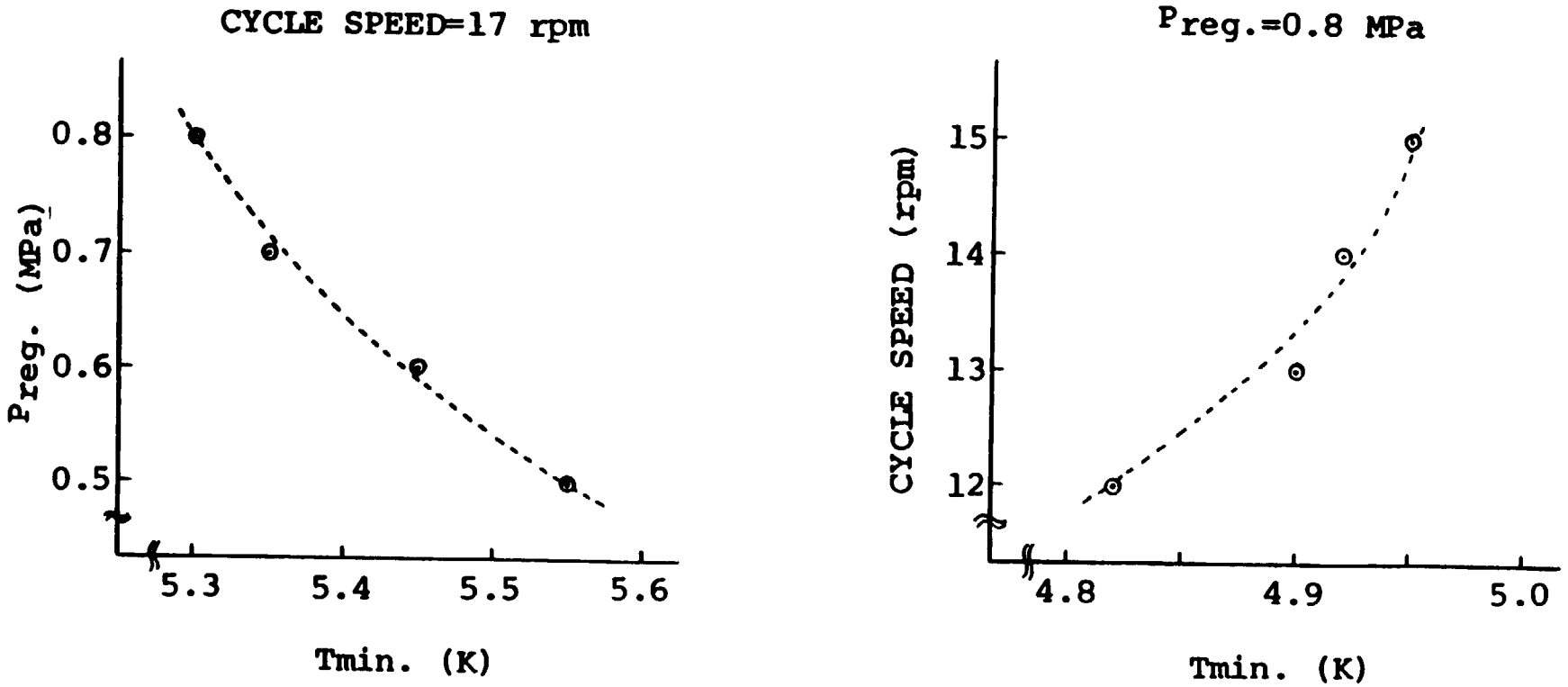

Fig.6 Measured minimum temperature at the cold end of the expander.

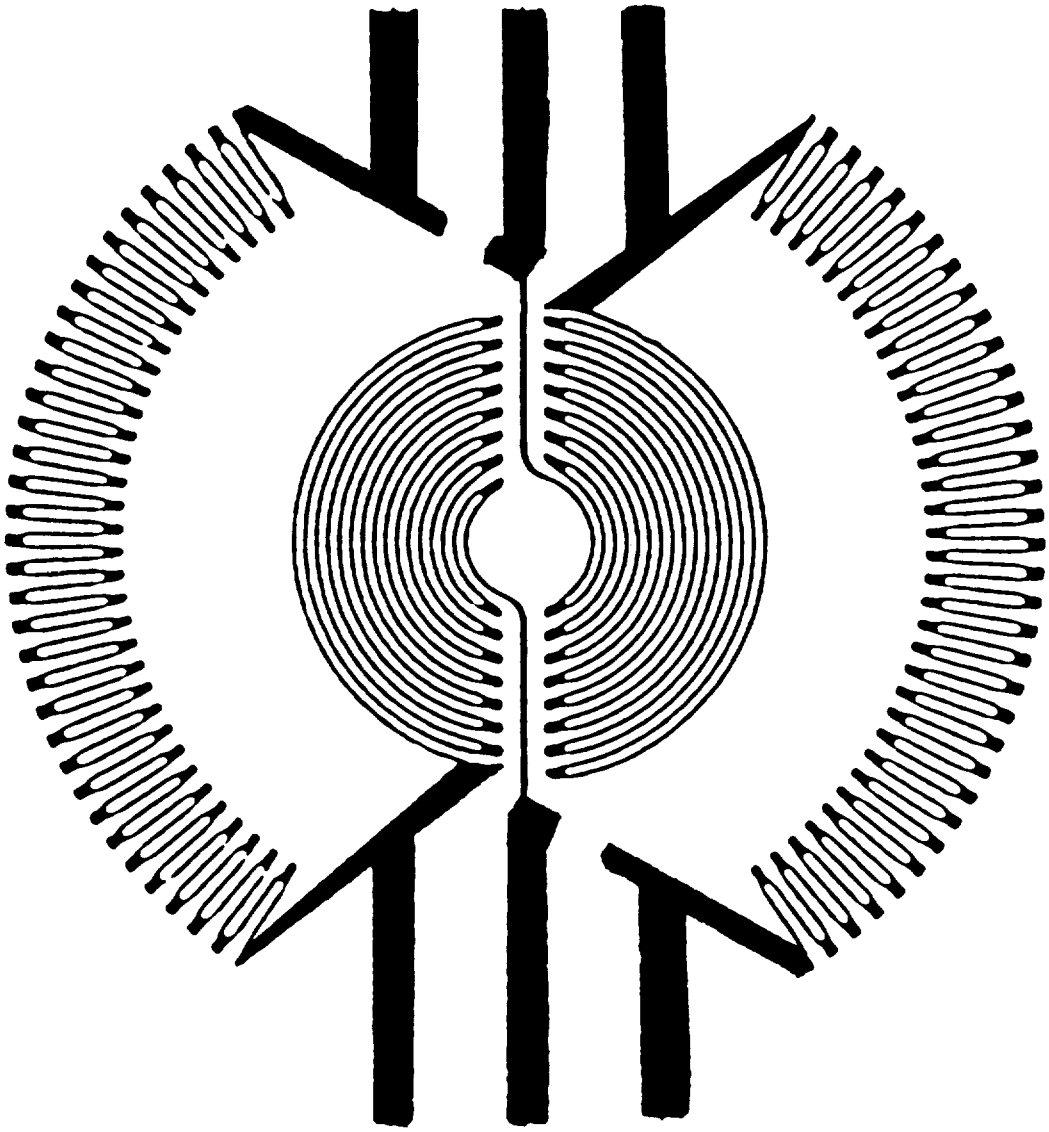

Figure 7. Strain gauge pressure transducer.

COMPACT CLAUDE CYCLE REFRIGERATOR FOR LABORATORY USE

Y. Hiresaki, M. Kaneko, T. Munekata and Y. Baba
Cryogenic Department, Suzuki Shokan Co., Ltd.

Y. Matsubara and K. Yasukochi
Atomic Energy Research Institute, Nihon University

ABSTRACT

A Claude cycle refrigerator with a three stage reciprocating expansion engine is described. Instead of a cam mechanism, valves are driven directly by magnetic solenoids operated by means of a micro processor control system. A swash plate mechanism is used to convert reciprocating motion of the expander pistons to rotary motion. A refrigeration capacity of 8 watts was achieved at 4.5 K with the operating pressure of 1.1 MPa and flow rate of 2.4 g/sec..

An effect of overintake operation was studied. Experimental results show that the efficiency of the expander has a peak point in the region of overintake operation with constant cycle speed, which agrees with theoretical results. The electrically controlled valve system is useful to vary the valve timing to achieve an optimum condition of operation.

INTRODUCTION

Recentry the demand for a compact helium refrigerator has been increased due to the development of applications of small scale superconducting technology such as NMR for medical applications, magnetically levitated trains, and Josephson-Junction computers.

In our previous theoretical study of the multi-stage Claude cycle helium refrigerator it was predicted that the existing optimum value of working pressure is lower than for commercial machines (1). To operate efficiently at low working pressure, such as below 1.0 MPa, three expanders are needed. This is shown in another study that the efficiency of a refrigerator increases by increasing the number of expanders while decreasing the operating pressure (2).

Simple mechanical design is an important factor for the three-stage Claude cycle refrigerator with three reciprocating expanders having six valves. Electronic control techniques are a powerful method to simplify the mechanical design. A micro processor control system provides not only a simple mechanism but also a flexible system such as variable valve timing

control system or variable cycle speed control system.

OUTLINE OF DESIGN

Figure 1 shows the main unit of the refrigerator without heat exchangers. The magnetic solenoid assembly with actuating valve rods is placed on the upper flange. The swash plate mounted in the crosshead housing is used to convert reciprocating motion to rotary motion. Roary motion of the swash plate is transmitted to a DC brake motor working as an electric generator by the V belt. Speed of revolution of the brake motor is maintained at a constant value by the speed control circuit. The DC motor works in its usual motor mode at starting time. Heat exchangers are of coiled finned tube using soldered copper finned tube. The cold box has a diameter of 40 cm and length of 1 m.

The electrical control system includes two micro processors, the valve driving circuit, the speed control circuit, the interface circuit to measure temperature and pressure and another interface circuits. The system is controlled by a host computer via a standard comunication line.

The compressor for a commercial model has an input power of 7.5 kW and a capacity of 52 Nm^3/hour with 1.05 MPa.

EXPANDER AND SWASH PLATE

The expansion engine has three identical cylinders with a bore of 50 mm, which are arranged symmetrically above the swash plate. Reinforced phenolic pistons are sealed by capseals at their warm end of them. A stroke of a piston is 30 mm. Fig. 2 shows a scheme of the expansion engine, representing the bottom part of the cylinder and piston, the swash plate and the flywheel which also servs as a pulley. The swash plate is lubricated by oil and connected to the rotary encoder not shown in the figure.

VALVE MECHANISM

The valves of the expansion engine are driven directly by DC solenoid coils which are actuated by the micro processor instead of the usual cam mechanism. The rotary encoder connected to the axis of the swash plate is an absolute value type encoder of which the output signal represents a three digit number corresponding to the angle of the axis. At every one degree of angle the encoder sends interrupt signal to the micro prosessor. The processor has a table in the memory containing values of the angle corresponding to the setting points of the valves. Comparing the angle obtained from the rotary encoder with the table, the processor operates valves through the driving circuit. This system responds with a resolution of 1 degree for engine speeds up to 350 rpm. The absolute value type

rotary encoder makes the system simple in comparison with the incremental type. Since set points of valves can be changed by changing the content of the table, valve timing can be changed even during operation.

Fig. 3 shows typical data of valve action recorded by an electromagnetic oscillograph along with data of the voltage across the solenoid coil and the signal of the angle marker. The upper level coresponds to a closed state of the valve. The osciration which appears during the rising and falling periods is due to a characteristic of the transducer. Time delay during closing is 10 to 20 m sec..

ELECTRICAL CONTROL SYSTEM

Fig. 4 shows the block diagram of the electrical control system for test operation of the prototype. The micro processor operates six valves on three expanders. The cycle speed of the expansion engine is varied by control of the DC brake motor. The speed control circuit compares the reference voltage with the output voltage from the tachometer on the brake motor, and maintains constant cycle speed by means of changing the electrical load of the brake motor. A PDP11/V03 was used as a host computer and also as a data acquisition system.

Fig. 5 shows the block diagram of the commercial model which includes another micro processor CPU-1. CPU-1 receives commands from the host computer through a standard comunication line, RS-232C, or an IEEE-488 bus. Main roles of the CPU-1 are

1. setting the cycle speed on the speed control circuit
2. changing the valve timing
3. monitoring temperature and pressure
4. operating the J-T valve and other valves
5. operating the compressor unit
6. performing emergent sequence
7. sending back infomation about the status of the refrigerator to the host computer.

The host computer contains an operator console and can be interconnected to another computer system. In addition to using the computer for these functions the user may also make other programs such as a time schedule or a data logging program on the host computer. This system is useful in both laboratory and industrial applications.

TEST RESULTS AND DISCUSSION

Fig. 6 shows typical experimental results of the test operation with 0.8 MPa pressure at the inlet of third expander. Refrigeration capacity of 8 watts at 4.5 K was obtained at 74 rpm and 2.4 g/sec. total mass flow rate. Expander efficiencies of 60, 70 and 74 % were obtained at inlet temperature of 129, 48, and 13 K respectively. Ideal isothermal compressor

work at 290 K is 3.5 KW, when the helium gas is compressed from 0.1 MPa to 1.1 MPa with a flow rate of 2.4 g/sec., therefore the actual input power will be less than 7 KW with the assumption that the overall efficiency of the compressor is more than 50 %. With this assumption the ratio of the refrigeration capacity to the input power is 1.1×10^{-3}.

Fig. 7 shows the efficiency of the third expander against the filling factor, X, with constant cycle speeds of 140 rpm and 180 rpm. Inlet temperature of the expander is 15 K and inlet and outlet pressure are 0.8 and 0.12 MPa respectively. Each curve has a remarekable peak in the overintake region, $0.34<X<1.0$. Fig. 8 shows theoretical results with same condition as the experiment for three different values of heat leak to the expander. The model for the calculation (3) is illustrated in Fig. 9 on a T-S plane. Helium gas at high pressure, point i, is expanded isentropically to point f. Heat leak is considered only on the process from f to ff and gas expands to pressure state Pe. The final state e is reached by the remaining gas at point el and leaving gas at point e2. In spite of the simplicity of this model, the theoretical results agree well with experimental results.

Fig. 10 shows cool down curves for each expander on the normal and the overintake mode. On the oveintake mode at 165 rpm the cool down time is 4.5 hours compared to 6 hours in the normal mode at 140 rpm. Improvement of operation in the overintake mode is clear even though there is a difference of speed between them.

SUMMARY

A compact three stage claude cycle helium refrigerator which produces 8 watts of refrigeration at 4.5 K has been made. The electrical control system with micro processors provides a flexible system which permits the operating mode to be changed, and is useful to simplify the valve mechanism. Overintake operation increases refrigeration capacity without decreasing the efficiency of the expanders.

REFERENCES

1. Matsubara, Y., Kaneko, M., Hiresaki, Y., and Yasukochi, K.: "Exergetic Analysis of Multi-staged Claude Cycle Helium Refrigerator", Cryogenic Processes and Equipment in Energy System, 131-134, ASME, Century 2 Publication, 1980.

2. Khalil, A. and McIntosh, G.: "Thermodynamic Optimization Study of the Helium Multi-engine Claude Refrigeration Cycle", Adv. Cry. Eng., vol. 23, 431-437, 1978.

3. Kaneko, M., Hiresaki, Y., Matsubara, Y., and Yasukochi, K.: "Performance of Reciprocating Expansion Engine with Electronic Control Valves", Proceedings of the 9'th Int'l Cryog. Eng. Conf., 355-358, 1982.

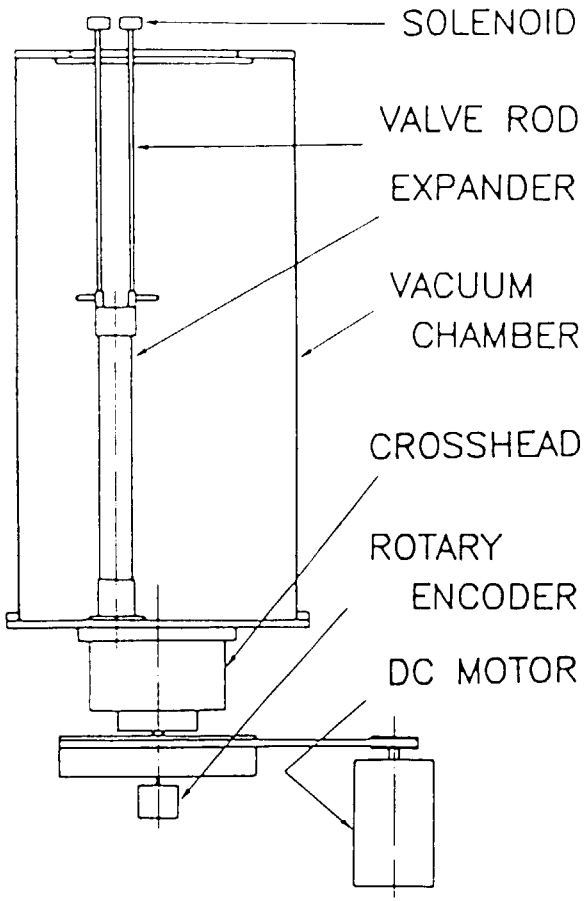

Fig. 1 Schematics of the expansion engine

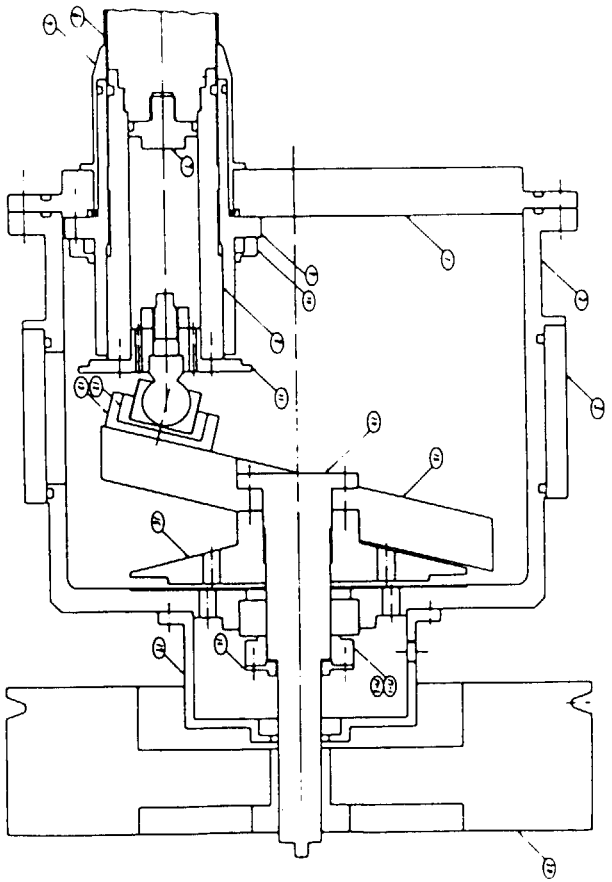

Fig. 2 Bottom end of the expansion engine and the swash plate mechanism.

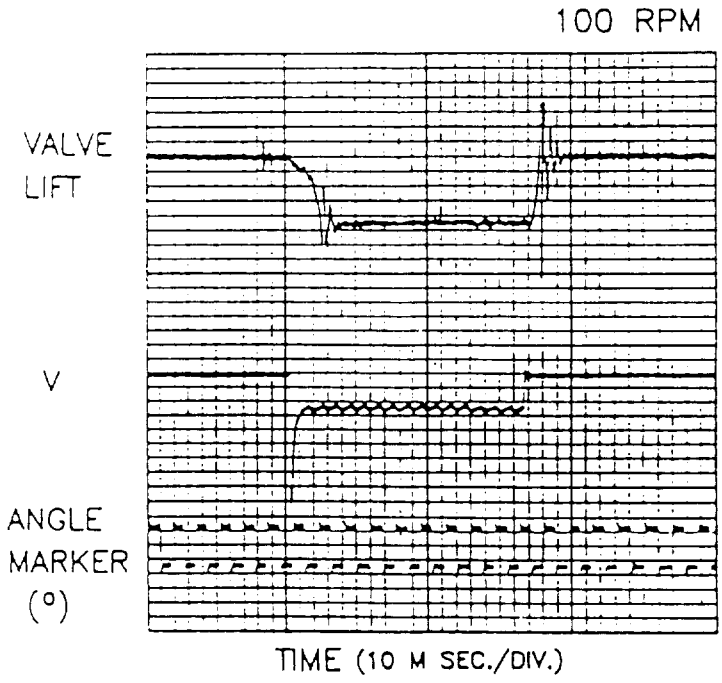

Fig. 3 Valve action compared with voltage V across a solenoid coil. One cycle of the marker coresponds to 10 degree of angle.

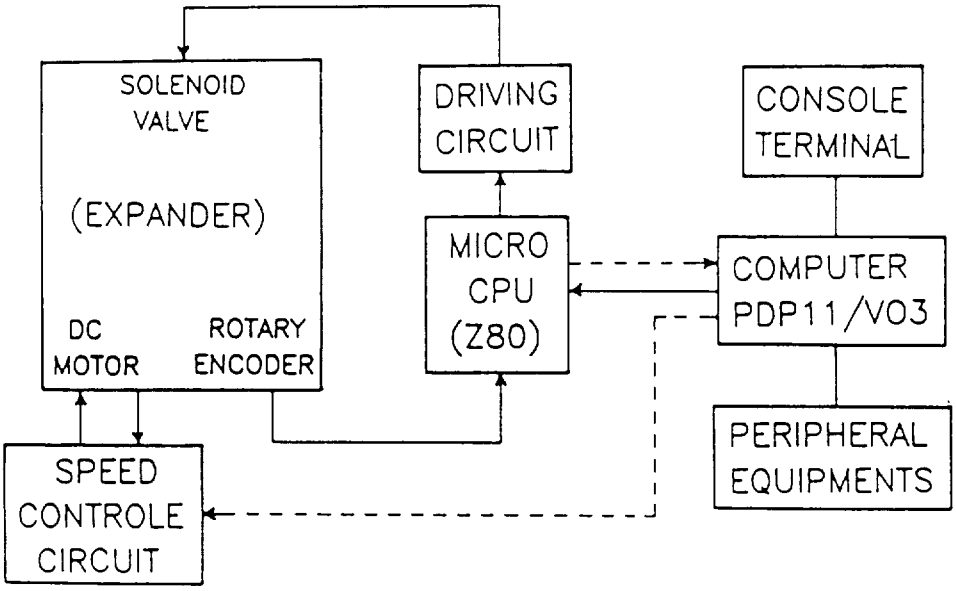

Fig. 4 Block diagram of the control system for experiments.

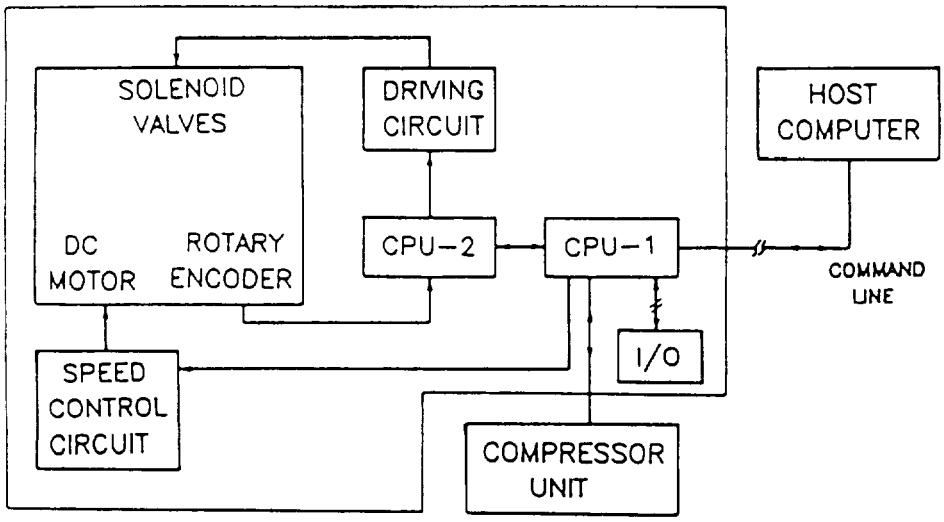

Fig. 5 Block diagram of the control system of the commercial model.

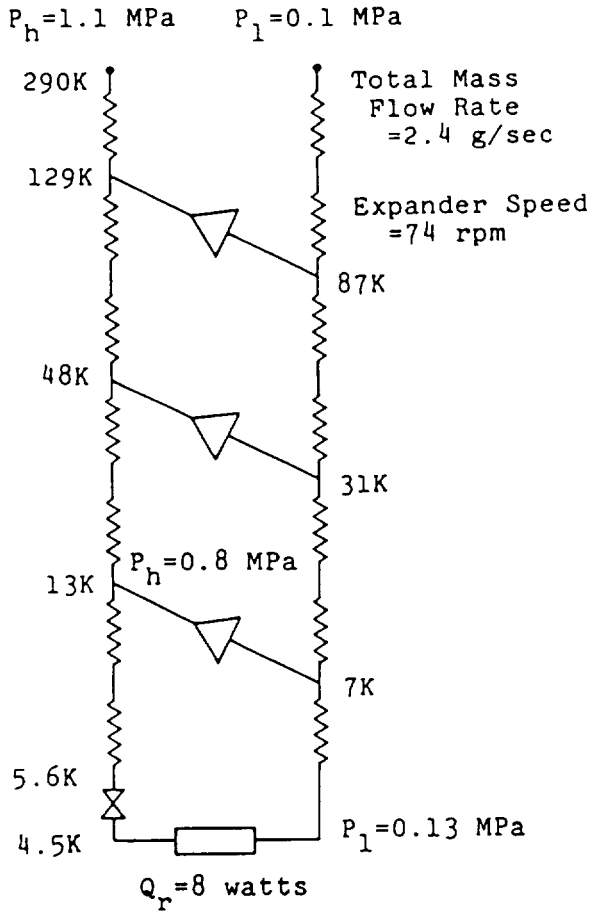

Fig. 6 Typical result of a test operation.

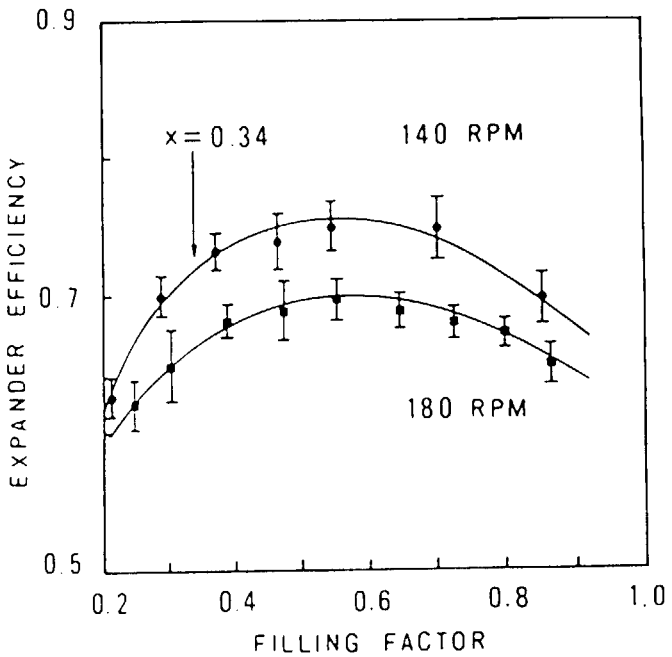

Fig. 7 Efficiency of the expansion engine against the filing factor X (Experimental results).
Inlet temperature = 15 K
Pressure = 0.8 MPa.

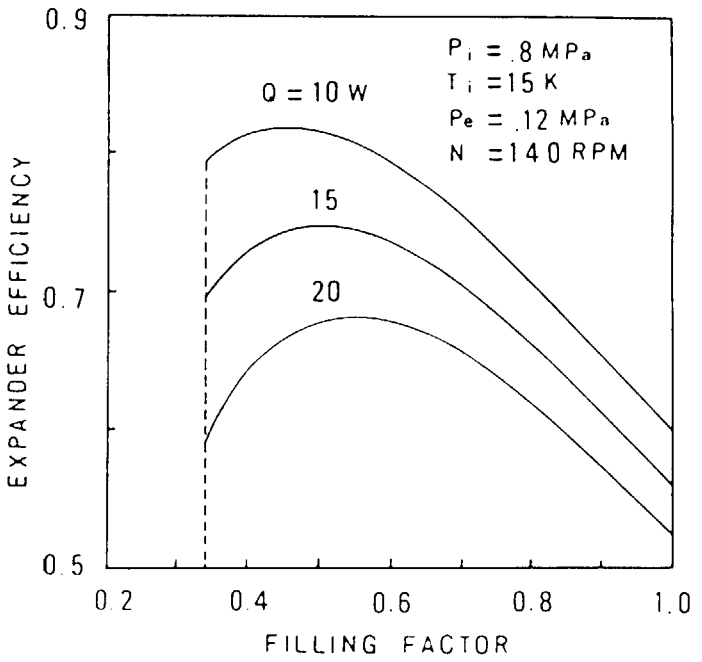

Fig. 8 Efficiency of the expansion engine against the filling factor (Theoretical results).

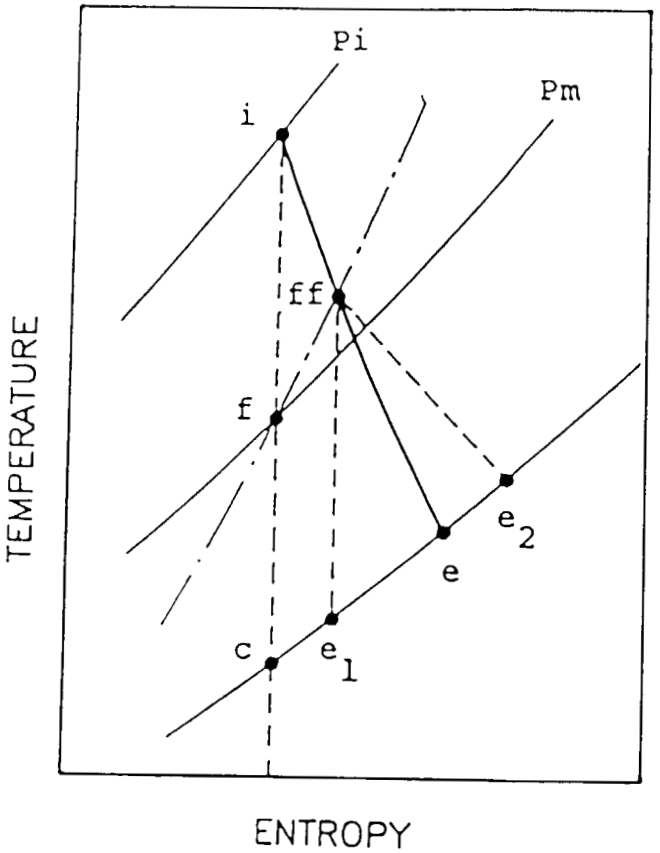

Fig. 9 Model of the expansion process on a T-S plane.

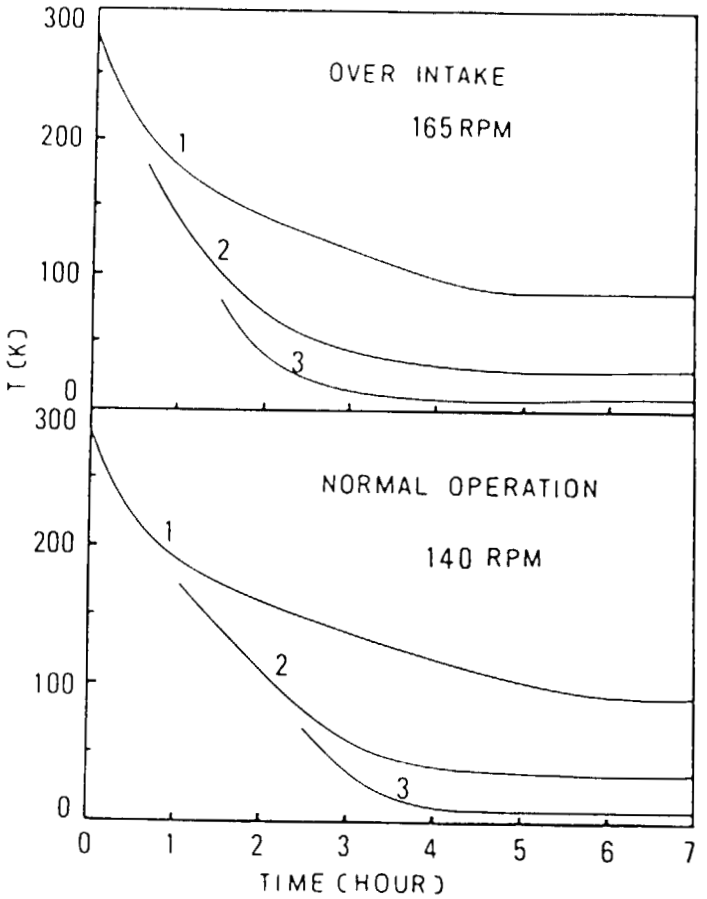

Fig. 10 Cool down characteristics for expandes.

A SMALL AND LIGHT WEIGHT HEAT EXCHANGER

FOR ON-BOARD HELIUM REFRIGERATOR

T. Koizumi, M. Takahashi, T. Uchida,
Y. Kanazawa, and M. Suzuki

Hiratsuka Research Laboratory,
Sumitomo Heavy Industries, Ltd., Japan

ABSTRACT

A small and light weight heat exchanger used for small helium refrigerator has been developed by Sumitomo Heavy Industries, Ltd.. This heat exchanger is a laminated metal heat exchanger which consists of perforated aluminum metal plates and glassfiber reinforced plastic separators. The size is from 100 mm to 28 mm in diameter and about 300 mm in length. The weight is from 2.5 kg to 0.6 kg. Also it can be used between room temperature and liquid helium temperature. The thermal efficiency obtained has been more than 96%. The heat exchanger has been practically used for on-board helium refrigerator in Japanese National Railways' superconducting magnetic levitated trains.

INTRODUCTION

Counterflow heat exchanger of high thermal efficiency is required for refrigeration and liquefaction systems. In recent years, many type heat exchangers, for example, Hampson, Collins and Plate-fin type have been developed. But these heat exchangers do not fit in with small refrigerators because the heat transfer area per unit volume of these heat exchanger is not large enough.

The small refrigerator, for example, on-board refrigerator in superconducting magnetic levitated trains, requires very small and high thermal efficient heat exchanger. Such heat exchanger must possess the following characteristics [1],[2].

1. Large heat transfer surface area per unit volume and per unit weight.

2. Very small longitudinal heat conduction through the walls in the exchanger.

3. Uniform distribution of flow throughout any cross section of exchanger.

4. High resistance to shock and vibration.

We have developed the small and light weight heat exchanger which fulfilled above requirements and applied it to on-board helium refrigerator in Japanese National Railways' superconducting magnetic levitated trains.

This paper describes the development of the laminated metal heat exchanger and its application for small refrigerator use.

CONSTRUCTION

The construction of laminated metal heat exchanger is illustrated in Fig. 1. This heat exchanger consists of a large number of parallel perforated aluminum metal plates, plastic separators and epoxy adhesives. The perforated metal plates and separators are alternately stacked and bonded with adhesives to build up the multilayer-body. Headers made of aluminum are bonded to both faces of the multilayer-body. Then, headers and multilayer-body are inserted into a thin walled stainless steel vessel with pipe fittings. One end of the fitting is welded to the stainless steel vessel and the other end is bonded to the header. Therefore, there is no gas leakage to the vaccum space, when the heat exchanger is installed in a vaccum space.

In this exchanger, gas flow passages are divided into eight sections and gas flows longitudinally in counterflow pattern. Heat transfers laterally from hot gas to cold gas through the perforated plates. The perforated heat transfer plate is made of aluminum which has high thermal conductivity and is 0.3 mm in thickness, with 0.5 mm diameter holes.

A thickness-to-diameter ratio is 0.6 in this perforated plate. It is represented that the desirable ratio is in the range 0.5 to 1.0 because thermal and hydrodynamic boundary layers are broken up before they have a chance to become fully developed, which results in high heat transfer surface coefficients [1].

The separator is made of glassfiber reinforced plastic which has low thermal conductivity and its thickness is 0.4 mm. Therefore, the longitudinal heat conduction through the walls in the heat exchanger is very samll.

Figure 2 is a photograph of this heat exchanger. This is applied to first stage heat exchanger for on-board refrigerator. The size is 80 mm

in diameter and 250 mm in length and the weight is about 2.2 kg. The heat transfer area per unit volume in this heat exchanger is about 1000 m^2/m^3.

PERFORMANCE

TEST APPARATUS

The heat transfer and friction loss performance test apparatus is shown in Fig. 3. The test has been performed by using helium gas between room temperature and the liquid nitrogen temperature. The pressure of the high pressure line and low pressure line are 1.57 MPa and 0.1 MPa respectively.

High pressure helium gas flows through test heat exchanger and is throttled to low pressure by throttle valve and flows back to helium compressor through the heat exchanger. The temperature of gas flow is measured by copper-constantan thermocouple. The pressure drop is measured by differential pressure gage.

EXPERIMENTAL DATA

The heat exchanger shown in Fig. 2 has been tested. The hole diameter of perforated plate is 0.5 mm and open area ratio of the high pressure passage is 15% and low pressure is 30%. The gap between perforated plates is about 0.6 mm. The effectiveness and pressure drop versus the mass flow rate of helium are plotted in Fig. 4. It shows that when helium gas flow rate is 1 g/sec, 96.5% effectiveness is obtained and pressure drop is 0.008 MPa.

Another type laminated metal heat exchanger which we have fabricated is shown Fig. 5. The size of this heat exchanger is 28 mm in diameter and 300 mm in length. Headers and multilayer-body are inserted into the stainless steel vessel and their weight is about 0.6 kg. Obviously, it is much small and light in weight compared with the heat exchanger shown in Fig. 2.

RELIABILITY

ADHESIVE

The construction of laminated metal heat exchanger which we have described above is very simple. But for heat exchanger it is important to possess the effective adhesive strength, gas tight and good durability, because this exchanger is constructed with adhesive bonding.

So, we have selected many kinds of adhesives and tested their adhesive strength and gas leakage at low temperature to choose the best adhesive among them. The test results of epoxy adhesive which we applied to fabricate the heat exchanger is explained in the following.

ADHESIVE STRENGTH

We measured the strength of two different test specimens, one is aluminum-aluminum adhesive bonded joint, the other is aluminum-GFRP-aluminum adhesive bonded joint.

The shearing strength versus temperature is shown in Fig. 6. The results indicate that the shearing strength increases as the temperature decreases. The shearing strength of Al-GFRP-Al at liquid nitrogen temperature is about 15 MPa and the specimens failed in the adhesive. Also shearing strength denoted by triangles shows the test results after 7 thermal cycles between room temperature and liquid nitrogen temperature.

Fig. 7 presents the tensile strength versus temperature. The tensile strength of Al-GFRP-Al specimens at liquid nitrogen temperature is about 50 MPa. Some specimens denoted by squares were cycled 235 times between room temperature and liquid nitrogen temperature after one year has passed since they were bonded. Their tensile strength were nearly equal to the other specimens. Also the failed surface displayed a cohesive failure in adhesive.

EFFECT OF THERMAL COOLING

The heat exchanger is also requested to have high reliability for gas leakage. The thermal cycle test of the heat exchanger has been performed and examined its reliability. The thermal cycle test apparatus is Fig. 8. The test was conducted by cooling the exchanger between room temperature and liquid nitrogen temperature. The test vessel in which test heat exchangers are put is immersed in liquid nitrogen and the heat exchangers are cooled to liquid nitrogen temperature. Then, the vessel moves to up and heat exchangers are heated up to room temperature by the heater. The temperature of the heat exchanger is measured by copper-constantan thermocouple. Also one thermal cycle between room temperature and liquid nitrogen temperature takes about 2 hours. During the test, high pressure and low pressure passages are pressurized with 1.57 MPa and 0.1 MPa helium respectively. Helium gas leakage flow is measured with a soap bubble flow meter attached to the low pressure side.

Table 1 summarizes results of the thermal cycle test. Before cooling the heat exchanger, helium gas leakage flow high pressure passages to low pressure passages was measured to be less than 1 X 10^{-4} Pa m^3/sec. After 235 cycles, helium gas leakage was constantly less than 1 X 10^{-4} Pa m^3/sec.

CONCLUSION

From these test results, it is confirmed that this heat exchanger can meet the requirements and fulfill the characteristics for " on-board refrigerator ".

A photograph of on-board helium refrigerator which we have developed is shown in Fig. 9. This refrigerator is Claude Cycle and consists of two reciprocating expantion engines and five laminated metal heat exchangers.

The refrigerator capacity is 5 W at 4.4 K. The size is 300 mm in diameter and 800 mm in length and the weight is about 40 kg. This refrigerator has been installed in the test vehicle and is presently being tested at Miyazaki Test Track in Japanese National Railways.

REFERENCES

1. R.B.Fleming, " A Compact Perforated-Plate Heat Exchanger " ; Adv. Cry. Eng., vol. 14, 197-204 (1968)

2. G.Vonk, " A Compact Heat Exchanger of High Thermal Efficiency " ; Philips Technical Review, vol. 29, no. 5, 158-162 (1968)

DISCUSSION

Question by W.L.Swift, Creare R&D; Have you tested shear strength, tensile strength and leakage of epoxy adhesive joints below liquid nitrogen temperature?

Answer by author; No, I have not.

Question by F.J.Kadi, Air Products & Chemical Inc.; Would you comment on any potential leakage of helium into vaccum space?

Answer by author; There is no leakage of helium into vaccum space, because headers and multilayer-body of heat exchanger are inserted into a thin walled stainless steel vessel.

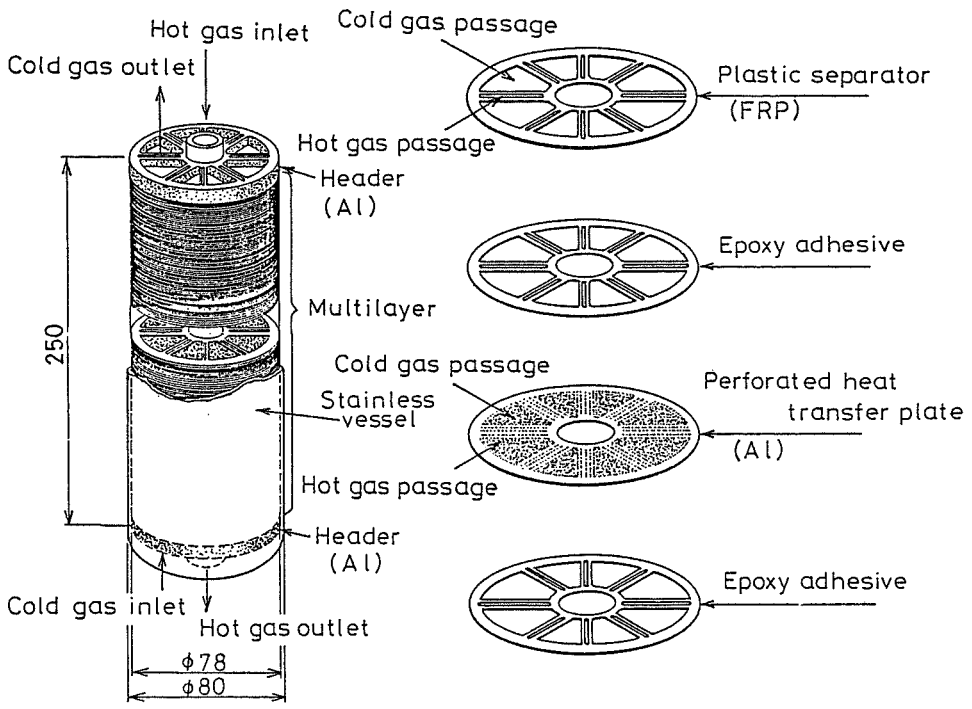

Fig. 1 The construction of laminated metal heat exchanger.

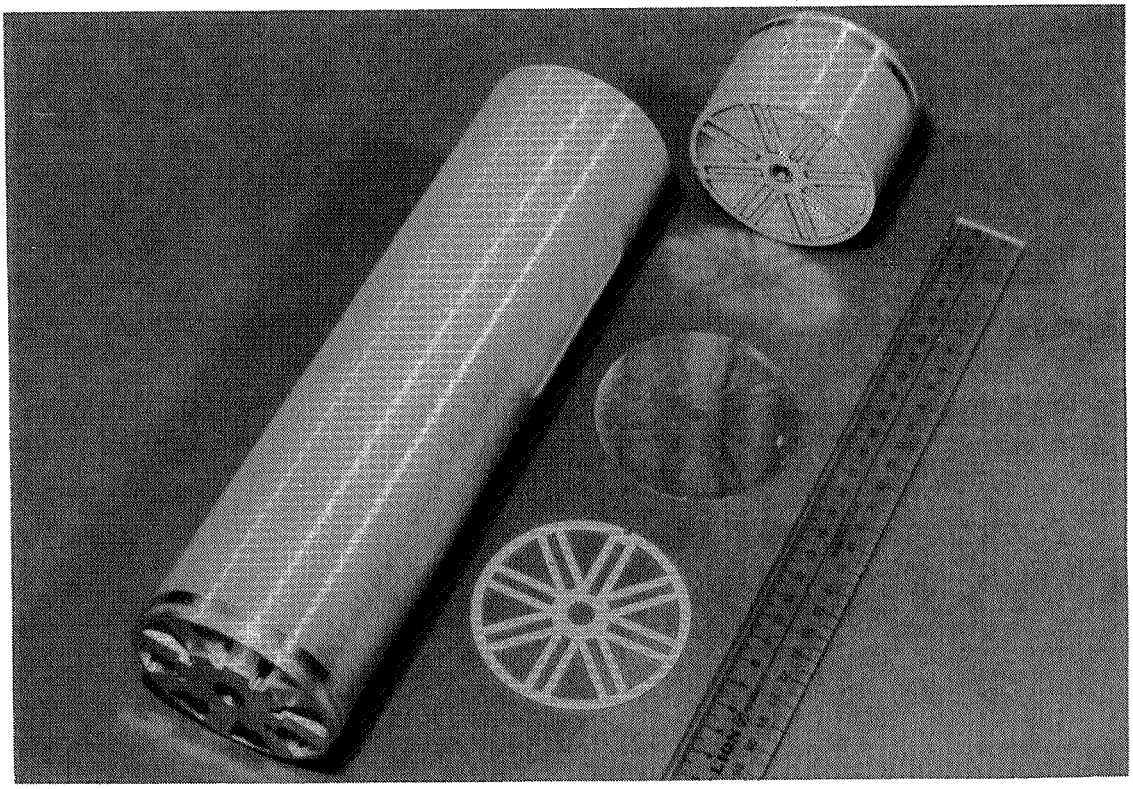

Fig. 2 laminated metal heat exchanger.

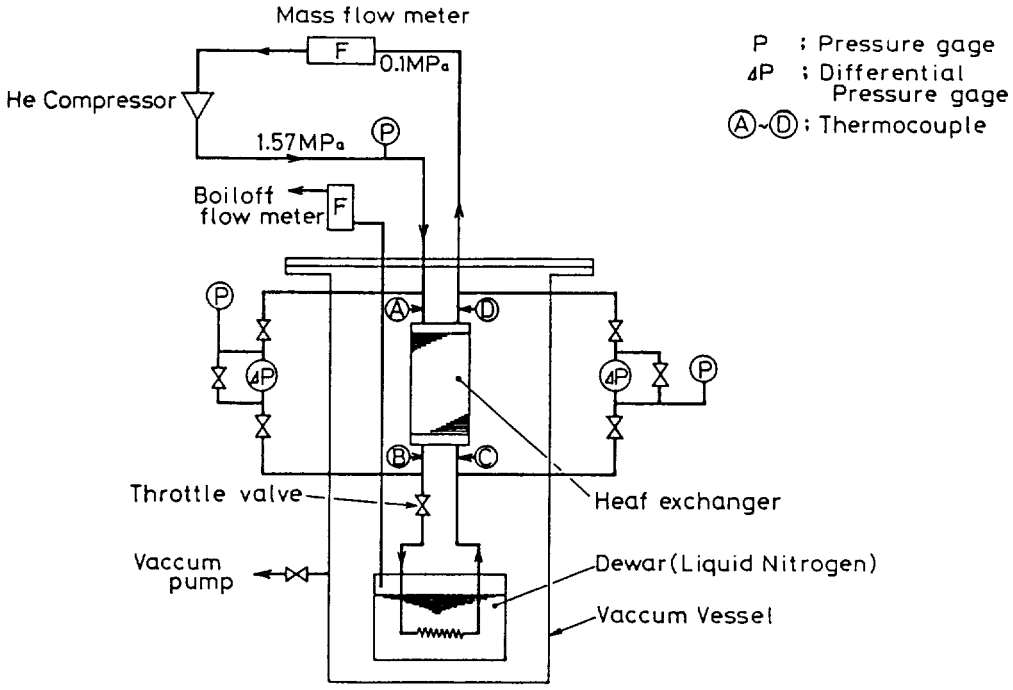

Fig. 3 Schematic diagram of heat transfer and friction loss performance test.

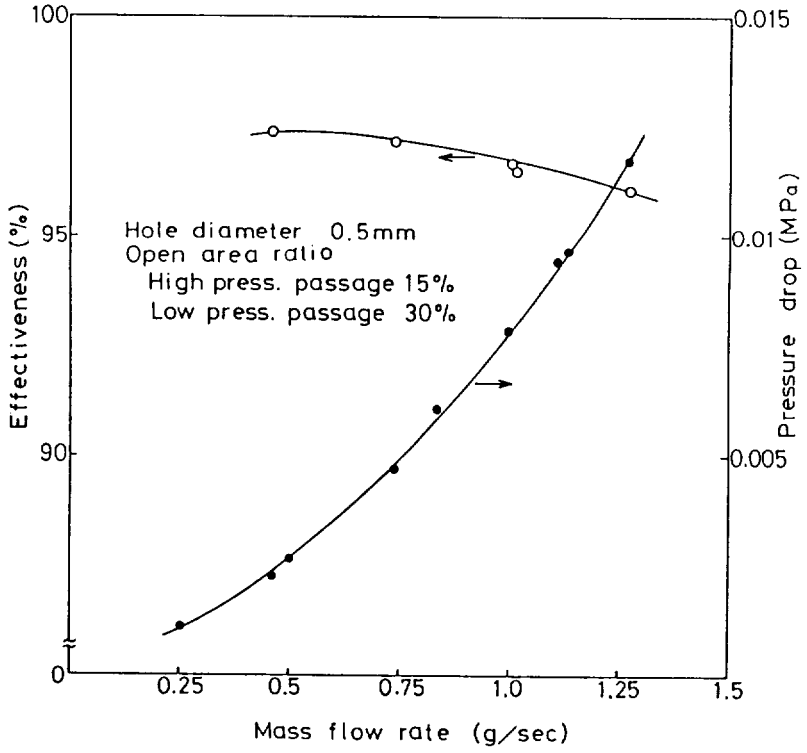

Fig. 4 Performance of laminated metal heat exchanger.

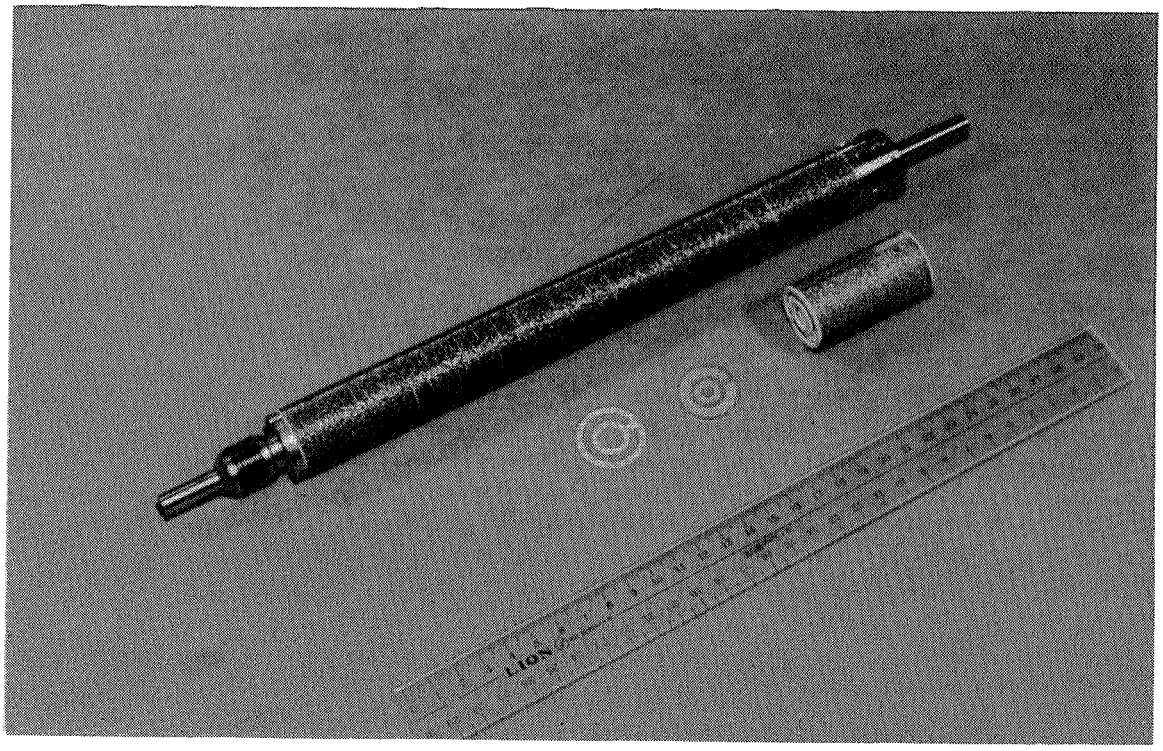

Fig. 5 Laminated metal heat exchanger.

Table 1. Result of thermal cycle test.

Item	Number of cycles	Pressure (MPa)		Helium gas leakage ($Pa\,m^3/sec$) (from high pressure passage to low pressure passage)
		High pressure passage	Low pressure passage	
Heat exchanger A	0	1.57	0.1	less than 1×10^{-4}
	235	1.57	0.1	less than 1×10^{-4}
		2.30	0.1	less than 1×10^{-4}
Heat exchanger B	0	1.57	0.1	less than 1×10^{-4}
	235	1.57	0.1	less than 1×10^{-4}
		2.30	0.1	less than 1×10^{-4}

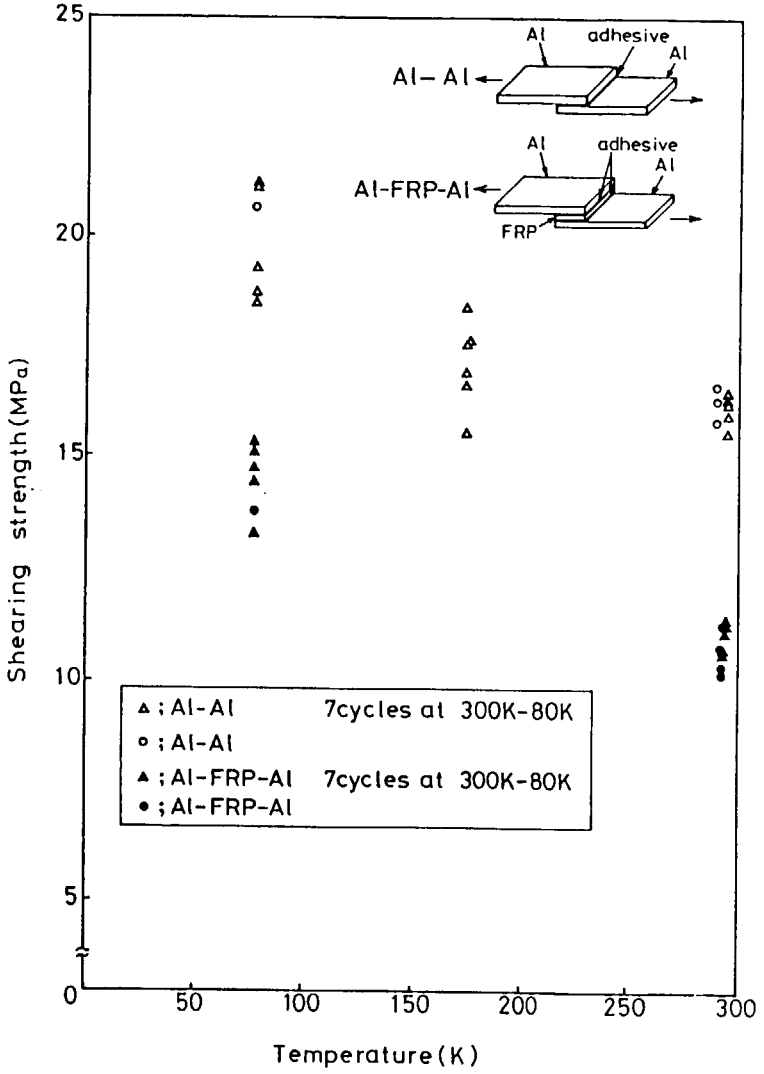

Fig. 6 Shearing strength of applied epoxy adhesive.

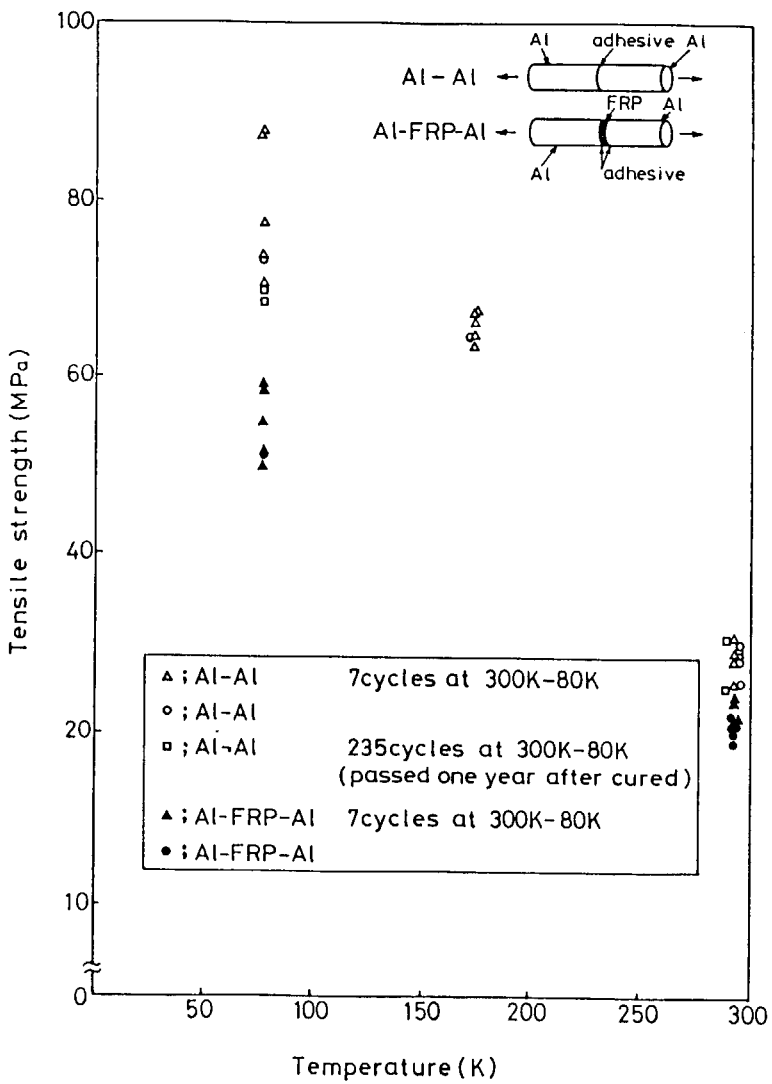

Fig. 7 Tensile strength of applied epoxy adhesive.

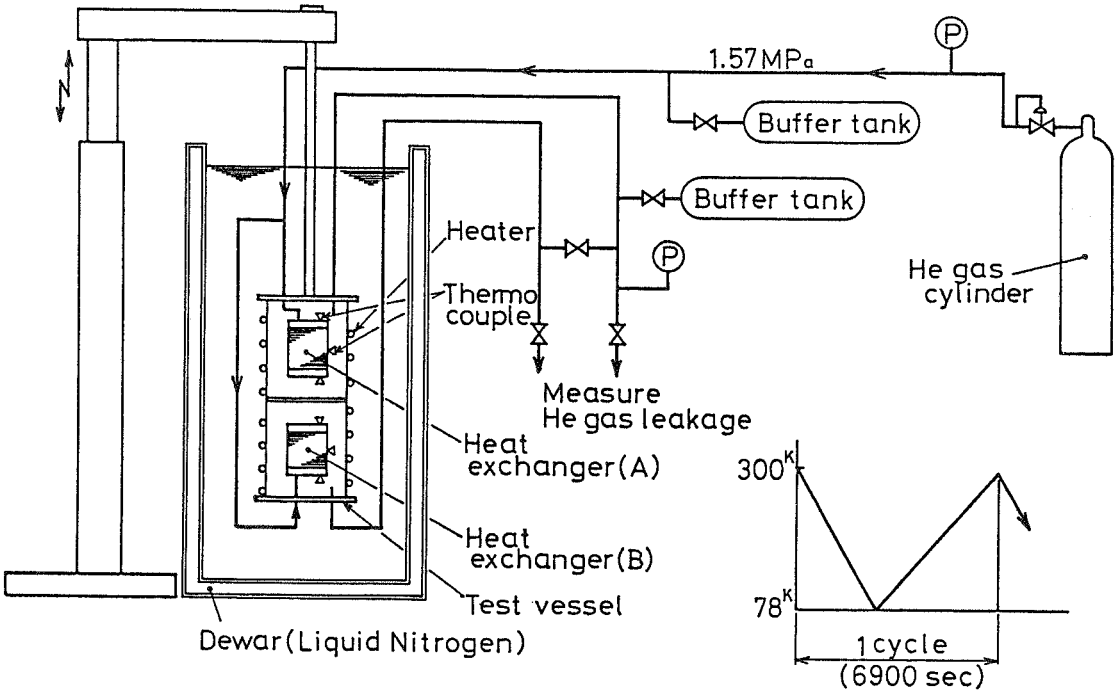

Fig. 8 Schematic diagram of thermal cycle test.

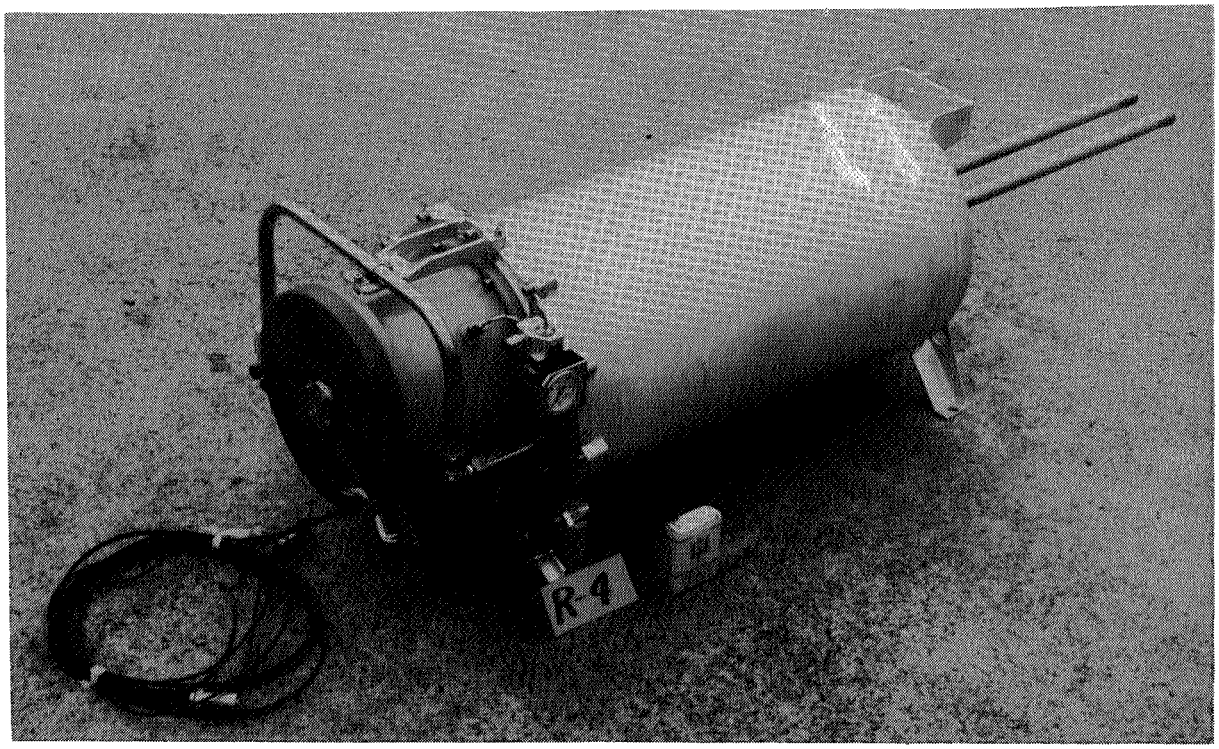

Fig. 9 Refrigerator

A MINIATURE TILTING PAD GAS LUBRICATED BEARING

Herbert Sixsmith and Walter L. Swift
Creare R&D Inc.

ABSTRACT

This paper describes the design and development of a miniature tilting pad gas bearing developed for use in very small turbomachines. The bearings have been developed for cryogenic turboexpanders with shaft diameters down to about 0.3 cm and rotational speeds up to one million rpm. Cryogenic expansion turbines incorporating this type of bearing should be suitable for refrigeration rates down to about 10 w.

INTRODUCTION

In helium refrigeration the adoption of compressors and expanders with gas lubricated bearings should eliminate wear and permit long life continuous operation with little or no maintenance. The present report describes a miniature tilting pad gas lubricated bearing which should be suitable for application in miniature cryogenic expansion turbines. The new design of bearing represents a further development of a tilting pad bearing which is described in References 1, 2 and 3. The major novel feature lies in the design which facilitates the manufacture of bearings down to internal diameters of 0.3 cm or less.

The successful operation of bearings of this size permits reductions in size and corresponding rates of refrigeration for cryogenic turboexpanders down to 10 w without appreciable loss of efficiency.

DESCRIPTION OF BEARING

The layout of the bearing is shown in Figure 1. The internal and external diameters are 0.317 cm and 1.27 cm respectively. The length is 0.33 cm. The pads are supported on elastic hinges the material of which is beryllium copper. The hinges are machined by spark erosion from a solid annulus at each end of the bearing. Each pad is given a bias in the direction of tilt to form a converging film by means of a helical compression spring. Each spring is provided with a shoe to make contact with the pad and a screw to adjust the pressure and the corresponding angle of tilt.

CONSTRUCTION

The various components of the bearing are machined and assembled ready for silver soldering as shown in Figure 2. The material of the outer housing and inner sleeve is leaded bronze. The material of the end discs is beryllium copper. After soldering, heat treating to temper the beryllium copper and cleaning, the bearing is turned to its final dimensions. A small

amount of metal is left in the bore which will be removed later by lapping to provide a smooth finish. Four offset slots are cut through the inner sleeve thereby forming four pads. The bore is then lapped out to size. The elastic hinges are then formed by removing unwanted metal by spark erosion. When the bearing has been cleaned, the springs and adjusting screws are inserted and the angle of tilt is adjusted. The bearing is now ready for operation.

THE TEST RIG

A pair of bearings have been tested in a rig as shown in Figure 3. The length of the shaft is 2.095 cm. The radial clearance between the shaft and the bearing along the hinge lines is less than 5 microns. The shaft is driven by a very simple turbine which consists of ten radial holes which break through into a recess 0.170 cm diameter in one end of the shaft. This is surrounded by a nozzle ring as shown in Figure 4.

A thrust bearing to position the shaft and support the thrust reaction from the turbine is located at the other end of the shaft. It consists of a conventional inherently compensated orifice 0.05 cm diameter. It is fed with a stream of compressed air to form a film of air between the end of the shaft and the thrust bearing. The flow restrictor in the outlet line from the thrust bearing serves to stabilize the shaft against pneumatic hammer.

A pair of capacitance probes are located one adjacent to each bearing to indicate the balance and stability of the shaft. A small flat on the shaft adjacent to the upper probe provides a signal once per revolution, which appears as a spike on the oscilloscope trace. The height of the sine wave due to shaft run-out can be compared with the height of the spike to provide an estimate of the run-out.

TEST RESULTS

In the first attempt to run the shaft whirling at exactly half speed commenced at about 5000 r/sec. The bearings were readjusted, with greater spring pressure to increase the angle of tilt of the pads. The adjustment was crude as equipment to measure the angle of tilt is not yet available. The method of adjustment consisted of screwing in the adjusting screws until the shaft would not slide freely in the bearing under the force of gravity. The screws were then backed out slightly until the shaft would again slide freely in the bearing. When the rig was reassembled the shaft was run up to 13,500 r/sec (810,000 rpm). At this speed whirling in the upper bearing commenced. The whirl speed was one quarter that of the shaft and the amplitude was quite small, about one tenth that of the spike. The whirling stopped when the rig was hit with a piece of wood which happened to be the back of a brush. After about an hour the speed was reduced to 12,500 rps (750,000 rpm). As this speed is sufficient for one potential application the rig was left running to demonstrate the absence of wear and to boost our morale. At the time of writing it has completed four weeks of continuous running.

REFERENCES

1. Sixsmith, H.; A HIGH SPEED TILTING PAD BEARING; Proceedings of the Gas Bearing Symposium at the University of Southampton, England, April 25-28, 1967.

2. Sixsmith, H.; A CENTRIFUGAL COMPRESSOR WITH GAS LUBRICATED BEARINGS; Proceedings of the 5th International Cryogenic Engineering Conference at Kyoto, Japan, May 7-10, 1974.

3. Sixsmith, H., Schlafky, A., and Swift, W.L.; A SMALL CENTRIFUGAL PUMP FOR CIRCULATING CRYOGENIC HELIUM; Presented at 1981 CEC/ICMC Conference, San Diego, CA, August 1981.

Question 1: Ralph C. Longsworth, Air Products & Chemicals, Allentown, PA
What is the anticipated efficiency of the 1/8" diameter expander?

Answer: We expect an adiabatic efficiency between 62% with a sub-critical shaft, and 70% if we can get a shaft to run above the first critical in bending.

Question 2: J. Zimmerman, National Bureau of Standards, Boulder, CO
What is the lowest power at which you can imagine a turbine expander being practical?

Answer: We believe that 10 watts is about the lowest practical power limit for expansion turbines. One can always go a bit smaller, but it gets more difficult and the efficiency decreases as the size is reduced.

Question 3: L. Lombardini, Officine Galileo, Florence, Italy
What is the material of the shaft?

Answer: Austenitic stainless steel.

Question 4: Robert D. Averill, NASA Langley Research Center, Hampton, VA
What pressure do the gas bearings operate at?

Answer: The bearings are self acting and not externally pressurized. Because the viscosity of gases is practically independent of pressure they will work satisfactorily over a wide range of pressures, from about half an atmosphere up to hundreds of atmospheres. In the test rig the pressure surrounding the bearings is about one atmosphere.

Question 5: G. Claudet, CEA, CENG/SBT, Grenoble, France
What is the start-up procedure for a dynamic gas bearing?

Answer: Because of the small size, gravity loads are very small and wear? due to friction at start up is negligible. All one has to do is to open the turbine inlet valve.

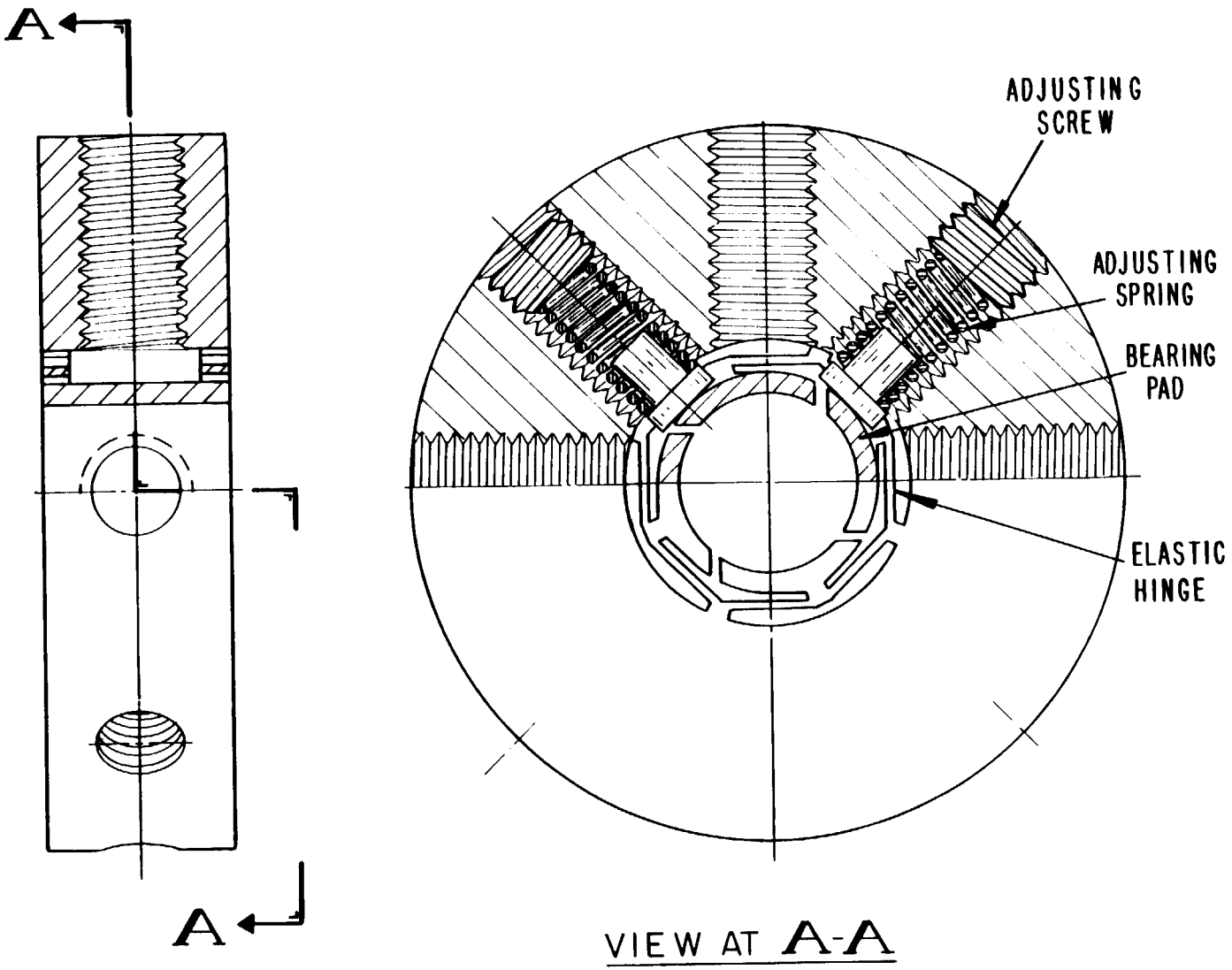

Figure 1 FINISHED BEARING SHOWING ANGLE-OF-TILT ADJUSTING SPRINGS

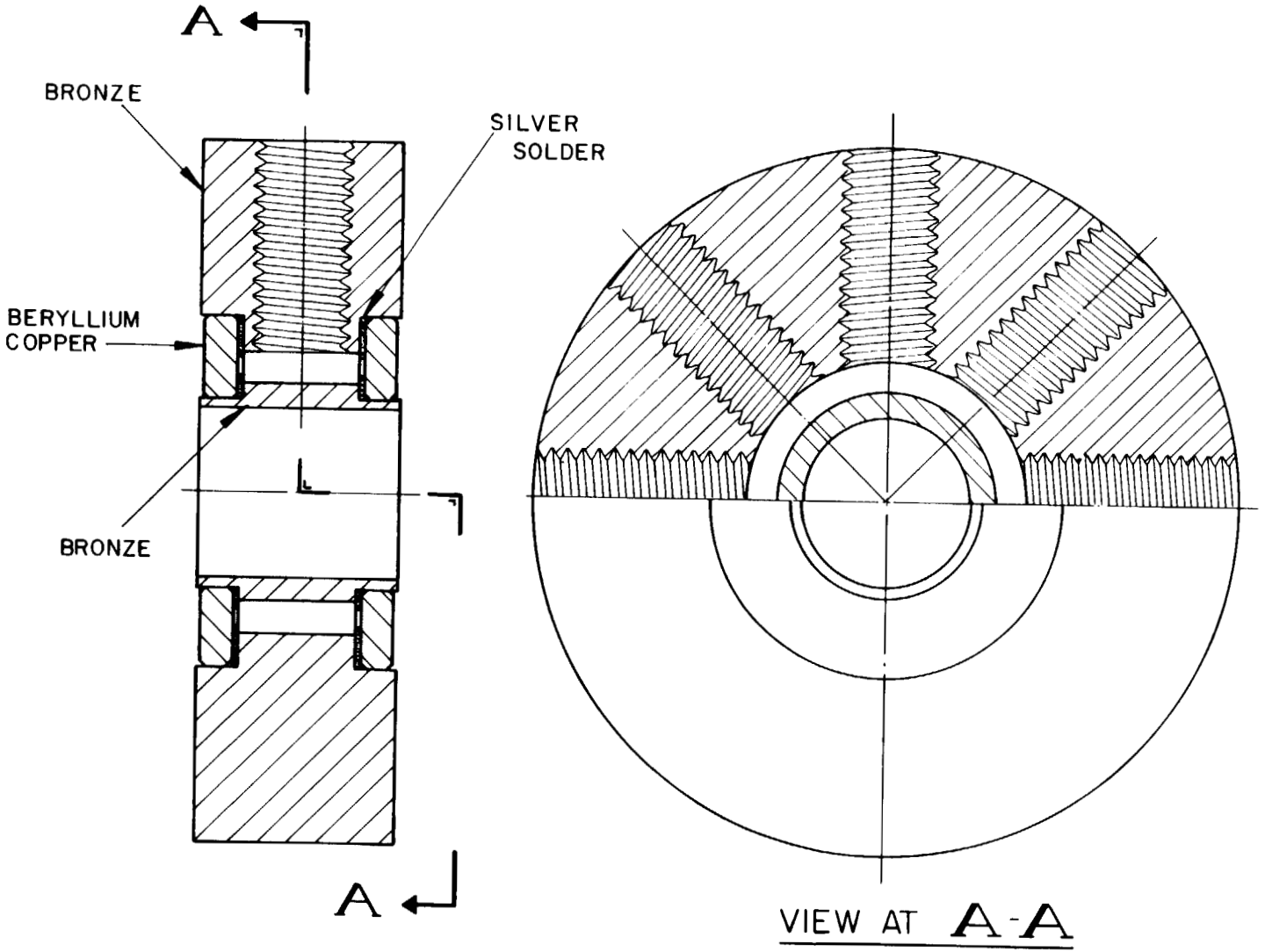

Figure 2 COMPONENTS OF BEARING ASSEMBLED READY FOR SILVER SOLDERING

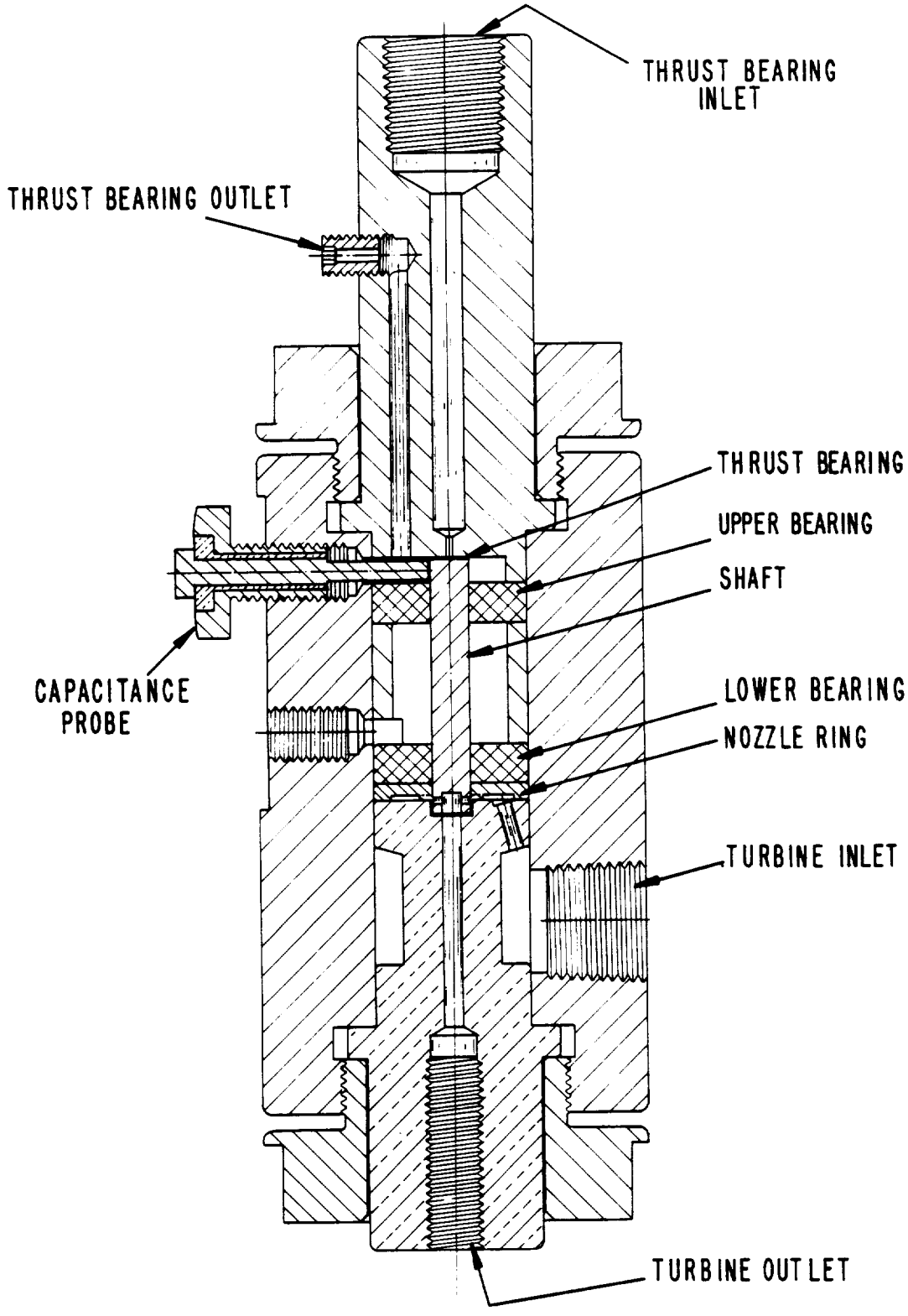

Figure 3 LAYOUT OF BEARING TEST RIG

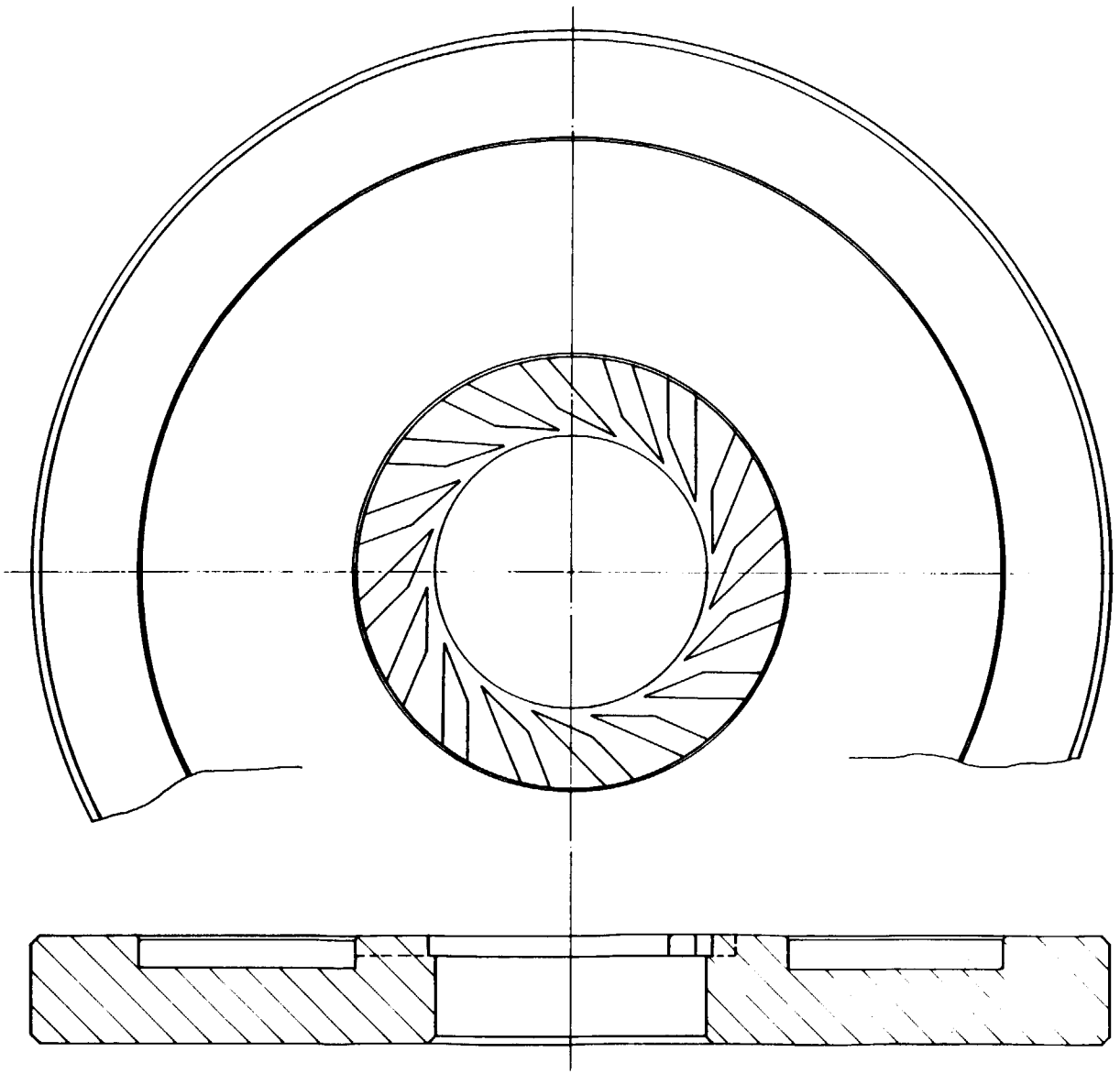

Figure 4 LAYOUT OF NOZZLE RING

LIFE TEST PERFORMANCE OF A PHILIPS RHOMBIC-DRIVE REFRIGERATOR WITH BELLOWS SEALS

E. Lindale
Philips Laboratories
Briarcliff Manor, New York 10510

D. Lehrfeld
Magnavox Electro-Optical Systems
Mahwah, New Jersey 07430

ABSTRACT

In February 1979, four Stirling cycle cryogenic refrigerators, developed by Philips Laboratories for the Johns Hopkins University/Applied Physics Laboratory, were launched into orbit aboard the P78-1 spacecraft. The refrigerators were designed to cool the detectors of two identical gamma-ray spectrometers to 77°K reliably for one year. Since launch, the refrigerators, still in orbit, have individually accumulated from 5,000 to over 20,000 hours of operation.

The refrigerators have met, and in some instances exceeded the predicted life. However, telemetry data indicates that the operating temperatures have been degrading with time. Specifically, the Lockheed Palo Alto Research Laboratory, the monitor of the spectrometers' performance, reported a 0.4°K/day short-term temperature degradation, and a 16°K increase per year. Although these increases are within acceptable limits, Philips Laboratories initiated efforts designed to minimize, or to eliminate the reported degradation.

As part of those efforts, a refrigerator identical to those in orbit was built, with one significant modification: flexible metal bellows between the crankcase and the working volume to prevent possible contaminants from migrating into the cold region. During the life test of the modified refrigerator, the temperature increase during the first three month run was 0.022°K/day, a negligible level. As of October 1982, the unit has accumulated over 12,300 hours of operation.

INTRODUCTION

Cryogenic refrigerators are normally subject to two failure modes: catastrophic mechanical breakdowns and degradation of the operating temperatures. The refrigerators addressed in this paper have operated in space for

three (3) years with no mechanical breakdown, the design goal having been one year. The operating temperatures, however, have degraded with time. This degradation has been attributed to two causes: a gradual loss of working gas by leakage past or through elastomeric static seals, and contamination of the working gas by volatile products originally present in the drive elements housed in the refrigerator crankcase.

The loss of working gas through the static seals can be significantly reduced or eliminated by using metallic seals or welded flanges, respectively. Maintaining the purity of the working gas, however, is a difficult problem. Philips Laboratories (PL), in an attempt to solve that problem, has modified the design of the four (4) refrigerators currently oribiting on the P78-1 spacecraft. Specifically, the new design approach makes use of metallic bellows to separate the working space from the crankcase, thus preventing contaminants from reaching the working space.

The new approach has been comparatively successful. This paper describes the new design and presents the experimental results attained. The work presented was fully funded by Philips Laboratories.

BACKGROUND

In 1973 Philips Laboratories, under contract to the Johns Hopkins University/Applied Physics Laboratory (JHU/APL), began to develop a miniature Stirling cycle cryogenic refrigerator capable of operating for one (1) year in space. The refrigerator was to cool the germanium detector of a gamma-ray spectrometer which was designed, flown and monitored by the Lockheed Palo Alto Research Laboratory. For maximum energy resolution, the germanium detector had to be cooled to approximately 77°K; this temperature level was to be reached and maintained as efficiently as possible using a mechanical refrigerator.

In addition to the operating life and efficiency requirements, the refrigerator had to be relatively free of vibrations. Specifically, the amplitude of its cold surface motion had to be less than 10 microns in any direction. To meet this requirement, the inertial forces induced by the reciprocating parts of the refrigerator, i.e., by the piston and by the displacer, were counterbalanced with the aid of a rhombic drive (ref. 1). The bearings of the drive, contained in the crankcase, were lubricated with a low vapor pressure grease; the low vapor pressure was to minimize the formation of gaseous contaminants; the use of a grease rather than a liquid was to help prevent lubricant migration away from the bearings.

One of the attractive features of the rhombic drive, in addition to its balanced configuration, is the absence of side loads on the reciprocating elements and seals. This feature helps minimize seal wear; it also enhances the use of bellows adjacent to the piston as a method of hermetically isolating the working space from the crankcase. Such isolation could prevent even the minimal gaseous contaminants generated by the lubricant

from migrating from the crankcase into the working space. Therefore, the original refrigerator design included bellows type metal seals.

However, several bellows failed during the preliminary performance tests. Diagnostic analyses suggested that the failures were induced by high stresses which resulted from non-uniform bellows cross-sections. The solution, obviously, was to select bellows having acceptably uniform cross-sections. However, a non-destructive selection method was time consuming, and its application would have jeopardized the timely delivery of the refrigerators. Therefore, it was decided to omit the bellows from the deliverable units, and rely solely on the conventional reinforced-Teflon compression type seals for separating the crankcase from the working space. The decision was confirmed by test results which indicated that the outgassing of the low vapor pressure lubricant, and the associated contamination of the working gas, was lower than anticipated, and could therefore be tolerated.

Indeed, tests with the first refrigerator without bellows showed no oil vapor contamination. However, after approximately 1,000 hours of operation, its cold production began to deteriorate, and its operating temperature continued to increase. Upon warm-up and disassembly of the refrigerator, several droplets of water were found on the displacer, suggesting that the temperature degradation was caused by water contamination. This was confirmed by the results achieved when more stringent purging and filling procedures were adopted. Specifically, by using a vacuum system to evacuate the working space, and by raising the refrigerator envelope to 140°F during the purging procedure, the rate of operating temperature degradation was reduced from 0.9°K/day to 0.4°K/day. The latter rate was acceptable to the ultimate user. Therefore, using the method just described, the remaining refrigerators were purged, successfully tested, and delivered.

Of the six refrigerators built (ref. 2), one was placed on life test at JHU/APL, four were integrated with the experiment on the P78-1 satellite (ref. 3), and launched into space in February 1979, and one was retained as a spare. No mechanical failures were experienced with any of the refrigerators (ref. 4, 5); however, the temperature degradation problem remained, although the rate of degradation was significantly lower than that experienced at the outset of the program. As expected, outgassing products were still being generated in the refrigerator crankcase, and the conventional seals did not prevent their migration into the working space.

It should be noted that following the removal of the bellows seals from the six deliverable refrigerators, Philips Laboratorires initiated a bellows testing program. Of the twenty pair of bellows available, six pair were randomly selected for endurance testing. The first two sets failed before achieving 1.0×10^6 cycles, which was determined to be the minimum number of cycles required to indicate the bellows reliability. One set having reached 1.0×10^6 cycles, continued on to exceed 5×10^8 cycles. These favorable results, and the failure to eliminate the contamination problem by

improved purging methods, suggested that the bellows sealing approach be reevaluated by conducting tests on an actual refrigerator.

DESCRIPTION OF REFRIGERATOR

To evaluate the performance of the refrigerator/bellows seal combination, Philips Laboratories fabricated the refrigerator shown in figure 1, which was both thermally and physically equivalent to those delivered to JHU/APL, except for the addition of bellows seals. As an aid to the reader, the major characteristics of the refrigerator and some of its performance parameters, although previously published, are given in table I. It should be noted that the cold production and input power levels can be tailored, within certain limits, to specific operational temperature requirements.

A cross-sectional view of the refrigerator is shown in figure 2a along with an enlarged view of the bellows seal area shown in figure 2b. As indicated, two bellows are used in a nested, or concentric configuration. One end of each bellows is hermetically connected to a stationary element of the refrigerator; the others are hermetically connected to the reciprocating elements, i.e., one to the piston rod, the other to the displacer rod. The major characteristics of the two bellows are given in table II. Each side of the bellows seal arrangement, that is, both the crankcase and the working space, are pressurized (with helium) to 4.8×10^5 Nm^2, reducing the pressure differential across the seal to essentially zero.

TEST PROGRAM AND RESULTS

The tests were run at a refrigerator speed of 1,000 rpm, with heat loads of 0.3 watts and 1.5 watts at the lowest and intermediate temperature levels respectively. The heat-rejection flange, the area where the heat of compression had to be dissipated, was maintained at 300°K $\pm$ 2°K. Testing commenced in January 1981. Although it was intended to run the test continuously, several interruptions were experienced, due to instrumentation failures, power outages, and the need to periodically recalibrate certain instruments.

For 800 hours of initial operation, data is available for comparing the output temperature stability of three (3) refrigerators which had no bellow seals, with the test refrigerator containing bellows. Specifically, the three refrigerators which had conventional seals were tested at Philips Laboratories prior to delivery to JHU/APL. The comparison is given in figure 3; it is obvious that the output temperatures of the refrigerators which had conventional seals, designated S/N 1 through S/N 3, degraded with use, while that of the test unit, designated PL, remained relatively constant. Since the four units were identical in every respect except for the method of separating the crankcase from ther working space, it is evident that the significant improvement in performance was due to the bellows seal.

It should be noted that a helium leak in the crankcase developed after the test was initiated. It was assumed that the leak was the result of static elastomeric seal relaxation. The associated loss of helium pressure, 3.5×10^4 Nm^2, was compensated for on a weekly basis. No attempt was made to repair the leak, since it had no effect on the bellows seal tests being conducted. However, as a precautionary step, the pressure in the working volume was monitored to insure no changes in the working pressure occurred. Indeed, no changes occurred; consequently there was no need to replenish the helium pressure in the working space.

The test described in this paper ran for over 12,300 hours. The performance of the refrigerator in that interval is summarized in the graph of figure 4. Some noteworthy events which occurred during the test period are highlighted next.

- During the first 3,064 hours of continuous running, the temperatures at both cold stages varied within a 5°K band. The monitoring instrumentation, the power input to the motors and to the cold finger heaters were reset, and testing resumed. During the next 1,360 hour continuous test period, the operating temperatures remained within the original 5°K band. At that point, that is, after a total of 4,424 hours of operation, the refrigerator was taken off the test stand for demonstration at a meeting.

- Following its reactivation, the test ran for another 1,702 hours (i.e., 5,944 total operating hours) before a power failure.

- The one year minimum expected operating life was attained with a temperature increase of 10°K on the lowest temperature cold surface and 7.5°K increase on the intermediate temperature cold surface. This translates to an average temperature rise of 0.027°K/day and 0.020°K/day, respectively. These rises were attributed to seal wear, inasmuch as no decrease in the operating pressure was experienced in the working space.

- After 1,660 additional operating hours, i.e., 10,420 hours total, the temperature increased at the coldest stage from 80°K to 87°K, and at the intermediate stage from 138°K to 142°K. The test was stopped; the refrigerator was allowed to warm up to ambient temperature, and the external surface of the cold finger checked for possible frost, since there was a suspicion that the vacuum level surrounding it was not adequate. No conclusions could be reached, and the refrigerator was placed on test again. Following 1,068 additional hours, i.e., 11,488 hours total, the temperatures were at 86.5°K (coldest surface) and 142°K (intermediate surface).

- After 854 hours of additional operation, i.e., 12,342 hours total, both cold finger temperatures showed a significant increase; this was accompanied by a light tapping noise from the cold finger. The testing was stopped, the refrigerator depressurized, and the cold finger removed to expose the displacers. Wear debris from the piston

and displacer seals appeared to be minimal, although some particles had evidently migrated through the first stage displacer to the second stage. However, part of the second stage displacer seal, which is a Rulon band, had lifted from the titanium shell, a failure ascribed to fatigue at the epoxy joint (figure 5). The motion of the displacer seal rubbing against the inner face of the cold finger forced a corner of the seal down over part of the first stage displacer shoulder. This corner formed a wedge between the displacer shoulder and the inner shoulder of the cold finger; hence the loss of cold production and the tapping noise.

- The piston and first stage displacer seals, although worn, showed potential for lasting perhaps a further twelve months of operation.

  The bellows will undergo further testing to determine their life capabililty.

  The second stage displacer seal was replaced, and the refrigerator placed on test again. At this writing, the unit, and the original bellows seal, have accumulated over a thousand hours of additional operation.

PERFORMANCE CHARACTERISTICS

Following the delivery of the six (6) refrigerators to JHU/APL, but prior to the initiation of the test described above, Philips Laboratories subjected the unit shown in figure 1 to off-design point tests. Specifically the off-design tests were to generate information for applications where the refrigeration requirements were different from those shown in table I. To generate such information, two major refrigerator parameters were varied: heat load on the cold stages, and operating pressure. The results are presented in figures 6, 7 and 8.

The effects of the heat load (including no load) on the operating temperatures of the two cold stages are given in figures 6 and 7. In the former, the heat load on the coldest stage was varied from 0 to 1 watt of heat, with the intermediate stage left unloaded. In the latter, the approach was reversed: the coldest stage was not loaded, while the load on the intermediate stage was varied from 0 to 2 watts of heat. In both instances, three operating pressures were used: 4.8×10^5 Nm^2, 5.5×10^5 Nm and 6.2×10^5 Nm^2, with the operating speed maintained constant at 1000 rpm.

Figure 8 illustrates the cold production capabilities of the refrigerator using different heat loads on both stages to obtain identical temperatures. This was accomplished by selecting various loads for the intermediate stage to achieve specific temperatures, i.e., 100°K, 120°K, and 140°K. The heat loads on the cold stage were adjusted so that these same temperatures were achieved, and heater power was measured.

SUMMARY

As of October 1982, the test refrigerator has accumulated over 12,300 hours of operation, including long periods of continuous runs. The bellows, with the initial life test data included, have flexed for 1.4×10^9 cycles. During the operational periods cited above the temperature of the cold surfaces remained within the range specified for the refrigerators which were delivered to JHU/APL.

TABLE I.--MAJOR REFRIGERATOR CHARACTERISTICS AND PERFORMANCE

Item	Results
Cold Production	0.3 W @ < 90°K; 1.5 W @ 140-170°K
Input Power	< 30 W
Speed	1000 rpm
Vibration of Cold Surface	3.3 μm
Acoustic Noise	< 48 dBA at 91 cm with a 40 dBA background
Size	15 cm x 18 cm x 30 cm
Weight	5.5 kg w/o electronics; 7.2 kg with electronics
Residual Torque Due to Starting/Stopping	Virtually zero

TABLE II.--MAJOR BELLOWS CHARACTERISTICS

Item	Outer Bellows	Inner Bellows
O.D. (mm)	44.2	24.1
I.D. (mm)	33.0	14.5
No. of Convolutions	16	21
Convolution Pitch (mm)	2.7	2.1
Wall Thickness (mm)	.14	.12
Material	Nickel, gold plated	

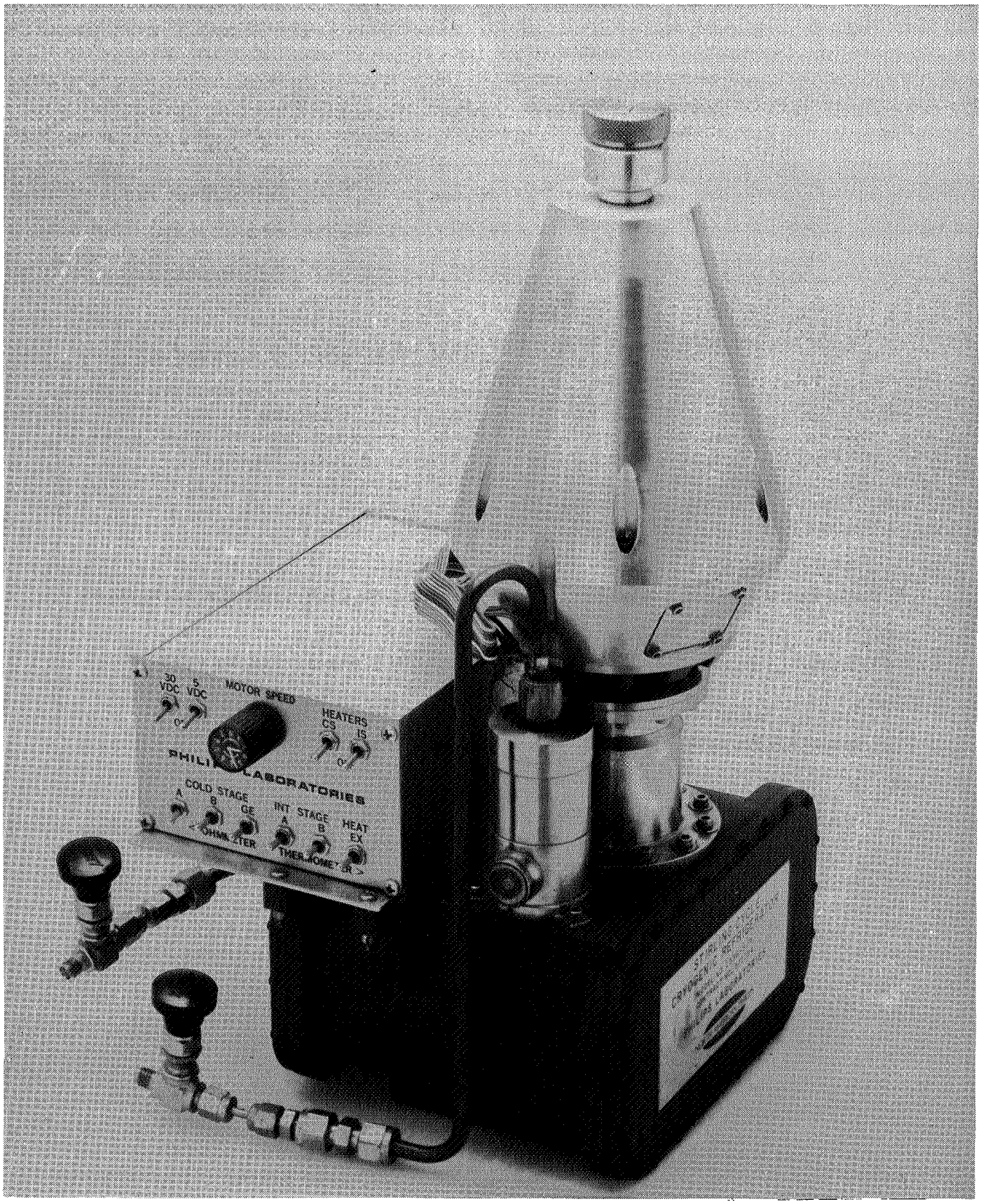

Figure 1. Fully instrumented Stirling cycle refrigerator used for testing.

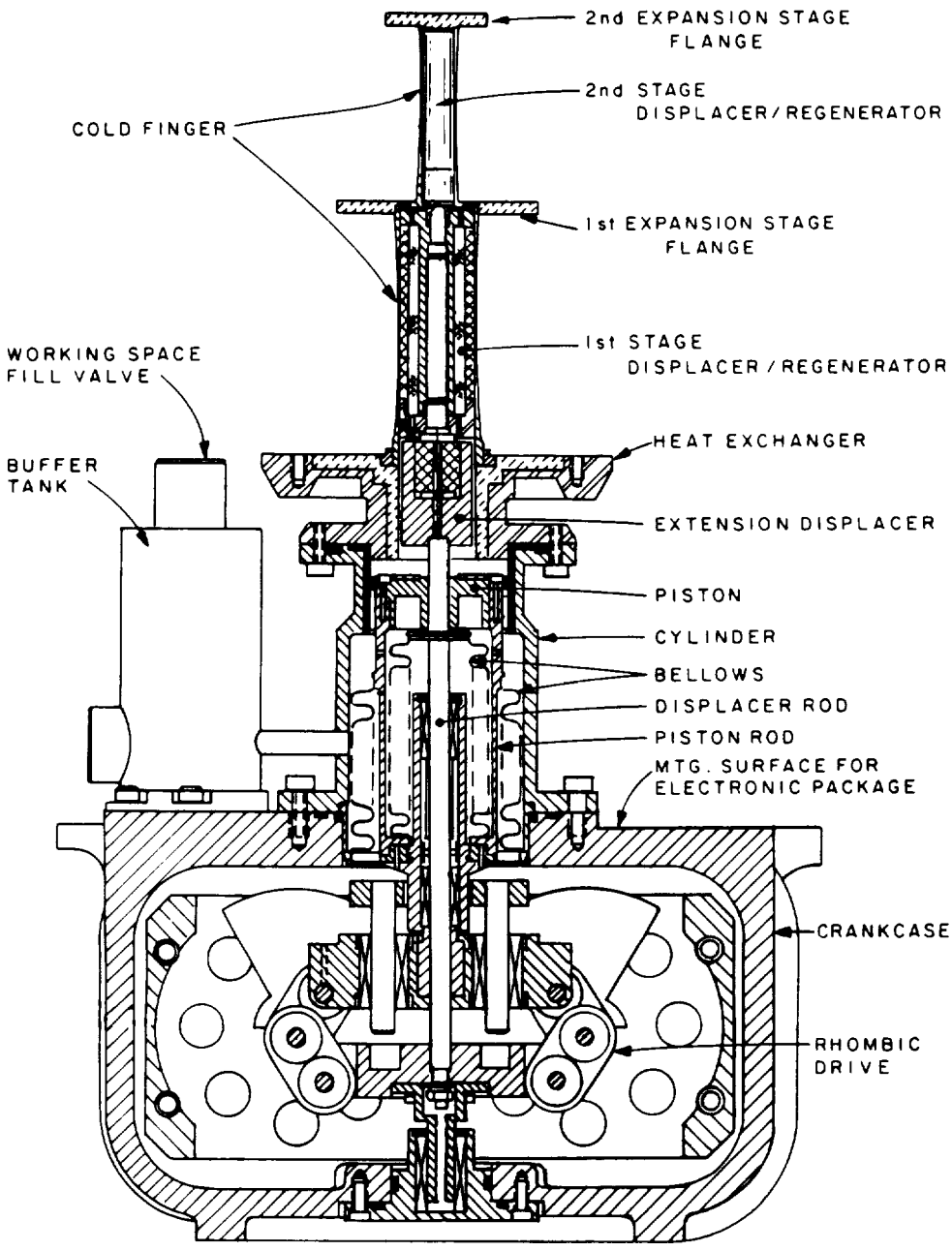

Figure 2a. Cross-sectional view of refrigerator.

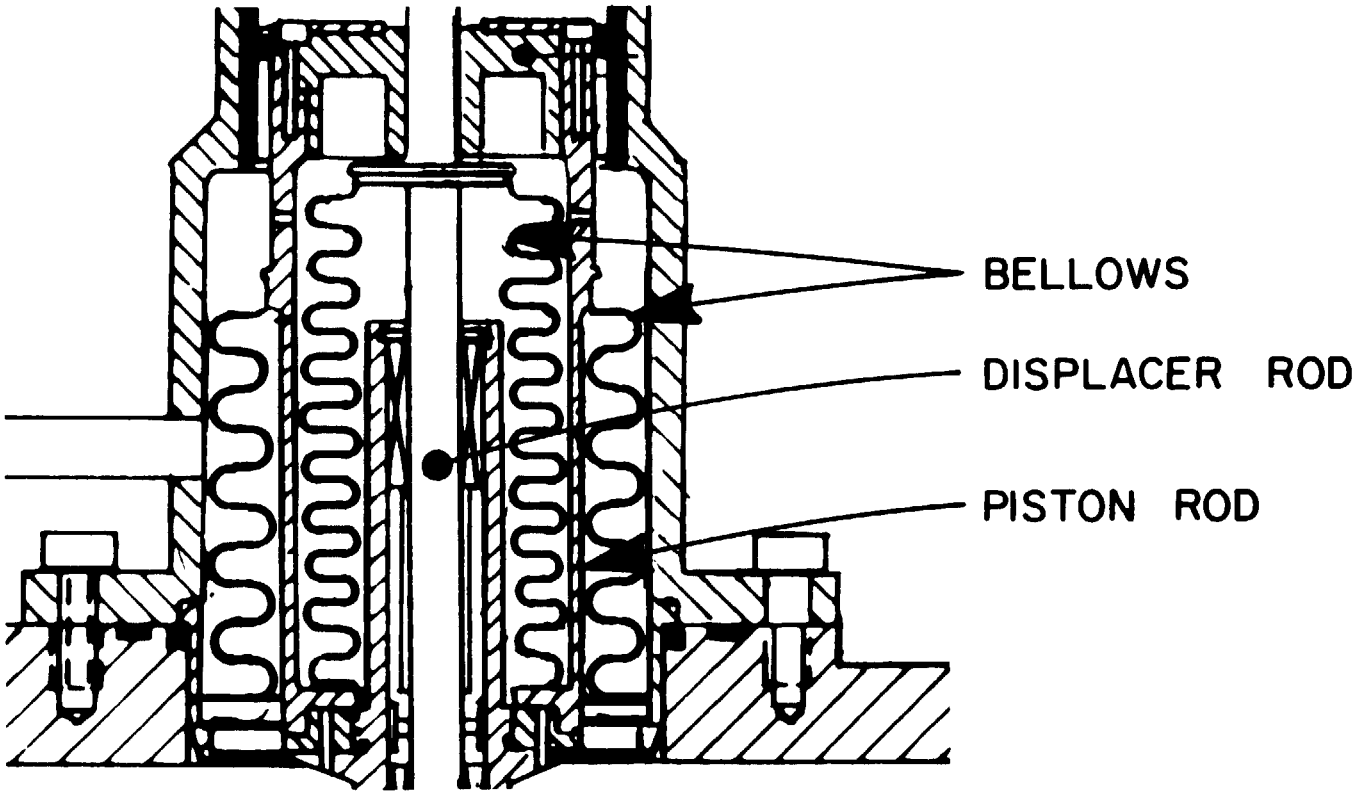

Figure 2b. Closeup of bellows seal area.

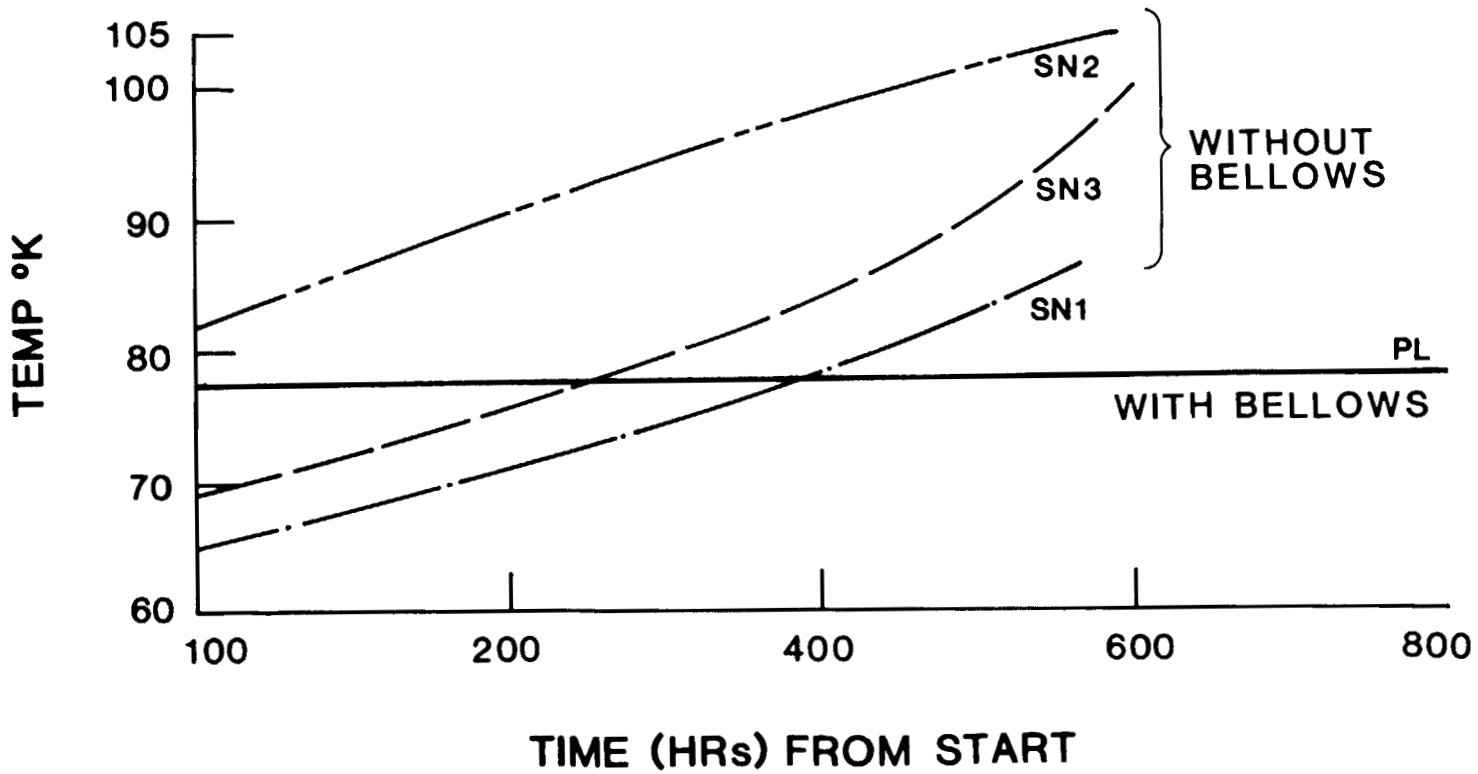

Figure 3. Cold-end temperature vs. operating time for first 800 hours.

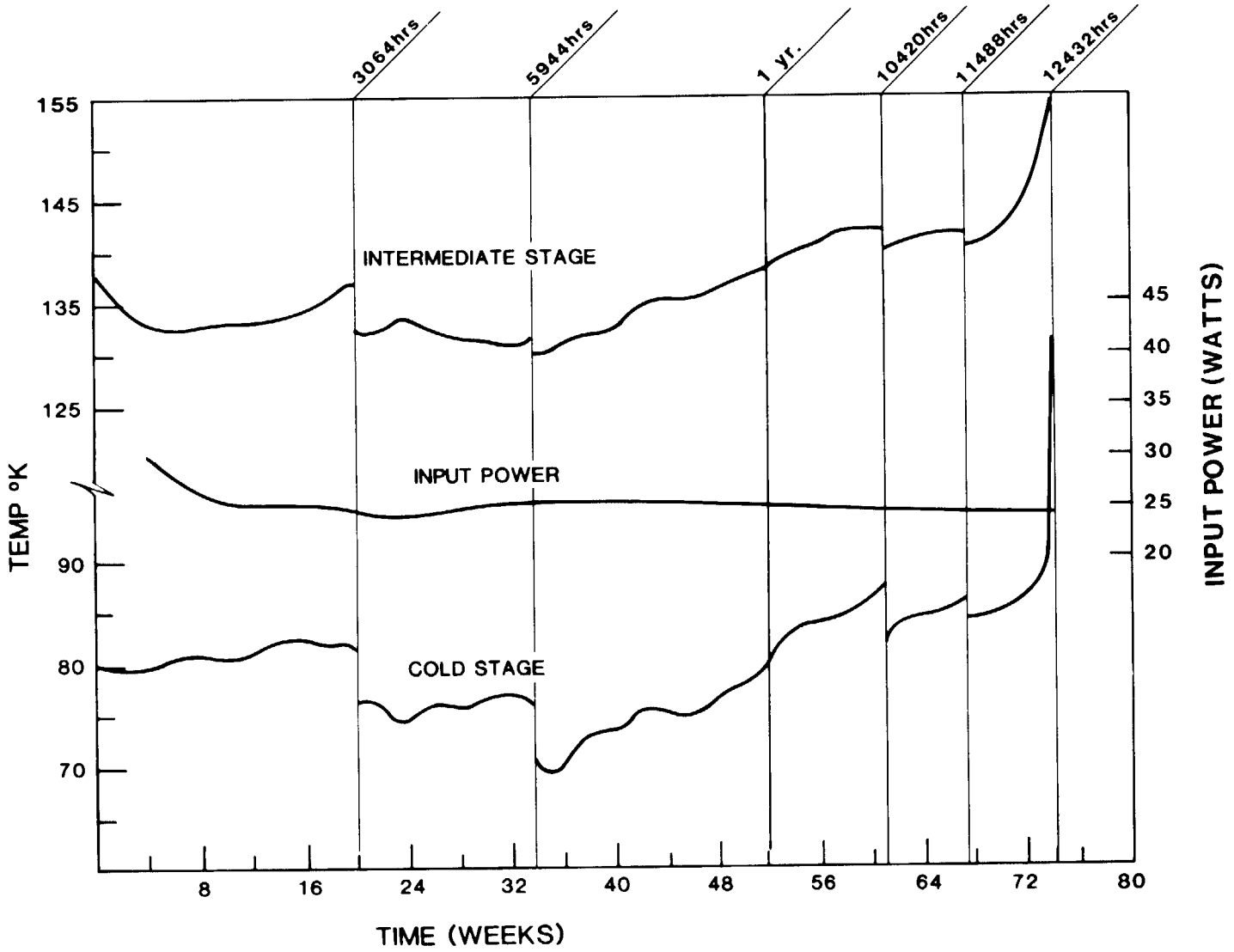

Figure 4. Operating temperatures and input power versus elapsed time.

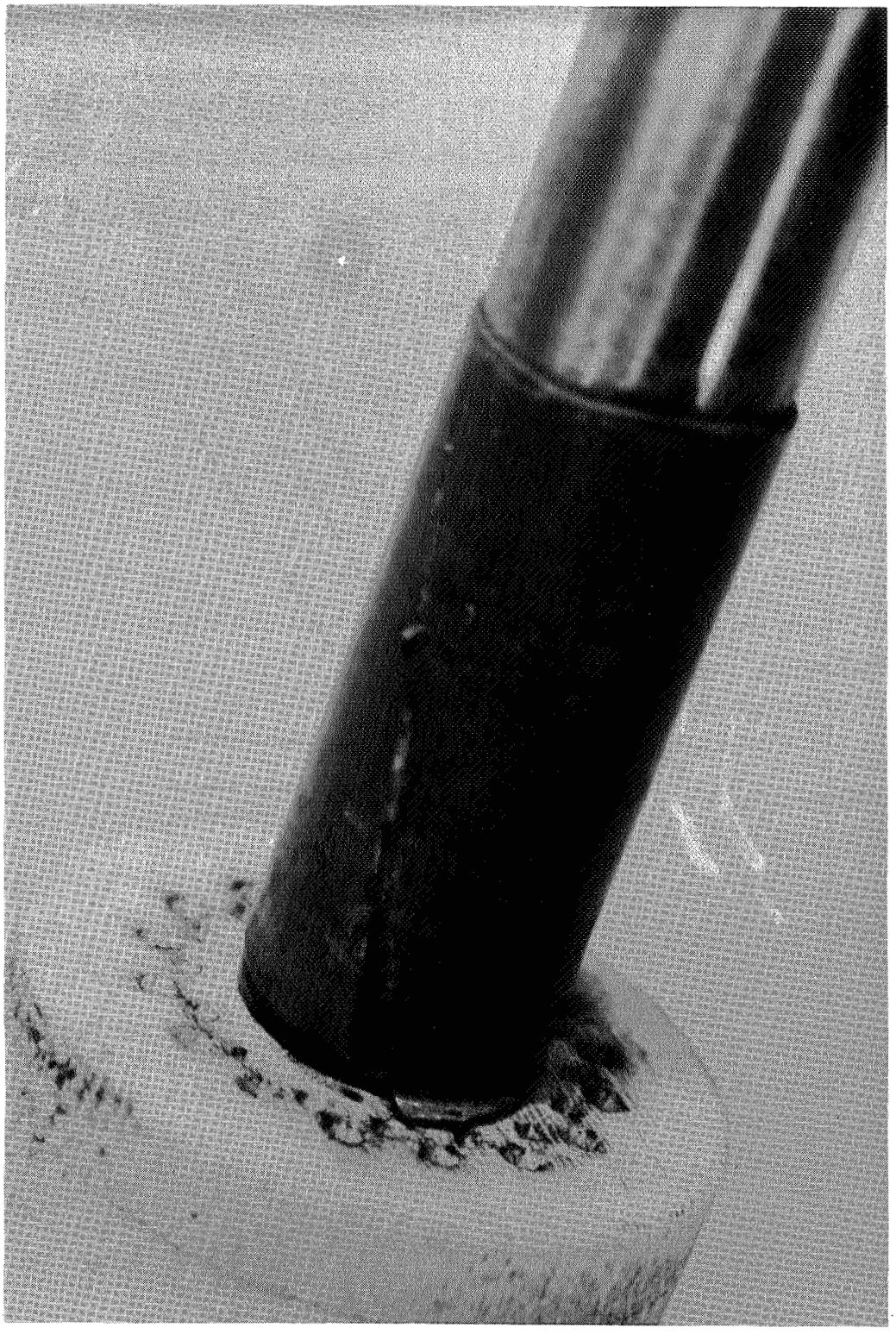

Figure 5. Photograph of the damaged seal.

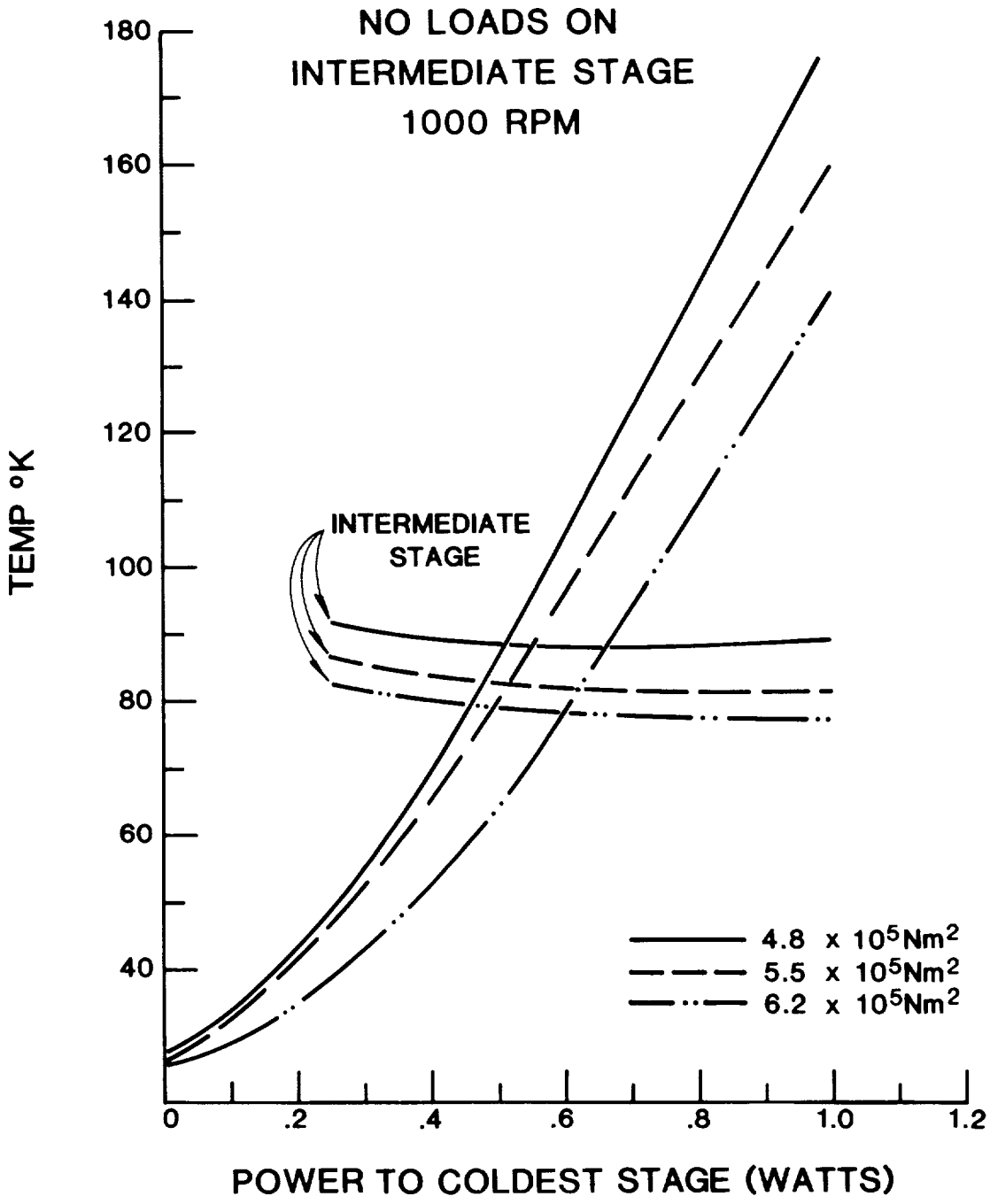

Figure 6. Intermediate-stage temperature vs. heater power to coldest stage.

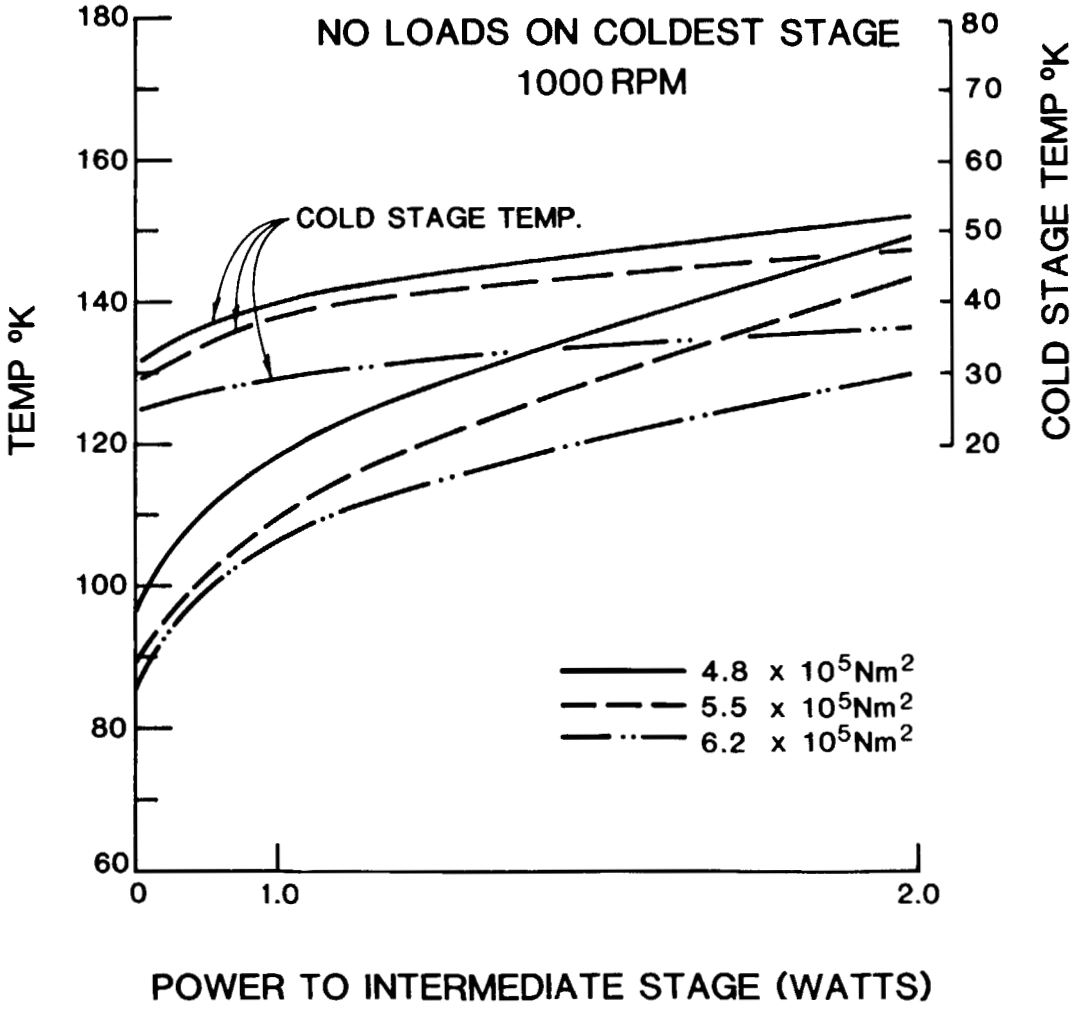

Figure 7. Coldest stage temperature vs. heater power to intermediate stage.

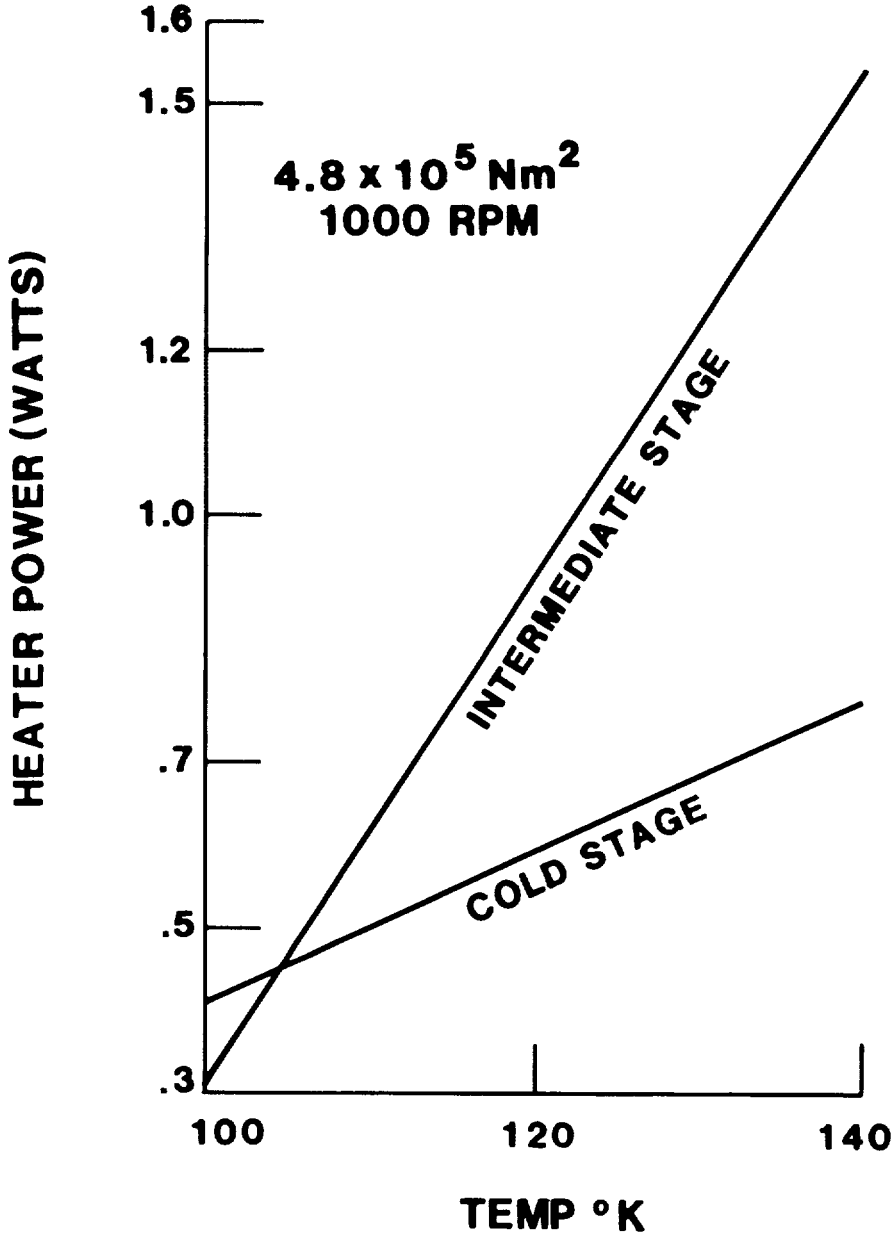

Figure 8. Cold production vs. heater loads.

REFERENCES

1. Meijer, R. J.: Philips Tech. Rev. 20, 245, 1958/59.

2. Balas, C., Jr. and Wingate, C. A., Jr.: An Efficient, Long-Life Cryogenic Cooling System for Spacecraft Applications. International Astronautical Federation (I.A.F.) XXXVIth Congress, Lisbon, Portugal, Sept. 1975.

3. Naes, L. G. and Nast, T. C.: Long Life Orbital Operation of Stirling Cycle Mechanical Refrigerators. SPIE 24th Annual International Technical Symposium and Exhibit, July 1980.

4. Leffel, C. S., Jr.: Performance of the Serial No. 1 Cryogenic Refrigerator, March 18, 1976 to November 3, 1976. JHU/APL QM-76-144, Nov. 1976.

5. Leffel, C. S., Jr. and Von Briesen, R.: The APL Satellite Refrigerator Program Final Report. JHU/APL QM-80-178, July 1981.

SPLIT-STIRLING, LINEAR-RESONANT, CRYOGENIC REFRIGERATORS

FOR DETECTOR COOLING

Daniel Lehrfeld

Magnavox Government and Industrial Electronics Company
Electro-Optical Systems
46 Industrial Avenue, Mahwah, N. J. 07430

ABSTRACT

Unfortunately, for user and manufacturer both, the closed-cycle cryogenic cooler to date has deserved its reputation as the "weak-link" in IR systems. When the cooler requires service at intervals of a few hundred hours at best, the quality of the system it serves is unfairly diminished.

This paper addresses technological advances in the art of Stirling-cycle coolers which will increasingly cause that image of military cryocoolers to change for the better.

For the past decade, military IR systems have preferred to see cryogenic coolers provided as "split" units; separating the functions of compressor and cold-end for system packaging and vibration isolation reasons.

A family of split-cycle coolers designed for long MTBF and in the final stages of development is the focus of the discussion. Their technological evolution, from multi-year-MTBF satellite system Stirling coolers developed in the U.S., and the UA 7011 cooler (the first all-linear, military, production cooler) developed in Holland, is explained.

Two new split-cycle machines are discussed. They provide 1/4 watt and 1 watt (nominal capacity) at 80°K and 85°K respectively. These linear-resonant, free-displacer Stirling coolers are designed for thousands of hours of service-free operation. They are designed to be compatible with standard U.S. 60 element and 120/180 element detector/dewars,respectively.

The technologies of linear-resonant compressor and free-displacer expanders as embodied in these machines is discussed in sufficient detail that the reasons for their superior performance (i.e., service-free life, low acoustic noise) will be clear.

INTRODUCTION

The Stirling refrigeration cycle, in its fifth decade of development, is by now well known to the technical community. One will recall that in

its simplest embodiment, two pistons (the compressor piston and the gas displacer) operating on a fixed charge of non-condensible gas (helium), cause the gas to be compressed, cooled, expanded and reheated repeatedly so that in a certain portion of the machine, net refrigeration at very low temperature is achieved.

The ideal Stirling cycle is "Carnot-limited", that is, its efficiency for cold production is the highest possible. It is not the intent of this paper to review the theory of operation; for that the reader is referred to the original references, Reference 1 and 2, or a number of later papers. Rather, we shall discuss new embodiments which have been developed recently from innovations introduced by the same research laboratories which "discovered" Stirling cycle technology in this century, the Philips Research Laboratories of N.V. Philips in Holland.

LIFE LIMITING CONSIDERATIONS IN STIRLING COOLERS

The most significant life-limiting mechanisms in conventional miniature Stirling refrigerators are wear and contamination.

Figure 1 is a schematic illustrating a conventional embodiment of the Stirling refrigerator, and useful for pointing out its weaknesses. The two pistons must reciprocate with a fixed phase relationship for the refrigerator to function; as shown, this is accomplished by using a kinematic mechanism to convert rotary motion from a motor/crankshaft into the required linear motion of the pistons. The mechanism requires bearings which in turn require lubricants. Since the dynamic seal around the piston is not hermetic, lubricant vapors can migrate and be "gettered" in the low temperature region of the machine. Alternatively, without adequate lubrication or lubricant containment in the bearing, bearing failure can result.

The kinematic mechanism inparts a side-load which must be carried by a dry-lubricated guide on the pistons. This load causes accelerated wear of the guide bearings and seals, which both decreases compression and produces particulate debris over time.

The processes of wear and contamination are inter-related. Particulate contamination is an obvious wear product, and can obstruct internal heat exchanger flow passages within the machine. Not as obvious are gases, which are evolved from freshly exposed wear surfaces, and vapors evolved from the lubricant under high shear stress and temperature. These gaseous contaminants freeze within the cold region of the machine and degrade cooling performance as well.

HISTORY OF THE PHILIPS LINEAR-RESONANT COMPRESSOR, FREE DISPLACER MACHINE

In 1968, recognizing that the weak-link in conventionally-driven embodiments of Stirling cryogenic coolers developed to date was the compressor (bearing, sealing, and contamination problems, as well as high cost to manufacture), work was begun in the Philips Research Laboratories in Holland on the concept of a linear-resonant compressor, driven by a linear motor,

for application to the Stirling cooler. This type of "free-piston, free-displacer" machine concept has far fewer moving parts, has eliminated crankshaft, bearings, and side-loads on dynamic seals, embodies clearance seals, eliminates lubricants, and can preserve the inherent efficiency of the Stirling cycle (the purpose of the "resonant" portion of its nomenclature), thus lending itself to long life and low cost in production. This new construction is discussed in a later paragraph.

The first generation of linear-resonant Stirling cooler product developed in Holland was the non-military MC-80 (Miniature Cooler, 80°,K), 1W @ 80°K cooler, brought into limited commerical production in 1975 by the Science and Industry Division of N.V. Philips.

In 1976, a second generation of linear-resonant Stirling coolers began in parallel in Holland and the U.S. In Holland, Philips Usfa B.V., a manufacturer of military infrared systems and products, undertook the development of a new cooler, in effect, a militarized version of the MC-80 machine. Initially dubbed the MMC-80 (Militarized Miniature Cooler, 80°K), and later officially designated the UA-7011 (see figure 2), this cooler was designed for and met full specifications for field, vehicle and aircraft use. Utilizing rare-earth cobalt magnets in its linear motor, and hermetic sealing of the helium, that cooler was brought into production and remains in production through the present day. Of particular significance is the fact that the cooler is sold with a 2500 hour guarantee on service-free MTBF.

The UA-7011 is distributed as the Magnavox MX7011 cooler in the U.S.; it is produced for Magnavox by Philips Usfa B.V. in Holland. While not readily compatible with standard U.S. military FLIR system components, there is interest in this highly reliable machine for use as a satellite-borne unit for cryogenic cooling in space.

In the U.S., Philips Laboratories Division of North American Philips Corporation, a Magnavox affiliate, began R&D for NASA and DARPA, applying the design concepts of the linear-resonant construction to satellite system coolers intended for three to five years of maintenance-free operation (reference 3.)

Figure 3 is a photograph of the NASA machine, designed for 5 W @ 65°K of refrigeration capacity. Its refrigeration performance has been proven in recent tests.

Currently at Magnavox, there is ongoing a program to design, fabricate, and prepare for test the first prototype operational cyrogenic cooler of this type for future use in multi-year satellite systems.

The third generation of linear-resonant cooler product development activities is ongoing at present and is the subject of this paper. The design experience and production know-how established in the development of the UA7011 cooler has been brought to bear on development of a family of split-cycle linear resonant coolers. This family consists of a standardized

compressor section and two cold fingers which are designed expressly to interface with U.S. 60 element and 120/180 element detector/dewar assemblies; the resulting coolers having 1/4 watt and 1 watt refrigeration capacities, respectively.

Magnavox/EOS is the U.S. distributor for these linear-resonant coolers. Currently, these coolers are produced in Holland.

DISCUSSION

The Stirling cycle requires the interphased reciprocating motion of its two major elements, the piston and the displacer. Traditionally, this motion was generated by either conventional crank-type mechanisms or by the special Philips rhombic drive. In both instances, the rotary motion supplied by an electric motor had to be translated into the required linear motions of the piston and displacer.

In the linear-resonant cooler, the piston is directly reciprocated by supplying an ac waveform to the coil of an electric motor. The piston, in turn, by fluidic coupling, drives the free-displacer.

Elimination of the direct-drive coupling to moving piston and displacer made the problem of analysis, optimization, and design of the coolers far more difficult. While formerly the analysis task was fundamentally a problem in thermodynamic modelling and analysis, the step to free piston-free displacer required the integration of equations of the dynamics of motion of the moving masses, the electrodynamic equations governing the performance of the linear-motor,and more careful analysis of the flow-losses in the system. Several years of research, experimentation, and development were spent in validating the design methods and principles applied to this new class of machines. References 4 and 5 discuss the thermodynamic/dynamic and electrodynamic theory and principle of operation of the machine in detail, and should be consulted by those desiring a detailed theoretical understanding of the linear-resonant, free displacer, free-piston Stirling cooler.

LINEAR-RESONANT COMPRESSOR

Figure 4 illustrates the construction of the linear-resonant compressor. The compressor contains a piston which is fixed to the moving coil of a rare-earth-cobalt permanent-magnet linear motor. The linear motor is an alternating current device, i.e., when a voltage of a given polarity is impressed across its coil windings it delivers a force proportional to the current in one direction, when the polarity is reversed the direction of the force is reversed.

A mechanical spring, connected between the base of the piston/coil subassembly and the housing, maintains the midposition of the piston.

A single piston seal/guide is needed to separate the compression space above the piston from the motor compartment below the piston.

All of the forces acting on the piston are in the direction of its motion; i.e., no side loads are imposed on the piston guide and seal. Hence, a clearance-type of seal design may be used, resulting in extremely low wear of the seal/guide surface. No lubricants are needed or used.

A spring/mass vibration absorber is incorporated in the compressor to automatically attenuate the momentum imbalance resulting from the reciprocating motion of the piston/coil assembly.

The helium transfer tube connects the compressor to the displacer. Through it, the pressure wave created by the piston can act upon the free-displacer inside the cold finger assembly.

The compressor unit is sealed by a closure weld in order to ensure helium containment.

FREE-DISPLACER COLD FINGER

Figure 5 illustrates the construction of the cold-finger and the free-displacer. The function of the displacer is to alternately move the gas from the expansion to the compression space. When the piston goes down (expansion) the displacer must be near its lower position, so that the expansion process occurs at the end of the cold-finger. When the piston goes up (compression) the displacer must be near its upper position.

A mechanical spring affixed to the displacer and the housing forms part of a spring-mass system which is tuned to help provide the proper phase relationship between the movement of the piston and that of the displacer.

Gas from the helium transfer tube flows alternately from the compressor space towards the expansion space through the body of the displacer, which is filled with a porous-metal regenerative heat exchanger.

Since the forces on the displacer, like that of the piston, act only in the directon of motion, the necessary seal at the base of the displacer is a simple clearance seal.

PERFORMANCE OF LINEAR-RESONANT, FREE-DISPLACER COOLERS

a) MX7011: 1 W @ 80K

The MX 7011 cooler currently in production (figure 2) as part of a complete product test program, was subjected to an endurance test. Five coolers were each tested for 5000 hours, preceded by a 400 hour "run-in" period. The purpose of this test was to demonstrate confidence in the 2500 hour MTBF warranted for the product.

The test was automatically controlled and each 24 hour cycle included a one hour warm-up to room temperature. Periodically, performance at temperature extremes was checked against specification.

None of the coolers exhibited mechanical problems during the test, impressively demonstrating the inherent reliability of the linear drive and the dry-running clearance seals. The worst degradation in cold-finger temperature observed during test was less than 5°K. At the end of the 5000 hour test, all coolers were still performing to specification, and the test was discontinued. Inspection of the units upon disassembly revealed negligible wear and tear.

Figure 6 is a comparison of the acoustic noise from a model HD1033, 1W @ 80°K Standard Common Module Cooler and the noise from an MX7011, as measured in an anechoic chamber. At a frequency of 1000 Hz, its noise level is 20 dB lower.

b) Magnavox MX7040 and MX7043 Coolers

The Magnavox MX7040 and MX7043 (figures 7 and 8) are the first split-cycle linear resonant coolers in existance. They are currently in the final stages of development testing, with initial production scheduled for 1983. These coolers are being produced for Magnavox by Philips Usfa B.V. for sale in U.S. markets. As with the MX7011, they are intended to deliver an MTBF of 2500 hours without service.

The MX7040 (figure 7) is a unit designed for 1/4 W of cold production at 85°K with less than 40 watts of input power required over full military ambient temperature extremes. It weighs 4.2 lbs.

The MX7043 (figure 8) is a unit designed for 1 W of cold production at 80°K with less than 55 watts of input power over full military ambient temperature extremes. It weighs 4.2 lbs.

Both coolers have a vibration absorber (passive countermass) contained within their common compressor.

Life tests of two prototype MX7040 coolers have each demonstrated over 6500 hours of operation without failure.

c) Magnavox MX7045 Cooler

The MX7045 Cooler was developed by Magnavox to provide a "form-fit and function" compatible, improved-reliability (true 1000 hour) cooler meeting the U.S. Government B2-Specification (#2104070122) for a "1/4 W-Split". It was developed for use in systems which could not employ the superior linear-resonant coolers. The design approach taken was to incorporate the same proven design principles embodied in the free-displacer portion of the linear-resonant coolers (mechanical restoring spring, clearance seal) into the MX7045 cold finger while utilizing the "U.S. Standard" brushless dc motor driven compressor design (with a few product improvements devised by Magnavox engineers).

Magnavox/EOS has demonstrated the life and reliability of this "hybrid" 1/4 W split-Stirling cryogenic cooler under a U.S. Army program. The unit

delivers 1/4 W of cooling at 85°K with less than 25 watts of input power over full military ambient temperature extremes.

CONCLUSIONS

The linear-resonant embodiment of the Stirling cooler has proven itself as synonymous with long-life and high reliability through two generations of production hardware. The newest generation of product, the split-Stirling coolers discussed herein, promises to retain all of the positive characteristics of its antecedents while providing as well the advantages of split-cooler construction.

The challenge remaining is for the system designer to exercise imagination and skill in utilizing this reliable, cost-effective component to best advantage in the IR systems of the future.

REFERENCES

1. J.W.L. Kohler and C.O. Jonkers, Fundamentals of the Gas Refrigerating Machine, Philips Technical Review, 16, p. 69, 1954.

2. R. J. Meyer, The Philips Stirling Engine, Engineer, Vol. 81, May 1969, p. W69-W81.

3. A. Daniels, et al, Magnetically Suspended Stirling Cryogenic Space Refrigerator Status Report, Cryogenic Engineering Conference, San Diego, CA., August 1981.

4. A. K. DeJonge, A Small Free-Piston Stirling Refrigerator, Proceedings of the 14th IECEC, Boston, August 1979.

5. A. Sereny, A. K. DeJonge, Analysis and Optimization of a Linear Motor for the Compressor of a Cryogenic Refrigerator, 1981 Cryogenic Engineering Conference, San Diego, CA., August, 1981.

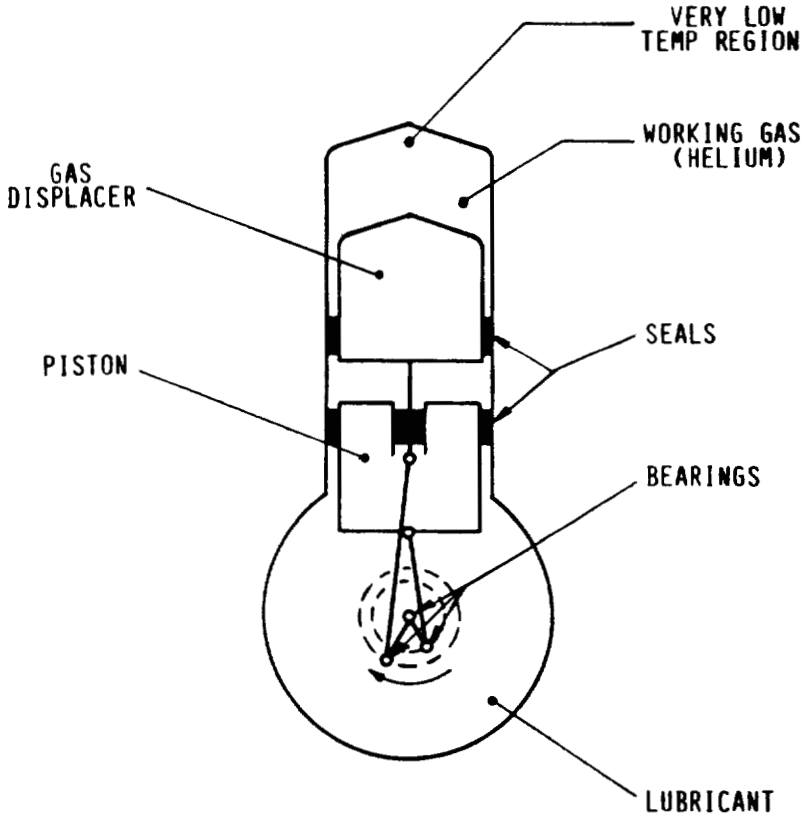

FIGURE 1. SCHEMATIC REPRESENTATION OF A CONVENTIONAL STIRLING REFRIGERATOR

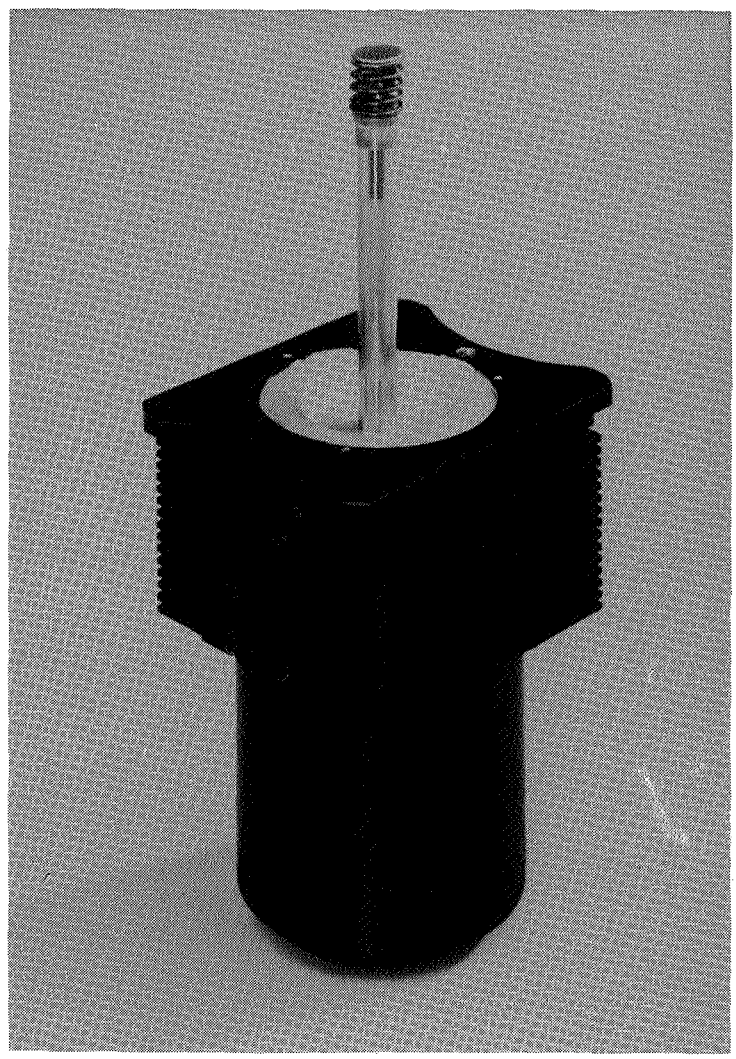

FIGURE 2. UA 7011/MX7011 LINEAR RESONANT COOLER

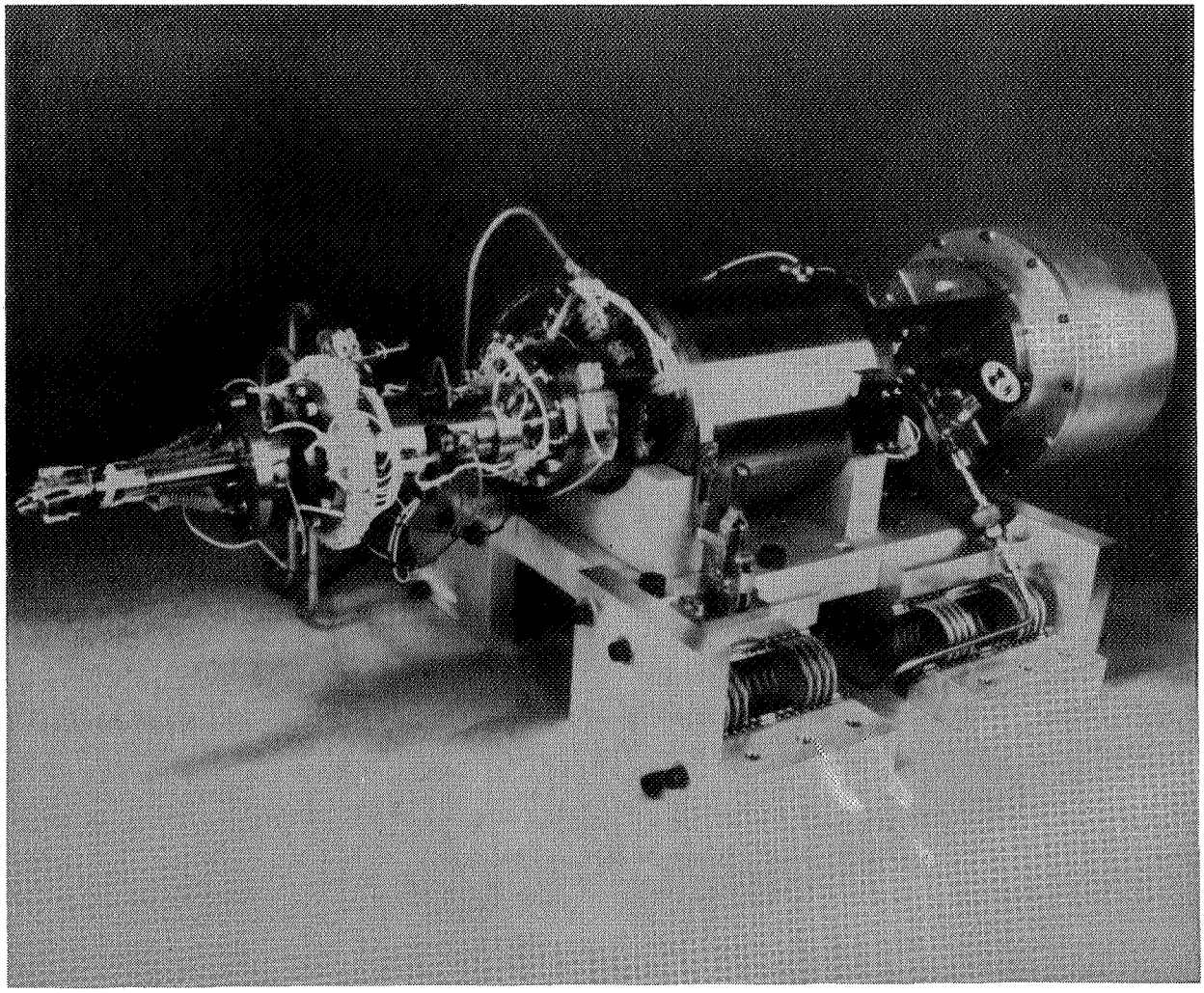

FIGURE 3. ULTRA-LONG LIFE PHILIPS LABS/NASA LINEAR-RESONANT, MAGNETIC BEARING STIRLING COOLER

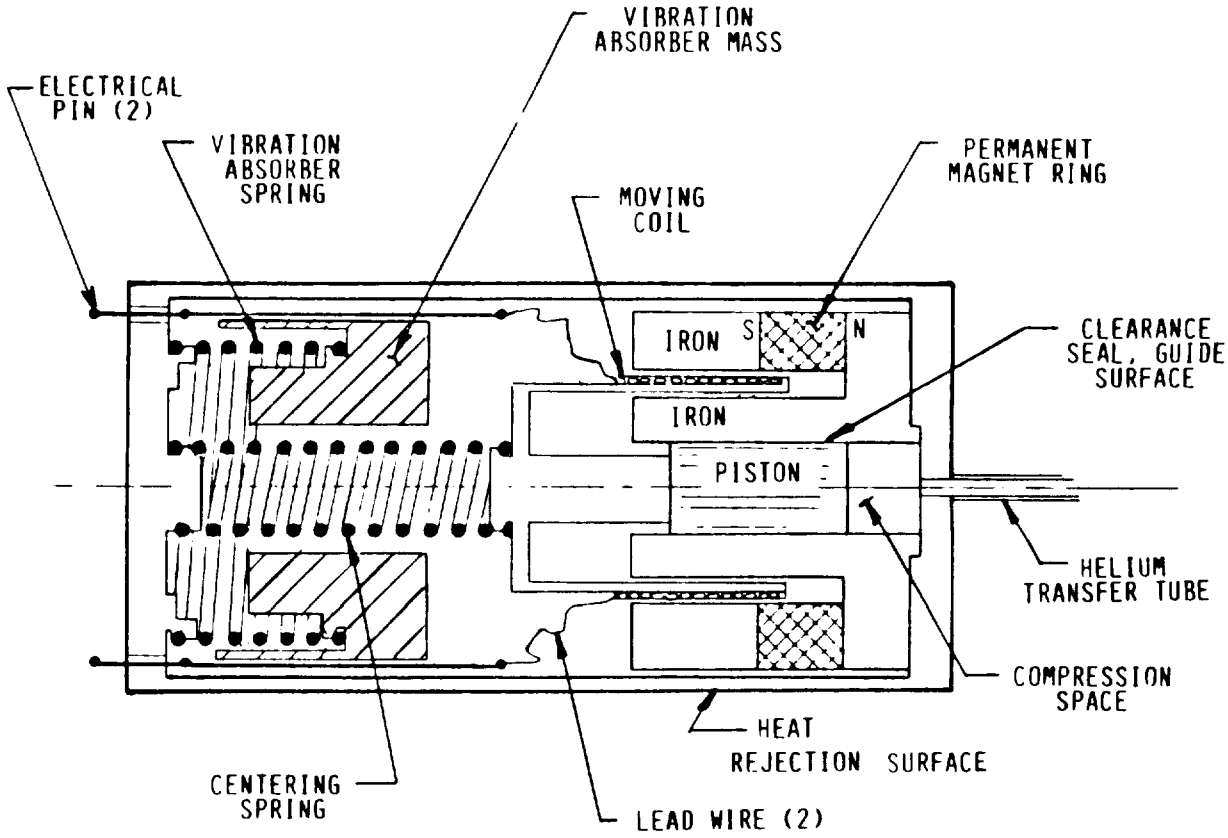

FIGURE 4. SCHEMATIC REPRESENTATION OF MAGNAVOX LINEAR-RESONANT COMPRESSOR

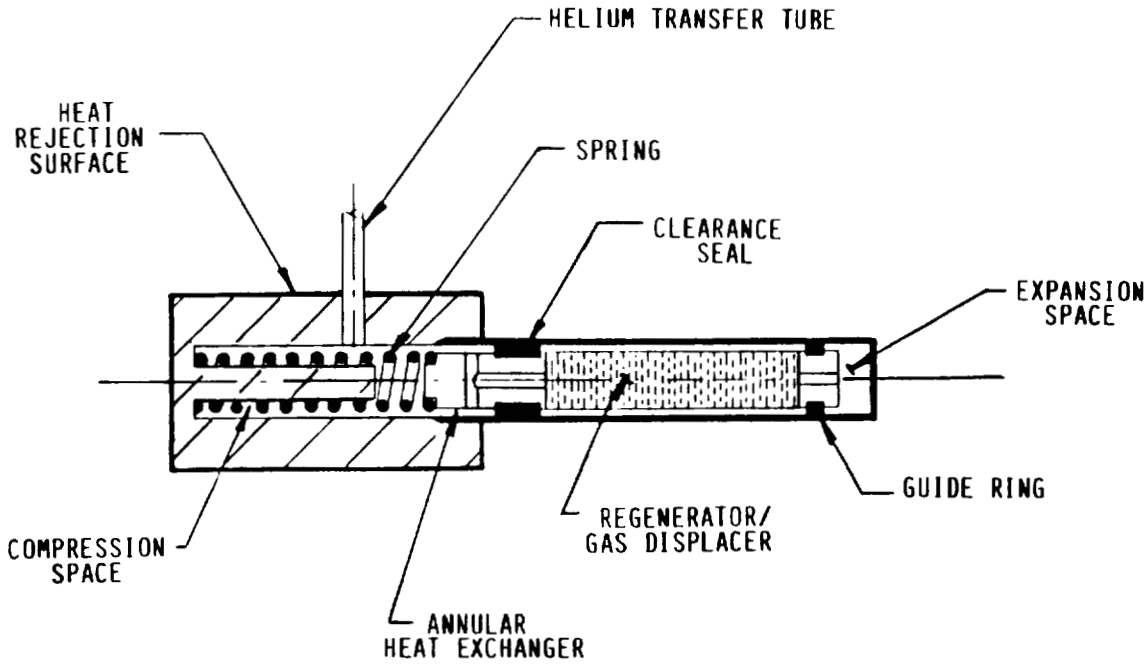

FIGURE 5. SCHEMATIC REPRESENTATION OF MAGNAVOX FREE-DISPLACER/COLD-FINGER CONSTRUCTION

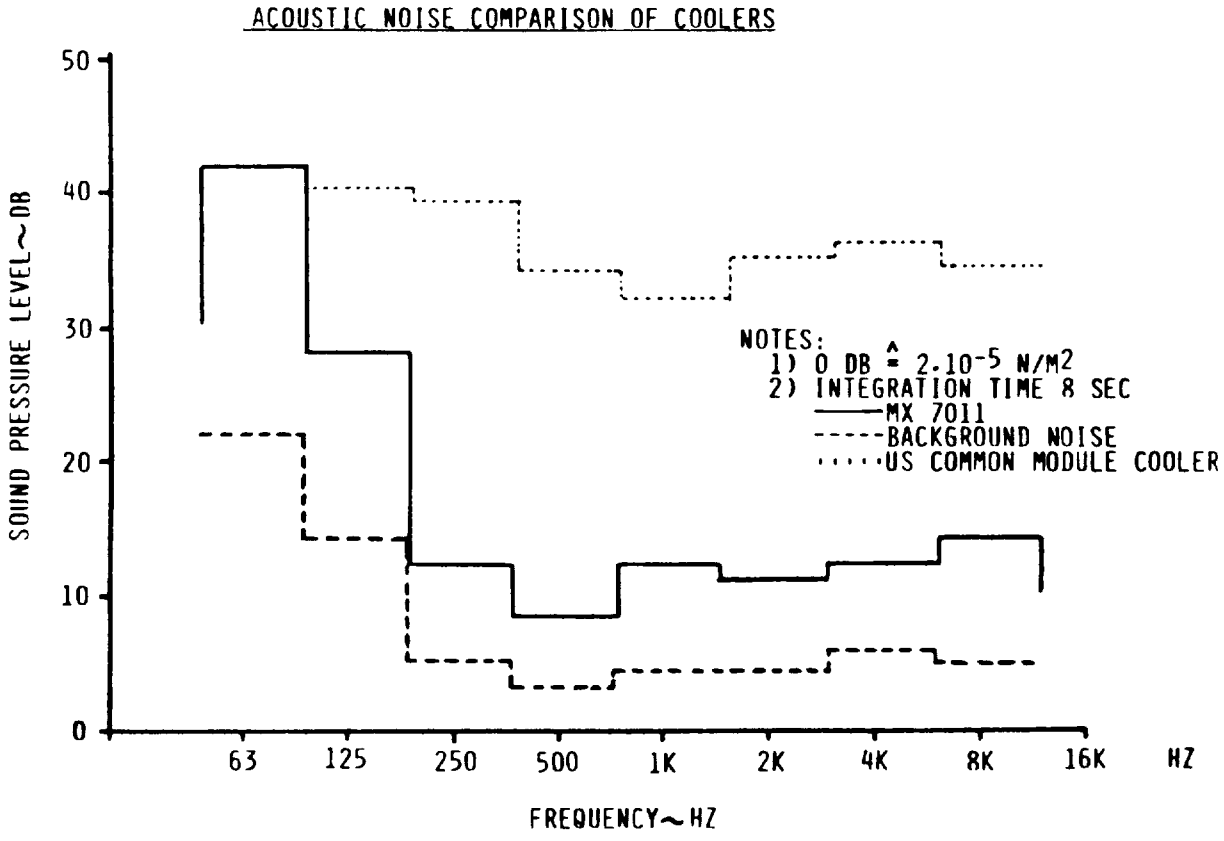

FIGURE 6. ACOUSTIC NOISE MEASUREMENTS

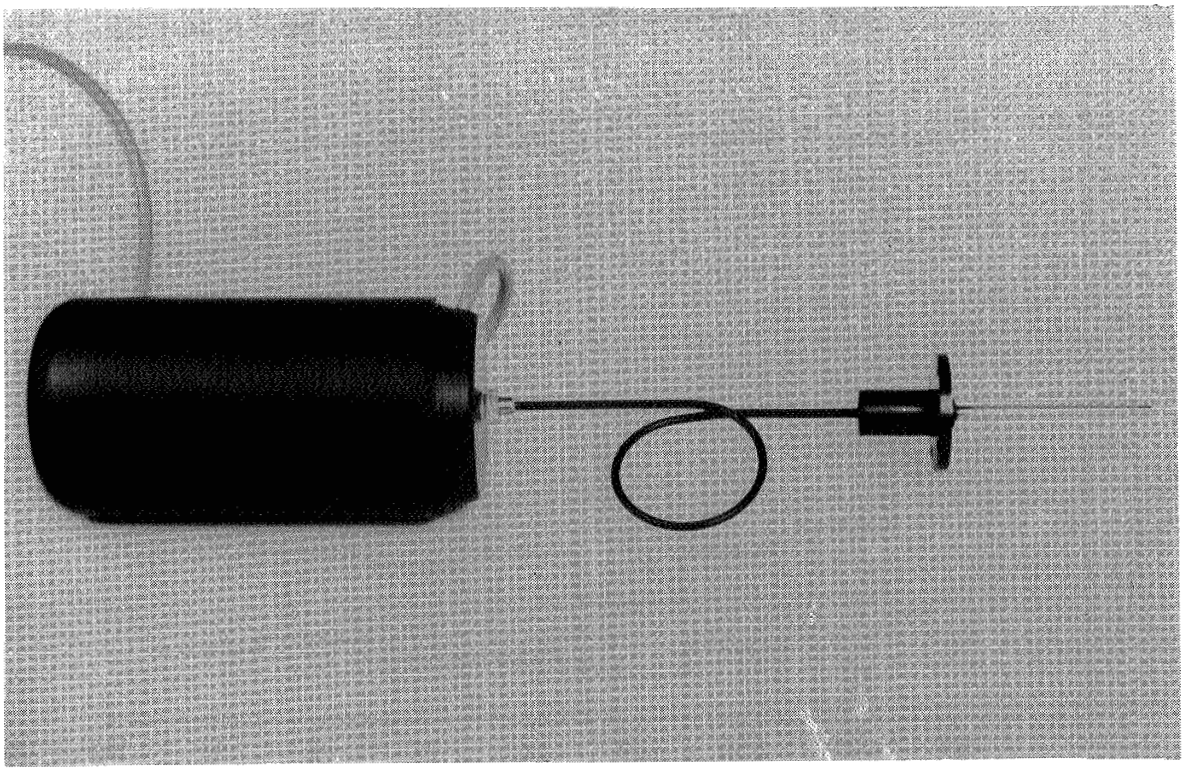

FIGURE 7. PROTOTYPE MX7040 SPLIT-STIRLING, 1/4 WATT LINEAR-RESONANT COOLER

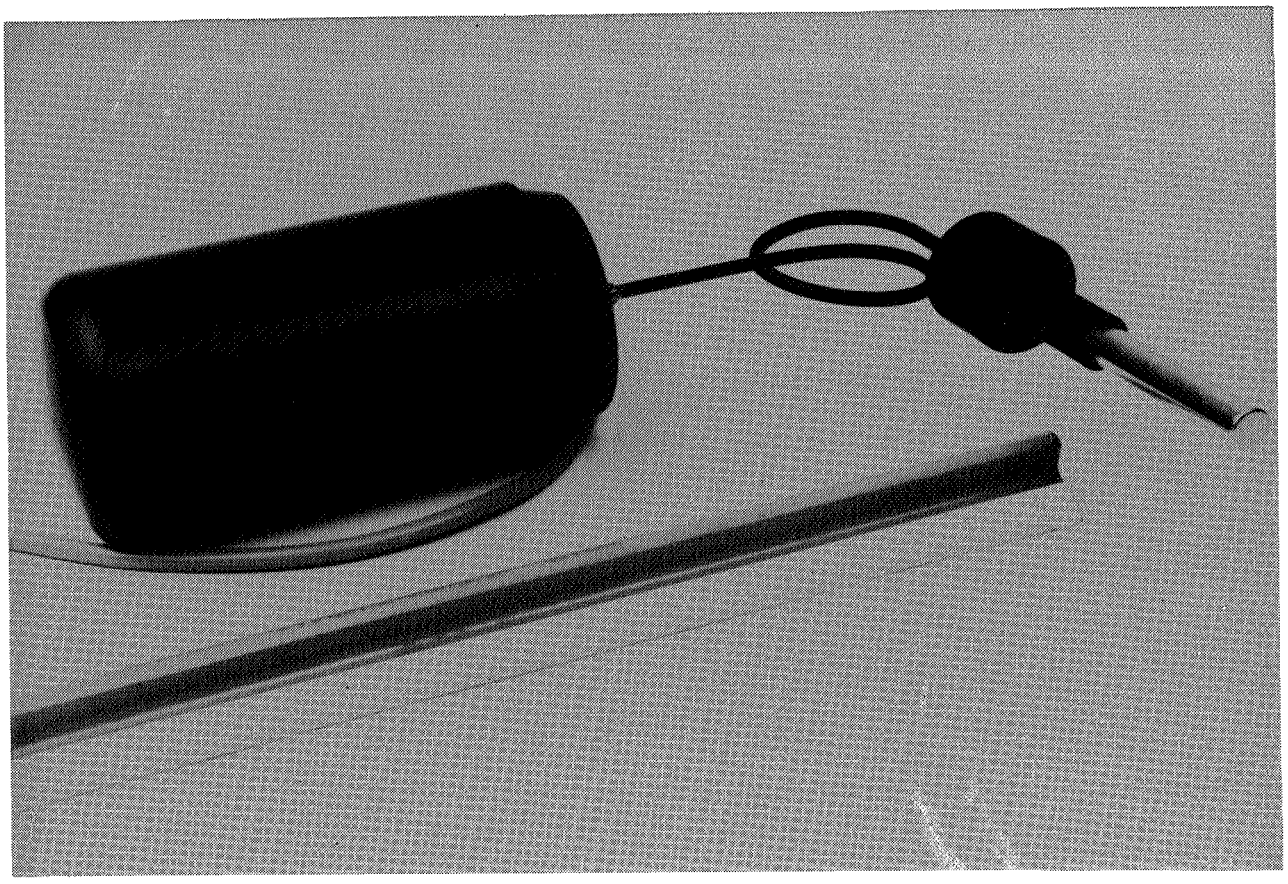

FIGURE 8. PROTOTYPE MX7043 SPLIT-STIRLING, 1 WATT LINEAR-RESONANT COOLER

SPLIT-STIRLING-CYCLE DISPLACER LINEAR-ELECTRIC DRIVE

R.A. Ackermann, S.K. Bhate, and D.V. Byrne
MECHANICAL TECHNOLOGY INCORPORATED

ABSTRACT

The retrofit of a 1/4-W split-Stirling cooler with a linear drive on the displacer was achieved and its performance characterized. The objective of this work was to demonstrate that a small linear motor could be designed to meet the existing envelope specifications of the cooler and that an electric linear drive on the displacer could improve the cooler's reliability and performance. The paper describes the characteristics of this motor and presents cooler test results.

INTRODUCTION

A recent in-house program at Mechanical Technology Incorporated (MTI) was directed toward retrofitting a 1/4-W split-Stirling-cooler displacer with a linear-electric drive. The cooler was supplied to MTI by the U.S. Army Chemical Systems Laboratory and the Honeywell Corporation with the objective of demonstrating the feasibility of adding a linear drive to the cooler. The in-house program involved:

- Designing a small linear motor to fit into the displacer bounce space
- Integrating the motor with the displacer
- Developing the control circuitry and logic to control displacer motion
- Testing the displacer with a standard 1/4-W cooler compressor.

COOLER DESCRIPTION

The 1/4-W split-Stirling cooler (Figure 1) was developed at the Night Vision Electro-Optics Laboratory. The retrofit to the cooler was made by adding a linear-electric drive to the displacer. The drive was designed to be added without changing the thermodynamics of the cooler, and to use all existing hardware. To achieve this, the linear drive was added to the displacer bounce space and attached to the displacer rod.

A layout of the retrofitted displacer is shown in Figure 2. This retrofit was assembled with existing components (shown to the left of line A-A) and the linear drive components (shown to the right of A-A). The drive components consist of a permanent-magnet linear motor, a housing, and a displacer rod connection. The linear motor has a radially energized, moving permanent-magnet plunger (which is attached to the displacer), and a laminated stator containing several circular coils. The housing, which provides a hermetic case for the motor, was designed for effective cooling of the motor, and to provide a rear bearing for radial support of the plunger.

In this retrofitted design, the motor was used to control the displacer motion by monitoring the pressure wave and triggering the displacer motion from this control parameter. The flexibility of the control scheme is shown in Figure 3. Control consisted of the ability to vary the phasing between the pressure wave and displacer motion (ϕ_d), the duration between intake and exhaust strokes (ψ_d), pulse width (τ), and the amplitude of the displacer forcing function (I_m). Through these four parameters, the effect of displacer phasing and motion on cooler performance can be evaluated. The control circuit (Figure 4) consisted of a pressure transducer mounted at the compressor outlet, the phasing circuitry, and a motor power supply.

MOTOR CHARACTERISTICS

The retrofit displacer motor is one of a family of permanent-magnet ($SmCo_5$) linear motors under development at MTI*. Figure 5 schematically shows a section of the motor with the plunger in the center position. The motor consists of stationary outer electrical coils wound on a steel bobbin and an inner permanent-magnet plunger. The magnets are radially magnetized with alternate magnets having north polarity on the outside diameter and south polarity on the inside diameter. The design characteristics for the motor are given below.

Frequency:	25.0 Hz
Stroke:	1.9 mm (0.075 in.)
Size:	25-mm dia x 25-mm long (1 in. x 1 in.)
Weight:	0.07 kg (0.15 lb_m)
Static Force at 0.8 A:	10.2 N (2.3 lb_f)
Electrical Input Power:	<3.0 W

RESULTS OF MOTOR BENCH TESTING

STATIC RESPONSE TEST RESULTS

As a first step in characterizing the performance of the MTI displacer linear motor, static force tests were conducted. The purpose of these tests was to determine available static force capability of the motor as a function of input current and plunger position. This information is particularly relevant to the operation of the motor to overcome friction effects as cooler wear and contamination progress.

---

*Bhate, S.K., "Linear-Oscillating Electric Machine with Permanent-Magnetic Excitation," U.S. Patent: 4,349,757, September 14, 1982, assigned to MTI, Latham, New York.

These tests were conducted with the apparatus shown in Figure 6. With this apparatus, the motor force is measured with a piezoelectric force transducer as a function of displacement measured with an LVDT and motor current. A plot of the motor force is given in Figure 7 for currents up to 1.6 A. An important characteristic defined by the force plot is the extraordinary force capability of this miniature motor. The motor can produce several pounds of force throughout the required stroke range, which is more than adequate to control the motion of the displacer.

DYNAMIC RESPONSE TEST RESULTS

A displacement test apparatus was used to measure the dynamic response of the motor to an alternating step-current input. This type of test is important because it determines the ability of the motor to quickly travel from one extreme stroke position to another. The data also provide the controls design team with dynamic response information necessary for the establishment of control system time constants and parameters. Figure 8 is a sketch of oscilloscope traces of a typical dynamic motor response test at 25 Hz. The plunger travels the stroke of 1.7 mm (0.065 in.) in approximately 3 ms*.

COOLER TEST RESULTS

Retrofitting of the cooler was recently completed. To determine cooler performance, preliminary tests with the following parameters were conducted:

- Operation of the cooler at a reduced stroke of 1.7 mm (0.065 in.) to determine control parameter settings
- Cool-down rate to 80 K
- Motor input power.

The oscillograph tracing presented in Figure 9 shows the system pressure motor current time history. For the run depicted, phasing between the pressure wave and displacer intake motion (positive current pulse) was 10 ms (approximately 48°), pulse width was 2 ms, and current amplitude was 0.8 A. Because of the limited testing conducted to date, sufficient data has not been taken to verify that these are the optimum control settings. However, the cooler did achieve the cool-down specification of 80 K in less than 10 min even at a reduced stroke. It is anticipated that in future testing at a design stroke of 1.9 mm (0.075 in.), the motor will enable the cooler to show a significant improvement over the cool-down specification.

The following analysis presents the motor power for the operating point described.

---

*Comparing favorably with a typical travel time of 6-8 ms in a pneumatically driven system.

Assumptions:

I_m - Displacer Motor Current = 0.8 A
R - Motor Coil Resistance = 27 Ω
F_f - Plunger Friction Force = 1.78 N (0.4 lb_f)
Δx - Motor Stroke = 1.7 mm (0.065 in.)
Δt - Plunger Travel Time = 0.002 s
F_A - Acceleration Force = 4.89 N (1.1 lb_f) (Assume $\ddot{x}$ constant over travel)

Peak Motor Power Calculation:

$$P_{peak} = \text{Heating Loss} + \text{Friction Loss} + \text{Acceleration Power}$$

$$= I_m^2 R + (F_f \times \Delta x)/\Delta t + (F_A \times \Delta x)/\Delta t$$

$$= (0.8^2 \times 27) + \left[(0.4 + 1.1)\left(\frac{0.065}{0.002} \times \frac{1\ \text{ft}}{12\ \text{in.}} \times \frac{1\ \text{W}}{0.74\ \text{ft-lb}_f/\text{sec}}\right)\right]$$

$$= (0.8^2 \times 27) + [(0.4 + 1.1)(3.67)] = 17.3 + 5.5 = 22.8\ \text{W}$$

Average Motor Power Calculation:

$$P_{avg} = P_{peak} \times \text{Duty Cycle}^* = (22.8\ \text{W})(0.13) = 3.0\ \text{W}$$

This analysis shows that because the duty cycle is low, average displacer motor power is approximately 3 W (about 10%) of the total power consumed by a typical 1/4-W cooler system. Ongoing tests indicate that further reduction in the power required to drive the displacer will be achieved by implementation of optimum control parameters. A displacer motor power reduction to less than 2 W in this prototype, and to approximately 1 W in an advanced design that eliminates the frictional rear bearing, is anticipated. Further, the flexibility gained in displacer control should lead to performance improvements through better selection of regenerator materials (now limited by displacer dynamics), displacer motion control, vibration elimination, and stroke modulation.

CONCLUSION

The conclusion reached from this work is that a small linear electric displacer drive can be developed for the 1/4 W split-Stirling cooler that will fit into the present cooler envelope. The benefits that will be gained from a linear drive are improvements in performance and reliability. Future work at MTI will be directed towards advancing the state of the art of linear coolers by building a linear drive compressor and coupling it with our retrofitted expander to demonstrate the feasibility of a total linear split-Stirling cooler.

---

*Calculated from Figure 9.

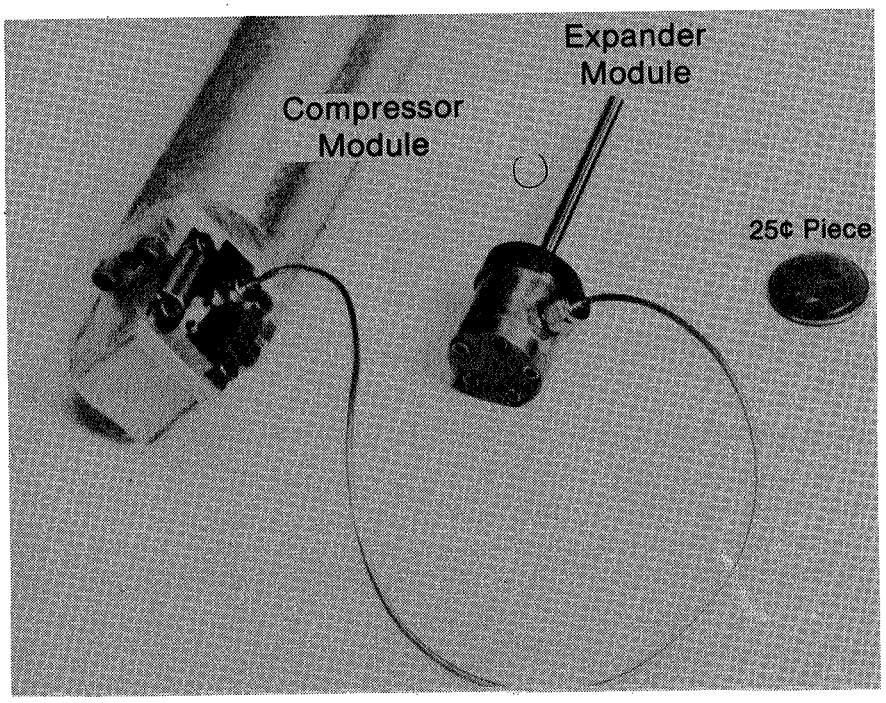

Figure 1 1/4-Watt Split-Stirling Cooler

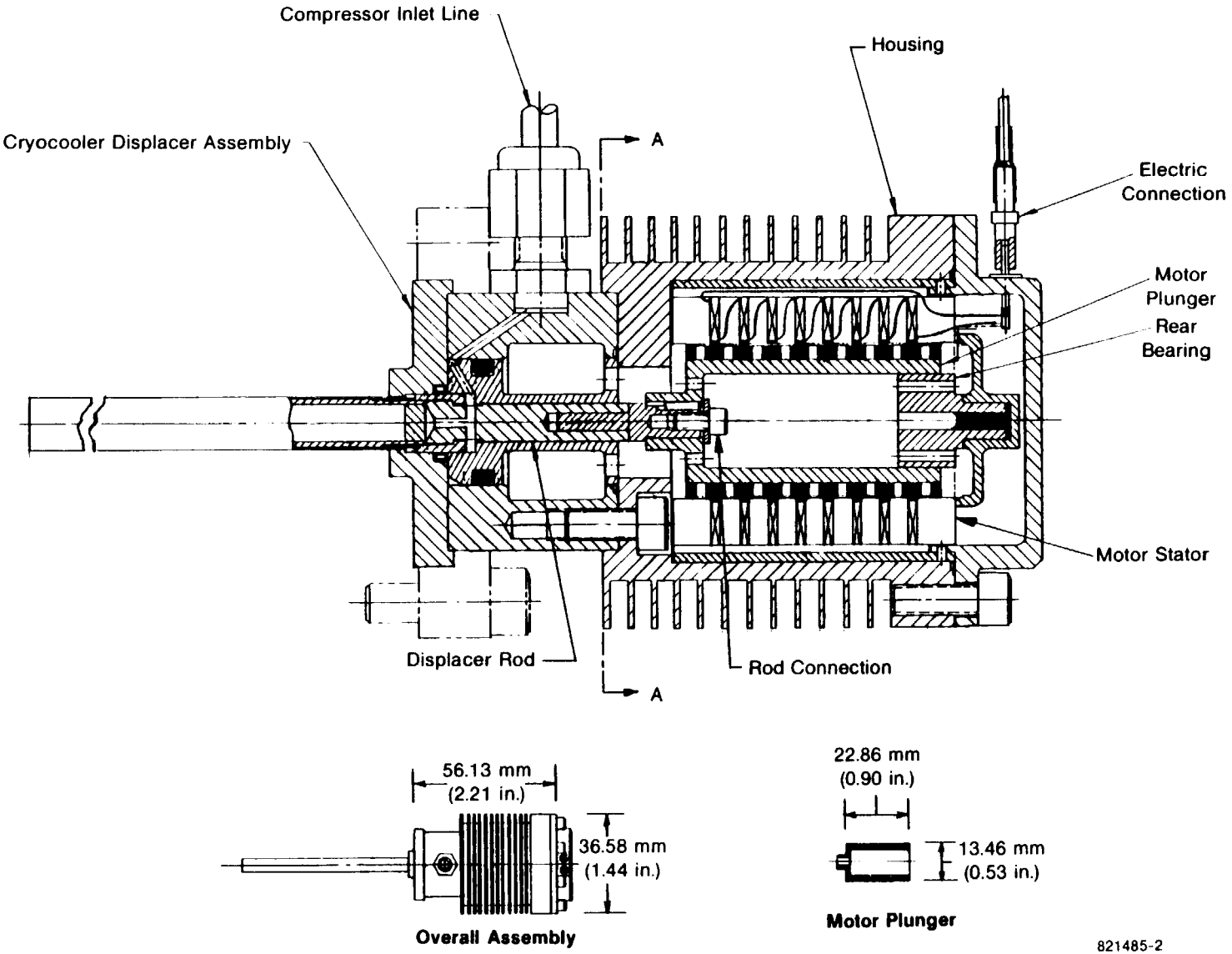

Figure 2 1/4-Watt Retrofit Cooler Displacer Design

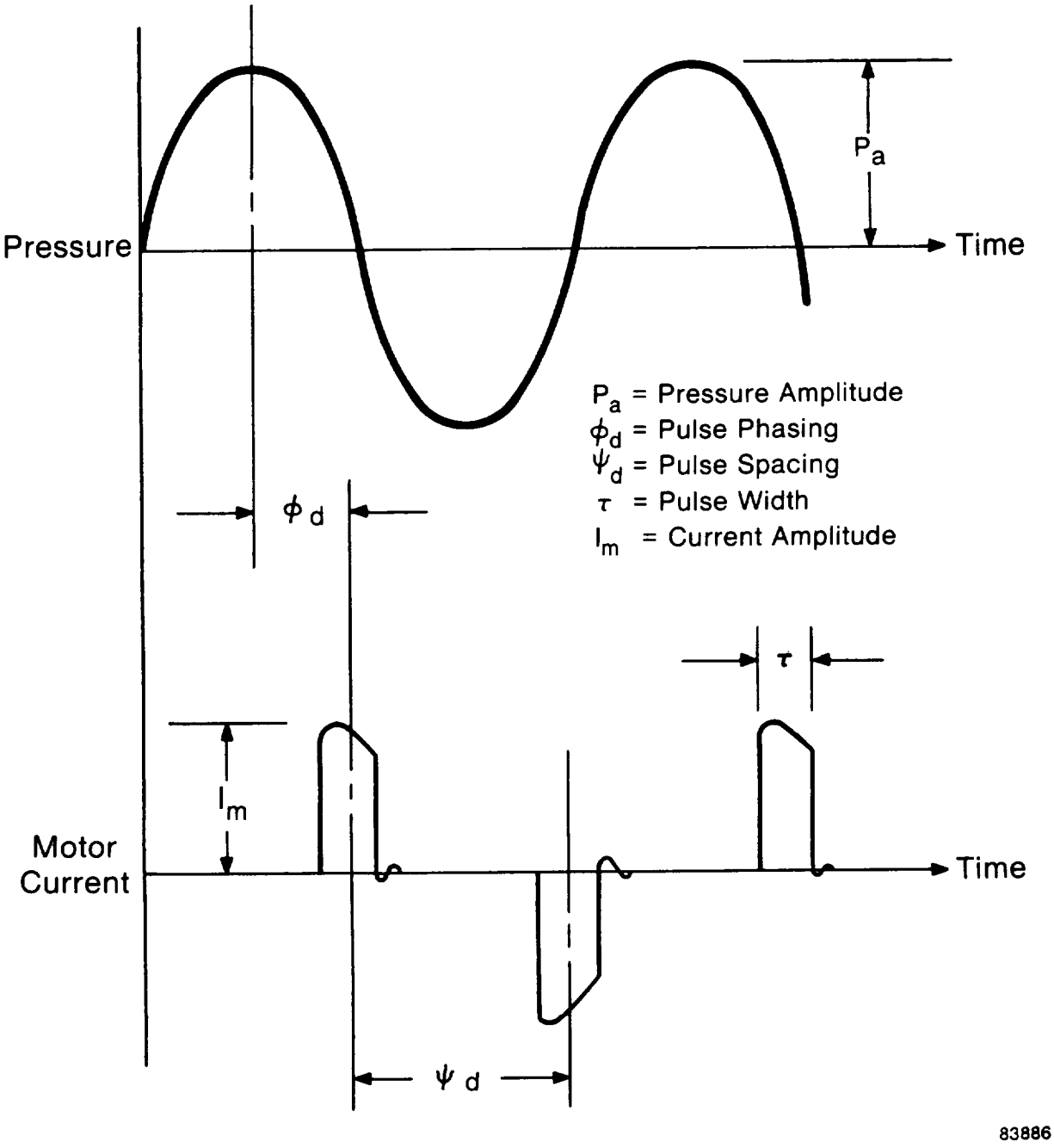

Figure 3 Displacer Motor Current Control Variables

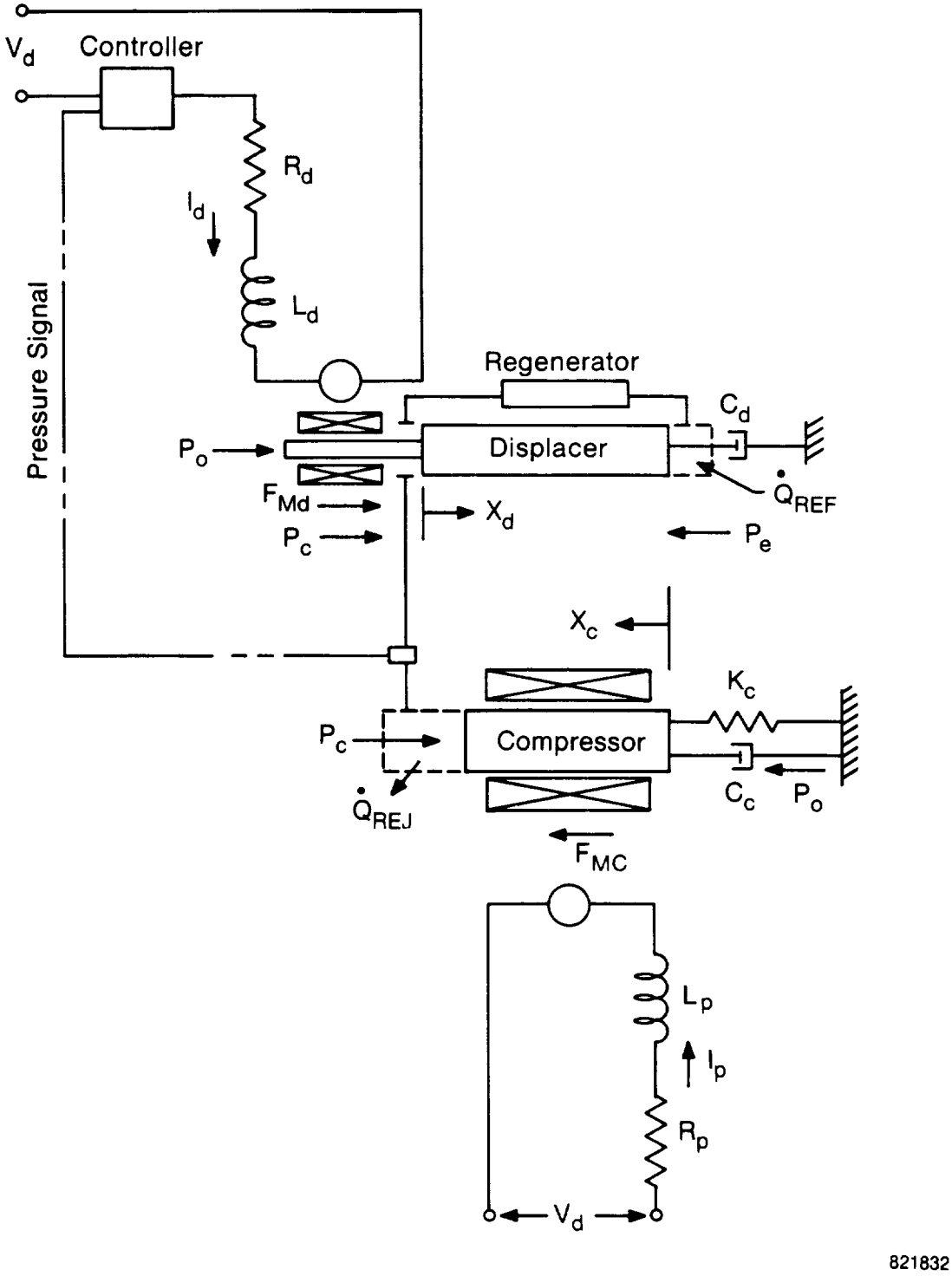

Figure 4 Linear Cryogenic Refrigerator with Pressure Control

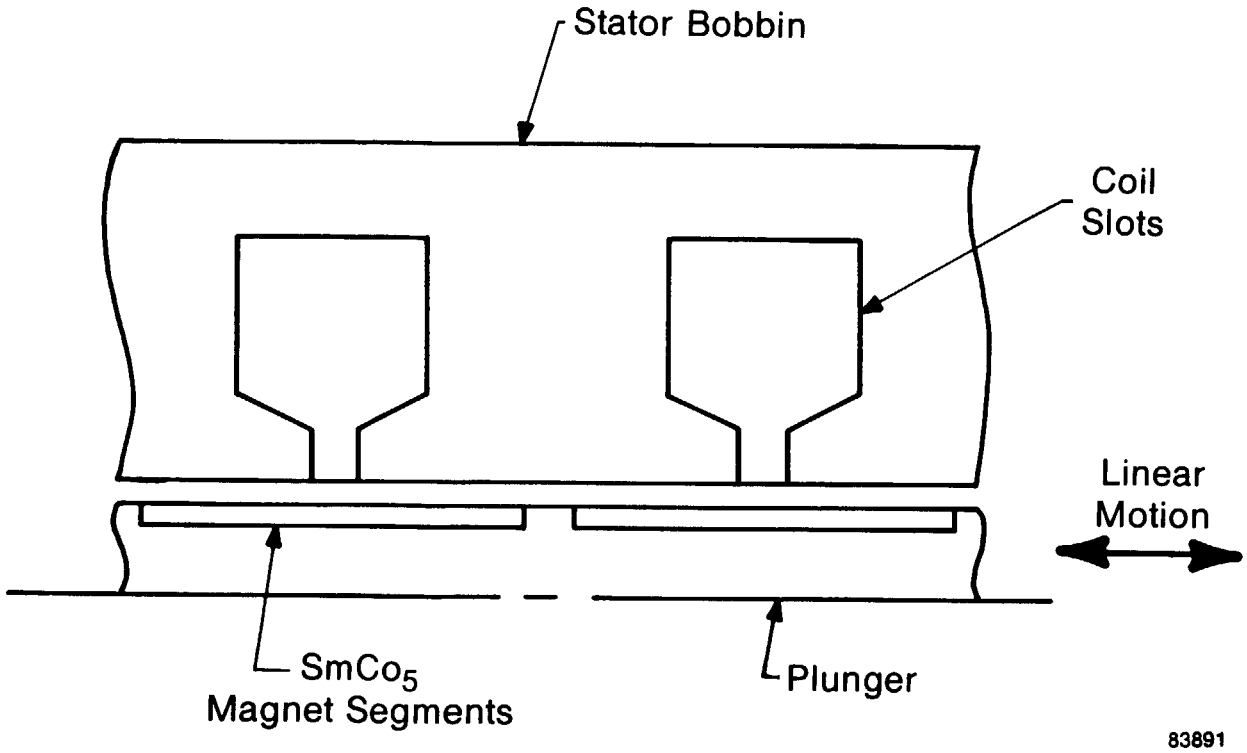

Figure 5 Schematic of Permanent Magnet Motor

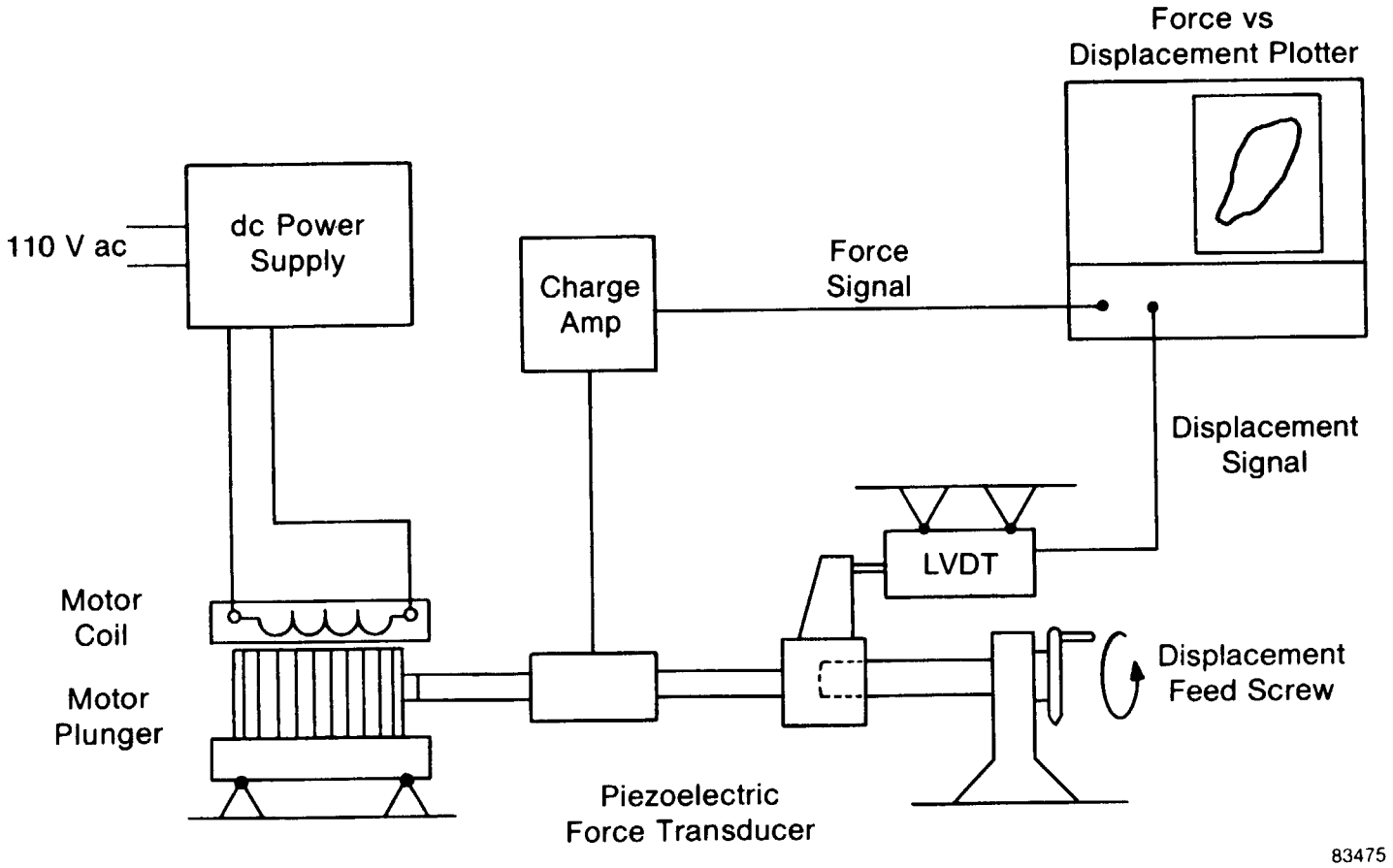

Figure 6 Displacer Motor Static Force vs Displacement Test Setup

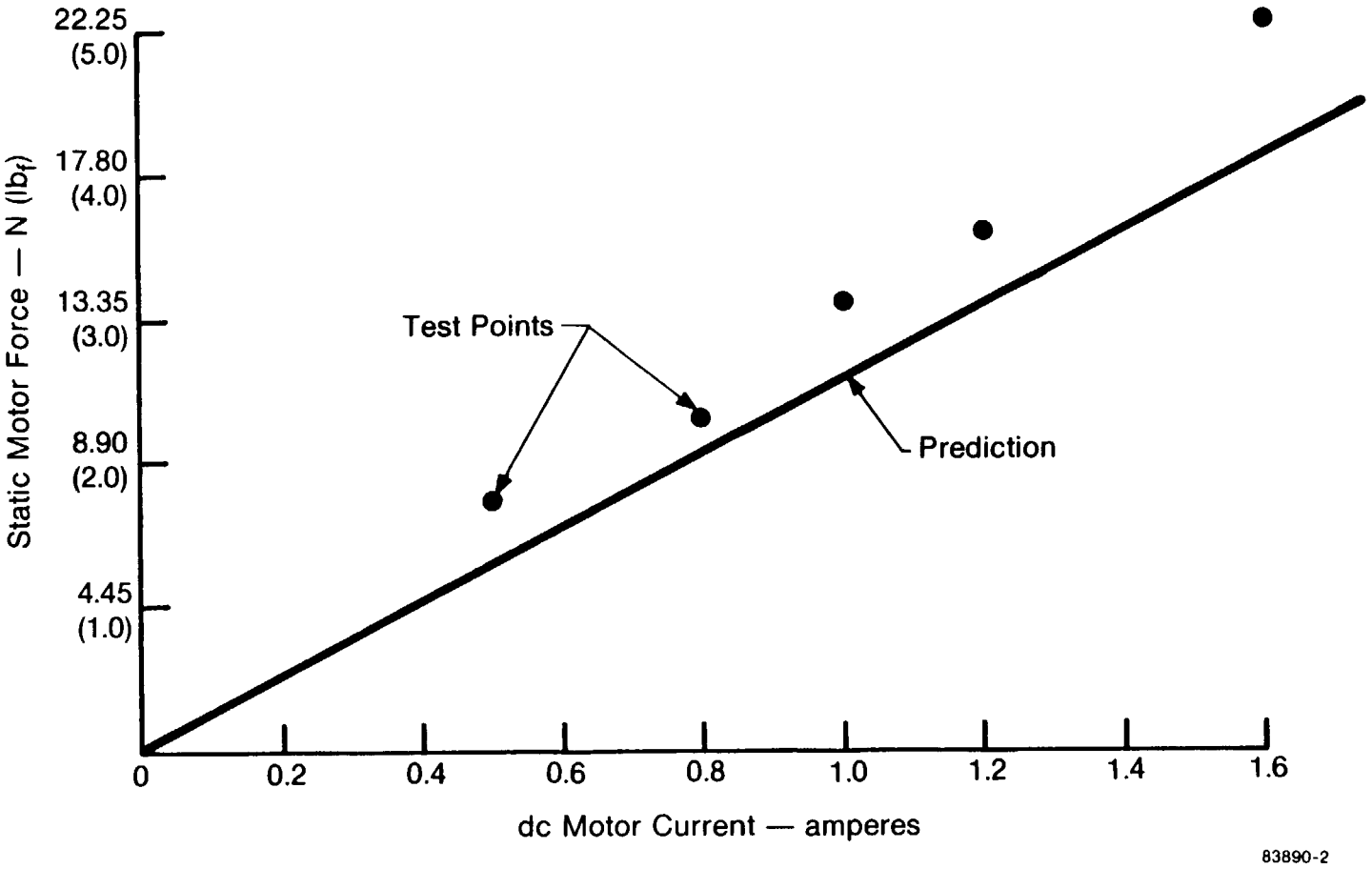

Figure 7 Comparison of Displacer Motor Test Data with Predictions

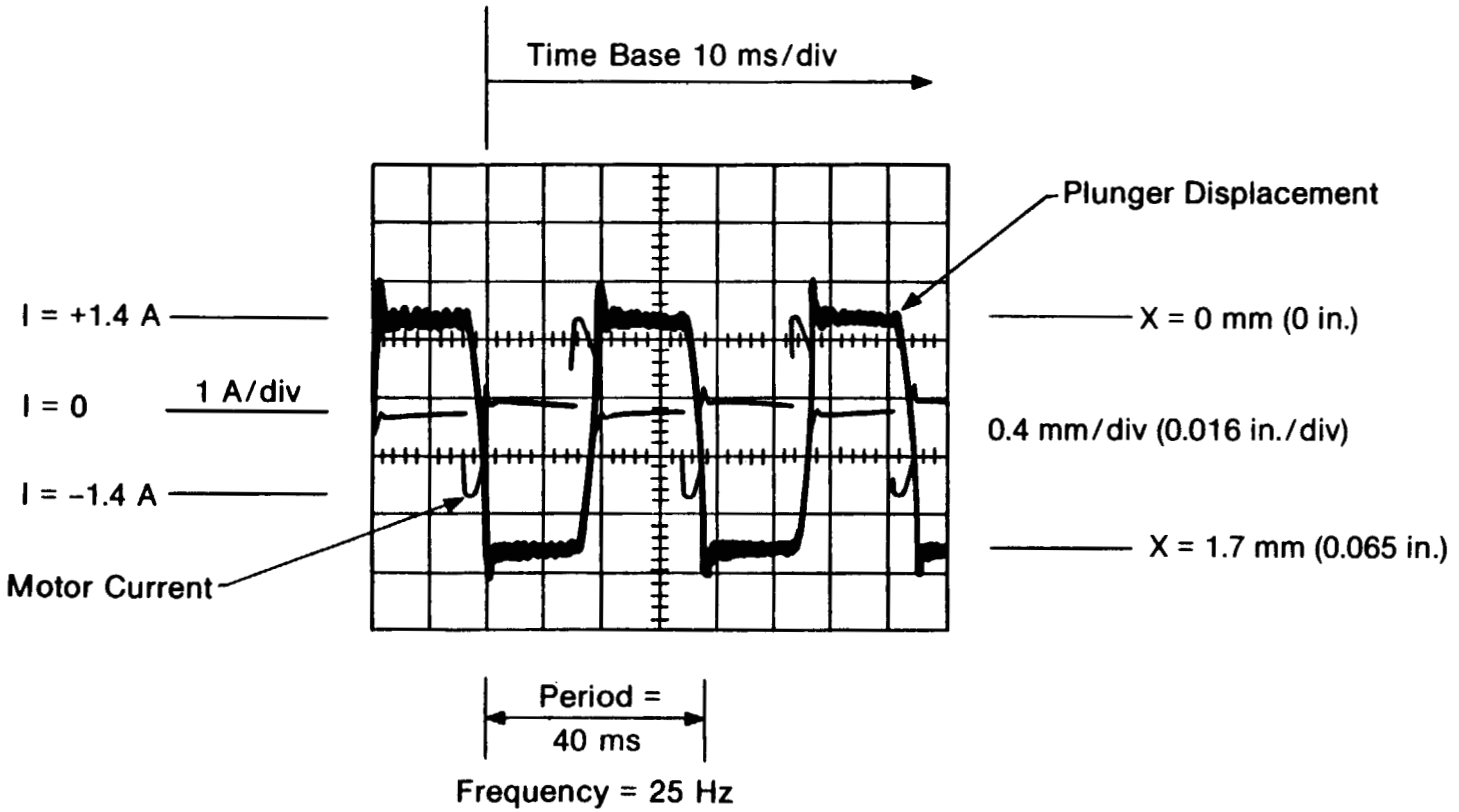

Figure 8 25-Hz Operation of Split-Stirling Displacer Motor

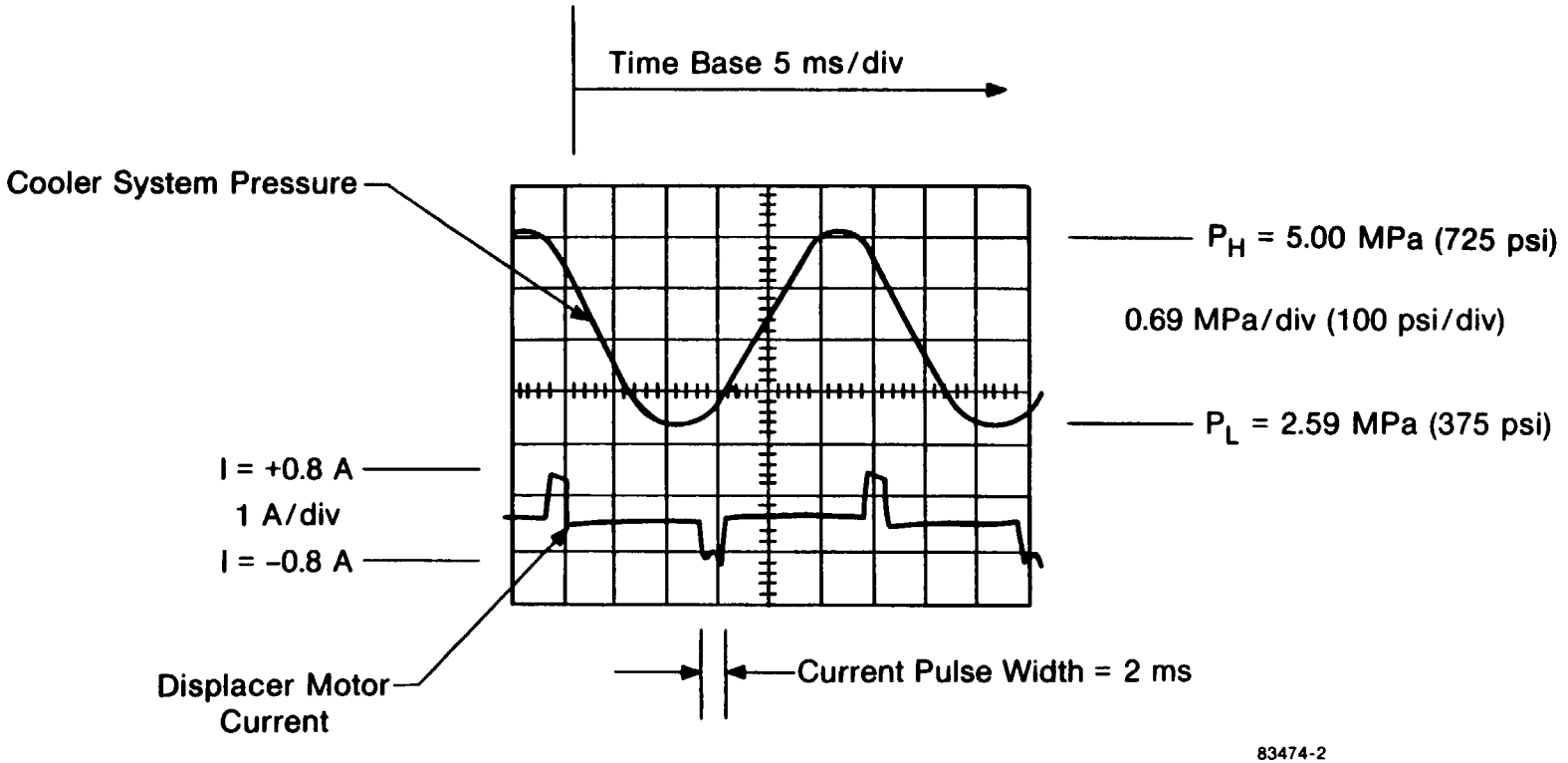

Figure 9 Cooler System Pressure/Displacer Motor Current Versus Time for Retrofit Cryocooler

COMPUTER PROGRAM FOR ANALYSIS OF SPLIT-STIRLING-CYCLE CRYOGENIC COOLERS*

M. T. Brown and S. C. Russo
Hughes Aircraft Company+

ABSTRACT

A computer program for predicting the detailed thermodynamic performance of split-Stirling-cycle refrigerators has been developed. The mathematical model includes the refrigerator cold head, free-displacer/regenerator, gas transfer line, and provision for modeling a mechanical or thermal compressor. To allow for dynamic processes (such as aerodynamic friction and heat transfer) temperature, pressure, and mass flow rate are varied by subdividing the refrigerator into an appropriate number of fluid and structural control volumes. Of special importance to modeling of cryogenic coolers is the inclusion of real gas properties, and allowance for variation of thermophysical properties such as thermal conductivities, specific heats and viscosities, with temperature and/or pressure. The resulting model, therefore, comprehensively simulates the split-cycle cooler both spatially and temporally by reflecting the effects of dynamic processes and real material properties.

The computer program was evaluated by modeling a small cryogenic cooler for which abundant test data was available. The accuracy of the computer program was verified by this comparison, and it provided an insight into the thermodynamic processes occurring in the cold regenerator. An important result of this effort is a clear idea of the further tests and research needed for those correlations which are not now well defined or whose application to small cryogenic coolers is questionable.

INTRODUCTION

In the late 1960's, it became obvious that a two-piece cryogenic refrigeration system offered a flexible approach to meeting the applications requirements, especially those typical of infrared sensor systems. In the split-cycle system, a primary power module is separated from the refrigeration module. Miniature, two-piece, split-Stirling-cycle refrigerators have been successfully developed and demonstrated.

The split-cycle refrigerator is a regenerative gas-cycle machine with its cyclic processes characterized by the Stirling cycle. The physical implementation of a split-cycle system requires a compression piston, an expander displacer, a thermal regenerator, and a gas transfer line to interconnect the expansion and compression spaces. Figure 1 is a schematic representation and typical pressure-volume curves of an actual split-cycle refrigerator. The

* This study was conducted under the direction of Robert E. Harris (technical monitor) of the Air Force Flight Dynamics Laboratory, Wright-Petterson AFB, under contract F33615-79-C-3402, "Cold Displacer Study Program."
+ Space and Strategic Engineering Division, El Segundo, California 90245

amount of refrigeration produced is proportional to the enclosed area in the cold expansion volume diagram. The compression required of the drive motor is proportional to the area of the compression volume in the diagram for mechanical compressor. The refrigerator employs a valveless compressor with a motor/crankshaft mechanism by which pressure pulses are transmitted to an expander consisting of a displacer joined to a push rod. Since this rod is sealed, it experiences drive forces that are proportional to the differences between the magnitude of the pressure pulse and the mean pressure in the sealed volume. When the pressure pulse is high, the push rod tends to stroke the displacer into the mean pressure volume; when the pressure pulse is low, the converse occurs. Because the expansion displacer in these modules is pneumatically driven, no electric power is needed at the expander.

CYCLE ANALYSIS

The techniques currently in use* for analyzing cryogenic coolers are typically based on an ideal isothermal model, which assumes isothermal expansion and compression. This method evaluates ideal cycle performance for the actual cycle on the basis of a quasi-steady-state solution; it then reduces this ideal refrigeration by the sum of the parasitic heat losses. It is assumed that each of these losses acts independently of the others and that the temperature of the gas in any volume of the refrigerator is constant. The most notable disadvantage of this process of uncoupling the cold head regenerator losses from cooler performance is in predicting the conditions and performance of the cold head displacer regenerator. Since the efficiency of the regenerator is critical, the dynamic process cannot be adequately modeled by means of an isothermal model. A complete analysis is needed in order to treat the more general case of dynamic heat transfer in the regenerator matrix and of heat conduction in all the refrigerator components, including the regenerator matrix.

The objective of this effort was to conduct a comprehensive analysis of all thermodynamic and dynamic processes occurring within the cold head displacer assembly. The resulting mathematical model presented in this paper is a general, nonisothermal cold head displacer model, with the thermal, frictional, and pressure losses treated as an integral part of the dynamic and thermodynamic analysis. Special attention was given to incorporating empirical correlations and data whenever this step was needed to increase the accuracy of the analytical definition of the dynamic and thermodynamic processes.

NONISOTHERMAL MODEL

This section presents the final equations for the nonisothermal model. How these equations were developed is discussed in detail in the Cold Displacer

* As far as is known by the authors only the ideal isothermal model common to the iterative design process is currently in use. The more detailed analytical tool of a non-isothermal model, although common to Stirling engine analysis, has not been applied and evaluated for the special requirements of cryogenic coolers.

Study Final Report.* The following equations are based on a consideration of conservation of mass, momentum, and energy. The sign conventions used in these equations are presented in Figure 2.

For the variation of the temperature of the working fluid with time (with the compressor crank angle θ used as a reference) for the control volume n, we have

$$\frac{dT_n}{d\theta} = \frac{1}{C_v m}\left[e\,\Sigma G(T_w - T_n) + C_{P_{n,n-1}}\,T_{n,n-1}\,\frac{dm_{ni}}{d\theta} - C_{P_{n,n+1}}\,T_{n,n+1}\,\frac{dm_{(n+1)i}}{d\theta} - \frac{PdV}{d\theta} - C_v T\,\frac{dm}{d\theta}\right] . \quad (1)$$

This equation neglects both potential and kinetic energy, and it assumes that the enthalpy and internal energy of the gas are provided by the ideal gas relations, i.e., by $C_p T$ and $C_v T$, respectively. These assumptions are very reasonable for the class of coolers to be modeled (relatively small and with cold expansion volume temperatures above 35K. In this equation, the term $\Sigma G\ (T_w - T_n)$ accounts for all of the heat transferred into the control volume, and the term $PdV/d\theta$ is the work performed on the control volume.

The variation in the pressure of the working fluid is

$$\frac{dP_n}{d\theta} = \frac{dm_i}{d\theta} \pm \left[\frac{1}{K}\,(P_n - P_{n+1})\right]^{1/2} \frac{ZRTe}{V} - \frac{dV}{d\theta}\frac{P}{V} + \frac{dT}{d\theta}\frac{P}{T} + \frac{dZ}{d\theta}\frac{P}{Z} . \quad (2)$$

where the compressibility factor Z is used to define the equation of state, which is

$$m = \frac{PV}{ZRT} \quad (3)$$

The pressure equation was derived by applying the Darcy flow resistance equation for mass flow between control volumes, whereby the mass flow rate is approximately proportional to a power function of the difference in the pressures of the control volumes. The flow resistances are denoted by the letter K.

Conservation of mass is expressed in terms of the mass entering a control volume. When the mass entering the first control volume is equal to zero (because the cooler is a closed system) the equation defining the mass flow into the n^{th} control volume is

---

* Cold Displacer Study Final Report, Volume I, AFWAL-TR-82-3010, Air Force Flight Dynamics Laboratory, AF Wright Aeronautical Laboratories, Air Force Systems Command, Wright-Patterson AFB, Ohio, 45433; April 1982.

$$\frac{dm_{ni}}{d\theta} = - \sum_{j=1}^{j=n-1} \frac{dm_j}{d\theta} \tag{4}$$

The working control volumes are defined by assuming a sinusoidal variation in the compressor volume and then writing an equation for the dynamic motion of the cold displacer in order to determine the expander volumes. The motion of the cold displacer depends on the resultant gas pressure on the displacer, the seal drag, and the external vibration forces. Figure 3 presents the dynamic model for the free displacer together with the terms for the acceleration of the displacer in relation to the acceleration of the cylinder. The associated equation is

$$\frac{d^2u}{dt^2} = \frac{1}{m_p}\left[F_P - F_S \text{ Sign } (\dot{u}) - m_p \frac{d^2w}{dt^2} \right] \tag{5}$$

This equation is integrated to produce the velocity of the displacer in relation to that of the cylinder.

The final equation represents the variation in the temperature of the regenerator. When it is written in finite-difference form, this equation is a heat balance for node i, where G_{ij} is the heat flow path between nodes i and j. These paths can represent either conductive or convective heat transfer between the respective nodes. By expressing t as a function of compressor crank angle, this equation can be expressed as

$$\frac{dT_i}{d\theta} = \frac{e}{C_{p_i} \rho_i}\left(\sum_{j=1}^{n} G_{ij}(T_j - T_i) + Q_i \right) \tag{6}$$

The solution of this equation yields a temperature/time history for each regenerator node.

NODAL REPRESENTATION

The thermal model is of the nodal network type, which divides the refrigerator into discrete structure and working fluid nodes that are interconnected by heat transfer and mass transfer energy flow paths. A schematic cross section of a typical split-cycle cold head divided into a discrete nodal network is shown in Figure 4. Details of a typical regenerator control volume are given in Figure 5.

The gas system is divided into control volumes, and the machine structure is divided into elements of corresponding size. In this way all internal gas volumes, machine elements, and boundaries are modeled as variable- or constant-

temperature regions that exchange energy with one another as defined by the fundamental equations of heat transfer. Modes of energy exchange between nodes include mass transport between the gas nodes, conduction across solid or gaseous material, and convection at gas/solid interfaces. Each volume of the nodal network is described by three sets of differential equations that are categorized as equations expressing the distribution of

1. Gas temperatures

2. Gas masses

3. Regenerator temperatures

The simultaneous digital solution of these three sets of equations by the nodal network representation is achieved by using the MIMIC program language (1). MIMIC is a high-level language used on a digital computer (in our case an Amdahl 580 and for Wright-Patterson a Control Data 6000) for simulation of continuous and sampled data systems. It is a simple way to express systems of ordinary differential equations since it allows the problem to be solved without requiring that the user formulate an algorithm. Working from this mathematical model, the user writes MIMIC statements describing the system; these statements can, in turn, be grouped into sets of statements that represent the various control volumes that make up the nodal network.

COMPUTER MODEL

To produce the computer program in final form, considerable attention was given to balancing the following three critical areas that affect the simulation accuracy and the size of the computer program needed.

1. The degree of complexity needed in the thermodynamic equations that define the conservation of energy and the conservation of mass of the working fluid.

2. The extent to which the nodal network should be divided, and what boundary conditions should be assumed.

3. The evaluation of the quantitative accuracy of the correlations used to define the various heat transfer mechanisms, gas-flow frictional pressure drops, and the frictional characteristics of displacer motion.

Each of these subjects was reviewed and was simplified as needed in order to devise a program that represents the physical system with an acceptable degree of accuracy and that is of manageable size (i.e., reasonable required core size for compiling and reasonable CPU time in which to conduct a complete simulation run).

THERMODYNAMIC EQUATIONS

Besides the simplifications made in the defining thermodynamic equations,

already discussed, the thermophysical properties of the helium working fluid as well as the regenerator matrix properties and the extent to which these properties affect the cooler performance was also considered. Provision was made for the variations in thermophysical properties as the pressures and temperatures vary during the refrigeration cycle. These variations become increasingly critical as the control volume temperatures decrease. The computer program therefore includes a means of accessing important thermophysical properties data by using pressure and temperature information.

NODAL NETWORK

The number of nodes to be used in a cooler simulation depends on the lowest temperature that the cooler to be simulated is expected to reach. In the present form of the program six regions along the regenerator length were used. This number was adequate for simulating the base cooler used for program verification and kept the computer simulation time below 6 minutes CPU on the Amdahl. Isothermality was also assumed as a boundary condition for the compressor and the warm expansion volumes.

CORRELATION ACCURACY

Item (3) listed above is the pacing item in terms of program accuracy. The other two items can be varied to reduce simulation errors to the extent required by the investigation, but the accuracies of the correlations have not yet been thoroughly investigated. Their applicability to the conditions in a small cryogenic refrigerator have yet to be rigorously concluded.

The set of correlations used in the program are presented in Table 1. These equations were chosen from the literature in the expectation that when the results from the computer program were correlated with the test data any need for further refinements of certain correlations would become obvious. The equations for two relationships are not given in Table 1. These are correlations for seal drag and heat transfer coefficient for the cold expansion volume and will be discussed later.

BASELINE COOLER SIMULATION

In order to verify that the software accurately simulates the actual split-cycle operation, software-generated data and hardware test data had to be compared. In this comparison, a test cooler was chosen as the baseline cooler, and the computer program was used to generate simulation data for a representative number of steady-state refrigeration loads.

The baseline cooler was simulated by inputting the program information defining the mechanical configuration of the cooler and specific operating conditions. The following two pieces of data remained to be determined for this simulation because they are not inherent in the program.

- The magnitude of the regenerator seal drag

- The heat transfer film coefficient between the gas in the cold expansion volume and the expansion volume wall.

These items were given special attention because they cannot yet be accurately defined and they have a significant effect on the simulation results. No accurate correlation has been defined that will yield the dynamic friction force characteristics of the expander seal. It was therefore assumed that the seal drag did not vary with velocity or with pressure drop across the seal. The seal drag was therefore estimated by measuring the force required to manually move the displacer at constant velocity within an ambient expander cylinder. This measured value may deviate from actual operational drag force. The convective film coefficient at the cold expansion volume is another parameter that is not accurately defined because it has not been possible to analytically define the extremely complex and variable flow patterns in the cold expansion volume nor is there enough test data available to develop an empirical relation. A best estimate of 1000 W/M^2-K was chosen as a constant for this factor.

PRESSURE VOLUME DIAGRAM COMPARISON

The validation of the pressure model was particularly detailed because of the availability of data from the test cooler. This data is in the form of a pressure-volume diagram. The linear motion of the displacer was monitored by a detector at the ambient spring volume, and the pressure was monitored at the compressor. The resulting plot pressure versus stroke position (a multiplying factor is all that is needed to determine the swept volume) is displayed on an oscilloscope. During data acquisition, it was noted that as the refrigerator expansion volume cooled down (the ambient temperature remained constant), the displacer stroke became shorter. This phenomena is shown in Figure 6 for two cold volume temperature levels (case 2 is 30K warmer than the minimum temperature case). Note that the test data (dashed line) shows a 30% decrease in stroke at its minimum temperature level. The computer program closely predicts this decrease. It is not surprising to see some deviations between the test and simulation data since the simulated motion of the displacer is handicapped by the need to assume seal frictional characteristics. The incorporation of a more realistic seal drag correlation (other than an assumed constant value) should provide an even better simulation of pressure and motion profiles.

NET CAPACITY COMPARISON

The net capacity test data available includes mean cooler performance as well as a range of performance results. A comparison of the cooler simulation data cooler plotted in Figure 7 with the range of cooler test data (also plotted) shows that the data from the simulation is slightly conservative. Since (as previously discussed) there are other parametric values that affect cooler performance (e.g., seal drag and cold head heat transfer correlation) that were not adjusted at this time, it is expected that correlations that predict the values of these parameters more accurately will provide predicted performance data that is consistent with the test data. The appraisal of the applicability of the correlations used during the program will require additional cooler

test data that can be obtained only from a completely instrumented test cooler.

Although the values of the thermodynamic design parameters require some additional fine tuning, the program can simulate cooler thermodynamic performance with great accuracy. The data obtained during these simulations for the cold regenerator and for the free displacer already provides a valuable insight into how these components affect cooler performance.

Additional simulation data profiles are presented in Figures 8 through 10 for one thermodynamic cycle (360° of rotation of the compressor drive). Figure 8 shows the variation in its pressure and volume of the cold end with time. The area within the cold expansion volume indicator diagram represents the gross cooling capacity available during a single thermodynamic cycle. After it is reduced by the thermal losses of the expander, this capacity represents the net refrigeration capacity. This net capacity is defined by the total heat flux across the cold expansion volume boundaries; see Table 2.

Figure 9 shows the variations in pressure with time during a complete cycle at the cold and ambient expansion volumes and at the compression volume. Aerodynamic frictional losses are the cause of the difference in the pressures of these volumes. Figure 10 shows how temperature, mass flow, and volume (displacement) at the cold expansion volume vary with time.

CONCLUSIONS AND RECOMMENDATIONS

The Cold Displacer Computer Program is an analytical tool that realistically simulates the performance and characteristics of cryogenic split-Stirling-cycle coolers. This program has already provided valuable qualitative information about cooler performance. The mathematical model employed appears to be entirely adequate for the tasks outlined in the abstract. It affords an opportunity for defining the intricate interrelationships of the thermodynamic and thermophysical properties and hence provides a better understanding of the performance of the split-cycle cooler. Quantitatively, this program simulates a test cooler very well. Further testing and research will make it possible to increase the accuracy of the program by providing data on the correlations that as yet are not well defined or whose application to small cryogenic coolers is questionable. The accuracy of the program as well as the extensive generalized modeling equations (especially those for the regenerator model) will give a realistic indication of how performance responds to design changes and to variations in the values of critical parameters.

NOMENCLATURE

A_w -Cross-sectional area of wall

BDC -Bottom-dead-center

C -Cylinder circumference

C_p -Specific heat at constant pressure

C_v -Specific heat at constant volume

D_c -Diameter, cylinder

D_p -Diameter, sphere

D_t -Diameter, regenerator bed

F_f -Force, mechanical friction

F_p -Force, resultant

F_s -Force, seal drag

F_v -Force, vibration and/or shock

G -Conductance

K -Flow friction coefficient

k_{cy} -Thermal conductivity, cylinder

k_{eff} -Thermal conductivity, effective

k_g -Thermal conductivity, gas

k_s -Thermal conductivity, matrix

L_{cy} -Length, cylinder

m -Mass of gas

m_p -Mass of displacer

N -Cyclic speed

P -Pressure

Q -Heat Flow

R -Gas constant

Re_h -Reynold's number based on hydraulic diameter

Re_s -Reynold's number based on sphere diameter

S -Radial clearance

T -Temperature

TDC -Top-dead-center

U -Velocity

V -Volume

W -Work

Y -Stroke

Z -Compressibility factor

Greek Letters

ϵ -Porosity

ρ -Density

θ -Crank angle

General Subscripts

n -node

a -ambient

c -cold

cv -control volume

e -exit

i -into

w -wall

Table 1. Correlations used within the cold displacer computer program

Item	Equation	Source
Regenerator Effective Conductivity for Sphere Matrix (bed axial heat conduction)	$k_{eff} = k_g * 1.72 \left(\frac{k_s}{k_g}\right)^{0.26} + \frac{0.071\ (Re_s)^{0.69}}{0.5} \left(\frac{D_p}{D_t}\right) (1 - \varepsilon)^{0.19}$	Reference 2
Regenerator Effective Conductivity for Screen Matrix	$k_{eff} = k_g\ 1.10 \left(\frac{k_s}{k_g}\right)^{0.25}$	Curve fit of Figure 11-7 Reference 2
Colburn Heat Transfer Modulus for Sphere Matrix	$j = 0.23\ Re_s^{-0.3}$	Curve fit of data in Reference 3
Colburn Heat Transfer Modulus for Screen Matrix	$j = 0.6 + Re_h^{-0.4}$	Curve fit of data in Reference 3
Darcy Friction Factor for Sphere Matrix	$f = 4 \left(0.43 + \frac{57.75}{Re}\right)^{0.97}$	Curve fit of data in Reference 3
Darcy Friction Factor for Screen Matrix	$f = 4 \left(0.4 + \frac{45}{Re}\right)$	Curve fit of data in Reference 3
Friction Loss of Perforated Header Plate	$\Delta P = \frac{A_D V_D Y}{A_f C} \frac{PD \left(1 - A_f A_D^2\right)}{2g}$	Reference 4 (see reference for nomenclature)
Pumping Heat Transfer Loss	$Q = \left[\frac{2\pi D_c L_{cy} S^3 (T_a - T_c)}{3.2kg}\right] * \left(\frac{(P_{max} - P_{min})\ C_p N}{R\ \frac{T_a + T_c}{2}}\right)^2$	Reference 5

Table 1 (Cont.)

Item	Equation	Source
Seal Frictional Heating Loss	$Q = 2\ Y\ N\ F_f$	Reference 5
Thermal Conduction Along Cylinders, Displacers and Other Structural Walls	$Q = \frac{k_{cy}\ A_w}{L_{cy}} (T_a - T_c)$ where $k_{cy} = \frac{1}{(T_a - T_c)} \int_{T_c}^{T_a} k_{cy}\ dT$	Reference 5
Shuttle Heat Transfer Loss	$Q = 0.186 * Y^2 \frac{K_g}{S} \frac{(T_a - T_c)}{L_{cy}}$	Reference 5

TABLE 2. RELATIVE CYCLIC ENERGY BALANCE FOR COLD EXPANSION VOLUME

WORK OF VOLUME CHANGE	(GROSS CAPACITY)	100%
THERMAL LOAD	(NET CAPACITY)	-36.6%
THERMAL LOSSES		
REGENERATOR INEFFICIENCY	35.0%	
CYLINDER CONDUCTION	8.7%	
DISPLACER CONDUCTION	0.6%	
SHUTTLE	8.9%	
PUMPING	10.2%	
SUM		-63.4%
CHANGE IN INTERNAL ENERGY FOR ONE COMPLETE CYCLE (STEADY-STATE ACHIEVED)		0.0%

*NUMBERS LISTED ARE FOR A SAMPLE SIMULATION OF THE TEST COOLER UNDER THE FOLLOWING CONDITIONS:
AMBIENT TEMPERATURE 22°C
MAXIMUM RATED HEAT LOAD
MOTOR SPEED 20Hz

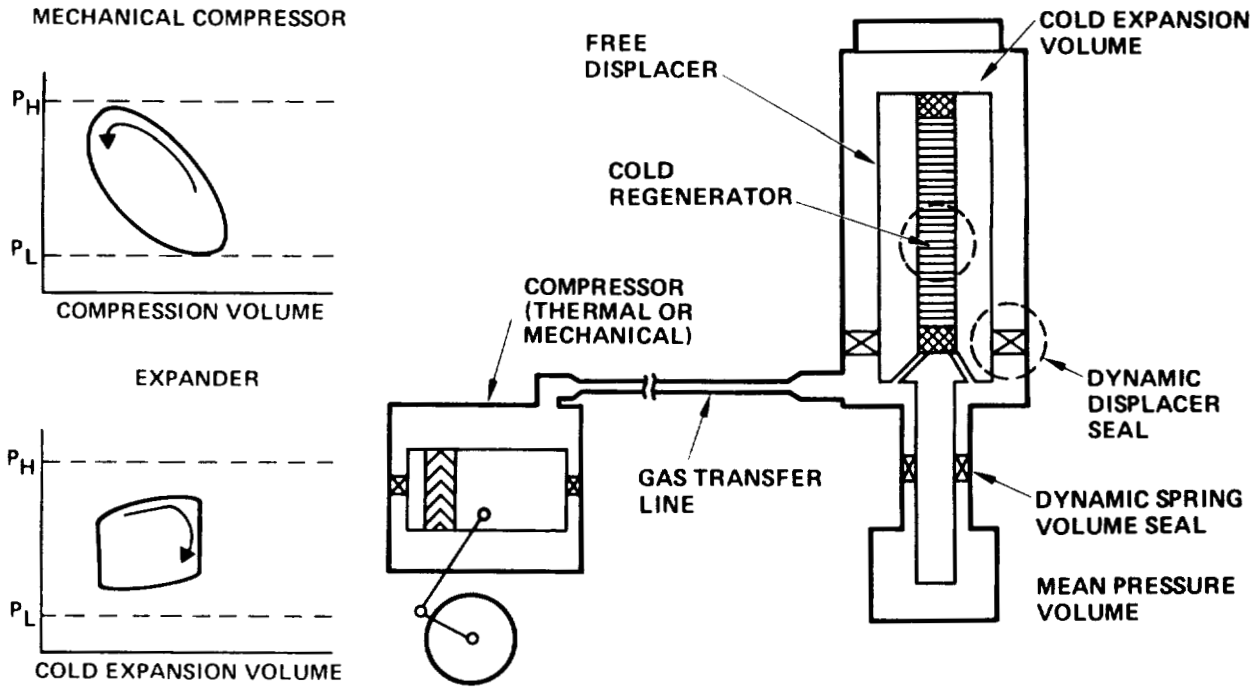

FIGURE 1. SCHEMATIC REPRESENTATION AND PRESSURE/VOLUME RELATIONSHIP OF SPLIT-CYCLE REFRIGERATOR

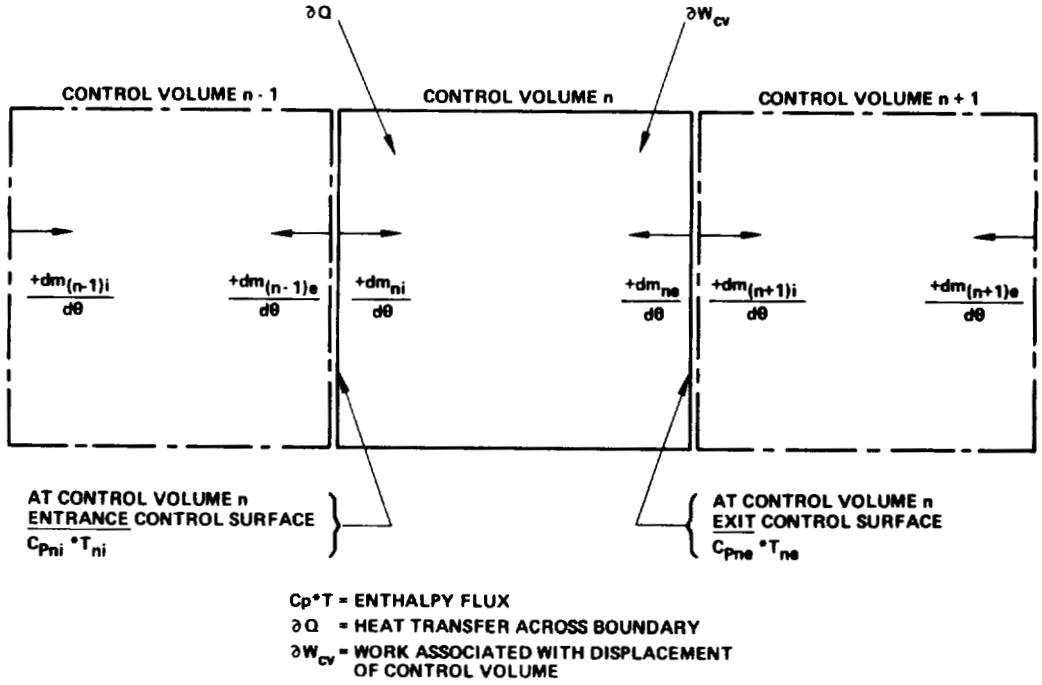

FIGURE 2. SIGN CONVENTION FOR THE ENERGY BALANCE OF A CONTROL VOLUME AND MASS FLOW CONVENTION FOR SEQUENTIAL CONTROL VOLUMES

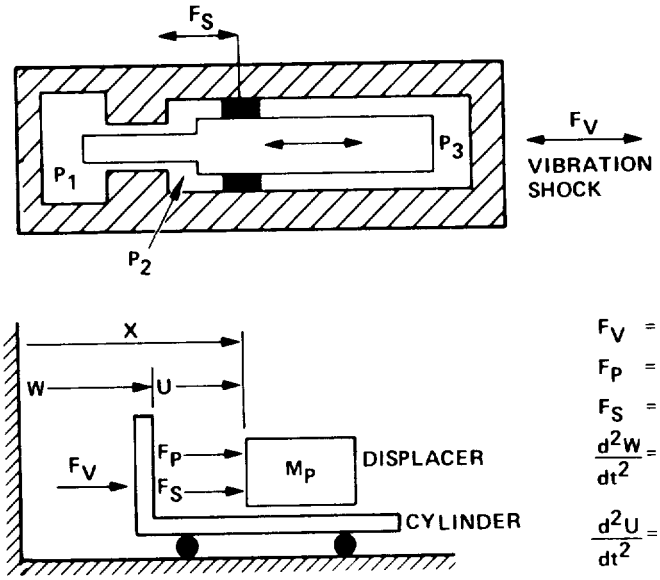

FIGURE 3. DYNAMIC MODEL OF THE FREE DISPLACER

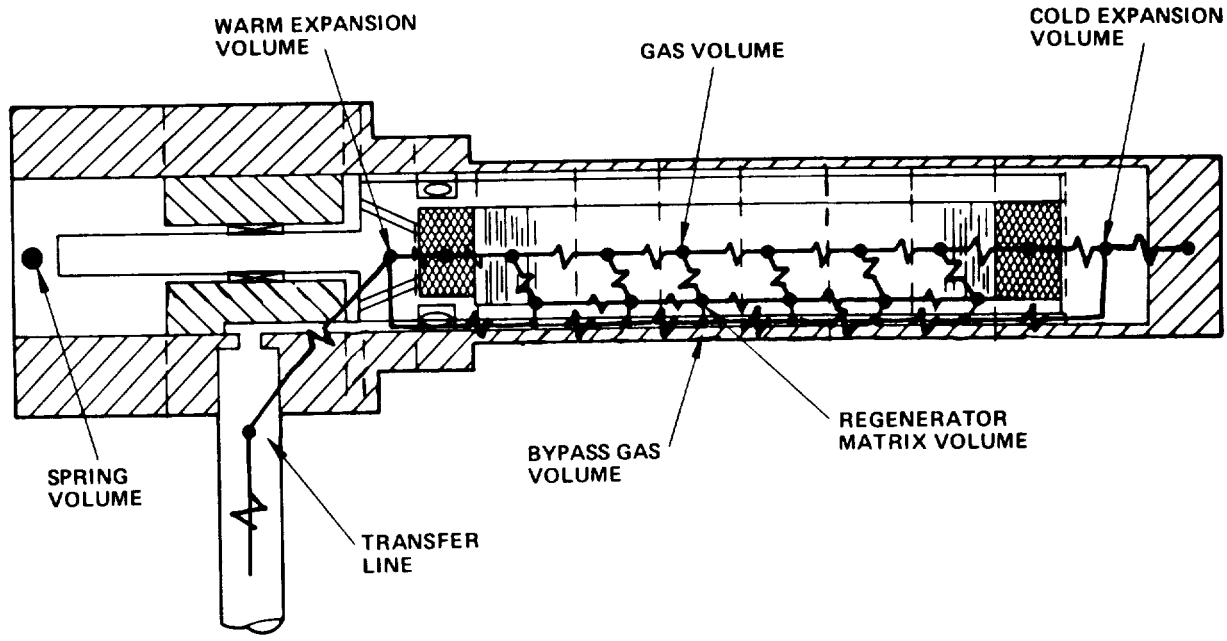

FIGURE 4. COLD HEAD NODAL NETWORK

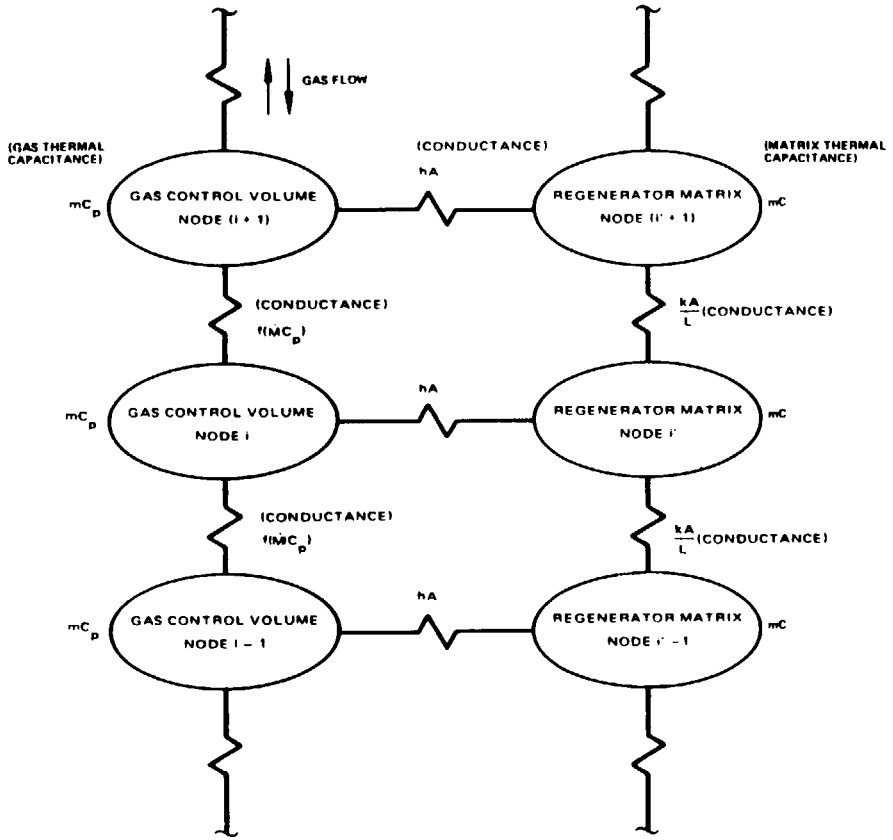

FIGURE 5. DETAILED NODAL NETWORK OF A TYPICAL REGENERATOR CONTROL VOLUME

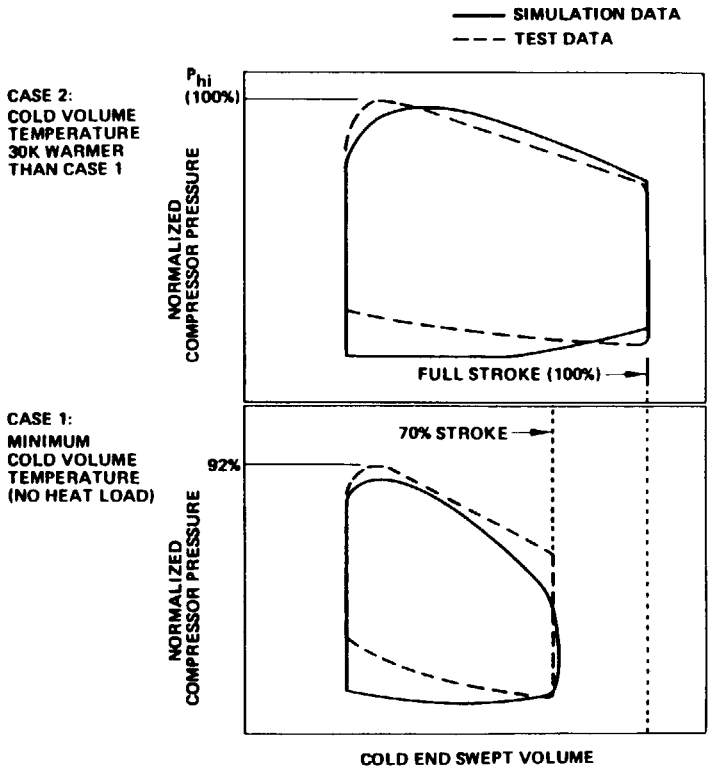

FIGURE 6. COMPARISON OF SIMULATION AND TEST DATA FOR VARIATION IN COLD VOLUME TEMPERATURE

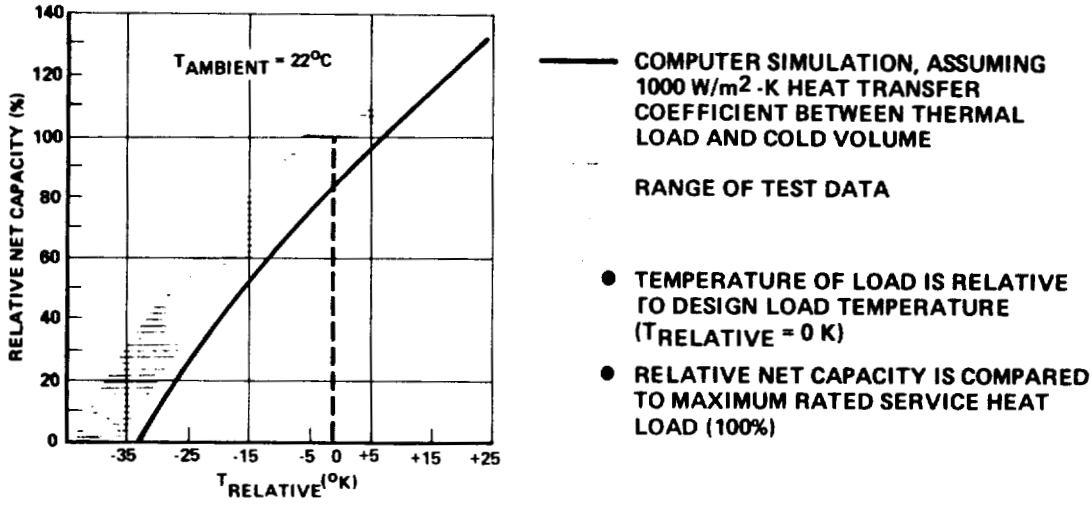

FIGURE 7. CORRELATION OF COMPUTER SIMULATIONS TO AVAILABLE DATA OF A SPLIT-CYCLE TEST COOLER

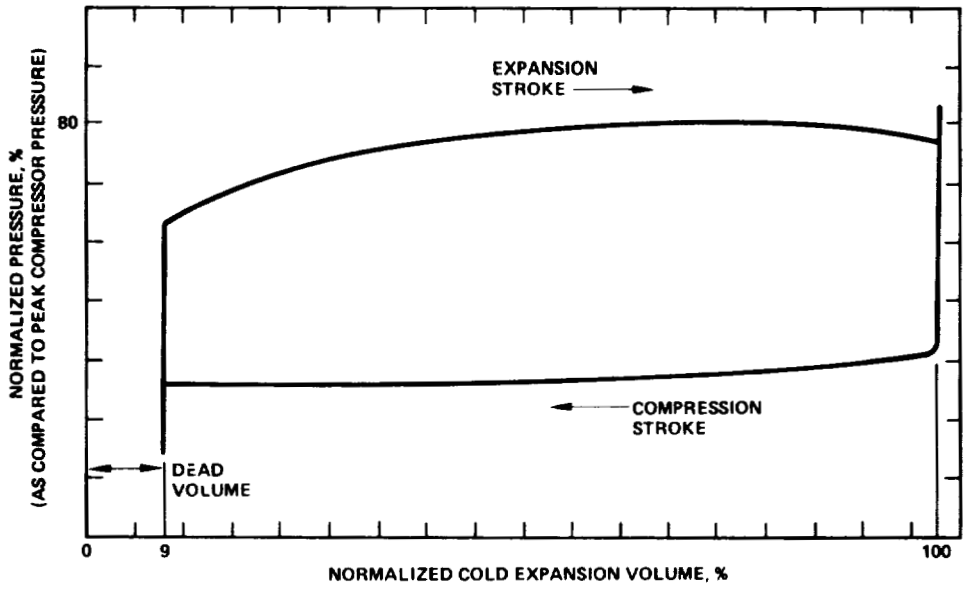

FIGURE 8. PRESSURE VERSUS VOLUME PLOT FOR THE COLD EXPANSION VOLUME

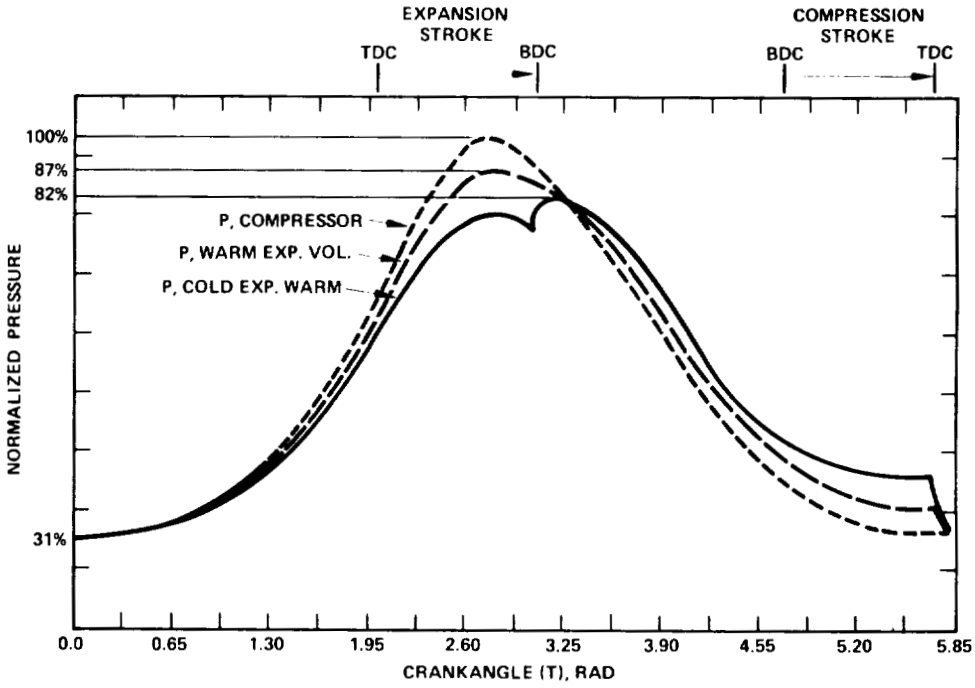

FIGURE 9. PRESSURE VERSUS TIME PLOTS FOR THE COMPRESSOR, AMBIENT EXPANSION VOLUME AND COLD EXPANSION VOLUME

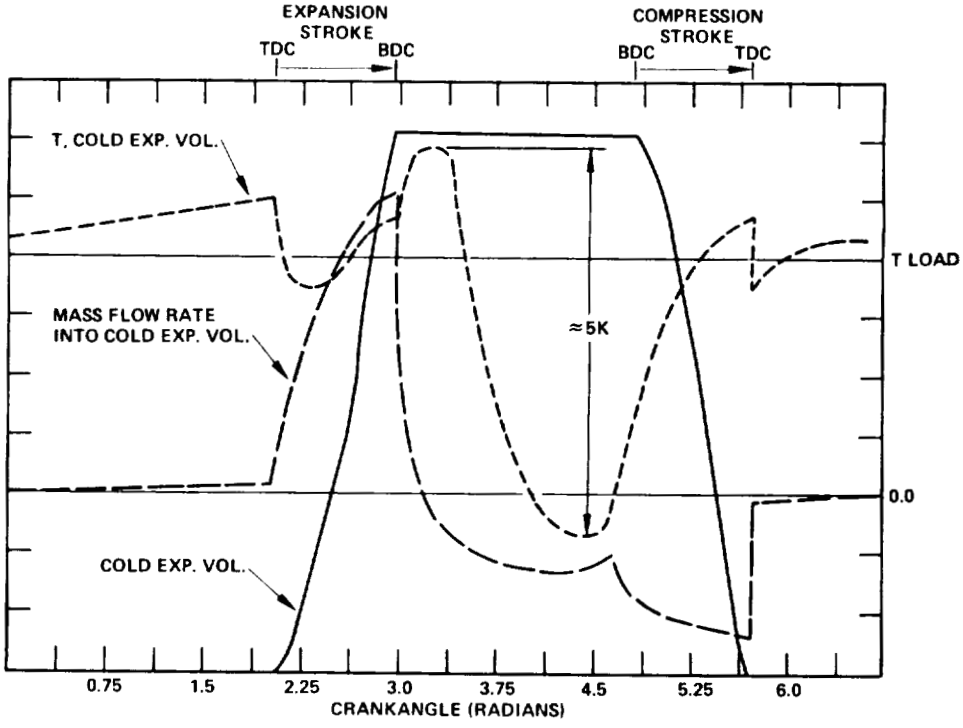

FIGURE 10. ENTRANCE MASS FLOW RATE, TEMPERATURE AND EXPANDER COLD WORKING VOLUME VERSUS TIME

REFERENCES

1. Control Data 6000 Computer Systems MIMIC Digital Simulation Language, Reference Manual, Revision E(1-1-72), Control Data Corporation, Sunnyvale, California 94086.

2. McAdams, W. H., Heat Transmission, McGraw-Hill Series in Chemical Engineering, 3rd ed., pgs. 290-295.

3. Kays, W., and A. L. London, Compact Heat Exchangers, McGraw-Hill Series in Mechanical Engineering, 2nd ed., pgs. 129-131.

4. Kolodize, P. A. and M. Van Winkle, "Discharge Coefficients through Perforated Plates", Reprinted from AICh. E Journal, Vol. 3, No. 3, 1957 by General Electric.

5. Leo, B. S., Designer's Handbook for Spaceborne Two-Stage Vuilleumier Cryogenic Coolers, AD No. 872-995, Air Force Flight Dynamics Laboratory, AF Wright Aeronautical Laboratories, Air Force Systems Command, Wright-Patterson AFB, Ohio, 45433

A MAGNETICALLY SUSPENDED

LINEARLY DRIVEN CRYOGENIC REFRIGERATOR*

F. Stolfi, M. Goldowsky,
J. Ricciardelli and P. Shapiro
Philips Laboratories
Briarcliff Manor, New York 10510

ABSTRACT

This paper describes a novel Stirling cycle cryogenic refrigerator which was designed, fabricated and successfully tested at Philips Laboratories. The prominent features of the machine are an electro-magnetic bearing system, a pair of moving magnet linear motors, and clearance seals with a 25 μm radial gap. The all-metal and ceramic construction eliminates long-term organic contamination of the helium working fluid. The axial positions of the piston and displacer are electronically controlled, permitting independent adjustment of the amplitude of each and their relative phase relationship during operation. A simple passive counterbalance reduces axial vibrations. The design of the refrigerator system components is discussed and a comparison is made between performance estimates and measured results.

INTRODUCTION

In 1978, Philips Laboratories proposed to design, fabricate and test a cryogenic refrigerator for spaceborne applications, under the sponsorship of the NASA Goddard Space Flight Center. Drawing on expertise developed at Philips over the last 40 years, the unit was based on the Stirling cycle but incorporated many novel electromechanical features which extended the operational life of the machine greatly beyond that of units built in the past. The ultimate goal is a system capable of producing 5 W of refrigeration at 65°K for 5 years or longer. The purpose of the first model, which was successfully tested in March 1982, was to prove the viability of the technology (Ref. 1).

(*) This work was performed under NASA Goddard Contract number NAS5-25172.

SYSTEM DESCRIPTION

GENERAL ASPECTS

The novelty of the refrigerator stems from the use of active magnetic bearings, clearance seals, and an electronically controlled direct-drive linear motion. The use of these three basic features leads to a design promising long mechanical life, comparatively high electromechanical efficiency and high thermo-dynamic stability. In short, it produces a refrigerator which is compatible with the ultimate intended spaceborne applications.

With active magnetic reciprocating bearings, the moving elements of the refrigerator are electro-magnetically suspended in small annular gaps. Friction, wear and particle generation are eliminated since there is no mechanical contact. Further, this approach allows the refrigerator to be made from only metal and ceramic components. There is no need for lubrication, either wet or dry. With the complete absence of organic materials and the associated contamination of the working gas, a principal cause of thermal degradation is avoided.

Clearance seals, an apparent contradiction in terms, is the designation given to the 25 μm radial gaps around certain sections of the moving elements. Since the amount of gas which can flow through these long narrow passages is limited, they effectively form dynamic pressure seals. This type of seal, accomplished without the use of organic materials or mechanical contact eliminates a traditional life limiting component in Stirling machines.

By using moving-magnet linear motors as the drive mechanism, linkages and flexing power leads are eliminated. The result is a design with high electro-mechanical efficiency, long life and high reliability. Since the motors are controlled with an electronic control system, the user has complete flexibility in adjusting the amplitude and the frequency of the linear motions. This gives the system a high degree of mechanical and thermodynamic versatility.

The development of the magnetic bearings and linear motors included the design, construction and use of dedicated test fixtures. The refrigerator is not an optimal test vehicle for these components since their individual design parameters could not be independently evaluated. However, since the bearings and motors are meant to perform a specific task, the test fixtures had to simulate the refrigerator as closely as possible. In the case of the bearings, this meant a fixture machined to close tolerances using materials and joining techniques equivalent to those used in the refrigerator. For the motor, this meant a fixture which utilized a gas spring and an air bearing.

Following a description of the refrigerator, the design and testing of the major subsystems (the bearings, linear motors, axial control system and

passive countermass) will be discussed. The paper concludes with the description and results of several thermodynamic parametric tests; work that is currently in progress.

CONFIGURATION

The cryogenic refrigerator, shown in cross section in Figure 1, is composed of three major sections. In the displacer section, gas is cyclically shuttled from the cold expansion end to the rear compression section which is held at ambient temperature with the aid of a water jacket/ heat exchanger. In the second major section, the gas is expanded and compressed through the action of a piston. Finally, the third section contains a spring-mass passive counterbalance, which minimizes axial vibrations when tuned to the refrigerator running frequency. The piston and displacer elements are supported on magnetic bearings, the countermass, on leaf springs. A photograph of the refrigerator is shown in Figure 2.

Displacer Subassembly

The displacer section is shown in detail in Figure 3. Helium gas, the working fluid, is free to flow from the expansion space at the 65°K flange, through the heat exchanger, which is maintained at 300°K with a water jacket, to the compression space in the piston section. A copper cap at the cold end serves as a heat exchanger and minimizes cyclic thermal variations. A moving regenerator maintains the temperature gradient along the length of the cold finger by storing heat energy in one half of the cycle to release it in the other half. The magnetic bearings and radial position transducers shown in Figure 3, form the first two clearance seals, forcing the helium to flow through the regenerator and through the heat exchanger. The axial motion of the displacer is driven by a moving magnet linear motor and transduced with a linear variable differential transformer (LVDT). The LVDT, described in greater detail in Section 5, requires no mechanical contact with the moving displacer.

Piston Subassembly

The piston section is shown in detail in Figure 4. The magnetic bearing on the left forms the third and final clearance seal; its function is to maintain the cyclic pressure in the compression space. The additional magnetic bearing at the rear of the piston supports the shaft but does not form a seal. The hollow vented piston shaft and the large volume in the center of this section constitute a buffer space for helium gas. As in the displacer, the axial motion control entails the use of a moving magnet linear motor and an LVDT.

Since there is no physical connection between the piston and displacer (such as a crankshaft and connecting rods), the refrigerator produces cold only through the action of an electronic control system which regulates the

amplitude and phase of each element. The displacer must lead the piston by a specific phase angle (about 60°) so that the gas is principally located in the compression (300°K) section when the piston compresses and in the expansion (65°K) section when the piston expands. Thermodynamic stability is achieved only if this phase and amplitude relationship is accurately maintained.

Countermass Subassembly

The countermass is shown in cross section in Figure 5. It passively reciprocates in vector phase opposition to the combined piston and displacer momentum when the coil spring/moving mass resonance is tuned to the refrigerator running frequency. Since the three subassemblies are bolted together on a common centerline, the action of the countermass minimizes the axial vibration of the refrigerator housing. The leaf springs provide radial support, adding little damping to the system. The countermass is tuned to the refrigerator operating frequency by changing the tuning mass shown in Figure 5.

MAGNETIC BEARINGS

DESCRIPTION

The configuration of the magnetic bearings is shown diagrammatically in Figure 6. Each ferromagnetic pole piece exerts a radial attractive force on the reciprocating shaft when current is applied to its coil winding. By situating poles diametrically opposite, one end of the shaft may be controlled in one plane by regulating the current in each pole (see Fig. 7). By positioning sets of poles at orthogonal planes on each end of the shaft, the shaft may be suspended (centered in the bore).

The radial position of the shaft is transduced with eddy current sensors. The eddy current probe consists of a flat coil which is situated parallel to the sensed shaft. By applying a high frequency voltage to this coil, eddy currents are generated in the shaft and the magnitude and phase of these eddy currents change as the magnetic air gap changes. The probe thus provides a dynamic measurement of shaft position. The probes are mounted differentially so that temperature-induced drift is substantially reduced.

FABRICATION

In the refrigerator, three of the magnetic bearings also form clearance seals. The dual nature of these sections, and the use of only metal and ceramic materials, means that special fabrication techniques are required in the construction. The 25 μm gap between the shaft and the housing requires the use of materials with high dimensional stability. Each cross section is radially symmetric to minimize thermal stresses. The ferromagnetic pole

pieces for the bearings are brazed hermetically to the housing wall, and the optimized magnetic properties of the pole pieces are still maintained. The eddy current probes are mounted behind ceramic windows with a thickness of 1 mm to prevent the organic insulation and potting compound used in their construction from contacting the working gas. Finally, the thermal expansions of the titanium alloy used for the housing, the iron alloy chosen for the pole pieces and the ceramic in the windows are closely matched, to prevent thermal stress and distortion.

BEARING CONTROL SYSTEM

The bearing electronic control system is shown diagrammatically in Figure 8. The pole piece magnetics are highly nonlinear: the force is porportional to the square of the current and inversely proportional to the square of the air gap. The electromagnetic field in the iron is influenced by the effects of eddy currents, hysteresis and magnetic saturation. The shaft dynamics includes a damping force caused by the gas squeeze film in the 25 μm gap.

The bearing controller can be modeled as a linear feedback regulator if it is assumed that the variations in the radial displacement and differential current are small about their nominal values. A reference center position of zero volts is compared to the transduced position voltage from the eddy current sensors. Any difference between these two signals regulates the current in the diametrically opposite pole pieces so as to reduce the error. The compensator is designed to provide large restoring signals for small errors over a wide frequency band in spite of the nonlinear nature of the magnetics and dynamics. A current amplifier is used so that the destabilizing phase shifts caused by the coil inductance and eddy currents are minimized.

TEST RESULTS

The magnetic bearing test fixture is shown in Figure 9. A linear shaker was connected to the center of the suspended shaft through a piezoelectric force transducer. The radial position of the shaft was dynamically measured with the eddy current sensors. The diameter of the shaft, the width and length of the clearance seal area, and the method by which the ferromagnetic materials were joined were chosen to simulate the piston section of the refrigerator.

The measured dynamic "stiffness" of the magnetic bearing is shown in Figure 10; the static load data in Figure 11. The dynamic stiffness increases at 200 Hz because the shaft inertia dominates the response. The test fixture also facilitated the development of the bearing electronic control system; Table 1 gives a summary of the control system and radial position sensor performance in refrigerator operation. This work demonstrated the feasibility of using linear magnetic bearings in the refrigerator, since, as the data shows, they exhibit a higher stiffness than many mechanical bearings.

LINEAR MOTORS

DESCRIPTION

The principle of operation of the linear motors used in this refrigerator is similar to that of the actuators used in most loudspeakers (Fig. 12 is an expanded view of the piston motor shown in Fig. 4). Permanent magnets, rather than a field coil, establish a steady magnetic flux field. The current through the coil interacts with the flux to produce a force between the coil and the permanent magnet. Since the flux is oriented radially and the coil is wound circumferentially, the force is directed along the axis of the motor, producing linear motion.

Figure 12 shows an inner and an outer coil section for each of the two "motor sections". The presence of substantial non-magnetic gaps (the coils) on each side of the magnet rings reduces the radial force generated between the moving-magnet armature and the stationary iron stator rings. Otherwise, these side forces can represent a significant load for the magnetic bearings.

An additional feature of this motor design is the ability to hermetically isolate the helium working gas from all possible sources of organic contamination. The hermetic seal is made by welding thin-walled titanium cans over the magnets and the coils. If the cans are relatively thin (0.3 mm), the reduction in the motor efficiency will be small.

Figure 13 is a photograph of the complete motor, with the armature mounted to the piston shaft and the stator assembly ready for insertion into the housing of the piston motor.

The displacer motor shown schematically in Figure 14 functions in the same manner as the piston motor. The geometry is somewhat different in that there is only one coil section for each magnet section, and the inner iron "stator" is actually part of the armature. The small size of this motor dictates these changes, but the small size also means that the side forces are relatively insignificant compared to those associated with the much larger piston motor.

The piston motor is required to provide real power output (equal to the thermodynamic load), with no reactive component. The gas compression and expansion in the Stirling cycle provides a gas spring for the piston mass, with the thermodynamic and dynamic parameters chosen so that the spring mass system is resonant at the cooler operating frequency. This results in the highest possible efficiency for the piston motor, since the motor does not have to accelerate the piston mass. See Reference 2 for a more detailed discussion of the refrigerator dynamics.

Conversely, the displacer is very nearly a purely reactive load. The motor force is actively used to accelerate and decelerate the displacer mass, while the damping load is fairly small, due only to the pressure drop

of the gas flowing through the regenerator and heat exchangers. The displacer motor, therefore, cannot be used in an efficient manner, since its power factor is near zero.

ANALYSIS

The electromagnetic force generated by a current flowing through a wire in a magnetic field is given by the relationship, $F = B\ L\ I$, where F is the force in Newtons, B is the magnetic flux density in Webers/m^2, L is the length of wire within the magnetic field in meters, and I is the current in Amperes. Estimating B, the magnetic flux density in the air gap occupied by the coil, is somewhat difficult. Magnetic materials are inherently non-linear, and the flux path of least resistance is not always apparent, since flux leakage is frequently significant. Philips Laboratories has available a proprietary finite-element computer package (MAGGY) which is designed specifically for the solution of magnetic problems. This program has been verified through extensive use by various Philips organizations, and is generally accurate to within a few percent. All calculations of magnetic performance, including estimates of motor inductance, were made using the MAGGY program. This allowed for the optimization of dimensions to obtain the maximum motor efficiency for a given motor weight, with the magnets operating at their peak energy product and the iron stator thickness minimized.

DESIGN PARAMETERS

Table II shows a comparison between the design values and the results measured during refrigerator operation for the piston and displacer motors. The refrigerator was producing 5 W at 65°K with a phase angle between piston and displacer motions of 60°. It should be noted that the force constant and losses in the displacer motor are substantially different than predicted. The effect of this on refrigerator performance is disussed in Section 7.

PISTON-MOTOR TEST DATA

As part of the effort to develop the linear motors, a task was undertaken to experimentally measure various characteristics of the piston motor. These included the electrical characteristics which affect the design of the control system and the mechanical characteristics which affect the design of the bearings supporting the piston.

The design of the fixture (see Fig. 15) can be divided into two major sections: the motor (on the left), and a gas spring (on the right). There is also a means for attaching the two and a rigid system to keep the apparatus aligned.

The motor, consisting of the stator (22) and the armature (23), is, of course, the motor to be tested. The armature is attached to a linear air bearing (25) which in turn is attached, through a force transducer (28), to the gas-spring mechanism. An air bearing was used for its low power dissipation, accurate location, and light-weight construction.

The gas spring consists of a cylinder (15) and a two-sided piston (16). The cylinder is pressurized so that in moving the piston, a considerable force is required to compress the gas, yielding its spring-like characteristic. This gas spring was designed so that its nonlinearities, inherent to all gas springs, would be comparable to those found in the cooler, thus producing a representative environment for testing.

Rulon sleeves were used on the piston as a combination clearance seal and bearing. The low coefficient of friction of Rulon assured low power dissipation, and a 8 μm radial gap produced an acceptable clearance seal.

A system of valves is used to change the mean pressure within the cylinder, which changes the stiffness of the gas spring and thus the dynamic resonant frequency of the motor fixture. The valve system can also dissipate energy by allowing gas to flow between the cylinder halves. By controlling this flow, any desired motor loading can be produced.

Incorporated into the fixture design are three piezoelectric force transducers and an LVDT. The two radial force transducers located at the ends of the shaft (27) measure the side forces which the magnetic bearings will encounter. The third force transducer (28), mounted between the armature and the spring mechanism, measures the axial force and torque. The LVDT (20, 18) is mounted inside the cylinder and measures the position of the oscillating system at any time. A photograph of the motor test fixture is shown in Figure 16.

Measurements taken with this fixture are summarized below.

Force Constant. The axial force constant was predicted to be 8.8 N/Amp, using the MAGGY computer program. The measured dc value, representing the average of 16 measurements, was 8.77 N/Amp $\pm$ 0.24 N/Amp standard deviation.

Efficiency. Motor efficiency was measured for a wide range of force output and stroke amplitude. In all cases, the measured efficiency was within 10% of the predicted value.

Temperature Rise. The average temperature of the motor coil during operation was obtained by measuring its resistance (since the resistivity of copper is a known function of temperature). Measurements showed a temperature rise of about one-half of a degree centigrade per watt of power dissipation in the coils, giving a coil temperature of 35°C at the design point.

Side Forces. The force transducer measurements indicated that the static side forces (due to magnetic assymetries) were less than 10 N on all axes,

and the dynamic side forces (due to coil and/or mechanical assymetry) were less than 5 N. This is well within the measured capability of the magnetic bearings.

Torque Generation. Although the motor is linear, it will generate some torque due to the same assymetries responsible for the side forces. The torque was somewhat difficult to measure, but a conservative upper bound was 5 N-m at 25 Hz. Given the large moment of inertia of the piston assembly, this level of torque would result in a torsional oscillation of only 1° peak rotation.

CONCLUSIONS

The design procedures described here have resulted in the successful development of linear motors which met all requirements of the current refrigerator program. Analytical and numerical performance-prediction techniques were validated to a high degree of accuracy.

AXIAL CONTROL SYSTEMS

GENERAL

The axial control loops of the piston and displacer motors are intended to ensure long-term, stable refrigerator operation and to minimize harmonic vibrations. In order to achieve this stability the control loop errors of amplitude, phase and center position had to be minimized over a wide frequency range. The control loop can be broken down into three major sections: axial position transducer (LVDT), motor driver, and compensation.

AXIAL POSITION TRANSDUCER

The position transducers used in the refrigerator are a slightly modified version of a commercially available transducer. The LVDT produces an electrical output proportional to the displacement of a non-contacting ferromagnetic core. The motion of the core varies the mutual inductance of the differential secondary windings of the transformer. In addition to the ac excitation of the primary, synchronous demodulation and filtering of the transformer output is needed to extract the position signal. Improvements to the commercial transducer system involved improving the frequency stability of the ac excitation.

MOTOR DRIVER

The piston and displacer motor drivers are linear amplifiers with a deliverable power capability in excess of 300 Watts RMS. The amplifiers were designed with a bridge output configuration in order to effectively increase the applied motor voltage capability above the 28 V power supply. This additional voltage "headroom" compensates for motor parameters which

change as a function of operating frequency. The disadvantage of the bridge configuration is that the load is in effect "floating" above ground, which makes closed-loop current control difficult. Further, the maximum efficiency of the amplifier is reduced by a factor of two because of the additional power transistor in series with the load.

In order to analyze the amplifier performance and provide stability to the closed loop current control the effective motor impedances, a function of the motor load, are required. To estimate these impedances, the equivalent circuits for the piston and displacer motor systems (see Fig. 17 and 18), which are a linear approximation of the refrigerator dynamics at the operating point, are derived. In the case of the piston, the motor will operate at or near mechanical resonance (power factor of 1). This is achieved as a result of the balance between the inertial force of the piston and the spring force of the gas. The mechanical/electrical analog is simplified by modeling the linear motor as an ideal transformer (using SI units). Therefore the reflected inductance and capacitance, at the primary of the transformer, will be in resonance and have an infinite impedance. The mechanical damper, when reflected, represents the dynamic motor load which is in series with the piston motor coil.

Since the displacer assembly was not designed to operate in resonance (there is no spring), the effective impedance at the operating point is a function of the displacer mass and the coupling of the piston force through the gas. The dynamic load of the displacer is primarily reactive and the net power delivered to the thermodynamics (excluding ohmic losses) is very small, on the order of a few watts. The effect of the mass is also small, and thus the equivalent circuit of the displacer motor and load is simply the motor coil impedance.

The equivalent circuits of the piston and displacer motors are used to determine the peak currents and voltages required at the operating point. Once the output requirements were defined, the driver and input stages were designed to meet specific amplifier operating requirements of stability and bandwidth. For both drivers a peak current of 25 amps at the operating frequency was specified with less than 1% gain sensitivity to internal component variations. The full power bandwidth of both current drivers is designed to be greater than 1.5 kHz.

COMPENSATOR

A general block diagram of the piston and displacer axial control loops is shown in Figure 19. The gain and frequency response of the position transducers and current amplifiers are determined. The compensator is designed to optimize the position loop response. The two major objectives for the control loops are to minimize the sensitivity of the system to internal changes in the dynamics and to achieve a phase margin of at least 40° for stability. The finite bandwidths of the amplifiers and position transducers, and the vibrational resonances of the piston and displacer

shafts are considered in the calculation of the achievable system frequency response. The final piston and displacer control loops resulted in less than 10% gain sensitivity to system changes at the operating frequency and a phase margin of 50° with bandwidths of 65 Hz and 105 Hz, respectively.

COUNTERBALANCING SYSTEM

DESCRIPTION

Axial vibrations induced by the motions of the piston and displacer are attenuated by a passive vibration absorber. This device, shown schematically in Figure 20, consists of a 3.0 kg mass suspended at its ends by leaf springs. This type of suspension was chosen to minimize damping and to provide radial centering accuracy. The mass is also attached to a stiff coil spring on which it resonates at the cooler operating frequency. The stroke amplitude is 5.0 mm.

After a short period of refrigerator operation, it was observed that small movements between the coil spring and its mount were causing the generation of particles by a process called fretting. This problem has been temporarily reduced by clamping the spring to the mount, but a permanent solution is needed. Although there is always a potential problem when moving parts have mechanical contact, relatively long life is still a possibility. Further, since the countermass housing is distinct from the working space of the refrigerator, lubrication is possible.

PREDICTED PERFORMANCE

To predict the performance of the balancer, a linear two degree of freedom vibration model is used (see Fig. 21). The mass of the balancer is connected by a damped spring to the refrigerator housing, which is in turn connected through a damped spring to inertial ground. Figure 22 is a plot of the predicted force transmission as a function of cooler frequency. In this case, maximum attenuation occurs at 26 Hz. The sharpness of the attenuation is a result of the low damping in the coil spring and the leaf spring mount of the countermass. If the refrigerator is run at frequencies other than 26 Hz, the transmitted force sharply increases. At 26.5 Hz, a natural frequency of the two degree of freedom system, the vibration is amplified because the countermass reciprocates in phase with the refrigerator piston and displacer. A second natural frequency, related to the resonance of the mount, is low enough to be of no concern. Note that the vibration absorber will remove only the fundamental frequency. Higher harmonics will not be attenuated significantly.

The 63 Kg refrigerator is mounted to the table through coiled-wire springs (see Fig. 2) and exhibits a measured natural frequency of 6 Hz with a damping factor, ζ_M of 0.07. Measurements taken on the countermass coil spring indicated a desirably low damping factor of only .0014. Using these

values a vibration attenuation of 22 dB is the calculated additional effect of the balancer.

PERFORMANCE DATA

An accelerometer was first mounted to the cooler without the countermass installed. Test data was obtained using a piston amplitude of 7.3 mm and a displacer amplitude of 3.0 mm with a phase shift of 67° at 26 Hz. Next, the countermass system was installed and the accelerometer data was retaken.

It can be seen in Table III that the agreement between actual and predicted performance is good. As a point of comparison, the piston and displacer masses exert a peak disturbance force (inertial) of 415 N. Thus, the counterbalancing system only transmits 0.3% of this force at the fundamental frequency. The small cooler motion and low force transmittal to the base is accomplished without the use of additional electrical input power.

REFRIGERATOR PERFORMANCE

The refrigerator was successfully operated beginning in March 1982. The cooldown curve (temperature vs. time) is given in Figure 23. Table IV shows a comparison between the predicted performance, calculated with the Philips Stirling Analysis Computer Program, and that actually measured. The lower operating frequency is used because the piston mass is higher than predicted. The charge pressure, which determines the gas spring stiffness, could also be raised to keep the system in resonance. The countermass was tuned to resonate at 25 Hz for operation with the refrigerator.

The discrepancy in the electrical input power to the motors can be explained in two ways. First, the measured power includes higher harmonics of the running frequency. The dissipation of power at these frequencies results from the action of the axial control system and is not included in the Stirling program.

Secondly, as noted in Section 4, the electrical input power to the displacer motor, at the fundamental frequency, is substantially higher than predicted. The measured dynamic force constant was lower than predicted, necessitating the use of higher input currents to generate the required force. The flux density of the Permendur in the motor armature was designed to be very close to magnetic saturation, with a magnitude as high as 2.4 Tesla. At this level of flux density, the uniformity of the material becomes critical, as does the manner in which it is annealed. Since the diameter of this motor was restricted by the small size of the displacer, no margin was available for a conservative design.

A resistive heater is used to apply the load power at the cold end of the refrigerator. Figure 24 shows the parametric effect on cold temper-

ature and input power of varying this heater load. For this test, the amplitude and phase of the moving elements, along with the operating frequency, were held fixed. The input power decreases with increased load since the Carnot efficiency increases with the higher temperature.

Figure 25 shows the effects of varying the phase shift between the piston and displacer motions while holding amplitudes and frequency fixed. For this test, the temperature was held constant by adjusting the load power of the heater.

FUTURE PLANS

Philips Laboratories is currently under contract with NASA-Goddard Space Flight Center to produce the second generation of this magnetically suspended refrigerator. Efforts will be directed at reducing electrical input power and at meeting flight qualification requirements. Additional attention will be given to the overall system interactions. The first step in the development is a parametric characterization of the present model, of which Figures 24 and 25 represent the first two tests.

REFERENCE

1. Philips Laboratories, Division of North American Philips Corp., Design and Fabrication of a Long-Life Stirling Cycle Cooler for Space Applications, Phase I and II - Engineering Model, Final Report: Sept. 1978 - Dec. 1982, by F. Stolfi, M. Goldowsky, C. Keung, L. Knox, E. Lindale, R. Maresca, J. Ricciardelli, P. Shapiro, NASA contract NAS5-25172, Briarcliff Manor, N.Y., March 1983.

2. A.K. de Jonge: A Small Free-Piston Stirling Refrigerator. The Fourteenth Intersociety Energy Conversion Engineering Conference, Boston, Mass, August 1979.

TABLE I.--MAGNETIC BEARING PERFORMANCE.

	Piston	Displacer
D.c. Offset (Due to Shaft Weight)	<.4 μm	<.5 μm
Peak a.c. Oscillations (During Operation)	<.7 μm	<2.5 μm
Control Loop Bandwidth	375 Hz	150 Hz
Control Loop Phase Margin	40°	40°
Calculated d.c. Stiffness	26 x 10^6 N/m (150,000 lbs/in)	5.3 x 10^6 N/m (30,000 lbs/in)
Worst Case Sensor Drift Observed While Operating	.25 μm	.75 μm
Wideband Sensor Noise Level	~.25 μm	~.25 μm

TABLE II. --MOTOR PARAMETERS.

Parameter	Piston Motor		Displacer Motor	
	Design	Measured	Design	Measured
Peak force (N)	150	189	35	37
Phase angle of force from displacement (°)	90	90	176	180
Operating frequency (Hz)	26.7	26.7	26.7	26.7
Stroke amplitude (mm)	7.0	7.0	3.0	3.0
Force constant (N/A)	8.8	8.8	5.0	3.7
Real power output (W)	88	110	0.6	
Peak applied voltage	15	16	12	18
Peak current (A)	17	22	7	10
Ohmic Loss (W)	29	46	40	91
Efficiency (%)	75	71	N/A	N/A

TABLE III.--COUNTERMASS TEST RESULTS.

	Fundamental (26 Hz)	2nd. Harmonic (52 Hz)	3rd. Harmonic (78 Hz)
Without Balance:			
Peak acceleration (m/sec^2)	6.6	0.51	0.11
Peak displacement (μm)	252.	19.3	4.1
Peak transmitted force (N)	24.	1.9	0.4
With Balance:			
Peak acceleration (m/sec^2)	0.35	0.44	0.14
Peak displacement (μm)	13.4	16.8	5.3
Peak transmitted force (N)	1.3	1.6	0.5

TABLE IV.--DESIGN VERSUS PERFORMANCE.

Quantity	Design Value	Measured Value
Piston moving mass (kg)	1.85	1.92
Displacer moving mass (kg)	0.32	0.35
Piston amplitude (mm)	7	7.3
Displacer amplitude (mm)	3	3.0
Phase between piston and displacer (deg)	60	67
Operating frequency (Hz)	26.7	25.0
Charge pressure (atm)	16	16
Ambient heat exchanger temperature (°C)	15	12
Electric input power to motors (W)	155	220
Cold production (W)	5	5
Cold temperature (°K)	65	64.6

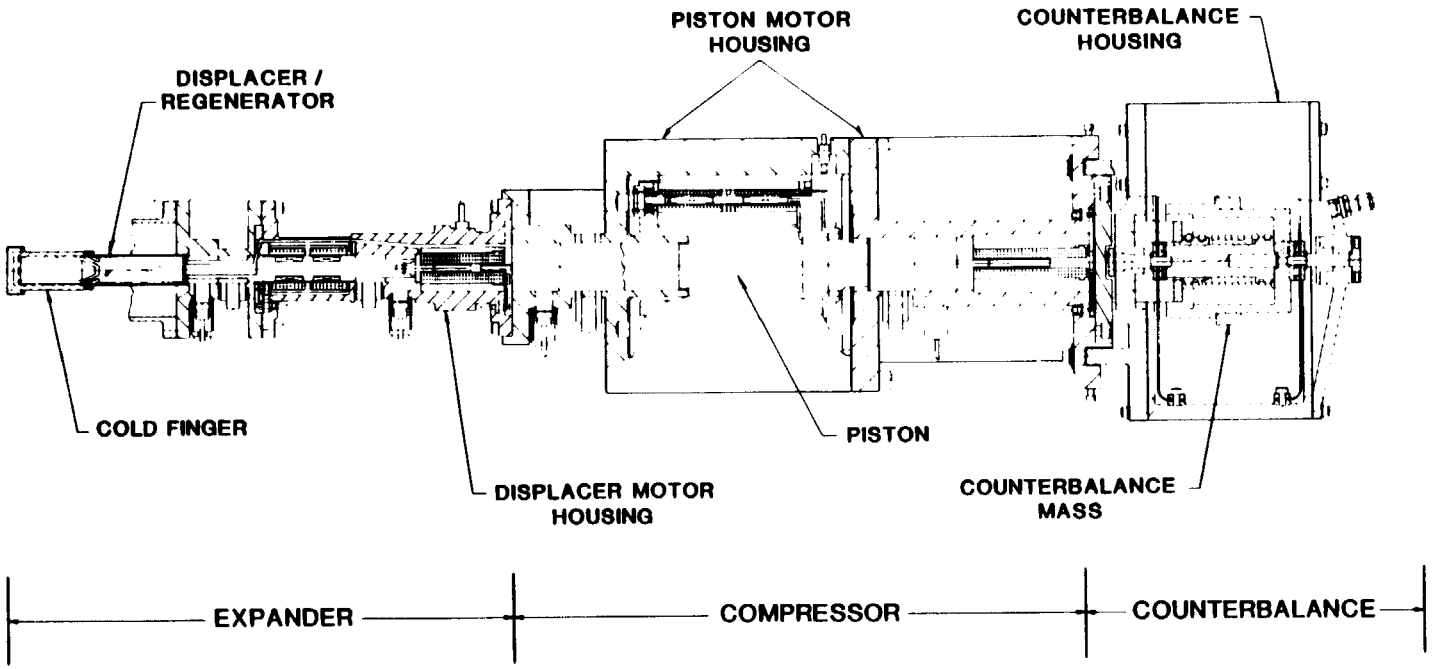

Figure 1. Cross-sectional view of refrigerator.

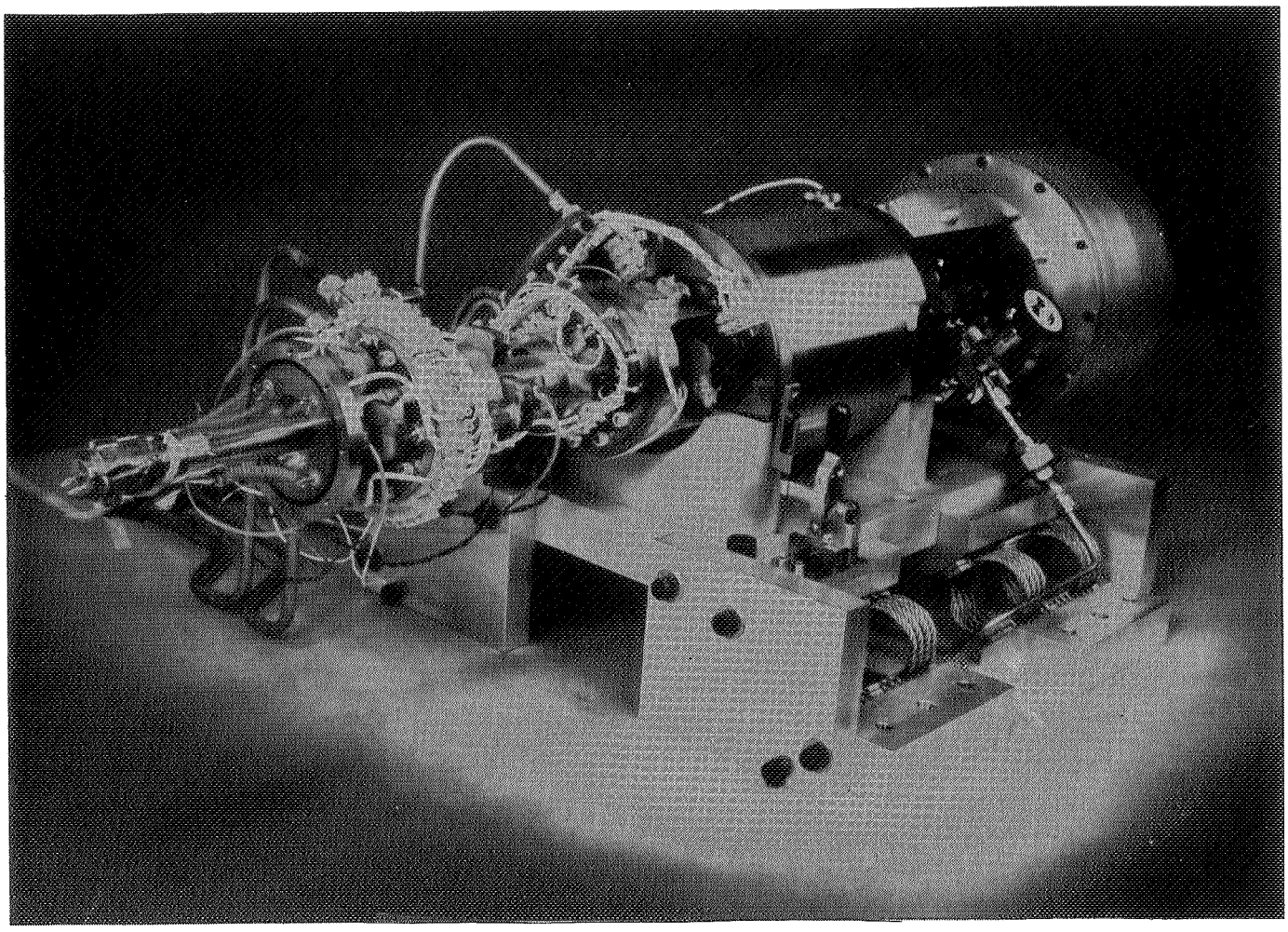

Figure 2. Cryogenic refrigerator.

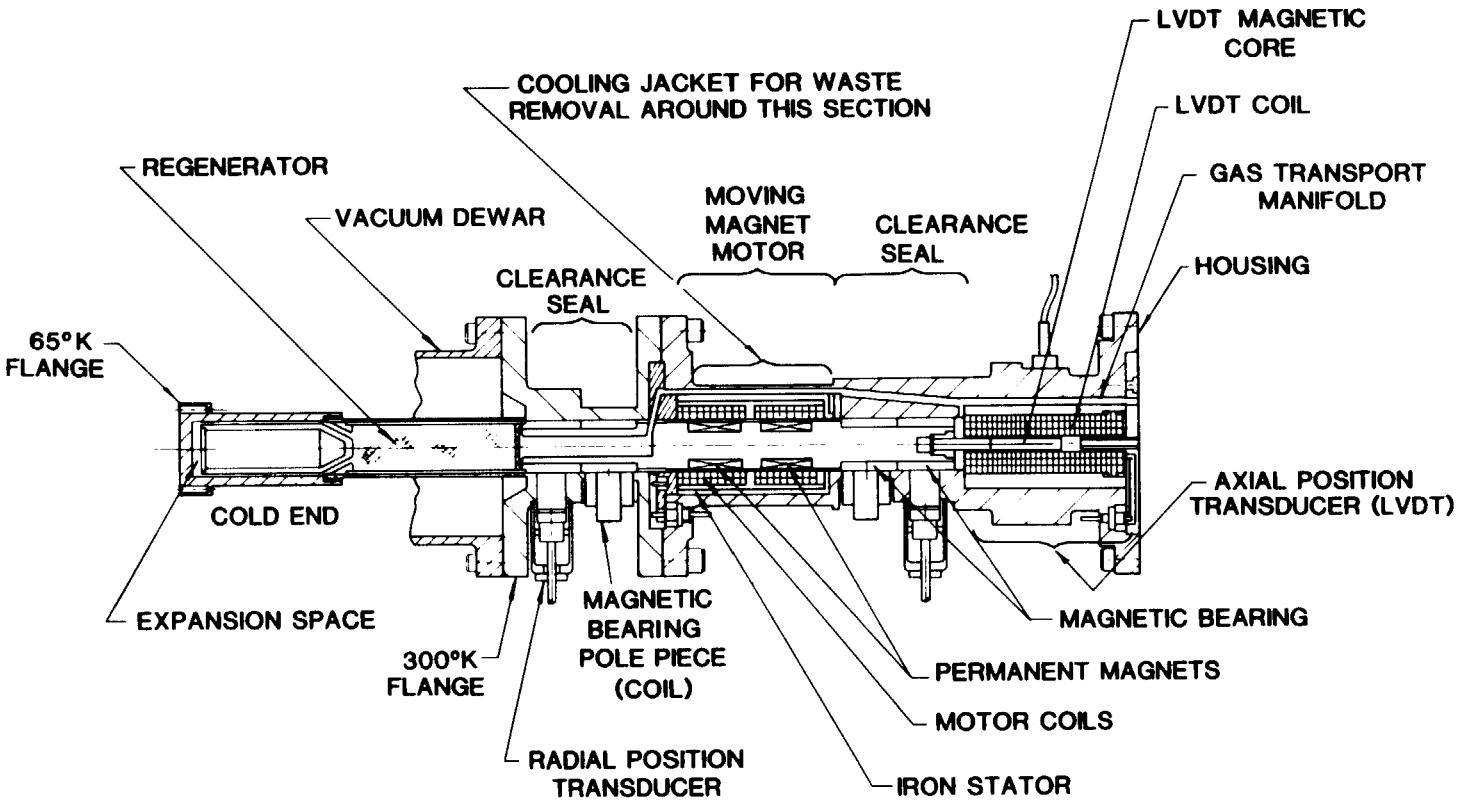

Figure 3. Displacer subassembly.

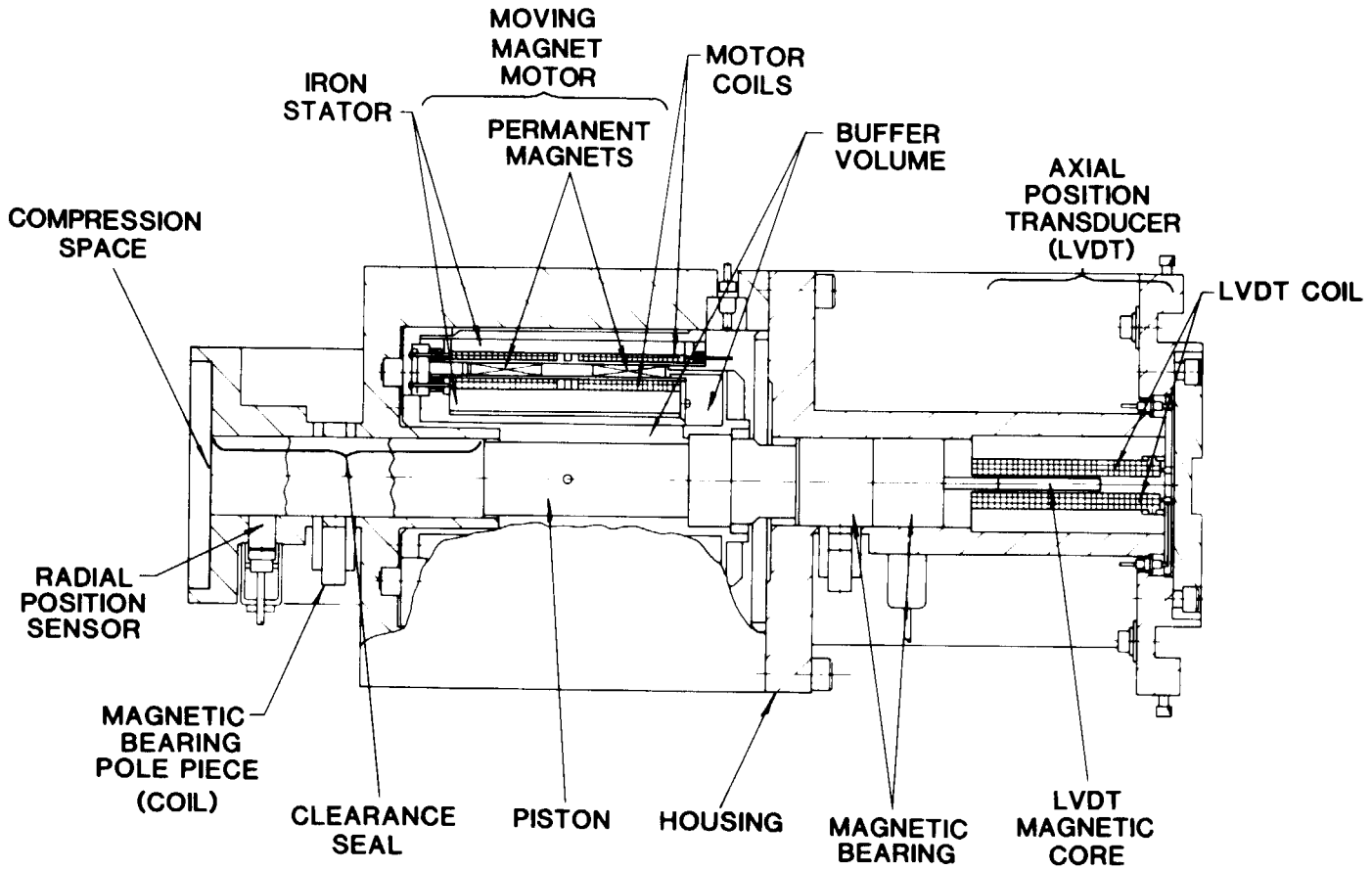

Figure 4. Piston subassemnly.

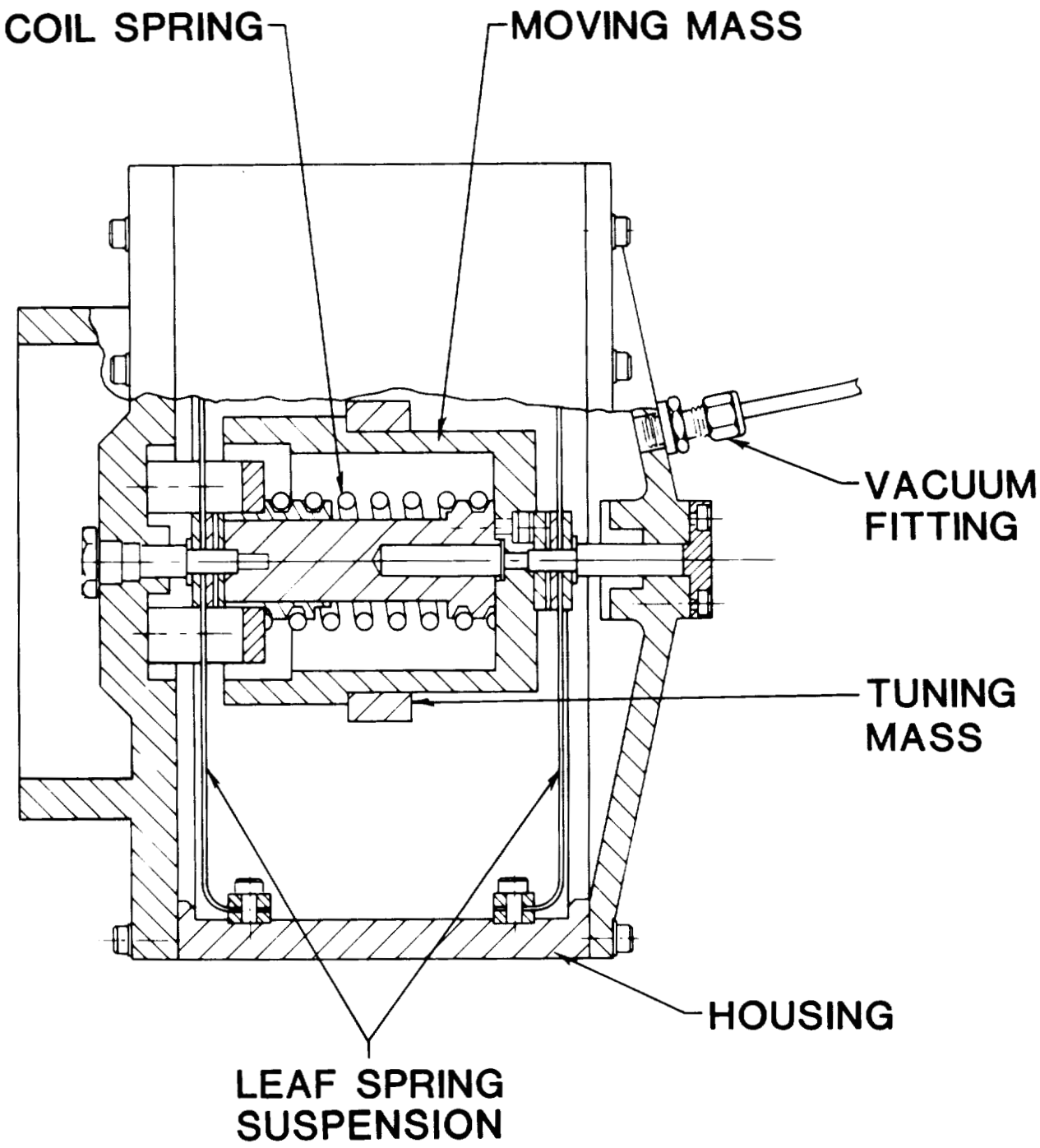

Figure 5. Countermass subassembly.

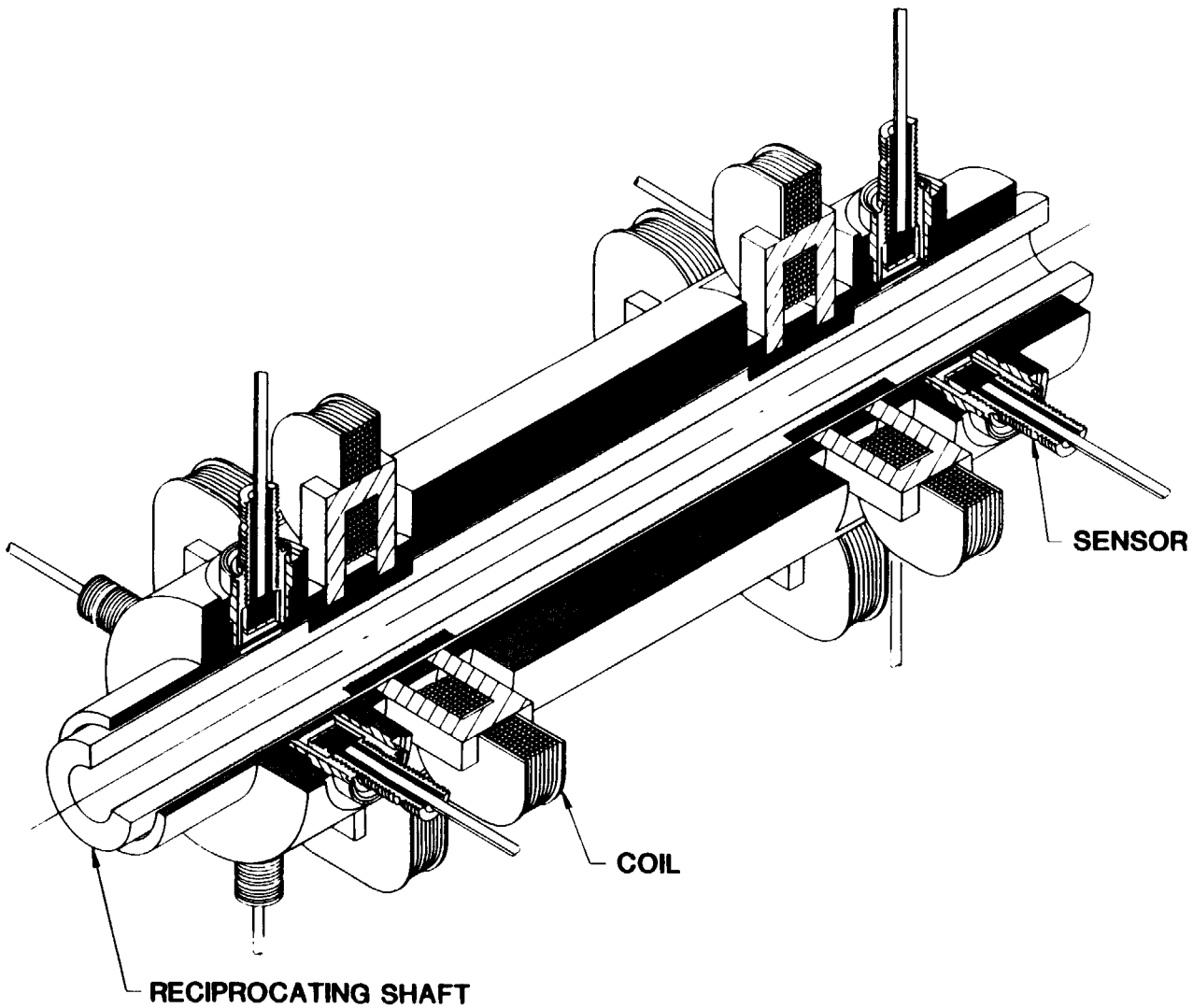

Figure 6. Schematic of magnetic bearing.

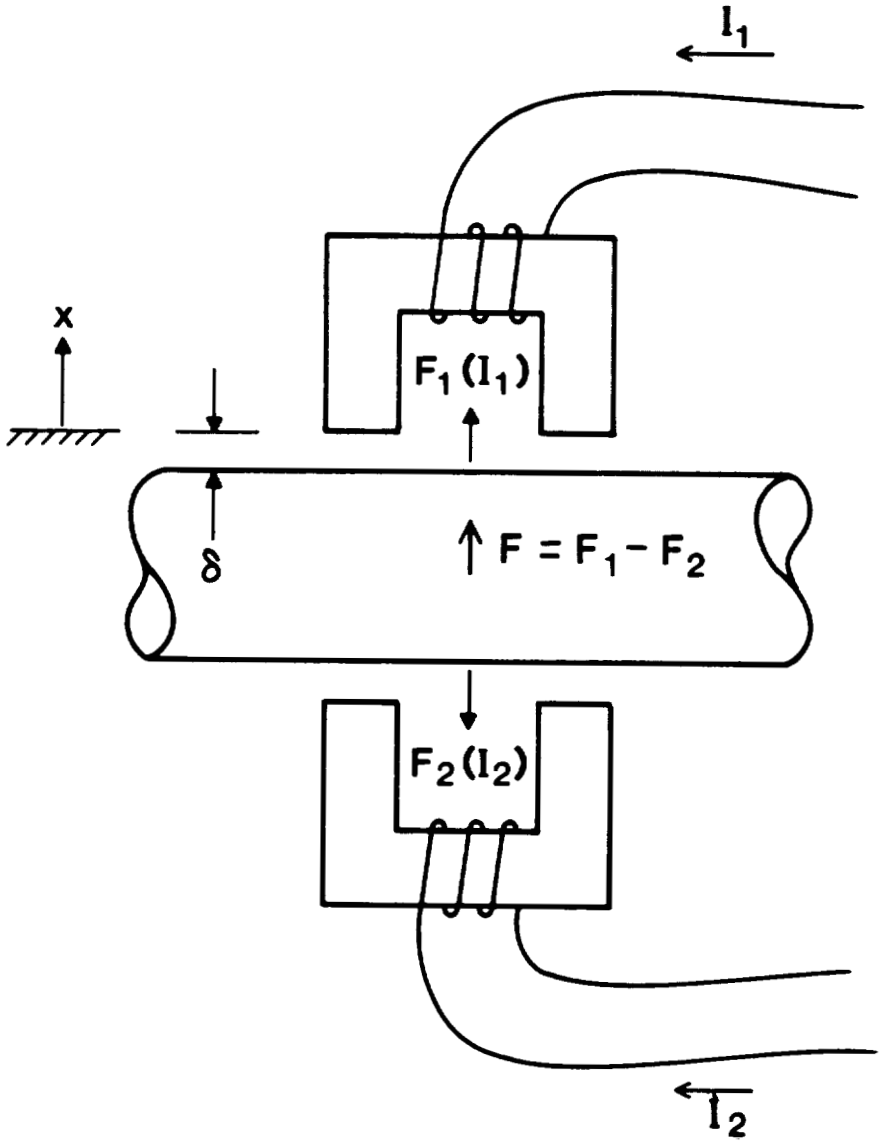

Figure 7. Radial force generation in magnetic bearing plane.

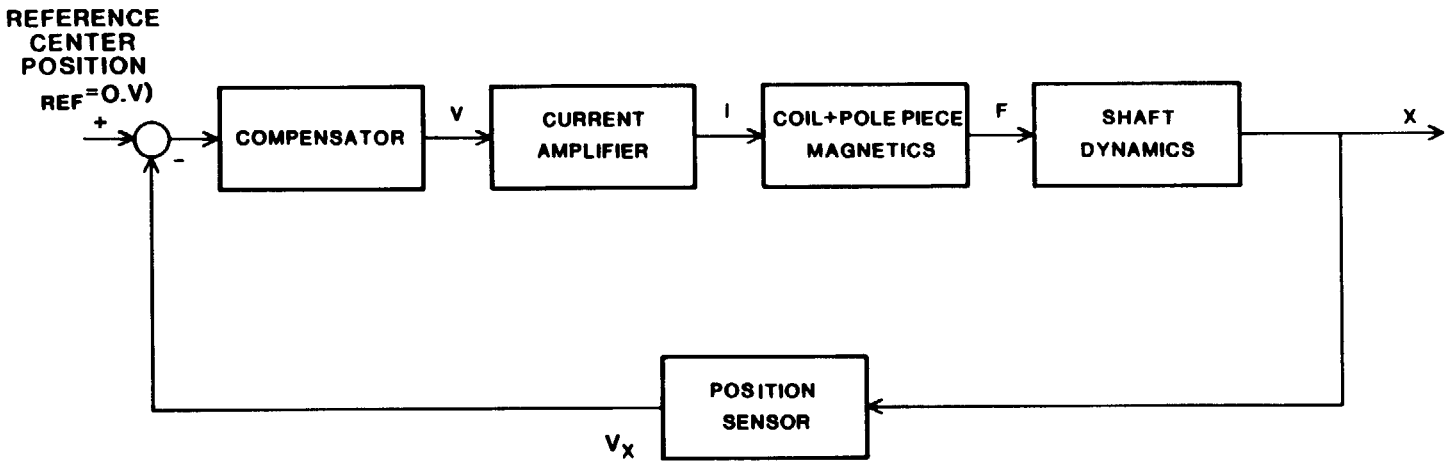

Figure 8. Bearing control sysytem block diagram.

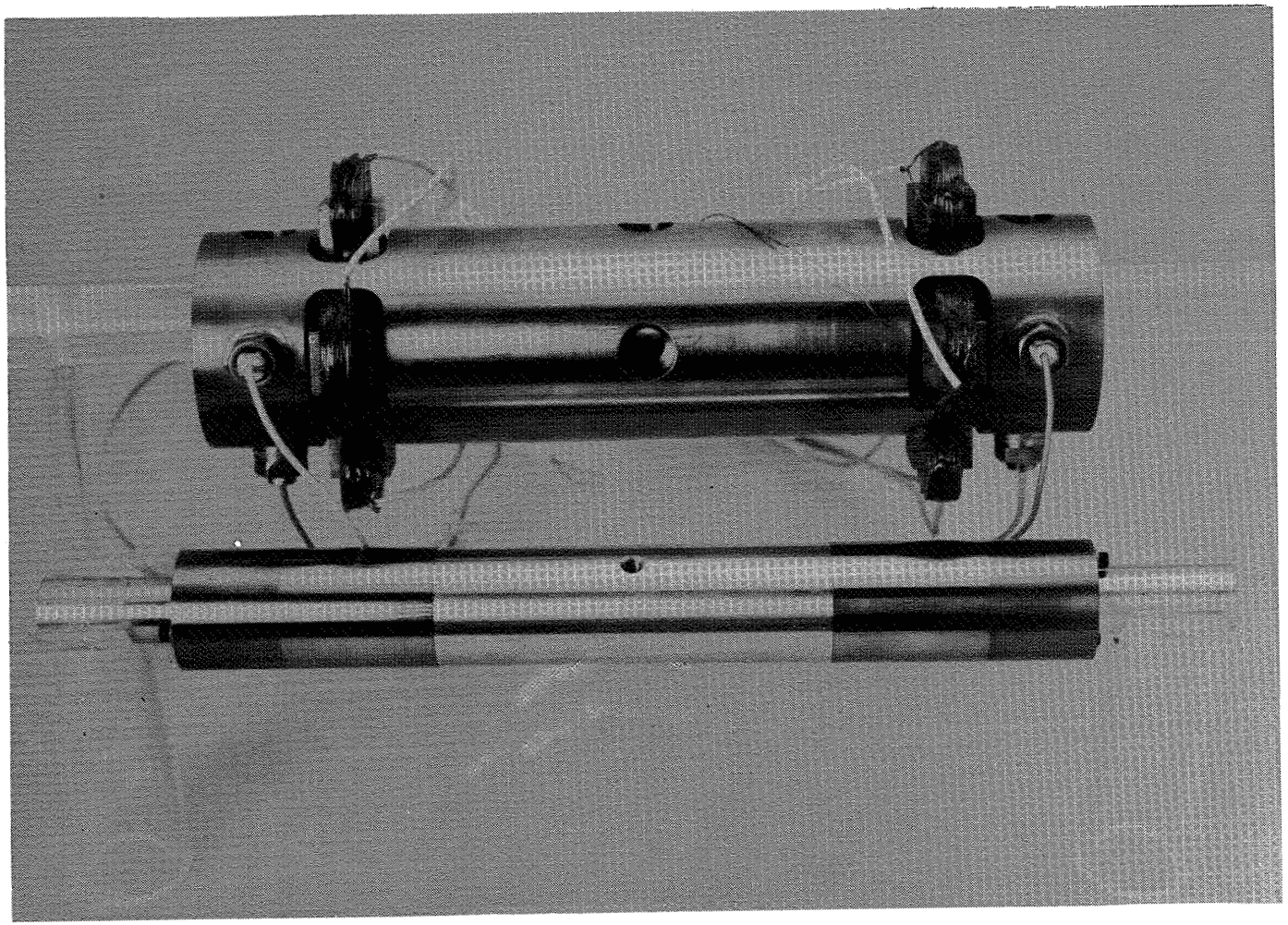

Figure 9a. Test fixture.

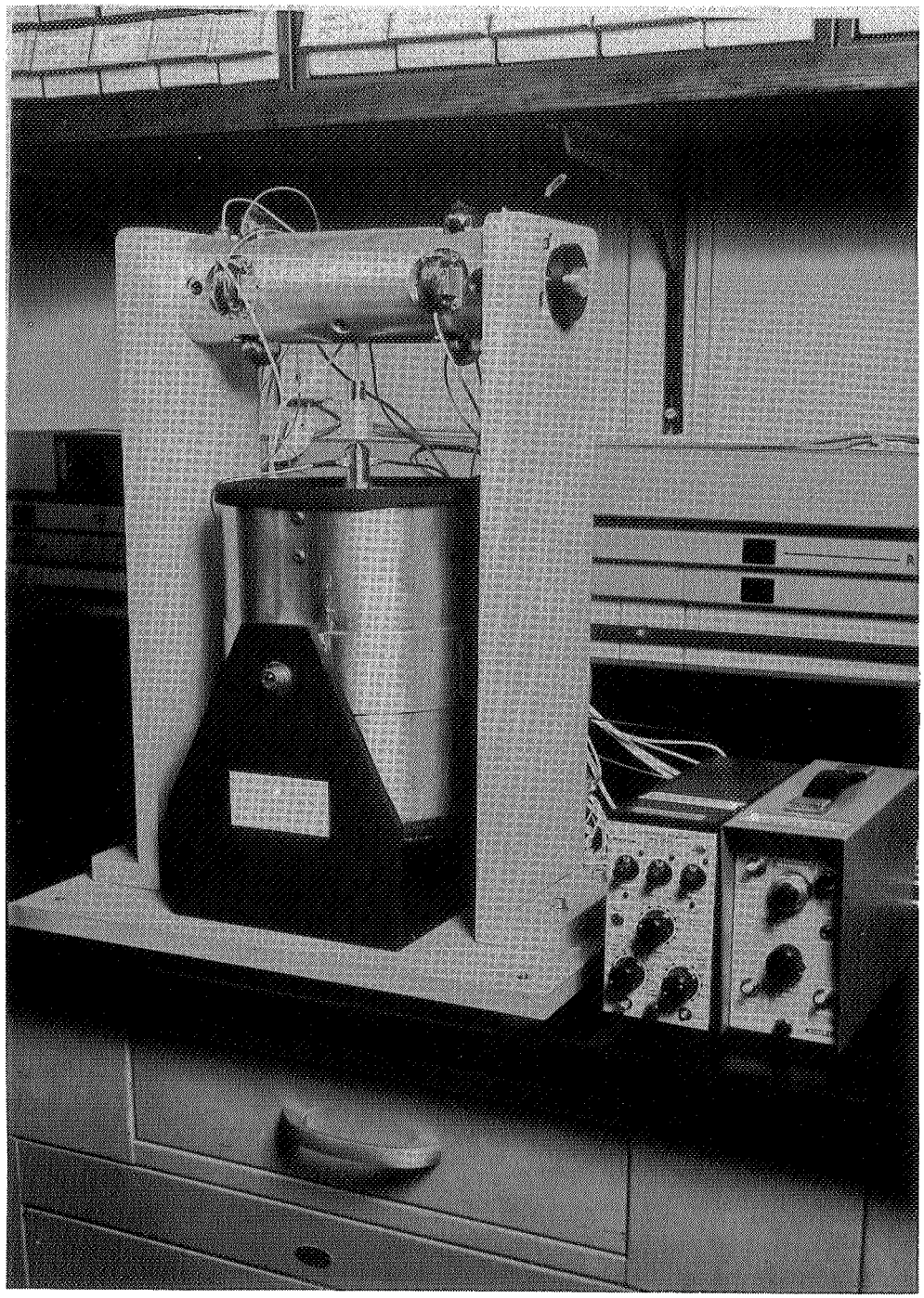

Figure 9b. Fixture on test stand.

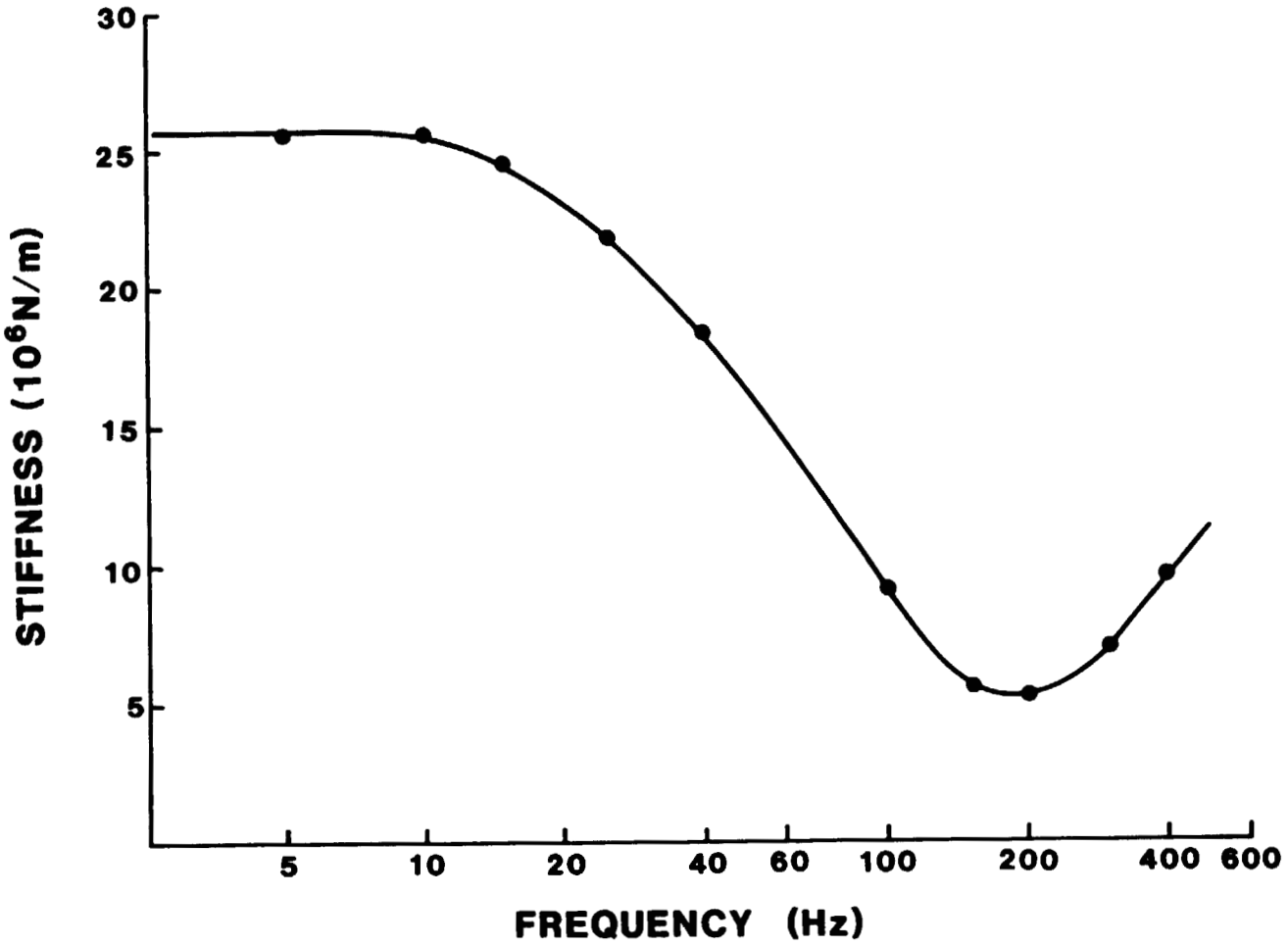

Figure 10. Magnetic bearing ac "stiffness".

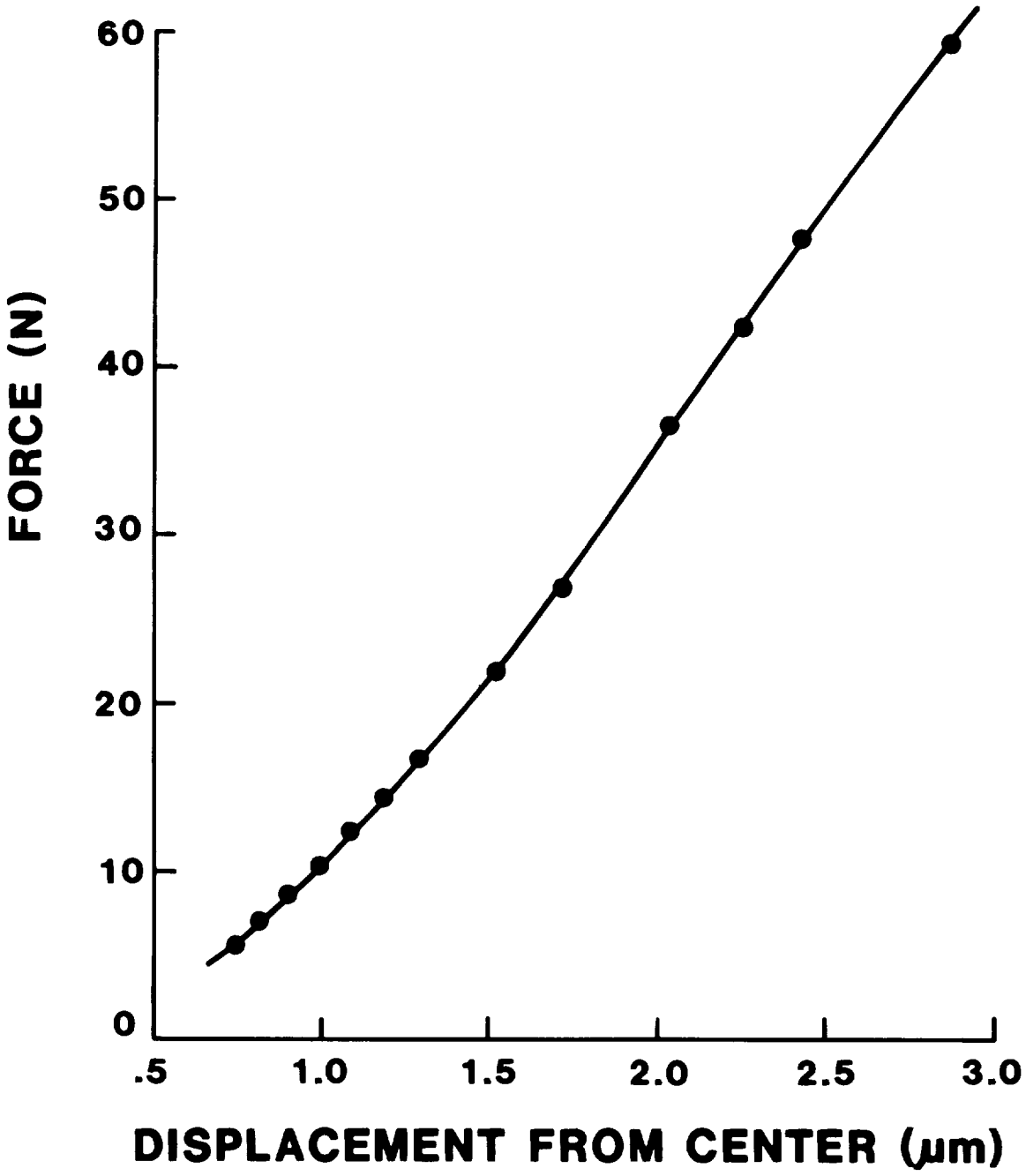

Figure 11. Magnetic bearing static load characteristics.

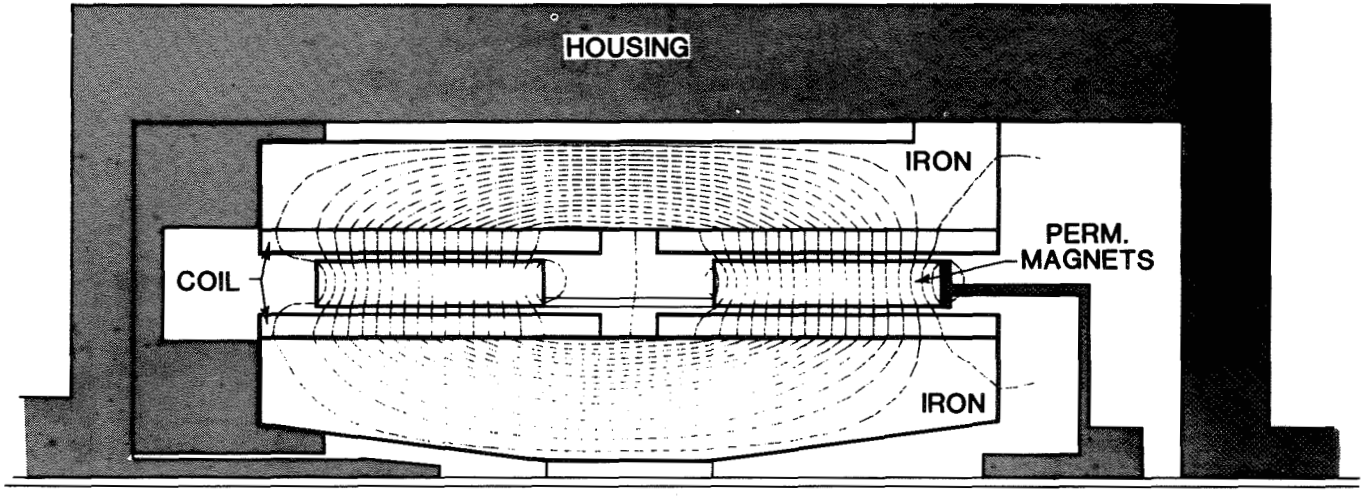

Figure 12. Schematic of linear motor for piston, showing lines of magnetic flux (armature in centered position).

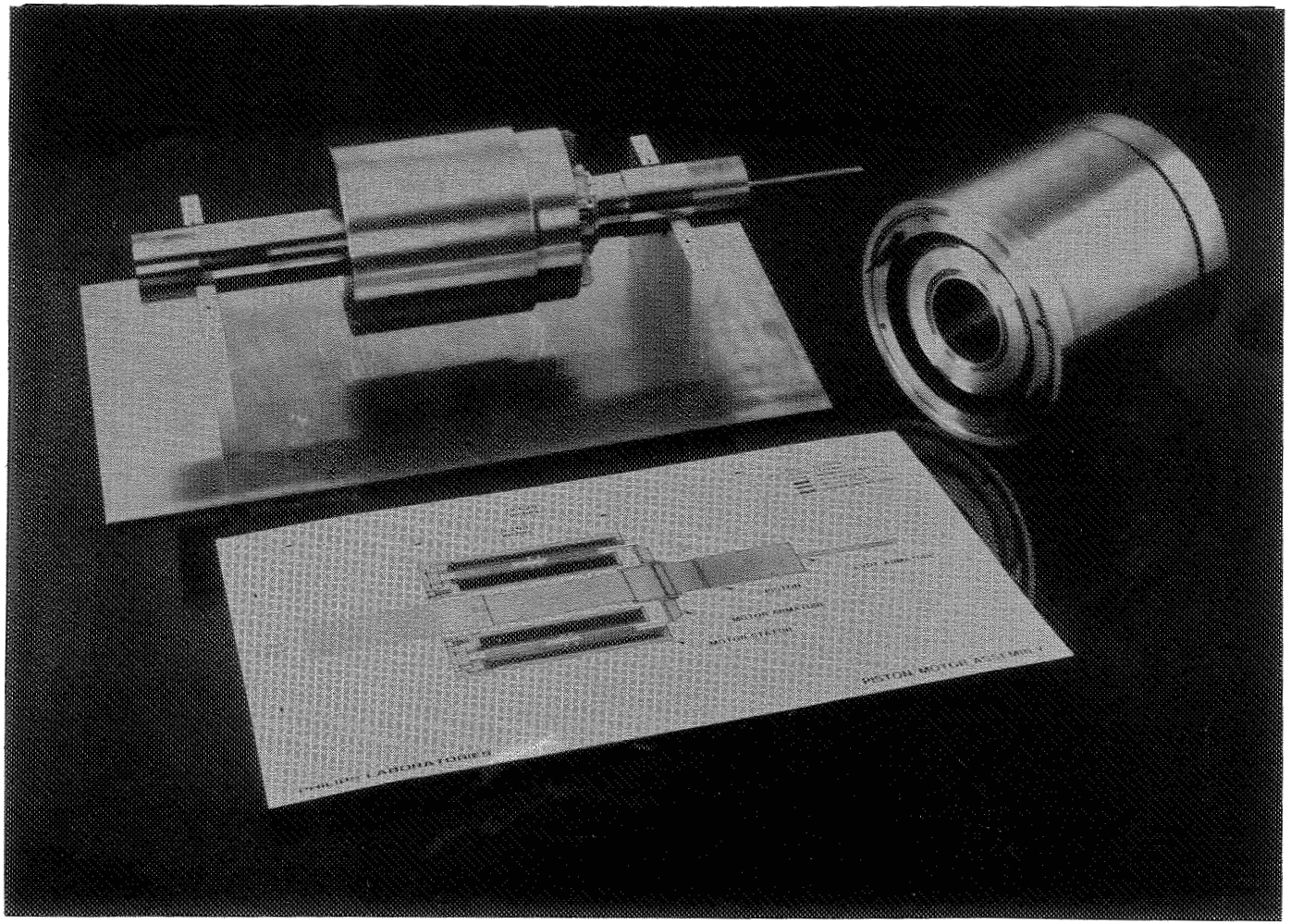

Figure 13. Completed piston armature on piston shaft, shown with stator assembly.

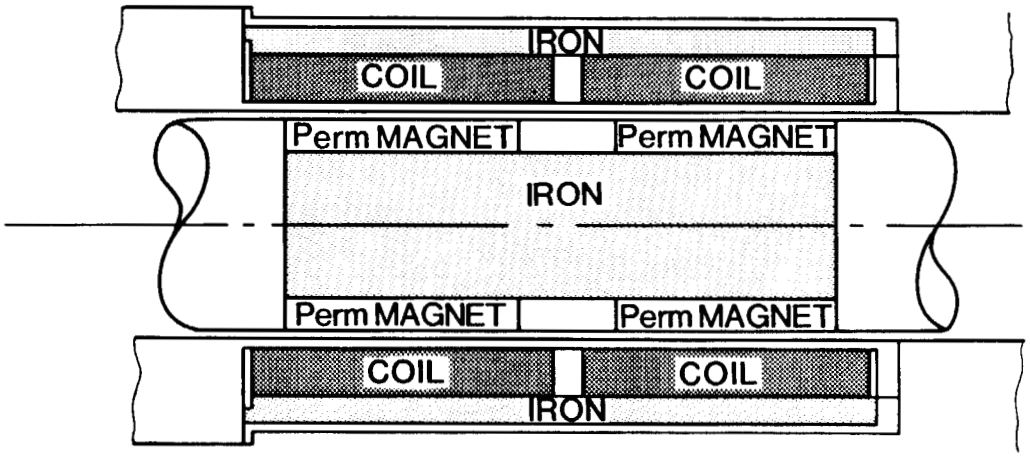

Figure 14. Schematic of linear motor for displacer.

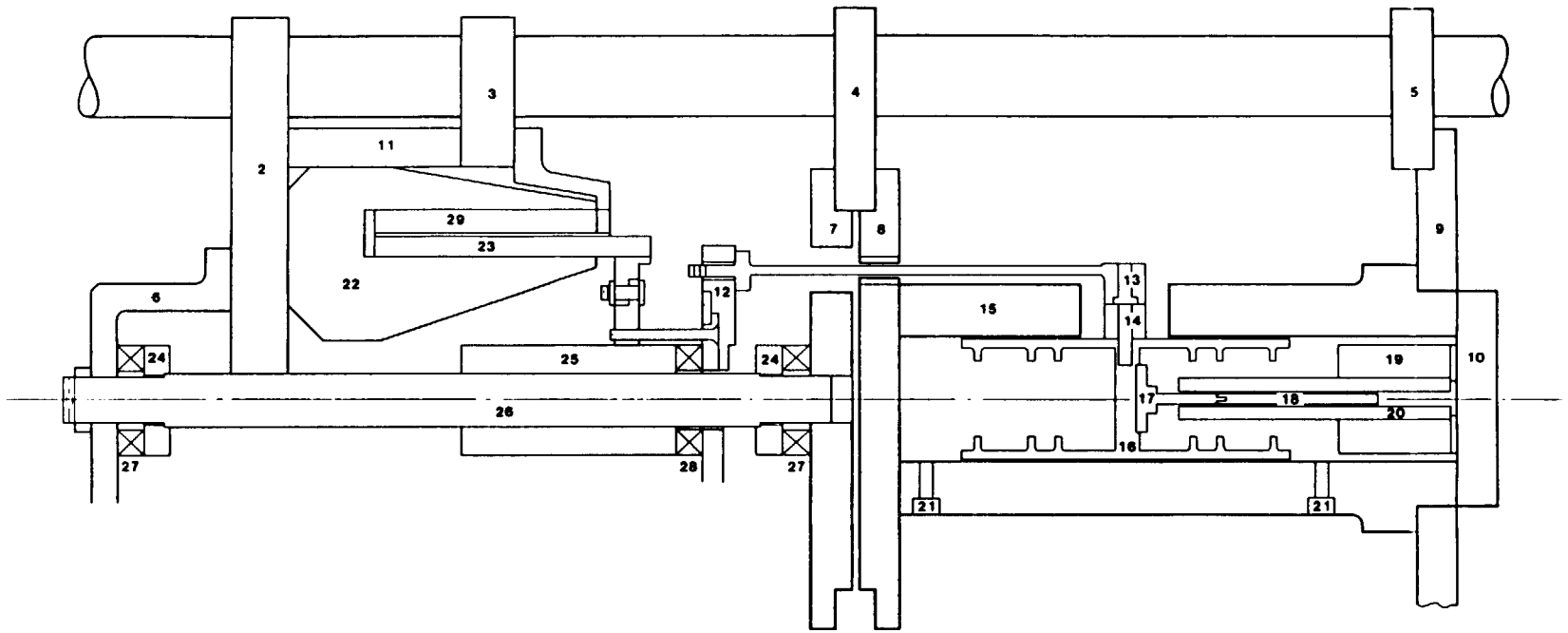

1) ALIGNMENT RODS (3)
2) MOUNTING PLATE
3) MOUNTING PLATE
4) MOUNTING PLATE, GAS SPRING
5) MOUNTING PLATE, GAS SPRING
6) MOUNTING PLATE
7) MOUNTING PLATE, GAS SPRING
8) MOUNTING PLATE, GAS SPRING
9) MOUNTING PLATE, GAS SPRING
10) END CAP
11) STATOR MOUNTING RING
12) SLIP RING LINKAGE
13) RODS (3)
14) ROD BUSHINGS (3)
15) GAS SPRING CYLINDER
16) PISTON
17) LVDT CORE SUPPORT
18) LVDT CORE
19) LVDT BODY HOLDER
20) LVDT BODY
21) PORTS (6)
22) STATOR
23) ARMATURE
24) F.T. CONNECTOR
25) BEARING
26) SHAFT
27) X-Y FORCE TRANSDUCER (2)
28) TORQUE-COMPRESSION F.T.
29) MAGNET ASSEMBLY

Figure 15. Schematic of piston-motor test fixture.

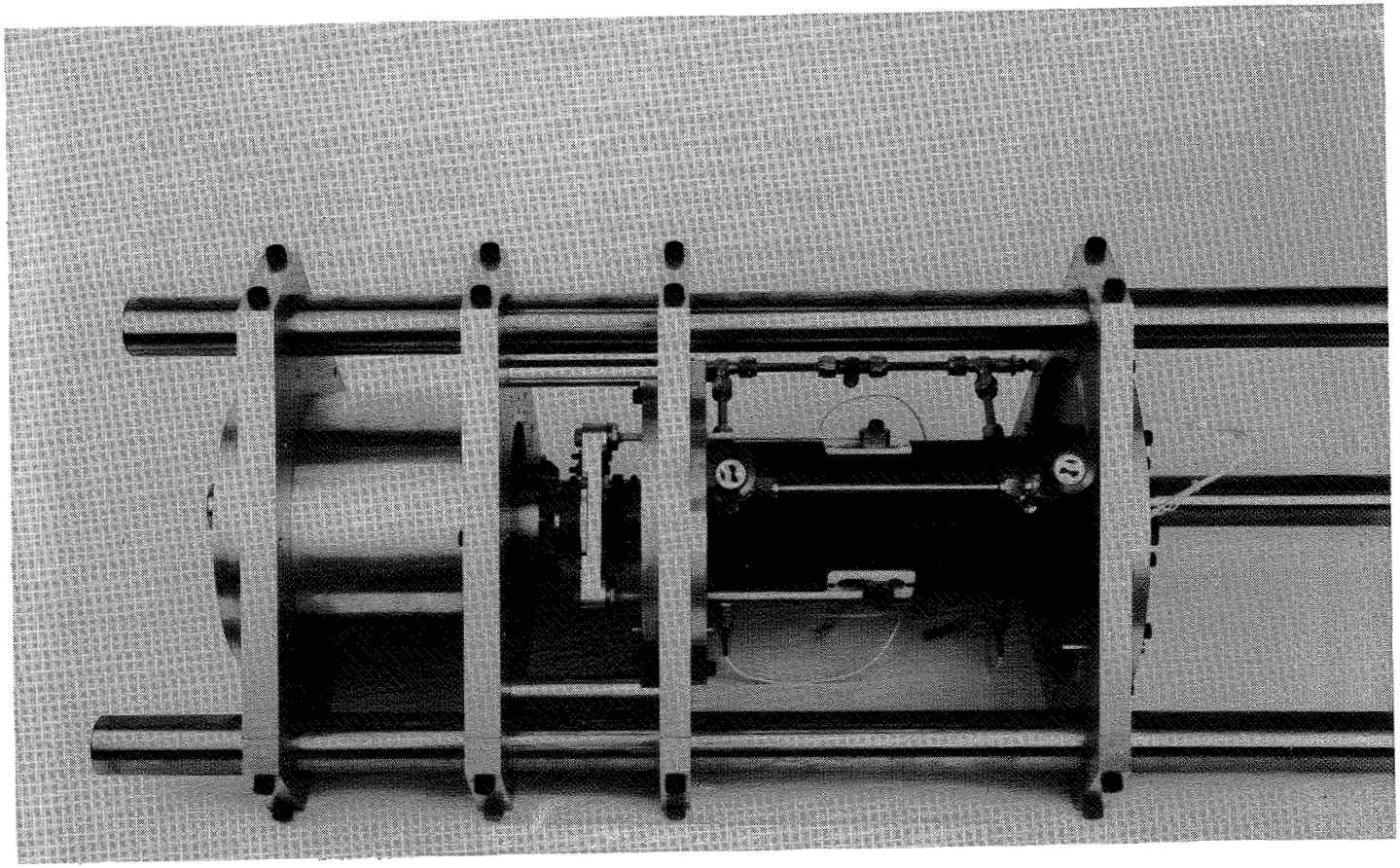

Figure 16. Piston-motor test fixture.

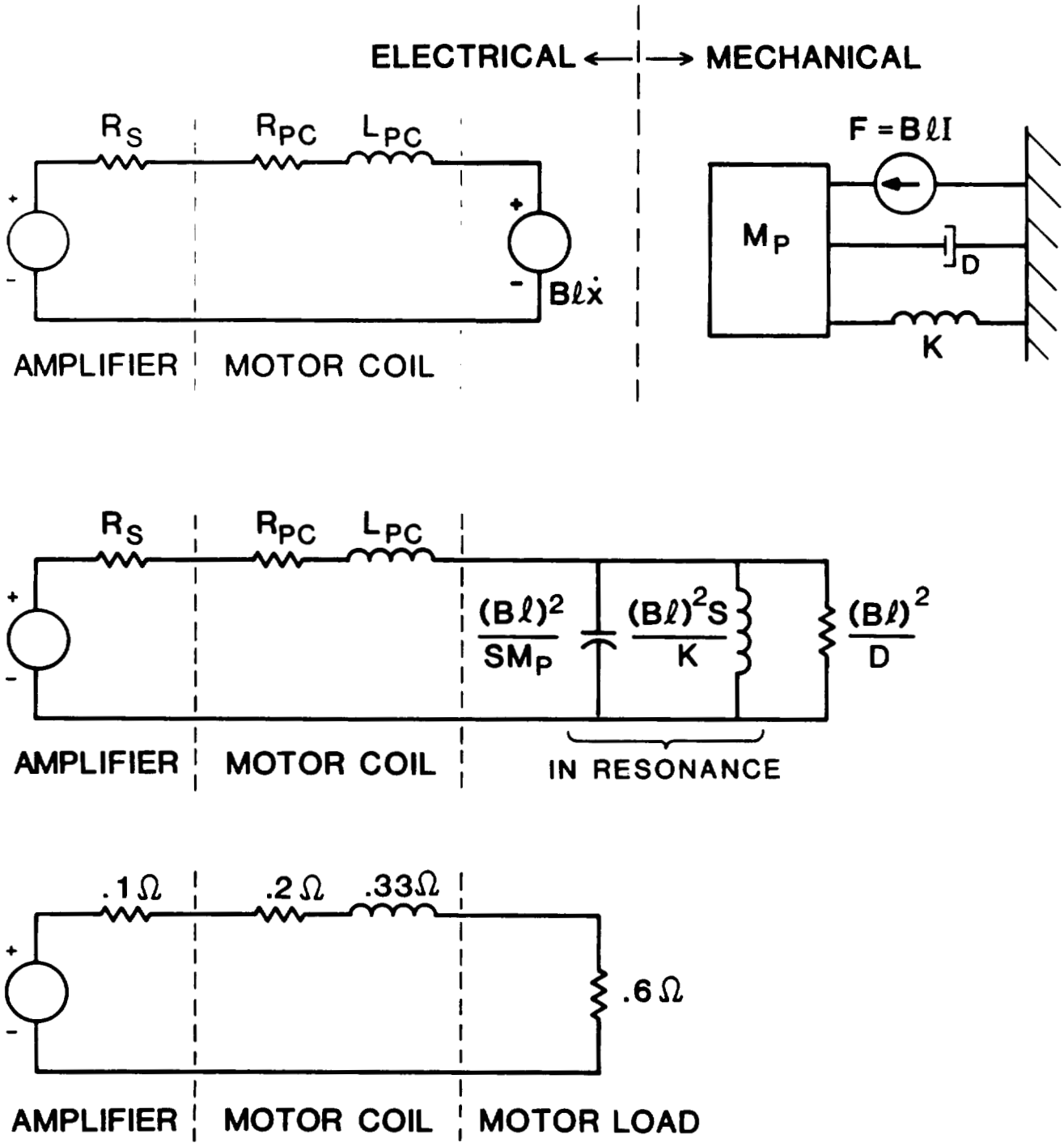

Figure 17. Derivation of effective piston system impedance.

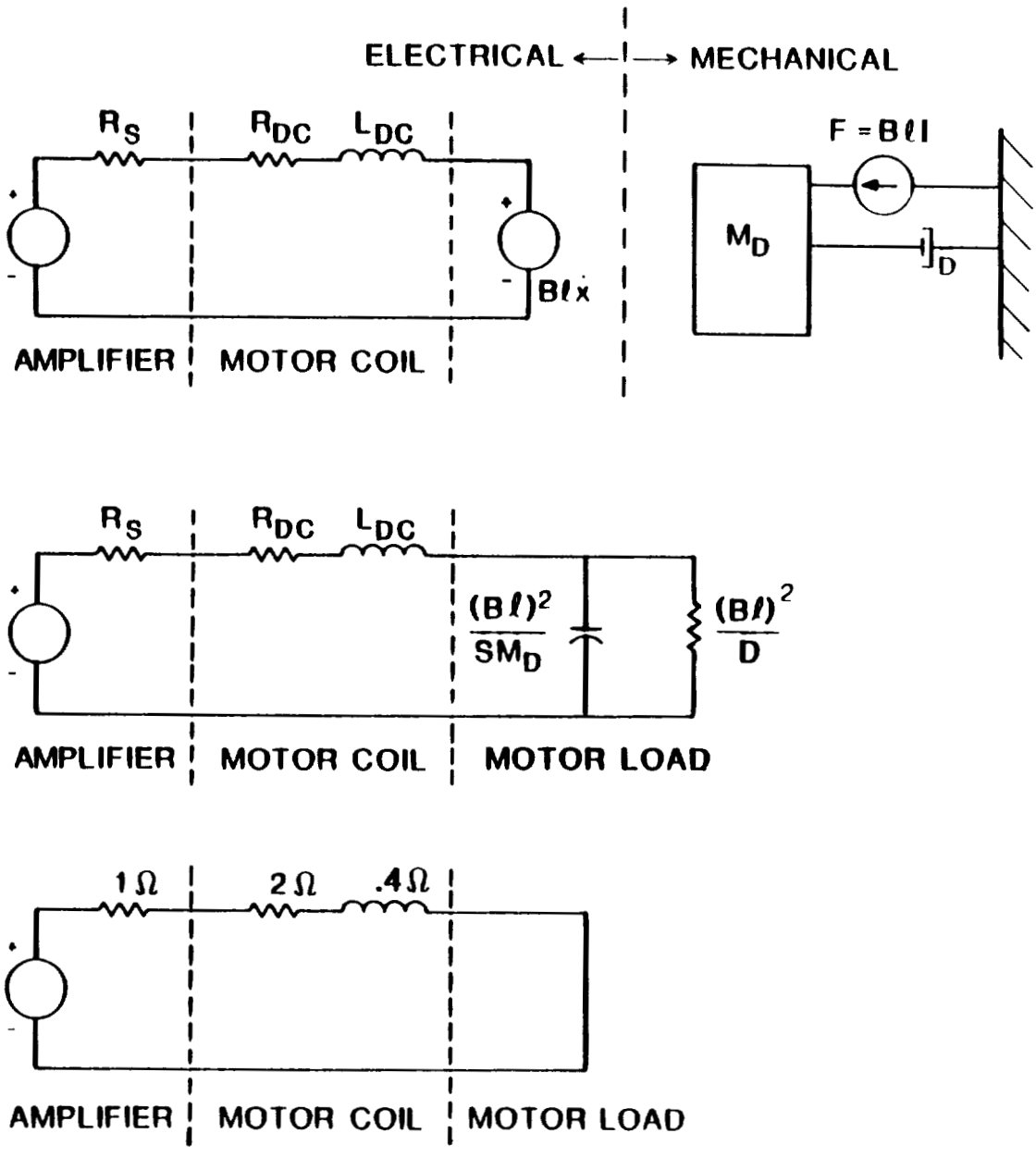

Figure 18. Derivation of effective displacer system impedance.

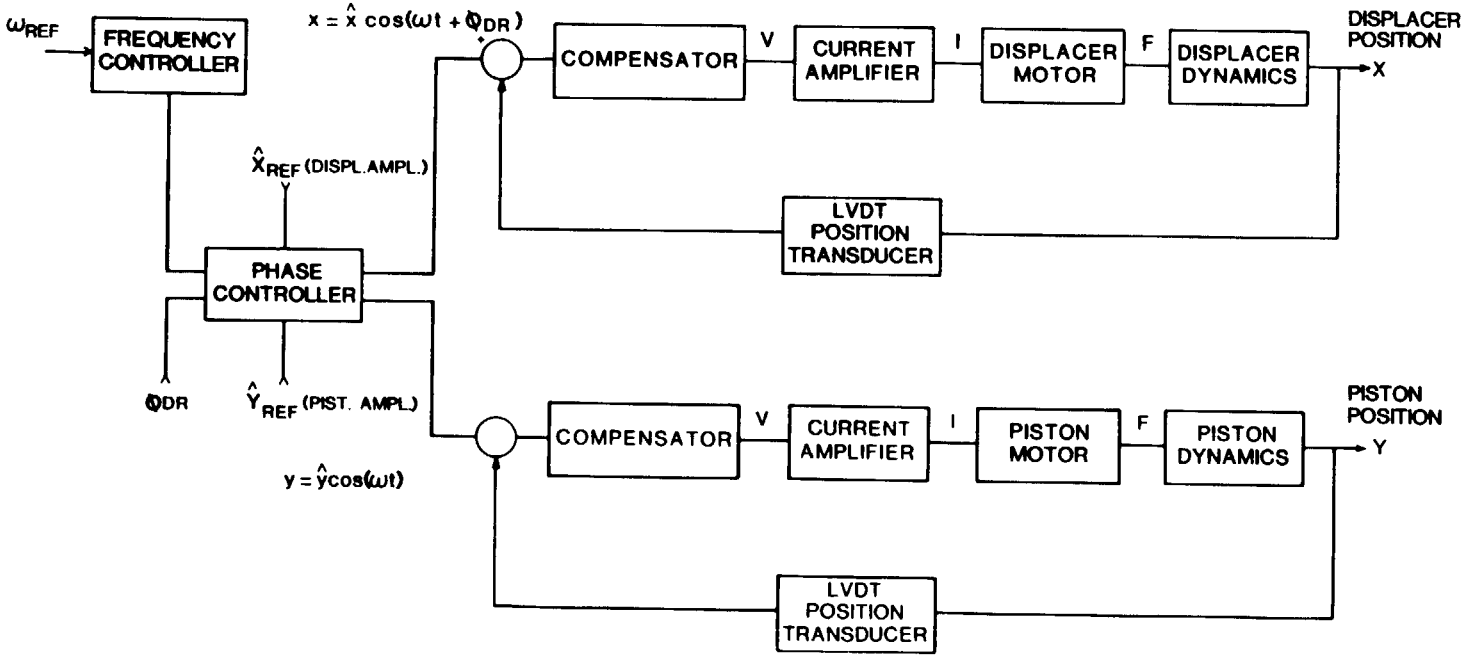

Figure 19. Piston and displacer axial control loops.

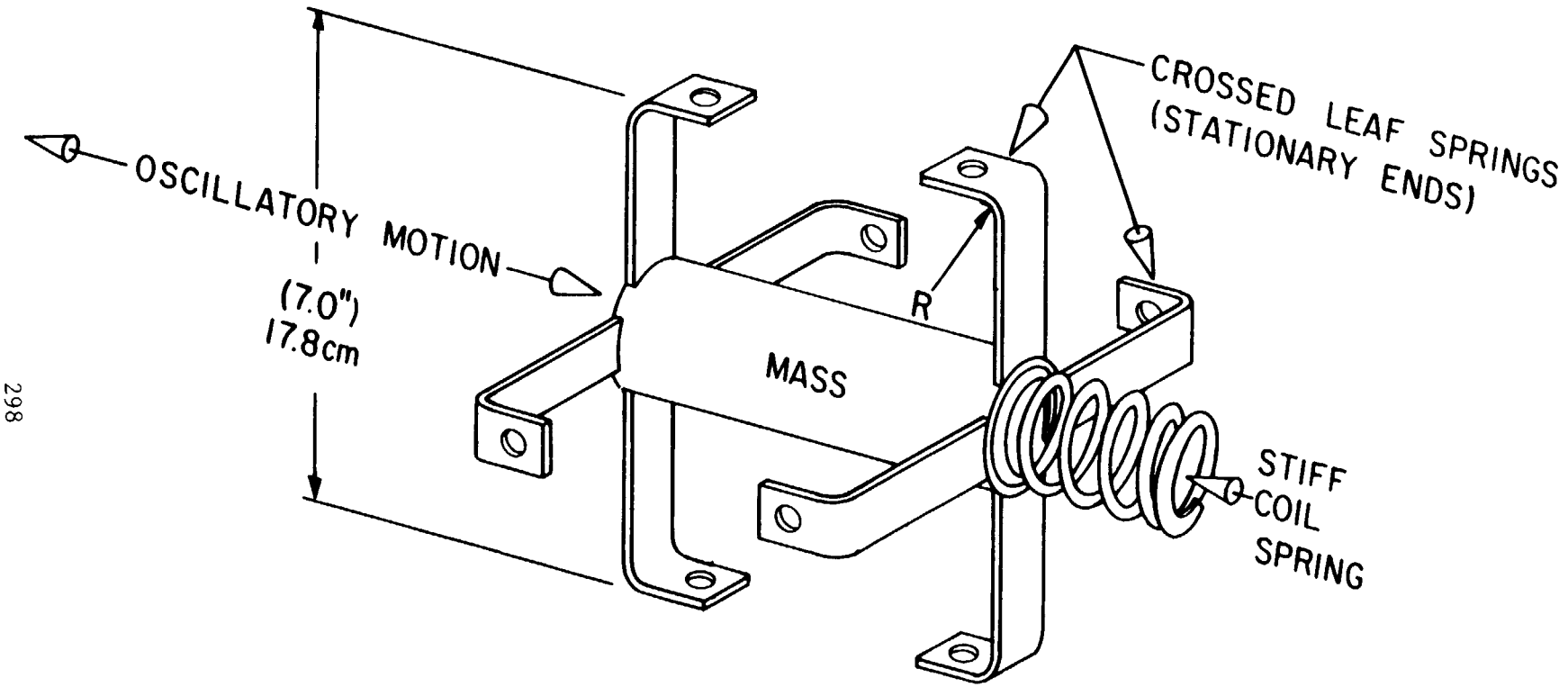

Figure 20. Schematic of vibration absorber.

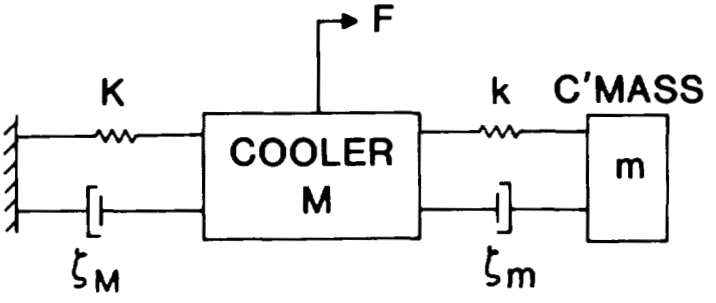

M = mass of refrigerator

K = spring constant of refrigerator mount

ζ_M = damping factor of refrigerator mount

m = mass of countermass

k = spring constant of countermass coil spring

ζ_m = damping factor of countermass coil spring

Figure 21. Vibration model of cooler/counterbalance system.

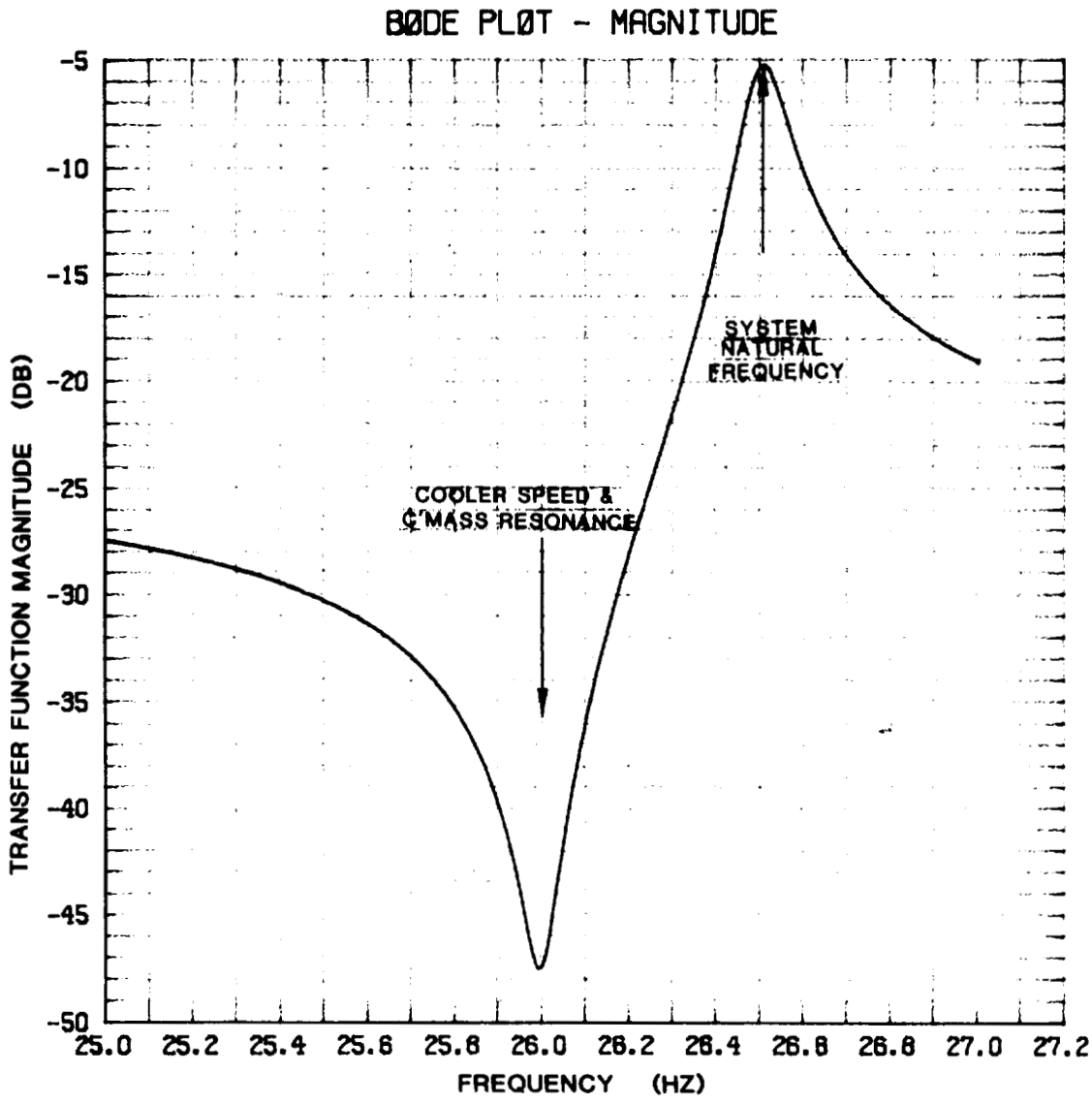

Figure 22. Calculated transmitted force imparted to refrigerator mount.

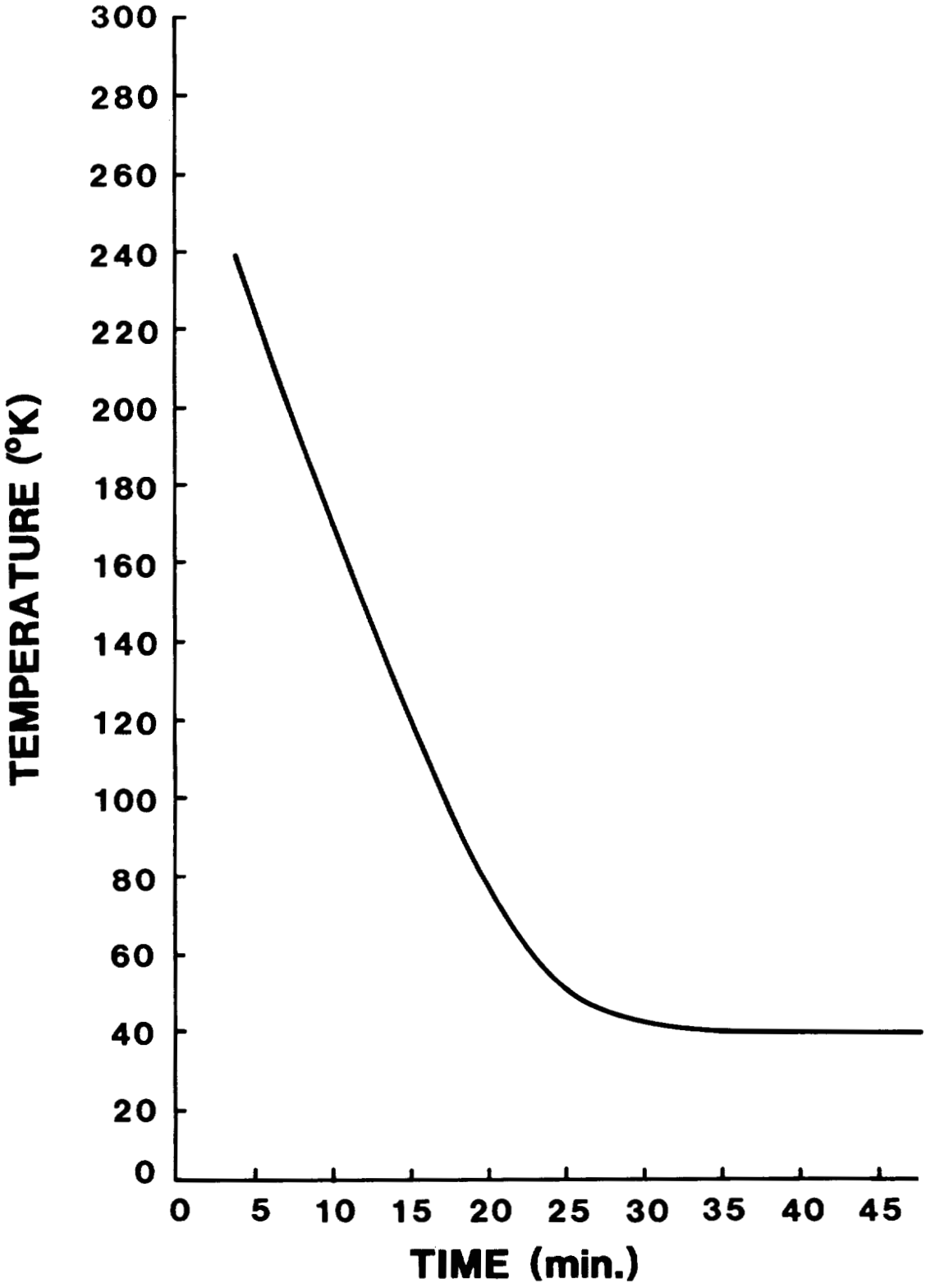

Figure 23. Cooldown time (temperature vs. time).

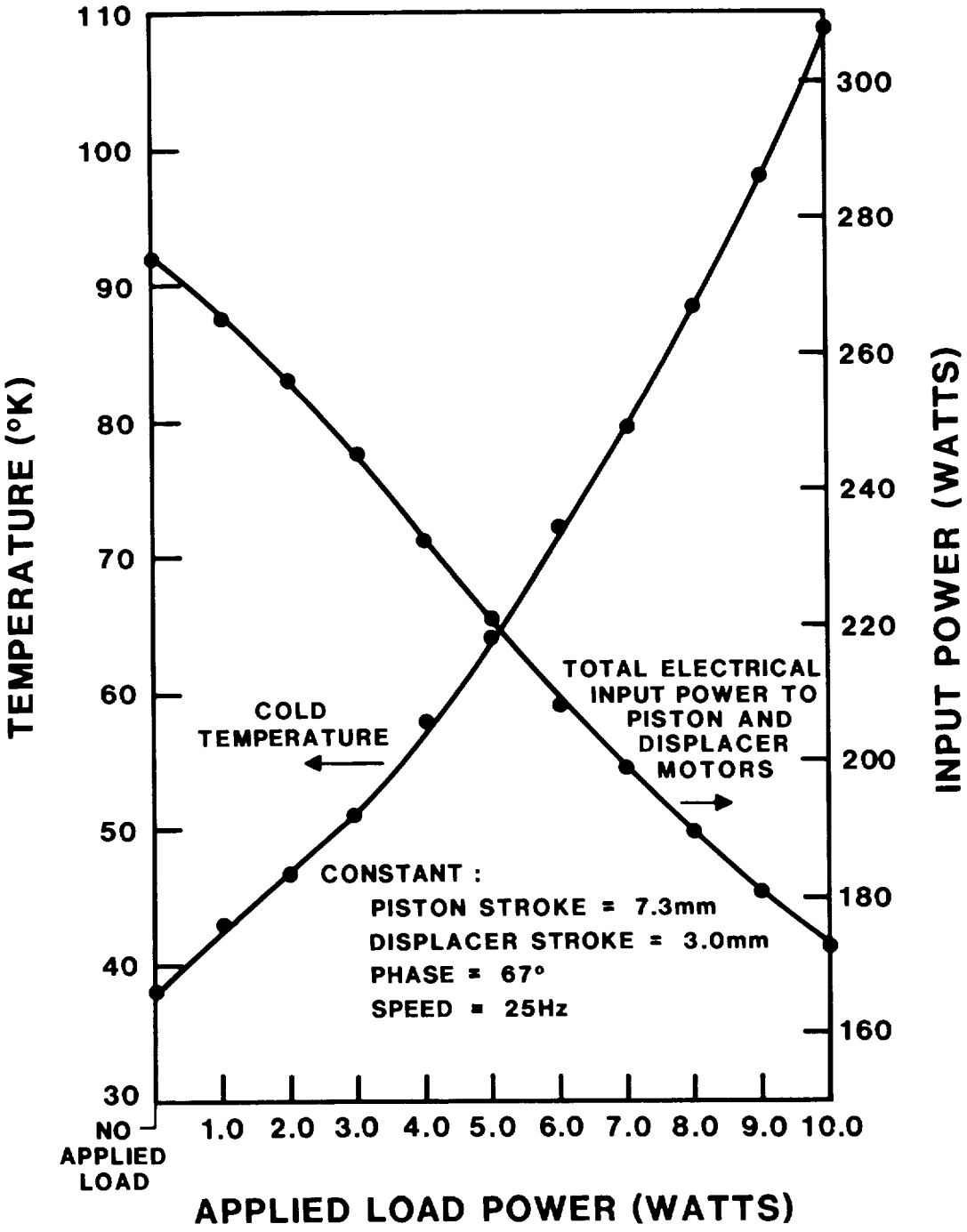

Figure 24. Load map.

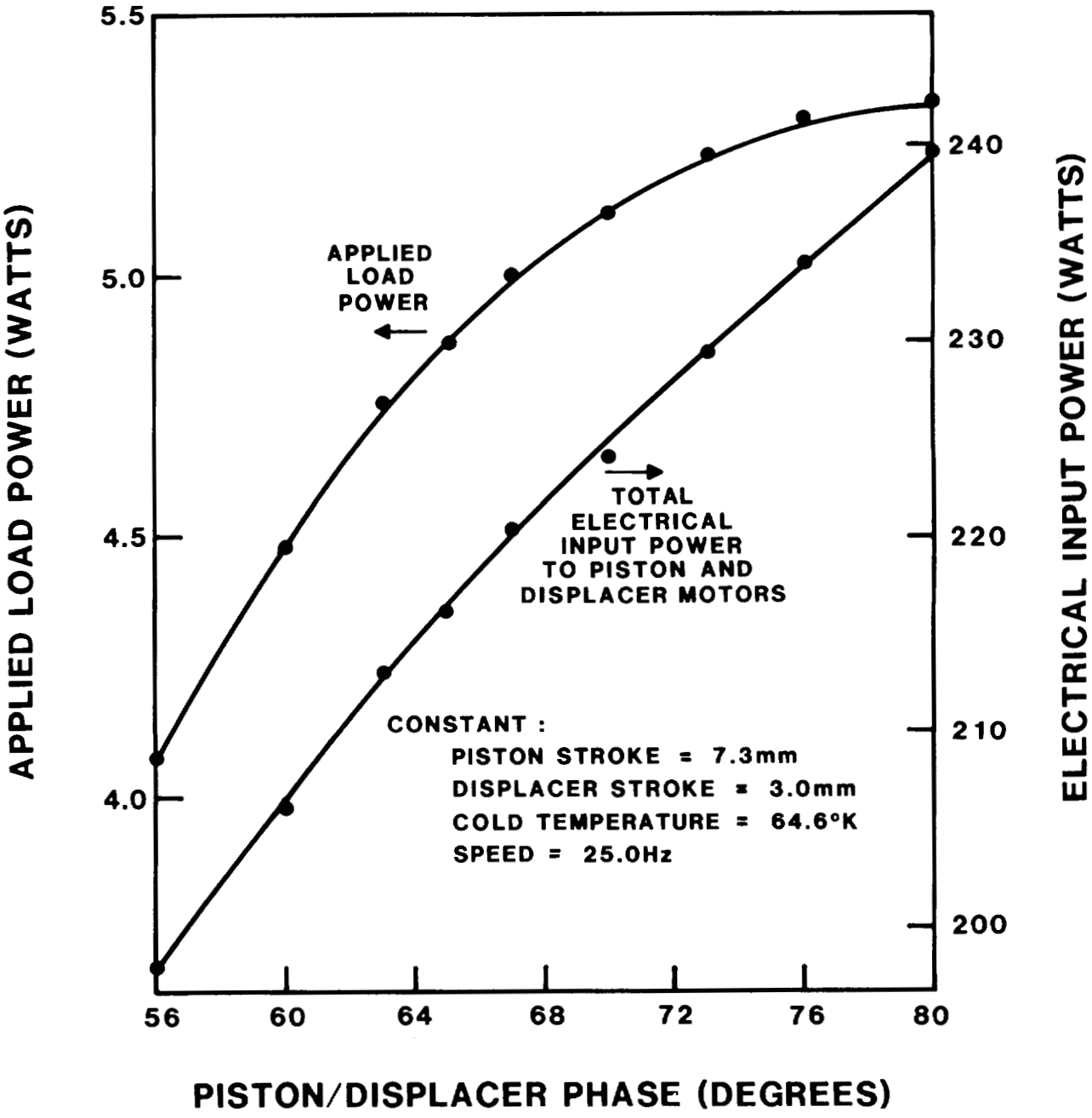

Figure 25. Parametric sensitivity piston/displacer phase.

GIFFORD-MCMAHON REFRIGERATOR WITH SPLIT COLD HEAD

H.-J. Forth, R. Heisig, H.-H. Klein
LEYBOLD-HERAEUS GMBH, Cologne, FRG

1. Introduction

The reason for the development of a split cold head has been the following problem:

In a vacuum vessel that consists of two separable hemispherical bowls a hydrocarbon-free vacuum of about 1.10^{-7} mbar (1.10^{-5} Pa) has to be produced. Due to the desorption rate of components situated inside the vessel an effective volume rate of flow of 10.000 ltr/s for H_2O, 500 ltr/s for N_2 and 1.000 ltr/s for H_2 is required for producing that pressure. The vacuum vessel is situated inside a magnet with a maximum magnetic flux density of c. 4 T. Access to the vessel is rather narrow and restricted. To each of the two cups a straight pipe of 5 m length and an inside diameter of c. 62 mm is fitted, but only one pipe is available for evacuation of the vessel. Because of its low flow conductance this tube cannot be used as a high vacuum line but only as a fore vacuum line. Consequently the high vacuum pump - whatever type this may be - must be situated inside the vacumm vessel itself, as a sort of integrated pump. Various types of pumps have been taken into consideration: The getter pump with water- or LN_2-cooled shield, the cryopump with LHe or refrigerator cooling. With respect to the relatively long operating periods of several weeks as required by the respective project all pumps that require LN_2 or LHe for their operation had to be ruled out. Discussion settled on a particular type of cryopump that is cooled by a two stage cold head of a Gifford-McMahon refrigerator.

2. Requirements on the cryocooler

In order to meet the requirements with respect to pressure and volume flow rates (and hence temperature) as given in section 1 the refrigerating capacity of the cryopump must be 10 W at 80 K (first stage) and 2 W at 20 K (second stage), and the ultimate temperature must be less than 14 K. The distance between compressor and expander (refrigerating part of the cold head) must be at least 5,5 metre,the strong magnetic field of 4 T must be taken into

consideration and no other electric and/or magnetic fields should be present. Other requirements are: small size, high reliability, long operation periods, low price etc. These requirements are similar to type of cryocoolers as used for cooling electronic devices.

Application to our special case implies:

- use of a split-cycle cryocooler
- small dimensions are required only for the expander assembly
- energy consumption is not particulary interesting
- low overall costs are important (investment, operating costs and maintenance)
- reliable operation with no maintenance for 8000 hours (1 year).

3. Checking the suitability of known devices

The following known devices which have separate expanders were investigated: the split Stirling cooler, the split Vuilleumier cryocooler and the Gifford-McMahon (GM) cryocooler.

a) The split Stirling cryocooler has a great advantage: it has no valves and only a single connecting line between compressor and expander. But this type of cooler reacts in his efficiency rather sensitive with respect to the length of the connecting line and the void volume. After Chellis (1) 5 feet long lines are possible, but lengths of 12 to 18 inches are practicable.

b) the split Vuilleumier cooler is virtually a Stirling cryocooler wherein the mechanical compressor component has been replaced by a thermal compressor. Thus the length of the connecting line is limited in analogy to that of the split Stirling cryocooler.

c) The Gifford-McMahon cryocooler has a widely separated compressor assembly and expander assembly (also called compressor unit and cold head). Two connecting lines join them. The cold head comprises a small motor to operate the valves and in some types the same motor moves also the displacer; other types have a gas drive.

The compressor unit may be seen as a gas source with nearly constant pressure levels. The valves isolate compressor unit and cold head from one another and allow that the connecting lines can be of almost any length. Their volumes are part of the gas reservoir of the compressor unit.

In conclusion: The split Stirling and split Vuilleumier cryocoolers had to be dischardedbecause of the long distance required between compressor and expander, the GM-cryocooler in its normal version because of the motor for the valve control. However, modification of the GM-cryocooler appeared to be feasible.

4. Ways of solving the problem

In view of the required operation of the cooling device within the strong magnetic field the usual valve control by means of a small electric motor had to be abandoned or moved outside the inaccessible zone or integrated in the compressor unit. The displacer movement has to be effected by means of a pneumatic drive.

As any type self-regulating operation is not available - in spite of several well known patent applications - and as - generally speaking - such self-regulation appears to be rather sensitive with respect to gas supply, gas consumption and friction of the sealing elements, we have deceided to displace valve control device and to split the cold head into expander and valve control device.

4.1 Solution

Fig. 1 shows diagrammatically various arrangements of the GM-cryocooler

Fig. 1a - normal GM-cryocooler

Fig. 1b - GM cryocooler with splitted cold head, with the valve control part outside the inaccessible zone

Fig. 1c - as Fig. 1b, but with the valve control part integrated in the compressor unit.

Based on the required refrigerating capacity - see section 2 - the standard LH Cryorefrigerator R 210 was used; this refrigerator has the cold head RG 210 with refrigerating capacity of 12 W/80 K and 2 W/20 K for the first and second stage respectively; the compressor unit type RW 2, 60 Hz has an electric power consumption of 1,5 kW. The maximal diameter of the first stage is 55 mm, which allows the expander to be built inside the fore-vacuum line with an inner diameter of 62 mm. The unit therefore becomes 30 % shorter and has by more than 30 % less weight as compared with the standard cold head.

4.2 Testing the realization

Is the solution described above in a position to satisfy the requirements mentioned at the beginning of this paper? To what extent do the mainparameters: length of connecting lines and void volume influence the behaviour of the device? Critical parameters are: Filling and draining of the expander, the effective pressure difference Δp_{eff} in relation to the pressure difference Δp_{cu} of the compressor unit. Furthermore:

- the heat of compression during filling of the expander and
- heat abduction from the expander.

4.2.1 Effective pressure difference Δp_{eff} in the expander

The filling and draining procedure of the gas filled volumes of the expander of GM-cryocooler with splitted cold head can be described as a filling of the expander volume from endless volume with constant pressure on high level through connecting line as a flow resistor and as a draining of the expander volume into the another endless volume with constant pressure on low level etc. The changes from low to high pressure happen very fast.

Already the qualitative comparison of the filling of the GM-cryocooler with splitted cold head with the filling of the expander of the split Stirling cryocooler occurs than in the case of the split Stirling cryocooler, more complete because of the virtually sudden change of the pressure in the case of split GM cryocooler.

The amount of gas required by the cold head RG 210 (see above) is about 20 $stdm^3/h$. The additional consumption of a line of for example ISO-size 4 amounts theoretically to 6.3 $stdm^3/h$. The higher gas requirement or - in other words - the smaller pressure difference $\Delta p = p_{high} - p_{low}$ of the system is partly compensated by the improved efficiency of the compressor. The applied measures might compensate the losses and increase the relative refrigerating capacity from 76 % to 84 % for this case.

4.2.2 Heat abduction from the expander

The nominal refrigerating capacity of the used cold head RG 210 amounts to 12 W/80 K plus 2 W/20 K; if one adds the unavoidable losses in the regenerator then the total thermal load on warm end of the expander amounts to c. 20 W. In the case of a normal GM-cryocooler this heat is removed by the discharged gas.
A cold head RG 210 has a temperature difference between high pressure and low pressure gas of about 4 K.

Things are much different in the case of cryocooler with split cycle and of GM cryocoolers with splitted cold head. The thermal load causes a warming up of the gas pipe and the expander housing.

Two ways are available for stabilising the system:

- additional air- or watercooling of the warm end of the expander
- introduction of a forced gas circulation as in normal GM cryocoolers by installation of a separate gas filling line connecting to high pressure valve and gas draining line connecting to low pressure valve (This however involves doubling of the void volume of the lines and corresponding losses as discussed above).

5. Experimental set-up

The simple set-up is shown in Fig. 2. The working and the control space of the cold head are supplied with gas via separate pipes. For the given length of line of 5,5 meter the following parameters were varied:

- inner diameter of the line leading to the working space: ISO-size 8, 6, 4, 2 mm
- inner diameter of the line leading to the gas drive: ISO-size 6, 4, 2, 1 mm
- cooling of the warm end of the expander
  - o air cooling with free convection
  - o air cooling with forced convection
- watercooling with forced circulation
- gas filling and gas draining through separate lines, connecting to high and low pressure valves

6. Experimental results

6.1 Dimension of the connecting lines

The experiments showed that the rating of the connecting line to the working space is determined by the small void volume requirement.

The void volume was smaller than the geometrie volume of the expander, the diameter was ISO size 6. For the diameter of the connecting line to the gas drive a diameter of ISO size 2 was found which ensures the pressure increase and fall and the correct timing of displacer motion.

6.2 Heat abduction from the expander

If the thermal load causes the temperature increase of the warm end of the expander, the refrigerating capacity of the first stage will be drastically reduces.

The influence of temperature of the warm end of the expander on the refrigerating capacity of the first stage at 80 K and second stage at 20 K give the Fig. 3. Cooling is necessary.

6.2.1 Air cooling

Cooling by air with free convection was not sufficient, the max. temperature of the warm end was nearly 85 °C. The refrigerating capacity was too low.

Air cooling with forced convection by fan was able to drop this temperatur level below 40 °C. The refrigerating capacity reached nearly 50 % and 80 % respectively of the nominal refrigerating capacity of the first and second stage. One bigger heat exchanger could not be realised (s. section 2).

6.2.2 Watercooling

Watercooling with forced circulation of the warm end of the expander showed the best results. The results obtained when watercooling, the expander housing or the end of the connecting line to the working space or both parts were only slightly different. The first and second stage refrigerating capacity of this GM cryocooler with splitted cold head reached 80 % and 85 % respectively of the nominal refrigerating capacity of the same GM cryocooler working in standard configuration.

6.2.3 Gas filling and draining through separarte lines

The losses caused by the void volume which is twice that of previous design, go-up in proportion to the void volume; the losses caused by the self-warming-up of the end of the expander can be neglected. The improvement of the efficiency of the compressor increases the relative refrigerating capacity of the first and second stage to 70 % and 82 % respectively of the nominal refrigerating capacity of the same GM-cryocooler in standard configuration.

The refrigerating capacity of the first and second stage of splitted cold head RG 210 is shown for the discusses arrangements at Fig. 4.

7. Conclusion

Leybold-Heraeus Co. have developed, built and succesfull tested a Gifford-McMahon cryocooler with splitted cold head for cooling a cryopump.

The refrigerating part of the cold head and the gas flow control device have been separated (splitted cold head) and the distance between them is bridged by only two thin lines for carrying the working gas. Due to this separation the size of the refrigerating part is virtually defined only by the size of the displacers whilst the gas flow control device can be of any desired design.

It has been shown that dimensioning of the connecting lines and the corresponding losses became less critical with increasing size of the expander, but additional cooling in proportion to the refrigerating capacity is required.

Such small and light-weight cryocooler, which does not produce any magnetic and electric fields nor is affected by strong magnetic fields appears ideal to be used:
as single-stage cryocooler for sensors to approx. 30 K (e.g. infrared detectors),
as two-stage cryocooler for objects down to approx. 10 K (e.g. cryopumps) and
to precool Joule-Thomson-cycle achieving temperature down to 4,2 K (e.g. SQUIDs, Josephson-junction-elements).

8. References

1) F. F. Chellis: Design Compromises in the Selection of Closed-cycle Cryocoolers
NBS Special Publication 508

2) H.-J. Forth, R. Frank, R. Heisig, H.-H. Klein: A new Development of Refrigerators of high operational Reliability for Use in Cryopumps
IVC, Cannes 1980

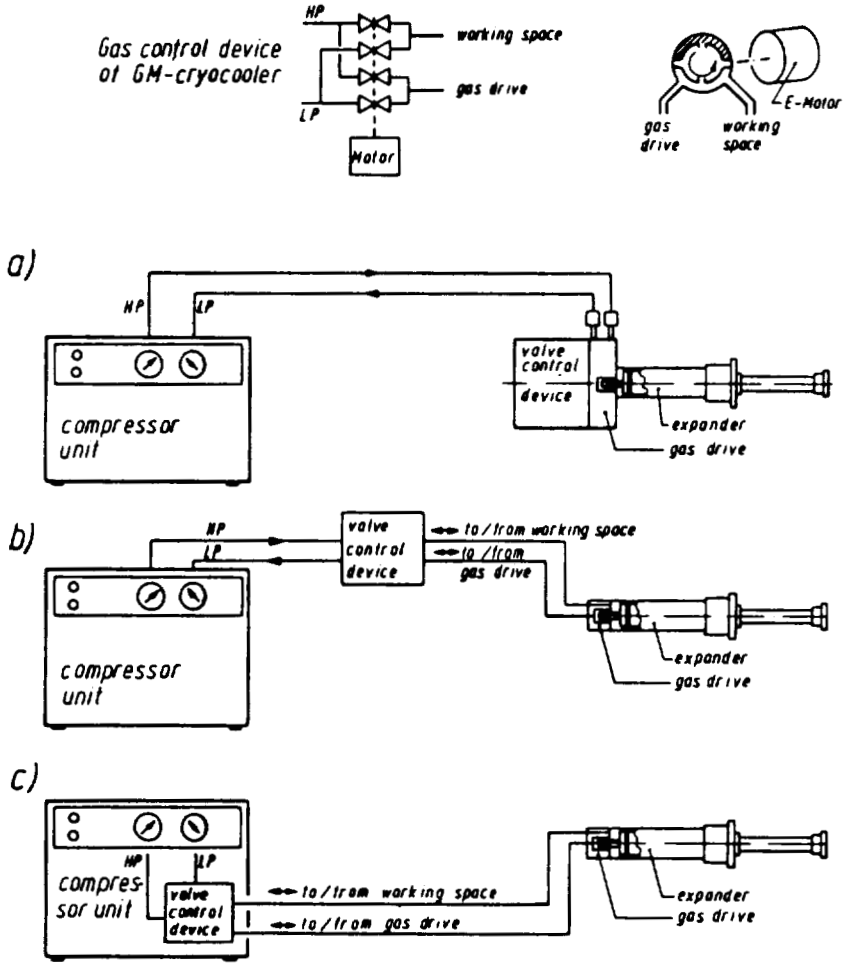

Fig. 1: Diagrammatically various arrangements of the GM-cryocooler.

Fig. 1a - normal GM-cryocooler.

Fig. 1b - GM cryocooler with splitted cold head, with the valve control part outside the inaccessible zone.

Fig. 1c - as Fig. 1b, but with the valve control part integrated in the compressor unit.

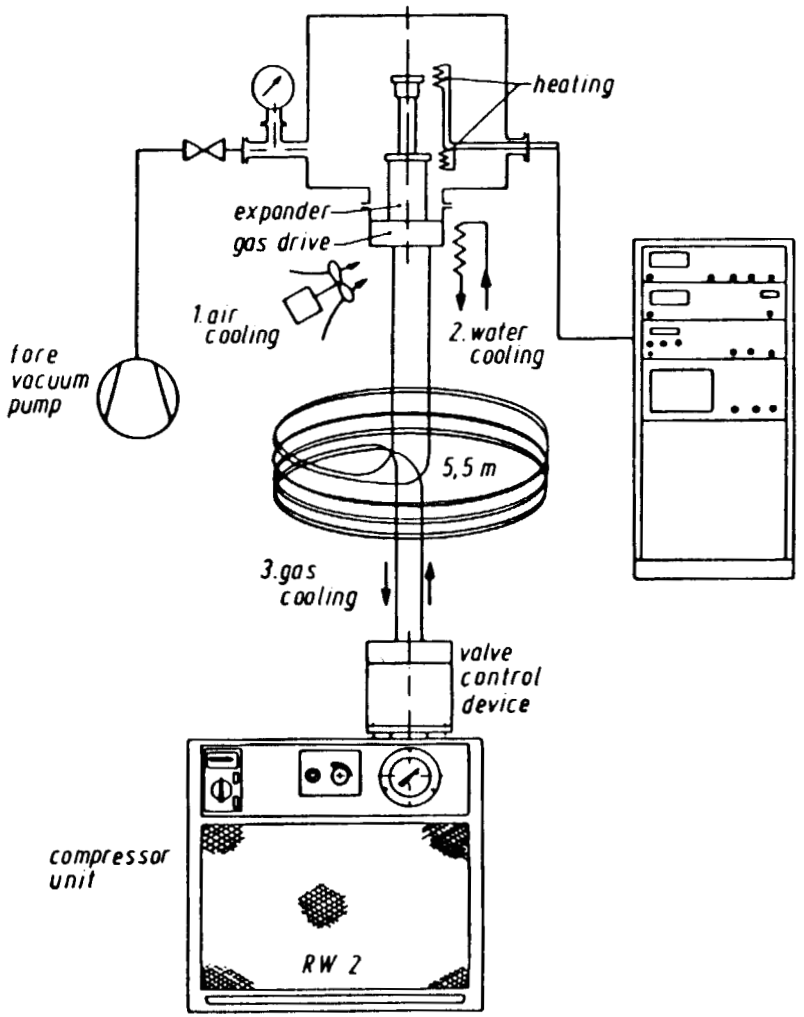

Fig. 2: Experimental set-up.

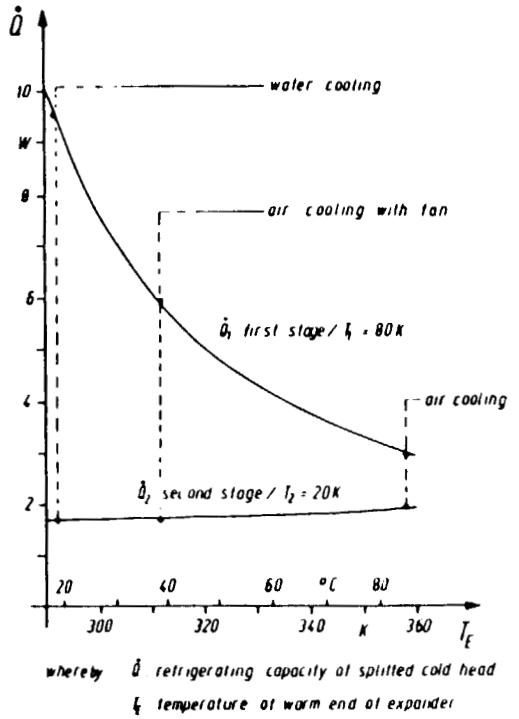

Fig. 3: Refrigerating capacity $\dot{Q}_1$ (80 K) of the first stage and $\dot{Q}_2$ (20 K) of the second stage of GM-cryocooler with split cold head independent of temperature T_E of warm end of the expander

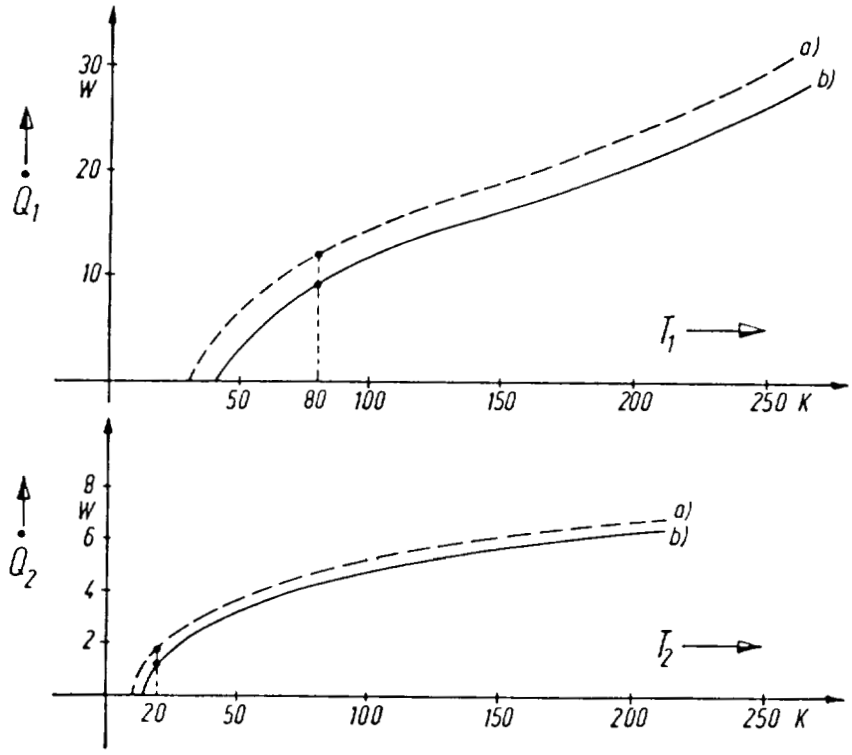

RG 210 a) standard cold head
b) splitted cold head $T_E \approx 300\,K$

whereby: $\dot{Q}$: refrigerating capacity
$T_{1,2}$: temperature of the stage
T_E : temperature of warm end of expander

Fig. 4: Refrigerating capacity $\dot{Q}_1$ of the first stage and $\dot{Q}_2$ of the second stage in dependance of their temperatures for standard cold head and splitted cold head RG 210

TESTING AND CHARACTERIZATIONS OF INFRARED SENSORS OVER THE TEMPERATURE RANGE OF 2 KELVIN TO 300 KELVIN

Robert G. Hansen

R. G. Hansen & Associates
1324 "C" State Street
Santa Barbara, CA 93101

ABSTRACT

To properly evaluate "state-of-the-art" electro-optic devices in a timely and convenient manner, various cryogenic techniques have been employed. As research, development, and production demands require more sensitive testing techniques, faster test results, and higher production through-put, the emphasis on supporting cryogenic systems increases.

This presentation discusses the three traditional methods currently utilized in electro-optic device testing, those being:

(1) liquid containment dewars
(2) liquid transfer systems
(3) closed cycle refrigeration systems.

Advantages, disadvantages, and the current "state-of-the-art" of each of these cryogenic techniques is discussed.

INTRODUCTION

With continued emphasis on the use of passive infrared sensors for both military and commercial applications, the need to evaluate semiconductor materials and devices through the various stages of material development, device testing and ultimate system checkout has placed considerable emphasis on the cryogenic aspects of device testing. Since the latter part of the 1960s, sensing systems have changed from active to passive techniques. Detecting techniques such as radar, microwave, acoustic and visual sensors have given way to "state-of-the-art" infrared semiconducting materials. As longer wavelength sensors are developed, the need for lower cryogenic temperatures has advanced the technical disipline of cryogenics in order to keep abreast with advancements in detector materials, semiconductor processing and electro-optic systems design.

As technology entered into the 1970s, detector materials such as doped germanium and doped silicon sensors required cryogenic systems capable of achieving and maintaining temperatures in the sub-20 Kelvin region. Through Federally sponsored research and development programs supporting end-use cryogenic refrigeration systems were developed. Recently, however, emphasis is being placed on the ability to rapidly test, evaluate, select, integrate and finally test electro-optic systems of varying complexities over the

temperature range 2K to 300K. The purpose of this presentation is to discuss the various cryogenic cooling techniques along with their advantages and disadvantages. Although hybrid systems comprising various cryogenic techniques have been developed, this paper will confine itself to the more traditional techniques:

(1) pour-fill type dewars
(2) liquid cryogenic transfer systems
(3) closed cycle cryogenic refrigeration systems.

DEWARS FOR ELECTRO-OPTIC DEVICE TESTING

Dewars, since first constructed by the Scottish chemist James Dewar (1842-1923), have changed little since their introduction in 1892. Dewars are designed to provide a means of conductively cooling samples by mounting them on the inner vacuum well of the storage dewar which is under an insulating vacuum. While working at liquid nitrogen temperatures, from 77K to 300K, dewars are not only convenient, but also the preferred method for evaluating devices in a conductively cooled cryogenic state. To use liquid containment storage dewars for testing below 77K presents problems of convenience and temperature stability. Conveniently speaking, the most commonly used cryogen employed to cool devices below 77K is liquid helium. In order to achieve dewar cooldown one must first precool the dewar flask with liquid nitrogen and then perform the liquid helium transfer via a siphon from the primary vacuum storage dewar to the research or test dewar. Once achieved, one experiences difficulty in achieving temperature controllability above 4.2K unless a thermal balance or heat station is designed with an appropriate heater circuit and cryogenic feedback sensor. An additional problem arises with the restricted orientation of liquid containment dewars. One may use them in either end-looking or side-looking configurations but each dewar is limited to its inherent design.

In recent years, multi-element infrared arrays have been traditionally tested by the use of rather sophisticated liquid containment dewars. Typically, test cycle times with traditional dewars resulted in the ability to test one or two devices per day at helium temperatures thereby restricting the production of electro-optic systems requiring helium temperatures.

In addition to problems associated with long test sequences was the inherent low yield factor on "state-of-the-art" electro-optic devices. The need arose to pre-test or evaluate semiconductor devices as early in their production cycle as possible so as to increase ultimate yield. Cryogenic testing on a rapid turnaround cycle was mandatory and, in most cases, dewars would not meet the demands.

LIQUID CRYOGENIC TRANSFER SYSTEM

Recognizing the inherent difficulties with conventional dewars, a series of liquid transfer systems was developed which employed the technique of direct transfer of cryogenic fluids from their storage dewars to cryogenic heat sinks or cold stations. These systems were designed to utilize very small flows of cryogen which allowed the user to integrate cryogenic sensors and heating circuits to rapidly and conveniently achieve temperature excursion from room temperature to helium temperature and in between with ease, convenience, and accuracy. The first such system developed in this country was the Heli-Tran^{R} designed and manufactured by the Advanced Products Department of Air Products and Chemicals, Inc. This system allowed the user to operate in any orientation, i.e.: end-looking, side-looking, horizontal, vertical, et cetera, without the fear of costly and dangerous cryogenic spills. By using the helium transfer systems, manual temperature stabilities of ±0.01K are achievable from 2-20K, ±0.1K from 20-77K and greater than ±0.3K from 77-300K. Through implementation of automatic temperature controllers, stability factors of ±0.01K can be achieved from 2-300K.

An additional feature responsible for the wide acceptance of the Heli-Tran^{R} was the rapid cooldown from ambient temperature to 4.2K in less than 20 minutes time. Liquid helium consumption rates of approximately 0.75 liters per hour at 4.2K with corresponding refrigeration capability of several hundred milliwatts is easily achieved. For requirements demanding higher refrigeration capacity, liquid transfer of up to three liquid liters per hour of helium can be provided with a corrsponding refrigeration capacity of two watts of refrigeration at 4.2K.

The schematic on the following page illustrates a typical liquid transfer system in a basic configuration. (Diagram A)

In the mid-1970s, requirements for infrared device testing of multi-element arrays necessitating up to 260 individual feedthroughs required the design of specially modified liquid transfer systems. Developments such as ribbon cable technology, microphonic dampening techniques, rapid cycling and ease of handling resulted in the further dependence of the electro-optic industry on the modified liquid transfer systems.

With the recent breakthroughs in CCD and CID devices, a demand was created for a low noise infrared device test station which could serve as an industry standard. A system was needed that would standardize on air industry accepted device carriers, exhibit low noise characteristics, have a minimum of 68 coaxial feedthroughs, cycle times of from 300K to 4.2K to 300K of one hour or less. Additionally, supporting temperature indication and control was required which provided computer interface and addressability.

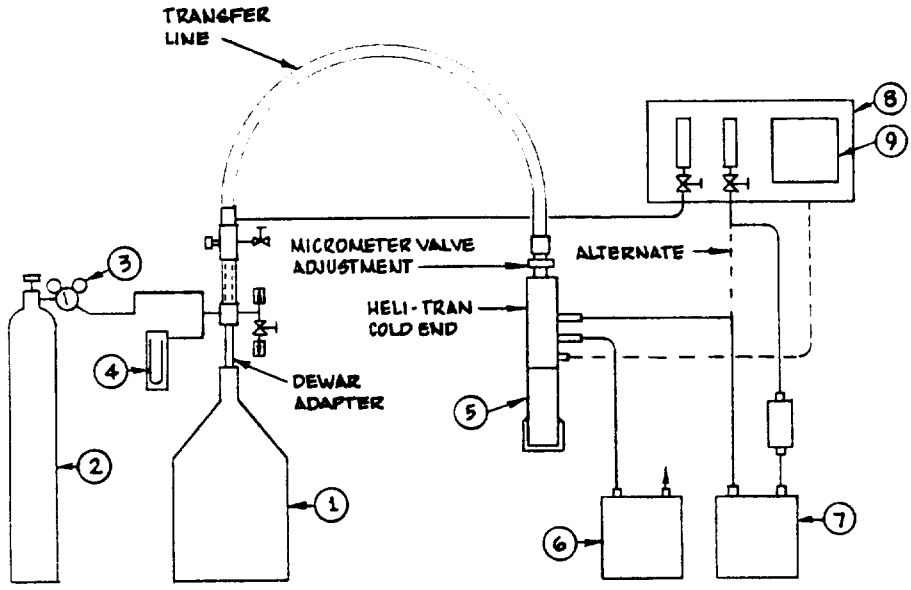

1. HELIUM DEWAR
2. HELIUM CYLINDER
3. PRESSURE REGULATER
4. MERCURY MANOMETER, 0 TO 20"Hg OR PRESSURE GAUGE ON HELIUM DEWAR
5. VACUUM SHROUD
6. VACUUM SHROUD PUMP
7. VACUUM PUMP FOR OPERATION BELOW 4.2°K
8. ACCESSORY FLOW CONTROL PANEL
9. ACCESSORY TEMPERATURE CONTROLLER, MANUAL OR AUTOMATIC

TYPICAL LIQUID TRANSFER SYSTEM

(Diagram A)

To satisfy these needs we developed a modified liquid transfer system which we believe is the answer to not only today's cryogenic device testing, but also meets the needs of the future.

The following interface outline depicts the salient features of our modified liquid transfer system. (Diagram B - 68-Pin Leadless Carrier Infrared Device Test Dewar).

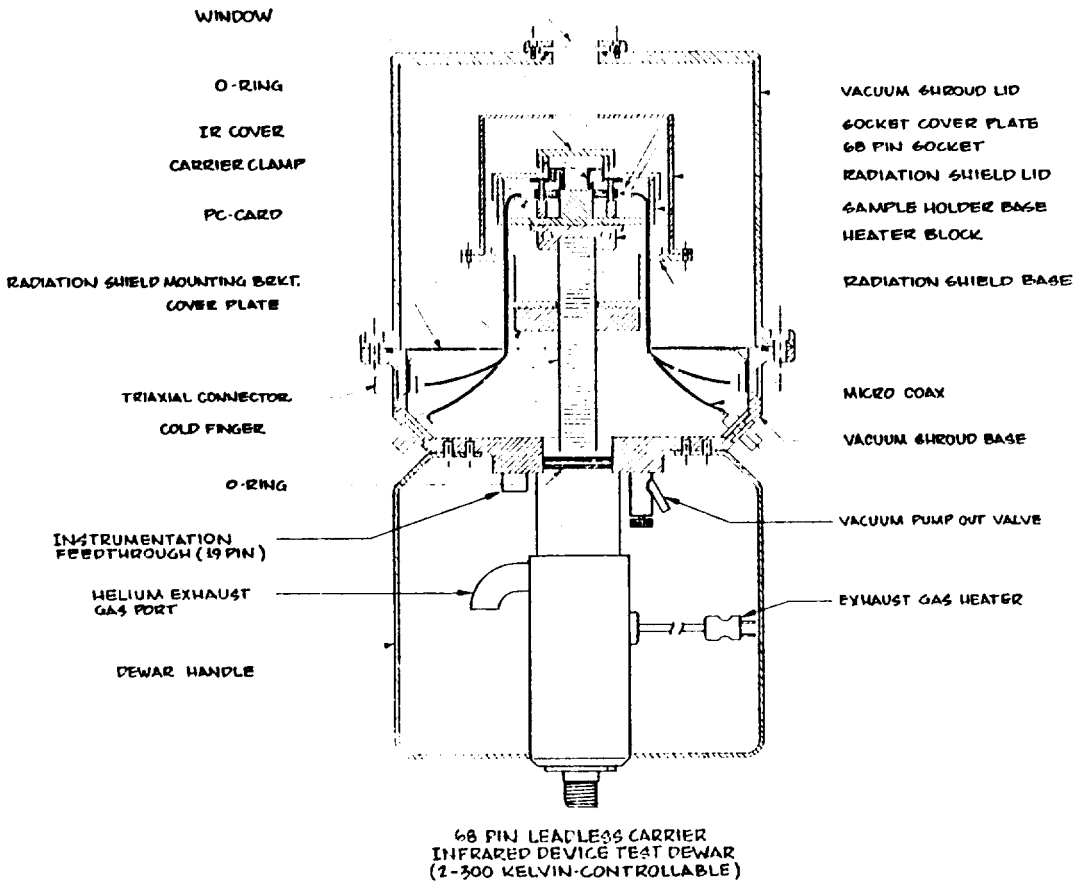

(Diagram B)

CLOSED CYCLE REFRIGERATION SYSTEMS

Although liquid transfer systems provide the necessary refrigeration stability for electro-optic device testing, the use of closed cycle refrigeration systems to perform device cooling over the temperature range of 10K to 300K is gaining wide acceptance. Although several manufacturers supply closed cycle refrigeration systems, each capable of achieving 0.250 watts of refrigeration at 10K, several distinct advantages have been realized by utilizing a pneumatically balanced, nonmechanically driven displacer design.

In testing sophisticated infrared arrays, charge couple devices and, in some cases, even individual detectors, the problem of microphonics is usually associated with mechanical refrigerators. This microphonics, being a generic term, defines two major constituents, i.e.: linear displacement and thermophonics. As the closed cycle refrigeration systems perform their

work cycle a very minute temperature cycle is generated which can alter the performance of sensitive electro-optic devices. Furthermore, linear displacement produced by the traveling mass of the displacer generates signals which can interfere with the desired sensing signal. In recent years this problem has been virtually eliminated by the incorporation of a lead attenuator on the base of the refrigerator, incorporation of a microphonic dampener or the unbalancing of the refrigerator's cold head by reducing the differential pressure between the inlet supply and return flow of helium. This latter technique is also an accepted technique for determining the threshhold level for acceptable microphonic levels in "noise" sensitive electro-optical systems driven by mechanical refrigerators.

The closed cycle refrigeration concept of detector device cooling offers similar advantages to the liquid transfer technique. The system may be operated in any orientation, may be left unattended for long periods of time, exhibits a meantime before maintenance interval of approximately 10,000 hours and requires no consummable cryogens to perform its cooling function.

Although the initial cost for a closed cycle refrigeration system is approximately twice that of a liquid transfer system or four times that of a conventional storage dewar, we are finding that more and more "state-of-the-art" detector development programs are using this technique. At the present time, the advent of closed cycle refrigerators into cryopumping technology has substantially increased inherent reliability of the systems as well as contributed greatly to the reduction of their price based on larger manufacturing throughput.

At the present time our firm is undergoing an internal development program whereby a 68-pin leadless carrier closed cycle refrigeration system is being developed which should provide device turnaround from 300K to 10K to 300K in less than one hour's timespan. Through the integration of this system with programmable temperature indicator/controllers, we believe that several test stations can be run in parallel which would allow a single operator to support and control multiple closed cycle cryogenic test stations.

An additional subcategory to closed cycle refrigeration systems is the single stage configuration of a closed cycle expansion module. By the elimination of the second stage of a two-stage expander one achieves rapid cooldown, higher refrigeration capacities, and the ability to perform device cooling over the temperature range of 40K to 300K. Depending on required capacities, various single stage refrigeration systems are available to provide approximately one watt of refrigeration at 77K or, in some instances, approximately 100 milliwatts at 77K a series of commercially available rather inexpensive refrigeration systems have been developed which provides many of the advantages of end-use cryogenic military systems.

For example, the single stage Air Products and Chemicals' Displex^{R} Model CS 1003 was recently integrated into a calibration laboratory to provide the cooling of a common module FLIR device. Although the specification for the end system is a refrigerator with a lifetime of approximately 1,000 hours, this particular system can be operated at lower noise levels, lower temperature, rapid cooldown and may be conveniently operated for 12,000 hours prior to maintenance interval. Associated cost with such a system is approximately comparable to that of a military cryogenic cooler yet provides a factor of 25 in the system's ultimate lifetime.

SUMMARY

In summarizing this presentation, we believe that many advancements have been made in the field of cryogenics over the last ten (10) years as a result of the industry's demand for highly reliable, rapid cooldown systems which may be conveniently operated by both skilled and unskilled test technicians.

With the rapid advancement of charge couple devices (CCDs), further progress will be made in the immediate future.

OPTIMAL DESIGN OF GAS ADSORPTION REFRIGERATORS FOR CRYOGENIC COOLING*

C. K. Chan
Jet Propulsion Laboratory
4800 Oak Grove Drive
Pasadena, CA 91109

ABSTRACT

The design of gas adsorption refrigerators used for cryogenic cooling in the temperature range of 4K to 120K has been examined. The functional relationships among the power requirement for the refrigerator, the system mass, the cycle time and the operating conditions were derived. It was found that the precool temperature, the temperature dependent heat capacities and thermal conductivities, and pressure and temperature variations in the compressors had important impacts on the cooling performance. Optimal designs based on a minimum power criterion were performed for four different gas adsorption refrigerators and a multi-stage system. The estimates of the power required and the system mass were within manageable limits in various spacecraft environments.

NOMENCLATURE

a	constant
b	Van der Waal's volume
c	constant
C	specific adsorptance, mass ratio of gas adsorbed to adsorbent
C_p	heat capacity
D	container diameter
h	enthalpy
k_g	gas conductance
m	mass
$\dot{m}$	mass flowrate
M	molecular weight
P	pressure
$\dot{Q}$	heat transfer rate
Q	heat
R	universal gas constant
t	time
T	temperature

* This paper represents one phase of research carried out at the Jet Propulsion Laboratory, California Institute of Technology, under NASA Contract NAS7-918.

ΔU heat of adsorption
V volume
x adsorption potential
x_m mass ratio of container to adsorbent
α correlating parameter
β parachor
γ correlating parameter
σ_y yield strength
ρ density
Δ difference
δ gas gap

SUBSCRIPTS

1, 2, 3, 4	compressor states illustrated in Fig. 2
a, b, c, d, e, f	thermodynamical states of gas illustrated in Fig. 3
cr	critical
C	heat sink, or cooling
H	high, or heating
L	low
p	precool
r	refrigeration chamber
s	container
α	adsorbent

INTRODUCTION

The potential use of gas adsorption compressors as a gas source for cryogenic refrigerators has become fairly promising for sensor cooling, because of their inherent merit of no moving parts and the fact that a low temperature heat source [1] can act as the power source. Conceptually, a Joule-Thomson (J-T) cooling device [2] can be coupled to a set of gas adsorption compressors which operate cyclically between desorption and adsorption modes. These compressors liberate and compress the gas during the desorption mode and readsorb the gas during the adsorption mode. A system design utilizing J-T cooling and two adsorbent compressors was proposed by Chan [1] while a multi-stage system to handle various refrigeration temperature requirements was proposed by Chan, Tward and Elleman [3].

This paper presents a generalized methodology to design such gas adsorption refrigeration systems and to evaluate their performance. In designing the J-T valve and heat exchanger, gas flow and other thermodynamical conditions such as pressures and temperatures will be determined for a given cooling load at a given refrigeration temperature. The gas adsorption compressor design will include the adsorbent mass, the temperature variation, the container volume, the cycle time and the power requirement. Optimization analyses will be emphasized for the power and the mass criteria. These analyses will provide information about the optimal operating conditions for various gas adsorption refrigerators.

GAS ADSORPTION REFRIGERATION SYSTEMS

The gas adsorption refrigeration system using a J-T valve and heat exchanger and two gas adsorption compressors is shown in Fig. 1, while the thermodynamical paths for the compressor and the J-T valve for an idealized system are shown in Figs. 2 and 3, respectively.

Starting from the state point 1 in Fig. 2, the adsorbent is at its lowest temperature T_1, the lowest pressure P_1 but highest adsorptance C_1 when the adsorbent chamber A in Fig. 1 is heated with no gas outflow (process 1-2 in Fig. 2). Both the temperature and the pressure inside the chamber would increase with little change of adsorptance concentration for an ideal compressor. At point 2 in Fig. 2 the pressure is high enough to push open the check valves 1 and 4 and close valves 2 and 3 in Fig. 1. The gas outflow causes the adsorptance to drop coupled with further temperature increase. In the ideal situation, the gas flows at a constant pressure as represented by the process 2-3 in Fig. 2.

When Chamber A is at the state point 1, chamber B will be at the state point 3, so when A is heated, heat is removed from chamber B. This will cause the temperature in B to drop and gas can be adsorbed as indicated by processes 3-4 and 4-1 in Fig. 2.

If the compression action of chamber A and the suction action of chamber B could be synchronized, then the high-pressure gas would flow through the precooler and the counterflow heat exchanger where it is cooled to a lower temperature before it expands through a J-T valve. Upon expansion, the gas enters the refrigeration chamber in the form of a two-phase mist. The thermodynamical states of the gas before the precooler, the counter-flow heat exchanger and the J-T valve are represented by state points a, b, and c, respectively, in Fig. 3. The throttling process moves the state point from c to d along a constant enthalpy process. The refrigeration load causes the vaporization of the liquid. Hence, the outlet of the refrigeration chamber is at state point 3 in Fig. 3. Upon the return passage through the counterflow heat exchanger, the outlet temperature of the gas at state point f is the same as the inlet temperature (state point b). The low pressure in the refrigeration chamber is maintained by the suction process in chamber B where the gas is being adsorbed.

At the state point 3, when the gas inventory in chamber A has been depleted, the heat flow of both chambers reverses direction. Chamber B now functions in the role of the compressor while chamber A functions as the suction pump. The state point of compressor A moves from 3 to 4 and then back to 1. Thus, the compressor completes its cycle by heating and then cooling. For the two-compressor system described here, there are two periods during the cycle when there is no gas flow (processes 1-2 and 3-4). This problem can be alleviated by combining this system with another similar set of two compressors which operates at ninety degrees out of the phase of the

first two, or by the use of ballast tanks so that continuous gas flow can be maintained at the J-T expander.

J-T COOLING

Considering the J-T expansion system with the precooler as shown in Fig. 1, the thermodynamic states of the gas downstream of the compressor are represented on the T-S diagram shown in Fig. 3. The state point of the gas after exiting the precooler is represented by the point b in Fig. 3.

The gas is further cooled to the state point c after it passes through the counterflow heat exchanger. The throttling of the high-pressure gas to the low-pressure region is represented by the path c-d. In the refrigeration chamber the refrigeration load causes the liquid to vaporize as shown by the path d-e. While passing through the counter flow heat exchanger, the gas is heated from point e to point f. From the total energy balance, the refrigeration load $\dot{Q}_r$ is related to the mass flow as:

$$\dot{Q}_r = \dot{m}(h_f - h_b) \tag{1}$$

where $\dot{m}$ is the mass flow rate through the J-T valve, h_f is the enthalpy of the outlet gas at the low-pressure side of the counterflow heat exchanger and h_b is the enthalpy of the inlet gas after the precooler. For a given refrigeration temperature T_r, the temperature at state point d must equal to T_r. This determines the low-pressure isobar at d, e and f because there is only one relationship between saturation pressure and saturation temperature.

From a designer's point of view there are two adjustable parameters: (1) the gas temperature, T_b after the precooler and (2) the pressure, P_c upstream of the J-T valve. As the pressure decreases and as T_b increases the required mass flow increases as shown in Fig. 4. The mass flow rate corresponds directly to the adsorbent mass in the compressor. However, a high-pressure condition would add structural mass to the system. As well, the maximum usable pressure is restricted by the isotherms and the thermal cycle of the compressor. The precooling temperature is restricted by the availability of the heat sink.

GAS ADSORPTION COMPRESSOR DESIGN

In the refrigeration cycle, a compressor provides the required gas flow at the desired pressure and temperature. Since the mass flow is related to the pressures of the gas from the compressors based on the refrigeration requirement as shown by equation (1), the parameters for the gas adsorption compressor such as the adsorbent mass, the container mass, the energy

required to power the compression, and the temperature swing of the adsorbent for the compression and decompression cycle, are expected to relate to the mass flow, the heat source, temperatures T_H and the heat sink temperature, T_C. If a gas heat switch [4] is used to control the heat into and out of the compressor, then the cycle time for the adsorption cycle may be controlled by the performance of the switch.

ISOTHERMS

The gas-adsorption compressor depends on the adsorption characteristics of the gas by the adsorbents at different temperatures. When the gas is brought into contact with the adsorbent, some of the molecules striking the solid surface will be retained for a finite period of time, resulting in a significantly higher molecular concentration at the surface than in the gas phase. The forces holding the molecules to the solid are due to molecular interactions. This process is known as physical adsorption and has been studied, both at ambient and cryogenic temperatures. A comprehensive review of the subject at cryogenic temperatures can be found in Reference [5]. However, much of the past experimental data for adsorption of various cryogenic gases by such adsorbents as charcoal, zeolite and silica gel are available only in the low pressure range. This is due to the fact that the main application of gas adsorption has been related to either low-pressure gas removal or to cryopumping. Gas adsorption at the higher pressures which are needed for a workable gas adsorption compressor, has only recently become available [6, 7].

For the design of an adsorption compressor, it would be convenient to express analytically the adsorption of the gas on the adsorbent as a function of pressure and temperature. For this reason, the isotherm data for hydrogen and neon, nitrogen and helium gases have been correlated with a similarity parameter, the adsorption potential x, given by

$$x = \frac{RT}{\beta} \ln \left(\frac{P_{cr}}{P} \left(\frac{T}{T_{cr}} \right)^2 \right), \tag{2}$$

where β is the parachor, R is the universal gas constant, T is the adsorbent temperature, P is the gas pressure, T_{cr} is the critical temperature of the gas and P_{cr} is the critical pressure of the gas.

The data were fitted to an expression of the form

$$C = \frac{M}{b} \alpha \, e^{-\gamma x} \tag{3}$$

where the specific adsorptance C is the gas mass adsorbed per unit mass of

charcoal, M is the gas molecular weight, b is the Van der Waal's volume, and α and γ are correlating parameters determined from the data.

POWER REQUIREMENT

The power requirement for the refrigeration cycle is best represented by the specific power which is defined as the ratio of the heat input for the cycle to the refrigeration load.

During the compression period, the total refrigeration load is

$$Q_r = m_\alpha \Delta C \, (h_f - h_b) \tag{4}$$

where m_α is the adsorbent mass and $m_\alpha \Delta C$ represents the gas mass liberated during the compression. The heat required for gas liberation is given by

$$Q_H = (m_\alpha C_{p\alpha} + m_s C_{ps}) \, \Delta T + m_\alpha \Delta C \Delta U \tag{5}$$

where m_α and m_s are the masses of the adsorbent and the container, respectively, $C_{p\alpha}$ and C_{ps} are the heat capacities of the adsorbent and container and ΔT is the maximum temperature swing of the adsorbent and ΔU is the isosteric heat of adsorption which satisfies an equation similar to the Clausius-Clapeyron equation, i.e.,

$$\Delta U = -R \left(\frac{\partial \ln P}{\partial \left(\frac{1}{T} \right)} \right)_C \tag{6}$$

In equation (5), the heat capacity of heat enhancement elements inside the adsorbent bed can be lumped into the $m_s C_{ps}$ term. Combining equations (4) and (5), the specific power of the refrigerator is given by

$$\frac{Q_H}{Q_r} = \frac{\left(C_{p\alpha} + x_m C_{ps} \right) \Delta T}{\left(h_f - h_b \right) \Delta C} + \frac{\Delta U}{\left(h_f - h_b \right)} \tag{7}$$

where x_m is the ratio of container mass to adsorbent mass.

Since h_f and h_b are functions of the high pressure P_H and the low pressure P_L, as well as the precooler temperature T_p, the specific power is a function of P_H, P_L, T_1, T_p, ΔT, and ΔC, but independent of the cycle time.

CONTAINER MASS

In estimating the container mass ratio in Eq. (6), a cylindrical container completely filled with the adsorbent is assumed for this model. By imposing the restriction that the Hooke stress of the cylindrical wall resulting from internal pressurization is limited by the yield strength of the container material, the mass of the container to the adsorbent mass can be expressed as [1]

$$x_m = \frac{m_s}{m_\alpha} = \frac{2\rho_s P_H}{\rho_\alpha \sigma_y} \tag{8}$$

where ρ_s is the density of container material, ρ_α is the density of the adsorbent, P_H is the maximum gas pressure in the compressor and σ_y is the yield strength of the material.

CYCLE TIME

Assuming a gas heat switch similar to the one mentioned in ref. [4] is used to conduct the heat out of the cylindrical compressor through a gas gap to the heat sink at temperature T_C, the time required to cool the compressor from T_3 to T_1 is given by

$$t_C = \frac{\rho_\alpha \bar{C}_p \delta D}{4k_g} \ln\left(\frac{T_3 - T_C}{T_1 - T_C}\right) \tag{9}$$

where

ρ_α = adsorbent density

$$\bar{C}_p = \left(C_{p\alpha} + x_m C_{ps}\right) \tag{10}$$

δ = gas gap

k_g = gas conductance

and D = diameter of the compressor cylinder.

The gas conductance k_g can usually be expressed as

$$k_g = \left(\frac{T}{a}\right)^c \tag{11}$$

where a and c are correlation constants (Table 1).

In our experience the cycle time of the heatup and the cooldown of the complete cycle is usually limited by the cooling period t_C. Hence, if the

cooling time equals the heating time because of the synchronization requirement, then the cycle time t_o is given by

$$t_o = 2t_C = \frac{\rho_\alpha \overline{C}_p \delta D}{2k_g} \ell n \left(\frac{\Delta T}{T_1 - T_C} + 1 \right) \tag{12}$$

When the adsorbent is heated at constant pressure (process 2-3 in Fig.2) the mass flow required for refrigeration comes from the liberation of the adsorbed gas. By assuming a uniform gas flow over the heating period, the mass flow rate $\dot{m}$ is related to the adsorbent m_α and the cooling period t_C by

$$\frac{\dot{m}}{m_\alpha} = \frac{\Delta C}{t_c} \tag{13}$$

By substituting equations (9) and (1) into equation (13), then the adsorbent mass for a unit of refrigeration load can be expressed as:

$$\frac{m_\alpha}{\dot{Q}_r} \left(\frac{4k_g}{\rho_\alpha \overline{C}_p \delta D} \right) = \frac{\ell n \left(\frac{\Delta T}{T_1 - T_C} + 1 \right)}{\left(h_f - h_b \right) \Delta C} \tag{14}$$

The total mass of the compressor is then

$$m = m_\alpha (1 + x_m) \quad . \tag{15}$$

Hence, the compressor mass, unlike the specific power, is a function of the cycle time which depends on the physical properties of the heat switch as well as the temperature swing of the cycle (ΔT) and the temperature difference between the heat sink and the minimum of the compressor cycle.

DATA

Four different refrigeration systems using charcoal as the adsorbent, have been studied. The adsorbed gases are nitrogen, helium, hydrogen and neon. The physical properties of these gases are shown in Table 1 which also includes the constants for the gas conductivity correlations of hydrogen and helium (eq. 11) and the constants for the isotherms (eq. 3).

Adsorption isotherms of hydrogen and neon on charcoal have been obtained in the pressure range from 1 to 100 atmospheres and in the temperature range from 77 to 200K [7]. These high pressure data compare well with the Kidnay and Hiza data [8] in the medium temperature and pressure ranges. Adsorption

of nitrogen in the high pressure range was obtained by Yang et al [6], Cook [9], and Tward [10]. The adsorptance from Yang's and Tward's data is about two times those found by Cook and Kidnay and Hiza. The correlating coefficients of the generalized equation (2) for the Kidnay and Hiza's as well as Tward et al isotherms, are presented in Table 1. The density, the temperature dependent heat capacities and the average heat capacities over a certain temperature range for charcoal, stainless steel and copper as well as the temperature dependent yield strength of stainless steel are presented in Table 2. It was found that the temperature dependent heat capacities can be expressed as

$$C_p = \left(\frac{T}{a}\right)^c \tag{16}$$

where C_p is the heat capacity in cal/g-K, T is the temperature in K, a and c are correlation constants which have the following values for charcoal; a = 775.57, c = 1.69877, for 20K < T < 500K. For stainless steel, a = 344.89, c = 2.0401, for 20K < T < 110K, whereas C_p = 0.1 cal/g-K for T > 110K.

OPTIMAL DESIGN

The mass flow rate, given by equation (1), provides the simplest way to have some insight into the optimal operating pressure conditions.

The mass flow rates per unit cooling power as a function of the compressor high pressure for four different gases is shown in Fig. 4. The low pressure for all these four cases is 1 atm while the precool temperatures for helium, hydrogen, neon, and nitrogen are 20K, 77K, 77K and 150K, respectively. Plots such as these which consider only the J-T cooler can be used to determine the minimum flowrate required.

It is always desirable to have a gas adsorption refrigerator that weighs the least, occupies the least space and requires the least power to operate. Specific power given by equation (7), is a good indication of the power required. For a given adsorbent material and container material,

$$\text{Specific Power} = f(P_H, P_L, T_1, T_3, T_p) \tag{17}$$

The mass of the compressor given by equations (14) and (15), is a function of the heat switch design parameters (δ, D, and k_g) in addition to the temperature and the pressure parameters:

$$\frac{\dot{m}}{\dot{Q}_r} = f\left(P_H, P_L, T_1, T_p, T_C, \frac{k_g}{\delta D}\right) \tag{18}$$

Among the six temperature and pressure parameters, the refrigerator chamber pressure P_L is determined by the refrigeration temperature T_r and the precool temperature T_p is determined by the availability of the heat sink (temperature T_C). The lowest temperature in the compressor cycle T_1 has to be higher than T_C. However, for a given P_L, higher adsorptance is obtained by having T_1 as low as possible. Hence, T_1 should be greater than but close to T_C.

In the present parametric study, the specific power and the compressor mass are determined for various values of P_H, P_L, T_1, T_3, T_p for helium, hydrogen, neon and nitrogen systems. In the calculation, the counter flow heat exchanger is assumed to be perfect, i.e., the inlet gas temperature is equal to the outlet gas temperature, the precool temperature and the sink temperature are equal and the difference between the temperature T_1 and the heat sink temperature T_C is 1^oK. The temperature dependent effects of the heat capacities (eq. 16) and the gas conductance (eq. 11) are incorporated into the calculations.

A computer program was written to perform the calculations. The outputs of the computer program include the specific power, the compressor mass and the mass flowrate for a unit of refrigeration load, the cycle time, the change of adsorptance, the container/adsorbent mass ratio, the heat capacities of the adsorbent and the container. In the compressor mass and the cycle time calculations, a gas gap of 0.01 cm and a compressor cylinder of 1 cm are used. It would be simple to calculate these two parameters for other heat switch dimensions because of the linear relationship between these parameters and those dimensions as illustrated by equations (9) and (14).

The results of a typical numerical calculation are illustrated in Fig. 5. It can be generally concluded that, for a given precooling temperature, a given low compressor pressure level and temperature, there exists a minimum specific power. For most efficient operation, one would like to operate the system at the pressure and temperature values corresponding to the minimum specific power. For example, the specific power for the helium system has a minimum value of 6.5 at P_H = 20 atm and T_H = 51K for T_p = 20K, T_C = 20K, T_1 = 21 and P_L = 1 atm. The minimum specific power decreases as the low pressure level increases and decreases with the precool temperature. The minimum power for the four systems and the corresponding compressor masses for unit refrigeration load, cycle time, and operating conditions are tabulated in Table 3. The compressor mass corresponding to the minimum power is not necessarily the minimum value in the parametric study. Thus, the optimal point based on minimum power is not necessarily the optimal point based on minimum mass.

MULTISTAGE DESIGN

A schematic diagram of a multistage refrigerator proposed by Chan, Tward and Elleman [3] is shown in Fig. 6. To illustrate the application of the optimal design method to the design of this multistage system, consider a helium refrigerator of 1 mW cooling at 4.2K. J-T output pressure must be at 1 atm corresponding to the vapor pressure of helium at 4.2K. For minimum Specific Power (S.P.) the high pressure should be 20 atm. If a hydrogen stage refrigerator can provide a heat sink of 20K for precooling the gas and cooling the helium compressor, then the maximum temperature in the helium compressor is 51K. Under these thermodynamic conditions, the S.P. for the helium compressor is 6.5 (Table 3). In other words, the total heat dumped into the hydrogen stage is 7.5 mW (i.e., 6.5 mW + 1 mW).

If a similar procedure is followed in designing the hydrogen stage, for a minimum S.P. of 66.6, the adsorption compression should be operated between 1 atm and 40 atm, for a temperature swing of the compressor between 78K and 218K with the gas precooling temperature at 77K. Hence, the heat dumped to the 77K heat sink is (66.6 x 7.5 + 7.5) or 507 mW.

The 77K heat sink is provided by the nitrogen stage. The S.P. for that stage is 54.2 for P_L = 1 atm, P_H = 60 atm, T_1 = 134K, T_3 = 474K and T_p = 133K. The 150K heat sink for the nitrogen stage can be provided by a passive radiator at 133K. The total heat load on the radiator will be 28W.

The total heat load on the radiator could be reduced if we adopted the following heat recovery schemes at each stage. Half of the heat for the heat-up process of the He compressor can be obtained from the cool-down process of the He compressor of the same stage. Hence, the total heat dumped onto the hydrogen stage will be (6.5/2 + 1) or 4.25 mW. This scheme is defined here as internal heat recovery. The other half of the heat to heat up the He compressor can be obtained from the cool-down phase of the upper stage compressor. This scheme is defined here as external heat recovery.

If a similar heat recovery procedure is followed in designing the hydrogen stage, for minimum power of 66.6, the adsorption compression should be operated between 1 atm and 40 atm, for a temperature swing of the compressor between 78K and 218K with the gas precooling temperature at 77K. Hence, the heat dumped to the 77K heat sink is $(66.6 \times \frac{4.25}{2} + 4.25)$ or 146 mW.

As before, the 77K heat sink is provided by the nitrogen stage, where the specific power is 54.2 for P_L = 1 atm, P_H = 60 atm, T_1 = 134K, T_3 = 474K and T_p = 133K. The heat sink for the nitrogen stage can be provided by a passive radiator at 133K. The total heat load on the radiator will be 4.1 W.

As shown in Fig. 7, the use of the internal heat recovery scheme reduces the heat load onto the radiator by a factor of 7. The use of the external

heat recovery scheme does not seem to greatly improve the efficiency of the overall system. Effects of additional control systems needed for the heat recovery to the multistage system design, remain to be examined.

The compressor mass calculated in the optimal design is based on a gas gap of 0.01 cm and the cylinder diameter of 1.0 cm. Suppose the gas gap is 0.1 cm instead of 0.01 cm, the mass and the cycle time will be simply 10 times those values tabulated in Table 3. If these 10 times conservative values were used to compute the two compressors for each system, then the compressor mass, the cycle time and the power for each stage are shown in Table 4. This corresponds well with some of the experimental results [11]. The mass of the J-T valve and the heat exchanger ($m_{J-T} + m_{H.E.}$) is estimated from the present miniature J-T technology; 14 gm per 40 cc (S.T.P.)/sec. gas flow [2].

Hence

$$m_{J-T} + m_{H.E.} = \frac{(14\ \text{gm})\dot{m}}{(40)\ M} \quad (22400) \tag{19}$$

where $\dot{m}$ is the mass flow rate (gm-s/W)

M is the molecular weight.

The mass of each (m_{sy}) system consisting of two compressors, the J-T valve and the heat exchanger is $2m + m_{J.T.} + m_{H.E.}$. The total power required by the three stages without heat recovery will be

$$\dot{Q}_r \left\{ \left[(S.P.)_{He} + 1\right] + \left[(S.P.)_{He} + 1\right]\left[(S.P.)_{H_2} + 1\right] + \left[(S.P.)_{He} + 1\right]\left[(S.P.)_{H_2} + 1\right]\left[(S.P.)_{N_2} + 1\right] \right\} \tag{20}$$

and total mass of the three stages is

$$\dot{Q}_r \left\{ \left(m_{sy}\right)_{He} + \left[(S.P.)_{He} + 1\right]\left(m_{sy}\right)_{H_2} + \left[(S.P.)_{He} + 1\right]\left[(S.P.)_{H_2} + 1\right]\left(m_{sy}\right)_{N_2} \right\} \tag{21}$$

For the case without heat recovery, the total heat rejected onto the radiator is 28.5 W and the total mass without the radiator is 1 K_g. However, with the internal heat recovery and the external heat recovery schemes, the heat rejected and the total mass are reduced by a factor of 7. Effects of heat recovery schemes on the multi-stage design are illustrated in Fig.7.

CONCLUSIONS

The design of gas adsorption refrigerators has been examined from the aspect of the minimum power criterion which is an important aspect, but it should not be the only one. The weight, versatility, and the interaction of the system with other spacecraft components should be considered in the merit evaluations of the design. The methodology and the functional relationships derived here, would provide the fundamental base for such merit evaluations. The weight and the power estimated for the multi-stage system seem to be manageable in spacecraft environments. From these design analyses, it is observed that gas adsorption systems could perform cooling below the 90K temperature range where radiators are ineffective, perform longer term cooling than stored cryogens, and offer better reliability and vibration-free operation in comparison to mechanical refrigerators.

ACKNOWLEDGEMENT

This paper represents one phase of research carried out at the Jet Propulsion Laboratory, California Institute of Technology, under NASA Contract NAS7-100. The author would like to thank Dr. E. Tward for his valuable suggestions and Mrs. G. McKay for her preparation of the manuscript.

QUESTIONS

Dr. H. P. Lee, NASA/GSFC

1. In your computer program, did you use empirical expressions or analytical relations for the charcoal adsorption coefficients for different media? If so, are they available?

2. How did you enter the temperature dependent thermophysics properties, such as thermal capacity, in your computation (based on what temperature to start)?

Dr. Al Sherman, NASA/GSFC

1. Have you run any system transient analyses for a space environment?

Author's Comments to Dr. Lee:

The adsorption coefficient used in the computer code was obtained from the generalized equation (eq. 3) which in turn was derived from the experimental data of References 6, 7 and 8. These references are available in the open literature.

The temperature-dependent thermophysical properties were incorporated in the computation process by averaging out the properties over the temperature swing of the complete cycle, (Reference 11).

Author's Comments to Dr. Sherman:

We have developed another program to analyze the transient behavior of the compressor. The results will be presented at the 1983 Cryogenic Engineering Conference in Colorado Springs.

Table 1. Gas Properties and Constants for Gas Conductivities and Isotherms Correlations

Gas	Helium	Hydrogen	Neon	Nitrogen
Molecular Weight (gm/g mole)	4.003	2.016	20.183	28.016
Inversion Temperature (^{o}K)	40	202	250	622
Critical Point				
Pressure, P_{cr}(ATM)	2.26	12.8	26.9	33.5
Temperature, $T_{cr}(^{o}K)$	5.2	33.3	44.5	126.2
Specific Volume, $V_{cr}\left(\frac{cm^3}{g}\right)$	14.4	32.2	2.067	3.21
Fusion Temperature K	2.17	13.9	24.57	63.
Van der Waal's Volume b (cm^3/g mole)	24	26.08	17	38.6
Parachor, 8 Cal/g mole	20.4	34.2	25.0	60.0
Constants for Thermal Conductivity Correlations				
a	0.7378	0.985	--	--
c	1.3258×10^{7}	7.81154×10^{5}	--	--
For Temperature Range	20K < T < 300K			
Constants for Isotherm Correlations Kidnay & Hiza [8]				
α	0.6722	0.40401	0.2961	0.40401
γ	0.0929	0.02870	0.0509	0.02870
	13<x<30	0<x<25	0<x<20	0<x<25
Tward et al [7]				
α	--	0.7875	0.304	--
γ	--	0.06466	0.0679	--
		12<x<50	10<x<50	

Table 2. Physical Properties of Charcoal, Stainless Steel and Copper

	Charcoal	Stainless Steel	Copper
Density, ρ gm/cc	0.466	7.82	8.94
Heat Capacity, C_p J/g - deg K			
$20^{o}K$	6.3×10^{-3}	4.6×10^{-3}	7.7×10^{-3}
$80^{o}K$	9.7×10^{-2}	1.6×10^{-1}	2.05×10^{-1}
$100^{o}K$	1.40×10^{-1}	2.4×10^{-1}	2.54×10^{-1}
$200^{o}K$	4.14×10^{-1}	4.1×10^{-1}	3.56×10^{-1}
$300^{o}K$	7.16×10^{-1}	4.8×10^{-1}	3.86×10^{-1}
$400^{o}K$	1.089		
$500^{o}K$	1.215		
Average Value J/g - deg K			
20-80K	0.045	0.0725	---
80-140K	0.166	0.267	---
140-200K	0.326	0.385	---
200-260K	0.505	0.448	---
260-300K	0.655	0.448	---
300-500K	1.03	0.532	---
Yield Strength, σ_y atm			
20K	--	4100	---
80K	--	3900	---
200K	--	2925	---
300K	--	2721	---

Table 3: Minimum Values of Specific Power, Compressor Mass for Unit Refrigeration Load and Cycle Time at Operating High Compressor Pressure P_H and Temperature T_3 for specified Precool Temperature T_p, Low Compressor Pressure P_L, and Temperature T_1

Gas	P_L atm	T_p K	T_1 K	T_3 K	P_H atm	Min Specific Power	m/Q_r g/W	t_o sec
Helium	0.68	25.5	26.6	67	20	20.	8.07	1.49
	1.00	25.5	26.5	67	20	17.7	6.91	1.49
	1.00	20	21	51	20	6.49	4.01	11.2
Neon	1.0	77	78	238	60	101.	6.54	7
	3.0	77	78	198	50	61.8	5.27	6.03
	5.0	77	78	178	40	49.7	4.87	5.2
Hydrogen	1.0	77	78	218	40	66.6	4.41	5.67
	3.0	77	78	198	40	41.3	3.31	5.45
	5.0	77	78	178	40	33.5	3.34	5.20
Nitrogen	1.0	150	151	501	70	104	1.92	9.64
	3.0	150	151	501	70	70.4	1.30	9.64
	5.0	150	151	471	70	60.7	1.26	9.34
	1.0	133	134	474	60	54.2	1.03	9.07
	3.0	133	134	474	70	39.1	0.92	9.45
	5.0	133	134	454	70	34.1	0.749	9.27

Table 4: Power, Cycle Time and System Mass for Helium, Hydrogen and Nitrogen Gas Adsorption Systems

Gas Adsorption System	Helium	Hydrogen	Nitrogen
Refrigeration Temperature, K	4	20	77
Precool Temperature, K	20	77	133
Compressor Operating Conditions			
P_L, atm	1.0	1.0	1.0
P_H, atm	20.0	40.0	60.0
T_1, K	21.0	78.0	134.0
T_3, K	51.0	218.0	474.0
Heat required (W) Per Unit Watt of Refrigeration Load	6.5	66.6	54.2
Cycle Time(s)*	110	56.7	90.7
Mass of Two (2) Compressors* (gm) Per Unit Watt of Refrigeration Load	80.02	88.2	20.3
Mass of J-T Valve and Counter Flow Heat Exchanger (gm/W)	227.4	4.31	2.54
System Mass (gm) per Watt of Refrigeration Load	307.42	92.51	32.84

* Based on δ = 0.1 cm

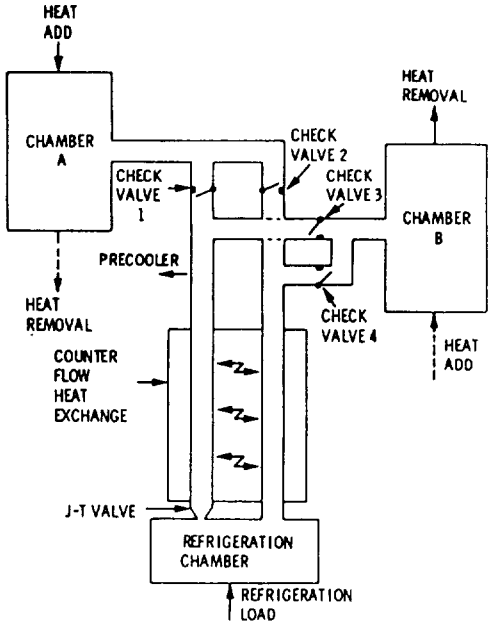

Fig. 1. Gas Adsorption Refrigeration System

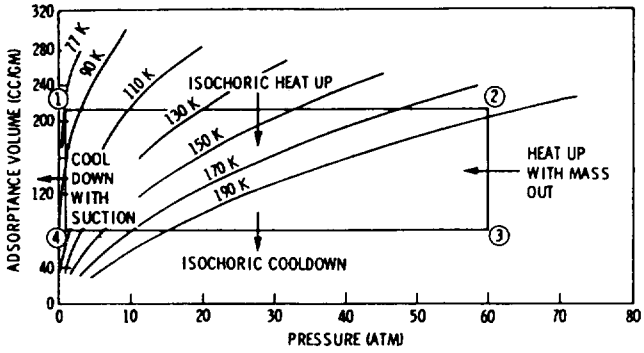

Fig. 2. Thermodynamical Cycle of Gas Adsorption and Desorption Processes for H_2

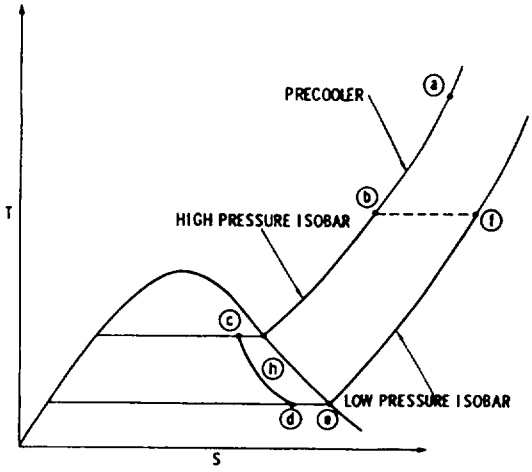

Fig. 3. Thermodynamical diagram of J-T Cooling

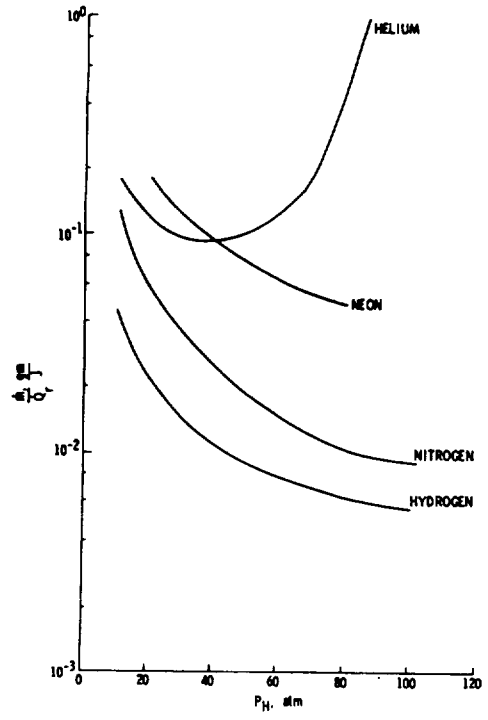

Fig. 4. Mass Flowrate for a Unit of Refrigeration Load for Four Different Gases

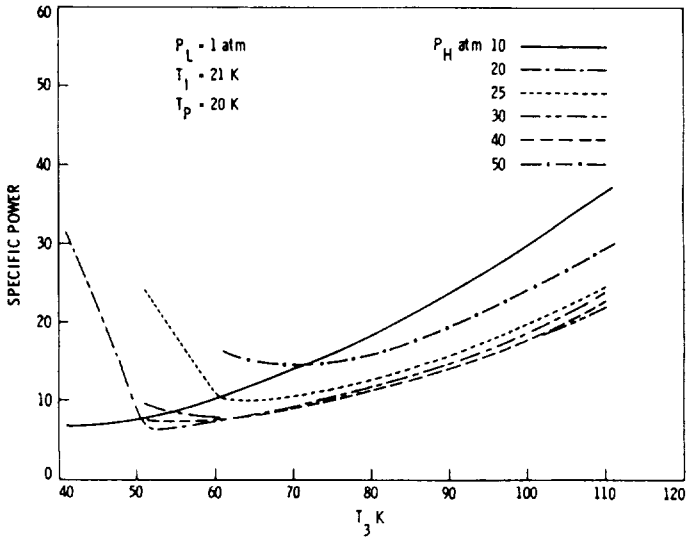

Fig. 5. Specific Power vs Maximum Compressor Temperatures for Various Nitrogen Compressor Pressures

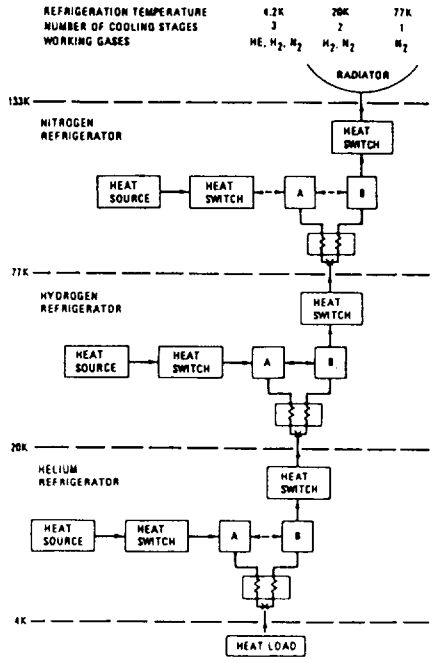

Fig. 6. Multistage Refrigerator Designs for Refrigeration Temperatures Varying from 4.2K to 77K.

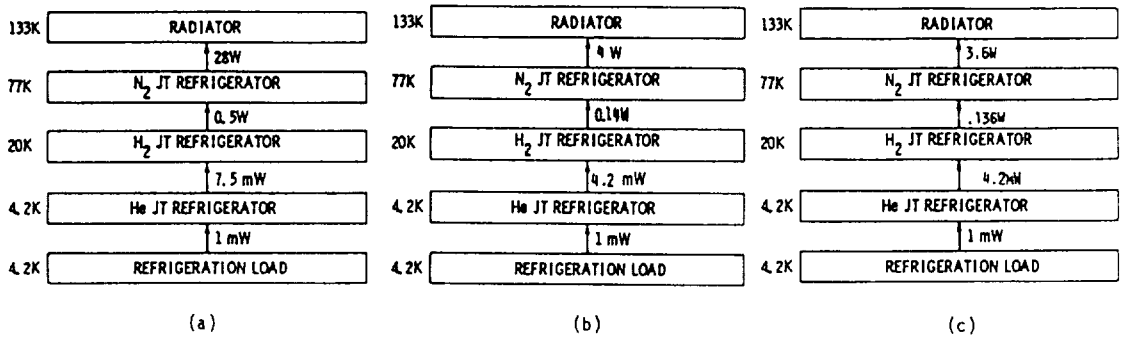

Fig. 7. Comparisons of Three Multi-stage Gas Adsorption Refrigerator Systems Performance for

(a) with no heat recovery

(b) with internal heat recovery

(c) with internal and external heat recovery

REFERENCES

1. Chan, C. K.: Cryogenic Refrigeration Using a Low Temperature Heat Source, Cryogenics, vol. 21, 1981, pp. 291-399.

2. Elleman, D. D.; Petrac, D.; Chan, C. K.;and Tward, E.: Thermal Stability and Noise of a Miniature J-T Heat Exchanger Refrigerator System, Proceedings of the 9th International Cryogenic Engineering Conf., (1982) p. 385.

3. Chan, C. K.; Tward, E.; and Elleman, D. D.: Miniature J-T Refrigerators Using Adsorption Compressors. Advances in Cryogenic Engineering, vol. 27, 1981, pp. 735-743.

4. Tward, E.: Gas Heat Switches. Refrigeration for Cryogenic Sensors and Electronic Systems, NBS Special Publication 607, 1981, pp. 178-185.

5. Kidnay, A. J.; and Hiza, M. J.: Physical Adsorption in Cryogenic Engineering. Cryogenics, vol. 10, 1970, pp. 271-276.

6. Yang, L. C.; Vo, T. D.; and Buriss, H. H.: Nitrogen Adsorption Isotherms in Zeolite and Activated Carbon, vol. 22, 1982, pp. 625-634.

7. Tward, E.; Marcus, C.; Chan, C. K.; Gatewood, J.; Steyert, W. A.; and Elleman, D. D.: High Pressure Adsorption Isotherms of H_2 and Neon on Charcoal, Proceedings of the 9th International Cryogenic Engineering Conf., (1982) p. 34.

8. Kidnay, A. J.; and Hiza, M. J.: High Pressure Adsorption Isotherms of Neon, Hydrogen and Helium at 76^{o}K. Advances in Cryogenic Engineering, vol. 12, 1966, pp. 730-740.

9. Cook, W. H.; and Basmadjian, D.: Correlation of Adsorption Equilibria of Pure Gases on Activated Carbon. Canadian J. of Chem. Eng., vol. 42, 1964, p. 146.

10. Tward, E.: (private communication)

11. Chan, C. K.; Tward, E.; Elleman, D. D.: Kinetics of Gas Adsorption Compressor, Accepted for oral presentation at Cryogenic Engineering Conference, August 15-19, 1983, Colorado Springs, CO.

A GENERAL COMPUTER MODEL FOR PREDICTING THE PERFORMANCE OF GAS SORPTION REFRIGERATORS*

Katherine B. Sigurdson
Jet Propulsion Laboratory
California Institute of Technology

ABSTRACT

Projected performance requirements for cryogenic spacecraft sensor cooling systems demand higher reliability and longer lifetimes than the state-of-the-art provides. The gas/solid sorption refrigerator is viewed as a potential solution to these cryogenic cooling needs. A generalized analytical software model of an entire gas sorption refrigerator system has been developed. The numerical model, generated from a systems point of view, is flexible enough to evaluate almost any combination and order of refrigerator components and any sorbent-sorbate pair for which the sorption isotherm data are available. Parametric curves for predicting system performance were generated for two types of refrigerators, a $LaNi_5$-H_2 absorption cooler and a Charcoal-N_2 adsorption cooler. It was found that precooling temperature and heat exchanger effectiveness affect the refrigerator performance significantly. Examination of the results indicates that gas sorption refrigerators are feasible for a number of space applications.

INTRODUCTION

Projected performance requirements for cryogenic sensor cooling systems demand higher reliability and longer lifetimes than the state-of-the-art can provide. A Joule-Thomson cryostat driven by a gas/solid sorption compressor, the "gas sorption refrigerator", is a potential solution. In support of the sorption refrigerator research program at JPL, a software analytical model of a general gas sorption refrigerator system has been developed. The numerical model was used to examine the relationships between heat exchanger effectiveness, cycle times, precooling temperature, total cooling power, system mass, and input power requirements. Two cases, a 30 K $LaNi_5$-H_2 absorption cooler and a 91 K Charcoal-N_2 adsorption cooler, with maximum compressor pressures of 40 and 60 bar, respectively, are presented here.

*The research described in this paper was carried out by the Jet Propulsion Laboratory, California Institute of Technology under contract with the National Aeronautics and Space Administration.

NOMENCLATURE

c	gas to sorbent concentration ratio
COP	coefficient of performance
C_p	specific heat
C_{p_c}	specific heat, compressor case
C_{p_m}	specific heat, metal foam
C_{p_s}	specific heat, sorbent
d	inside diameter of compressor
d_{JT}	J-T valve diameter
f_o	sorbent packing factor
f_{micro}	volume fraction of solid sorbent per particle
f_{solid}	volume fraction of micropores per particle
h	heat transfer coefficient
h_{co}	enthalpy, heat exchanger cold side outlet
h_{hi}	gas enthalpy, heat exchanger hot side inlet
H^o	isosteric heat of adsorption/absorption
k	thermal conductivity
K	ratio of gas specific heats
L	length
$\dot{m}$	gas mass flow rate
m	mass
m_c	mass, compressor case
m_g	mass, gas
m_m	mass, metal foam
m_s	mass, sorbent
M	gas molecular weight
NTU	number of transfer units, heat exchanger
P	maximum pressure in compressor
P_{ho}	pressure, heat exchanger hot side outlet
Pr	Prandtl Number
Q_{ij}	heat input from point i to j in compressor
$\dot{Q}_L$	cooling power
$\dot{Q}_{heat}$	time averaged input power, total compressor
R	universal gas constant
Re	Reynolds Number
t_{ij}	time from point i to j in compressor cycle
Δt_{sorp}	desorption time in compressor cycle
T_{ci}	temperature, heat exchanger cold side inlet
T_{co}	temperature, heat exchanger cold side outlet
T_{hi}	temperature, heat exchanger hot side inlet
V	volume
x	volume percent of metal foam in compressor
η	heat exchanger effectiveness
ρ_g	mass density of gas
ρ_s	mass density of sorbent
σ_y	maximum yield strength of compressor metal

GAS SORPTION REFRIGERATOR SYSTEMS

The basic components of a gas sorption refrigerator are the gas sorption compressor, a precooling radiator, a counterflow heat exchanger, and a J-T expansion valve. A typical block diagram is shown in Figure 1. The gas sorption compressor is a non-mechanical compressor which utilizes the phenomenon of gas absorption or adsorption to pressurize the gas. The sorbent material in the compressor absorbs/adsorbs the gas in large quantities when cooled at low pressure and desorbs the gas at higher temperatures and pressures when heated. The flow through the compressor is controlled with self-operating check valves. The high pressure gas from the compressor is precooled below the inversion temperature upon passing through the radiator and is further cooled in the counter-flow heat exchanger in the J-T cryostat before being isenthalpically expanded through the J-T valve. The heat load is absorbed upon evaporation of the condensate.

NUMERICAL MODEL APPROACH

A previous numerical model (ref. 1) evaluated one refrigerator system design with a $LaNi_5$-H_2 absorption compressor. The current, modified version has the capability to evaluate a wide range of combinations and orders of refrigerator components and any sorbent-sorbate pair, for which the data are available, in the compressor. Generated from a systems point of view, the model is a steady-state program that evaluates the characteristics of each refrigerator component from the state properties of the working fluid at the corresponding nodes. The program evaluates the component masses and pressure drops; the required fluid mass flow rate; the required J-T valve diameter; and the gas to sorbent concentration ratios, temperatures, and pressures in the compressor based upon the input refrigerator performance requirements and constraints. The program starts by evaluating the J-T cryostat and then proceeds to evaluate the remaining components in an order opposite to the gas flow. The $LaNi_5$-H_2 cooler schematic, Figure 1, illustrates the node numbering scheme and component order. The Charcoal-N_2 cooler is similar but with only one radiator and no intermediate heat exchanger. All the temperatures and pressures throughout the system are found and any required gas properties such as enthalpy and thermal conductivity are evaluated through a gas properties look-up code (ref. 2). Currently the capability of the model is restricted to one fluid loop with one J-T cryostat and only data for Charcoal-N_2 adsorption (ref. 3) and $LaNi_5$-H_2 absorption (ref. 4) have been entered into the program.

J-T CRYOSTAT

The J-T cryostat is a combination of a counterflow heat exchanger, a J-T

expansion valve, and an evaporator. The required fluid mass flow rate through the system is found from the given cooling heat load and the change in enthalpy through the J-T cryostat. The change in enthalpy is a function of the precooling temperature, T_{hi}, and the heat exchanger effectiveness, η. The heat exchanger cold side outlet temperature is found from the precooling temperature, the cooling temperature, and the effectiveness

$$T_{co} = (T_{hi}-T_{ci})\eta + T_{ci} \tag{1}$$

$$\dot{m} = \dot{Q}_L/(h_{co}-h_{hi}) \tag{2}$$

The maximum JT valve diameter is found as a function of the mass flow rate and the gas properties, assuming choked isentropic expansion:

$$d_{JT} = 2\left[\frac{\dot{m}}{\pi P_{ho}}\right]^{.5}\left[\frac{T_{ho}R}{MK}\left(\frac{K+1}{2}\right)\left(\frac{K+1}{K-1}\right)\right]^{.25} \tag{3}$$

The mass of the J-T cryostat is assumed to be the mass of the counter-flow heat exchanger because the mass of the J-T valve is negligible in comparison. The masses of the refrigerator components tend to increase linearly with fluid mass flow rate, therefore the system mass increases nearly linearly with the cooling load. Consequently, minimizing the fluid mass flow rate will tend to optimize the coefficient of performance, COP, and minimize the system mass.

COUNTERFLOW HEAT EXCHANGER

The hot and cold inlet temperatures of the heat exchanger are determined by the adjacent components in the system. The hot and cold outlet temperatures are determined from the heat exchanger effectiveness and an energy balance across the heat exchanger. The required length of the heat exchanger is determined as a function of the number of transfer units, NTU, and the heat transfer coefficient, h,

$$L = \frac{NTU\ \dot{m}\ Cp}{\pi dh} \tag{4}$$

The mass of the exchanger is determined from the passage size, the required wall thickness, and the required length. As the effectiveness increases, the change in enthalpy through the cryostat increases, decreasing the fluid mass flow rate. As the masses of the system components are all dependent upon this mass flow rate, the total system mass is reduced as the heat exchanger effectiveness increases, as shown in Figure 2. Also the COP is

improved as the effectiveness is increased due to the reduce mass of the compressor.

SPACE RADIATOR

The compressor heat rejection component and the gas precooling component are both passive space radiators. Assuming a constant heat load, an estimate of the radiator masses was made by based on the equations developed for JPL's advaced radiator (ref. 5,6). The COP is shown as a function of the precooling temperature in Figure 3 for a 30 K $LaNi_5$-H_2 system and a 91 K C-N_2 system. Reducing the precooling temperature increases the change in enthalpy across the JT valve thus reducing the required fluid mass flow rate to heat load ratio and improving the COP. As the mass of the entire system is nearly linearly dependent upon the fluid mass flow rate, the refrigerator system mass also decreases with the precooling temperature, Figure 4.

SORPTION COMPRESSOR

The gas sorption compressor is made up of a set of compressor sub-units cycled sequentially to supply an essentially continuous stream of high pressure gas to the J-T valve. The inlet and outlet pressures and temperatures are determined by the adjacent components in the refrigerator. The compressor cycle consists of a heating phase and a cooling phase. Each phase is assumed to be made up of a constant gas concentration pressure change and an isobaric gas concentration change, thus there are four states in the idealized compressor cycle. Consequently, the pressures, temperatures and concentration ratios can be found at all points in the idealized cycle from the sorption isotherms and the compressor inlet and outlet conditions. The required mass of sorbent is directly related to the fluid mass flow rate, the desorption time, the gas concentration change in the compressor, and the void volume in the lines

$$m_s = (\dot{m}/\Delta c)\Delta t_{sorp} \tag{5}$$

The void volume, or dead volume, increases the required sorbent mass as additional sorbent is required to pressurize this volume as well as the gas that is being passed through the compressor. At higher pressures and temperatures, this effect becomes predominant and the refrigerator efficiency degrades.

The heat transfer within each compressor unit is enhanced with a copper foam. Thus the components of the compressor unit are the sorbent, the metal

foam, and the pressure case. The total volume is a function of the sorbent packing factor, the volume percent of metal foam, and the case thickness. The heat input between any two points i and j in the compressor cycle is the sensible heat transfer to the sorbent, metal foam, compressor case, and gas, and the isosteric heat of adsorption/absorption

$$Q_{ij} = (mCp)(T_j - T_i) + m_s(c_j - c_i)H^o + m_g(h_j - h_i)_g \quad (6)$$

$$mCp = Cp_m m_m + Cp_c m_c + Cp_s m_s \quad (7)$$

The coefficient of performance is determined from the calculated total heat rejection requirement and the cooling heat load

$$COP = \dot{Q}_L / \dot{Q}_{heat} \quad (8)$$

The coefficient of performance is a strong function of precooling temperature, as shown in Figure 3. This is expected as the mass of the compressor decreases nearly linearly with fluid mass flow rate which is reduced by lowering the precooling temperature. It was found that by staging the compressor for the Charcoal-N_2 system, illustrated in Figure 5, the COP can be improved somewhat at intermediate to high precooling temperatures, Figure 3. However, at low precooling temperatures a cross-over occurs and the single stage C-N_2 system becomes superior to the two-stage C-N_2 system, Figure 4.

The system masses shown include the estimate masses of the supports, insulation, and the compressor heat addition-rejection component. Using Table 1, the masses of each system without these extras can be deduced.

CONCLUSIONS

A numerical model has been developed and is available to size and evaluate gas sorption refrigeration systems for spacecraft applications. Two refrigerator types, $LaNi_5$-H_2 and Charcoal-N_2, have been studied to demonstrate the versatility of the model. It was found that the heat exchanger effectiveness and the precooling temperature have significant effects on the predicted refrigerator performance. It was also determined that staging the compressor with an intermediate radiator improves the performance of the Charcoal-N_2 adsorption refrigerator at higher precooling temperatures. Further studies need to be completed with different adsorption systems in order to characterize the effect of staging the compressor.

Although the COP's of the systems presented here are somewhat non-competitive with conventional mechanical refrigerators, the non-mechanical aspect of the sorption refrigerator makes the sorption refrigerator more attractive for long-life applications when excess waste heat is available.

Table 1

Component Mass Fraction (in percent) at Constant Precooling Temperature
1 Watt Heat Load

Component	Precooling Temperature 80 K	100 K	120 K
$LaNi_5$-H_2 Refrigerator:			
Compressor	3.9	5.7	6.5
Compressor heat add/rej component	41.0	60.2	68.4
High temperature radiator	2.2	3.3	3.8
Heat exchanger	1.0	3.3	5.2
Precooling radiator	42.1	19.5	9.0
JT cryostat	0.1	0.1	0.5
Support, plumbing, insulation, etc.*	10.0	10.0	10.0
	150 K	200 K	250 K
C-N_2 Refrigerator (2-Stage Compressor):			
Compressors	0.2	0.8	2.8
Intermediate radiator	5.8	3.1	0.9
Compressor heat add/rej component	78.5	83.7	86.3
Precooling radiator	6.5	3.3	0.9
JT Cryostat	-	-	-
Support, plumbing, insulation, etc.*	10.0	10.0	10.0

* assumed constant mass fraction of 0.1

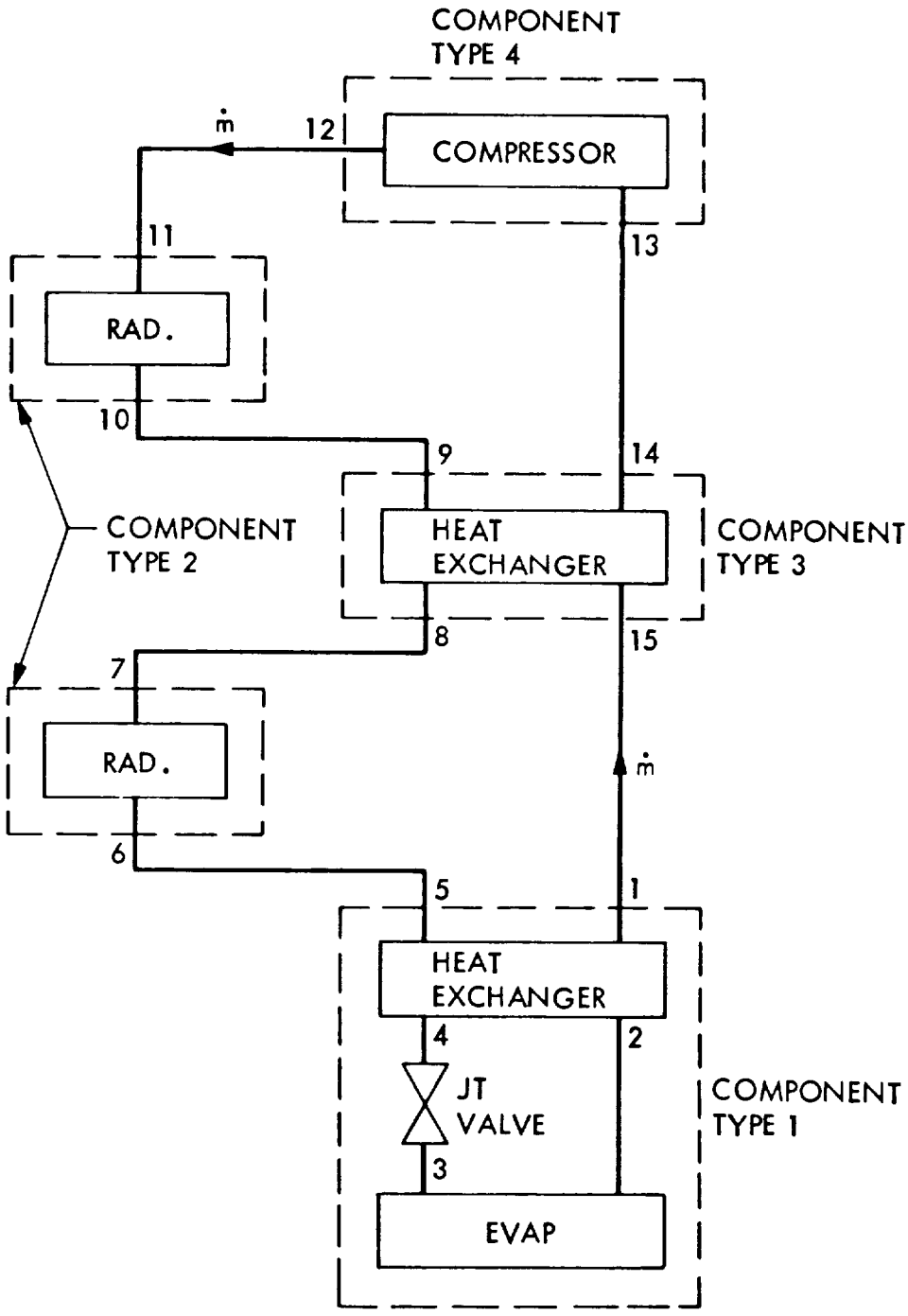

Figure 1. $LaNi_5$-H_2 System Block Diagram

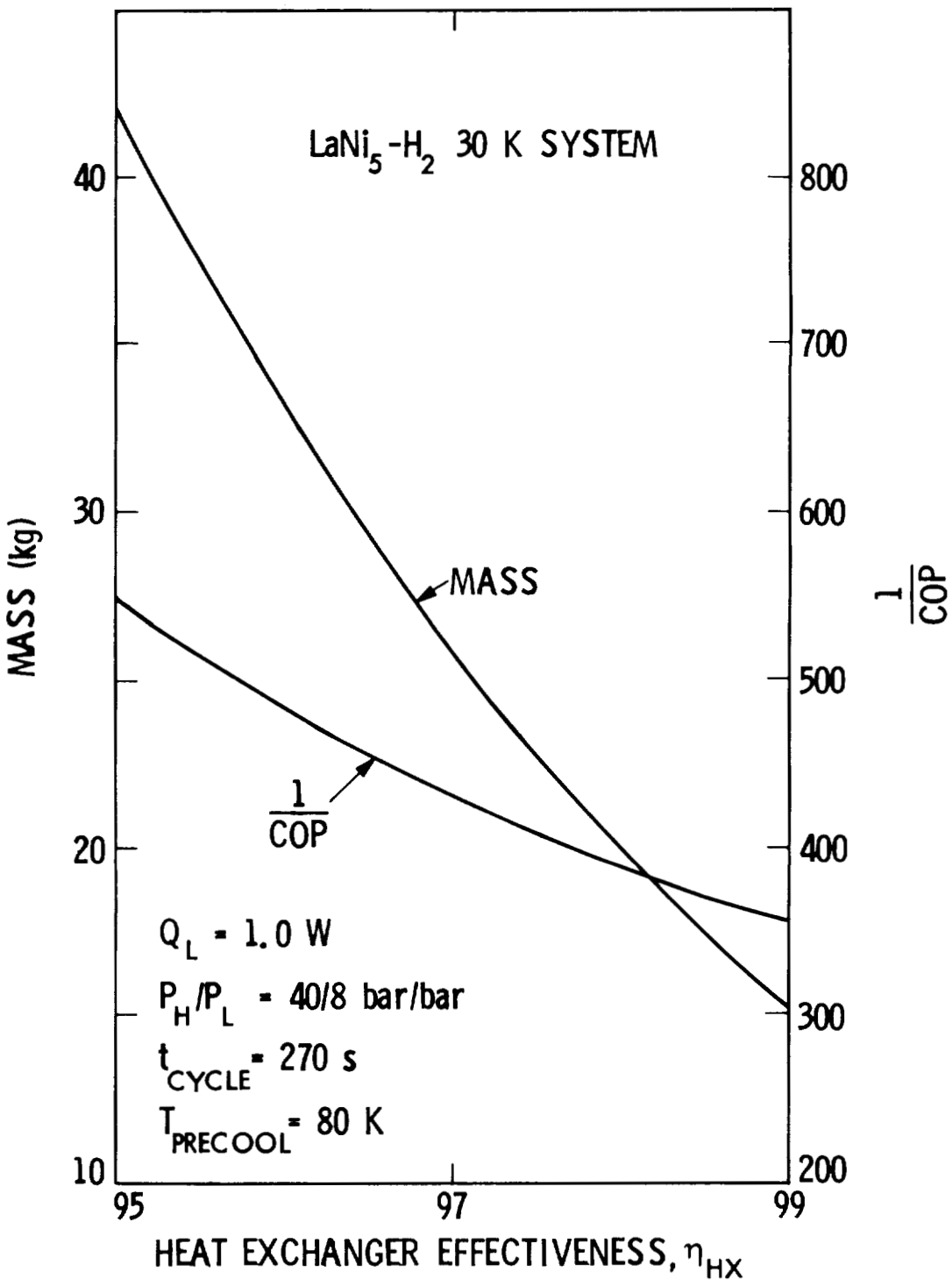

Figure 2. System Mass and COP versus Heat Exchanger Effectiveness

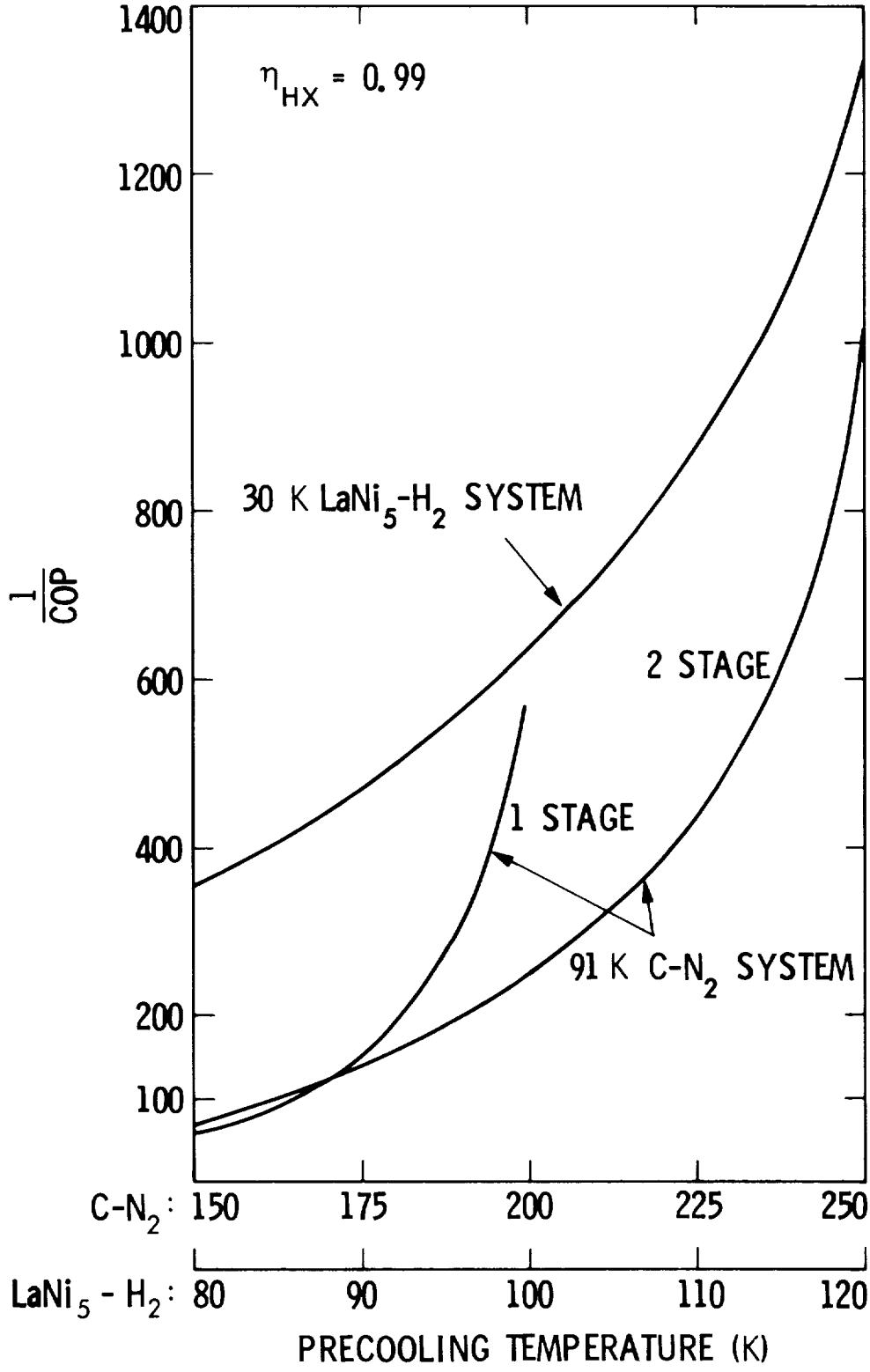

Figure 3. COP versus Precooling Temperature

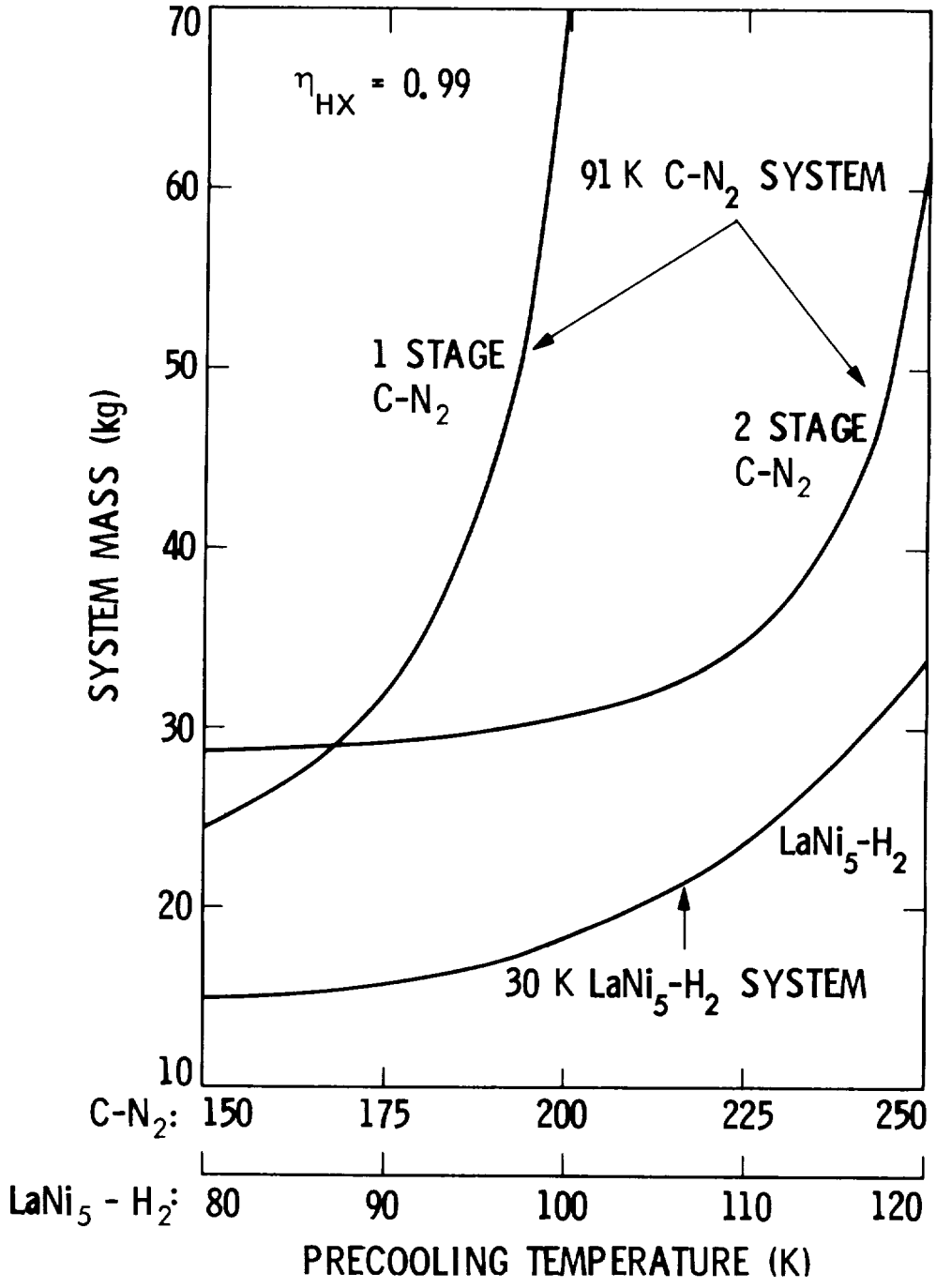

Figure 4. System Mass versus Precooling Temperature

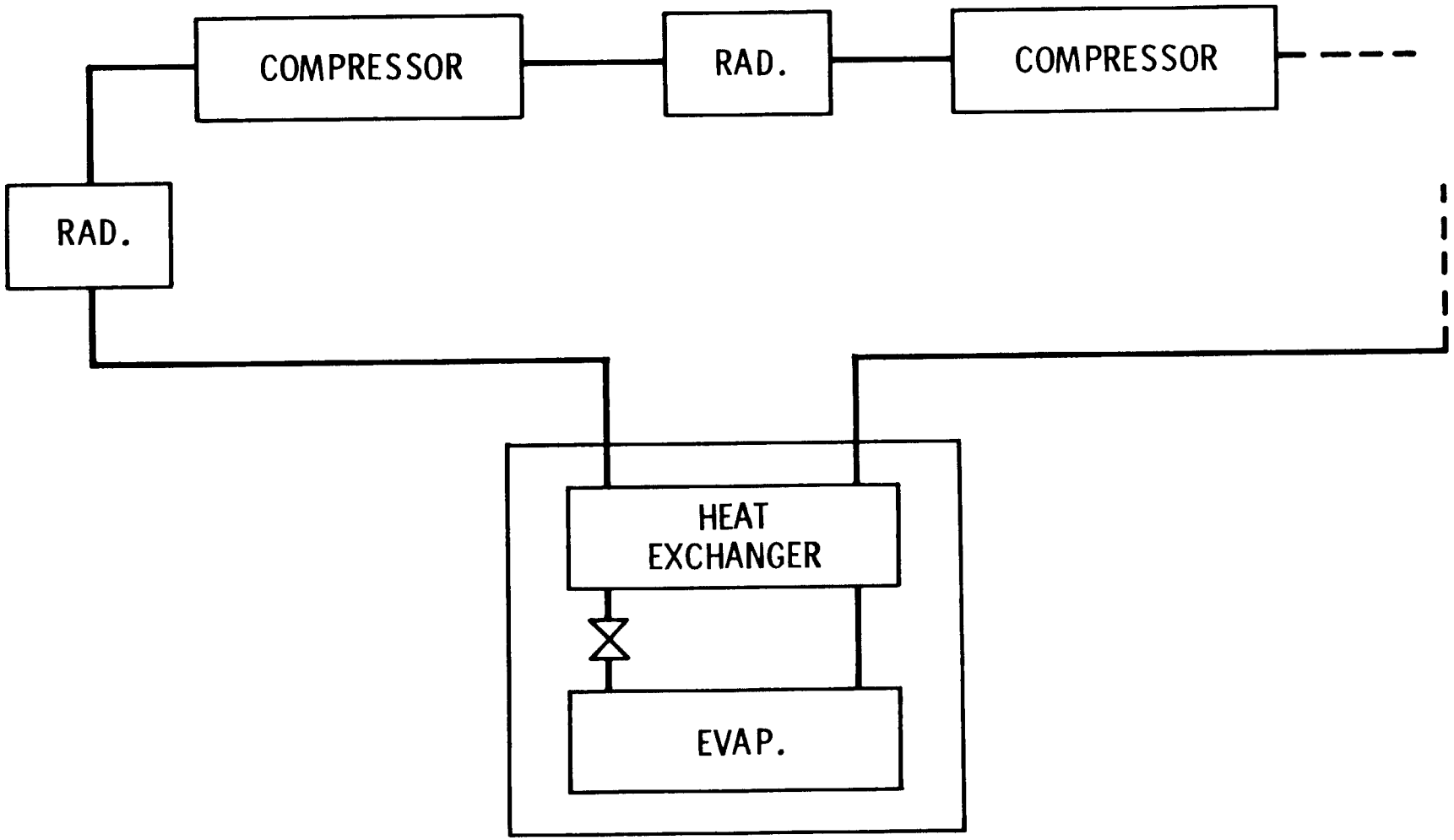

Figure 5. Schematic of Staged Compressors with Intermediate Cooling.

REFERENCES

1. Klein, G. A., Jones, J. A.: Molecular Absorption Cryogenic Cooler for Liquid Hydrogen Propulsion Systems. Paper # AIAA-82-0830, AIAA/ASME 3rd Joint Thermophysics, Fluids, Plasma and Heat Transfer Conference, June 7-11, 1982, St. Louis, Missouri.

2. McCarty, R.: Interactive Fortran For Computer Programs for the Thermodynamic and Transport Properties of Selected Cryogens. NBS Technical Note 1025, 1980.

3. Yang, L. C., Yo, T. D., Burris, H. H.: Nitrogen Adsorption Isotherms in Zeolite and Activated Carbon. Cryogenics, Vol. 22, No. 12, December 1982, pp 625-634.

4. Jones, J. A.: $LaNi_5$ Hydride Cryogenic Refrigerator Test Results. Second Biennial Conference on Refrigeration for Cryogenic Sensors and Electronic Systems, NASA CP - , 19 . (Paper of this compilation.)

5. Bard, S.: Development of an Advanced Passive Radiator for Cryogenic Cooling of Spaceborne Instruments. AIAA Journal of Spacecraft and Rockets, in press, 1983.

6. Bard, S., Stein, J., Petrick, S. W.: Advanced Radiative Cooler with Angled Shields. Spacecraft Radiative Transfer and Temperature Control, Vol. 83, Progress in Astronautics and Aeronautics, 1982.

$LaNi_5$ HYDRIDE CRYOGENIC REFRIGERATOR TEST RESULTS

Jack A. Jones
Jet Propulsion Laboratory/California Institute of Technology

ABSTRACT

A complete $LaNi_5$ hydrogen absorption cryogenic refrigerator system has been developed and life tested for 300 continuous hours at 29 K. The system uses low temperature waste heat of approximately 100°C (373 K) as a power source, and has no moving parts other than self-operating valves. The refrigerator's three alternately cycled compressors provide approximately 650 mW of cooling for a given average waste heat power of 250 watts. The total weight of $LaNi_5$ in all three compressors is 288 gms. The $LaNi_5$ compressor units operate by absorbing 16 standard liters each of hydrogen gas at room temperature and low pressure. When heated to 100°C (373 K), most of the hydrogen gas is liberated at 40 atmosphere pressure and is driven through a standard heat exchanger - Joule Thomson expansion valve cooling loop until cooled to liquid hydrogen saturation temperatures (20 K at 1 atmosphere or 29 K at 6 atmosphere pressure). The returning hydrogen is then absorbed back into the water-cooled $LaNi_5$ compressor units. The cycle continues automatically by means of an electronic sequencing timing mechanism which provides 3 minutes of heating and 3 minutes of cooling to each of the three compressors which are phased such that a constant supply of high pressure hydrogen gas is provided.

Although some contamination due to impure hydrogen was initially experienced, the first life test (June, 1983) exceeded 300 hours of continuous operation, and longer periods are expected in the future. Recent research has indicated that with a fully clean hydrogen system, hundreds of thousand cycles should be attainable, even though some degradation may eventually occur. Simple vacuum reactivation of the hydride can be performed if contamination effects are experienced. Due to the lack of moving parts, other than self-operating, long-life valves, the refrigerators predicted life is extremely long, and, in fact, should potentially attain at least 10 years of continuous operation.

INTRODUCTION

This paper describes the results of preliminary testing performed on the hydride compressor for the Molecular Absorption Cryogenic Cooler (MACC). As explained in References 1 and 2, the overall purpose of the MACC compressor

is to pump gaseous hydrogen at high pressure through a series of heat exchangers and a Joule-Thomson (J-T) valve such that the net cooling effect due to expansion of the gas at the J-T valve lowers the hydrogen temperature to its liquefaction point (20 K at one atmosphere pressure).

The basic theory of the compressor operation relies on the fact that the intermetallic compound $LaNi_5$ absorbs about six atoms of hydrogen per unit formula at an equilibrium pressure of a few atmospheres at room temperature. The density of the absorbed hydrogen at room temperature is almost twice the density of free liquid hydrogen at cryogenic temperatures. The equilibrium pressure of the absorbed hydrogen is a very strong function of temperature, and thus the hydrogen static pressure can be increased from 4 atmospheres at $40^{o}C$ to about 60 atmospheres at $120^{o}C$ (393 K).

The basic advantages of this type of system are that it provides considerably lower temperatures (as low as 20 K) than those from passive radiator systems (approximately 80 K), and yet it still has no mechanical moving parts, other than self-operating check valves (Figure 1). It is much simpler and has a much longer life expectancy than present orbiting mechanical refrigeration systems, and it can be operated using low temperature waste heat, e.g., RTG waste heat, or direct solar heat.

In the example shown in Figure 2, $LaNi_5$ sorption compressors are heated by a black plate facing the sun, and they are cooled by a room temperature space radiator. Switching between heating and cooling is provided by thermal gap switches which are alternately filled with a conductive gas for conduction, and then evacuated for non-conduction. A two phase lithium canister (not shown) on the black solar heating plate allows for solar heat retention while in the shady portion of a low earth orbit. The particular system shown is for cooling large liquid hydrogen refueling tanks for NASA's future Space Station, and includes a $120^{o}K$ low earth orbit directional advanced radiator. The radiator, or some first stage refrigeration device, is necessary to insure an overall good coefficient of performance. Because hydride refrigeration can use heat from lightweight solar heating plates or waste heat from radioisotope thermal generators (RTGs) instead of electricity from heavier solar electric power systems, the overall spacecraft system weight is significantly lighter than for any other $20^{o}K$ refrigeration system (Reference 3).

HARDWARE

An overview photograph of the tri-compressor refrigerator test breadboard system is shown in Figure 3 and schematically in Figure 4. The control panel is visible in the far right position of Figure 3 and is

adjacent to the three compressors. The Joule-Thomson/heat exchanger assembly is contained in the one gallon silvered dewar, while the rest of the lines on the board are plumbing interfaces. Each of these portions of hardware is described in detail below.

COMPRESSORS

A sketch of a single hydride compressor appears in Figure 5. The primary consideration in the design of this compressor is to add and remove heat as quickly as possible in order to produce the highest possible hydrogen flow rate for a given mass of hydride. A MINCO resistance heater is bonded to theoutside of the 5/8" stainless steel tube. Using the heater manufacturer's suggested bonding method (RTV) resulted in a detached heater after a number of cycles, possibly due to high thermal shock stresses. Application of Epoxy 2850/11 with catalyst #11, however, has proven much more successful after repeated thermal cycling.

The heat is transferred into the low-conductivity powder by means of a close fitting cylinder of high purity copper foam that is placed inside the tube. During the cooling cycle, the heater power is turned off, and water is pumped through the annulus between the water housing and the compressor tube. In order to keep the very fine $LaNi_5$ powder from leaving the compressor tube and contaminating the system plumbing, a fine porous sintered stainless steel filter (2 micron nominal pore size) is inserted inside the compressor. The potential problem of long term filer clogging does not occur, as the hydrogen flows both ways through the filter.

PLUMBING

As shown in Figure 4, the plumbing interface consists of all lines, and valves as well as the holding tank, and hydrogen reservoirs. As the high pressure hydrogen leaves any of the heated compressors, it is directed to a common line by means of the indicated check valves. This high pressure hydrogen is then stored in a "holding tank" which is attached to the Joule-Thomson (J-T) cryostat assembly. Thus, the J-T assembly is supplied with a continuous flow of high pressure hydrogen. The pressure-activated solenoid valve is set at a very high pressure (850 psi) and is used as a safety in case the J-T valve fails.

After the hydrogen passes through the J-T assembly (described in next section), it is at a low pressure (typically about 6 atmospheres for this operation) and is then absorbed by a cooled compressor. The one gallon

reservoir is used to even out any small pressure pulses due to the somewhat non-uniform, hydrogen flow.

It should be noted that the relatively large surface area of the plumbing system upstream of the J-T assembly allows the hydrogen gas to cool from about $110^{o}C$ (383 K) to room temperature by simple natural convection cooling.

JOULE-THOMSON ASSEMBLY

A schematic of the Joule-Thomson cryostat assembly appears in Figure 6. Room-temperature hydrogen gas enters a two meter long 1/16" counterflow coiled heat exchanger and is lowered to about 80 K at the cold exit. The heat exchanger coils are surrounded by closed cell insulation to minimize parasitic heat leaks. The hydrogen is cooled to about 77 K when it passes through an additional one meter section of 1/16" heat exchanger loops that are submerged in the LN_2. It is necessary to insure that the hydrogen temperature is below its inversion temperature of 202 K in order for the J-T expansion to result in a net cooling.

For actual deep space operation, the 77K LN_2 bath heat exchanger submersion would be replaced by a cold space radiator below the hydrogen inversion temperature of $202^{o}K$. The lower the radiator temperature, the better the hydride refrigerator's coefficient of performance (References 1 and 3). As an alternative, a first stage refrigerator system could be used instead of the LN_2 bath. For sizing purposes, approximately one watt of heat must be removed by the first stage refrigerator, for every watt of heat removed at $20^{o}K$ by the hydride refrigerator.

The heat exchanger coils then enter into a high vacuum container that is also submerged in the LN_2. An additional two meter counterflow heat exchanger length allows the GH_2 to cool to slightly above its boiling temperature. Expansion through the J-T valve, which is actually a modified adjustable flow-through check valve (Figure 7), drops the 40 atmosphere pressure to about 6 atmospheres and causes partial liquefaction of the hydrogen. A small chamber collects the LH_2, which can be boiled to provide constant temperature cooling at 29 K or lower if lower GH_2 pressures are used. The returning hydrogen gas then precools the entering hydrogen gas.

CONTROL PANEL

The control panel (barely visible on the right side of the Figure 3 photograph) has an electrical timing mechanism that allows each compressor

to be heated for three minutes and cooled for three minutes. The compressors are phased such that they provide a nearly uniform flow of hydrogen gas through the system. At present, all switches and relays are high-lifetime mechanical types, although even longer life, lightweight solid state electrical devices would be used for spacecraft operation. For the breadboard design, a mechanical override system exists independent of each automatically timed operation, so that independent tests could be made and controlled for each compressor.

TEST RESULTS

HYDRIDE ACTIVATION

Before actually building a test set-up, it was necessary to "activate" the $LaNi_5$ so that it would absorb and desorb hydrogen in the proper manner. As received from the manufacturer, Ergenics, the $LaNi_5$ is in the form of 1/4 inch chunks and has little hydrogen absorbing properties. In order to be broken down into a fine powder so that large quantities of hydrogen can be absorbed, it was necessary to cycle the powder several times between high pressure hydrogen (200 psi) and a near vacuum, allowing at least two hours for each portion of the cycle.

Each compressor contains 96 grams of $LaNi_5$ and was found to absorb 16 liters of hydrogen gas. This translates to approximately 6 atoms of hydrogen being absorbed onto each molecule of $LaNi_5$, as previously reported in the literature (Reference 2).

ISOTHERM DATA

In this portion of the testing it is desired to obtain the temperature-pressure relationships for various concentration levels of hydrogen in the powder. This information is necessary for further compressor performance sizing and for comparison to previous results (Reference 2). After the compressor had absorbed as much hydrogen as possible at the cooling water temperature of 21°C (294 K), its heater was activated at low power (37.5 watts) and the pressure regulator on the board (Figure 4) was set open, i.e., no hydrogen-gas was allowed to flow back to the reservoir. Core temperature versus line pressure measurements were then made for increasing core temperature readings. At 100°C (373 K), the estimated pressure was just over 40 atmospheres, while lower temperatures resulted in much lower pressures. Following this, about 4 standard liters of hydrogen-gas were allowed to flow back into the hydrogen reservoir and the hydrogen supply

valve (Figure 4) was closed. Similar T versus P measurements were made on the remaining gas in the compressor, which was then at a density of about 4.5 atoms of hydrogen per molecule of $LaNi_5$.

Similar measurements were then made for other hydrogen concentrations and the results are plotted in Figure 8. The JPL data showed somewhat higher pressure readings for any given temperature and hydrogen concentration than those published by Van Mal et al (Reference 2). A partial explanation of this may be due to slight variations in the La/Ni ratio of the absorbent.

The indicated boxed cycle in Figure 8 is an actual typical operating cycle of the powder. The horizontal lower line represents a three minute cooldown, during which the hydrogen heat of absorption is removed. This is followed by a 40 second heating temperature rise during which no hydrogen gas is pumped. Next, a 100 second heating outgassing occurs during which the hydride temperature increases only slightly, while high pressure hydrogen gas is driven off the hydride powder. The left-side pressure-temperature drop corresponds to the short time when the hydrogen gas traverses the J-T-heat exchanger assembly.

OPEN CYCLE OPERATION

In the preliminary open-cycle operation tests, the hydrogen exhaust gas was allowed to exit the system to an outdoor vent. The system was rapidly prechilled to about 30 K by supplying a high flow of 40 atmosphere GH_2 to the J-T valve from a K-Bottle of supplied hydrogen. The K-Bottle source pressure was then reduced, and a slight temperature decrease was noted, presumably due to a lowering of the back pressure with corresponding reduced saturated vapor temperature. The pressure was continuously reduced until a slight temperature rise was noted. At this point, the parasitic heat loads became slightly larger than the available cooling load, and net heating resulted.

The minimum upstream supply pressure required to maintain 20 K was thus found to be approximately 9.5 atm absolute with a resulting flow rate of approximately 100 scc/sec. The corresponding calculated heat load is 150 mW, assuming a highly efficient heat exchanger. The net cooling load is calculated as the mass flow rate times the difference between the cold heat exchanger inlet and outlet enthalpies, as further explained in Reference 5.

CLOSED CYCLE OPERATION

After each of the compressors had been confirmed to achieve their expected performance, the entire system was operated in a closed cycle mode. The J-T assembly was precooled for two hours with a small GN_2 internal pressure to aid in its convective cooldown time from room temperature. A full internal vacuum (10^{-5} Torr) was then drawn inside the J-T chamber and the three compressor system was activated. The net average flow rate of hydrogen gas was measured to be approximately 100 scc/sec with a pressure drop from approximately 39 atmospheres to 6 atmospheres. The flow rate was measured by means of measuring the pressure rise in the one gallon reservoir (Figure 4) during separate heating cycles. The J-T temperature finally reached approximately 30 K in about an hour and remained below 30K for the following 300 hours. Although two of the check valve rubber seats failed (metal seats have since been installed), the compressors showed no measureable degradation even after 300 hours of continuous operation. With a predicted life of at least one million cycles at room temperature, the new metal seat check valves should last at least 10 years.

It should be mentioned that recent research by Cohen and Wernick (Reference 4) has indicated that for very clean systems, intrinsic degradation of the $LaNi_5$ powder below 100°C should not be significant unless hundreds of thousands of cycles are attained. Furthermore, the $LaNi_5$ powder is readily reactivated, even after severe contamination. Further research by Goodell (Reference 5) has shown that although 300 psi pressure cycling results in some measurable degradation after 1500 cycles, the exponential limit of degradation even after hundreds of thousands of cycles, appears to be only about 50%. Goodell has also found that other hydride compounds such as $LaNi_{4.7}Al_{0.3}$ apparently have no measurable degradation after thousands of cycles (Reference 5).

SUMMARY AND CONCLUSIONS

A $LaNi_5$ hydride absorption cryogenic refrigerator has been built, and preliminary testing to 20 K open cycle and 29 K closed cycle has been performed. The refrigerator compressors consist of three units which are cooled by water and heated by electrical resistance heaters. High purity copper foam inside the compressors enhances heat transfer into and out of the enclosed $LaNi_5$ powder. During cooldown to room temperature, six atoms of hydrogen are absorbed at low pressure onto each $LaNi_5$ molecule, and during heatup to 110°C, the hydrogen is driven off at 40 atmospheres pressure. The pressure isotherm data for the $LaNi_5$/hydrogen system is similar to that previously obtained (Reference 2), although slightly higher, possibly due to a somewhat different La/Ni ratio.

During refrigerator operation, high pressure gas passes through a Joule-Thomson valve/heat exchanger assembly, and provides open cycle cooling, i.e., venting to ambient, to 20 K. Closed cycle cooling has provided a calculated 650 mW of cooling at 29 K for 6 atmosphere bottom cycle pressures. Contamination due to 50 ppm hydrogen gas impurities initially prevented long term operation (in excess of two hours per test period), but switching to UHP hydrogen, however, has allowed test periods in excess of 300 hours with no measurable degradation in compressor performance. If accidentally contaminated, the $LaNi_5$ powder is quickly reactivated by heating the powder while under high vacuum. The predicted lifetime for very clean hydride systems below 100°C (373 K) is hundreds of thousands of cycles (Reference 3), although some degradation may eventually occur (Reference 4). Use of $LaNi_{4.7}Al_{0.3}$ in place of $LaNi_5$ could potentially increase hydride life even further, since $LaNi_{4.7}Al_{0.3}$ has exhibited no measurable degradation even after thousands of cycles (Reference 4).

Due to the lack of moving parts, other than self-operating, long-life valves, the JPL refrigerator's predicted life (with clean hydrogen) is extremely long, and based on predicted check valve life, should potentially last at least 10 years.

QUESTION

J. Verdier, CEA/CENG, Grenoble, France

1. What is the amount of time that each compressor is on during cycling?

Authors response to J. Verdier

Each compressor is heated for three minutes and cooled for three minutes. The three compressor cycles are phased 120° relative to each other such that a continuous flow of high pressure hydrogen is supplied to the Joule-Thomson cooling assembly.

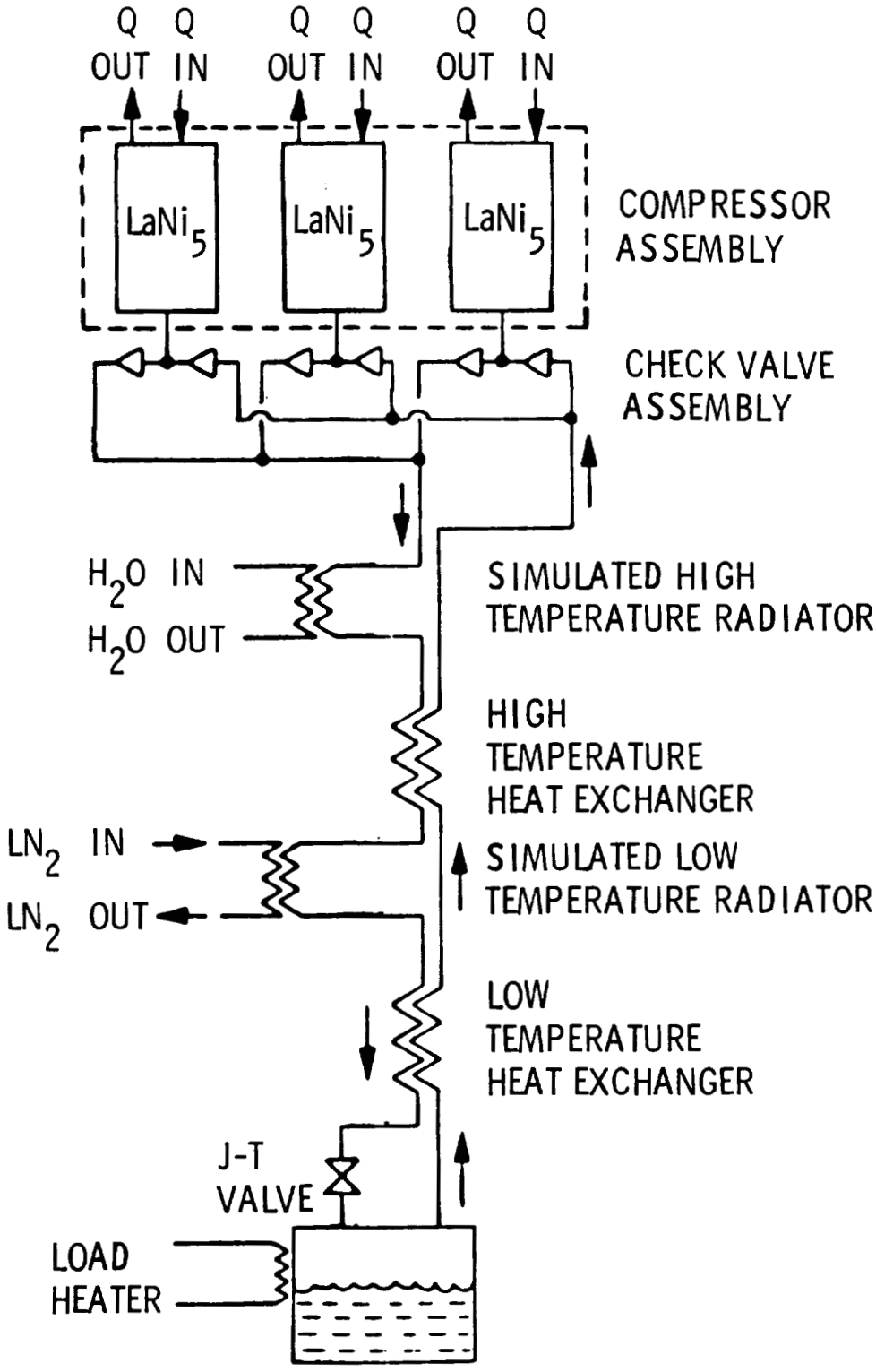

Figure 1. Hydride refrigerator operational schematic.

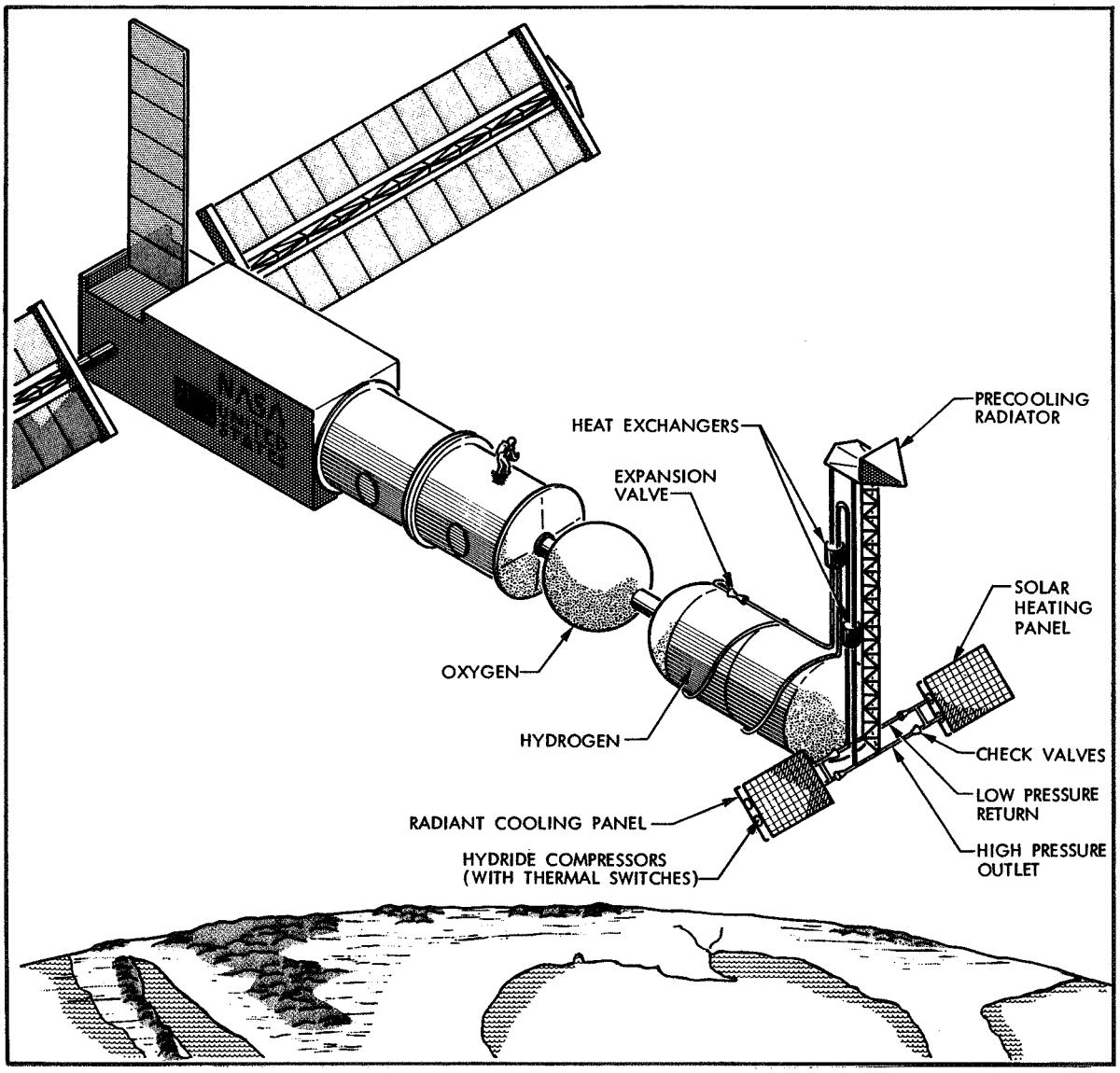

Figure 2. Space station refueling port with hydride refrigeration.

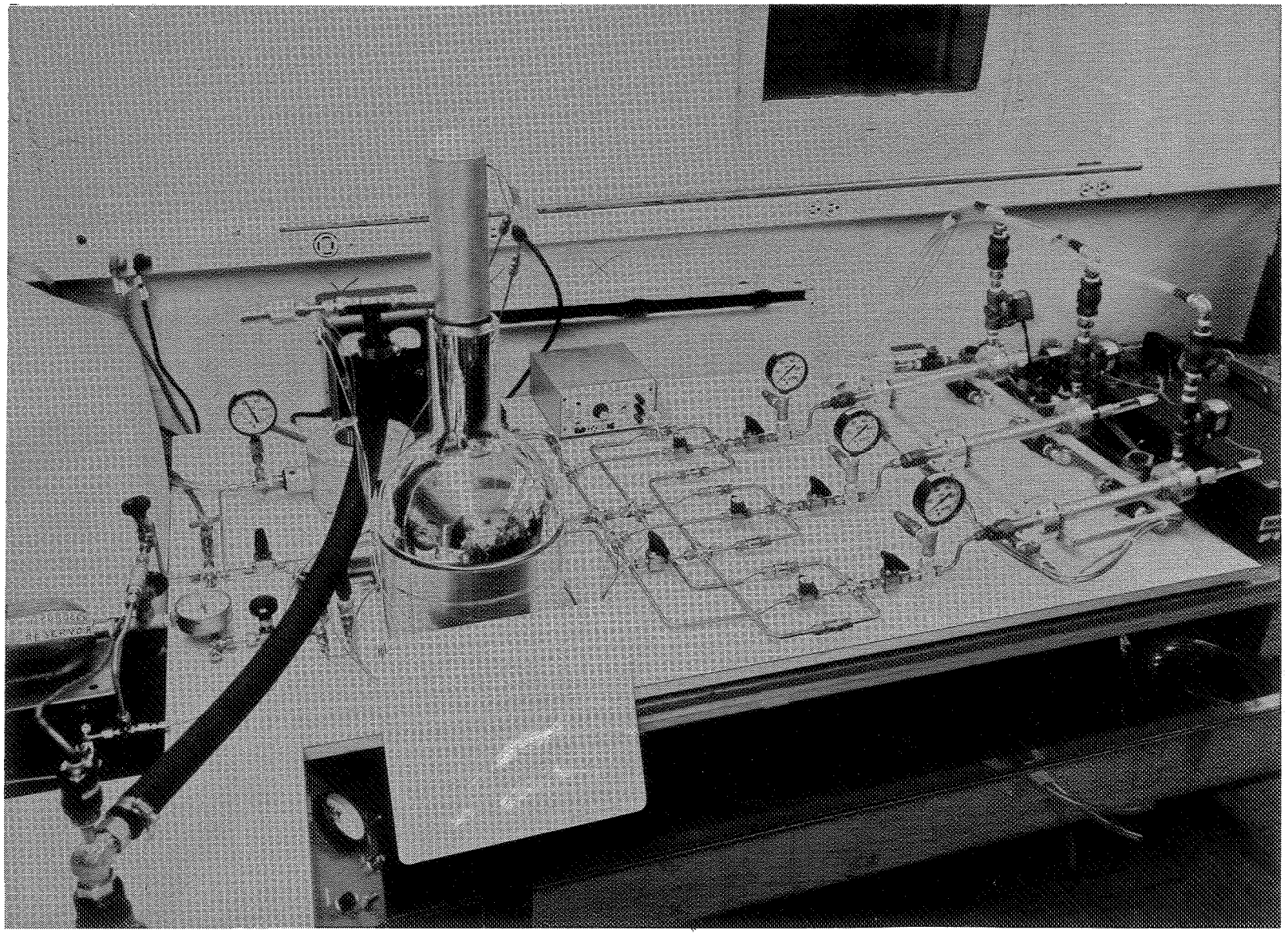

Figure 3. JPL Hydride Absorption Cryogenic Refrigerator.

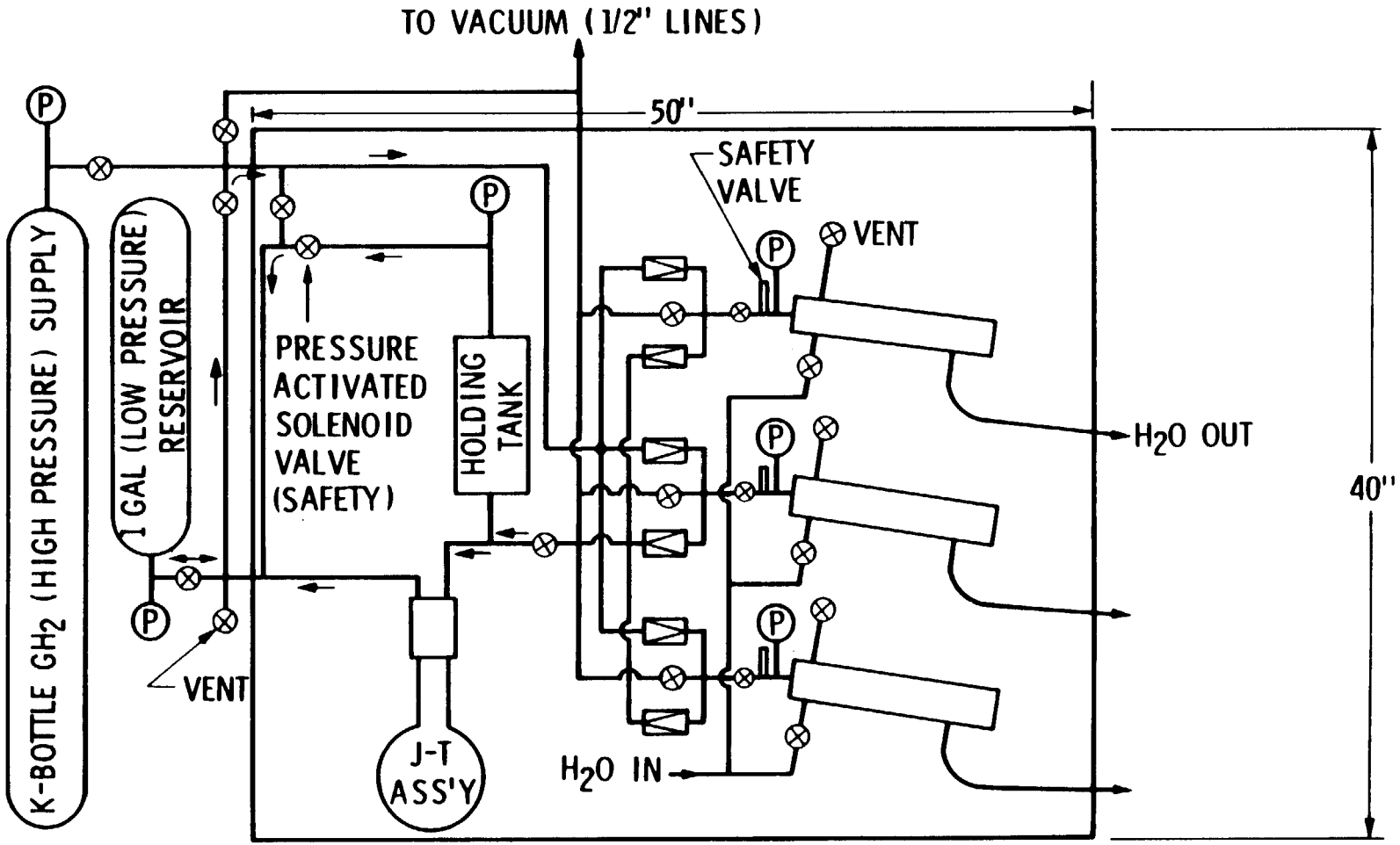

FIGURE 4 HYDROGEN ABSORPTION CRYOGENIC REFRIGERATOR-BOARD LAYOUT

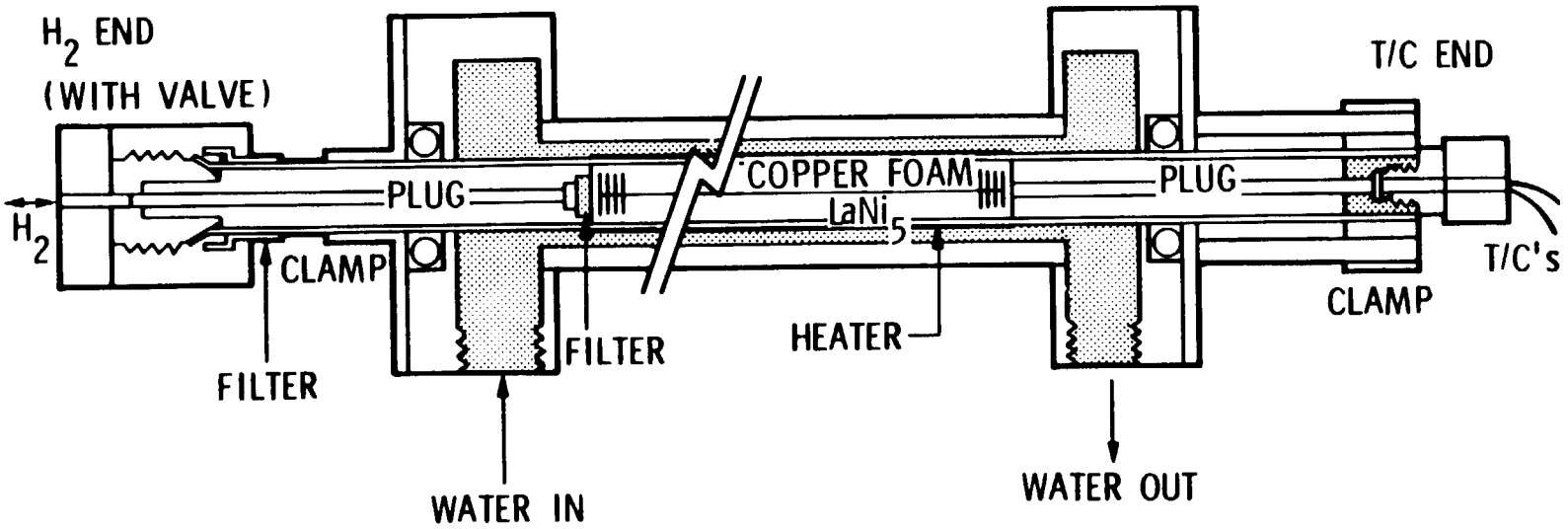

FIGURE 5 MACC COMPRESSOR ASSEMBLY

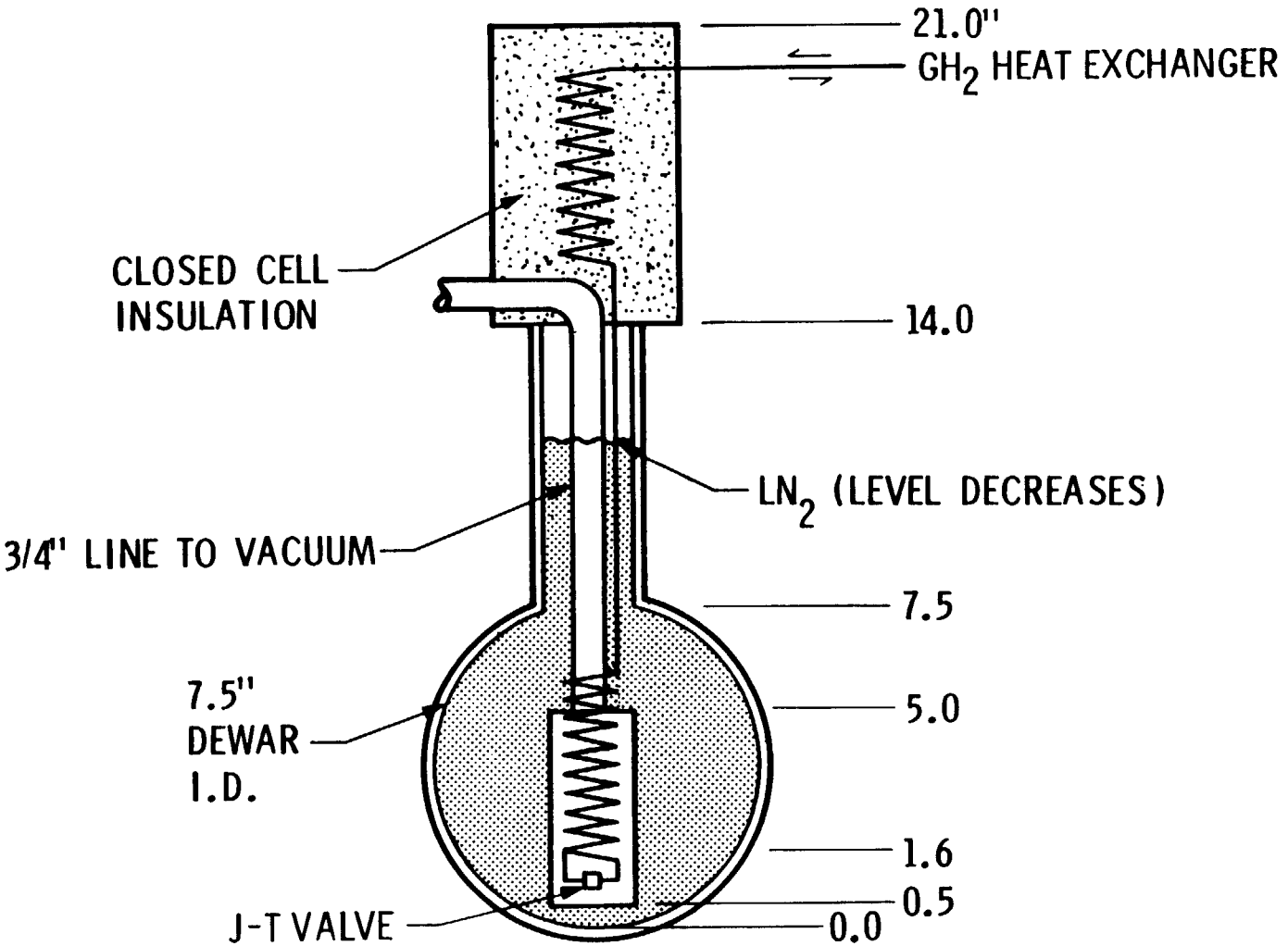

FIGURE 6 JOULE THOMSON/HEAT EXCHANGER ASSEMBLY

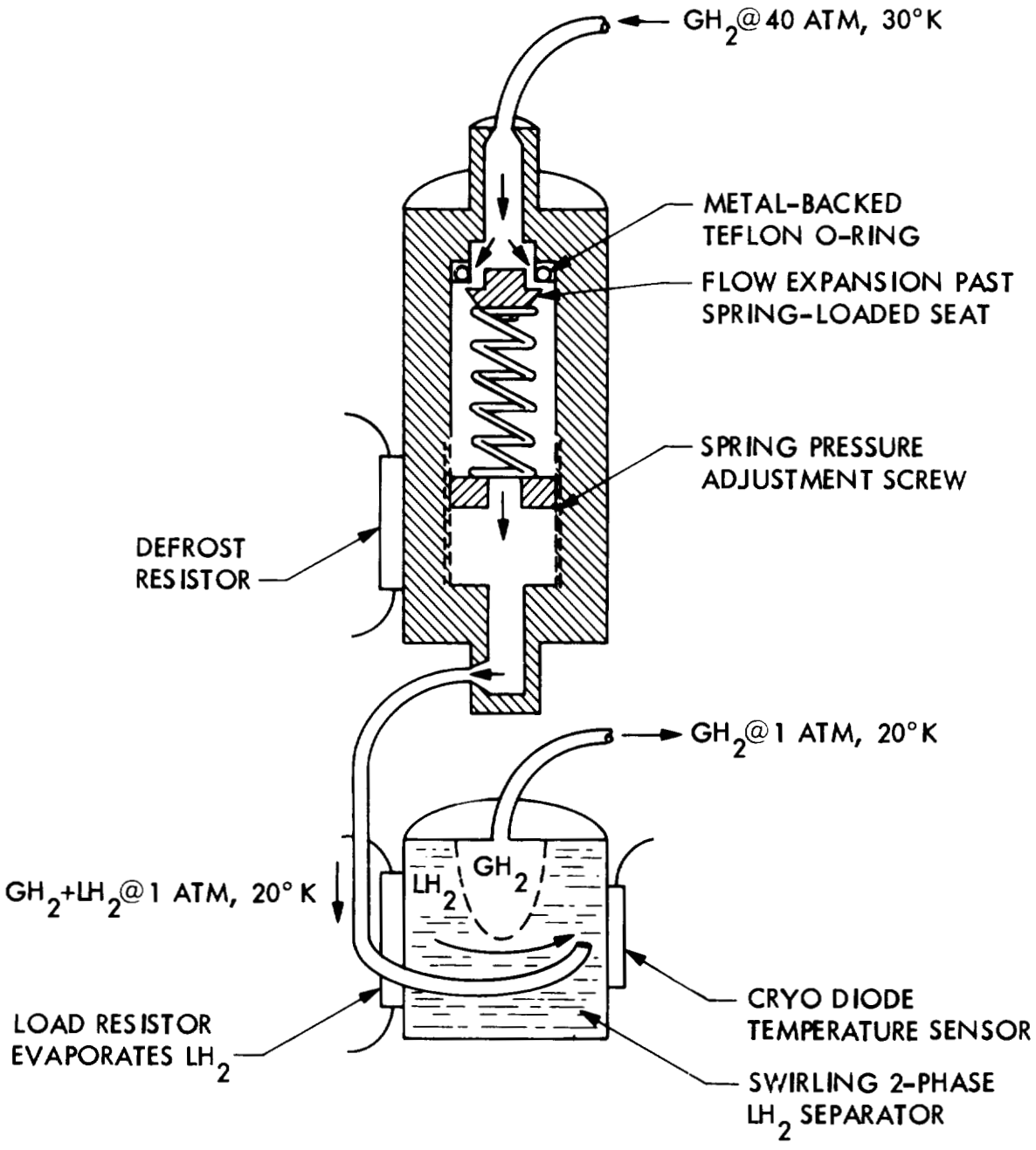

Figure 7. Joule Thompson Valve and Cryostat Assembly.

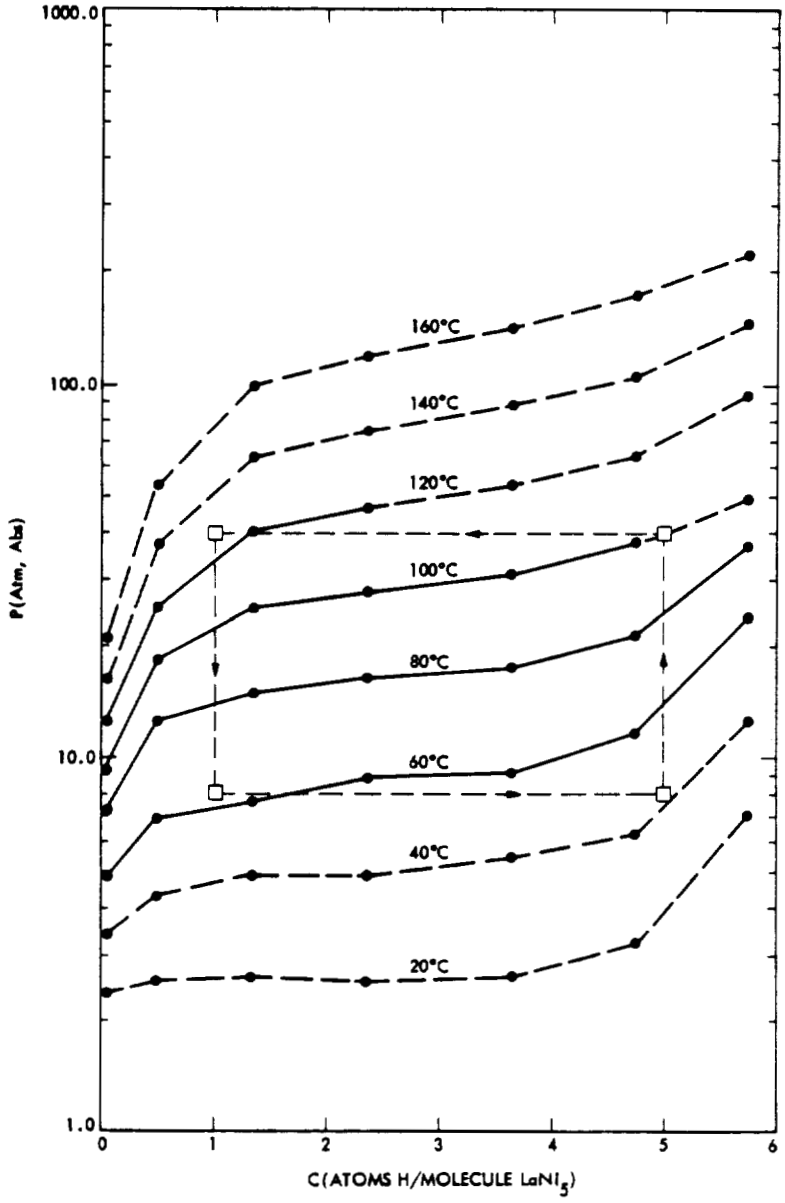

FIGURE 8 $LaNi_5$-H_2 ABSORPTION ISOTHERMS

REFERENCES

1. Klein, G.A., and Jones, J. A., "Molecular Absorption Cryogenic Cooler for Liquid Hydrogen Propulsion Systems," Paper No. AIAA-82-0830, AIAA/ASME 3rd Joint Thermophysics, Fluids, Plasma and Heat Transfer Conference," June 7-11, 1982/St. Louis, Missouri.

2. Van Mal, H. H., and Maynheer, A., "Hydrogen Refrigerator for the 20K Region with a $LaNi_5$-Hydride Thermal Absorption Compressor for Hydrogen,"
Proceedings of the Fourth International Cryogenic Engineering Conference, IPC Science and Technology Press, Surrey, England, 1972.

3. Klein, G. A. and Jones J. A., "Cryogenic Propellant Storage Study," Submitted to AIAA 22nd Aerospace Sciences Meeting, Reno, Nevada, January 9-12, 1984.

4. Cohen, R. L., and Wernick, J. H., "Hydrogen Storage Materials Properties and Possibilities," Science, Volume 214, Number 4525, 4 December, 1981.

5. Goodell, Doug, "Stability of Rechargable Hydriding Alloys During Extended Cycling" International Nickel Co., White Plains, New York. Publication pending in Journal of Less Common Metals.

6. Sigurdson, Katherine B., "A General Computer Model for Predicting the Performance of Gas Sorption Refrigerators," Second Biennial Conference on Refrigeration for Cryogenic Sensors and Electronic Systems," December 7 and 8, 1982, Goddard Space Flight Center, Greenbelt, Maryland.

THE THEORY OF AN ACTIVE MAGNETIC REGENERATIVE REFRIGERATOR*

J. A. Barclay
Los Alamos National Laboratory

ABSTRACT

The adiabatic temperature change with field is limited to about 2 K/Tesla for ferromagnets near their Curie temperatures by the change of magnetization with temperature and the lattice heat capacity. Hence, practical magnetic refrigerators operate on a regenerative cycle such as the Brayton cycle. One way to execute this cycle is through the use of an active magnetic regenerator, i.e. a regenerator composed of magnetic material that is cycled in an out of a magnetic field with appropriate fluid flows. The theory of these devices can be predicted by solving the partial differential equations that describe fluid flow combined with heat transfer between the fluid and the magnetic solid. The active magnetic regenerator is described along with the method of calculation. Temperature profiles for a normal regenerator and a magnetic regenerative refrigerator are shown.

INTRODUCTION

Many applications of advanced technology require low-temperature refrigeration for proper operation. Devices ranging from superconducting magnets and generators, infrared sensors, maser amplifiers to Josephson-junction computers and SQUID detectors all need a variety of refrigeration power at temperatures ranging from $\sim$4 K to $\sim$60 K. Each application puts a slightly different set of constraints on the refrigerator but some of the more desirable features are high reliability and long lifetime, small volume and mass, and, of course, high efficiency. Conventional gas-cycle refrigerators have been used for most present refrigeration needs but with the push for less massive, higher efficiency coolers, especially for some space missions, there is a necessity to explore new ways to obtain better refrigerators.

One promising method is magnetic refrigeration where the magnetocaloric effect is used in place of gas compression and expansion.[1-5] In contrast to regenerative gas-cycle stages, magnetic-refrigerator devices tend to perform best at low temperatures particularly from 4 K to 20 K

*This work was performed under the auspices of the U.S. D.O.E. and support from D.O.E., DARPA, WPAFB, and NASA (K.S.C.) is gratefully acknowledged.

but may also perform well from ∿20 K to ∿77 K. In this paper, I describe the active magnetic regenerator concept that may be useful in practical designs in the 20 to 77 K range.

THEORY

MAGNETOCALORIC EFFECT

Above ∿20 K ferromagnetic materials near their Curie temperature must be used to achieve the entropy change required for refrigeration of a load. Figure 1 shows calculated entropy-temperature curves for a typical ferromagnet with a Curie temperature of 40 K. Typical gas entropy changes are included for comparison. The entropy changes on this figure are calculated using the molecular field model for the magnetic equation of state[6] and the Debye-model for the heat capacity.[7] With these models the entropy changes as a function of temperature and magnetic field can be found according to

$$dS = \frac{C_B}{T}\,dT + \left(\frac{\partial M}{\partial T}\right)_B dB \quad . \tag{1}$$

The isothermal entropy changes or adiabatic temperature changes can be obtained from these curves. Figure 1 also shows that a single magnetic material can only span a limited temperature range, typically 20 to 40 K. Therefore, to span a temperature range from 20 K to 75 K, at least two or three different materials must be used. The materials can be in separate stages or combined in a single-stage active magnetic regenerator.

MAGNETIC REGENERATOR

Descriptive Theory[4]

The active magnetic regenerator comprises several magnetic materials that are thermodynamically cycled to provide the refrigeration over an extended temperature range. The basic theory is that of an ordinary regenerator except that the temperature of the materials can be changed by the application or removal of a magnetic field and a displaced thermal wavefront propagates back and forth in the regenerator. The materials that might be used in a magnetic regenerator are gadolinium intermetallic compounds that are prepared by arc melting and are relatively cheap and stable to oxidation. In order to achieve excellent heat transfer, the material could be put into a chip geometry with an effective particle diameter of ∿0.5 mm. Because the pressure drop across an efficient regenerator would have to be very small, typically 10^4-10^5 Pa, there is no equivalent pressure wave problem as in normal regenerators dealing with compressed and expanded gas movement. This also should avoid the "dust" problem that comes from the continual pressure pulsing in ordinary Pb shot regenerators. Each material completes a small Brayton cycle near its Curie temperature, but when all the materials are combined, they yield

a Brayton cycle over an extended temperature range, e.g., 20-75 K. The basic cycle, illustrated in Fig. 2 is described below.

Consider a porous-bed regenerator composed of a series of different ferromagnetic materials with Curie temperature T_o gradually decreasing from the sink temperature T_H to the load temperature $T_C - \Delta T_C$, as shown in the top frame of Fig. 2. Also consider that the temperature gradient is uniform except for the constant temperatures at the ends of the regenerator, as shown in the second frame of Fig. 2. (For start up from a warm condition, i.e., T_H everywhere, several cycles are also required to reach the condition assumed above, so for simplicity we start with an established temperature gradient.) Upon application of a magnetic field, the temperature along the bed adiabatically increases by ΔT, which is about 15-20 K for a 10-T field, as shown in the third frame of Fig. 2. After the field is applied, helium or hydrogen gas, at temperature T_C, is pushed through the bed from the cold end, which is now at T_C. As the gas at T_C enters the bed, the gas warms as the bed cools and a thermal wavefront of magnitude $T_H + \Delta T_H - T_C$ is established, as shown in the fourth frame of Fig. 2. The overall wavefront propagates through the regenerator (to the right in the fourth frame of Fig. 2) as gas continues to flow into the bed at T_C. The gas leaves the regenerator at $T_H + \Delta T_H$ until the thermal wavefront arrives at the end of the regenerator. When this happens, the gas flow stops and the regenerator is adiabatically demagnetized. The temperatures all along the bed drop by ΔT, as shown in frame 5 of Fig. 2, in preparation for the reverse flow of gas. The gas that came out of the regenerator at $T_H + \Delta T_H$ during the magnetized stage is put through a heat exchanger and cooled to T_H before it is pushed back into the regenerator after demagnetization. Another thermal wave of magnitude $T_H - T_C + \Delta T_C$ is established, but it travels in the opposite direction to the first thermal wavefront, as shown in the bottom frame of Fig. 2. The gas exits the cold end at $T_C - \Delta T_C$ and is heated when it contacts a load at T_C. When the thermal wave reaches the cold end of the regenerator, the gas flow stops and the cycle now repeats as the regenerator is again magnetized. This concept can be incorporated into both reciprocating and wheel modes. In both modes, the rate of magnetization and demagnetization is limited in practice to <1 Hz by the heat transfer coefficients. If the heat transfer could be improved, the frequency could be increased but eventually the eddy current power would become significant; probably near 5-10 Hz. If the eddy current and heat transfer problems could be eliminated, the upper limit on cycle frequency is given by the spin-lattice relaxation rate; typically to $\sim$1 kHz for gadolinium compounds.

The efficiency of the active magnetic regenerative refrigerator is potentially quite high for several reasons. The basic process, magnetization/demagnetization, is inherently highly reversible compared to the compression/expansion of a gas. The work for the cycle can be put in via a $\sim$90% efficient motor rather than through a 60-70% efficient compressor as in a gas cycle. The external heat exchanger and other losses are comparable in the gas and magnetic systems. In the magnetic system the heat transfer during the regenerative stages will be the dominant

inefficiency, thereby requiring excellent regenerator design with respect to heat transfer, viscous flow dissapation, and longitudinal conduction. If the regenerator can be made highly effective, the overall magnetic refrigerator efficiency can approach 50-60% of Carnot efficiency. This would be significantly higher than existing gas refrigerators such as Stirling-cycle devices.

Mathematical Theory

The basic theory of thermal wavefront propagation through a porous bed was first presented approximately fifty years ago.[8] The temperature span across the bed was considered small enough so that the bed and gas properties could be taken as constant. Also, momentum and mass-continuity effects were ignored leaving only a set of energy-balanced equations to describe the problem. The one-dimensional, partial differential energy equations are

$$\text{fluid:}\quad \alpha\rho_f C_f \frac{\partial T}{\partial t} = -\dot{m}_f C_f \frac{\partial T}{\partial x} + ha(\theta - T) \tag{2}$$

$$\text{solid:}\quad (1-\alpha)\rho_s C_s \frac{\partial \theta}{\partial t} = ha\,(T - \theta) + (1-\alpha)\lambda_s \frac{\partial^2 \theta}{\partial x^2} \tag{3}$$

where α is the porosity, ρ_f, ρ_s are the fluid and solid densities, respectively, C_f, C_s are the fluid and solid heat capacities, respectively, m_f is the fluid mass flow rate, T is the fluid temperature, h is the conductance between the fluid and solid, θ is the solid temperature, a is the contact area per unit volume of the bed, and λ_s is the effective axial thermal conductivity of the bed. When Eqs. (2) and (3) are numerically solved by finite difference techniques, they give a thermal wavefront propagating as a function of time.

For the prediction of the thermal-wavefront propagation in a regenerator with a large temperature gradient when all properties are temperature dependent, the one-dimensional equations for a porous bed are given by[9]

$$\frac{\partial \rho'}{\partial t} + \frac{\partial \rho' u}{\partial x} = 0 \tag{4}$$

$$\frac{\partial \rho' u}{\partial t} + \frac{\partial (\rho' u^2)}{\partial x} + \alpha \frac{\partial P}{\partial x} - \rho' g + \frac{f \rho\, (1-\alpha)\, |u|\, u}{d_p} = 0 \tag{5}$$

$$\frac{\partial \rho' U}{\partial t} + \frac{\partial \rho' u U}{\partial t} + P\frac{\partial (\alpha u)}{\partial x} + \frac{6(1-\alpha)h}{d_p}(T-\theta) +$$

$$\frac{4\alpha h'}{d_i}(T-\psi) - \frac{f\rho(1-\alpha)|u|u^2}{d_p} - \frac{\partial}{\partial x}(k_f \alpha \nabla T) = 0 \qquad (6)$$

$$\rho'_s \frac{\partial U_s}{\partial t} - E_s - \frac{6(1-\alpha)}{d_p} h (T-\theta) - \frac{4(1-\alpha)h''}{d_i}(\psi - \theta) -$$

$$\nabla \cdot [k_s(1-\alpha)\nabla\theta] = 0 \qquad (7)$$

$$\rho_w \frac{\partial U_w}{\partial t} - E_w + \frac{4(1-\alpha)d_i}{(d_o^2 - d_i^2)} h''(\psi - \theta) - \frac{4d_i \alpha h'}{(d_o^2 - d_i^2)}(T-\psi) -$$

$$\nabla \cdot (k_w \nabla \psi) = 0 \qquad (8)$$

where ρ' is the effective fluid density, u is the velocity, P is the pressure, f is the friction factor, g is the gravitational constant, k_f, k_s, and k_w are the thermal conductivities of the fluid, magnetic solid, and wall, respectively, ψ is the wall temperature, h' and h" are the fluid to wall and solid to wall conductance, respectively, d_i and d_o are the inner and outer diameters of the regenerator container, respectively, U is the internal energy, and E_s and E_w are heat sources or sinks such as eddy currents, heat leak from surrounding, and magnetocaloric effect.

RESULTS

The coupled non-linear, partial differential equations that describe the one-dimensional processes in the porous magnetic bed can be solved only by numerical techniques. Equations (4) through (8) have been solved by using the finite difference method. As a model a stainless steel container 0.05 m inner diameter by 0.0025 m (.010") wall and 0.05 m long was chosen. The container was filled with lead spheres with a 0.0005 m (0.5mm) diameter to a porosity of 40%. For the calculations described here the initial conditions of the bed were stationary helium gas at 25 K and 1.013 MPa. To establish a thermal gradient across the bed, a pressure increase of 0.03 MPa was introduced suddenly on the right end of the bed where the input gas temperature was fixed at 75K. A thermal wavefront propagated across the bed until the temperature on the left end of the bed started to rise slightly above 25 K. At that point the pressure difference was reversed and the inlet gas temperature on the left was fixed at 25 K. The net mass flow per cycle was constrained to be zero. Figure 3 shows the

gas, lead spheres, and wall temperature profiles as a function of distance across the bed after several complete cycles of gas flow reversal. The solid temperature profile is characteristic of a regenerator where the bed-material heat capacity decreases as a function of temperature.

The behavior of a magnetic regenerator was calculated by using the same model as previous except that now it was assumed that the bed was composed of a series of magnetic materials whose combined adiabatic temperature change upon magnetization or demagnetization was a uniform 10 K across the entire bed. The magnetic regenerator cycle was started from a normal regenerator profile between 25 and 75 K. The magnetic material temperature was then increasing rapidly by 10 K after which gas was introduced from the left at 35 K. The gas exited the right end of the bed at between $\sim$85 and 80 K. After an arbitrary mass flux such that the outlet temperature started to drop, the pressure difference was removed and the magnetic material demagnetized everywhere by 10 K. Upon completion of the demagnetization the flow was reversed with the temperature of the inlet gas fixed at 75 K. The exiting gas on the left end of the bed was between $\sim$25 and 28 K. When the net mass flow at the left end of the bed was zero, the cycle was repeated. Figure 4 illustrates the temperature profiles at various stages of the cycle after approximately ten cycles.

DISCUSSION AND CONCLUSIONS

There are many interesting observations that come from these calculations but I will only mention a few. The effect of the variation in heat capacity as a function of temperature is very obvious during magnetization or demagnetization because the wall to solid temperature difference remains larger longer at the higher-temperature end of the regenerator. The choice of a thin container wall reduces the shuttle effect in this model but with thicker walls more distinct influence would be apparent. A second obvious effect is the longitudinal conduction in the bed. The solid temperature at either end of the regenerator tends to be a degree or two from the corresponding gas inlet temperature. With a 35 to 75 K temperature difference across the bed, a slightly longer bed would probably be a better choice.

Another observation was that after the pressure difference across the bed was removed, during magnetization or demagnetization, the gas undergoes substantial movement due to temperature gradients. This gas movement has very little effect in this temperature range because the thermal mass of the gas is small compared to the solid. However, in the 4-10 K temperature range where helium has a larger volumetric-heat-capacity than most materials, the effects of moving helium could be significant.

The calculations described in this work indicate that a magnetic regenerator can be cycled successfully to provide cold gas for refrigeration between 25 and 35 K. The exhaust gas can be used to reject heat between 85 and 75 K. Many questions about a detailed magnetic regenerative refrigerator design remain unanswered at this time but calculations of the kind described in this paper should help obtain a successful design.

Q1. Yes. In both the reciprocating and wheel modes there is a definite requirement for force compensation as the magnetic material is moved into and out of the magnetic field. At 9T with 1 liter of gadolinium, the forces are in the many ton range.

Q2. Yes, we have looked at staging of the refrigerator so the maximum amount of heat leak is intercepted at the highest possible temperature. This is clearly required to obtain high efficiency.

Q3. The source of field is a superconducting magnet. The best way to incorporate a superconducting magnet into a refrigerator is to put the magnet in persistent mode once it is charged and to leave it alone. Cycling the magnet requires careful attention to an energy storage device at room temperature and is definitely not recommended on the first designs.

Q4. Very small pressure ratios are used because the porous bed has only a small pressure drop if it is highly effecient. The cycle time for the gas in a typical AMR is about 0.1 to 1 Hz. The pressure ratio has to be different at the cold end and hot end of the regenerator to have mass conservation for a complete cycle.

ACKNOWLEDGEMENTS

It is a pleasure to thank Frank Harlow for several hours of discussion on the problems of finite-difference methods.

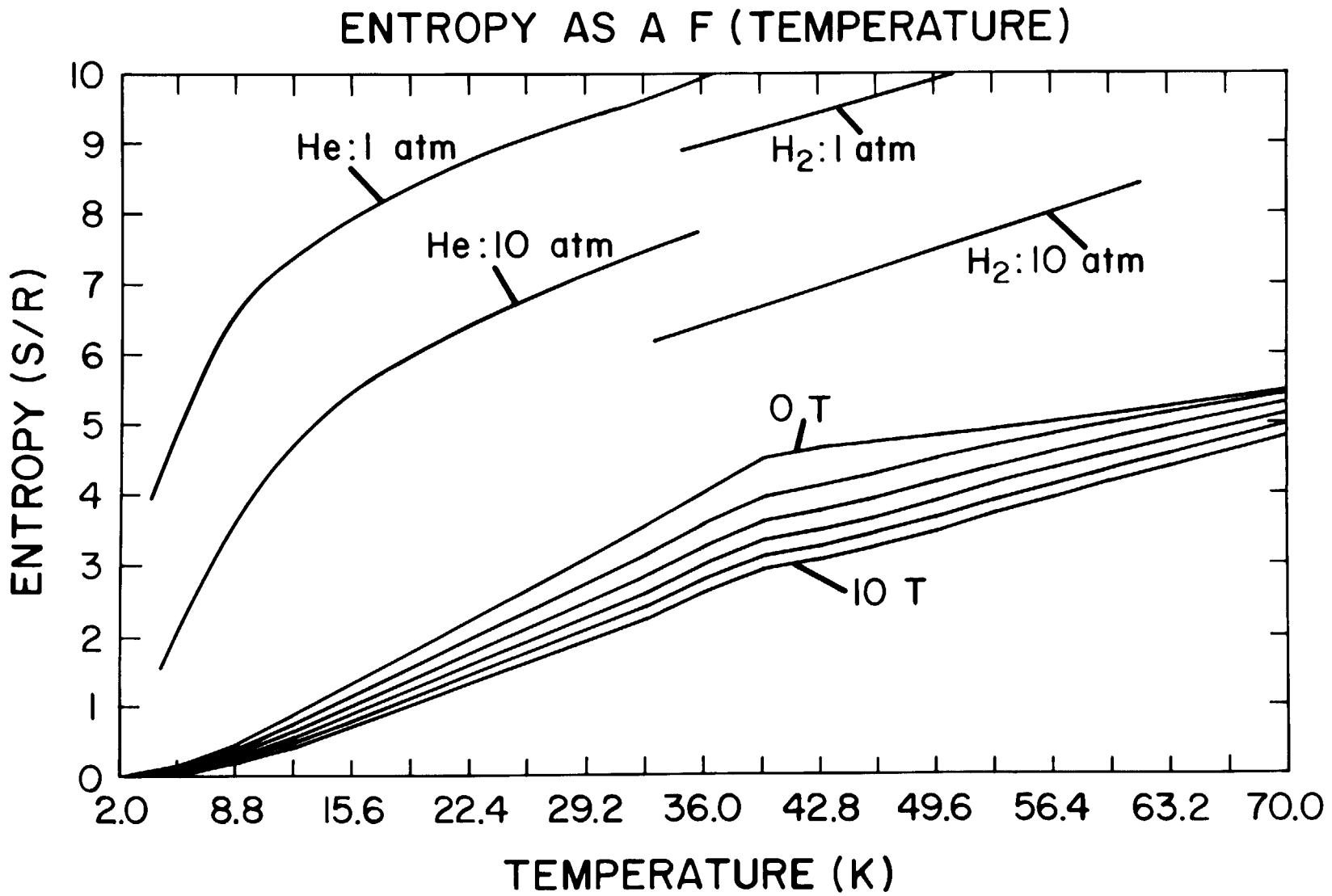

Figure 1. Calculated Entropy-Temperature curves for a typical ferromagnetic with a Curie temperature of 40 K. The curves for the helium and hydrogen gas are added for comparison.

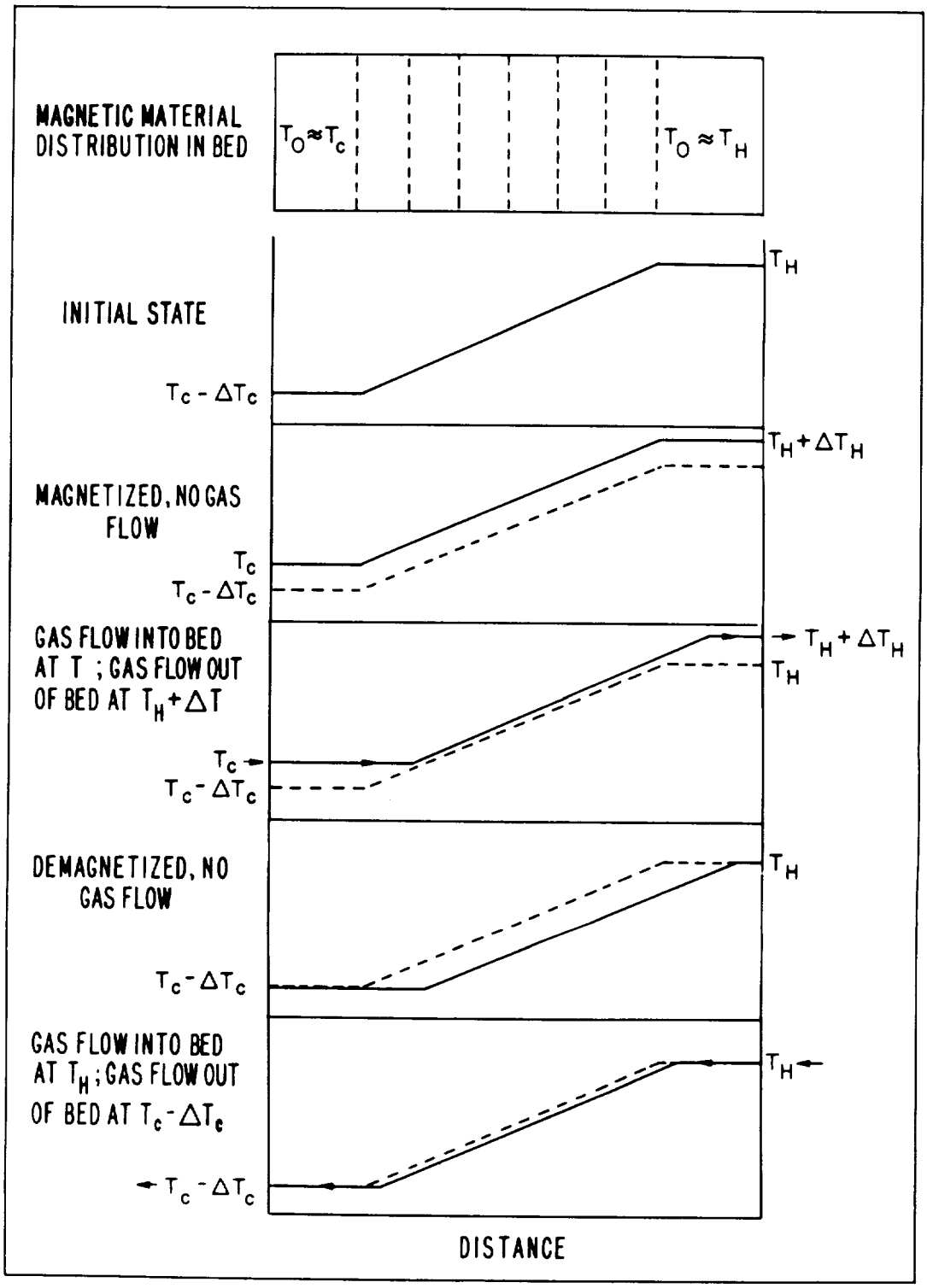

Figure 2. A schematic of the various parts of an active magnetic regenerative refrigeration cycle.

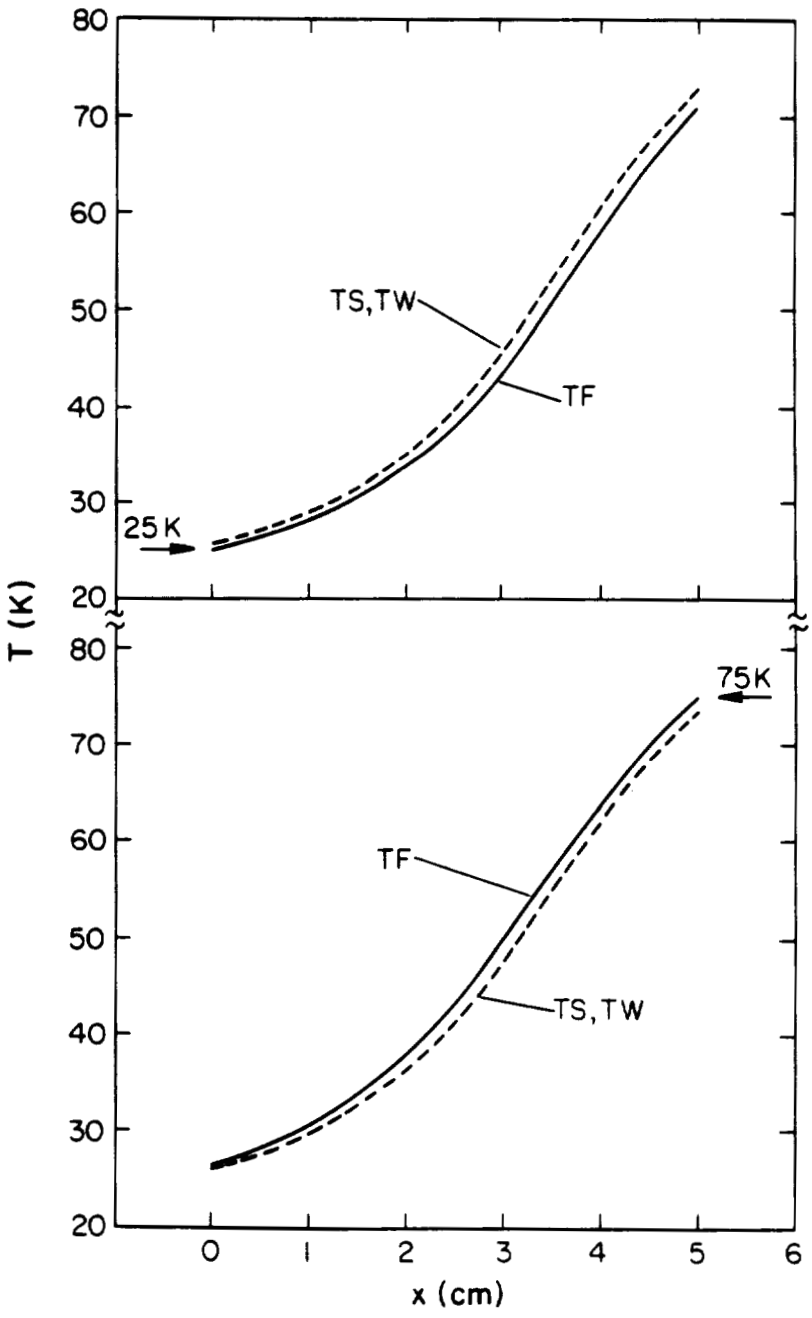

Figure 3. The temperature profiles of the gas, solid, and wall as a function of distance in a ordinary regenerator after cycling between 25 and 75 K.

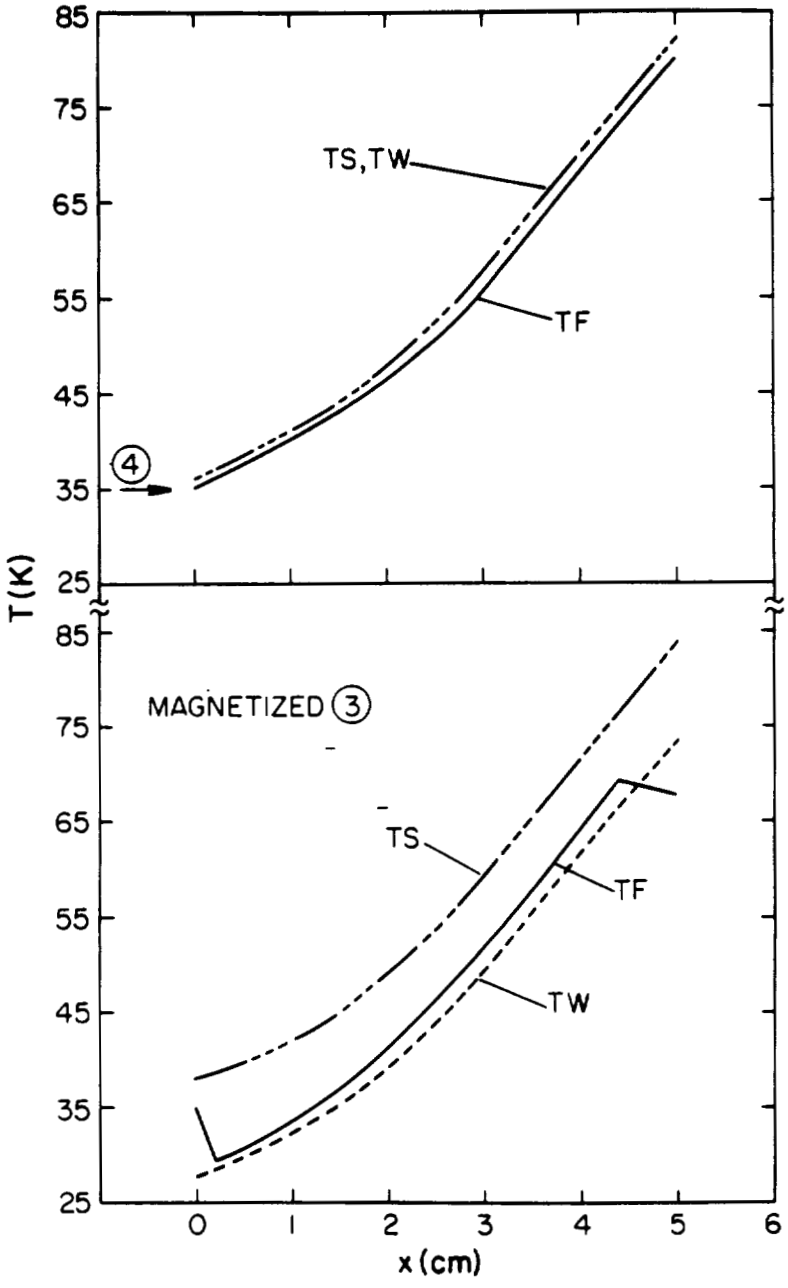

Figure 4. The temperature profiles of the gas, magnetic solid, and wall as a function of distance in a magnetic regenerator. Frame 3 indicates temperatures after magnetization and frame 4 after gas flow from the left end.

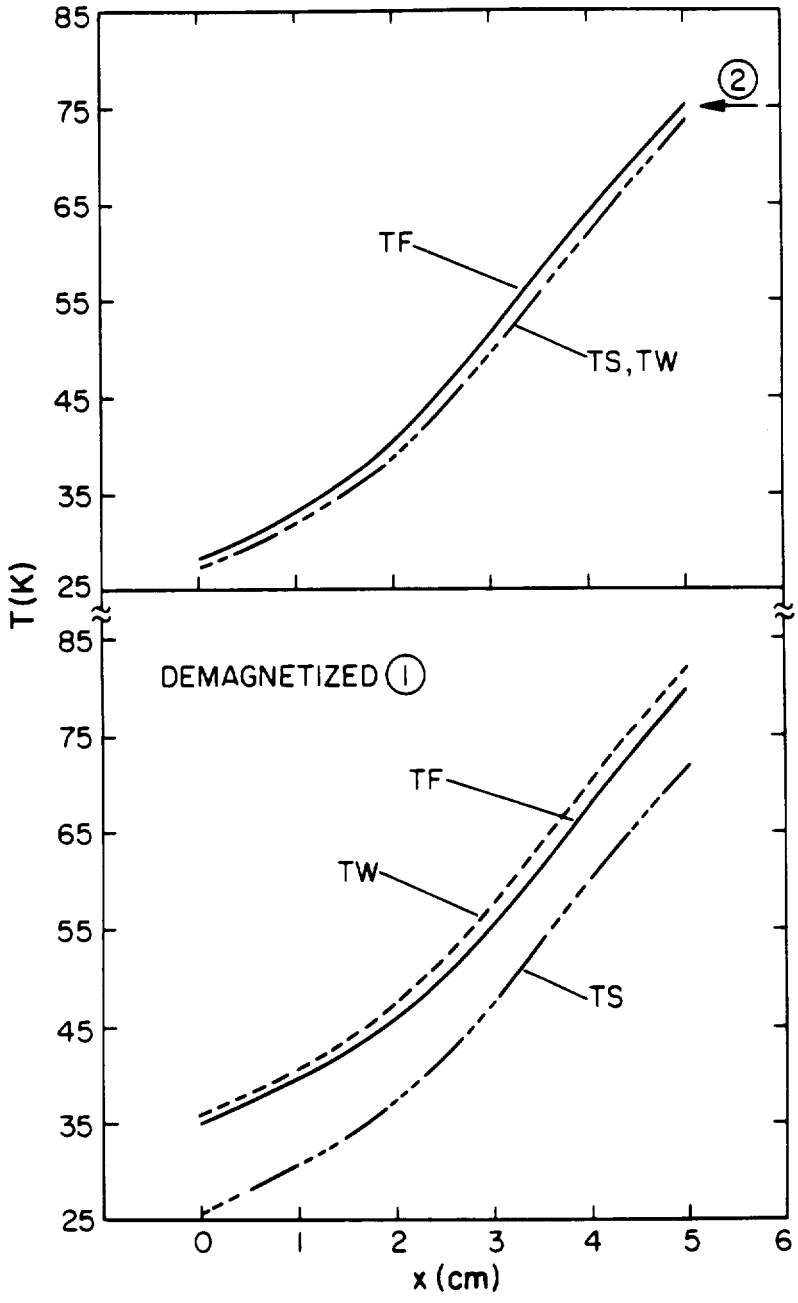

Figure 5. The temperature profiles of the gas, magnetic solid, and wall as a function of distance in a magnetic regenerator. Frame 1 indicates temperatures after demagnetization and frame 2 after gas flow from the right end.

REFERENCES

1. J. R. van Geuns, "A Study of a New Magnetic Refrigerating Cycle," Philips Res. Rep. Suppl. 6 (1966).

2. G. V. Brown, "A Magnetic Heat Pump Near Room Temperature," J. Appl. Phys. 47, 3673 (1976).

3. W. A. Steyert, "Stirling Cycle Rotating Magnetic Refrigerators and Heat Engines for use near Room Temperature," J. Appl. Phys. 49, 1216 (1978).

4. J. A. Barclay, "Can Magnetic Refrigerators Liquefy Hydrogen at High Efficiency?," Trans. Am. Soc. Mech. Eng. 1981, paper 81-HT-82.

5. T. Hashimoto, T. Numasawa, M. Shino, and T. Okada, "Magnetic Refrigeration in the temperature range from 10 K to room temperature: the Ferromagnetic refrigerants," Cryogenics 21, 647 (1981).

6. J. S. Smart, Effective Field Theories of Magnetism (W. B. Saunders Co., Philadelphia, 1966) Chp. 3.

7. C. Kittel, Introduction to Solid State Physics (John Wiley and Sons, Inc., New York, 5th ed., 1976), Chp. 5.

8. T. E. W. Schumann, "Heat Transfer, A Liquid Flowing through a Porous Prism," J. Franklin Inst. 208, 405 (1929).

9. F. H. Harlow and A. A. Amsden, "Numerical Calculation of Multiphase Fluid Flow," J. Comput. Phys. 17, 19 (1975).

DESIGN OF AN ADIABATIC DEMAGNETIZATION REFRIGERATOR FOR STUDIES IN ASTROPHYSICS

by

Dr. Stephen Castles
Cryogenics, Propulsion and Fluid Systems Branch
Space Technology Division
National Aeronautics and Space Administration
Goddard Space Flight Center
Greenbelt, Maryland

ABSTRACT

An adiabatic demagnetization refrigerator has been designed for cooling infrared bolometers for studies in astrophysics and aeronomy. The design has been specifically tailored to the requirements of a Shuttle sortie experiment. The refrigerator should be capable of maintaining three bolometers at 0.1 K with a 90 percent duty cycle. There are great advantages in operating the bolometers at 0.1 K rather than at the 1.5 K that can be attained with a space-pumped liquid helium cryostat. These advantages are: greater sensitivity, faster response time, and the ability to use larger bolometer elements without compromising the response time.

The design presented in this paper is the first complete design of an ADR intended for use in space. The requirements of space, as well as the requirements of the bolometers that are being cooled, create a number of specifications that have not been incorporated into previous ADR designs. The most important of these specifications are to survive a Shuttle launch, to operate with 1.5 K - 2.0 K space-pumped liquid helium as a heat sink, to have a 90 percent duty cycle, and to be highly efficient.

The first unit, called the engineering model, has been designed and fabricated. This engineering model will satisfy the basic operational and structural requirements for flight. It will be functionally tested at the GSFC in the near future.

INTRODUCTION

The adiabatic demagnetization refrigerator (ADR) described herein was designed specifically for cooling infrared bolometers to 0.1 K. There are great advantages in operating the bolometers at 0.1 K rather than at the 1.5 K that can be attained with a pumped liquid He^4 cryostat. These advantages are: greater sensitivity, faster response time, and the ability to use larger bolometer elements without compromising the response time. The latter two advantages result from the decreased heat capacity of the bolometer at the lower temperature. In addition, the photon noise of the sensor is reduced, which improves its sensitivity.

In the absence of the photon noise, the detector sensitivity is limited by the Johnson noise and the temperature fluctuation noise. This sensitivity can be characterized by the detector noise equivalent power (NEP). For a bolometer with a given time constant, the NEP that may be achieved varies with the detector temperature T as:

$$NEP \sim T^{5/2} \tag{1}$$

It can also be shown that

$$t^5 \sim NEP^2 \tag{2}$$

where t is the observing time necessary to obtain data with a certain accuracy. From equation (1) and (2), one finds that operation of bolometers at 0.1 K with an adiabatic demagnetization refrigerator, rather than at 1.5 K with pumped liquid helium reduces the NEP by a factor of 870 and reduces the observing time by a factor of 700,000.

As mentioned, equations (1) and (2) are valid only for bolometers with time constants independent of the temperature. Unfortunately, the time constant of certain types of bolometers increases at low temperatures as the temperature is decreased. For these bolometers, the decrease in the NEP and the observing time will be less than the decrease derived from equations (1) and (2). However, for an infrared bolometer properly designed for use at low temperatures, the improvement in the NEP and the observing time should be considerable.

Due to the great advantages of operating bolometers at lower temperatures, the 0.1 K adiabatic demagnetization refrigerator (ADR) development program was initiated at the GSFC. The goal is to develop a highly reliable ADR capable of withstanding a Shuttle launch and capable of operating in the 0-g environment of space.

The first unit, called the engineering model, has been designed and fabricated. Final assembly and testing is on-going. This engineering model will satisfy the basic operational and structural requirements for flight. However, some modifications will be required for a flight unit. The following sections describe the design of the engineering model ADR and the modifications that will be required for the flight unit.

OPERATING CHARACTERISTICS

The operating characteristics for the GSFC engineering model adiabatic demagnetization refrigerator were developed in meetings with infrared astronomers, namely Dr. Michael Hauser and Dr. John Mather. These operating characteristics are summarized in Table 1. They include an operating temperature of 0.1 K, better than 10μK temperature stability, 50μW cooling power, and observing time for the cooled bolometers of at least 90 minutes. To achieve a 90% duty cycle, the time necessary to recycle the ADR is limited to 10 minutes. Also, since the total cooling capacity of the stored liquid helium in the spacecraft is limited, the heat load expelled to the helium by the ADR must be held to a minimum. To accomplish this goal, the ADR should be highly efficient.

Table 1

Adiabatic Demagnetization Refrigerator

- Operating Temperature is 0.1°K
  - Higher operating temperatures possible with greater cooling power
  - Excellent temperature stability
- 50μW Cooling Power
- Operating Time Greater than 90 Minutes
  - Recycle time of 10 minutes
- Highly Efficient
  - Thermodynamic efficiency approaches Carnot
  - Expels less than 2mW to the liquid helium bath
- High Reliability
  - No moving parts
- Mechanical Design Appropriate for a Shuttle Launch

PRINCIPLE OF OPERATION

The key component in an ADR is the paramagnetic salt. This salt contains ions of metals that have a net magnetic moment. The magnetic moments of different ions interact with one another, the strength of the interaction being dependent on, among other factors, the spacing between the ions. This interaction will cause the magnetic moments to "order" below some temperature. The paramagnetic material (a salt crystal in our case) will then be ferromagnetic or antiferromagnetic. For example, in iron the spacing is small and the magnetic moments are ordered at room temperature. In paramagnetic salts used in an ADR, the spacing must be large so that the magnetic moments will not be ordered at the operating temperature of the refrigerator. For this reason, hydrated salt crystals are generally utilized in an ADR. Hydrated crystals containing cesium, chromium, iron, manganese, and gadolium have been utilized with ordering temperatures ranging from a few milli-Kelvin (mK) to a few Kelvin.

When the magnetic moments are not ordered, the collection of magnetic moments has associated with it a relatively large quantity of entropy, S. However, the magnetic moments of the ions can be aligned (ordered) by applying a sufficiently large magnetic field. As the magnetic moments align, the entropy associated with the collection of magnetic moments decreases. If this decrease in entropy, ΔS, occurs at a constant temperature, T, a quantity of heat, ΔQ, given by

$$\Delta Q = -T \Delta S$$

is produced by the alignment of the magnetic moments. If the magnetic field is removed, an equal quantity of heat, $\Delta Q = T \Delta S$, will be absorbed by the collection of magnetic moments as the moments unalign. This heat absorbed by the change in entropy associated with the magnetic moments of the metal ions, provides the cooling power of the ADR.

An ideal adiabatic demagnetization cycle is depicted in Figure 1. The entropy-temperature diagram for ferric ammonium sulfate is presented in Figure 1a for various magnetic fields. The dashed line connecting points 1, 2, 3 and 4 represents the cycle through which an ADR operates. Figure 1b presents four sketches of an ADR illustrating the position of the heat switch (conducting or nonconducting) and the strength of the magnetic field at the four stages of the demagnetization cycle. These stages correspond to points 1, 2, 3 and 1 again in Figure 1a.

At the beginning of the demagnetization, point 1, the heat switch is closed and the magnetic field has its maximum value. The heat switch is then opened and the field rapidly decreased until the desired operating temperature (0.1 K in this case) is reached (point 2 in Figure 1a). Then the field is slowly decreased such that the heat absorbed, Q_A, by the spin system equals the heat load on the refrigerator. The dashed line between point 2 and point 3 corresponds to this isothermal demagnetization.

When the magnetic field reaches zero (point 3), the heat switch is closed and the salt is rapidly magnetized, corresponding to the dashed lines from point 3 to point 4 to point 1. The heat expelled from the spin system, Q_B, is conducted to the helium bath between point 4 and point 1. Once the heat is removed, the cycle can be repeated. It should be noted that the efficiency of the ideal adiabatic demagnetization cycle is equal to the Carnot efficiency. Therefore,

$$\frac{Q_A}{Q_B - Q_A} = \frac{Q_B}{T_B - T_A}$$

NEW DESIGN REQUIREMENTS FOR THE GSFC REFRIGERATOR

The design presented here is the first complete design of an ADR intended for use in space. The requirements of space, as well as the requirements of the bolometers that are being cooled, create a number of specifications that have not been incorporated into previous ADR designs. The most important of these specifications are the following:

- Survive a Shuttle launch.
- Operate with 1.5 K - 2.0 K space pumped liquid helium as a heat sink.
- Produce a minimum heat load on the stored helium to extend the cryogen lifetime.
- Have a 90% duty cycle.
- Have a temperature stability of better than μ10 W, with a goal of 1μW.
- Incorporate a superconducting magnet that can be easily qualified for spaceflight.

SUMMARY OF THE DESIGN FEATURES

A sketch of the GSFC refrigerator as it will be operated in the laboratory is presented in Figure 2. The part of the ADR that is cooled to 0.1 K is called the "cold section" (see figure 3). It consists of the lower part of the heat switch, the paramagnetic salt-copper wire structure in its cylindrical container (often called the salt "pill"), the detector mount, and the copper wires and stainless steel stiffeners connecting these

elements (see figure 3). The continuous fill He^4 refrigerator will be pumped with a vacuum pump to obtain 1.5 K to 2.0 K. The superconducting magnet and the vacuum can containing the cold section will be submerged in liquid helium at 4.2 K.

Since the design of the ADR is lengthy and complicated, a summary of the finalized design is presented here. A more detailed description of the design features of each subsystem can be obtained from the author.

a. Demagnetization System: Magnet, Salt, and Magnet Control Loop:

The ADR is designed to utilize a reliable and inexpensive NbTi superconducting magnet. The rated field in the paramagnetic salt varies from 3.4 T (1 Tesla = 10,000 Gauss) to 4.5 T and averages over 4.0 T.

The cylindrical salt pill is 8.89 cm long and 5.08 cm in diameter. It has a layered construction alternating slabs of salt 1.6 mm thick with sheets of 0.2 mm diameter, 99.999% pure copper wire. All voids are filled with Apiezon J-oil to ensure good thermal conductance. The pill contains 175 gm of ferric ammonium sulfate salt, $Fe(NH_4)(SO_4)_2 \cdot 12H_2O$. This amount of salt can provide 50μW of cooling for 95 minutes at 0.1 K with a 25% margin for cooldown losses.

To obtain adequate temperature stability to operate bolometers at 0.1 K, it is advantageous to control the temperature of the salt by controlling the demagnetization with a feedback loop. The elements of the feedback loops are shown in Figure 2. A calibrated germanium resistance thermometer is thermally anchored to the salt pill. Its electrical conductance is measured with an S.H.E. Model PCB conductance bridge. The off-balance signal from the bridge is then tailored with a Linear Research Model LR-130 temperature controller and fed into an active integrator. The active integrator provides a ramp voltage signal to the HP 6260 D.C. programmable power supply, which in turn provides the current to operate the superconducting magnet.

The temperature stability provided by this feedback loop is determined primarily by two factors:

1. The sensitivity of the Model PCB bridge in conjunction with the germanium resistance thermometer. This sensitivity is on the order of 0.01% of the temperature at 100 mK.

2. The time constant of the feedback loop.

The smaller the time constant of the feedback loop, the smaller the temperature excursions will be before they are corrected. In an ADR, the magnetic moments of the metal ions, often called the "spin system," responds very rapidly to small changes in the magnetic field. Also, the

time constant between the spin system and the lattice of the salt is negligible at 0.1 K. In addition, the relatively high thermal conductivity (for 0.1 K) of the salt crystals causes the thermal time constant of the salt to be very short. The only remaining time constant, the thermal time constant between the salt and the germanium resistance thermometer will, therefore, be the longest single time constant in the feedback loop. This time constant can be made quite short by ensuring that good thermal contact is made between the salt and the resistance thermometer, and that no significant heat capacity is thermally anchored to the germanium resistor.

The relatively short time constant of this feedback loop results in superior temperature stability. This short time constant is one of the important assets of an ADR.

b. Structural Design:

As mentioned, the primary purpose of this ADR is to provide reliable refrigeration for bolometers in the 0-g environment of space. To meet this requirement, the refrigerator must be able to survive a Shuttle launch. The GSFC design has incorporated this requirement.

The cold section of the refrigerator is attached to the nominally 2 K He^4 pot by the nylon cylinder connecting the two ends of the gas gap heat switch. Additional support is provided by 32 Type 101 nylon wires attached to nylon rings located at various points along the cold section. Nylon is not the optimum material but rather was chosen for its ready availability.

The end of the nylon wires at 2 K are also attached to nylon rings. These rings are supported by four sturdy rods spanning the length of the cold section and equally spaced around it. The nylon cylinder and wires must provide less than a 50 μW heat leak to the cold section. For this reason, they are the critical elements in the mechanical design. Other parts of the structure can be made quite rigid. For example, the cold section is made both sturdy and rigid by placing thin wall stainless steel tubing between the salt pill and the heat switch, and between the salt pill and the detector mounting plate.

The critical components of the structural support system have been analyzed by M.T.P. Chan of the GSFC Structural Loads and Analysis Section. The structural analysis shows that the support system will survive a Shuttle launch with a margin of safety of 5.7.

c. Thermal Design:

c.1 The Cold Section:

Temperature differences between various sections of an ADR may significantly degrade the performance of the refrigerator. Therefore, the most important consideration in the thermal design of an ADR is to limit these temperature differences. The temperature differences result from and are maintained by the heat load on one section of the refrigerator being conducted to another section. Since these heat loads differ for each part of the demagnetization cycle, the temperature differences must be calculated for each part of the cycle.

During the isothermal demagnetization at 0.1 K, the heat load on the bolometers is conducted to and absorbed by the salt. Taking the total heat load on the bolometer mount to be 25μW (a very conservative assumption), the temperature difference between the salt and the bolometer mount is calculated to be less than 8 mK. An 8 mK temperature difference will require the salt to be maintained at 92 mK in order to maintain the bolometer mount at 100 mK. This would reduce the cooling power of the salt by 8%. But, the salt pill in the GSFC refrigerator is designed with a 25% margin on the cooling power so the ADR will still meet its design goals.

For the demagnetization of the salt from 2 K to 0.1 K, the primary heat load on the refrigerator is due to eddy current heating and due to the removal of the enthalpy of the refrigerator (other than the enthalpy of the spin system). Fortunately, the enthalpy of the entire cold section of the refrigerator, exclusive of the salt spin system, is much less than the enthalpy of the spin system itself. Furthermore, the eddy current heating is also small. The calculated total loss of cooling power due to these parasitic heat loads will be less than 2%. Since this loss is so small, the details of the thermal design during this phase of the demagnetization are immaterial.

Only the essential features of the thermal design of the cold section have been presented here. By historical standards, an unusually thorough thermal design was performed on the GSFC refrigerator.

c.2 Thermal Conduction of the Mechanical Support Structure:

The thermal conductivity of type 101 nylon (density = 1.141 gm/cc) has been well characterized at low temperature.[1] At 2 K, its conductivity is given (conservatively) by K = 50μW/cm K. Using this value of K as $\bar{K}$ (another conservative approximation) in

$$Q = \frac{\bar{K}A}{L}\Delta T$$

[1] R.J. Kolouch et al, J. Apl. Phys. 39, 3999 (1968)

we find that the heat leak through the 32 nylon support wires is less than 9 μW when the support bracket is at 2 K. The heat leak through the 40 mil thick nylon cylinder of the gas gap heat switch is less than 18 μW. Thus, the total heat leak through the mechanical support system is less than 27 μW.

d. Gas Gap Heat Switch:

The GSFC refrigerator is designed specifically for flight on a Shuttle sortie mission. To store liquid helium for a Shuttle sortie requires a relatively long lifetime storage dewar. With present dewar technology, all such dewars have at least one vapor cooled shield to intercept the radiation between the liquid helium and the typically 300 K outer shell of the dewar. Due to the appreciable tubing length required by such vapor cooled shields, long lifetime storage dewars have appreciable flow impedance in the vent lines. It is estimated that this flow impedance will, in general, be sufficient to prevent space from pumping liquid helium to much less than 1.5 K. Therefore, if the ADR is not to impact the liquid helium dewar design, it must be capable of operating with liquid helium in the range from 1.5 K to 2.0 K.

In contrast to this requirement, all ADRs have historically operated either with an He^3 refrigerator or with an He^4 refrigerator at 1.0 K. At these temperatures, a lead superconducting heat switch can be utilized. However, with space pumped helium at 1.5 K or above, the superconducting heat switch has a very poor on/off ratio. Therefore, a new heat switch capable of functioning at higher temperatures was required. To fill this need, a getter-operated, gas gap heat switch was designed. The heat switch consists of two copper end pieces separated by a narrow "gas gap." The volume in the gap is connected to a small zeolite getter capable of pumping helium to a pressure of less than 10^{-6} torr. At these pressures, the conduction across the gas gap is much less than the 9 μW/K thermal conductance through the nylon cylinder connecting the two copper end pieces. By heating the getter to 10 K to 20 K, enough helium can be driven off to raise the pressure of the gas gap to 10^{-1} torr. With this pressure in the gas gap, the heat switch has a thermal conductane of approximately 100 mW/K. Thus, the on/off ratio of the switch is approximately 10,000.

e. Features for Laboratory Testing:

It should be emphasized that the GSFC refrigerator is a development model. As such, it will be extensively instrumented. Specifically, heaters and calibrated resistance thermometers will be placed on strategic locations throughout the ADR. This instrumentation will provide access to sufficient experimental data to thoroughly analyze the performance of the refrigerator.

To provide a convenient and flexible method of simulating space pumped helium, a continuous fill He^4 refrigerator has been included in the test cryostat. This refrigerator would not, of course, be part of the flight model ADR.

f. Impact of New Requirements on the Design:

As indicated earlier, to provide cooling power for bolometers in a Shuttle launch experiment, an ADR must satisfy several new requirements. The impact of these requirements on the design of the ADR can be seen in the preceding design summary. In particular, the most important of these impacts are the following:

- To survive the Shuttle launch, the ADR must have a strong and rigid support system. The dominant heat load on the ADR is the heat conducted through this support structure.

- To operate with the liquid helium at 1.5 K to 2.0 K requires a heat switch capable of functioning at higher temperatures than is possible with the standard superconducting heat switch. This requirement necessitated the design of a getter operated gas gap heat switch.

- To produce a minimum heat leak on the stored cryogen, the efficiency of the ADR has been maximized. To achieve this efficiency, the thermal paths within the refrigerator were designed with great care.

- To obtain a 90% duty cycle, severe constraints were placed on the physical construction of the ADR. Specifically, the rapid magnetization and demagnetization will create excessive eddy current heating in any large piece of highly conductive metal within the field. This requirement resulted in the use of fine copper wires for thermal conductance.

- To satisfy the temperature stability requirements, the cylindrical paramagnetic salt "pill" was designed for higher internal thermal conductance. In addition, the programmable power supply was servocontrolled to produce an isothermal demagnetization.

- To ensure that the superconducting magnet could be easily space qualified, the ADR was designed to use a limited magnetic field.

MODIFICATIONS REQUIRED FOR A FLIGHT MODEL ADR

Due to the relatively large costs associated with them, several requirements for a flight model ADR are not incorporated in the engineering model. These include flight qualified electronics, a space qualified superconducting magnet, an automated operating system, and elimination of fringing magnetic fields at the bolometers. Each of these areas have been or will be addressed by various programs both in and outside NASA.

Electronic systems not presently qualified for space include the electronics associated with high sensitivity resistance thermometry and the superconducting magnet charging system. Excellent temperature sensitivity could be obtained by using a non-observing bolometer as a resistance thermometer. The electronics associated with this bolometer could be essentially identical to the electronics associated with the observing bolometers. Bolometers and their associated electronics have been flown on a number of balloon experiments, and space qualified bolometers and the associated electronics are presently being developed for the Cosmic Background Explorer satellite.

Space qualification of a superconducting magnet charging system for an ADR should not be a difficult undertaking. Magnet charging systems with very simple circuit designs have been flown on a number of balloon flights. Furthermore, the magnets flown on these balloon programs required over 100 amps to charge them. The magnet for a space qualified ADR would require only a fraction of this current. It should also be mentioned that the total energy required to charge the magnet is very small, namely 10,500 J (about 3 watt hours). The superconducting magnet must also be qualified for use in space. Primarily, this requires that it must withstand Shuttle loads (but it does not need to be magnetized during launch). It is also highly desirable that the magnet be able to operate without being submerged in liquid helium to alleviate 0-g fluid management problems. The first of these requirements is almost no requirement at all, for any well constructed laboratory superconducting magnet will survive the Shuttle loads. As for the second requirement, small modern magnets similar to those required by ADRs are often potted in epoxy. These magnets do not utilize direct contact to liquid helium to provide cooling. Several potted magnets have even been operated in a vacuum. For example, Johnson Space Flight Center used a superconducting magnet operated in a vacuum to study the moon rocks. Finally, it should be mentioned that there are proposals to fly two large (770 kg) superconducting magnets on the Shuttle for a cosmic ray experiment. If these magnets were to fly and perform well, it would certainly end any doubts about the appropriateness of flying the much smaller magnet required by an ADR.

Before leaving this discussion of the superconducting magnet, another requirement resulting from the need to conserve the stored liquid helium should be addressed. The magnet leads used to charge and discharge the superconducting magnet must pass from the electronics at room temperature to the magnet at roughly 2 K. Since a solid copper wire large enough to carry the current required by a typical superconducting magnet would conduct too much heat from room temperature to the liquid helium, special vapor cooled leads have been developed by the commercial superconducting magnet manufacturers. For example, American Magnetics, who supplied the

magnet for the GSFC refrigerator, also provided 50 amp vapor cooled leads that consume only 0.14 liters/hour of liquid helium. This is equivalent to 3.36 liters/day, which is an appreciable but acceptable boil-off rate for the shuttle sortie mission. However, this boil-off rate can easily be reduced as follows. Any reasonable sized liquid helium storage dewar that would be launched on the Shuttle will have a boil-off rate roughly 1 liter/day or more. Some of the cooling power of this boil-off can be used to decrease the heat load due to the magnet leads by routing the leads through the dewar wall inside the vent line. Even more important the boil-off rate can be greatly reduced by designing, a magnet to draw much less current than that used in the present GSFC refrigerator. This would be accomplished by simply using small diameter superconducting wire. A magnet using only 4 amps could be constructed, reducing the heat load on the cryogen from the magent leads by a factor of 150.

Another feature of a flight model ADR not presently incorporated into the GSFC refrigerator is automated operation. But, a microprocessor controller for an ADR has been developed by J.P. Eisenstein et al[2] and is presently in use at the University of California, Berkeley. This controller appears to be quite similar to that needed for a flight model ADR.

It would be essential that a flight model ADR not produce any appreciable magnetic field at the bolometers since the magnetoresistance of the bolometers might interfere with their operation. These fields can be eliminated by any combination of the following techniques. First, a superconducting "bucking" coil could be put in series with the demagnetization magnet and positioned so as to cancel the fringing magnetic field of the demagnetization magnet in the region of the bolometers. Second, a superconducting shield could be put around the bolometers. And finally, the bolometers could be physically separated from the demagnetization magnet to reduce the fringing fields at their location. Using these three techniques in concert will virtually eliminate the magnetic field in the region of the bolometers.

CURRENT STATUS

The design and fabrication of the GSFC refrigerator has been completed. The test dewar and the superconducting magnet and its support structure have been designed, fabricated, and delivered to the GSFC. The electronics to control the demagnetization have been designed and assembled. Final assembly and testing of the refrigerator is in process.

Preliminary tests of the adiabatic demagnetization refrigerator have been completed. While quantitative measurements of performance have not yet been performed, some qualitative statements can be made. The cooling power of the salt pill is approximately as described here. The thermal conudctance between the detector mount and the salt pill is excellant, as is the thermal conductance between the salt pill and the gas gap heat switch. In its conducting state, the heat switch has a thermal conductance of roughly half the design goal of 100 m W/K. However, this conductance is sufficently high to allow the salt to be magnetized in 3 minutes with minumum thermal loses. The design requirement for the system was for a 5 minute magnetization. In the isolating state the thermal conductance of the heat switch is so small that a good determination of its thermal conductivity is somewhat difficalt. However, the on/off ratio appears to be in excess of 10,000.

The only difficulty encountered to date is an anomalously long time constant for the gas gap heat switch when going from the conducting state to the nonconducting state. The cause of this long time constant is presently being investigated.

CONCLUSION

The detailed design of the engineering model refrigerator has not uncovered any potential problem areas that might prevent an ADR from being used in space. When and if this design is proven by laboratory testing of the refrigerator, we will have come a long way toward a flight model ADR, for this refrigerator incorporates most of the features that are necessary for a flight model. (The cold section of the engineering model incorporates all the features that are necessary for the flight model.) Features necessary for the flight model that, due to cost limitations, have not been incorporated into the engineering model either have been developed elsewhere or appear likely to be developed in the near future.

Improved bolometers are presently under development at the GSFC and other locations. These advanced bolometers, together with the adiabatic demagnetization refrigerator, will provide astronomers with a powerful long wavelength detector system.

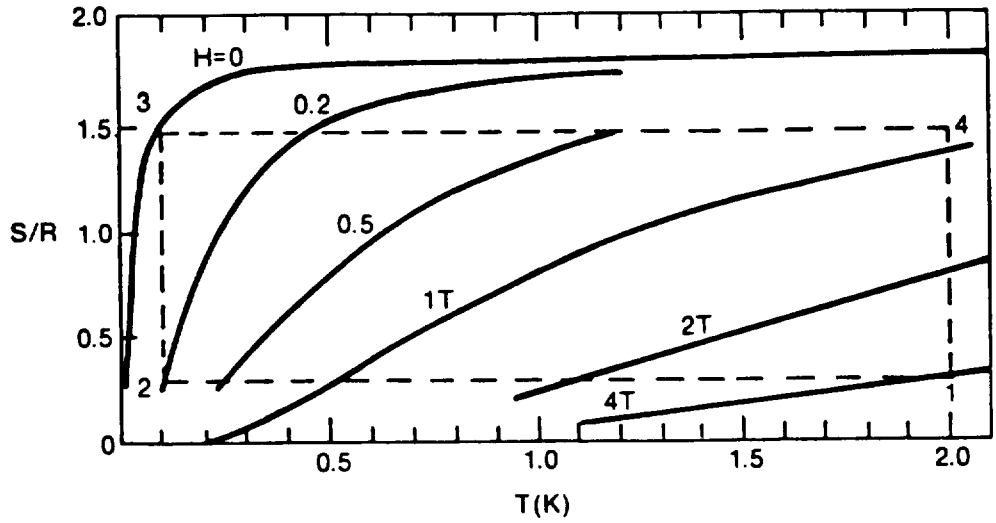

FIGURE 1a.

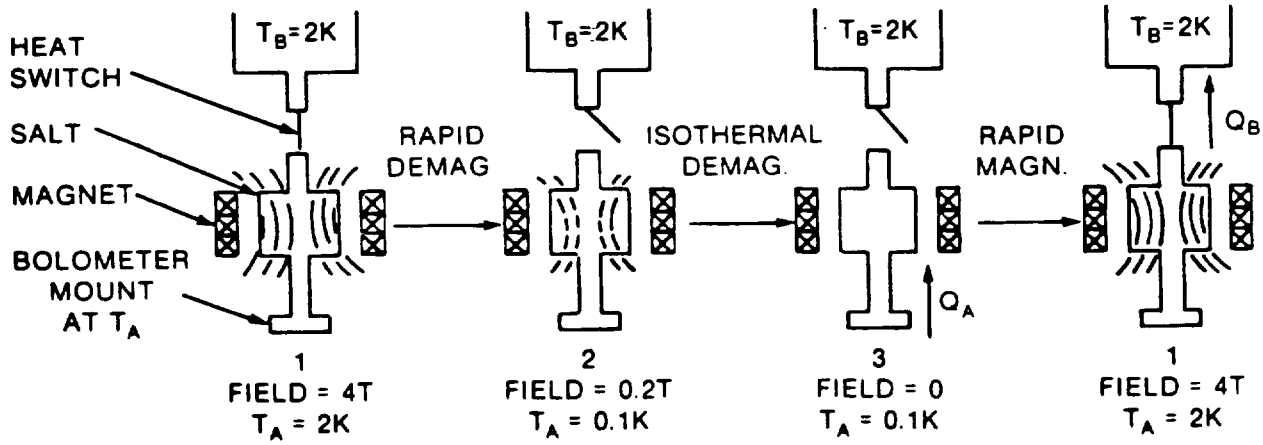

FIGURE 1b.

Figure 1. Ideal Adiabatic Demagnetization Cycle.
Numerical Parameters are for Ferric Ammonium Sulfate.

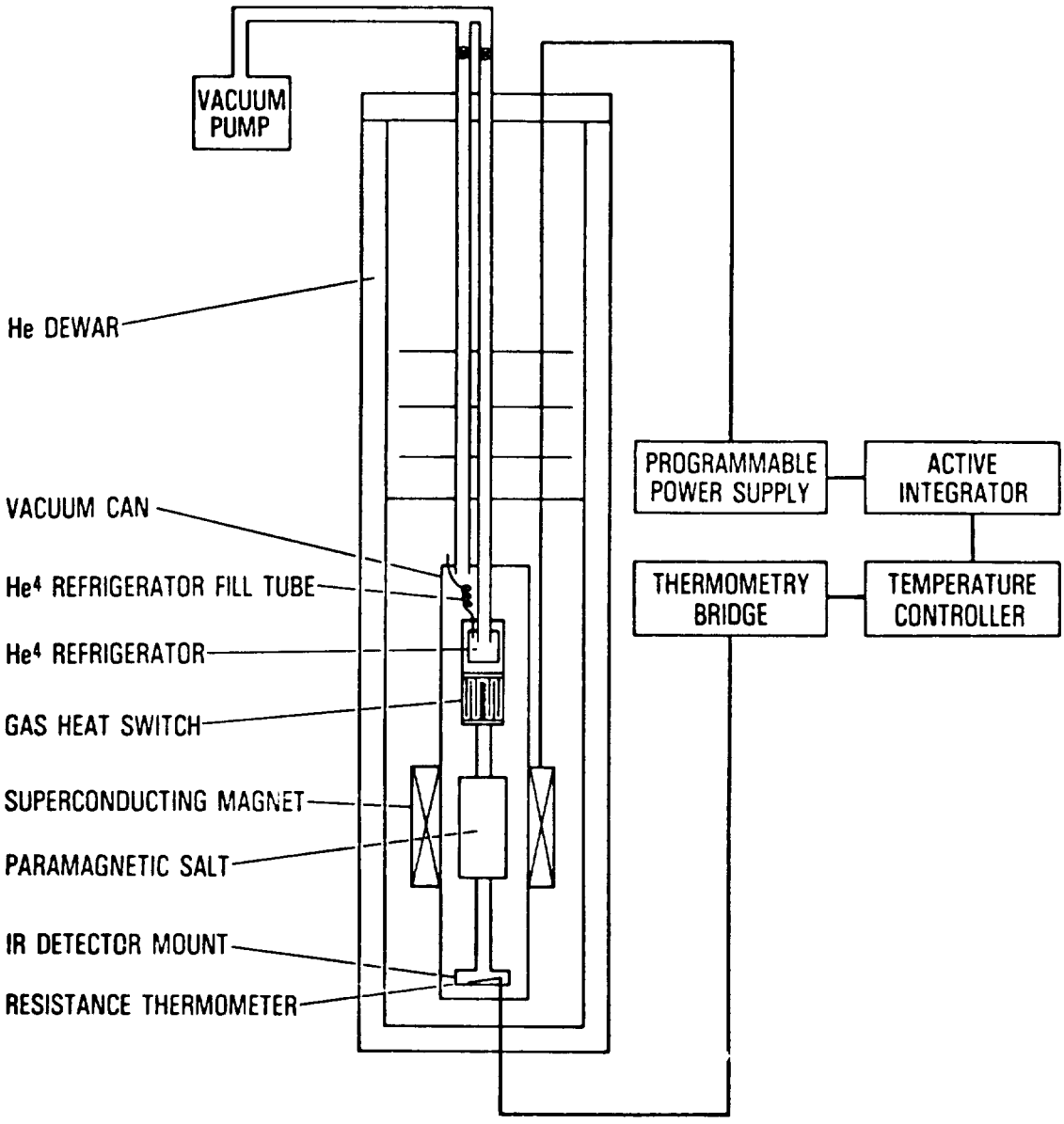

Figure 2. GSFC Adiabatic Demagnetization Refrigerator

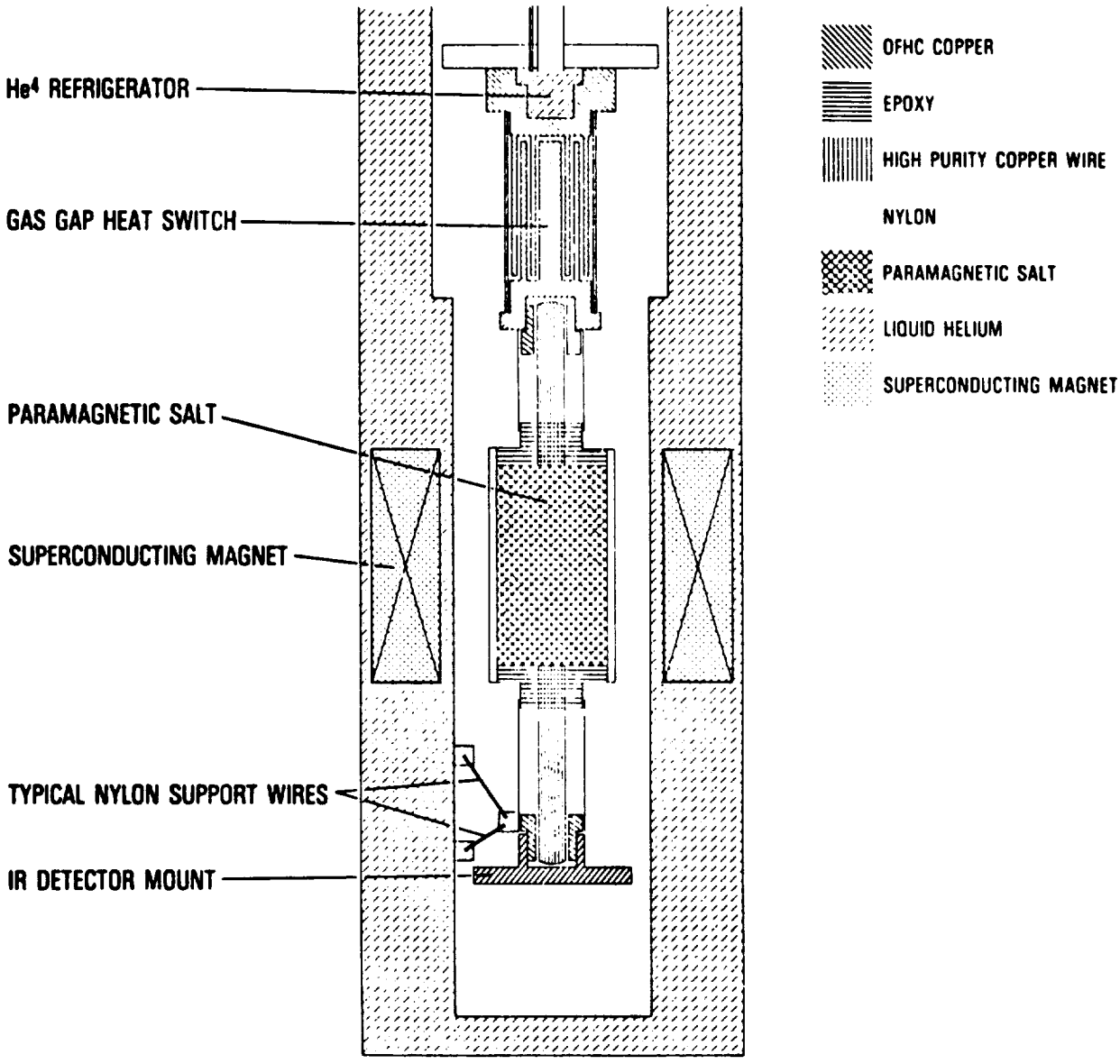

Figure 3. GSFC Adiabatic Demagnetization Refrigerator

A HELIUM-3 REFRIGERATOR EMPLOYING CAPILLARY CONFINEMENT OF LIQUID CRYOGEN

D.J. Ennis, P. Kittel, W. Brooks, A. Miller
Ames Research Center
NASA
Moffett Field, CA

A.L. Spivak
Transbay Electronics
Richmond, CA

ABSTRACT

A condensation refrigerator suitable for operation in a zero-gravity space environment has been constructed. Unlike conventional cryostats, the condensed liquid refrigerant is confined by surface tension inside a porous metal matrix. Both helium-4 and helium-3 gases have been successfully condensed and held in a copper matrix. Evaporative cooling of confined liquid helium-4 has resulted in a temperature of 1.4K. Using a zeolite adsorption pump external to the cryostat, a temperature of 0.6K has been achieved through evaporative cooling of liquid helium-3. The amount of time required for complete evaporation of a controlled mass of liquid helium-4 contained in the copper matrix has been measured as a function of the applied background power. For heating powers below 18 mW the measured times are consistent with the normal boiling of the confined volume of liquid refrigerant. At background powers above 18 mW the rapid rise in the temperature of the copper matrix- the signature of the absence of confined liquid- occurs in a time a factor of two shorter than that expected on the basis of an extrapolation of the low-power data.

INTRODUCTION

Refrigerators operating at cryogenic temperatures on the order of 1K or less will be required for several classes of future NASA space missions. Cooled infrared detectors will be used in conjunction with infrared astronomical telescopes- notably the Shuttle Infrared Telescope Facility (SIRTF) and the

Large Deployable Reflector (LDR), Earth resources remote sensing satellites, and high-frequency commercial communications systems. In addition, spaceborne physics experiments studying liquid helium critical phenomena will require a cryogenic working surface. By performing such experiments in space improvements in temperature resolution of several orders of magnitude can be achieved [1].

Possible refrigeration processes compatible with the zero-gravity space enivironment are helium-3/helium-4 dilution, adiabatic demagnetization, and liquid helium evaporation [2]. Dilution refrigeration in space presents difficulties since no gravitational field is present to maintain the crucial cooling interfaces. Recent proposals for circumventing this problem have concentrated on determining the effect of a controlling electric field on the phase boundary [3]. Gravity-independent adiabatic demagnetization refrigerators show promise for space applications and are an active area of research, but engineering problems- including magnetic torques and power/mass requirements- still remain [4].

Ground-based helium-3 evaporation refrigeration technology is not directly transferable to space refrigeration since the Earth's gravitational field is used to direct and confine the liquid cryogen during and after condensation from the gas phase [5]. A proposed alternate approach replaces the gravitational force with liquid/metal surface tension to confine the cryogen. Theoretical calculations [6] have addressed the feasibility of this approach and preliminary experimental research with various liquid cryogens in a porous metal matrix have been successfully performed [7].

In this paper, a low-temperature cryostat in which surface tension forces confine the liquid helium cryogen to the micron-sized capillaries of a copper sponge is described. Both helium-3 and helium-4 gases have been successfully condensed; evaporative cooling of the resulting liquids have resulted in temperatures of 0.5 K and 1.4 K respectively. Since in any realistic experimental or astronomical application the low temperature working surface will be subject to a background power load, the response of confined liquid helium-4 to a range of heat loads was measured. As discussed in detail below, it was found that for heating powers less than 18 mW, the liquid cryogen underwent normal evaporation but that for powers above this value the temperature of the copper sponge rose in a time faster than the evaporation time suggesting a possible physcial ejection of

the liquid cryogen from the sponge interior.

INSTRUMENT DESCRIPTION

Figure 1 is a schematic diagram of the capillary confinement cryostat. The critical component of the system is the porous copper matrix or sponge (A). In operation, the liquid cryogen is held in the interstitial spaces of the sponge by the surface tension between the copper strands and the liquid helium. Foametal Inc. manufactures the sponges by sintering a granular powder into a reticular celluar structure. The results reported in this paper were obtained with a sponge having 60% the density of pure copper and containing an average pore size on the order of 9 microns. The cylindrical sponge is indium soldered along its rim to a copper working surface.

Surrounding the copper sponge and working surface is the transfer gas volume (B). The gas in this volume acts as a thermal switch between the sponge and helium-4 reservoir (D). The sponge and working surface are attached to the end of the U-shaped test gas delivery tube (E) through which the gas to be condensed flows from an external gas supply to the sponge. To insure that the test gas will condense at the sponge and at no other point along the length of the delivery tube, the tube must not be in thermal contact with the helium reservoir. For the bottom part of the tube, the thermal isolation is provided by an inner vacuum can (C). The remainder of the tube which passes through the dewar is double-walled. As a further step to prevent condensation in the delivery tube, a heating coil was attached to the horizontal section of the U-tube (see Figure 1). Finally, conventional liquid nitrogen and outer vacuum jackets provide a thermal shield to the room temperature laboratory environment.

Also shown in Figure 1 as black dots are the locations of the sensors used to monitor the status of the cryostat. Thermometry is provided by germanium resistance thermometers in thermal contact with the helium reservoir, working surface, sponge, and test gas delivery tube. With liquid helium in the sponge, it was found that the temperature of the working surface was typically only 10% higher than the sponge temperature, thus indicating that the thermal conductance between these points was as high as desired. The purpose of the test gas delivery tube thermometer was to verify that no helium gas had condensed in the tube as opposed to in the sponge. Three manometers were also

employed to measure the helium gas pressure over the helium-4 reservoir, in the transfer gas volume, and over the copper sponge. A plumbing manifold connected to the top of the cryostat enabled the evacuation of the test gas delivery tube, the transfer gas volume, and the inner vacuum can. Both the pressure of the helium gas above the sponge and in the helium-4 reservoir were maintained at a fixed value by automated, motor-driven valves.

It should be pointed out that the ultimate application of a refrigerator employing capillary confinement would be in the low-gravity space environment. Although, of course, this situation cannot be simulated in an earth-based laboratory, the geometrical configuration of the cryostat shown in Figure 1 represents a more stringent test of the surface tension confinement principle. This is due to the fact that the flow of the condensing gas is opposite to the gravitational vector; the confined liquid must be held by the surface forces against a gravitational acceleration of 1 g.

EXPERIMENTAL RESULTS

In this paper, two sets of experiments will be described each aimed toward characterizing the performance of the capillary confinement technique for zero-gravity helium refrigeration. The first experiment was to establish that helium gas could both condense on the copper fibers and that surface tension could confine the resulting liquid cryogen during evaporative cooling. During condensation the transfer gas volume was filled with helium-4 gas to a pressure of 4 torr, thereby allowing the sponge to attain the temperature of the helium-4 reservoir (2.5 K). The test gas was delivered to the sponge at a controlled pressure greater than the helium condensation pressure. It was established that the test gas had condensed when the sponge temperature and the test gas pressure were consistent with the known helium vapor pressure relation. Both helium-4 and helium-3 gases have been sucessfully condensed. For helium-4 the gas supply used was the boil-off from a commercial helium-4 dewar. For helium-3 a closed cycle control system was constructed in which high pressure gas is expanded into low-pressure volumes before passage into the test gas delivery tube.

To achieve the desired low-temperature performance, the liquid cryogen in helium refrigerators must undergo evaporative

cooling by lowering the pressure of the gas in equilibrium with the liquid. In order to enable evaporative cooling of the liquid held in the sponge, the transfer gas volume was evacuated and the test gas delivery tube was attached to a pump. For helium-4 the pump used was a conventional diffusion pump. For helium-3 a zeolite absorption pump cooled to 4.2 K was employed. The lowest pressures and temperatures achieved with the present system are shown in Table 1. These temperatures are consistent with the the operating temperatures of germanium bolometers presently used for ground and air based far-infrared/millimeter obeservational astronomy [8,9]. It should be noted that the limiting factor in achieving the lowest sponge temperature for the present system is the pumping capacity of the zeolite in the adsorption pump. Increasing the volume of the present external pump should allow temperatures of 0.3K to be obtained.

The second set of experiments involved establishing the performance of the capillary confinement technique when the copper sponge was subjected to a range of background heating powers. The first step in the experimental procedure was the condensation of a controlled volume of helium-4 gas. This input volume was regulated at 3.0 liters using a conventional dry gas meter. Heating loads were applied to the sponge through Joule heating of three sets of resistors attached to the working surface (schematically shown in Figure 1). After condensation of the test gas, the heating power was applied and the gas pressure above the sponge was maintained at 50 torr which corresponded to a sponge temperature of 2.5 K. For a given heating power, P_H, the time, t_e, between the onset of heating power application and the point at which liquid cryogen was no longer present in the sponge was measured with a strip chart recorder. The signature that the sponge no longer contained liquid helium was a rapid sponge temperature increase. A secondary indicator was the sudden decrease in the rate of gas flow leaving the sponge as measured with a flowrate meter attached to the test gas delivery tube.

In Figure 2 the results obtained from heat load experiments performed on four separate days are presented. For each day the inverse of t_e is plotted against heating powers ranging from 2 to 20 mW. The error shown in t_e is dominated by the finite time width of the temperature rise signature. As is illustrated by Figure 2, the data obtained for low heating powers- $P_H < 18$ mW are well fit by the solid lines shown. The slope and intercept of these lines were obtained from a least squares analysis. In the second column of Table 2, the reduced chi-squared resulting from

this analysis are shown; the values obtained reflect the excellent quality of the fit of the data to a straight line.

A linear relationship between inverse t_e and P_H pertains if the liquid confined to the sponge is undergoing evaporation due to the heating power. Specifically, energy conservation gives the following equation

$$1/t_e = (1/LV_o)\, P_H + P_R/LV_o \qquad (1)$$

where L is the latent heat of evaporation of helium-4, P_R is the residual or parasitic power continually absorbed by the sponge from its surroundings, and V_o is the volume of confined liquid cryogen. This liquid volume is converted into the volume of gas evaporated- V_G - by the liquid/gas density ratio. In Table 2 the values of V_G and P_R calculated, respectively, from the slope and intercept of the least-squares fit lines are presented. As required by mass conservation, the value of V_G agrees well with the input gas volume of 3.0 NTP liters. The negative values of P_R obatained on two days probably reflect the inadequacy of the assumption that all of the power applied to the heating resistors is transferred to the liquid helium.

It is apparent in Figure 2 that for each of the days shown the high heating power data points deviate significantly from the evaporation line. For applied heating powers above 18 mW, t_e is considerably shorter than the anticipated evaporation time; the sponge temperature increases on a faster timescale. In Figure 3 the data from all four days have been plotted on the same graph. It can be seen in Figure 3 that there is reasonable agreement between data obtained on various days. The larger reduced chi-squared obtained for the composite data (see Table 2) is a reflection of the variation of the parasitic power from run to run. More importantly, the data shown in Figure 3 indicate that deviation of t_e from the evaporation value has a sharp dependence upon the heating power; the effect cuts-on quite rapidly at 18 mW. The possible physical explanations of the observed effect- such as the ejection of the confined liquid during the transition between nucleate and film boiling at high powers- will be discussed in a future paper.

FUTURE WORK

In terms of fully investigating the capillary confinement

technique for zero-gravity helium refrigeration, several avenues and questions still remain open. In addition to theoretically understanding the physical processes involved in the high heating power effect discussed above, more experimental data - especially at $P_H > 20$ mW- is required. Heat load data using liquid helium-3 have been obtained and are presently under analysis. In addition, the effect of the variation of sponge parameters such as composition, interior geometry, and pore size on cryostat performance needs to be established.

Actual operation of the capillary confinement refrigerator in a zero-gravity environment would completely establish its performance. This could be especially critical if the high power heating effect is a boiling phenomenon since, unlike the situation on earth, the role of buoyancy forces is diminished by several orders of magnitude in the space environment. Aircraft parabolic trajectories and ground-based drop towers can produce low-gravity simulation but are severly time constrained. For extended testing a space shuttle or space station experiment is required.

Table 1. Capillary refrigerator performance.

CAPILLARY REFRIGERATOR PERFORMANCE

CRYOGEN	PRESSURE (TORR)	TEMPERATURE (K)
HELIUM-4	1.8	1.4
HELIUM-3	0.3	0.55

Table 2. Evaporation data.

EVAPORATION DATA

DATE	χ_ν^2	$V_G(\ell)$	P_R(mW)
5/11/82	1.3	2.7±0.3	-3.0±1.2
5/3/82	0.1	3.2±0.2	-0.8±0.3
5/12/82	0.4	3.2±0.5	1.4±2.0
3/29/82	-	3.4±0.3	0.2±0.6
COMPOSITE	6.0	3.1±0.1	-0.8±0.2

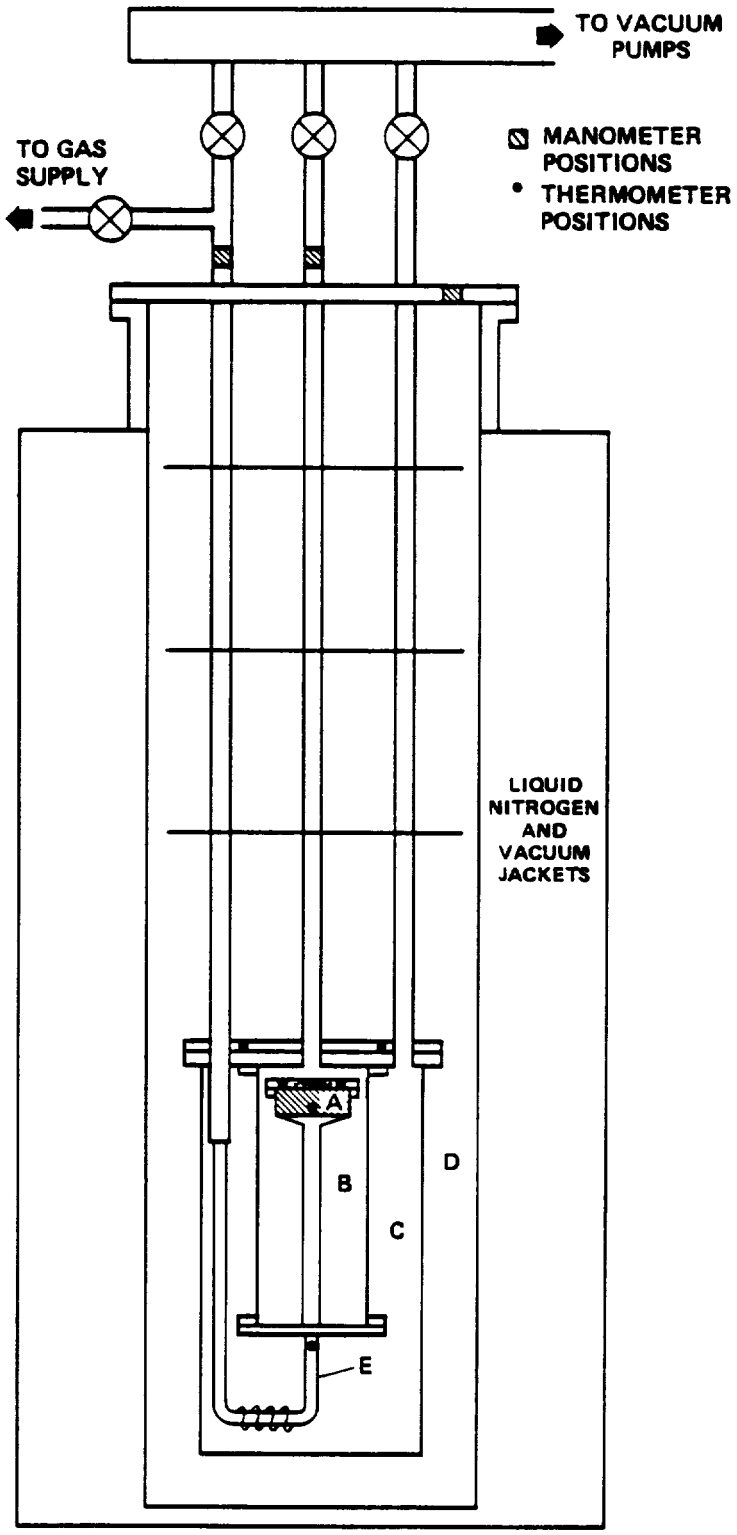

Figure 1. Schematic diagram of the capillary confinement cryostat

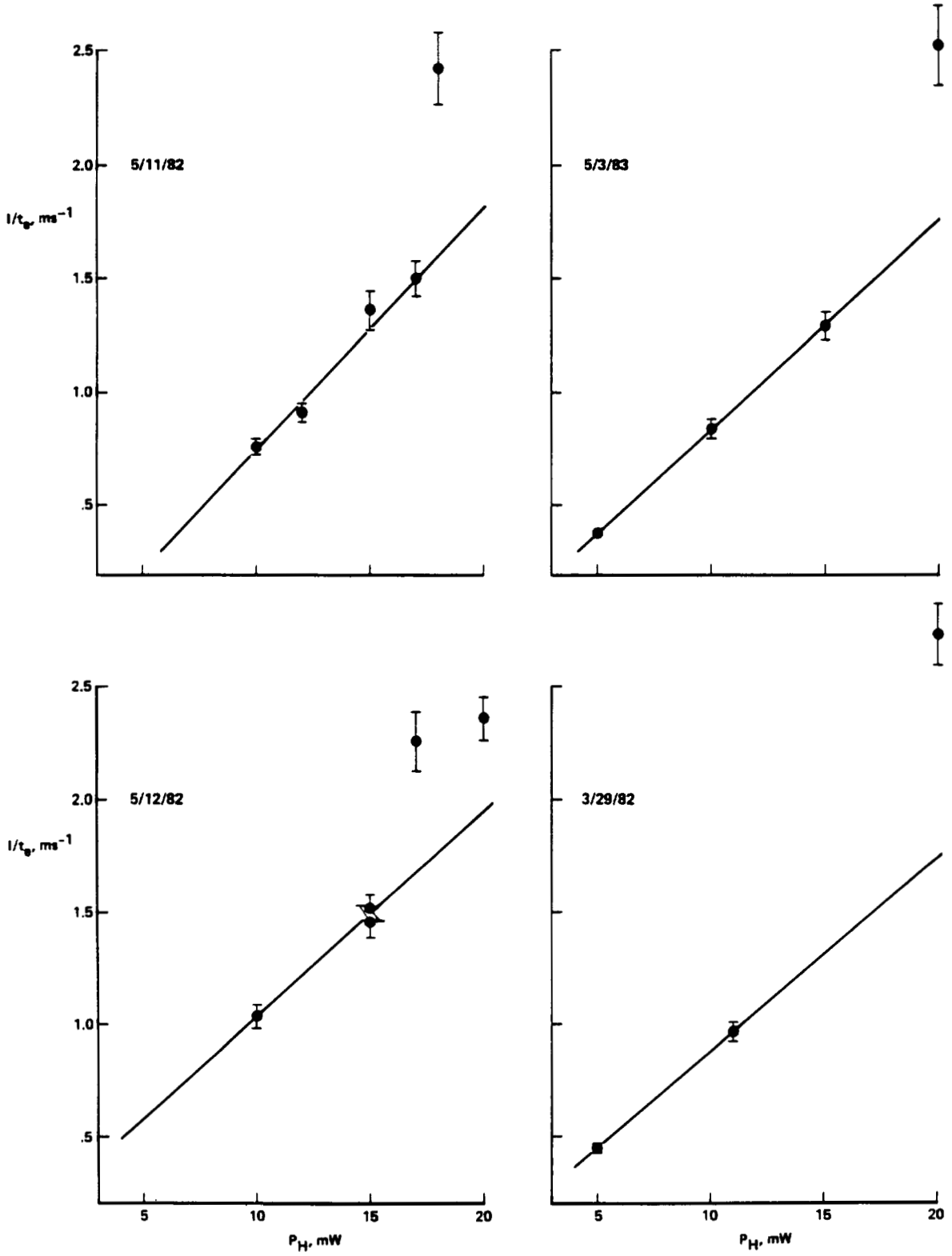

Figure 2. Inverse evaporation time versus applied heating power for four runs

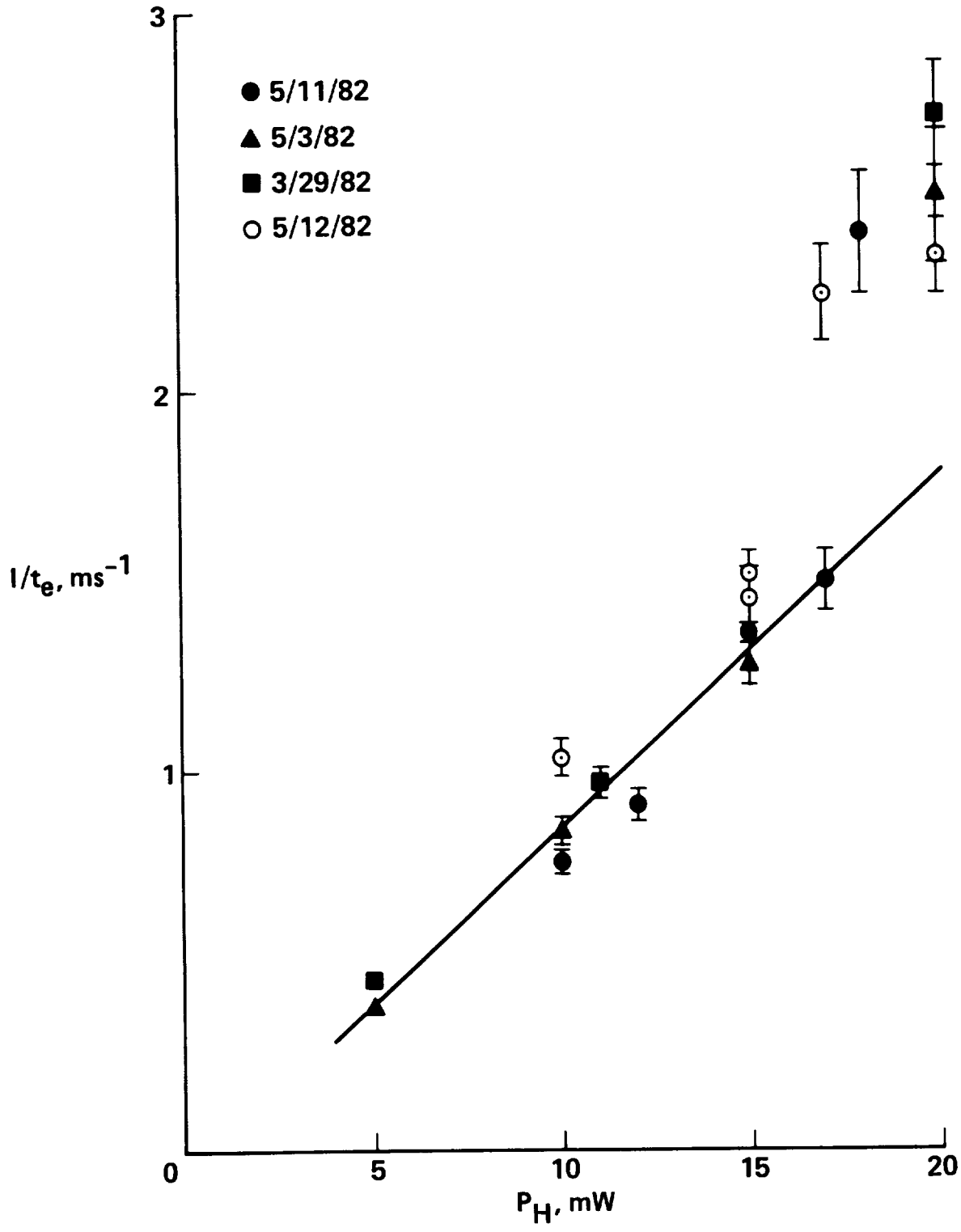

Figure 3. Composite Evaporation Curve

REFERENCES

1. Fairbank, W.M., van Kann, F.J., and Lipa J.A.: The Possibility of Performing in Space an Improved Measurement of the Lambda Point Heat Capacity Singularity. Quantum Fluids in Space, 1975, pp. 35.

2. Kittel, P.: Refrigeration Below 1K in Space. Physica, vol. 108B, 1981, pp. 1115.

3. Jackson, H.W.: Can Helium-3 - Helium-4 Dilution Refrigerators Operate Aboard Spacecraft? Cryogenics, vol. 22, 1982, pp. 59.

4. Kittel, P.: Magnetic Refrigeration in Space- Practical Considerations. J. of Energy, vol. 4, 1980, pp. 266.

5. Roellig, T.P.L., and Houck, J.R.: A Helium-3 Cooled Bolometer System for One Millimeter Continuum Observations. International Journal of Infrared and Millimeter Waves, 1983, in press.

6. Ostermeir, R.M., Nolt, I.G., and Radostitz, J.V.: Capillary Confinement of Cryogens for Refrigeration and Liquid Control in Space, I. Theory. Cryogenics, vol. 18, 1978, pp. 83.

7. Donnelly, R.J.: A Study of Confinement and Heat Transfer Properties of Cryogens. NASA Grant NSG-2208, June 1979.

8. Ennis, D.J.: One-Millimeter Continuum Observations of Quasars. Ph. D. Thesis, California Institute of Technology, June 1982.

9. Roellig, T.P.L.: One-Millimeter Continuum Observations of Extragalactic Thermal Sources. Ph. D. Thesis, Cornell University, June 1981.

CASCADE JOULE-THOMSON REFRIGERATORS*

E. Tward and W. A. Steyert+
Jet Propulsion Laboratory
4800 Oak Grove Drive
Pasadena, CA 91109

ABSTRACT

The design criteria for cascade Joule-Thomson refrigerators for cooling in the temperature range from 300K to 4.2K have been studied. The systems considered use three or four refrigeration stages with various working gases to achieve the low temperatures. Each stage results in cooling to a progressively lower temperature and provides cooling at intermediate temperatures to remove the substantial amount of parasitic heat load encountered in a typical dewar. With careful dewar design considerable cooling can be achieved with moderate gas flows. For many applications, e.g., in the cooling of sensitive sensors, the fact that the refrigerator contains no moving parts and may be remotely located from the gas source is of considerable advantage. A small compressor suitable for providing the gas flows required has been constructed and tested. Performance of the system is described.

* This paper represents one phase of research carried out at the Jet Propulsion Laboratory, California Institute of Technology, under NASA Contract NAS7-918.
+ Present address: Air Products and Chemicals, Inc., Box 538, Allentown, PA 18105

INTRODUCTION

The applications for electronics operating at cryogenic temperatures are continually expanding, particularly for military applications. Examples include infrared detectors, Josephson junction computers, communication receivers, precise navigation devices and magnetic sensors. With the advent of nuclear magnetic resonance imaging systems, the production of liquid helium temperatures even in medical instrumentation will soon be routine. Unfortunately, the actual use of cryogenic electronics has been hampered by the expense, complexity, size, and power requirements of the cryogenic refrigerators. In addition, cryogenic refrigerators, in most circumstances, require highly trained maintenance personnel to keep them operating.

The Joule-Thomson (J-T) refrigerator is extremely simple and has no moving parts at cryogenic temperature. In a small J-T refrigerator very high pressure gas flows through a capillary sized tube to a valve or flow restriction where it expands to a lower pressure and cools. This, now cool, gas is used both to provide the required refrigeration and to precool the high pressure gas moving in the capillary tube. This very simple refrigeration method is based entirely on simple energy conservation and requires no intricate or speculative design. Apparently, two factors have limited the use of J-T refrigerators for cryogenic applications. First, very high pressure gas and very clean gas is required, and second, J-T refrigerators are theoretically not as efficient as other types of refrigerators. In order to provide clean high pressure gas researchers have been trying for several years to develop a compressor to meet the very exacting requirements of J-T refrigerators. At the Jet Propulsion Laboratory, a need for long-lived refrigerators (up to 10 years) for use on spacecraft has resulted in a considerable effort to develop non-mechanical adsorption and absorption compressors [1] for use with J-T refrigerators. It is anticipated that such systems could deliver the long lifetime required because of the absence of motion induced wear which is the chief performance degradation mechanism in conventional refrigerators.

In the meantime, W. A. Little, at Stanford, has developed a method of producing tiny J-T refrigerators for electronics applications on small glass slides using photolithographic techniques.[2] These small refrigerators are now produced commercially [3] and are very promising for high volume, inexpensive mass production. Currently, these refrigerators are run "open cycle" from a compressed gas cylinder with the exhaust gas being vented to the atmosphere. The development of a small reliable compressor would open up many more applications for use of small J-T systems. Cross, Lawless, and Steyert have designed, but not built, a J-T compressor which uses new electrostrictive materials developed at Pennsylvania State University. In addition, a prototype small mechanical compressor which appears to meet the exacting requirements of J-T systems has been built and tested at the Jet Propulsion Laboratory.

There are two important features of J-T systems which are of particular importance for many applications and should be emphasized. The first is that the J-T refrigerator itself can be made very small. This means, that for the cooling of devices such as sensors the dewar can also be made small. For many sensor applications the major load on the cooling system is due to parasitic heat leaks which scale with the size of the dewar system. Therefore, one often would require smaller cooling powers for a J-T system than if either a mechanical refrigerator system or a stored cryogen system is chosen. Secondly, for sensors that are vibration sensitive, the J-T cooler itself has no moving parts and the compressor can be remotely sited. This leads to potentially very low vibration at the sensor for J-T refrigerators with small gas flows [4].

JOULE-THOMSON REFRIGERATION

J-T refrigerators operate on a simple conservation of energy principle. This is illustrated with the aid of Figure 1. High pressure gas of enthalpy h_h with mass flow rate $\dot{m}$ enters the high pressure side of the heat exchanger where it is precooled before it expands through the J-T valve to a low pressure and cools. The gas then picks up the heat load $\dot{Q}$ and exits through the low pressure side of the heat exchanger so that it precools the incoming high pressure gas. The gas exits the heat exchanger with an enthalpy h_l. From energy conservation,

$$\dot{Q} = \dot{m} \, (h_h - h_l) \tag{1}$$

if there are no additional parasitic heat loads.

This simple expression is valid independent of the quality of the heat exchanger, although, obviously the better the heat exchanger the larger is $(h_h - h_l)$ and therefore the larger the cooling power. Many gases can be used to provide J-T cooling over a wide temperature range. The primary physical constraint on the cooler is that for a particular gas which is to be used, the inlet temperature to the heat exchanger must below the inversion temperature of that gas. It is this constraint that limits use of a single working fluid design for an all J-T cooler operating to liquid helium temperatures and at room temperature. He^4 has an inversion temperature of 51K and therefore to reach temperatures around 4K requires upper stage refrigeration to well below 51K in order to precool the high pressure He gas. Therefore, in order to reach $\sim$4K with an all J-T cooler design one requires a cascade process in which one has a few stages of cooling using appropriate working gases. For example, in order to reach 4.2K starting at room temperature one could design a three-stage J-T system using the working gases N_2, H_2 and He.

A N_2 gas source provides high pressure gas to a N_2 J-T cooler which reaches 77K. A H_2 gas source provides high pressure gas which is precooled by heat exchange with the N_2 J-T cooler before it enters the H_2 J-T cooler and provides cooling to approximately 20K. The last cooling stage uses He gas precooled by both the N_2 and H_2 refrigerators before entering the He J-T refrigerator and achieving the 4.2K low temperature. For each cooling stage one must include additional cooling power in order to handle the inevitable parasitic heat loads encountered in a real system. However, nature is kind to the designer in the following way. For a given flow rate, the cooling power available from a N_2 cooler is far larger than that available from the H_2 which is in turn far larger than that available from a He cooler. This means that per unit of cooling power less is demanded of the compressor for the higher temprature stages.

In a related paper at this conference [5] we give an example of a cascade J-T refrigerator which is designed for a very long lifetime. In this system non-mechanical adsorption compressors are used as the high pressure gas sources. The long lifetime is expected because of the absence of moving parts in the refrigerator. A feature of these compressors is that they must also be precooled to their appropriate operating temperatures. Therefore, for this design an upper stage refrigerator has to provide, in addition, cooling for the lower stage compressor. This differs from the example given later in this paper, where room temperature gas sources are assumed. Therefore, for adsorption J-T systems, the upper refrigeration stages would require larger cooling power than a comparable cascade J-T refrigerator using a room temperature compressor. In some applications, however, such as for a long space mission where the cooler is inaccessible for maintenance, cascade J-T refrigerators using adsorption compressors are very promising, especially given the history of lifetime problems with mechanical cryocoolers.

CASCADE J-T REFRIGERATOR

To illustrate the performance requirements of a cascade J-T refrigerator, we consider for simplicity a two-stage design operating between 300K and 84K rather than a four-stage design operating down to 4.5K. A schematic of the cascaded J-T system is shown in Fig. 2. The upper temperature CF_4 stage is used for precooling the gas to the lower temperature N_2 stage. In addition, the CF_4 stage is used to trap parasitic heat leaks into the dewar system. If required, sufficient additional cooling capacity may be included for a specific cooled instrument. In Table I we show some performance characteristics for a two-stage system. The available cooling power is calculated conservatively, assuming that the heat exchangers are not perfect resulting in 85% of ideal efficiency for each J-T heat exchanger system. As well, the heat load

on the CF_4 refrigerator for precooling the N_2 gas has been included. Therefore, the available cooling power represents the cooling which can be used for both dewar parasitics and instrument heat loads. Note that even with these modest flow rates we have quite reasonable cooling powers available.

Table I

Two-stage Refrigerator Performance

	CF_4 stage	N_2 stage
Input pressure (atm)	68	68
Output pressure (atm)	3	2
Flow rate STP cm^3/sec	15	15
Precool temperature (K)	300	165
J-T temperature (K)	163	84
Total cooling power (W)	2.0	1.0
Precool power (W)	0.8	---
Available cooling power (W)	1.2	1.0

Such a refrigerator can be run either open or closed cycle and additional cooling stages to lower temperatures could be added. The addition of H_2 and He stages would provide temperatures down to <5K with cooling powers at the lowest temperature approximately 25mW.

A real closed cycle refrigerator requires a small high pressure compressor for the gas source. We have built such a small mechanical compressor which is oilless and provides almost isothermal compression. This single-stage compressor is capable of providing compression ratios of 40:1 with flow rates larger than those used in the previous example. We have operated this compressor for periods of weeks as a gas source for a small J-T refrigerator using argon as the working fluid. In that period we had no failure or blockage in the small refrigerator. From data taken with the cooler we can make the following estimates on its performance. Because of the low flow rates a simple parallel capillary tube heat exchanger can easily be made to give refrigerator efficiency of at least 85% relative to ideal values. The compressor and drive combined are 60% efficient and a motor of at least 70% efficiency can be used. Therefore, the refrigerator of the example for an 85% efficient J-T and heat exchanger would have available cooling powers of 1.2W at 165K and 1.0W at 84K with an input power of 19W.

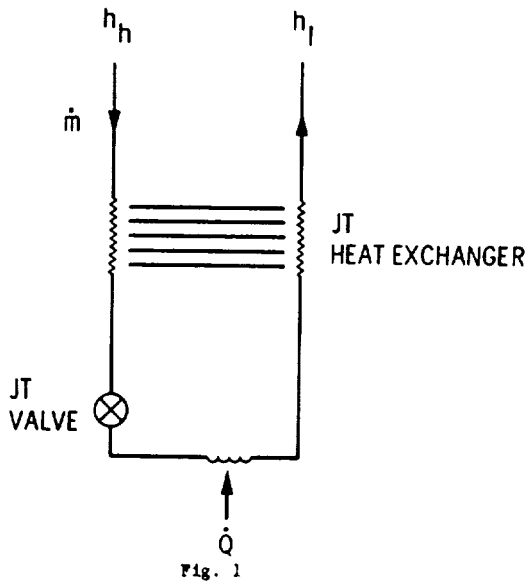
h_h
h_l
$\dot{m}$
JT
HEAT EXCHANGER
JT
VALVE
$\dot{Q}$

Fig. 1

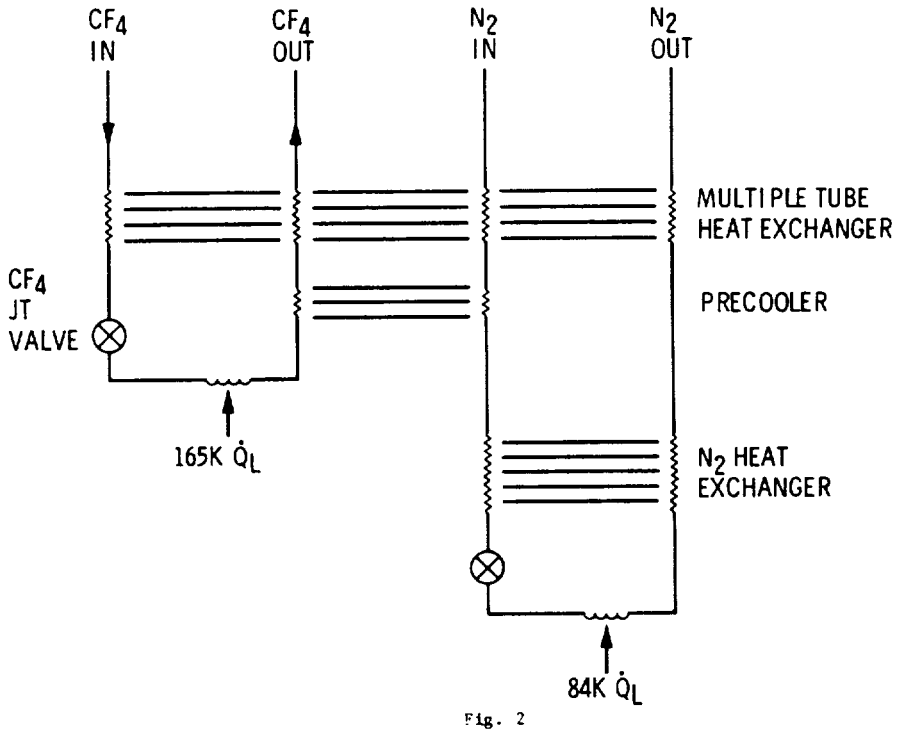
CF_4
IN
CF_4
OUT
N_2
IN
N_2
OUT
MULTIPLE TUBE
HEAT EXCHANGER
PRECOOLER
CF_4
JT
VALVE
165K $\dot{Q}_L$
N_2 HEAT
EXCHANGER
84K $\dot{Q}_L$

Fig. 2

QUESTIONS

K. B. Sigurdson, JPL

1. For a 4.2K, .01W, 4-stage cascaded J-T refrigerator, is 18W input power the total required for all 4 compressors?

Author's reply:

Yes. The calculation assumes the same efficiencies as given in the two-stage example of the text, a particular dewar design whose small parasitic heat loads are handled by the refrigerator, and no excess cooling capacity at the upper stages.

REFERENCES

1. Chan, C. K.; Tward, E.; and Elleman, D. D.: Miniature J-T Refrigerators Using Adsorption Compressors, Adv. in Cryogenic Engineering 27, 735, 1982.

2. Little, W. A.: Scaling of Miniature Cryocoolers to Microminiature Size. NBS Special Publication 508, 75, 1978.

3. NMR Technologies, Mountain View, CA 94043.

4. Elleman, D. D.; Petrac, D.; Chan, C.K.; and E. Tward: Thermal Stability and Noise of a Miniature J-T Heat Exchanger Refrigerator System. Proceedings of the 9th International Cryogenic Engineering Conference, p. 385, Butterworth 1982.

5. Chan, C. K.: Optimal Design of Gas Adsorption Refrigerators for Cryogenic Cooling, Proceedings of this conference.

SUITABILITY OF COMMERCIALLY AVAILABLE LABORATORY CRYOGENIC REFRIGERATORS TO SUPPORT SHIPBOARD ELECTRO-OPTICAL SYSTEMS IN THE 10 - 77 KELVIN REGION

R. G. HANSEN

R. G. Hansen & Associates
1324 "C" State Street
Santa Barbara, CA 93101

E. A. BYRD

Naval Surface Weapons Center
White Oak
Silver Spring, MD 20910

ABSTRACT

The primary development of cryogenically cooled infrared systems was accomplished by the Air Force for its various FLIR (Forward Looking Infrared) systems designed for airborne, passive night vision. Essential to the development of these FLIR systems was a family of closed cycle refrigerators which had to meet a limited envelope requirement, utilize a nonlubricated compressor module, and be light in weight. These refrigeration systems proved not only costly but also were characterized by a rather short meantime before maintenance interval. Although commercially available closed cycle refrigerators accomplished the same cooling function, they use modified oil-lubricated reciprocating compressors which are limited in their axis of orientation to an angle of approximately 15-20 degrees maximum from horizon. This restriction quickly eliminated them from being considered for use aboard naval vessels for passive infrared systems.

Recently, manufacturers of commercial cryogenic refrigeration systems initiated product lines featuring oil-lubricated, rotary type compressors which, as a result of preliminary tests, indicate an acceptable tilt tolerance of up to 45 degrees.

INTRODUCTION

Over the past 15 years considerable emphasis has been put forth by various agencies within the United States Government to develop closed cycle refrigeration systems for the cooling of infrared and optical devices. The primary application has been Forward Looking Infrared Systems (FLIR) which operate on the principal of cooled (sub-77 Kelvin) infrared sensors operating in a passive mode.

Primary emphasis on developing closed cycle refrigeration systems has been undertaken by the U.S. Air Force for airborne FLIR systems and the Army for ground-based mobile vehicles. Both users share the common requirement for a miniature, dry-lubricated compressor module with a lifetime of approximately 1,000 hours and the capability of being field maintainable.

It is the purpose of this paper to introduce the concept of utilizing commercially available laboratory cryogenic systems to support and sustain the longterm operation of electro-optic systems over the temperature region of 10 - 77 Kelvin for shipboard use.

CURRENT STATE OF MILITARY TECHNOLOGY FOR ELECTRO-OPTIC SYSTEMS

In an effort to provide commonality for the defense requirements, attempts were made to establish a common mod refrigeration system which would be interchangeable within various service requirements. This system, however, was designed for compact mobile use with size, weight, and nonrestrictive orientation being paramount design considerations. With this in mind, dry-lubricated compressors, of small size and short lifetime, have been utilized. Although they perform their intended function and have greatly enhanced the capabilities of our airborne and ground-based military forces, it is our opinion that naval requirements can use less sophisticated, although highly reliable, closed cycle refrigerators to support shipboard electro-optic systems with appreciable savings in economy and downtime for maintenance.

LABORATORY CRYOGENIC SYSTEMS

To perform the necessary cooling function for a variety of laboratory cryogenic sample cooling needs, a typical system comprises a compressor module, interconnecting ambient temperature gas lines, and a cryogenic expansion head (more commonly referred to as a cold head assembly). Commercially available, these systems have specifications of 10,000-20,000 hours of operating time before maintenance interval with projected meantime before failure of 25,000 operating hours. Additionally, the cold head assembly can be separated from the compressor module by as far as 100-200 feet by utilizing rigid plumbing for the supply and return of ambient temperature gas to the expansion module from the compressor.

Although the refrigerator cold head assembly presents no design constraints other than that of size, the typical laboratory system provides long term cooling with temperature stabilities of $\pm$ 0.01K over the temperature range of 10K to 77K.

The compressor module is the primary area of concern for shipboard

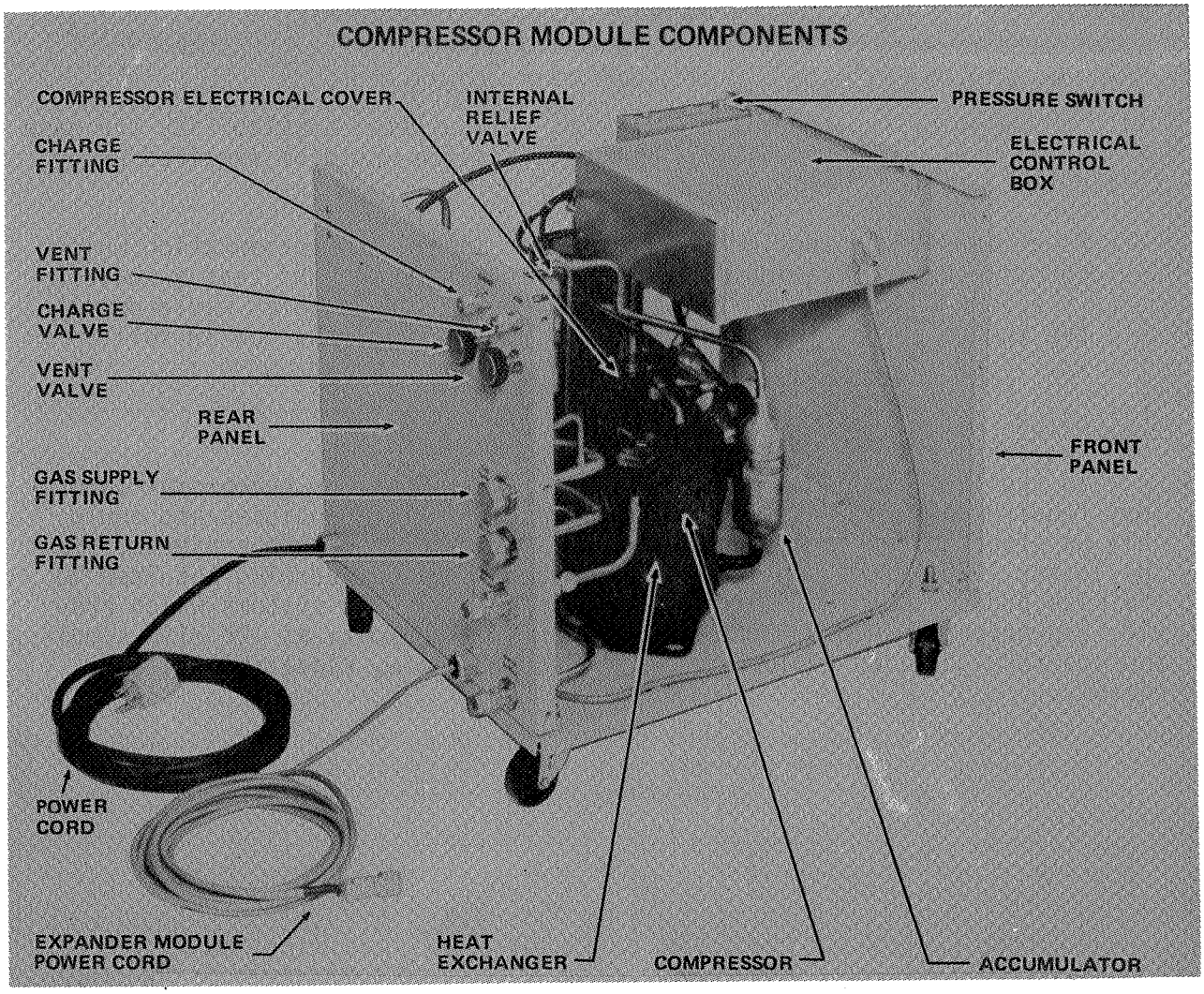

Air Products & Chemicals Model 1RO2W Rotary Compressor.

applications. The compressor is an oil-lubricated compressor which may be of reciprocating or rotary design with a weight of approximately 90 kg and may be oriented in up to a 14-20^0 list on reciprocating type compressors and 45^0 on rotary type compressors. This factor was established by elevating an Air Products and Chemicals, Inc. Model 1RO2A rotary compressor in such a manner as to allow the unit's orientation to be positioned at varying angles and the compressor's performance monitored on the inlet and outlet helium pressure gauges. Results indicated that orientation changes of up to 45^0 were tolerable to the compressor's function with no adverse effects in performance.

The changes in orientation were for five (5) minute duration and were accomplished in both the X and Y axis. After these tests, the compressor was operated for 1 1/2 hours. Should further testing on the part of the authors be undertaken, it would be our intent to monitor the compressor's temperature at varying positions to determine if any specific orientation or tilt angle restricts oil lubrication and thus overheats the compressor. With this in mind, it is our belief that future naval requirements should pursue the relatively attractive merits of commercially available refrigeration systems for the benefit of economy, reliability, availability and ease of maintenance. Of course, Mil-Spec certification would be required prior to fleet use.

As a means of protecting the compressor module from orientation which would provide nonlubrication of moving parts, it is thought that a conical mercury switch be integrated into the compressor module which would deactivate the compressor during times of excessive list, pitch, yaw or roll.

CONCLUSION

In the 1970's closed cycle refrigeration systems for commercial laboratory requirements were costly, manufactured in small quantities and could only be afforded by heavily endowed laboratories or research projects. In the latter 1970's, the application of cryogenic vacuum pumping resulted in the mass production of commercially available cryogenic systems which provide approximately 0.250 watts of refrigeration capacity at 10K with simultaneous refrigeration of 10.0 watts at 77K with ease, repeatibility and economy.

LOW COST MICROMINIATURE REFRIGERATORS FOR LARGE UNIT VOLUME APPLICATIONS

Robert M. Duboc, Jr.
MMR Technologies, Inc.
1400 Stierlin Road, Suite A-5
Mountain View, California 94043

ABSTRACT

Photolithographic techniques have been employed to fabricate small Joule-Thomson refrigerators in laminated substrates. The gas passages of a J-T refrigerator are formed by etching channels as narrow as 50 microns and as shallow as 5 microns in glass plates which are then laminated together. Circular refrigerators on the order of 1.5 centimeters in diameter and .75 millimeters thick have been produced which cool down to cryogenic temperatures in a few seconds, using Argon or Nitrogen, with no vacuum or radiation insulation. Even smaller refrigerators are being developed for both faster cooldown and low refrigeration capacity applications.

By using this technology, custom refrigerators can be designed to meet specific application requirements. These refrigerators can then be mass produced in a high yield process, which is expected to lead to low unit costs for large volume applications.

INTRODUCTION

Novel photolithographic techniques have been used to produce miniature cryogenic gas refrigerators. In this paper, I discuss the significant design capabilities and inherent low cost nature of this new microminiature refrigeration technology.

BACKGROUND

In the early 1970's, Little [1] recognized the need for refrigerators with cooling capacities much smaller than any then commercially available. Many electronic components such as infrared detectors, low noise amplifiers, solid state lasers, SQUID sensors and Josephson devices either require or significantly benefit from low temperature operation. Such components typically dissipate only a few microwatts to a few milliwatts while commercially available refrigerators have capacities ranging from one watt to many watts. This obvious mismatch between the refrigerators and the needs of the cryogenic electronic components suggested the need for a refrigeration cycle which could be scaled down to microminiature size and capacity [2].

After evaluating the numerous refrigerators which had been developed to achieve temperatures of 80K and below, Little focused on the Joule-Thomson refrigerator because it had no moving parts in its cold stage. This simplified the scaling problems and had the additional advantage of being free of vibration at the cold end. The advantages and disadvantages of the Joule-Thomson refrigerator as well as the scaling laws subsequently developed by Little have been presented in a series of articles [3], [4], [5], [6]. These scaling laws indicated that channel dimensions of a few microns would be required in the lower capacity J-T coolers, which effectively ruled out the small capillary tubing used in conventional coolers and provided the impetus for developing the photolithographic techniques to produce the micron sized channels.

The first microminiature refrigerators were constructed in silicon; however, this proved only partially successful because the silicon wafers used for the heat exchanger had to be made excessively thin due to the high thermal conductivity of silicon and proved to be too fragile to hold the high operating pressures. Glass was then selected due to its high strength and low thermal conductivity.

A set of novel photolithographic techniques have subsequently been developed to etch and bond together the thin slides of glass to form the present generation of microminiature Joule-Thomson refrigerators [7].

FABRICATION-TECHNIQUES

To form the heat exchanger, channels of 50 microns width and 10 microns depth are precisely etched in thin glass plates by an abrasive etching technique. This is done by the application of a special photo resist to the glass slides which is then exposed and developed to define the pattern of channels for a J-T refrigerator. These channels are then etched using a fine particle sandblasting technique, Figure 1. Next, the slides are cleaned and bonded together to form the encapsulated gas passages of the refrigerator.

In mass production, a step and repeat process is used to produce a mask of many images of the channel pattern. This allows one to generate multiple copies of the refrigerators on one large sheet of glass. These are then diced and laminated. Figure 2 shows a plate of multiple slides for a fast cooldown refrigerator discussed later in this paper. This fabrication process has proven to be reliable and consistent, leading to low unit costs for high volume production runs.

DESIGN CAPABILITIES

Figure 3 shows an early model microminiature refrigerator produced with the techniques described above. During operation, high pressure gas, such as N_2 at 1800 psi, is introduced to this device through one of the holes at the right. It then flows through the narrow channels in the counterflow heat exchanger to the single capillary channel where it drops to a low pressure approaching one atmosphere. This isenthalpic reduction of gas pressure causes the temperature of the gas to fall a few degrees. The cooler gas then flows into the boiler cavity at the left end of the refrigerator, continues through a hole in the central plate of glass, and finally flows out through the wide, shallow outflow channel. During initial cooldown, the outgoing gas in the counterflow heat exchanger causes regenerative cooling of the incoming gas until liquefaction occurs in the boiler cavity. The temperature of this liquid is determined by the pressure at the boiler,

which in turn is determined by the pressure drop of the gas as it flows through the outflow channel. For example, LN_2 at one atmosphere boils at 77K, while at two atmospheres it boils at 84K. Hence, as in all Joule-Thomson refrigerators, the pressure drop in the outflow channel limits the minimum temperature.

The scaling laws developed for MicroMiniature Refrigerators indicate that as the mass flow through the channels drop, turbulent flows cannot be maintained without a significant increase in the pressure drop. While in conventional heat exchangers, turbulent mixing of the gas is essential for adequate heat transfer; in these planar microminiature refrigerators, adequate heat transfer can occur in relatively wide, shallow outflow channels through conduction alone because of the small mass flow.

As an example, one should note that in the refrigerator of Figure 3 there are twenty narrow inflow channels in parallel which are bracketed together to feed the single capillary channel. This type of interconnecting would be difficult and costly with traditional plumbing techniques, but with photolithography, the only difficulty lies in preparing the initial artwork. More advanced models of microminiature refrigerators have been produced which rely on complex networks of interconnecting channels, which accomplish a number of design objectives not practical in 'standard plumbing' Joule-Thomson refrigerators. For instance, most microminiature refrigerators have redundant inflow channels to minimize the clogging problems normally associated with J-T refrigerators. Also, a two J-T stage Linde refrigeration cycle is often designed into refrigerators which must operate at temperatures near the 1 atmosphere boiling temperature of the refrigerant [8].

Microminiature refrigerators with Linde cycles, or even more complex cycles, can be fabricated for only slightly more cost then ones with single J-T stages.

NEW REFRIGERATOR MODELS

Most microminiature refrigerators produced to date are similar in size to the one in Figure 3 and are typically designed to achieve 80K using N_2 at 1800 psi at 1.5 liters per minute (STP) with a net refrigeration capacity of 250 milliwatts and a cooldown time of 8 to 12 minutes.

However, the potential commercial and non-commercial applications for this technology have stimulated development in two directions:

Lower Flowrate Models: These refrigerators are designed to minimize the gas flow required for a particular application. Hence, efficiency is maximized by retaining the long thin design which isolates the cold end from the warm end by a narrow counterflow heat exchanger of low thermally conductive glass. Figure 4 shows the inflow slide of such a device designed to have 25 milliwatts capacity using 1800 psi N_2 with a flow of about 0.1 liter per minute. The cooldown time will vary from one to several minutes depending on input pressure and the mass being cooled.

Figure 5 illustrates a low flowrate refrigerator cooling an electronic device in a hermetic package. The planar nature of the refrigerator lends itself to this type of hybrid packaging. Such packages are potentially lower in cost than the double walled glass/metal dewars used with traditional J-T coolers.

Fast Cooldown Models: In many applications such as cooling IR detectors in tactical missiles, the primary objective is rapid cooldown. Efficiency is of secondary importance. In these cases, cooldown rate is optimized by changing the refrigerator configuration so that the amount of material being cooled, including that in the refrigerator itself, is minimized -- while at the same time maximizing the cooling capacity in the refrigerator. These objectives are achieved in the fast cooldown model shown in Figure 6. The cooling in this model takes place in the central portion of the disc shaped refrigerator, with the heat exchanger extending radially outward so that the outer perimeter is at room temperature. Hence, this refrigerator can be supported around its perimeter, providing a sturdy device capable of withstanding the high 'g' forces that occur during launch of tactical missiles. The device in Figure 6 has a cooldown rate under 4 seconds using 3500 psi Argon with a 9 liter per minute (STP) flowrate. This performance is in the absence of any vacuum insulation.

One possible way of packaging a fast cooldown refrigerator for cooling an electronic device is illustrated in Figure 7. Since no vacuum insulation is required with these devices, this package could be backfilled with a dry gas which will yield a longer shelf life package than one with a vacuum shroud.

CONCLUSION

The use of photolithography to produce microminiature refrigerators has enabled the production of refrigerators with cooling capabilities on the order of 10 to 100 times smaller than those of other commercially available refrigerators. A few significant side benefits have also resulted from this approach. The fabrication process is ideal for mass production with high yields, leading to low unit costs for high volume applications. J-T coolers can now be custom tailored for particular applications and packaged in low cost hybrid packages.

Open cycle microminiature refrigerators are finding applications in laboratories, certain scientific equipment and tactical missile guidance systems, where gas cylinders or small gas bottles can be used. Also, MMR Technologies is currently developing a miniature diaphram compressor under ONR contract N00014-78-C-0514 which will allow for closed cycle operation of microminiature refrigerators. The initial compressor prototype is designed to produce 2 liters/minute gas flow at 1400 psi while operating at 2 hz. If a miniature compressor such as this can achieve reliable life performance in excess of 2,000 hours, then closed cycle microminiature refrigerator systems are likely to find broad applications in military and commercial instruments for cooling low heat dissipating devices and specimens.

Acknowledements

I wish to thank W. Little for his helpful comments on this paper and his continuing innovative contributions to this technology. I also wish to thank S. Garvey, R. Wolfe, S. Logan and the numerous others on the staff of MMR Technologies who have contributed significantly to the rapid developments of this technology. We are indebted to the Office of Naval Research for its early support of the technology at Stanford University (grant N00014-78-C-0514).

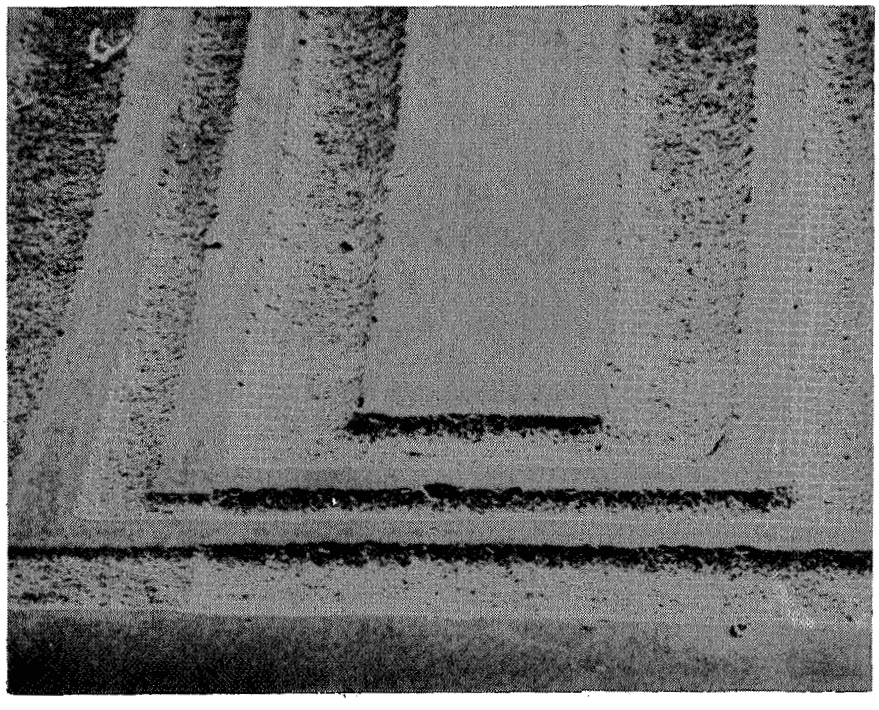

Figure 1. Scanning electron microscope picture of portion of etched glass plate used to form the heat exchanger. The wider grooves are about 200 um in width.

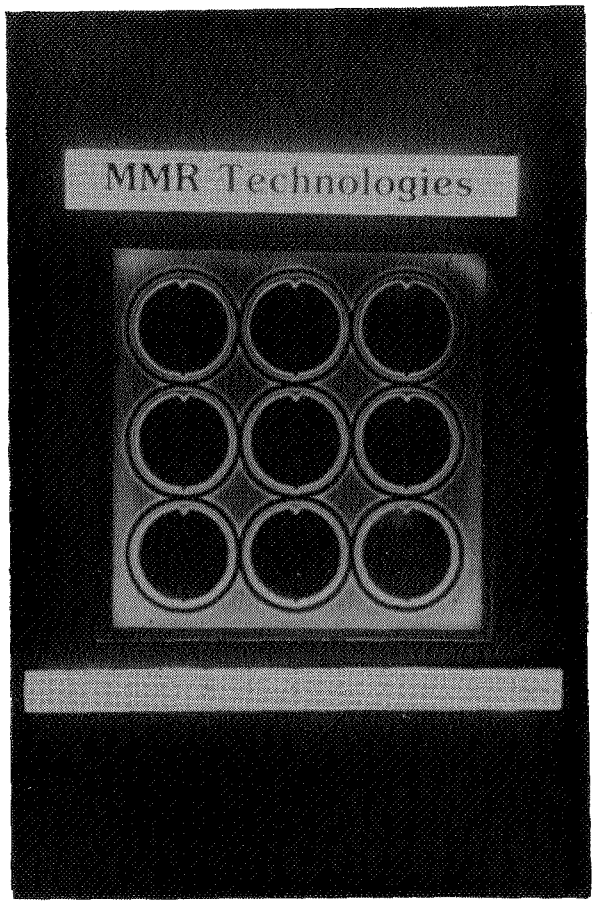

Figure 2. Plate of outflow channels for fast cooldown refrigerators before they are etched and laminated to other etched plates.

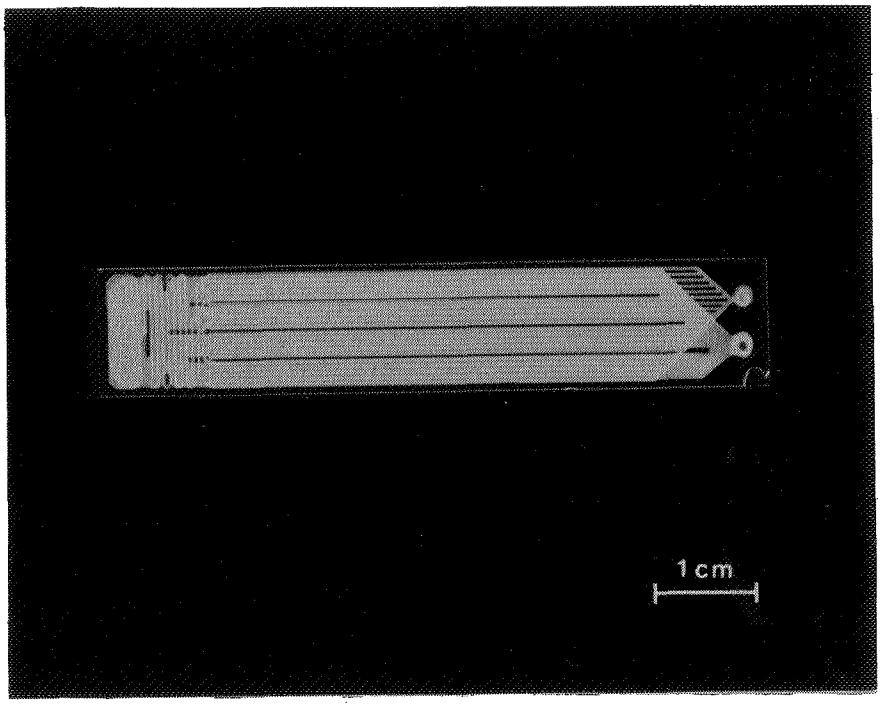

Figure 3. Original laminar flow glass Joule-Thompson refrigerator showing high pressure inflow channels, capillary, boiler and low pressure return.

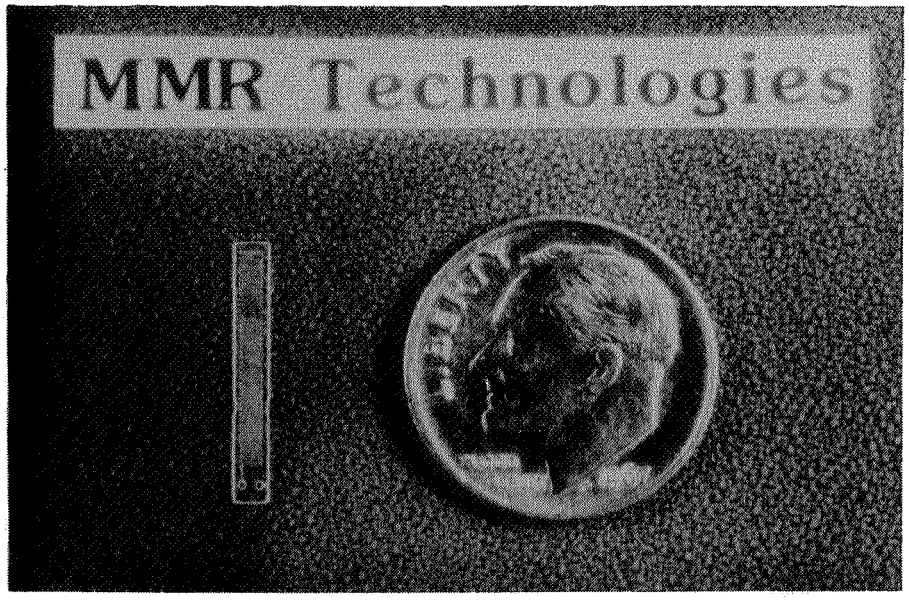

Figure 4. Inflow slide for low flowrate Microminiature Refrigerator.

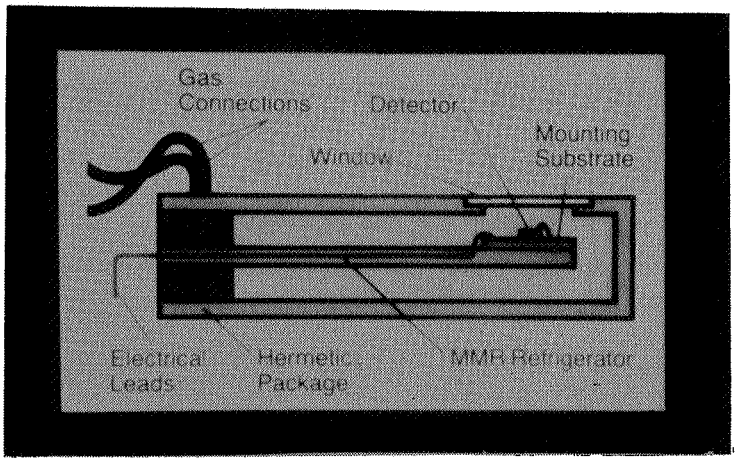

Figure 5. Possible package configuration for low flowrate model.

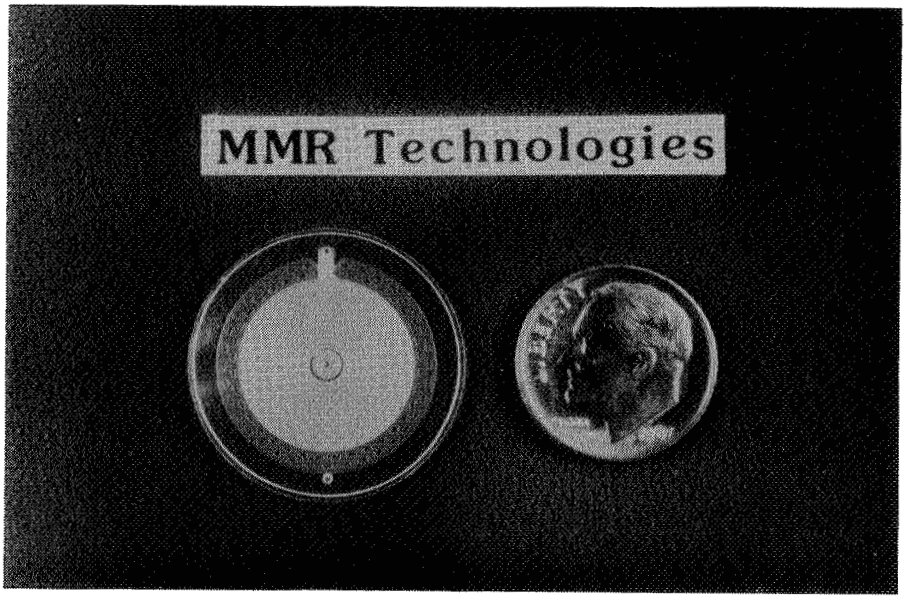

Figure 6. Fast cooldown Microminiature Refrigerator which cools in its center with heat exchange occurring radially outward.

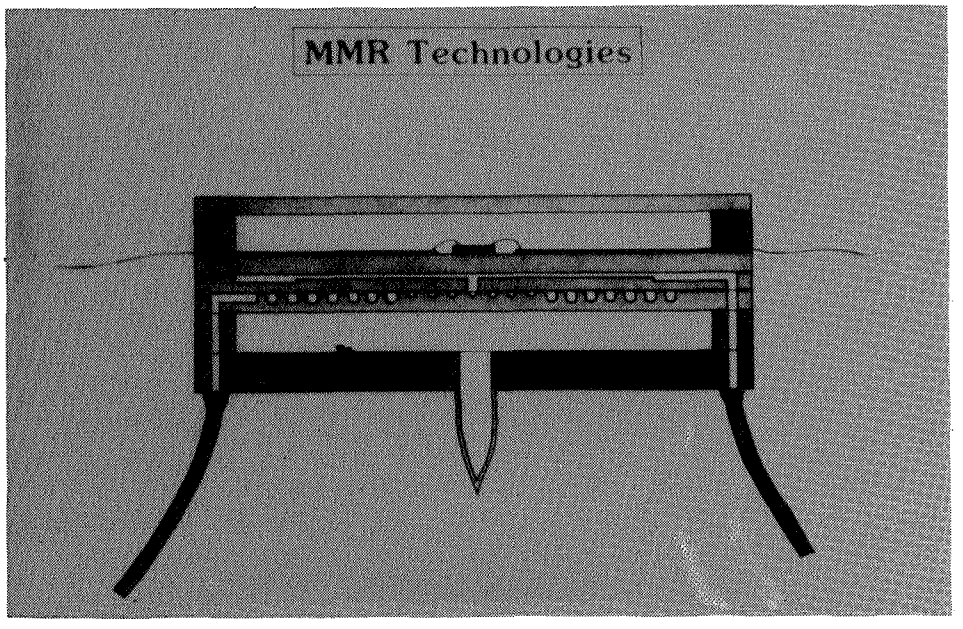

Figure 7. Possible package configuration for fast cooldown Microminiature Refrigerator with component being cooled mounted on the center cold spot and the electrical leads extending radially outward.

REFERENCES

[1] W.A. Little, (private communication).

[2] W.A. Little, MicroMiniature Refrigeration - "Small is Better", Physica 109 & 110B (1982) 2001-2009

[3] W.A. Little, "Scaling of Miniature Cryocooler to Microminiature Size", Proc. NBS Cryocooler Conf., J.E. Zimmerman and T.M. Flynn, eds. Special Publication 508 (April 1978) p. 75.

[4] W.A. Little, "Design and Construction of Microminiature Cryogenic Refrigerators", in Future Trends in Superconducting Electronics, B.S. Deaver et al, ed. APS Conf. Proc. 44 (1978) p. 421

[5] R. Hollman and W.A. Little, "Progress in the Development of Microminiature Refrigerators Using Photolithographic Fabrication Techniques", Proc. NBS Conf. Refrigeration for Cryogenic Sensors and Electronic Systems, J.E. Zimmerman et al, eds. Special Publication 607 (May 1980) p. 160.

[6] W.A. Little, "Design Considerations for Microminiature Refrigerators Using Laminar Flow Heat Exchangers", NBS Conf. Refrig. for Cryogenic Sensors and Electronic System, J.E. Zimmerman et al, eds. Special Publication 607 (May 1980) p. 154.

[7] U.S. and foreign patents are pending on these techniques and on the refrigerators themselves.

[8] J. G. Daunt in Encyclopedia of Physics, ed Flugge, Vol. XIV, Low Temperature Physics, Springer-Verlag, Berlin (1956) p. 1.

1. Report No.	2. Government Accession No.	3. Recipient's Catalog No.
NASA CP-2287		

4. Title and Subtitle	5. Report Date
REFRIGERATION FOR CRYOGENIC SENSORS	December 1983
	6. Performing Organization Code: 713

7. Author(s)	8. Performing Organization Report No.
Max Gasser, Editor	83F5158
	10. Work Unit No.

9. Performing Organization Name and Address	11. Contract or Grant No.
Goddard Space Flight Center Greenbelt, MD 20771	
	13. Type of Report and Period Covered: Conference Publication

12. Sponsoring Agency Name and Address	14. Sponsoring Agency Code
National Aeronautics and Space Administration Washington, D.C. 20546	

15. Supplementary Notes

16. Abstract

This document contains the proceedings of the Second Biennial Conference on Refrigeration for Cryogenic Sensors and Electronic Systems held at Goddard Space Flight Center, Greenbelt, Maryland on December 7-8, 1982. The Conference was attended by manufacturers, users, and government representatives interested in the latest results of cryogenic technology as they relate to aerospace use.

The Conference dealt with various topics including low temperature, closed cycle cooler technology, high temperature coolers, and low temperature coolers.

This document contains the formal papers presented at the Conference.

17. Key Words (Suggested by Author(s))	18. Distribution Statement
Cryocoolers Closed Cycle Cooler Refrigeration	STAR CATEGORY 31 Unclassified-Unlimited

19. Security Classif. (of this report)	20. Security Classif. (of this page)	21. No. of Pages	22. Price
Unclassified	Unclassified	455	A20

For sale by the National Technical Information Service, Springfield Virginia 22161

NASA-Langley, 1983